CHITOSAN-COATED PLGA NANOPARTICLES FOR OCULAR DRUG DELIVERY

By

Madhuri Dandamudi

A dissertation submitted to SETU for the degree of Doctor of Philosophy

2023

Prepared under the supervision of Dr. Sweta Rani, Dr. Lee Coffey, Dr. Gautam Behl, Prof. Anuj Chauhan, Prof. Peter McLoughlin, and Dr. Laurence Fitzhenry

Ocular Therapeutics Research Group

Pharmaceutical and Molecular Biotechnology Research Centre

Department of Science

South East Technological University

DECLARATION

I hereby declare that this material, which I now submit for assessment is entirely my own work. It is based on research carried out in the Department of Science, South East Technological University, Ireland.

Signed: Madhuri Dandamudi

Date: 17/04/2023

ACKNOWLEDGMENTS

I would like to express my thanks and sincere gratitude to my supervisor Dr. Larry Fitzhenry for his continuous guidance, invaluable advice, support, and encouragement during my PhD study. His positive attitude and approach towards research inspired me. I'm extremely grateful for the freedom and trust he had in me to try, learn, and achieve things.

I would like to extend my thanks to my entire supervisory team, Prof. Peter McLoughlin, Dr. Gautam Behl, Prof. Anuj Chauhan, Dr. Sweta Rani and Dr. Lee Coffey for their continuous advice, guidance, and training. Their immense knowledge and experience have encouraged me all the time in my academic research.

I would also like to thank my friends at OTRG and PMBRC for being kind and supportive along this journey. I am also thankful to the staff and technicians of the Department of Science for their support and help throughout.

I am forever thankful to my husband, Krishna, for encouraging and motivating me towards my goals. He is my rock who stood beside me during the ups and downs of my journey. Thanks to my daughter, Niya, for her smiles and love which made my PhD journey easier than it could have been. Words cannot express my love and gratitude to my wonderful parents and my sister for their continuous encouragement towards my higher education.

ABSTRACT

Age-related Macular Degeneration (AMD) is a disease of the back of the eye and the most common cause of vision loss in elderly people. Existing therapies involve repeated intravitreal injections with poor patient compliance, which can be associated with serious side effects such as retinal detachment and haemorrhage. In light of the need for the development of a non-invasive treatment option for AMD, this study aims to develop a topically applied nanoparticulate system encapsulating a corticosteroid and a flavonoid for extended drug release. Triamcinolone acetonide (TA)-loaded chitosan-coated poly (lactic-co-glycolic acid) (PLGA) nanoparticles (NPs) were fabricated using the thin-film hydration and oil-in-water emulsion techniques and characterized to assess their suitability.

The particle size of uncoated and coated PLGA NPs fabricated using thin-film hydration ranged from 411 nm to 456 nm, with an encapsulation efficiency of 63%. The zeta potential of PLGA NPs was -4.10 mV increasing to +44.05 mV upon chitosan coating, indicating the formation of stable NPs with polydispersity indices ranging from 0.08 to 0.19. *In-vitro* TA release from the NPs was 28% in 32 hours, subsequently reaching a plateau, suggesting controlled release of the drug. An emulsion formulation technique was also used to optimize the chitosan-coated PLGA NPs encapsulating TA, using the Box-Behnken response surface statistical design. The optimized surface-modified NPs were stable with a particle size of 334 to 386 nm, PDI between 0.09 and 0.15 and zeta potential between +26 mV and +33 mV. These NPs encapsulated 55% – 57% of TA and displayed a controlled release of the drug that reached a plateau in 27 h.

Different pathological conditions were simulated using ARPE-19 cells and exposed to various concentrations of TA and quercetin (QCN), in an attempt to investigate their potential for the treatment of AMD. The concentrations utilised were non-toxic on ARPE-19 cells and showed no signs of synergetic toxicity and changes in morphology of the cells (with cell viability >80%). The ARPE-19 cells treated with combination decreased the cytokines expression by 3.4, 5.2, 1.7, and 2.2 folds for IL-6, IL-8, MCP-1, and VEGF-C, respectively, indicating the anti-inflammatory and anti-VEGF effects. The combination drugs exhibited a synergetic antioxidant effect compared to the individual treatments ($P < 0.05$). Investigated dual drugs were successfully encapsulated into the optimised NPs. Future work will focus on investigating the stability and transport of the dual drug-loaded NPs in *in-vitro* and *ex-vivo* conditions. The size of the NPs in conjunction with the biodegradable and biocompatible properties of the polymers suggest these particles might be promising for topical ocular drug delivery.

TABLE OF CONTENTS

LIST OF FIGURES

LIST OF TABLES

LIST OF ABBREVIATIONS

AMD	Age Related Macular Degeneration
ARPE-19	Adult Retinal Pigment Epithelial Cell Line-19
BAB	Blood-Aqueous Barrier
BRB	Blood-Retinal Barrier
CNV	Choroidal Neovascularization
DED	Dry Eye Disease
DSC	Differential Scanning Calorimetry
EE	Encapsulation Efficiency
FTIR	Fourier-Transform Infrared Spectroscopy
HCECs	Human Corneal Epithelial Cells
LOD	Limit of Detection
LOQ	Limit of Quantification
NPs	Nanoparticles
PDI	Polydispersity Index
PLGA	Poly (Lactic-Co-Glycolic Acid)
RPE	Retinal Pigment Epithelium
TA	Triamcinolone Acetonide
TGA	Thermogravimetric Analysis
VEGF	Vascular Endothelial Growth Factor
WHO	World Health Organization
ZP	Zeta Potential
LPS	Lipopolysaccharide
H_2O_2	Hydrogen peroxide
APA	Acid phosphatase assay
ELISA	Enzyme-linked immunosorbent assay
DPPH	1,1-diphenyl-2-picrylhydrazyl
DCFH-DA	Dichloro-dihydro-fluorescein diacetate

Chapter 1: Literature Review

1.1 Introduction

The eye is an important organ that gathers significant information about our surroundings. It is designed for protection from foreign bodies, with a range of physiological and anatomical barriers. It is these barriers, as well as its complex structure that makes it so challenging to treat many ocular diseases. Anatomically, the eye is divided into two segments: the anterior and the posterior segments. The anterior segment is the visible part of the eye whereas, the back of the eye is known as the posterior segment [1].

According to the World health organisation (WHO), the majority of people with vision loss and vision impairment are aged over 50 [2]. As the percentage of aging in the global population continues to increase, the number of people suffering from age-related ocular diseases will also significantly rise (>21.1% of Europe's population are now over 65) [3]. Diseases of the posterior segment of the eye, such as age-related macular degeneration (AMD), diabetic retinopathy and macular edema, are the most common causes of vision loss [4].

AMD is a multifarious degenerative disease with gradual loss of central vision in people aged over 50 years. At present, there is no cure for this disease, but treatment will slow down its development [5]. AMD is classified into two types: wet AMD (neovascular and exudative) and dry AMD (atrophic and non-exudative), ~67 million Europeans are suffering from AMD and the numbers are expected to increase by 15% in the next 25 years [6]. This condition is typically treated by regular intravitreal (IVT) injections of expensive monoclonal antibodies (bevacizumab and ranibizumab), where the injection is given into the vitreous of the eye [7]. This can be associated with serious side effects, such as retinal detachment [8], retinal haemorrhage [9], endophthalmitis [10] and an increase in intraocular pressure [11]. Together with an increased financial burden, this treatment leads to poor patient compliance and a significant number of patients not turning up for follow-up injections [12,13]. As such, there is an unmet clinical need for the development of both new therapeutics and controlled-release drug delivery systems for the treatment of AMD and similar diseases of the posterior segment of the eye.

Targeted drug delivery systems with controlled release properties could provide benefit in the treatment of posterior segment disorders [14–16]. To this end, emerging drug delivery systems include implants [17], polymeric-controlled release injection [18], nanoparticles (NPs) [19] and genetic medicines [20], etc. The current study aims to investigate new combination therapy and to develop an effective nanoparticulate system that can deliver dual drugs in an extended-

release manner to treat AMD, thereby reducing the listed side effects. In this chapter: ocular diseases, routes of drug delivery to the eye, polymers and methods used to fabricate NPs and their characterization are discussed along with previous investigations.

1.2 Ocular Diseases

The eye can be broadly divided into anterior and posterior segments, where the latter constitutes about two-thirds of the eye [21]. The anterior segment includes the tear film, cornea, conjunctiva, iris, ciliary body, lens, and aqueous humor, while the posterior segment encompasses the sclera, choroid, retina, Bruch's membrane, vitreous humor, optic nerve, and retinal blood vessels, as represented in Figure 1.1.

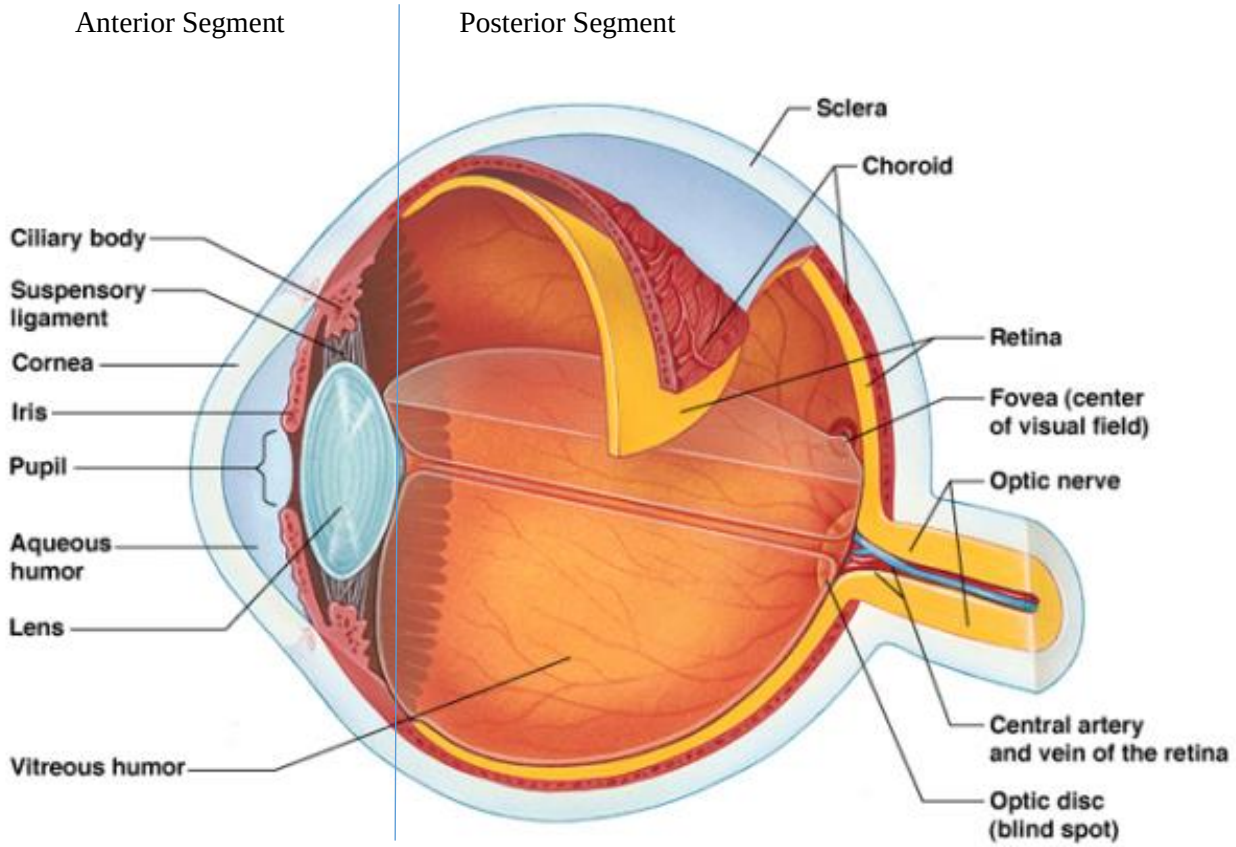

Figure 1.1: Schematic representation of the eye [22].

Several diseases can affect the structure of the eye with outcomes starting from discomfort to vision loss. Globally there are at least 2.2 billion people with vision impairment and the common diseases resulting in vision impairment include glaucoma, cataract, AMD and diabetic retinopathy [23].

1.2.1 Anterior segment diseases

Diseases that can affect the front of the eye include cataract [24], conjunctivitis [25], and dry eye disease [26], etc. The development of opacification or cloudiness within the lens due to damaging of the crystallin protein leads to cataracts [27], which, if left untreated leads to vision loss and which is one of the common causes of blindness [28]. The most frequently performed ophthalmic operation is cataract surgery, where the cataract is extracted [29]. Conjunctivitis occurs due to infection or inflammation to the conjunctival tissue. It is the most common ocular disease, which occurs by bacterial, viral, fungal infections, irritants and allergens and is commonly called ‘pink eye' or ‘red eye’. Meibomian gland dysfunction (MGD) is blockage of the Meibomian glands, which impacts the production of enough tear film lipids and which can lead to the rapid evaporation of tears. [30]. MGD is the leading cause of dry eye disease (DED) and both have similar symptoms [31].

DED is a multifactorial disorder of the tears and ocular surface resulting in discomfort, visual obstruction, and unstable tear film with possible ocular surface damage. It is characterized by the elevated osmolarity of the tear film accompanied by subacute inflammation of the eye surface. The disease can be of two types: dry eye with less tear production (aqueous deficient) and rapid evaporation of tears (hyper evaporative). The location of the tear film and tear glands in the eye are shown in Figure 1.2. Around 10% of cases arise from aqueous deficiency whereas 80% is accounted for by hyper evaporation, mostly caused by Meibomian gland dysfunction and mixed cases of both types of DED [32]. Although the complete pathology of DED is unknown, the unstable tear film and osmolarity can damage the ocular surface, initiating an inflammatory cascade, which generates immune responses. These immune-inflammatory responses continue to damage the ocular surface by developing self-regulating inflammatory cycles until treated [33].

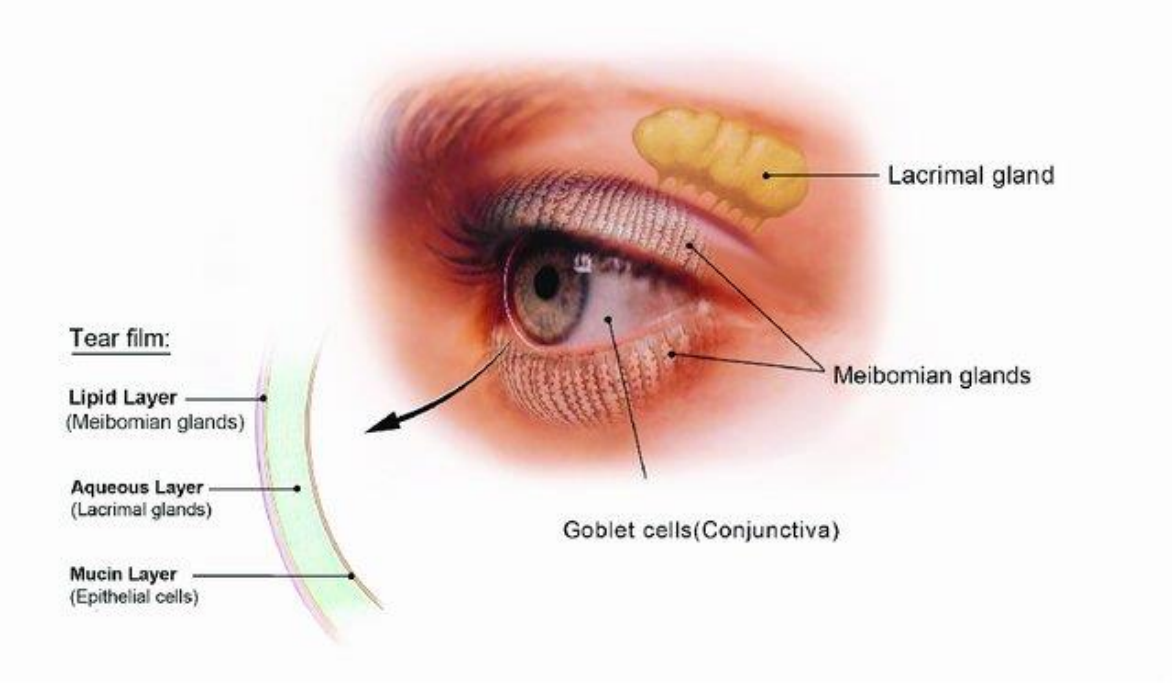

Figure 1.2: Representation of tear film made of lipid, aqueous and mucin layers along with tear (lacrimal) glands [34].

1.2.2 Posterior segment diseases

Posterior segment eye diseases commonly affect the retina, choroid and optic nerves and include retinitis pigmentosa [35], glaucoma [36], diabetic macular oedema (DME) [37], diabetic retinopathy [38], AMD [39], etc. Glaucoma is a condition, which effects the tissues of both anterior and posterior segments, it is characterized by an optic neuropathy that leads to the gradual degeneration of optic nerve axons and the death of retinal ganglion cells [40]. It is generally caused due to elevated intraocular pressure because of abnormal production or blockage of the aqueous humor, which may damage the optic nerve. An irreversible disease, the signs of glaucoma begin with a gradual loss of vision leading to complete blindness [41].

1.2.2.1 Diabetic retinopathy

Diabetic retinopathy (DR) is one of the leading causes of blindness in working age adults and it is a future health problem due to the increase in the diabetic population [42]. It is a specific vascular complication of Type I and II diabetes mellitus, with around 60% of Type II diabetics and almost all Type I diabetics showing some signs of DR [43]. DR is of two types based on its development: proliferative and non-proliferative. Non-proliferative DR is characterized by increased permeability of retinal vessels, exudate deposits, basement membrane thickening, and micro-haemorrhages. Proliferative DR is complicated and includes the same clinical symptoms as non-proliferative DR, but with the inclusion of pathologic angiogenesis. These

new vessels are delicate and leak fluid and blood into the eye. Blood in the vitreous can obstruct the path of light to the retina, resulting in spots within the visual field [38].

1.2.2.2 Age-related macular degeneration (AMD)

AMD is a degenerative, posterior segment disease and it is the leading cause of vision loss in developed countries with gradual loss of central vision in people over 50 years [44]. Millions of people suffer from severe retinal diseases like AMD and glaucoma and globally the numbers are increasing every year, 243.4 million people are expected to have AMD by 2030 as seen in Figure 1.3 [45].

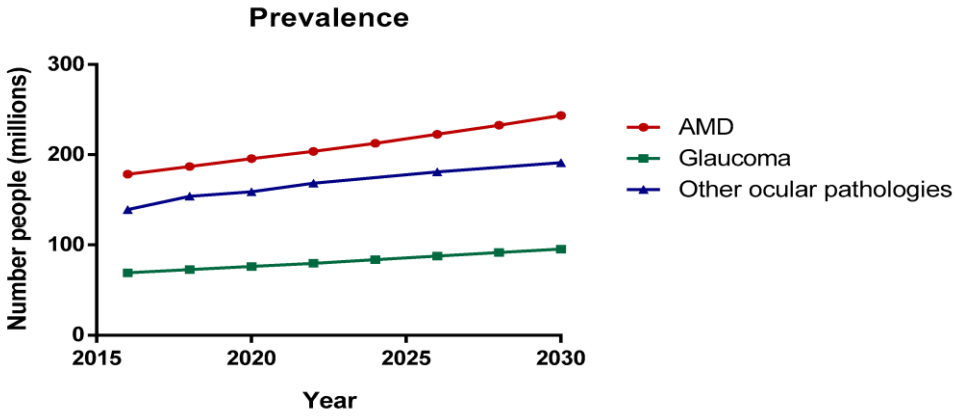

Figure 1.3: Estimated number of people globally with AMD and glaucoma projection for 2025 and 2030 [45].

Our vision is generated by conversion of light into electrochemical signals by the retina and the macula, which is the centre part of the retina and consists of light sensitive cells responsible for sharp central vision [46]. The damage to the macula in AMD affects the central vision of the patient (Figure 1.4), which plays a vital role in leading an independent life.

(a) (b)

Figure 1.4: Vision of (a) normal person and (b) AMD patient [47].

Taylor *et al.* have documented the experiences of AMD patients regarding diagnosis of their disease and the effect of loss of central vision on their everyday life, as well as strategies for coping with AMD [48]. The progression of AMD is characterized by the evolution of new blood vessels (angiogenesis) in the retinal pigment epithelium (RPE), which results in atrophy, and detachment of Bruch's membrane as seen in Figure 1.5. As stated in Section 1.1, no cure has been developed for this disease, but treatment may slow down its development [49].

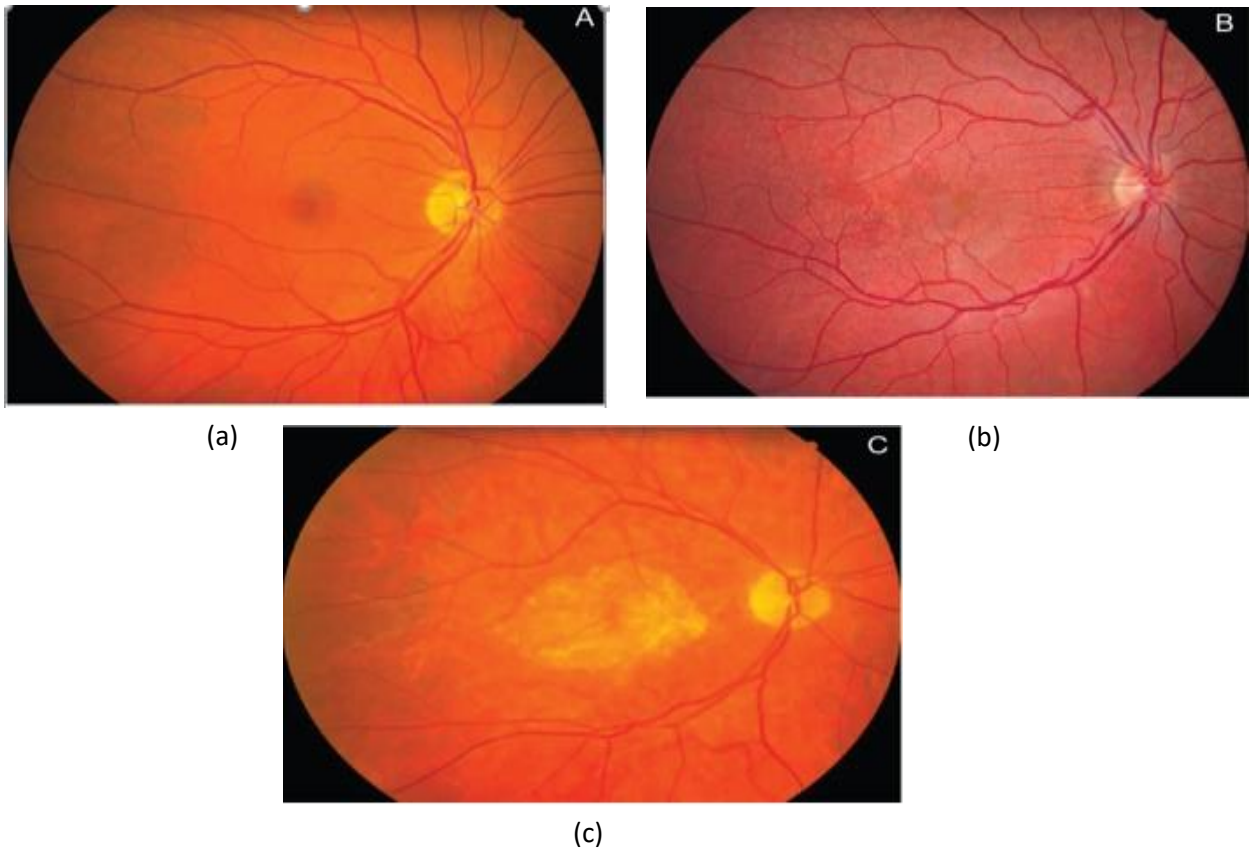

Figure 1.5: Fundus photographs showing the macula and optic nerve: (a) Normal subject; (b) Patient with multiple drusen within the posterior pole; (c) Patient with advanced AMD showing geographic atrophy within the macula [49].

AMD is generally classified into two types: wet AMD (neovascular and exudative) and dry AMD (atrophic and non-exudative). The characteristic lesions of dry AMD are smooth drusen, as seen in Figure 1.5 (drusen are round, discrete, multiple, and various sized sub-RPE deposits in the macula) and changes with the pigmentation of RPE. In wet AMD, new blood vessels developed, leading to leakage of fluid and blood under the macula. This may result in scarring, retinal detachment, and irreversible vision loss [50]. The pathogenesis of AMD includes: oxidative stress, lipofuscin build-up in the RPE, abnormal extracellular matrix, apoptosis and atrophy [51].

The AREDS (Age-Related Eye Disease Study) categorised AMD based on the characteristics of the drusen, neovascularization, and atrophy [52]. According to their clinical trial studies, drusen measuring 63 μm, 63-124 μm and larger than 125 μm in diameter were considered as small, intermediate, and large, respectively. ARED subtypes of AMD were listed as: (1) if there were less than five small drusen considered as no AMD; (2) mild AMD if the presence of numerous small drusen or one intermediate-sized drusen was seen; 3) intermediate AMD involves the appearance of multiple intermediate-sized drusen along with large drusen, or non-central geographic atrophy (GA); and 4) advanced AMD includes central GA or CNV causing vision loss (4 (a) involves categories 1, 2, and 3 whereas 4 (b) associated with low visual acuity <20/32).

1.2.2.3 Age related macular degeneration therapeutics

The current standard treatment for AMD is through IVT injections with anti-VEGF (vascular endothelial growth factor) agents. These anti-VEGF agents control choroidal neovascularization (CNV), which occurs in the late stage of AMD where branching and development of new blood vessels evolve from the choroid (these blood vessels reach the RPE and damages central vision). Marketed anti-VEGF agents include: pegaptanib, ranibizumab, bevacizumab, aflibercept, conbercept, abicipar-pegol, brolucizumab, faricimab, ziv-aflibercept, and Tarcocimab tedromer. According to their molecular structures and synthesis procedure, these anti-VEGF agents can be aptamers, monoclonal antibodies (mAbs), or recombinant fusion proteins. [53].

While these anti-VEGF treatments have revolutionized the therapy for this complicated disease, as mentioned in Section 1.1 they require regular IVT injections, which are associated with many side effects [54]. Together with an increased financial burden, this treatment leads to poor patient compliance, with an estimated 1 in 4 patients not returning for follow up treatment [55]. This creates a defined need for new advanced therapeutic approaches, which can either reduce or negate the need for current IVT injections. Novel therapies could include those given topically or long-acting controlled release approaches that have a suitable safety profile [56].

1.2.2.3.1 Glucocorticoids for AMD

The strong immune protection of the eye, while guarding the retinal tissue against any damage, can also expose it to autoimmune targeting [57]. Autoantibodies in response to retinal antigens have been traced for many ocular diseases including AMD [58]. The inflammation causes

frequent damage to adjacent cells and the immune system cannot protect tissues with low regenerative capacity, like the retina. A detailed understanding of the pathogenesis of autoimmune retinopathy will be needed for the development of novel and effective therapies for AMD [59]. Drusen contains amyloid P, vitronectin, apolipoprotein E, IgG immune complexes, factor X, complement factors (C5 AND C5b-9 complexes), interleukins, carboxyethyl pyrrole protein adducts and tissue metalloproteinase 3 (TIMP-3) [60]. Most of these components are found to be inflammatory and immune factors. These findings point to the fact that both immunity and inflammation have a role in drusen formation [61,62]. Morohoshi *et al*. found that 94% of patients with early AMD and 83% of late AMD patients displayed high amounts of retinal autoantibodies and also noticed that several retinal antigens are being targeted by autoantibodies in the serum of AMD patients [63].

The importance of glucocorticoids (GCs) for the treatment of ocular inflammatory disorders was initially noticed in the early 1950s [64]. GCs are extremely important steroid hormones, which regulate various homeostatic and metabolic functions in the physiological systems [65]. These can be considered as a therapeutic option for many posterior segment eye disorders for their antiangiogenic, anti-inflammatory and anti-proliferative properties [58]. An anomalous proliferation of cells is triggered and associated with inflammation with intra-retinal fluid accumulation related to blood-retinal barrier dysfunction, which may be restored with steroidal treatment. Proliferation of intraocular tissue is one of the major problems left unsolved in clinical ophthalmology and GCs have been shown to suppress the proliferation of cells [66]. Synthetic GCs are one of the most commonly used drugs for the treatment of allergy, autoimmune and inflammatory diseases [67]. They are mainly used for their immunosuppressive and anti-inflammatory properties, which are regulated through signal transduction by the glucocorticoid receptors in the human body. In ophthalmology, GCs such as dexamethasone, triamcinolone, fluocinolone, prednisolone and their derivatives have shown to be useful in treating disorders like uveitis, macular edema and AMD [68–70]. Recently, Gaballa *et al.* reviewed corticosteroids usage for ocular diseases, their route of delivery, adverse effects and future perspectives [71]. One such adverse effect is an increase in intraocular pressure (IOP) with topical administration of corticosteroid. As the trabecular meshwork cells drain around 90% aqueous humour, it contains high amounts of corticosteroid receptors. It has been hypothesised that the interaction between corticosteroid and these receptors could be the reason for elevated IOP. The authors suggested these adverse effects can be negated by regular ocular examinations for patients on long-term treatment with

corticosteroids, by choosing a suitable dosage form with the right route of drug delivery based on the disease and by preferring targeted therapy instead of generalized therapy.

Jonas *et al.* studied the effect of IVT triamcinolone acetonide on 67 AMD patients using an interventional case series study [72]. Results of the study revealed that IVT injection of 25 mg of triamcinolone acetonide showed maximum visual acuity in 66.2% and unchanged visual acuity in 19% of AMD patients. The remaining patients encountered side effects of triamcinolone acetonide IVT injections. Cataract and increased intraocular pressure were noticed, which increased with the number of IVT injections. As stated by the authors of the work, these complications are treatable with cataract surgery and topical antiglaucomatous therapeutics and post-injection side effects like retinal detachment and endophthalmitis were not reported in any of the patients.

1.2.2.3.2 Flavonoids for AMD

In the 20th century, most approved drugs were natural products or analogues derived from them [73]. Natural source-derived antibiotics such as penicillin, immunosuppressants for organ transplants such as cyclosporine, and anticancer drugs such as Taxol®, revolutionized medicine and improved quality of life [74–76]. The functions and structures of natural products and their molecular targets are believed to have evolved to interact with one another, suggesting that natural products might serve as optimal small molecule ligands for some human targets [77]. Flavonoids are widely distributed in the plant kingdom and are categorized as flavanol, flavanone, flavones, anthocyanidin and isoflavone (Figure 1.6) [78].

Quercetin is a typical flavanol-type flavonoid abundantly present in fruits and vegetables. It has been shown to have antioxidant properties with anti-inflammatory [79], anti-proliferative [80] and gene expression changing capacities [81] and found to be effective for AMD in primary research [82–84].

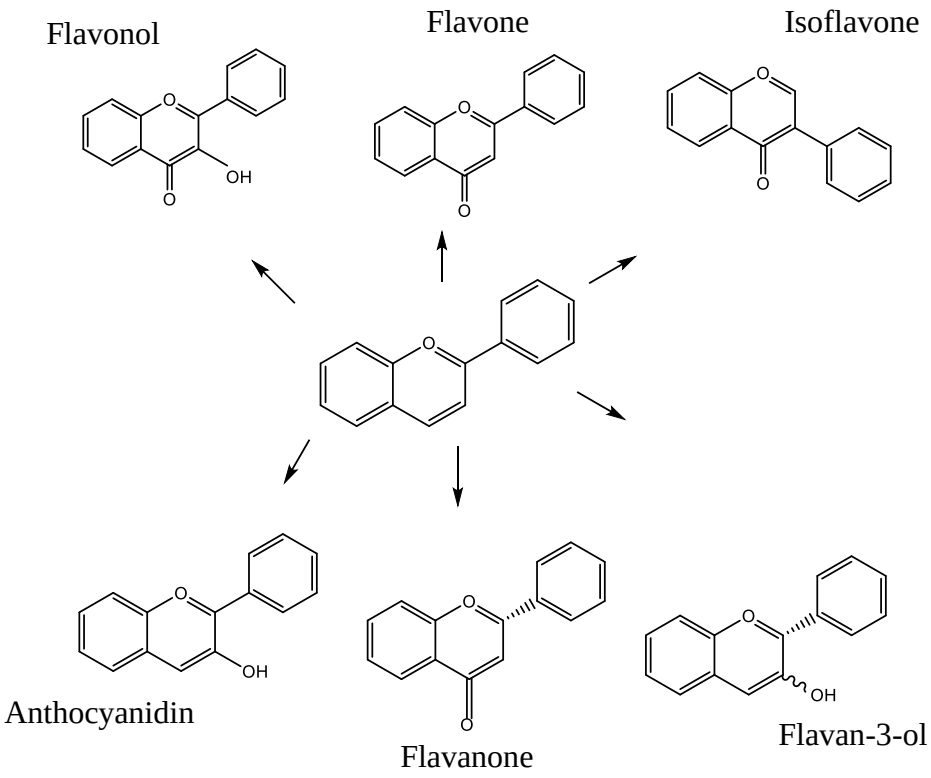

Figure 1.6: Chemical structure of flavonoids.

Chen *et al.* studied the effect of quercetin on choroidal and retinal angiogenesis and it has shown dose dependant inhibition (by inhibiting the growth of vascular endothelial cells) on a rhesus choroidal-retina endothelial cell line [85]. With the increase in quercetin concentration from 10 μM to 100 μM, inhibition elevated from 10% to 65%. Migration and tube formation of the choroidal-retina endothelial cell line was also inhibited in a dose dependent way. Several mechanisms such as inhibition of lactate transport [86], suppression of glycolysis and ATP production [87], inhibition of protein kinases [88], interference with ion pump systems [89], and various signal transduction pathways [90] have been associated with anti-proliferation activity of quercetin.

Wang *et al*. studied the protective effect of quercetin and chlorogenic acid (polyphenols) on visible light induced retinal degeneration in rabbits [83]. Experimental rabbits were divided into four groups: normal group (NG), model group (MG), quercetin group and chlorogenic group (CA). The rabbits from the MG, quercetin and CA groups were treated daily with PBS, quercetin, and CA respectively for 21 days. Rabbits in the MG, quercetin and CA groups were exposed to 18,000 lx light to induce retinal degeneration. All rabbits were euthanized after the study and the retinas were isolated for further analysis. Upon light exposure, inflammatory

cytokines (MCP-1, IL-1β and IL-8) were upregulated in the MG group whereas quercetin treated groups showed a decrease in cytokines, as seen in Figure 1.7. The mRNA and protein levels of the cytokines expressed were analysed by PCR and western blot.

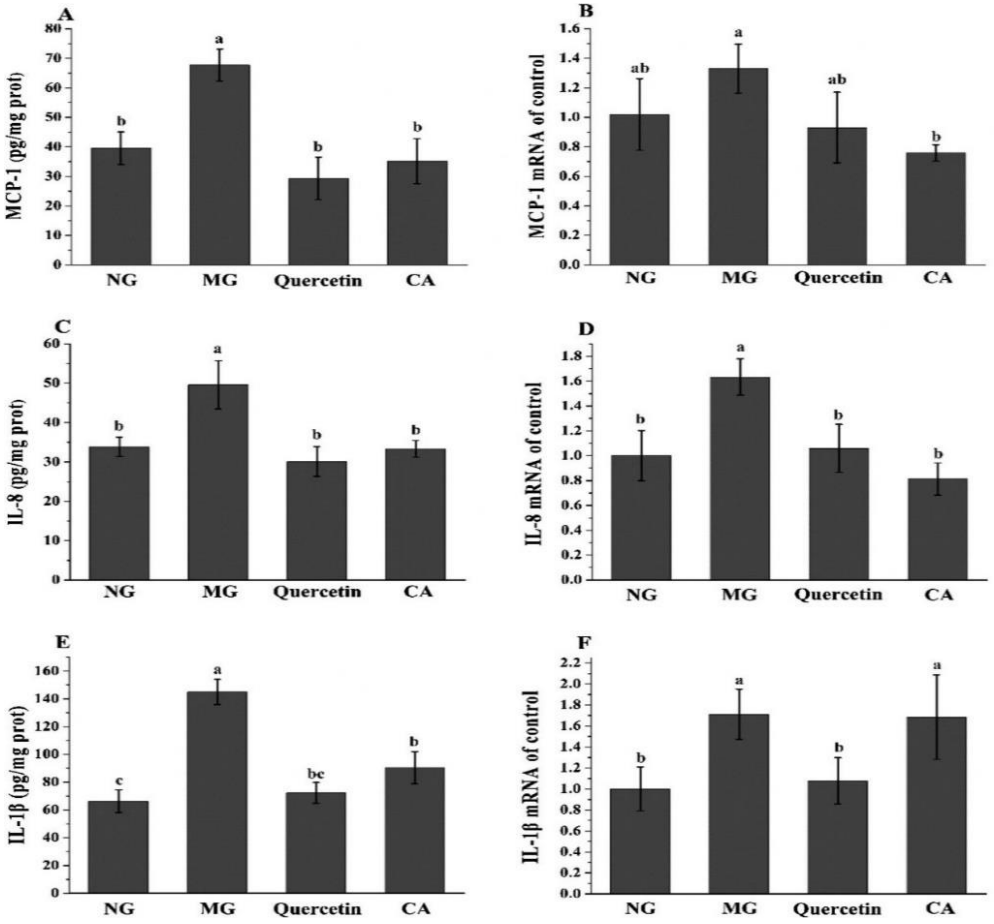

Figure 1.7: Effects of quercetin and chlorogenic acid on [A, B] monocyte chemoattractant protein 1 (MCP-1), [C, D] interleukine-8 (IL-8), and [E, F] interleukin-1 β (IL-1β). (A, C, E) protein and (B, D, F) mRNA levels in rabbit retinas after light exposure [83]**.**

To determine the inhibitory effect of quercetin and CA on CNV, the levels of VEGF and hypoxia-inducible factor-1α (HIF-1α) were quantified in the retinas of rabbits. Quercetin and CA reduced the VEGF and HIF-1α expression levels compared to the MG group as depicted in Figure 1.8.

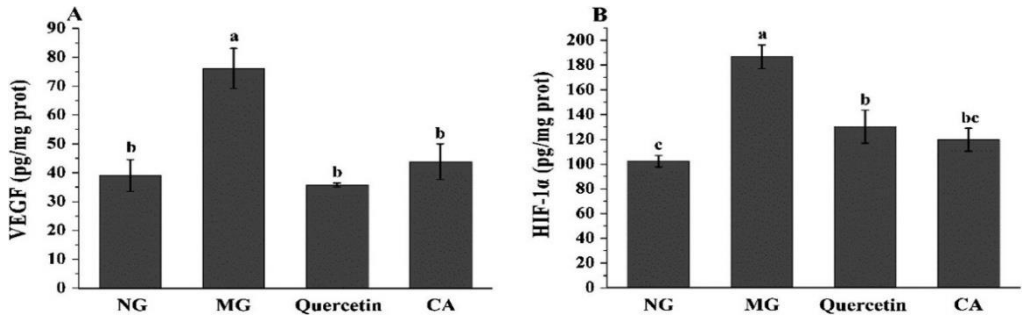

Figure 1.8: Expression levels of [A] VEGF and [B] HIF-1α determined using ELISA in the four experimental groups [83]**.**

The outer nuclear layer (ONL) thickness of retinas was measured through histological examination to track the changes in retinal morphology (Figure 1.9). Thicker ONL (35 μm) was observed for the quercetin group ($P < 0.05$) compared to MG (30 μm) and CA groups (32 μm) indicating the potential of quercetin in protecting retinal morphology from light induced damage.

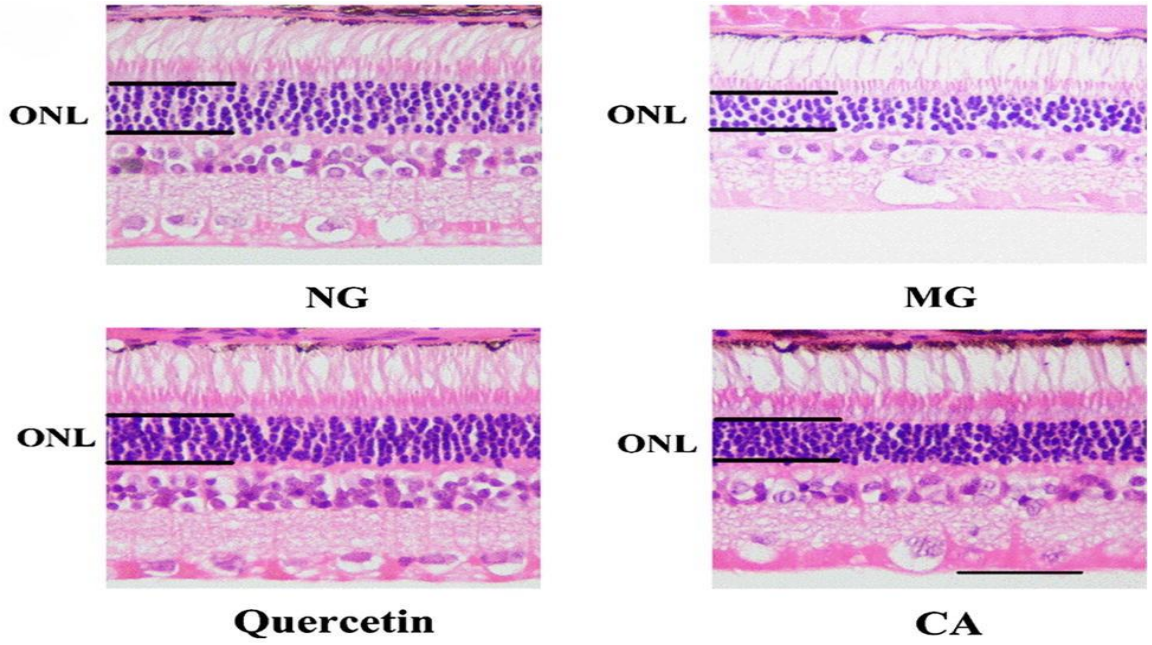

Figure 1.9: Histological image showing the effect of quercetin and chlorogenic acid (CA) on the retinal outer nuclear layer (ONL) thickness in rabbits after light exposure [83]**.**

The properties of quercetin together with a proper dosage form may help to treat multifactorial diseases such as AMD. The use of natural products on sensitive organs like the eye could minimise side effects and may protect the retina while healing or prolong eye health [91].

1.3 Ocular drug delivery

Ocular drug delivery is one of the most challenging tasks for formulation development experts. The eye is a complex organ with vast anatomical, biochemical, and physiological barriers restricting the entry of drug molecules to the site of action. Considering these features, it may be beneficial to design an ocular formulation with some requirements to efficiently compensate for the associated limitations. Generally ophthalmic drugs are administered topically, which are suitable for anterior segment eye diseases [92]. Whereas for posterior segment eye diseases alternative routes have been evolved (periocular and IVT routes) considering the clearance mechanisms and poor bioavailability associated with the topical route [93]. As mentioned in the earlier sections, the invasive nature of these treatments along with serious side effects can lead to poor patient compliance. Developing a non-invasive treatment option for posterior segment diseases is a great challenge for drug delivery researchers. Understanding the various routes of drug administration with their related challenges is of utmost importance to overcome this challenge.

1.3.1 Routes of ocular drug delivery

There are three main ways of delivering therapeutics to the eye: topical, local delivery (IVT [94], periocular [95], implants [96], etc.) and the systemic route as represented in Figure 1.10. The selection of drug delivery route depends on the type of disease, the area of the eye to be treated and patient compliance.

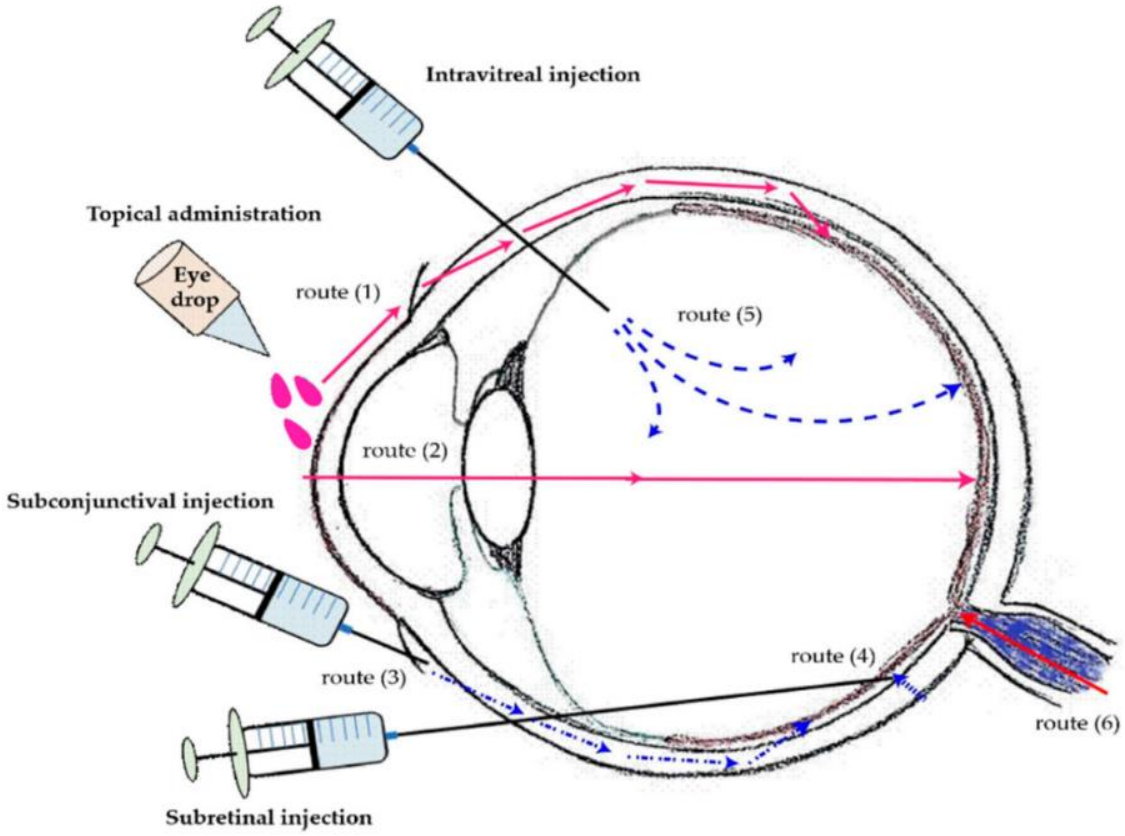

Figure 1.10: Routes of drug transportation via topical administration (1 and 2), subconjunctival injection (3), subretinal injection (4), intravitreal injection (5), and drug transportation from systemic circulation (6) [97]**.**

1.3.1.1 Topical

Due to ease of application and patient compliance, topical instillation is the most widely chosen route to treat anterior segment ocular diseases with topical methods accounting for 90% of commercial eye formulations [98–100]. Addo *et al.* detailed the anatomical and physiological limitations of the eye (Figure 1.11) resulting in poor ocular bioavailability of the drug with topical instillation resulting in difficulty to attain a therapeutic concentration of the drug in the posterior segment [101]. Precorneal fluid drainage is one of the key reasons for low drug absorption into the ocular tissues [103]. After topical instillation, the instilled volume is drained into the nasolacrimal duct which maintains only 7-10 µl of the precorneal fluid, the excess fluid is lost due to physiological nasolacrimal drainage [104].

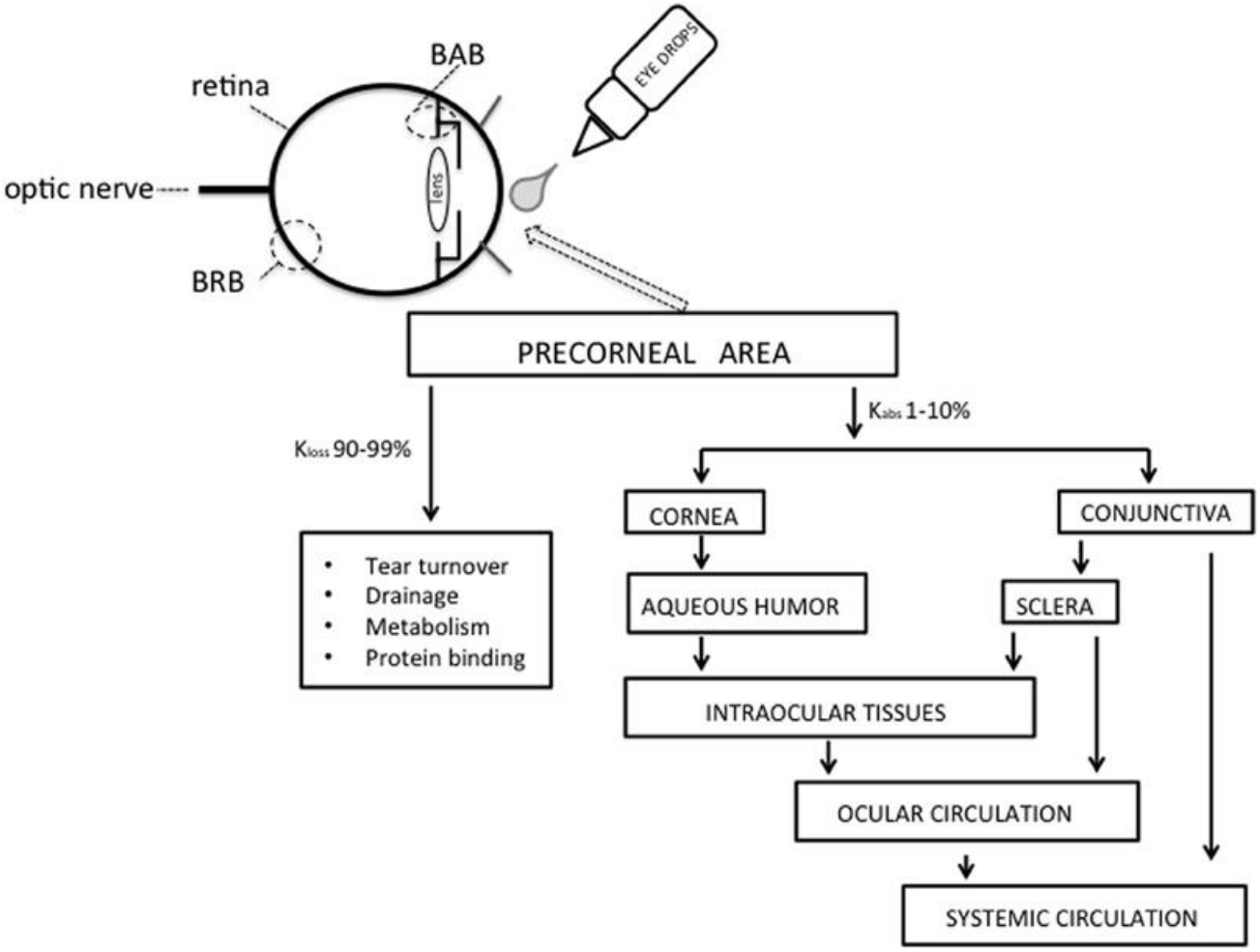

Figure 1.11: Illustration of movement of the drug into the eye crossing the blood-aqueous barrier (BAB) and blood-retinal barrier (BRB) after topical administration [102].

The administered drug reaches the tear film, which is the first barrier of the topical route, where the drug is diluted by tears and cleared from the ocular surface through tear turnover rate and blinking [105]. A majority of the topically administered drug is cleared from the corneal surface in 2–3 min, this reduces drug residence time on the cornea. The thickness of the tear film is between 4–7 μm and is composed of lipid, aqueous, and mucin layers [106]. The outer lipid layer prevents the tear film evaporation of the tear film and controls the tear overflow. The middle aqueous layer contains proteins and enzymes that can bind and metabolize the active drug, impacting the drug's bioavailability. High sulfate and sialic acid groups in the mucin layer provide a negative charge, therefore mucins can repulse or attract drugs via electrostatic interactions based on the charge of the drug or nanoparticulate system. The tear film volume is 7.0–30.0 μL with an average tear turnover rate of 1.2 ml/min, hence topical formulations with a minimal volume containing high drug concentration might achieve effective bioavailability.

The drug permeates through the corneal route and the conjunctival route as shown in Figure 1.11. An avascular, transparent dome like structure, the cornea sits at the front of the eye measuring 11.5 mm in diameter, 500 µm thick in the centre and 700 µm towards the periphery. The cornea consists of five different layers: epithelium, Bowman's membrane, stroma, Descemet's membrane, and endothelium, as represented in Figure 1.12 [107].

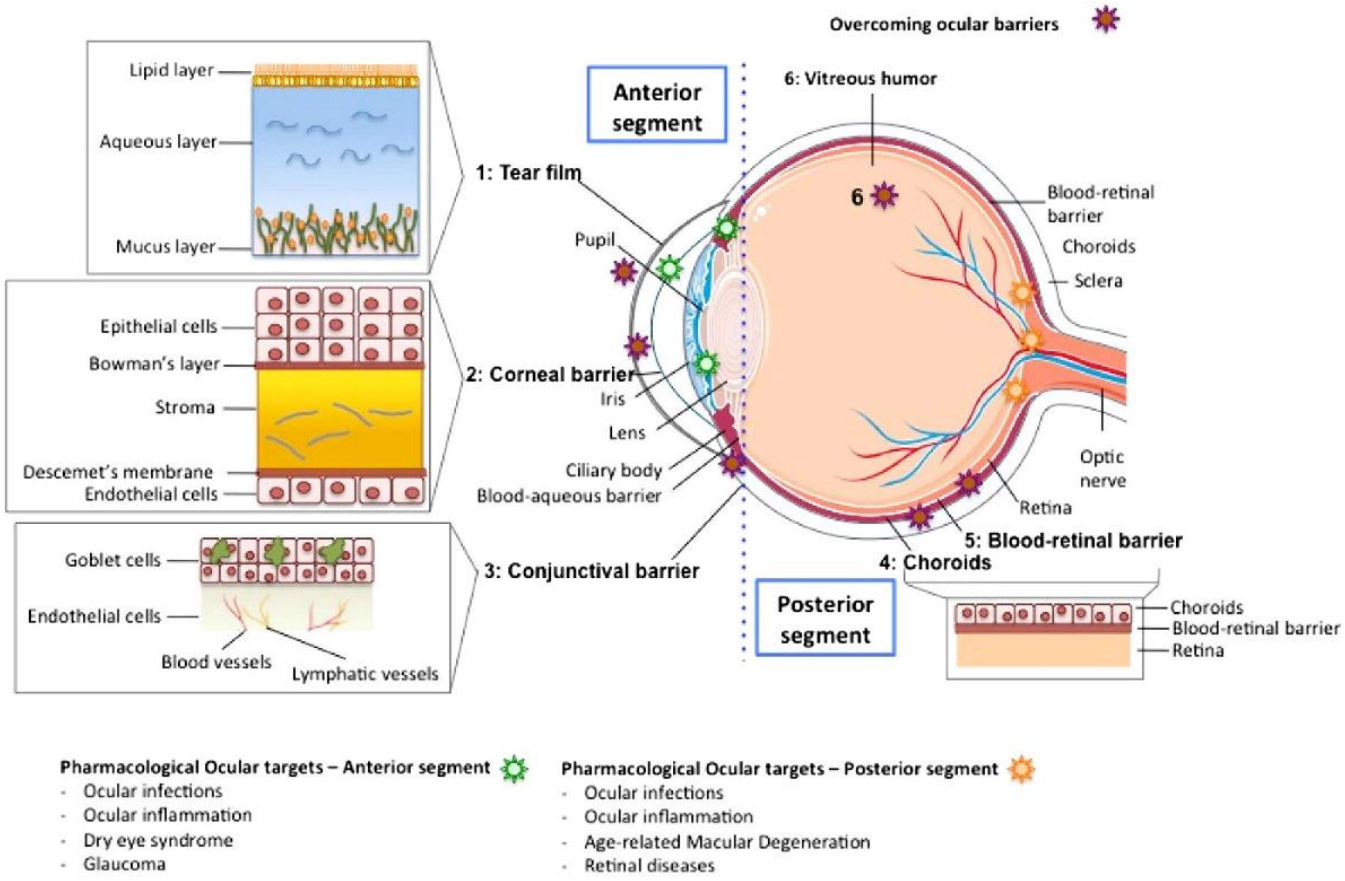

Figure 1.12: Representation of ocular barriers with pharmacological targets [108].

Among the five layers of the cornea, the epithelium plays a vital role in drug permeation. The corneal epithelium is lipophilic with tight junctions, which restricts the permeation of hydrophilic molecules. Epithelial tight junctions have a paracellular pore measuring 2.0 nm in diameter, therefore molecules with a molecular radius <5.5 Å or with a molecular weight of 500 Da generally pass through corneal epithelium *via* the paracellular route [109]. Apart from molecular weight and lipophilicity of molecules, corneal permeability is also affected by the charge of the solute. The surface of the cornea is negatively charged above its isoelectric point of 3.2, where cationic compounds bind and permeate more effectively than anionic molecules [110–112]. The corneal epithelium and endothelium prevent the passage of hydrophilic

molecules into the aqueous humor while allowing permeation of small-sized lipophilic molecules. On the other hand, the stroma allows permeation of hydrophilic molecules but restricts lipophilic molecules. Considering all these factors, only small molecules with optimal lipophilicity can permeate effectively through these barriers [113]. Due to the corneal barriers and pre-corneal factors, <5% of the administered drug reaches the aqueous humor, resulting in poor ocular bioavailability of most compounds [114–116].

In humans, the conjunctiva has a 17-fold larger surface area than the cornea, which allows for higher drug absorption across the tissue. Intercellular spacing in the conjunctival epithelium is wider than the cornea (3.0 nm in bulbar and 4.9 nm in the palpebral conjunctiva) [117]. Due to this, penetration of drugs through the conjunctiva is higher than through the cornea, but still, the drug absorption is minimal due to the presence of conjunctival blood vessels and lymphatics, which may cause loss of drug into systemic circulation [118].

The aqueous humor in the intraocular environment is protected by the blood-aqueous barrier (BAB). The non-pigmented ciliary epithelium and the endothelium of the iris-ciliary blood vessels form the BAB in the anterior part of the eye. It regulates the transfer of solutes between anterior and posterior segments and is less permeable due to the presence of tight junctions [119]. The BAB restricts the permeation of plasma-derived albumin and hydrophilic drugs into the aqueous humor from plasma and the permeation of drug molecules from the anterior to posterior segment is further limited by constant aqueous humor drainage (2.1 to 3.4 µl/min) [120].

1.3.1.2 Systemic route

After systemic injection, the drug permeates through the scleral pores and passes to choroidal circulation, posterior choroid and finally to RPE from the choroidal blood vessels [121]. The BRB and the BAB with tight junctions are the major barriers for drugs administered through the systemic route (Figure 1.13). The sclera acts as a physical barrier to many drugs due to its dense nature, given that drug permeability depends on molecular weight (smaller molecules up to 150 KDa diffuse easily) [122]. The choroid has more blood vasculature delivering oxygen and nutrients from the blood flow into the outer retina. There are two barrier functions associated with the choroid: on the one hand, it acts as a molecular filter and on the other, choroidal blood flow has a clearance mechanism [123]. Lipophilic molecules have proved to have increased choroidal delivery due to the bonding of lipophilic molecules to binding sites such as membranes and melanin [124].

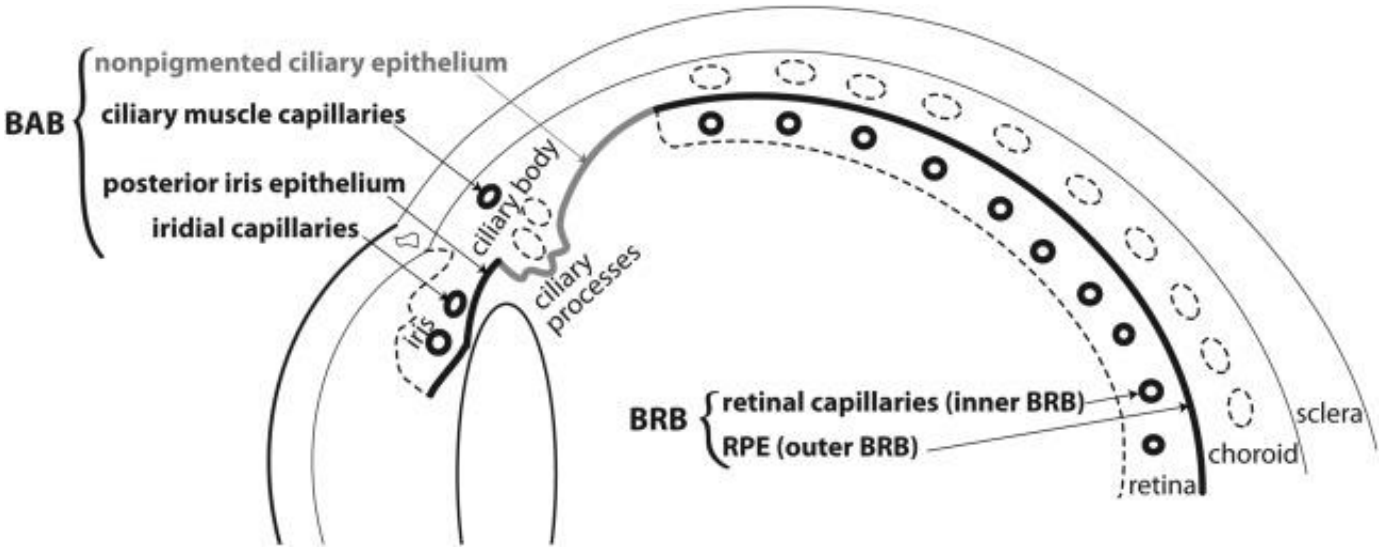

Figure 1.13: Illustration of blood ocular barriers, blood-retinal barrier (BRB) and blood-aqueous barrier (BAB) [125]**.**

The BRB mainly obstructs substance diffusion from the systemic circulation into the retina. There are two portions of the BRB, the inner and outer BRB. The inner BRB consists of retinal capillary endothelial cells (RCE), it possesses intercellular tight junctions and protects the retina from foreign substances present in systemic circulation. The outer BRB consists of RPE, which governs the diffusion of compounds [126]. Hydrophilic molecules permeate through tight junctions via the paracellular route, while lipophilic molecules traverse through the transcellular route [127]. Verteporfin (Visudyne®) is the commercially available systemic drug given intravenously to treat wet AMD by photodynamic therapy [128].

1.3.1.3 Intravitreal route

As stated in Section 1.1, the most commonly used route to deliver drugs or drug delivery systems to the posterior segment (choroid, retina and vitreous chamber) of the eye [129–131]. The drug, in the form of solution, particles, suspension or emulsion is injected through the ocular surface to intraocular tissue. Mostly, injections are directed in the pars plana region due to its lesser innervation. In the case of implants, vitreoretinal surgery is required for installing, removing, or replacing the implants. As highlighted in Section 1.1, frequent use of this route leads to retinal detachment, retinal haemorrhage, endophthalmitis and increase in intraocular pressure. The IVT route provides direct local treatment with enhanced bioavailability hence despite the disadvantages, it is used in the present day [132–134].

There are also other routes such as the periocular route where the drug is delivered to periocular tissue for local effects or may travel to intraocular tissues. It consists of other specific routes

like subconjunctival, subtenon, peribulbar, retrobulbar, suprachoroidal and trans-scleral [135]. Peribulbar and retrobulbar are generally used for giving anaesthesia and the remaining routes are for delivering drugs to the posterior segment [136].

In the subconjunctival route, the injection or implant is placed under the conjunctiva. A bleb is formed for injection, which slowly acts as a depleting depot and the drug overcomes the elimination by conjunctival blood and lymphatic system as it will pass to the sclera and choroid to reach the retina [137]. The suprachoroidal route is used to diffuse drugs slowly from the suprachoroidal space to the choroid or retina. It does not interfere with the optical path and also has lesser side effects and more bioavailability than other periocular routes [138].

1.4 Nanotechnology: A strategy for ocular drug delivery

Scientists have achieved remarkable success in the field of nanoscience and nanotechnology since their discovery in the twentieth century. Nanotechnology is any technology on the nanoscopic scale, which has diverse applications in everyday life. It is an interdisciplinary field including, physics, chemistry, material science, biology, etc., where materials and functional systems are created with special properties. Nanotechnology has a wide range of applications in the fields of textiles, agriculture, engineering, electronics, forensic science, space, medical therapeutics, etc. [139].

Nanotechnology in drug delivery deals with an entire range of nanomaterials that have specific size dependant characteristics related to biological and biomedical applications. Nanoscale materials have evolved in various forms with unique characteristics for ocular drug delivery. Different forms of nanomaterials being tested for anterior and posterior segment eye diseases include: NPs [19], nano-micelles [140], nano-suspensions [141], liposomes [142], dendrimers [143], nanoparticle-loaded contact lens [144] and sub-conjunctival implants with nanostructures [145], etc. NPs are poly-colloidal particles with sizes ranging from 10 to 1000 nm [146]. Drug can be dissolved, wrapped, embedded or adsorbed within the NPs [147]. For the use of ocular drug delivery, NPs are generally composed of proteins, lipids, synthetic polymers ((poly (D, L-lactic-co-glycolic acid) and polycaprolactone) and natural polymers (albumin and chitosan) [148–150].

NPs can be tailored to have important biological properties like biodegradability [151], biocompatibility [152], non-toxicity [153], mucoadhesiveness [154] and can be designed to improve drug targeting, drug penetration and controlled release [147]. Additionally, NPs with good physical stability can be formulated with simple techniques. Considering all of these combination of properties, NPs have been chosen widely in recent times to overcome the

drawbacks of delivering the drug through the barriers of the eye [155–157]. Drug-loaded NPs are often depicted as being either nanocapsules or nanospheres as seen in Figure 1.14.

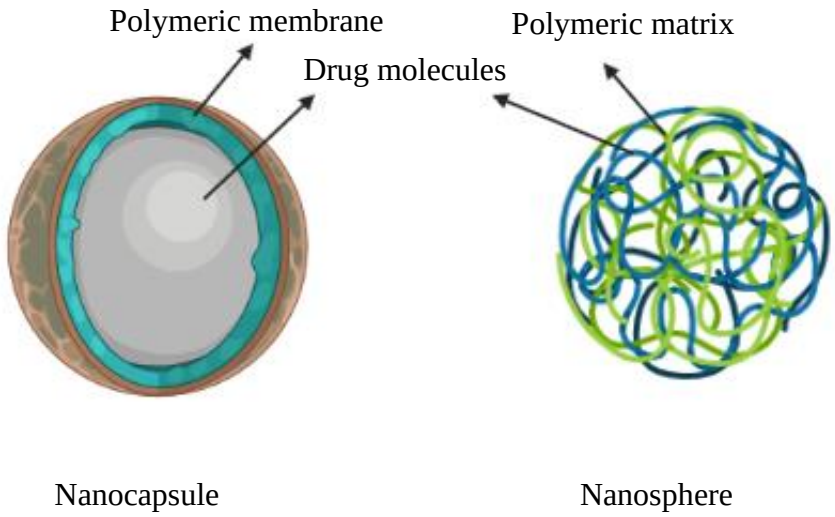

Figure 1.14: Diagrammatic representation of nanocapsule and nanosphere.

The drug is enclosed inside the polymeric shell for nanocapsules, whereas drug is dispersed uniformly in the polymer matrix for nanospheres [158].

1.4.1 Synthetic polymeric nanoparticulate systems

Synthetic polymers have well-defined structures, which can be altered for functionality and degradability. Due to the tailorable structure and modification, they have many biomedical applications [159]. Synthetic polymers such as poly (lactic-co-glycolic acid) (PLGA) [160], polylactic acid (PLA) [161], poly (epsilon-caprolactone) (PCL) [162] and poly (alkyl cyanoacrylate) (PACA) [163] are widely used in drug delivery due to their drug release properties [164].

1.4.1.1 Poly (lactic-co-glycolic acid) nanoparticles

Poly (lactic-co-glycolic acid) [PLGA] is a copolymer of PLA and poly (glycolide) (PGA). PLGA is one of the most explored polymers for ocular drug delivery due to its biocompatibility [165], biodegradability [166] and sustained release characteristics [167]. Hydrolysis of PLGA results in glycolic and lactic acids as seen in Figure 1.15, which further enter the tricarboxylic acid cycle where these acids get metabolized into carbon dioxide, energy, and water, making PLGA degradable *in-vivo*. There is a wide range of PLGAs available with varying molecular weights and PLA:PGA ratios. Generally, polymers with high molecular weight show slow degradation as more time is needed to degrade polymer chains [168].

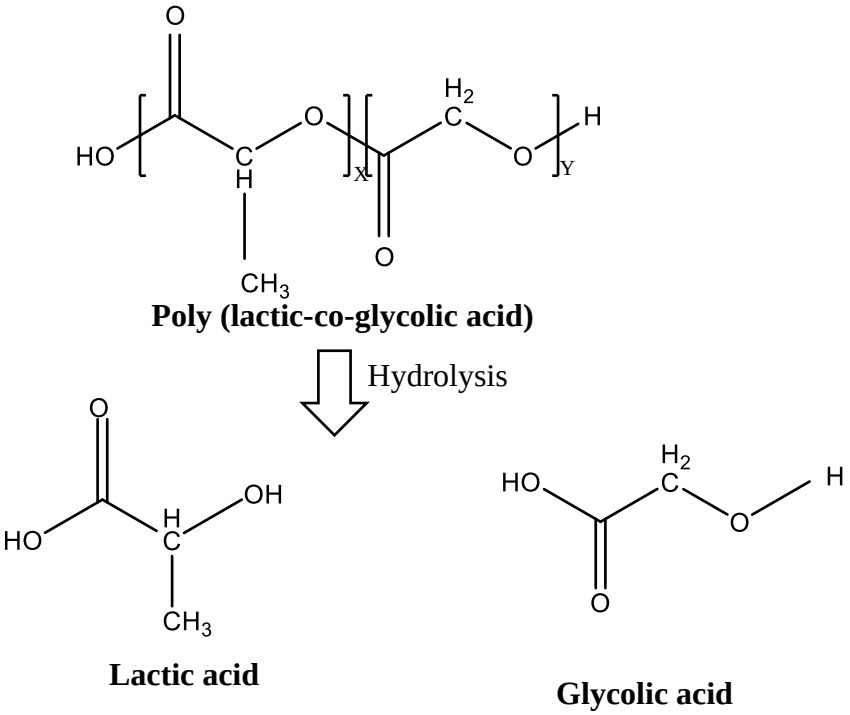

Figure 1.15: Structure of PLGA and its hydrolysis. x = number of units of lactic acid, y = number of units of glycolic acid.

There is a wide range of procedures for the formulation of PLGA NPs, which have both advantages and disadvantages. The nature of the drug, nanoparticle size, size distribution and preparation procedure play a vital role in PLGA NPs. Work on PLGA NPs in the 90s, by Yoo HS *et al*. formulated doxorubicin (an anti-cancer drug) conjugated (the hydroxyl terminal group of PLGA was activated by p-nitro phenyl chloroformate and reacted with a primary amine group of doxorubicin for conjugation) and unconjugated PLGA NPs using an emulsion-solvent diffusion technique [169]. They reported that doxorubicin conjugated to PLGA NPs demonstrated a 96.6% loading/encapsulation efficiency (amount of drug encapsulated into the particles compared to the initial weight of drug taken) and 3.5% loading percentage (% weight of the drug going into the particles compared to the total weight of the system). Sustained release was achieved over 25 days, whereas doxorubicin unconjugated to PLGA NPs achieved only 6.7% loading efficiency with around 5 days of sustained release. This shows that the method of preparation of the NPs has a high impact on drug loading and release.

Jayamanti *et al*. prepared chitosan-coated PLGA NPs containing bevacizumab using a double emulsion solvent evaporation technique to target the retina [170]. The prepared chitosan-coated PLGA NPs obtained had a particle size of 222 nm with a charge of +32 mV and encapsulation efficiency of 69%. *In-vitro* drug release was performed by incubating the formulation in phosphate buffer saline (PBS) containing antibacterial and antifungal agents, 0.1% sodium

azide and 0.02% thiomersal, respectively. Both the PLGA and chitosan-coated PLGA NPs (chitosan-coated NPs showed reduced initial burst release) showed 25% drug release in 72 h whereas 90% of drug suspension was released within 24 h. Transscleral permeation was carried out on excised goat sclera with a diffusion area of 0.80 cm^2 using a Franz diffusion cell. The flux, a measure of permeability of the particles/drug through the sclera, of the drug from chitosan-coated PLGA NPs was significantly increased (0.32 $\mu g/cm^2/h$) compared to the free drug (0.25 $\mu g/cm^2/h$). Egg hen's test chorioallantois membrane (HET-CAM) was used as an alternative to the Draize test to determine ocular irritation and tolerance. The chitosan-coated PLGA NPs showed less vascular damage compared to the positive control as seen in Figure 1.16.

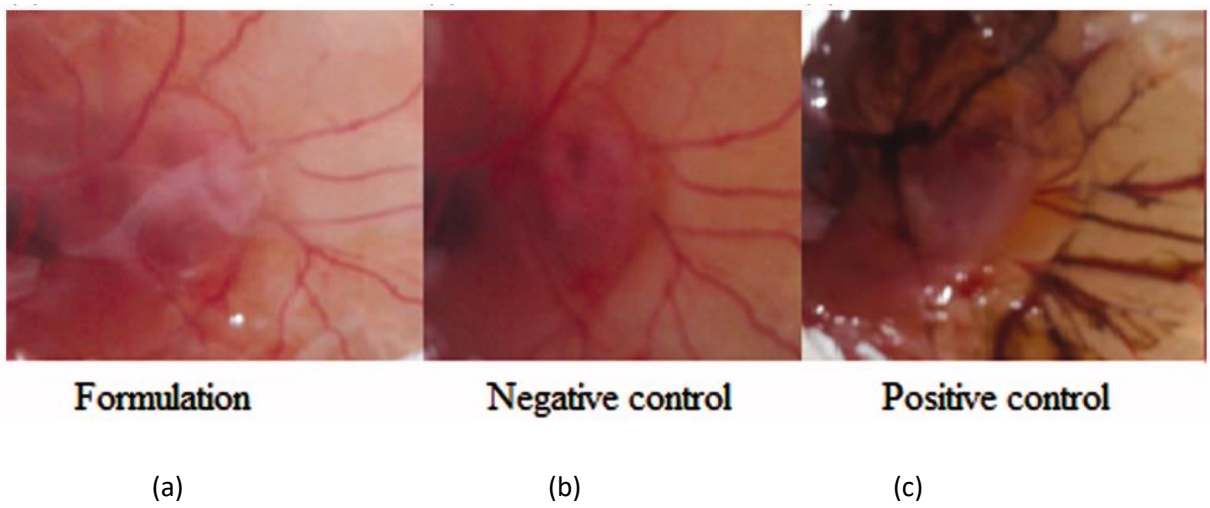

Figure 1.16: HET-CAM study images of (a) formulation, (b) negative control-saline and (c) positive control-0.1 M sodium hydroxide [170]**.**

Controlled release of drug from the NPs and the ocular tolerance exhibited in the study suggested chitosan and PLGA as suitable polymers for ocular drug delivery.

1.4.1.2 Polylactide nanoparticles

Polylactide (PLA) is a synthetic, aliphatic, biodegradable (by enzymatic activity and hydrolysis), hydrophobic polyester formed by lactide polymerization [171]. Different molecular weights of PLA with varying crystallinity can be formed by altering polymerization conditions. PLA is prepared from renewable sources, which makes it affordable and easily available for biomedical use. PLA's wide range of physical and chemical properties can be altered depending on the application [172].

Bourges *et al*. synthesised PLA NPs containing the fluorochromes Rh-6G (Rh) and Nile red (Nr) to investigate the cellular localization and kinetics of these NPs in intraocular tissues after

IVT injections to rat eyes [173]. IVT injection of 5 µL Rh NPs (140 nm, -60 mV), Nr NPs (310 nm, -6 mV), blank NPs and free dyes were applied to the rat eyes. At specific time intervals (1, 6, 18, 24, 48 h, and 4 weeks) rats were sacrificed and the eyes were subjected to examination using confocal microscopy, immunohistochemistry, and electron microscopy. The fluorescence and confocal microscopy showed the appearance of Rh NPs settling on the internal limiting membrane after one hour of injection, while no NPs were identified in the retina. After 6 h, Rh NPs were detected on the retinal surface and retinal layers, as Rh dye had diffused into the RPE. After 18-24 h of injection, Rh NPs localised in the RPE and at this time point, NPs were noticed in the vitreous and the red staining diffused into the retina, RPE and the rods outer segment. At later time points (48 h and 4 weeks) and up to 4 months, Rh NPs, Rh diffused from degrading NPs and Rh leaked from NPs was noticed on RPE cells and neural retinal tissues. A similar pattern of kinetics was seen for Nr NPs except for the prominent Nr dye and diffusion of dye from NPs authors suggested this could be due to the low aqueous solubility of the Nr dye. Immunohistochemistry and histology studies revealed the inflammatory reaction post IVT injection of all the NP samples and control with a significant increase of infiltrating cells, but the reaction improved after 48 h. The authors stated anti-inflammatory treatment might be useful along with injection. Along with the post-inflammatory reaction non-specific activation of the glial cells was also noticed, which could be a side effect of IVT injection. This activation could affect the integrity of the retina as glial cells maintain stability. .

In the above study, NPs were seen in RPE up to 4 months after injection. These systems may benefit the extended and controlled release of the active agents. But the side effects of the IVT injection noticed might be minimised by delivering these particles *via* the topical route in a suitable platform.

1.4.1.3 Poly (epsilon-caprolactone) nanoparticles

Poly (epsilon-caprolactone) [PCL] is a synthetic, aliphatic, semi-crystalline polymer formed by the polymerization (ring opening) of epsilon-caprolactone. This polymer is negatively charged due to the terminal carboxyl group and degraded hydrolytically with ester bond cleavage in aqueous media resulting in biocompatible products [174].

Lee *et al*. studied the effect of pilocarpine-loaded PCL nanocapsules and nanospheres on treating glaucoma in rabbits [175]. The particle size of both NPs was around 200 nm, nanocapsules had a hollow uniform barrier of 50 nm thickness (analysed using transmission

electron microscopy) around the particle whereas the nanospheres had a PCL matrix. The hollow structure of nanocapsules loaded 90% of the drug, which was 3 times more than nanospheres (30% - drug loading). The nanocapsule barrier diffused the drug in a controlled manner up to 42 days and reduced the intraocular pressure in rabbits but the nanosphere treated group of rabbits returned to the hypertensive stage after 7 days (electroretinogram was used to determine changes in intraocular pressure). This study showed the importance of selecting the correct type of nanoparticle for the application.

1.4.2 Natural polymeric nanoparticulate systems

Polysaccharides, proteins, and polyesters extracted from plant and animal kingdoms constitute the natural polymers. Among the wide range of natural polymers, polysaccharides are the most studied for drug delivery, due to their high stability, biodegradability, biocompatibility, hydrophilicity and low toxicity [176]. They have an added advantage compared to synthetic polymers of being a renewable resource, cost effective and environmentally friendly [177].

1.4.2.1 Alginate nanoparticles

Alginate is an anionic natural polymer obtained from the extraction of algae and soil bacteria. Alginate is an unbranched, linear polysaccharide consisting of α-L-guluronic acid (G) and β-D mannuronic acid (M), which are arranged as both homopolymers (G or M blocks) and heteropolymers (MG block) as shown in Figure 1.17 [178].

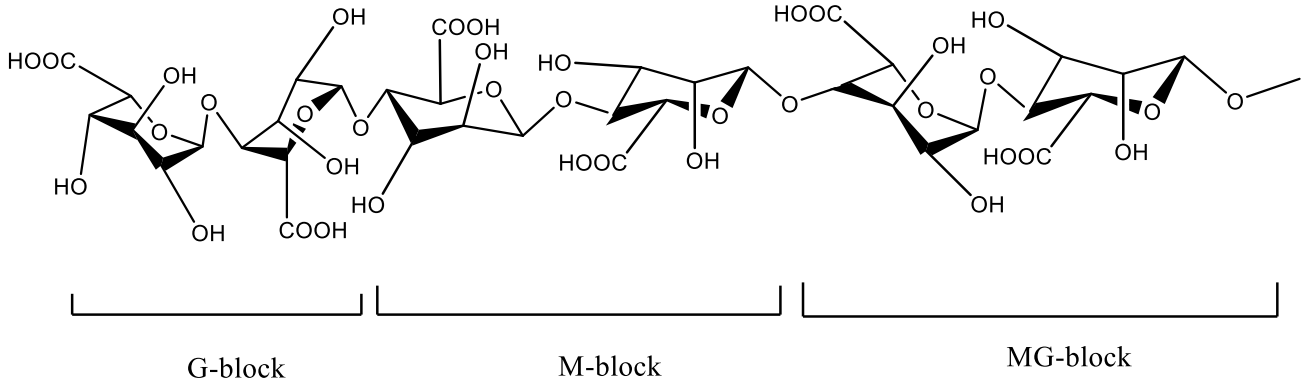

Figure 1.17: Structure of alginate showing α-L-guluronic acid (G) and β-D mannuronic acid (M).

Addition of alginate to cross-linkers like calcium chloride and polyelectrolytes with opposite charge produces hydrogel, alginate beads or nano/microparticles, which can encapsulate hydrophobic and water-soluble drugs [179]. The capacity of alginate to produce hydrogels under mild pH and temperature conditions and their inherent biocompatibility makes them capable of biomedical usage including drug delivery [180], implantation of living cells [181]

and tissue engineering [182]. Alginate has many hydroxyl groups to form H-bonds with carboxyl groups present on mucin glycoproteins, which is the major component of the inner ocular mucosa, this could increase the residence time for alginate carriers. Additionally, due to the hydrophilic nature of the alginate, it swells in aqueous media leading to high exposure to target sites. Also, the distance between the chains leading to effective penetration and higher molecular weight polymer contributes to mucoadhesion [183]. Considering these beneficial properties several alginate based carriers were developed for ocular drug delivery [184,185].

Ibrahim *et al*. prepared brimonidine-loaded alginate NPs for topical ocular drug delivery using an emulsification solvent diffusion technique and tested them against commercial eye drops (Alphagen P®) in mice [186]. The particle size of the NPs varied between 115 nm and 157 nm with a zeta potential of +35 mV and –37 mV; encapsulation efficiency and loading capacity of the drug was 74% and 11% respectively. The time to decrease IOP and duration of drug action were 7 and 21 h for alginate NPs and 2 and 5 h for commercial eye drops, respectively. The commercial eye drops showed Newtonian flow behaviour whereas the prepared system had non-Newtonian pseudoplastic flow (measured using plate rotatory viscometer), which is suggested for topical ocular drug delivery as it does not interfere with the pseudoplastic properties of the tear film. This non-Newtonian flow and bioadhesive properties of alginate when combined with polymers like PLGA, which can control the release of therapeutics, might be beneficial in developing topical formulations for back of the eye diseases.

1.4.2.2 Albumin nanoparticles

Albumin is a natural polyanionic protein extracted from a wide range of sources like bovine (BSA) [187], egg white (ovalbumin, OVA) [188] and human plasma (human serum albumin, HSA) [189]. Albumin is a single polypeptide chain consisting of 575 amino acids, including large amounts of aspartic acid, cysteine, lysine, glutamic acid and arginine and small amounts of methionine and tryptophan [190]. It has various functional groups, which can bind to complex drugs and different ligands. In terms of safety, albumin is biocompatible, biodegradable and it is produced within the body. These characteristics have encouraged the use of albumin for ocular drug delivery [191–193].

Redin *et al*. formulated bevacizumab-loaded HSA NPs (B-NP) employing the desolvation process and freeze-drying (without any physical or chemical cross-linking processes) as represented in Figure 1.18 [194].

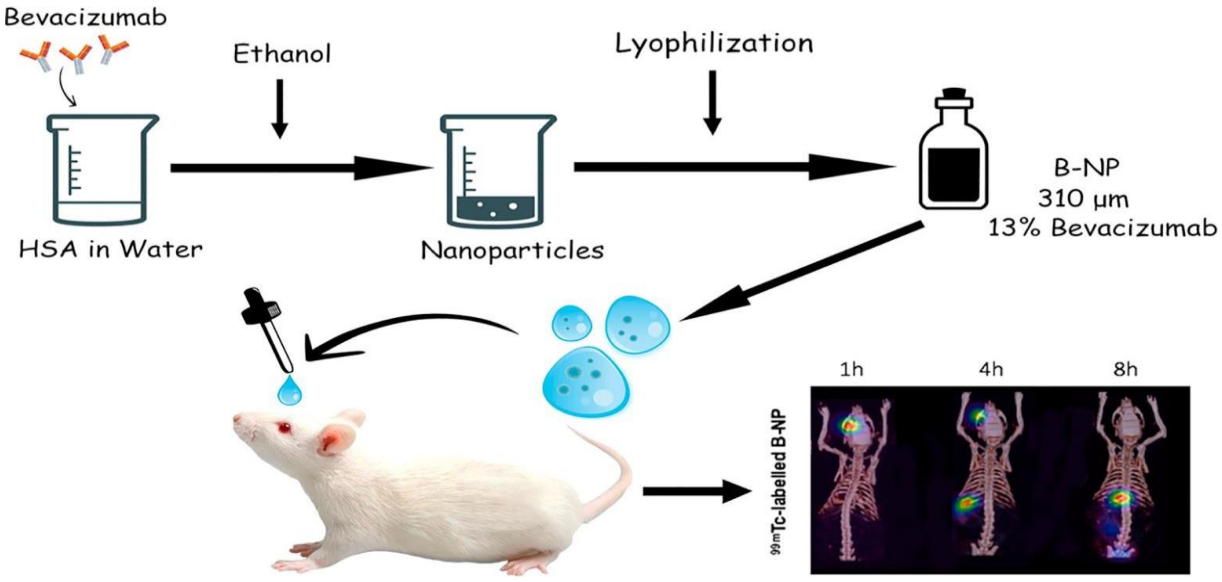

Figure 1.18: Preparation and testing of bevacizumab NPs [194]**.**

The prepared NPs were compared with HSA NPs cross-linked with glutaraldehyde (B-NP-GLU). The B-NP encapsulated approximately 13% of bevacizumab with more residence time whereas B-NP-GLU showed very low encapsulation (0.1 µg/mg). The authors suggested this may have been due to inactivation of bevacizumab while interacting with glutaraldehyde (from XRD and FTIR analysis). B-NPs were radiolabelled and topically instilled on rat eyes with the NPs remaining in the eye for 4 h and progressively moved towards the gastrointestinal tract whereas the radiolabelled free drug was visualized in the gastrointestinal tract after 1 h. In this study, NPs fabricated by protein-protein interaction were suggested for topical ocular drug delivery.

1.4.2.3 Chitosan nanoparticles

Chitosan is a polycationic polysaccharide obtained from chitin by chemical deacetylation (Figure 1.19). It is the second most abundant natural polymer after cellulose and is mainly extracted from crustaceans. The molecular weight, composition, and purity of chitosan varies with the source, extraction and processing methods [195]. Chitosan is an unbranched and linear polymer consisting of β-linked D-glucosamine with N-acetyl glucosamine groups. Deacetylation provides amino groups and makes it soluble at pH ≤ 6 leading to the formation of the polycationic polymer, which can interact with both anionic cross-linking agents (e.g. tripolyphosphates [196] and anionic polymers (e.g. alginate and hyaluronic acid [197,198]) resulting in polyelectrolyte-based systems for drug delivery.

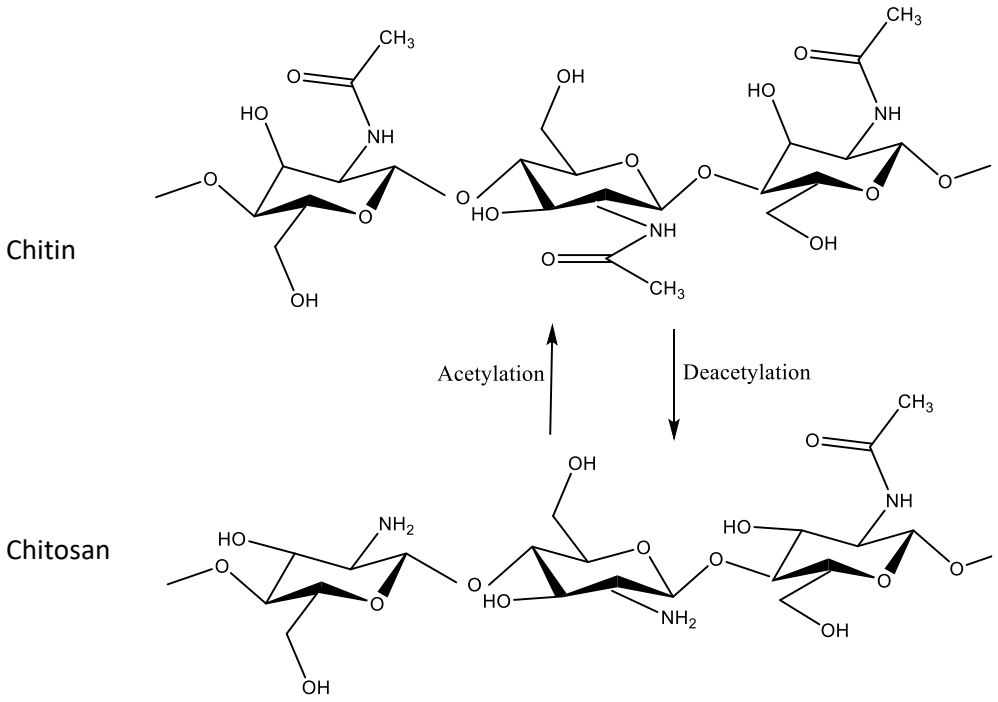

Figure 1.19: Structure of chitin and chitosan.

Biodegradation of chitosan occurs through a broad range of hydrolytic enzymes, which are found in human beings and animals. The degradation products are monosaccharides or oligosaccharides and natural metabolites of glycosaminoglycan or glycol-amino proteins [199]. The positive charge in the chitosan provides it with its mucoadhesive property, due to the interaction with negatively charged mucosa. Another property of chitosan, which might be useful in ocular drug delivery is its ability to open the tight junctions between epithelial cells, improving drug permeation via the paracellular route [200–202]. A schematic representation of this process is presented in Figure 1.20.

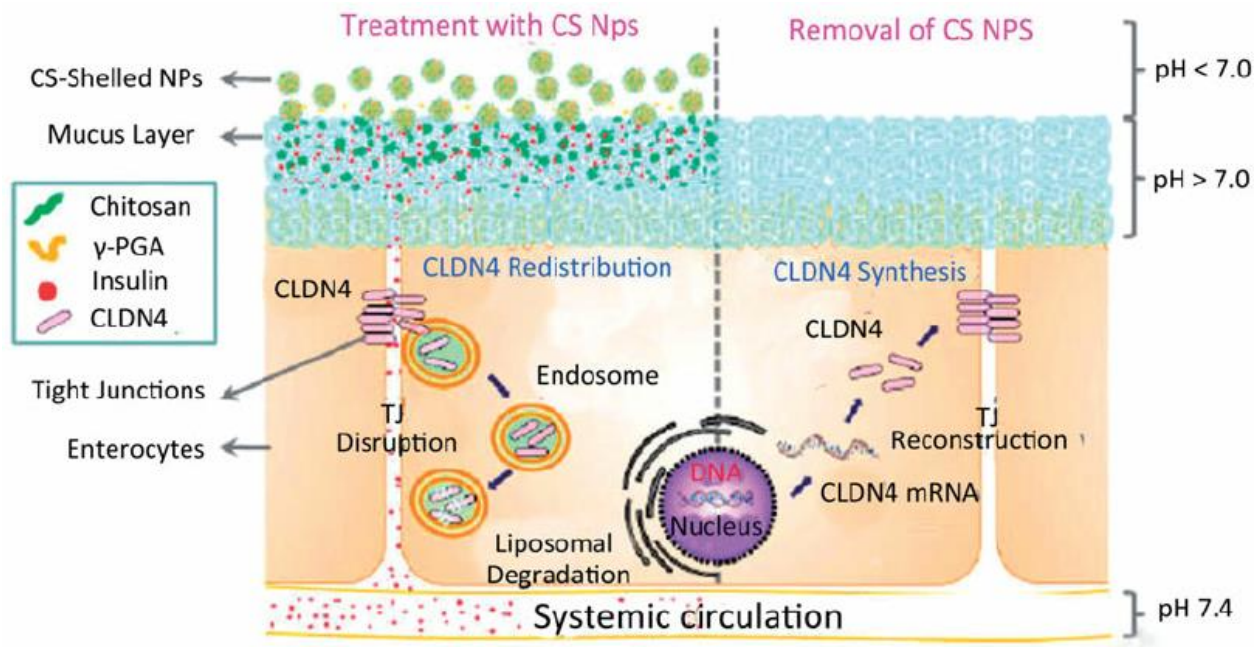

Figure 1.20: Schematic representation of chitosan mediated opening of reversible tight junction [203].

Sung *et al.* studied the mucoadhesive and permeating enhancing behaviour of insulin-loaded chitosan NPs on a Caco2 epithelial monolayer using TEM micrographs [203]. Insulin-loaded NPs were prepared by the addition of an aqueous poly (γ-glutamic acid) with insulin into an aqueous chitosan solution under magnetic stirring. Electrostatic interaction between these two polyelectrolytes in an aqueous environment (pH 6.0) induced the formation of neutralized complexes, which segregated into colloidal NPs. The positively charged chitosan NPs were shown to interact with negatively charged sialic acid groups on the mucin layer. Claudin-4 is a transmembrane protein present in the epithelium, which maintains the integrity of tight junctions. Upon reaching the epithelium, chitosan lowers the expression of claudin-4 and dilates the intracellular spaces; claudin-4 expression was significantly increased upon the clearance of chitosan (Figure 1.20).

Chaiyasan *et al*. developed chitosan-dextran sulphate NPs (with the mean size of 400 nm and a surface charge of +48 mV) employing a polyelectrolyte complexation technique for sustained ocular delivery [204]. The stability of NPs in tear fluid was assessed by incubating in lysozyme (as chitosan may be hydrolysed with lysozyme present in tears) and there was no change in size and charge after incubation. The mucoadhesion of fluorescein dye tagged chitosan was studied on excised porcine eyes. After 6 h of topical instillation, NPs were accumulated in the corneal epithelium but not found in the corneal stroma. However, when the corneal epithelium was removed, NPs penetrated through the stroma, which highlights the binding of positively charged chitosan particles to the negative corneal epithelium. This reveals the increase in

corneal residence time of nanoparticles leading to improved ocular bioavailability, particularly for anterior segment diseases, and highlights the mucoadhesive property of cationic chitosan towards the corneal epithelium.

1.4.3 Nanoparticle formulation techniques

NPs can be prepared from polymers directly or by polymerization of monomers. Preparation techniques with preformed polymers include: solvent evaporation [205], salting out [206], supercritical fluid technology [207], dialysis [208], etc. For polymerisation of monomers, NPs can be prepared using mini-emulsion [162], micro-emulsion [209], interfacial polymerization [210], etc.

1.4.3.1 Solvent evaporation

In the solvent evaporation method, polymer solutions are prepared using volatile organic solvents (e. g. dichloromethane [211], chloroform [212] and ethyl acetate [213]) and the emulsion is formed when the organic solvent is added to the aqueous solution. Upon evaporation of the organic solvent, the emulsion turns into a nanoparticle suspension, as seen in Figure 1.21. In some instances, the mixture of organic and aqueous solutions is subjected to ultra-sonication or high-speed homogenization to form a nano emulsion. Subsequently, the organic solvent is evaporated under reduced pressure or by continuous magnetic stirring and solidified NPs are collected with the help of centrifugation or filtration [214].

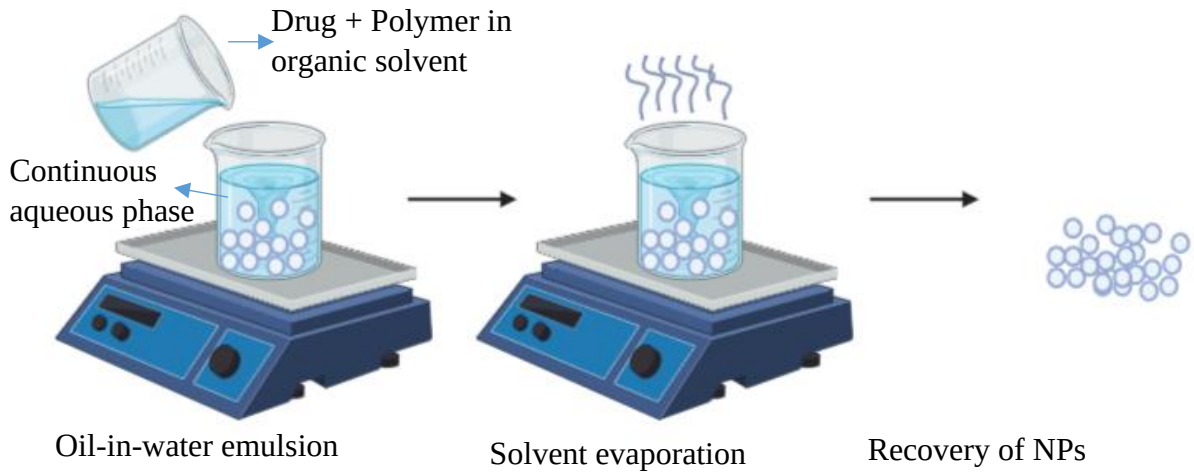

Figure 1.21: Representation of the solvent evaporation method.

Salama *et al.* formulated ofloxacin-loaded bioadhesive NPs utilising a solvent evaporation technique to treat ocular inflammation [215]. Dichloromethane was used as an organic solvent to dissolve drug and polymer (PCL), which was added to an aqueous surfactant (Kolliphor P188) phase under homogenisation and followed by evaporation of organic solvent using rotary

evaporation. During the optimization of NPs, the authors reported an increase in particle size with an increase in molecular weight of the polymer and surfactant concentration (possibly due to a higher number of polymer chains and accumulation of surfactant molecules around/within the nanoparticulate system [216]). The optimized NPs showed a particle size of 195 nm with +55 mV of zeta potential and 90% encapsulation efficiency. *In-vitro* drug release displayed 60% drug release in 6 h. These NPs were incorporated into the *in-situ* gel system made of Pluronic F-127 (PG), methylcellulose and fructose (MCFG). All these formulations (NPs, NPs -loaded on PG and MCFG gels) and marketed formulation (Oflox®) were instilled on rabbit eyes to investigate anti-microbial activity and permeation across the cornea, conjunctiva and sclera using confocal laser microscopy. Both the NPs and NPs incorporated onto PG gel demonstrated no significant difference whereas the NPs in MCFG gels showed maximum penetration across ocular barriers and exhibited 8 times more anti-microbial activity compared to Oflox®. This investigation demonstrated the effectiveness of NPs incorporated in MCFG gels in reducing the dosing frequency compared to commercial eye drops.

1.4.3.2 Nanoprecipitation

The nanoprecipitation method is also known as the solvent displacement method [217]. Diffusion of the polymer solution into non-solvent decreases the interfacial tension between two phases leading to an increase in surface area and the formation of droplets of organic solvent (Figure 1.22). This system consists of three main components: the polymer, the polymer solvent and the non-solvent [217].

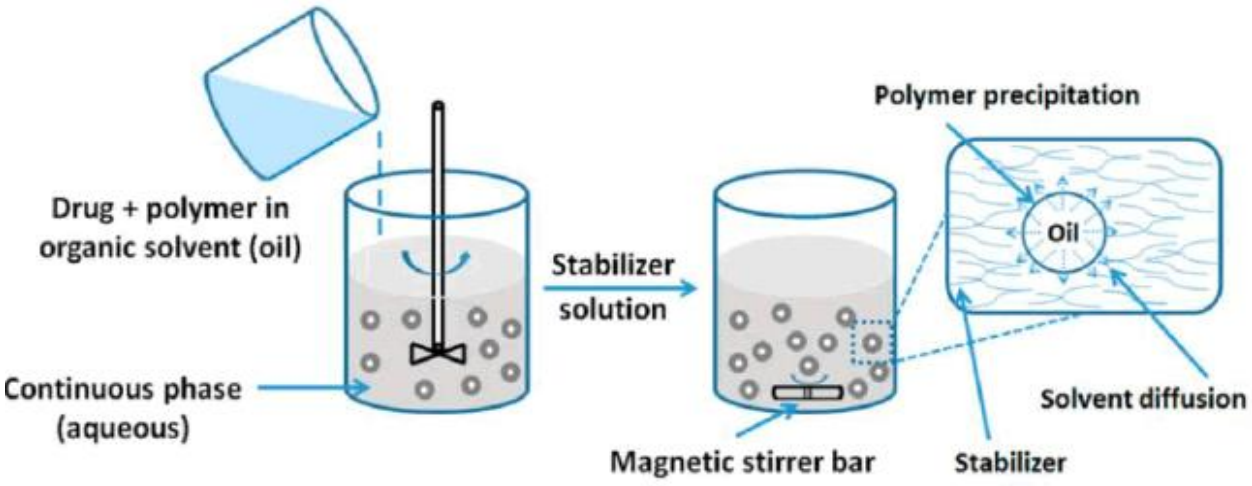

Figure 1.22: Illustration of nanoprecipitation technique [218].

Ahuja *et al*. prepared a chitosan-itraconazole nanosuspension using the nanoprecipitation technique for ocular delivery [219]. Itraconazole encapsulated chitosan NPs were formulated

by controlled co-precipitation of itraconazole and chitosan from aqueous acetate solution with non-solvent addition and pH change. It was noticed that co-precipitation with poloxamer-188 as a stabilizer yielded smaller particle size (100 nm) with a 12-fold increase in itraconazole aqueous solubility. A comparative permeation study of formulated itraconazole nanosuspension (1% (w/v)) with commercial itraconazole suspension (1% (w/v)) was carried out on goat cornea. The formulated itraconazole nanosuspension displayed 1.73-fold higher corneal permeability compared to the commercial suspension. This increase in corneal permeability may have been due to the smaller size of the NPs along with the positive charge of chitosan NPs. Using the nanoprecipitation method, smaller size NPs were produced that had 90% encapsulation efficiency with poloxamer-188 maintaining stability, without agglomeration of the NPs.

1.4.3.3 Ionic gelation

In ionic gelation, NPs are formed by electrostatic interactions and involve noncovalent cross-linking between the polymer and cross-linking agent. Electrostatic interactions occur between polycations and polyanions [220], as seen in Figure 1.23. The size and surface charge of NPs can be altered by changing the ratios of polymer and the cross-linking agent. This can be as simple a process as mechanical stirring at room temperature followed by ultracentrifugation.

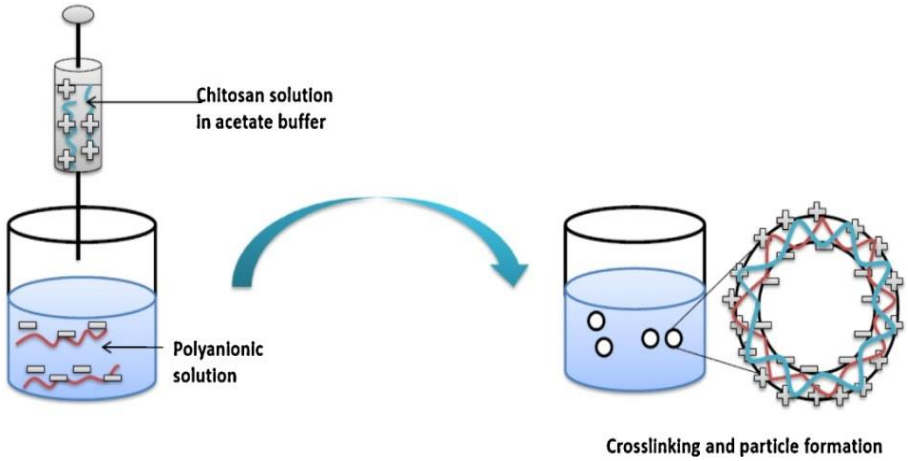

Figure 1.23: Representation of ionic gelation method [221]**.**

Silva *et al.* formulated daptomycin-loaded chitosan NPs using sodium tripolyphosphate as a cross-linking agent via the ionic gelation technique for the ocular treatment of bacterial endophthalmitis [222]. The spontaneous formation of complexes resulted in the formation of stable chitosan NPs of 200 nm with charge +35 mV and encapsulating 97% of the drug. The stability study of nanoparticles in precorneal fluid (lysozyme and mucin) showed no interaction

with lysozyme, possibly due to electrostatic repulsion between cationic lysozyme and chitosan. If the chitosan interacted with lysozyme, it would degrade the polymer before reaching the cornea. The chitosan NPs incubated in mucin turned the overall charge negative because of the ionic interactions between chitosan and mucin. These findings further suggest that chitosan NPs may increase the contact time with the ocular surface.

1.4.3.4 Dialysis

In the dialysis method of fabricating NPs, the polymer dissolved in an organic solvent is placed inside the dialysis tube having the appropriate molecular weight cut-off, as seen in Figure 1.24. The dialysis tube is placed in a non-solvent, which leads to displacement of the polymer solvent followed by polymer aggregation due to its loss of solubility. This leads to the formation of a homogeneous suspension of nanoparticles [223].

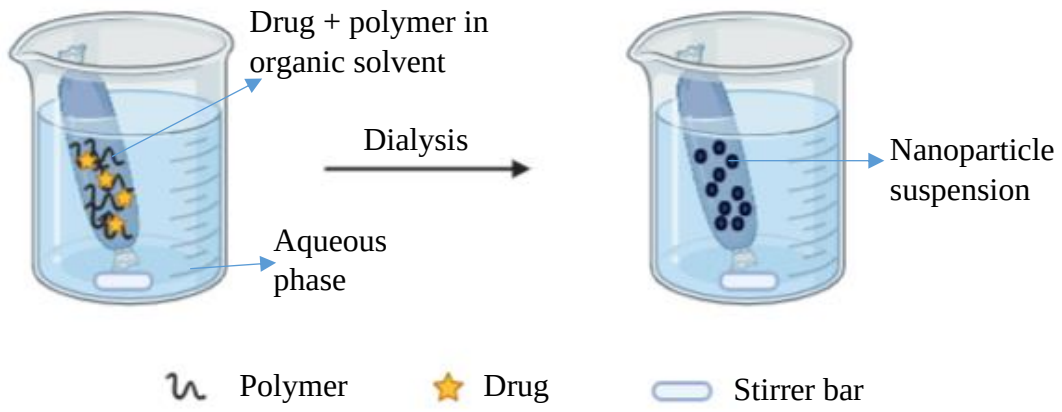

Figure 1.24: Synthesis of NPs using a dialysis method.

Chronopoulou *et al.* formulated homogenous chitosan-coated PLGA NPs containing dexamethasone using an osmosis/dialysis method and studied their release on cell culture models [224]. The negatively charged PLGA NPs (-58 mV) of 200 nm became positively charged (+18 mV) after chitosan coating. There was no significant change in spheroidal morphology upon chitosan coating as pictured in Figure 1.25, indicating the formation of a thin layer of chitosan on PLGA NPs, which was not detected in SEM analysis.

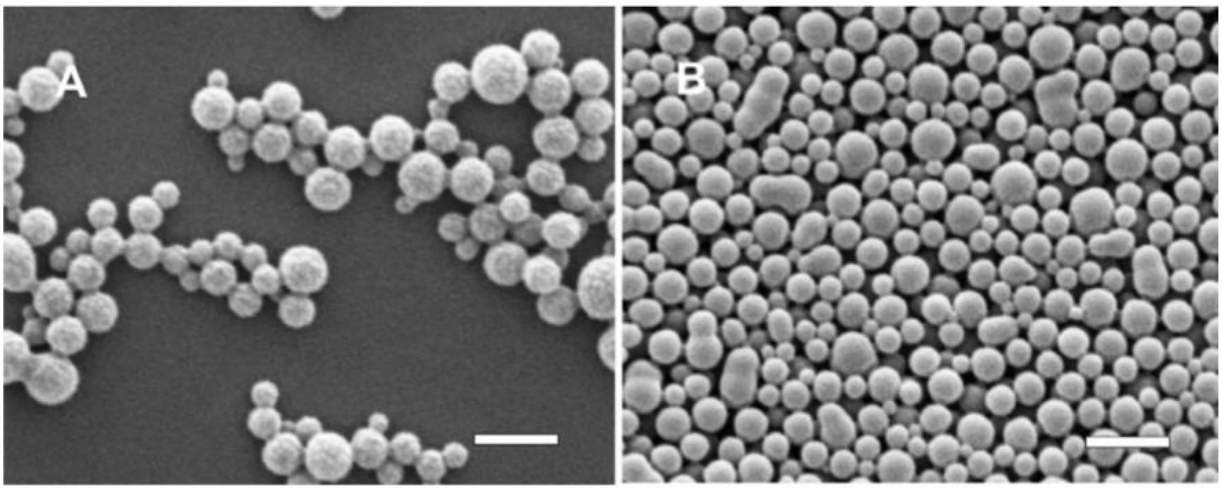

(a) (b)

Figure 1.25: SEM micrographs of dexamethasone encapsulated (a) PLGA NPs and (b) chitosan-coated PLGA NPs, the scale bar is 500 nm [224]**.**

Mouse fibroblast and human hepatocyte cell lines were used for *in-vitro* cell studies. The cell internalization study was performed using fluorescent coumarin-6 dye by confocal microscopy. The cellular uptake of chitosan-coated NPs appeared to be faster than uncoated NPs. The authors noted that internalization of cationic chitosan NPs occurs mainly by adsorptive endocytosis as these NPs adhere to the negatively charged cell membrane. An antiproliferative study was performed using dexamethasone and dexamethasone-containing PLGA and chitosan-coated PLGA NPs. The chitosan-coated PLGA NPs showed highest inhibition of cell proliferation, due to faster internalization of these particles leading to an effective cellular response.

1.4.3.5 Microfluidic technique

Microfluidic devices are fabricated to control the flow of fluids in channels on the microscale, these devices can be single-phase or multiphase flow systems [225]. Nanoparticles are prepared in microfluidic systems with the help of microreactors that have dimensions of less than 1 mm. Microreactors consist of tubular designs or lab-on-chip designs where the chips are prepared using silicon, glass, or polymers such as poly(methyl methacrylate), poly(dimethyl siloxane), or Poly(methyl methacrylate), etc. The laminar flow is attained at the microscale and the mixing of fluids occurs by diffusion at the interface of laminar layers. To achieve homogeneous particles, the nucleation should occur in a short time with slow addition of materials. As the concentration of materials should be lower than the critical concentration for the nucleation to

occur. The microfluidic technique proved to be advantageous in achieving high reaction yield with improved particle size and distribution when compared to bulk synthesis [226].

1.4.4 Characterization of nanoparticulate systems

NPs and nano-based formulations have occupied an important place in drug delivery. As such, it is essential to characterize these NPs for physical, chemical, thermal and biological properties for both storage and in order to administer them into living systems [227–229].

1.4.4.1 Particle size and surface charge

NPs are evaluated for their particle size distribution and morphology as these characteristics play a major role in drug delivery [230]. Electron microscopy can be used to evaluate the particle size and morphology of the NPs [231]. The shape and size of NPs will affect how cells in the body receive them and it impacts their distribution, targeting ability and toxicity [232]. Spherical polymeric NPs of smaller particle size have been found to be non-toxic on ocular cell lines [150]. It has been mentioned previously how important the nanoparticulate systems are, but these systems would not be beneficial if the drug is not released effectively. As the particle size gets smaller, their surface area to volume ratio gets higher. This would imply that most of the drug is closer to the surface of the particle compared to a bigger particle [233–235].

Dynamic light scattering (DLS) or Photon-correlation spectroscopy (PCS) is the most used approach to measuring the hydrodynamic particle size and the distribution of the particles. When the spherical particles in Brownian motion are exposed to monochromatic light, a Doppler shift is created. The monochromatic light hits the particles in motion and leads to a change in wavelength of the incoming light; the range of wavelength change determines the particle size [236]. This feature aids in the determination of particle size distribution and it is represented as the polydispersity index (PDI). PDI values vary between 0 and 1, where 0 is a highly homogenous nanosuspension and 1 is a highly heterogeneous distribution [237]. DLS instruments have three major components: laser, sample and light detector as shown in Figure 1.26. The laser source produces a consistent beam of monochromatic light, and an attenuator alters the strength of the laser. The sample should be homogenous and clear without any aggregates and precipitates. DLS instruments are equipped with avalanche photodiode detectors having ~65% quantum efficiency in red wavelengths thus, lasers of 633 nm are utilised. The detectors are placed at a 173^{o} angle for measuring backscattering and removes extra scattered light. This helps to uncover scattered light signals of less intensity generated from smaller particles [238]. The fluctuations of the scattered light are converted into electrical

pulses by the avalanche photodiode detector or photomultiplier tube and are processed into a digital correlator, which generates the data.

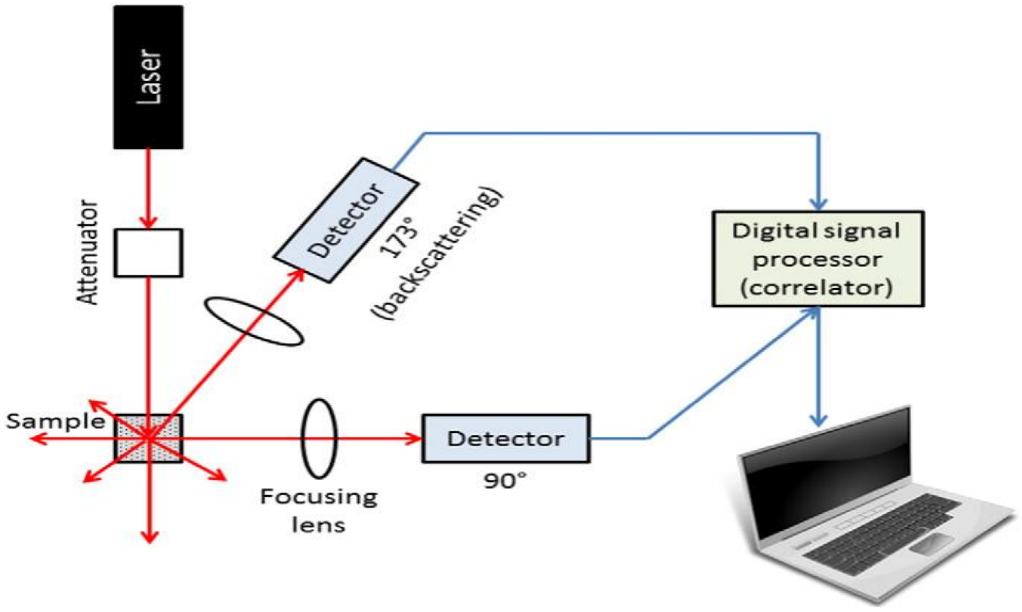

Figure 1.26: Instrumentation of DLS [239]**.**

The surface charge helps to determine the electrostatic interaction of particles with biological components [240]. Zeta potential (ZP) is an important parameter for knowing the surface charge of NPs and for predicting their stability in suspension. It is also known as the electro-kinetic potential, which is the potential at the slipping/shear plane of a moving colloid particle under an electric field [241]. An electric potential of a surface is the amount of effort that is needed to bring a unit positive charge from infinity to the surface without acceleration. ZP reflects the potential difference between the EDL (electric double layer) of electrophoretically mobile particles and the layer of dispersion media around them at the slipping plane as shown in Figure 1.27 [242].

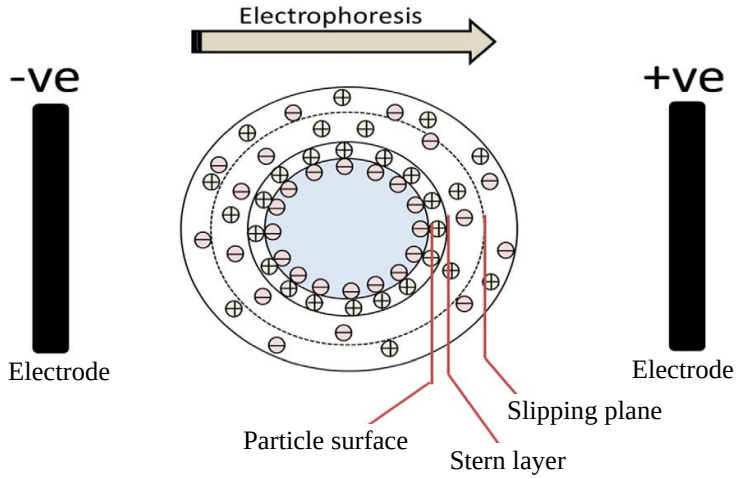

Figure 1.27: Representation of electric double layer of a negatively charged particle [239]**.**

When a charged particle is dispersed in a solvent, an adsorbed double layer known as the EDL is formed on its surface. The inner layer comprises of ions and molecules with the opposite charge to that of the particle known as the stern layer. Beyond the stern layer, the electrostatic effects caused by the surface charge on the particles decrease as per Debye's law (The law states that with the distance of each Debye length the field decreases by a factor of 1/e) [243]. NPs with ZP higher than +30 mV or less than -30 mV are considered to be highly stable [244].

Mohd *et al*. formulated hyaluronic acid (HA)-coated chitosan NPs for topical eye delivery of dexamethasone [245]. The HA coating acts as a protein repellent and facilitates the free flow of the NPs whereas chitosan aids in mucoadhesion and permeation through the ocular barriers. Using DLS the particle size and zeta potential of the prepared NPs were determined. Chitosan and HA-coated NPs were found to be 305 nm and 400 nm, respectively, and the polyanionic nature of HA altered the zeta potential from +32 mV to –33 mV. 72% of the drug was encapsulated and the *in-vitro* drug release study (using simulated tear fluid as release medium) showed 75% cumulative drug release in 12 h with Fickian diffusion. Stability studies revealed no change in NPs (particle size, charge, encapsulation efficiency, drug release and physicochemical characteristics) after 3 months of storage at 25 ºC. This study highlights the importance of DLS to study the stability and surface modification of the NPs used for drug delivery.

1.4.4.2 Scanning electron microscopy

Scanning electron microscopy (SEM) determines the shape, size, and surface morphology of NPs with direct visualization. SEM images the NPs by scanning it with a high energy beam of electrons [246]. The beam of electrons strikes the surface of the sample and interacts with

atoms of the sample leading to the generation of signals (in the form of backscattered electrons, secondary electrons, and X-rays), which contain information about surface topography, electric conductivity etc. In the typical SEM, the beam passes through a pair of deflector plates or scanning coils to the final lens in the electron column. The beam changes into horizontal and vertical directions to scan the sample surface in a rectangular shape; image displayed is the representation of the signal intensity emitted by the scanned area of the sample [247].

Park *et al*. studied the effect of silica NPs (SiNPs) on human corneal epithelial cells (HCECs) [248]. They prepared SiNPs of 50 nm, 100 nm and 150 nm sizes and evaluated the toxicity on cultured HCECs for 48 hours. The morphology of the prepared SiNPs was analysed by SEM (Figure 1.28). SiNPs were internalised by HCECs inside cytoplasmic vacuoles and SiNPs of all the three sizes up to a concentration of 100 µg/mL did not show any cytotoxicity on HCECs, as determined by changes in the cell and cell membrane. A cell viability study on HCECs showed 93.54%, 91.45% and 92.11% cell viability for 50 nm, 100 nm, and 150 nm NPs respectively, while the smaller particles displayed high viability with intact cell membrane.

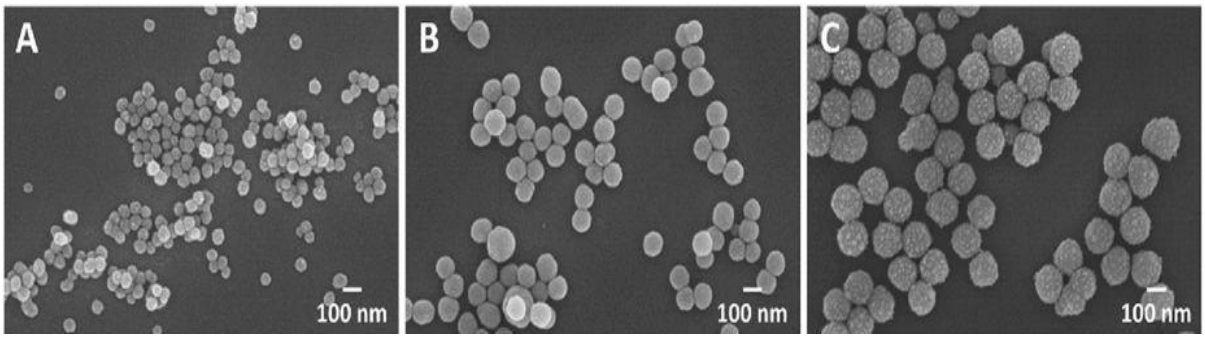

(a) (b) (c)

Figure 1.28: SEM images of silica NPs (a) 50, (b) 100, (c) 150 nm.

Whereas silica NPs of 600 nm have shown toxicity with cell wall damage, the 100 nm particles remained nontoxic [249].This study is in agreement with other studies where smaller spherical NPs were shown to have less cytotoxicity but the larger NPs may cause cell membrane distortion leading to cell rupture [250,251].

1.4.4.3 Transmission electron microscopy

TEM is used for the analysis of morphology and structure of samples. The core components of the TEM microscope consist of an electron gun, electrostatic lenses and a transmitted electron detection system [252]. The electron gun present in the TEM accelerates electrons (accelerating voltage = 80-300 kV) to give them enough energy to pass through up to 1 µm of material.

Condenser lenses present before the specimen focus the electrons into a beam of controlled diameter and the objective lens focuses the transmitted electrons for the formation of a diffraction pattern or first image. The transmitted electrons pass the sample and are focused by the post sample lenses to generate the image and the formed image can be tracked live on a phosphor screen or using a wide-angle camera.

Ameeduzzafar *et al*. formulated levofloxacin-loaded chitosan NPs for topical ocular delivery [253]. The size of NPs increased from 79 to 456 nm with an increase in chitosan concentration from 0.05 to 0.3% (w/v) with varying zeta potential from +21 to +30 mV. The prepared NPs were imaged using both SEM and TEM and compared with particle size analysed by DLS (Figure 1.29) and observed similar particle sizes from the three instruments.

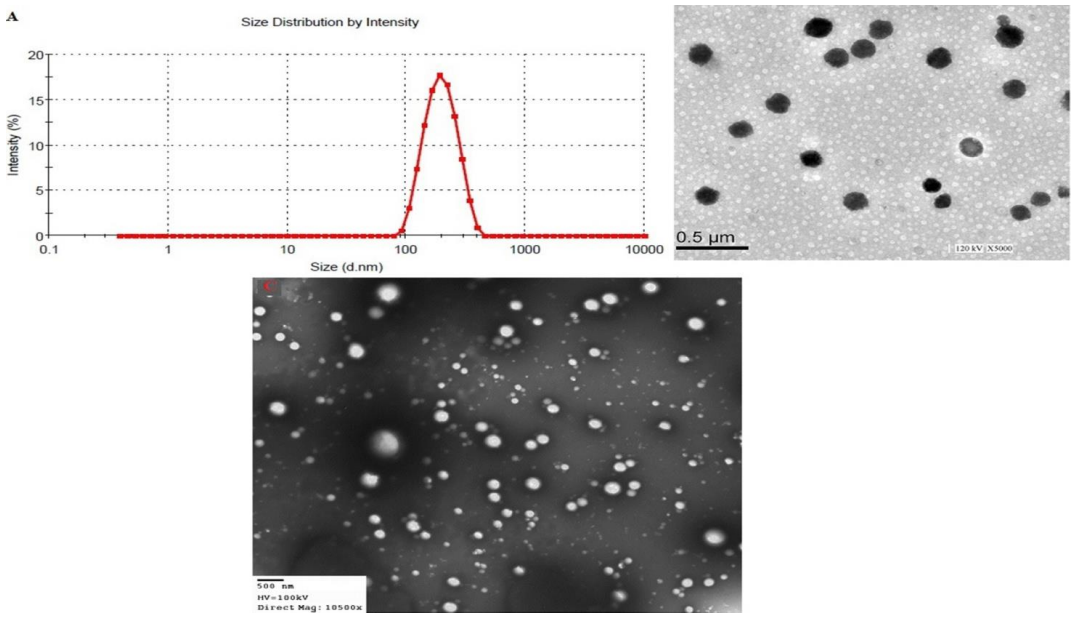

Figure 1.29: Levofloxacin NPs examined by PCS, SEM and TEM [253]**.**

The HET-CAM (Hen's Egg Test Chorioallantoic Membrane) test and histopathology study on excised goat cornea revealed that levofloxacin NPs were non-irritant and safe for ocular delivery (no change in integrity/anatomy of goat cornea upon instillation of NPs). The *in-vivo* gamma scintigraphy study on rabbits showed rapid elimination of levofloxacin solution from the ocular region to systemic circulation through nasolacrimal drainage (in 30 min) whereas levofloxacin NPs were retained for a long duration on the topical ocular region (over 6 h) and showed sustained release.

1.4.4.4 Stability studies

The ability of nanoparticles to retain their physical and chemical properties over a period in different storage conditions describes their stability. Agglomeration [254], sedimentation [255] and change in crystallinity [256] are the common physical stability issues in nanosuspensions. The specific functional groups of molecules and the nanoparticle preparation procedures might affect the chemical stability in suspension form with conversion of the suspension to dry powders leading to stable dosage forms [257].

Sah *et al.* formulated loteprednol etabonate-loaded PLGA NPs using the solvent evaporation method for ocular drug delivery [214]. The particle size, ZP and encapsulation efficiency of the prepared PLGA NPs were found to be 167 nm, -16 mV and 96%, respectively. The *ex-vivo* transcorneal permeation on goat eyes showed 55% of the nanoformulation and 38% of the drug suspension permeated across the cornea in 4 h. A stability study on the NPs was performed at three storage temperatures: ambient (25 ℃), refrigerated (4 ℃) and accelerated temperature (45 ℃) for three months and the observed changes in particle size and encapsulation efficiency monitored. There was negligible variation in particle size at refrigerated and ambient temperature (+2 nm) and slight variation at accelerated temperature (+9 nm). The encapsulation efficiency remained the same at refrigerated temperature and reduced by 1% and 12% for ambient and accelerated temperatures, respectively. At high temperature there could be a rupture of the polymer sheath, which resulted in lower encapsulation efficiency. This study highlighted the importance of stability studies for nanoformulations to identify their ideal storage conditions.

1.4.5 Drug release studies

Assessing the drug release kinetics from nanoparticles gives important information about their capability to alter drug release. As mentioned in Section 1.4, polymeric NPs can be nanocapsules or nanospheres based on their preparation method. The release of drug from these polymeric NPs is based on desorption of surface adsorbed or bound drug (in some instances, there will be an initial burst release of drug [258]), diffusion from particles [259], and erosion/degradation of polymeric NPs along with diffusion [260]. NPs composed of biodegradable polymers release the drug by enzymatic degradation, polymers like PLGA [261], PCL [262] undergo hydrolytic degradation leading to drug release.

1.4.5.1 *In-vitro* and *ex-vivo* drug release studies

Nanoparticles can be designed to regulate drug release to have a controlled/sustained release of the drug which may result in minimal side effects on non-targeted sites. In-vitro drug release kinetics are mostly represented by 'cumulative drug release Vs time', which shows the ability of NPs to release the encapsulating drug [263–265]. Drug release studies from NPs can be performed by different methods. In the dialysis technique of drug release, the nanoformulation is placed inside the dialysis bag with the specific molecular weight cut off and the drug that passes through the dialysis membrane into the release medium is quantified at regular periods [266]. A drawback for the drug release study using dialysis membrane is accounting for the actual release from the particles as the released drug is quantified from the release compartment, but there is a dialysis membrane barrier between the particles and release media [267]. Translocation of the released drug takes time to reach the outer compartment and the dialysis membrane also acts as a second barrier apart from the actual polymeric matrix of the NPs [268]. To address this issue mathematical models have been developed to predict the actual release kinetics of the drug from the particles [269].

Alternatively, nanoparticles are suspended in a certain volume of release medium and incubated under agitation. At specific time intervals, the suspension is centrifuged and the supernatant is analysed to quantify the drug release [270]. Complete separation of the free drug from the NPs might be a challenge considering the smaller particle size, however, syringe filtration [271] and centrifugation [272] have been used for the separation of the released drug. *In-vitro* drug release is also performed using Franz diffusion cells where the donor and receptor chambers are separated by a dialysis membrane. The nanosuspension is placed in the donor compartment and the drug released into the release medium is quantified from the receptor compartment over time [273]. Abouelmagd *et al*. investigated the importance of studying the stability, saturated solubility of the drug in the release media and volume of the release media to be taken based on the concentration of drug present in the NPs [274]. If the solubility of the hydrophobic drug in release media is not considered there is the possibility of reporting an underestimate of drug concentration resulting in a misleading controlled or sustained release estimate.

Ex-vivo drug release studies are similar to *in-vitro* but instead of dialysis membrane excised animal/human tissue is used in the diffusion cell [275]. The whole organ excised from the living system can also be used to study drug release and drug permeation by maintaining

physiological conditions [276]. These studies can give valuable information about the potential of a formulation before animal studies [277]. Maintaining the integrity of the animal tissues and layers is a challenge for *ex-vivo* drug release. Integrity can be checked by staining the tissue followed by histological examination [278].

1.4.5.2 *In-vivo* evaluation

Once the formulation shows effectiveness in preliminary *in-vitro* studies they are further evaluated in biological species. The proposed use of the drug and route of administration together with similarity in anatomy will determine the model and animal species for *in vivo* evaluation. The pharmacokinetic [279], pharmacodynamics [280] and toxicity profile of drug encapsulated NPs [281] have been analysed in living systems.

Lopez *et al.* formulated PEG-ylated PLGA nanospheres using the solvent displacement technique for ocular delivery of dexibuprofen to treat corneal inflammation [282]. The nanospheres measured 200 nm with a negative charge (-15.9 mV) and encapsulated 99% of dexibuprofen (DXI). *In-vitro*, *ex-vivo* and *in-vivo* analysis of the nanospheres and the drug was performed. *In-vitro* drug release was performed using a bulk equilibrium reverse dialysis technique (the dialysis sacs were equilibrated before the experiment using dissolution medium) and phosphate buffer saline as release medium. The excised corneal and scleral tissues were placed in a Franz diffusion cell, the receptor compartment was filled with bicarbonate Ringer's solution and maintained at 32 ℃ and 37 ℃ for corneal and scleral permeation respectively. New Zealand rabbits were used for assessing *in-vivo* ocular bioavailability. To achieve a steady-state concentration, 50 µL of the formulation was instilled every 8 hours for 2 weeks. The animals were sacrificed at the end to quantify the DXI in the aqueous and vitreous humor and the drug retained in the cornea and sclera. An *in-vitro* drug release study showed that 100% of free drug was released in 3 h whereas nanospheres showed 55% release in 12 h. The free drug showed similar permeation in the cornea and sclera by an *ex-vivo* study but nanospheres exhibited high corneal permeation compared to the sclera as seen in Figure 1.30.

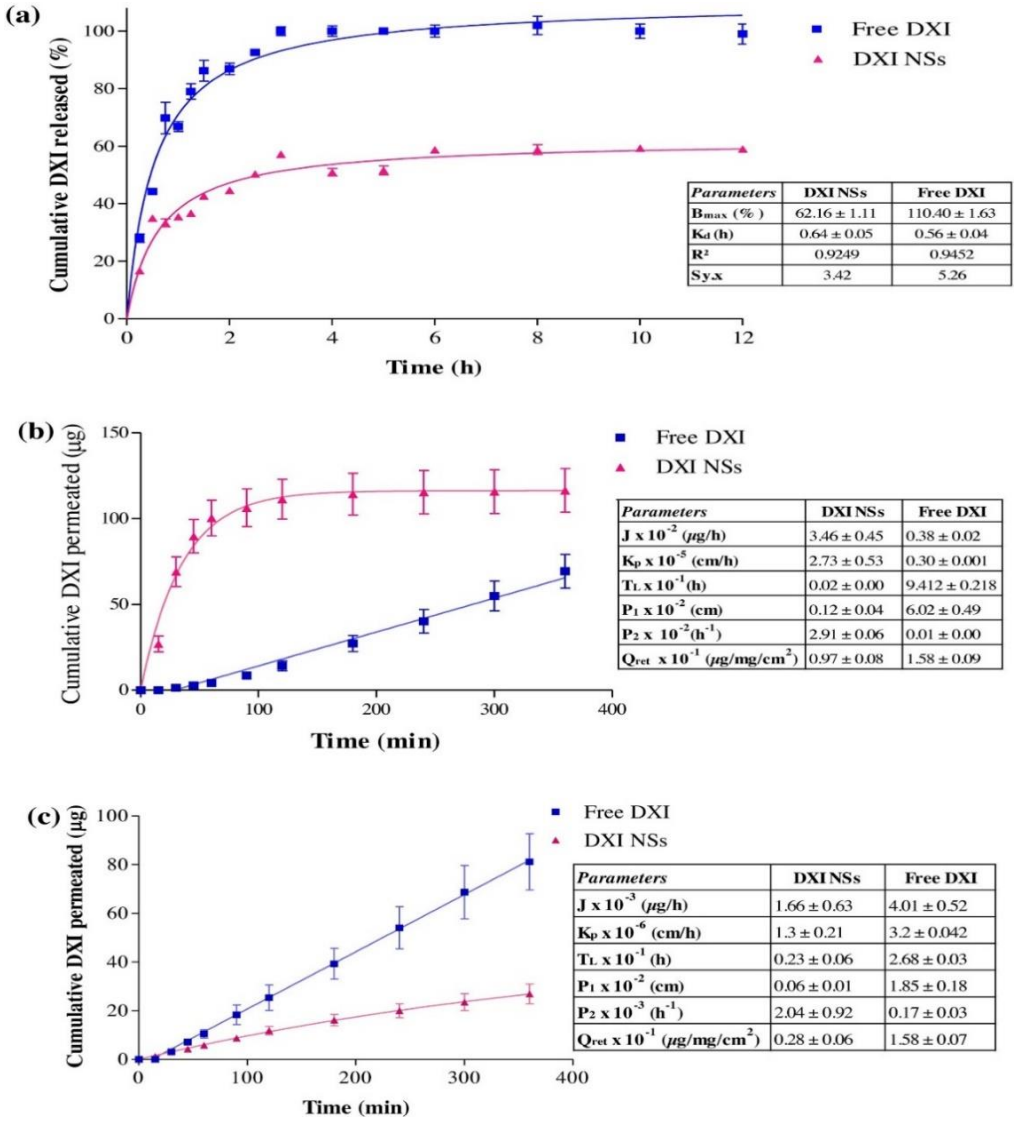

Figure 1.30: The release trends of free DXI suspension and DXI nanospheres [a] in-vitro release [b] ex-vivo corneal permeation [c] ex-vivo scleral permeation.

The *in-vivo* ocular bioavailability analysis showed higher amounts of the drug in the cornea (3.08 µg/mL) when compared to other tissues, including the sclera (1.28 µg/mL). The *ex-vivo* corneal and scleral permeation study was in accordance with *in-vivo* permeation, which highlights the importance of *ex-vivo* studies before animal studies. DXI nanospheres have been suggested for treating corneal inflammation as the drug retention is higher in the cornea and could release in a steady manner to inner tissues.

1.5 Nano-formulations for posterior segment ocular diseases

As mentioned earlier, nano-formulations have many advantages, such as enhanced permeation and retention ability, passage through the reticuloendothelial system, biocompatibility, and rapid internalization. Various tunable and biodegradable polymers and lipids are currently

being used to develop formulations via different routes for controlled and sustained release. Many nano-formulations have been investigated preclinically to deliver drugs to the posterior segment, for example, NPs [283], nanoparticle-loaded *in situ* implants [284], liposomes [285], nanostructured lipid carriers (NLC) [286] and solid lipid NPs [287] etc. and have demonstrated positive results. The nano-formulations synthesised with the drugs mentioned in previous sections are summarised in Table 1.1.

Table 1.1: Nano-formulations targeting posterior segment diseases.

Drug/route of administration	Components	Characteristics	Outcome	Ref
microRNA-150 and quercetin lipid NPs/IVT	dioctadecyl dimethyl ammonium bromide, asparagine-glycine-arginine, PEG, Cholesterol	Size: 209 nm, PDI: 0.15, ZP: +21 mV, EE: quercetin 85% and mRNA-150 99%	NPs effectively suppressed CNV in mice by downregulating HIF1α and CXCR4 target genes. Use of peptide (asparagine-glycine-arginine) significantly enhanced cellular uptake of the dual drugs (due to peptide's high affinity for CD13)	[288]
Bevacizumab NPs/IVT	PLGA, albumin	Size: 190 nm, PDI: 0.17, ZP: -24 mV, EE: 84%	Sterile stable formulation. Vitreous concentration sustained over 500 ng/mL (for 56 days) and 3.3 times more residence time compared to control.	[289]
Dexamethasone nanomicelles/topical	Polysorbate 80, polyoxy-40-sterate	Size: 14 nm, ZP: 0.23 mV	Stable sterile formulation at 4 ℃ and 25 ℃ for 6 months. No irritation was observed at 43.27 ng/g and 67 ng/g on retinal tissue of albino rats (on single/multiple applications).	[290]
Bevacizumab-loaded hydrogel/IVT	Silk fibroin	not reported	Initial burst release followed by sustained *in-vitro* drug release. Showed sustained release in rabbit for 3 months.	[291]
Avastin® thermosensitive hydrogel/IVT	PLGA, PEG	Pore size: 100-150 µm, gelatin temp: 22 ℃	*In-vitro* sustained release for 14 days. Pharmacokinetic study on rats for 6 weeks using ELISA showed no toxicity to retina.	[292]
Avastin® liposomes/topical	Annexin A5, Phosphatidyl serine, PC, tocoferol	Single layered, size: 163 nm, PDI: 0.203, ZP: -7.2 mV,	Annexin A5-liposome enhanced transcytosis (on HCE, 127 ng/g Avastin® in posterior segment of rat eye and 18 ng/g in rabbit retina	[293]

			was quantified after topical application.	
Dexamethasone nanomicelles/topical	Caprolactone, mPEG, $SnCl_2$	Size: 27 nm, PDI: 0.125, DEX solubility:1.36 mg/ml	2.5 days controlled *in-vitro* drug release, 1.3×10^6 cm/s permeability across HCE cell, and 3×10^6 cm/s permeability across excised rabbit sclera. MTT and LDH assays revealed no toxicity.	[294]
Rapamycin micelles/IVT	PCL, monomethoxy PEG	Size: 40 nm, ZP: 0.89 mV	1000-fold increase in water solubility of rapamycin. Retention of micelles in RPE up to 14 days. Good intra-ocular biocompatibility in Sprague Dawley (SD) rats.	[295]
Triamcinolone acetonide NLC/topical	Precirol®ATO5 (solid lipid), Squalene® (liquid lipid), Lutrol F68 (hydrophobic surfactant)	Size: 173 nm, PDI: 0.10, ZP: -46 mV	Ocular deposition study conducted on mice eye for 3 hour using Nile red dye with fluorescence microscopy revealed NLC access to retina.	[296]
Dasatinib micelles/IVT	poly (ethylene glycol)-block-poly(ε-caprolactone) (PEG-b-PCL)	Size: 54.3 nm, PDI: 0.14, ZP: 0.06 mV, EE: 95%	Solubility of dasatinib increased to 190 μg/ml. More than 75% cell proliferation inhibition at 137.7 μM on ARPE-19 (immortal RPE cell line).	[297]
Indomethacin SLN and NLC/topical	CompritolATO888 (glyceryl behenate), tween 80, 3M, miglyol (triglyceride), chitosan	SLN size: 226 nm, ZP: -2 mV, PDI: 0.17, EE: 91.5% NLC size: 227 nm, ZP: -12.2 mV, PDI: 0.23, EE: 99.8%	Stable for 3 months at 4 ℃, 25 ℃ and 40 ℃. Sustained drug release over 6 hours. *In-vivo* bioavailability study on male NZL albino rabbit revealed superiority of NLC over other tested formulations in terms of drug loading and drug deposition in the eye.	[153]

The effectiveness of ciliary neurotrophic factor has been researched as a novel drug delivery system for implant based technology, which can deliver the active agent up to 2 years [298]. It contains a humanized cell line, which was genetically engineered to produce and express the desired therapeutic protein (Ciliary neurotrophic factor) for a prolonged time. A semi-permeable matrix was used to encapsulate this cell line and placed in the vitreous cavity. The estimated half-life for this system in the vitreous was around 51 months. In a study by Solanki *et al*., humanin, a novel neuronal peptide encapsulated in chitosan NPs reduced retinal

apoptosis, while suppressing VEGF expression on RPE and protected the cells against oxidative cytotoxicity. The free humanin and humanin NPs suppressed VEGF by 59% and 71%, respectively with desirable biocompatible and pharmacokinetic properties, highlighting its potential for AMD treatment [299].

Nanoparticles for drug delivery commonly consist of biodegradable polymers such as PLGA, PEG, chitosan, etc., but considering the complex ocular barriers, one or two polymers having multiple properties are cross-linked, conjugated or co-polymerized, which can improve the effectiveness of the NPs. The other strategy is the use of natural polymers such as chitosan, alginate, and silk fibroin for surface modification. Surface modification is mainly used to obtain the desired charge for the NPs to suit the application, which can prolong the retention of drugs inside the eye and improve bioavailability [216,300].

1.5.1 Platforms to deliver nano-formulations to the back of the eye

To increase the efficiency of NPs and the bioavailability of the loaded drug they need to be delivered to the eye using appropriate platforms. Every drug delivery system has its own advantages and disadvantages but when multiple systems are combined, the ultimate drug delivery system can have added benefits. Hence identifying an effective platform based on the application of NPs is of utmost importance. Some of the drug delivery platforms implemented for ocular drug delivery are discussed below.

As highlighted in Section 1.3.1.1, some of the major obstacles for topical delivery of drugs to treat posterior segment eye disease are nasolacrimal drainage, tear fluid, blinking and poor ocular surface retention [301]. Nanomaterials, when loaded onto platforms like *in situ* gels, could be more effective in increasing retention and precorneal residence time. *In-situ* gels upon instillation converts into a gel upon phase transition. The transition occurs by variation in factors such as temperature, pH, ion-induced etc. Hirani *et al.* formulated thermo-reversible gels by dissolving polymers (PLGA–PEG–PLGA) in distilled water at cold temperatures in a slow process [302]. These gels containing NPs were in solution form at lower temperatures and converted to a gel phase within the eye at a biological temperature. Sustained release of the drug with local targeting is possible with thermo-gels due to the rapid formation of a gel *in-vivo*. Previously prepared thermo-gels containing bevacizumab released the drug over 17 weeks on ocular cell lines (fresh primary bovine corneal cells and human retinal pigmental epithelium cells-ARPE-19) in *in-vitro* conditions [303]. The other form of *in-situ* gel is an ion-activated *in-situ* gel system; it consists of polymer, which converts into a gel upon cross-linking

with mono/divalent cations present in the tear fluid (Na^+, Ca^{2+} and Mg^{2+}), leading to increased pre-corneal residence time and reduced loss of drug upon topical instillation. Polymers like gellan gum [304], sodium alginate [305] and pectin [305] have been used previously for ion-activated gels.

In addition to thermosensitive and ion-activated gel systems, pH trigged *in-situ* gelling systems consist of pH-sensitive polymers, which are polyelectrolytes containing an acidic or a basic group that either accepts or releases protons in response to changes in pH in the surrounding environment. At lower pH, the formulation exists as a solution and undergoes gel formation at pH 7.4, that is, the pH of tear fluid [306]. pH activated gels made with polymers like Carbopol 940 [307] and polycarbophil [308] have shown promising results for topical ophthalmic drug delivery.

Nanoparticles can be incorporated into eye drops and contact lens. Permeation enhancers can be used in eye drops and contact lens to enable drug/NPs to pass through the poorly permeable ocular barriers such as the cornea and retina. These penetration agents act by altering the stability of the tear film and mucus layer, opening tight junctions and modifying cell membrane components [309]. Benzalkonium chloride, Brij® 78, ethylenediaminetetraacetic acid, cremophor, dimethyl sulfoxide, etc. have been used as ocular permeation enhancers [310,311].

Wang *et al.* formulated photo-targeted NPs and introduced them intravenously to mice to treat choroidal neovascularization. These NPs were formed by self-assembly of a chemically modified PEG-PLA block copolymer. The nanoparticle surfaces were modified with Tat-C (cell penetrating peptide) as the targeting moiety due to its high cellular uptake. Accumulation of the NPs near the retina of the eye was noted after intravenous injection following laser application [312].

1.5.2 Clinical trials

Despite the enormous research effort on nanoformulations for ocular drug delivery, few formulations make it to clinical trials. This is due to drawbacks they experience during the development stages with regards to formulation parameters optimization, quality control, stability issues, cytotoxicity profiling, and outcomes from *in-vivo* animal studies (inability of rabbit and mouse eye to completely mimic human eye, etc.) [313]. Effective preclinical efficacy outcomes from *in-vitro* and *in-vivo* experiments will lead to the progression to clinical trials.

Despite the various advantages of natural product-based new drugs and associated drug delivery systems, pharma companies are cautious to invest, being more inclined towards libraries of chemical compounds to discover new drugs [314]. However, natural products are now being investigated to treat various diseases, such as diabetes, inflammatory, cardiovascular, and immune-related diseases, etc. Despite having a great therapeutic potential and the advantage of low cost, the biocompatibility and toxicity of these compounds appear to be a challenge for the clinical trial phase [315]. Utilising large molecules for drug delivery is also a challenge in terms of *in-vivo* stability, bioavailability, solubility, and absorption in the body. In overcoming the challenges associated with natural products, hydrophobic drugs and large molecules, nanotechnology plays a significant role.

Ocugen investigated the effectiveness of brimonidine tartrate 0.2% nanoemulsion, alone and in combination with loteprednol 0.2% eye drops for dry eye disease (eye drops administered two times a day for 4 weeks in 252 participants) [316]. In Phase two clinical trials, there was no significant enhanced effect with the addition of loteprednol therefore, for the Phase three clinical trial, brimonidine tartrate 0.2% alone is being investigated. Systane®, an eye drop containing nanoemulsion made of propylene glycol-hydroxypropyl guar has completed phase four clinical trial and is commercially available for the treatment of dry eye disease treatment [317]. The nanoemulsion showed a sustained effect up to 8 h upon one eye drop application and well tolerated by patients. A cationic emulsion containing 0.1% cyclosporin is currently marketed as Ikervis® to treat DED . This emulsion consists of excipients such as triglycerides, glycerol, poloxamer 188, etc. The cationic emulsion displays enhanced permeation across negatively charged corneal and conjunctival cells leading to enhanced bioavailability compared to anionic treatments.

An ophthalmic suspension comprising of dexamethasone-cyclodextrin NPs formulation (OCS-01) for the treatment of anterior inflammation is in phase 2 clinical trial [318]. In the phase one clinical trial, the nanoformulation was effective and well tolerated compared to the placebo. Momin *et al*. reviewed the nanoformulations in the clinical stage, such as NPs, polymer matrices, liposomes, nano micelles, etc. [319]. The authors suggested that the growing number of drug delivery systems in the clinical stage created hope for the availability of nanoformulations in the near future. Though there is a pressing need to explore new and novel ocular therapies with better outcomes, collaborations between formulation scientists and

clinicians are required to achieve successful nanoformulations with good safety profiles and to meet clinical needs [320].

1.6 Scope of thesis

Previous sections of this chapter and the cited literature highlight the benefits and characteristics of nanoparticulate systems, which might be a suitable strategy to overcome the challenges associated with topical ocular drug delivery. With the need for the development of non-invasive treatment options for AMD, this study aims to develop topically applied chitosan-coated PLGA nanoparticles. The NPs will encapsulate the novel combination of a corticosteroid (triamcinolone acetonide) and natural antioxidant (quercetin), which could help treat the disease and additionally strengthen the retina. The polymeric matrix of PLGA supports controlled diffusion of encapsulated drug, while the mucoadhesive property of chitosan may enhance permeation across the barriers of the eye.

Results from this study highlight the combination of formulation development and the investigation of the drugs on human retinal pigment epithelial cells to know the effect on targeted disease (AMD). This study will give preliminary information on the suitability of drug delivery systems along with the safety and therapeutic activity of the encapsulated drugs on human cell lines. The first part of the study utilises thin-film hydration and emulsion formulation techniques to fabricate the non-coated and coated NPs. To develop and optimise the parameters of the nanoparticulate system design of experiments (by Minitab software) was used. The optimised NPs were investigated for drug and components compatibility. In-vitro drug release of NPs was performed to identify the release profile of the encapsulated drug.
The second part of the study involves the process of investigating the synergetic effect of combination drugs on the disease conditions stimulated in ARPE-19 cells. Identifying the non-toxic drug concentrations and selecting the combination concentrations was described. Various studies were performed on ARPE-19 to know the effect of dual drug therapy on inflammation, VEGF secretion and oxidative stress. Research involving multidisciplinary studies like the above will move a step closer to pre-clinical and clinical studies promoting translational research.

Chapter 2: Triamcinolone Acetonide-loaded chitosan-coated PLGA nanoparticles prepared by thin-film hydration

2.1 Introduction

As outlined in Chapter 1, age related macular degeneration (AMD) is a leading cause of vision loss in people aged over 50. Clinically, it is being treated with expensive monoclonal antibodies *via* IVT injections associated with serious side effects. Developing non-invasive treatment options such as a topical formulation is a great challenge, as the eye is a complex organ with vast anatomical, biochemical, and physiological barriers restricting the entry of drug molecules to the site of action. Nanomedicine, the merging of nanotechnology and medicine is a promising approach to tackle challenges related to conventional drug delivery techniques. Since the initial use of nanoparticulate systems in medicine to date, they have revolutionised drug delivery and have also shown promising research outcomes for treating complex ocular diseases like AMD [321–323].

Considering the size of nanoparticles, they are likely to have greater diffusivity through biological membranes like corneal epithelium. Previous research on NPs for ocular drug delivery has demonstrated an increase in corneal permeability of the drugs they have used [324–326]. Also, the higher surface area of nanoparticulate systems enables enhanced interaction with the epithelial layers of the eye leading to increased retention time of topically administered drug delivery systems [327]. In the past few years, drug delivery systems designed from polymeric NPs have played a vital role in the progress of nanomedicine. As mentioned previously in Chapter 1, several polymeric materials such as PLGA, PLA, PGA and PCL have been researched extensively for nanoparticulate drug delivery applications. PLGA is one of the most explored polymers for ocular drug delivery due to its biocompatibility [165], biodegradability [166] and sustained release characteristics [167]. There is a wide range of PLGAs available with varying molecular weights and PLA:PGA ratios. Generally, polymers with high molecular weight show slow degradation as more time is needed to degrade polymer chains into lactic and glycolic acids, as shown in Figure 2.1 [168]. Sheshala *et al.* reported the sustained *in-vitro* release of triamcinolone acetonide from a PLGA implant for 42 days [328]. As this type of PLGA has shown promising results in tailoring NPs for drug delivery [329,330], Resomer® RG 504 H (lactide: glycolide 50:50, M_w 38,000-54,000) with carboxylic acid terminated moiety was used in the current study to enhance the binding to the cationic coating polymer.

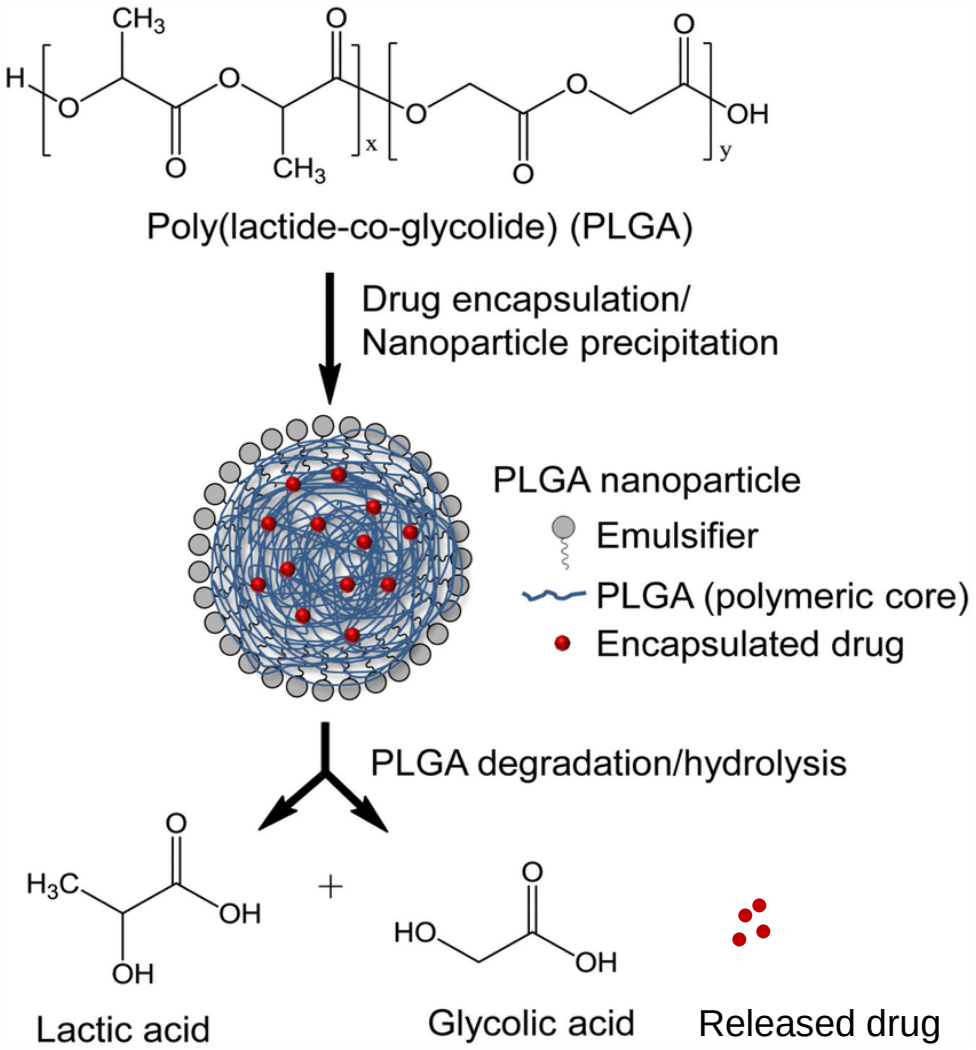

Figure 2.1: Representation of the drug encapsulated PLGA nanoparticle and polymer degradation pathway [331]**.**

Emulsifier or surfactant, such as poloxamer, used in the nanoparticle preparation forms a steric barrier around the nanoparticle with both PEO (polyethylene oxide) and PPO (polypropylene oxide) moieties (Figure 2.1). The emulsifier helps keep the nanoparticles uniformly suspended with low PDI (polydispersity index) values [332].

PLGA NPs have shown good stability with prolonged release of the drug in many studies but they can lack mucoadhesion [333]. This property enhances the ocular retention time, which plays a vital role when targeting the topical route for posterior segment diseases [334]. The surface modification of PLGA NPs with natural and biodegradable polymers like chitosan has proven to be beneficial for ocular drug delivery [160,224,335]. Polymers with mucoadhesive properties bind to mucin by various mechanisms such as hydrogen bonds, electrostatic interactions, polymer chain inter-diffusion and van der Waal forces [336]. These surface modified NPs may have the potential to increase the stability of the encapsulated drug, reducing

initial burst release of the drug and the targeting ligands may conjugate with the free amine groups of chitosan [337,338]. Conversion of charge from negative to positive, may enhance cellular adhesion and retention time of the formulation at the target site [339]. The adsorption of chitosan onto PLGA NPs follows a multilayer behaviour with the reason for adsorption being found to be the cationic nature of chitosan and also the non-uniform porous surface of PLGA NPs [340]. Xu *et al*, reported the entrapment of the positively charged particles in the bovine vitreous humour due to its anionic nature, whereas the negatively charged particles diffused through the vitreous [341]. This need to be further investigated hence in the current study negative and positive-charged NPs were formulated and characterised.

By considering all of these parameters and the findings summarised in Chapter 1, the current research focused on working with chitosan-coated PLGA nanoparticles encapsulating a corticosteroid (represented in Figure 2.2)

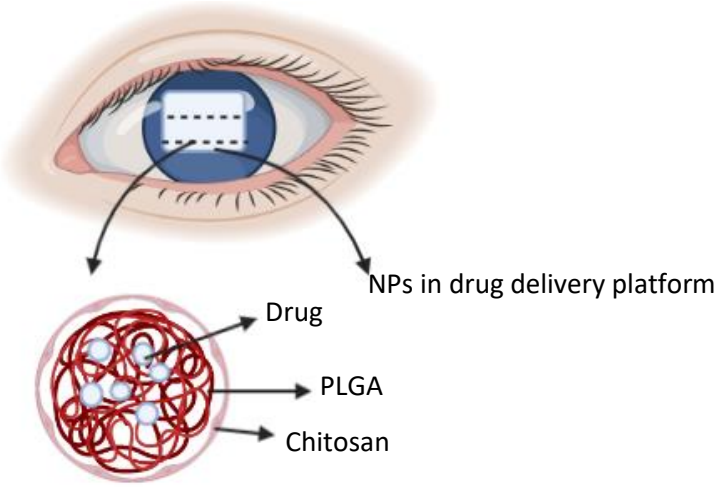

Figure 2.2: Diagrammatic representation of drug delivery platform loaded with NPs on the ocular surface.

The hypothesis under investigation is whether PLGA helps in controlled and sustained release of the encapsulated drug, and if using chitosan for surface modification will aid in mucoadhesion and permeability (both trans and paracellular transport of the NPs). Additionally, corticosteroidal lipophilicity could further drive permeation across the barriers of the eye. Small, lipophilic, positively charged NPs loaded in a suitable drug delivery platform (discussed in Section 1.5.1) may benefit topical delivery to treat posterior segment diseases such as AMD. As the research on nanoparticulate systems proceeds with ocular use, the scalability, safety, and robustness of these systems will be established leading to a new and highly efficient nanoparticulate system available for patient use.

In the current study, chitosan-coated PLGA NPs were fabricated by a thin-film hydration technique and optimised by design of experiments using Minitab software. The designed nanoparticles were characterised for particle size, polydispersity index (PDI) and zeta potential (ZP) using dynamic light scattering (DLS). *In-vitro* drug release of the optimized NPs was performed under different conditions while maintaining sink conditions. Toxicity assays were performed on human corneal epithelial cell lines to assess the safety of the developed system on ocular cell lines.

2.2 Experimental

2.2.1 Materials

Triamcinolone acetonide (TA) (MW: 434.50 g/mol with purity >99%) and water-soluble chitosan (MW: 10-100 KDa with a deacetylation degree >90%) were procured from Carbosynth Ltd, UK. PLGA (DL-lactide/Glycolide copolymer, ratio M/M%: 50/50, MW: 38,000-54,000), Pluronic® F-127 (MW: ~12600 g/mol), Fetal bovine serum, MTT (MW: 414.32 g/mol with purity >98%) and phosphate buffer saline tablets, were purchased from Sigma Aldrich, Ireland. Dulbecco's Modified Eagle Medium (with high glucose, GlutaMAX™ Supplement), trypsin (with EDTA (0.25%) and phenol red) and T75 cell culture flasks (Nunc™ Cell Culture Treated Flasks with Filter Caps) were purchased from Fischer Scientific, Ireland. 96 well plates (F-bottom (chimney well), white, CELLSTAR® TC, lid with condensation rings, sterile) were obtained from Cruinn diagnostics Ltd, Ireland.

2.2.2 Equipment

The following equipment was used throughout the experimental work: Rotary Evaporator (Stuart RE300-Keison, UK), Ultrasonic-probe sonicator (VCX 130-SONICS®, US), Shaking incubator (S1500-Stuart, UK), Refrigerated centrifuge (Sigma 3-18KS, Focus scientific, Ireland), DLS - particle size analyser (Microtrac, Nanotrac Wave II, US), High performance liquid chromatography (Agilent 1200 Series, Ireland), Differential scanning calorimetry (TA Instruments Q2000, UK), Thermogravimetric analysis (TA Instruments Q50, UK), Fourier-transform infrared spectroscopy (Varian 660-IR & 610-IR), Freeze dryer (Freezone 2.5, Labconco, UK), and plate reader (HTS Plate Reader-MSD Model 1250 Sector Imager, US).

2.2.3 Preparation of PLGA nanoparticles encapsulating triamcinolone acetonide (TA)

Blank nanoparticles (BNPs) were prepared by a previously reported thin-film hydration method with some modification [216], where the polymer (PLGA) and surfactant (poloxamer) were dissolved in 20 mL acetonitrile (Figure 2.3). The organic solvent was evaporated by rotary evaporation leading to the formation of the thin-film. Hydration of the thin-film formed was carried out with 10 mL of Millipore water, leading to the formation of a nanosuspension. The suspension was centrifuged at low speed (3000 rpm at 4 ℃ for 30 min) to remove any larger particles (and unentrapped drug for drug-loaded formulations) [342].

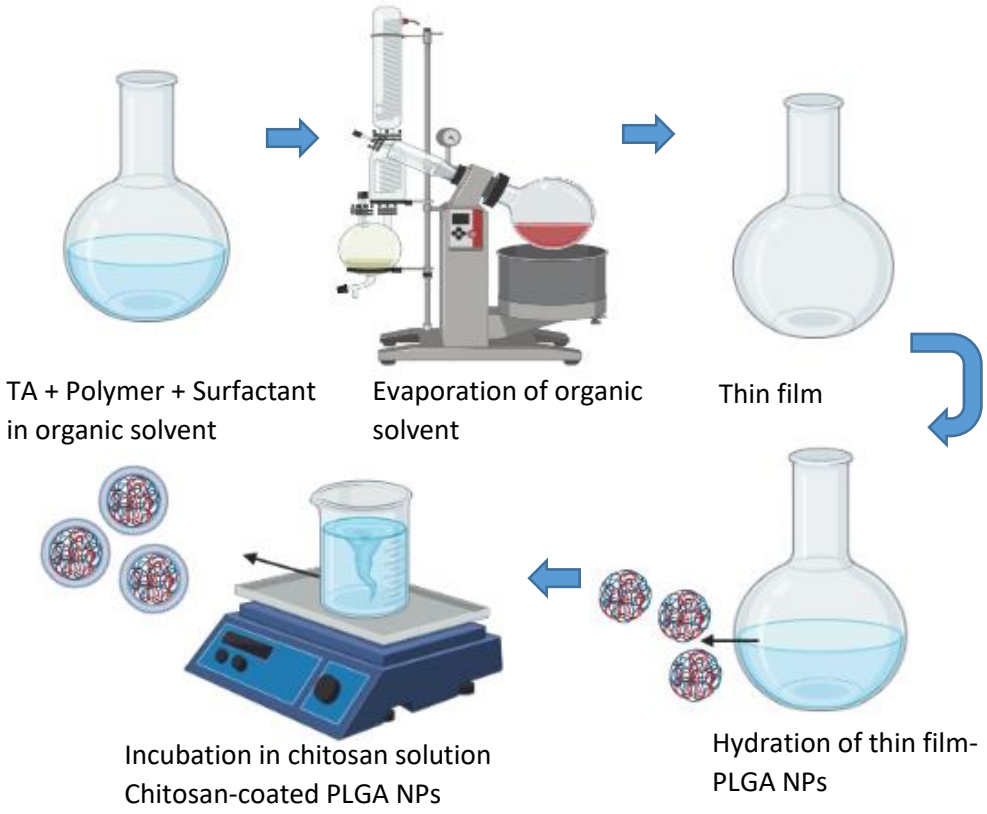

Figure 2.3: Representation of thin film hydration procedure for preparation of TA-loaded NPs.

Following the same procedure, TA encapsulated NPs were prepared using different concentrations of drug, 2.5, 5, 7.5, and 10 mg for F1, F2, F3 and F4 NPs, respectively. Where the drug, polymer and surfactant were dissolved in acetonitrile and both the polymer and surfactant concentrations were kept constant (1:10).

2.2.4 Experimental design study

Design of experiments (DOE) was used to conduct the minimum number of experiments while obtaining the maximum amount of information. Plackett-Burman factorial design was selected

for this study due to the generation of significantly fewer experiments [343]. The drug (2.5 – 7.5 mg), polymer (50 – 100 mg) and surfactant (500 – 1000 mg) were the three factors taken with three levels of concentrations for each and one centre point, as represented in Table 2.1.

Table 2.1: Plackett-Burman design of experiments for triamcinolone acetonide loaded PLGA NPs.

Formulation code	Composition (mg)			Drug: polymer: surfactant
	TA	PLGA	Poloxamer	
AA 1,	2.5	50	500	1:20:200
AA 1,2	2.5	50	500	1:20:200
AA 1,3	2.5	50	500	1:20:200
AA 1,4	2.5	50	500	1:20:200
AA 2,1	2.5	50	1000	1:20:400
AA 2,2	2.5	50	1000	1:20:400
AA 3,1	2.5	100	500	1:40:200
AA 3,2	2.5	100	500	1:40:200
AA 4,1	2.5	100	1000	1:40:400
AA 4,2	2.5	100	1000	1:40:400
AA 4,3	2.5	100	1000	1:40:400
AA 4,4	2.5	100	1000	1:40:400
AA 5,1	5	75	750	1:15:150
AA 5,2	5	75	750	1:15:150
AA 6	7.5	50	500	1:6.67:66.67
AA 6,1	7.5	50	500	1:6.67:66.67
AA 7,1	7.5	50	1000	1:6.67:133.33
AA 7,2	7.5	50	1000	1:6.67:133.33
AA 7,3	7.5	50	1000	1:6.67:133.33
AA 7,4	7.5	50	1000	1:6.67:133.33
AA 8,1	7.5	100	500	1:13.33:66.67
AA 8,2	7.5	100	500	1:13.33:66.67
AA 8,3	7.5	100	500	1:13.33:66.67
AA 8,4	7.5	100	500	1:13.33:66.67
AA 9,1	7.5	100	1000	1:13.33:133.33
AA 9,2	7.5	100	1000	1:13.33:133.33

TA-loaded PLGA nanoparticles were prepared with the same procedure but instead of acetonitrile, a combination of acetone and acetonitrile was used as the solvent. The NPs have been assigned formulation codes starting from AA 1,1 to AA 9,2 for the experiments generated by the statistical model.

2.2.5 Preparation of chitosan-coated PLGA nanoparticles

The formulations selected from the DOE were coated with chitosan. Chitosan solutions of concentration 0.5, 1, 2 and 3% (w/v) were used in initial screening experiments. For coating, chitosan solution was added to the prepared PLGA nanoparticle suspension in a 1:1 ratio under magnetic stirring and left overnight. The NPs were separated from unbound chitosan by centrifugation at 15,000 rpm, 4 ℃ for 30 minutes. Upon centrifugation the pellet was redispersed in water.

2.2.6 Nanoparticle Characterisation

2.2.6.1 Particle size, polydispersity index and zeta potential

The particle size, PDI and ZP were determined using DLS (Nanotrac Wave II). The analysis was performed at 25 ℃ with an angle of detection of 180° with the heterodyne-backscatter arrangement. 1 mL of nanosuspension was placed in a sample cell and the FLEX software was used to analyse electrophoretic mobility (for ZP) and particle size distribution using Brownian motion. Nanosuspensions were measured in triplicates, each of the measurements was recorded as an average of three runs.

2.6.6.2 Encapsulation efficiency:

The encapsulated drug was quantified by high-performance liquid chromatography (HPLC) using a C18 column, mobile phase of phosphoric acid buffer:Acetonitrile (50:50 (v/v), pH 3), 1.2 mL/min isocratic flow rate, injection volume of 20 µL and a 240 nm detection wavelength. TA was quantified using a calibration curve with demonstrated linearity in the range of 0.1-0.9 µg/mL.

The limit of detection (LOD) and limit of quantification (LOQ) of TA were determined based on the standard deviation (Sy) and slope (S) of the HPLC calibration curve using Equations 2.1 and 2.2:

$$LOD = 3.3\ (Sy/S) \qquad \textbf{Equation 2.1}$$

$$LOQ = 10\ (Sy/S) \qquad \textbf{Equation 2.2}$$

2.6.6.3 Thermal analysis:

Thermal gravimetric analysis (TGA) was measured using a nitrogen gas flow rate at 50 mL/min and a heating rate of 10 ℃/min. Thermal decomposition analysis was performed from room

temperature to 500 ℃ with a sample weight between 5-10 mg. The weight loss and onset of degradation were simultaneously recorded as a function of temperature/time. Resulting TGA thermograms were analysed using TA universal analysis software.

Calibration using indium was performed to ensure the accuracy and precision of the differential scanning calorimetry (DSC) thermograms obtained. Accurately weighed samples of 5-10 mg were loaded in T zero aluminium pans with a pinhole. The analysis was performed up to 350 ℃ under a nitrogen atmosphere at a heating rate of 10 ℃/min. For modulated DSC analysis repeated heating and cooling cycles were performed at a heating rate of 0.5 ℃/min to separate the glass transition and relaxation peaks of the polymer.

2.2.7 Cytotoxicity testing on human corneal epithelial cell lines:

2.2.7.1 Cell culture

Human corneal epithelial cells (HCECs) were cultured in T75 cell culture flasks under conditions of 5% CO_2 and 37 ℃ in the incubator. The cell culture media (Dulbecco's modified eagle medium [DMEM]) was supplemented with 10% FBS (Fetal bovine serum) and 1% penicillin and streptomycin. For subculture, HCE cells were passaged when 70-80% confluent, where the cells were detached from the flask by trypsinization followed by centrifugal separation of cells (800 rpm for 5 min). The cells obtained after centrifugation were resuspended in fresh media in a new T75 cell culture flask.

2.2.7.2 *In-vitro* cytotoxicity assay:

The 96 well plate was seeded with 10,000 cells/well in DMEM medium (containing 10% FBS and 1% penicillin-streptomycin) and cultured for 24 hours. After 24 hours cells were treated with varying concentrations of drug and nanoparticles (5, 10, 20, 50, 100 µM) for 4 h and after that treatments were replaced with fresh media for further incubation for 20 h. After completion of the specified time, 15 µL of MTT (3-(4, 5-Dimethylthiazol-2-yl)-2, 5-diphenyltetrazolium bromide) dye was added to each well and incubated for 4 h. After 4 h, the media in each well was replaced with 200 µL of DMSO to solubilise formazan crystals formed after MTT treatment. The plate was left overnight in the incubator and absorbance was measured using a microplate reader at 570 nm. The % cell viability was calculated using Equation 2.3.

$$\%\ Cell\ viability\ = \left(\frac{test\ absorbance}{control\ absorbance}\right) \times 100 \qquad \textbf{Equation 2.3}$$

2.2.8 *In-vitro* drug release study using dialysis membrane

2.2.8.1 Solubility of TA in PBS and PBS with 1% tween 80

2 mg and 10 mg of TA was incubated in 5 mL of PBS and PBS with 1% tween 80 at 37 ℃ with agitation. After 24 h the samples were centrifuged at 10,000 rpm and the supernatant was syringe filtered prior to HPLC analysis to determine the saturation solubility of TA.

2.2.8.2 Use of dialysis membrane for *in-vitro* drug release:

Dialysis membrane with a molecular weight cut off 14,000 KDa and a length of 10-15 cm was filled with drug and nanoparticle suspension (TA-25 µg/mL). These dialysis bags were dialyzed in 20 mL of PBS with 1% tween 80 (pH 7.4) at 37 ℃ under 200 rpm stirring. At predetermined intervals, 100 µL of the sample was withdrawn from the release medium and the same amount of fresh medium was replaced. The extracted sample was analysed using HPLC to determine the quantity of TA released. All the experiments were performed in a closed, dark environment and the vials are closed to prevent evaporation of PBS. The %drug release and %cumulative drug release were calculated by using the following formulae:

$$\%\ Drug\ release\ = \left(\frac{Released\ drug}{total\ drug}\right) * 100 \qquad \textbf{Equation 2.4}$$

$$\%\ Cumulative\ drug\ release\ = \left(\frac{Volume\ of\ sample\ withdrawn}{bath\ volume}\right) * P(t-1) + P \qquad \textbf{Equation 2.5}$$

P = % release at time ‘t’

P (t-1) = % release previous to ‘t’

2.2.8.3 *In-vitro* release study in PBS with 1% tween 80:

The drug release study using PBS with 1% tween 80 as release media was performed in two different methods as follows:

Microcentrifuge tube drug release method: Nanosuspension equivalent to 1 mg of TA was mixed with 40 mL of release media (25 µg/mL). The release medium was distributed into 20 microcentrifuge tubes containing 2 mL each with 50 µg of TA. These microcentrifuge tubes were placed in a shaker with continuous agitation at 37 ℃. At every sampling point, a new microcentrifuge tube was taken and centrifuged at 15000 rpm for 15 min and the drug present in the supernatant was quantified.

Centrifugation drug release method: Nanoparticles equivalent to 500 µg were mixed with 20 mL of release media (TA-25 µg/mL) in a beaker. The beaker was placed in the incubator at

37 ℃ under stirring and at every sampling point, the release media was transferred into a centrifuge tube. The media was centrifuged at 15,000 rpm for 15 min and the supernatant was analysed to quantify the drug released. The pellet was re-dispersed in the same release media and kept for further incubation.

Student's t-test was used to calculate p-values and $p < 0.05$ was taken as statistically significant.

2.3 Results and discussion

2.3.1 Method optimisation for PLGA nanoparticles

The thin-film hydration technique used to prepare nanoparticles was a modification of a previously published method [216]. This method of fabricating nanoparticles does not involve ultrasonication and high-speed homogenisation which might need further optimization of parameters like sonication time, power etc., and also have potential risk of metal contamination *via* probes [344].

The use of poloxamer in the PLGA NPs was not only for stabilisation of the nanoparticle suspension; it consists of physically bonded PLGA and PEO moieties of poloxamer, thus giving better drug protection and stable NPs [345]. Gupta *et al.* designed paclitaxel-loaded PLGA and poloxamer NPs to treat cancer *via* an intravenous route [346]. Particle size, ZP and PDI of the NPs were found to be 179.4 nm, -22.7 mV and 0.3, respectively, with 48% of drug release in 3 days with a sustained release mechanism. There was no change in characteristics of the particles after being stored at accelerated conditions for 3 months. The authors suggested the non-ionic poloxamer may act as a co-emulsifier resulting in smaller particle size. Poloxamer also provides steric stabilisation (polypropylene oxide chains bind to the NPs surface and polyethylene oxide moieties extend into the solvent medium creating a steric barrier) resulting in uniform distribution of NPs with low PDI values. Considering these benefits of poloxamer, in the present study it was considered as an ideal surfactant for formulating PLGA NPs. To investigate the nanoparticles prepared by TA, PLGA and poloxamer, the effect of different concentrations of TA on nanoparticles was studied with results summarised in Table 2.2.

Table 2.2: Particle size, polydispersity index (PDI), zeta potential and %encapsulation efficiency values for PLGA NPs with carrying concentrations of TA.

Formulation Code	Particle Size (nm)	PDI	Zeta potential (mV)	%Encapsulation efficiency
BNPs	305	0.119	- 4.7	-
F1	266	0.119	- 5.5	26.60
F2	415	0.130	- 5.5	10.46
F3	150	0.160	- 4.7	6.98
F4	94	0.155	- 4.8	9.53

The particle size and encapsulation efficiency of the nanoparticles decreased from 266 nm to 94 nm and 26.6% to 9.53% respectively with increase in the concentration of the TA from 2.5 mg (F1) to 10 mg (F4) as seen in Table 2.3 and Figure 2.4. The F2 formulation is an exception, where particle size increased to 415 nm (the DLS histogram showed monodispersed NPs) this could be due to the limitation of the thin-film hydration method where achieving control over particle size is a challenge (during the hydration of film into aqueous media) [347]. Hou *et al.* formulated betaxolol hydrochloride-encapsulated chitosan NPs using ionic gelation [348]. They noticed a decrease in encapsulation efficiency with the increase in drug concentration with the authors postulating that it might be due to saturation kinetics (with high concentration of drug it reaches a limit). In the present study the encapsulation of drug at high concentration might have been affected due to saturation kinetics and also due to limited solubility of the drug in acetonitrile, where there is a chance of precipitation of the drug. In this case, the poloxamer formed nanodroplets, due to its self-assembly nature in an aqueous solvent (during redispersion of the thin film), may result in smaller particle sizes and low drug encapsulation efficiency [349].

(a) (b)

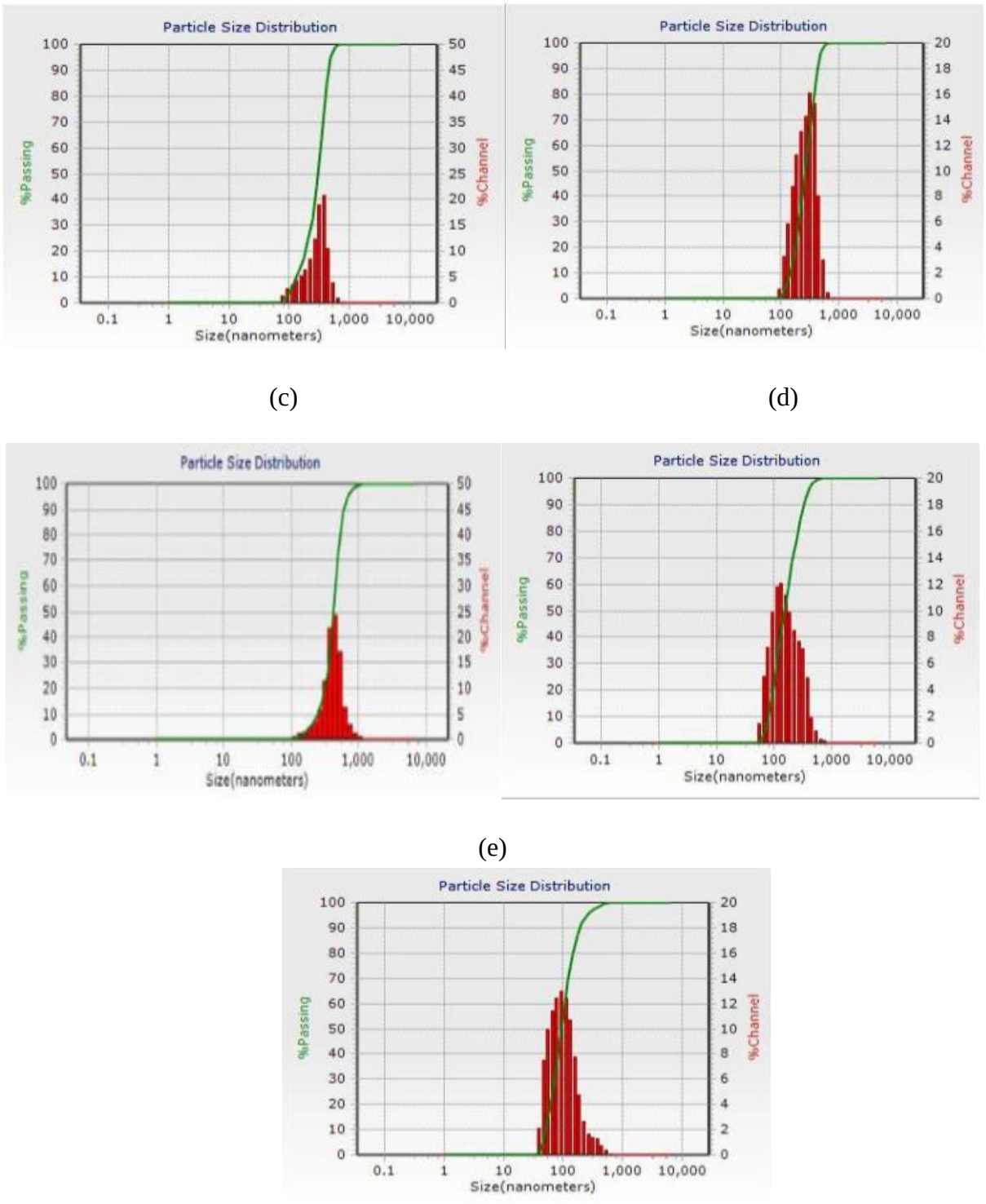

(c) (d)

(e)

Figure 2.4: Histograms demonstrating the particle size distribution of (a) BNPs (b) F1 (c) F2 (d) F3 (e) F4 nanoformulations.

The low polydispersity index values (0.119 – 0.160) of all the nanoparticles indicate that NPs are homogenously suspended as seen in Figure 2.4 [230]. This may be due to the formation of a steric barrier by poloxamer, as mentioned previously in this chapter. Similar results were

observed in a previous investigation by Menon *et al.*, who studied the effect of surfactants (poloxamer and polyvinyl alcohol (PVA)) on the physical properties of PLGA NPs [350]. Both the surfactants, poloxamer and PVA yielded smaller particle sizes of 150 nm with 0.13 PDI and 157 nm with 0.18 PDI, respectively. However, poloxamer yielded smaller particles with a more uniform distribution (also observed in their TEM images) compared to PVA. The authors reported no change in the properties of the NPs when incubated in PBS and FBS for a period of 5 days. This suggests that NPs might remain stable without aggregation during *in-vivo* investigation as already being tested in physiological conditions. Also, lyophilised formulations need to be investigated and compared to the aqueous formulation in terms of stability.

The ZP values of PLGA and TA encapsulated nanoparticles were negative in charge, which was expected because of the terminal carboxylic acid groups of the PLGA [351]. The amount of TA present in NPs was determined using HPLC. Initially, the calibration curve with different concentrations of TA was constructed as shown in Figure 2.5 (b); TA showed linearity between 0.1 and 0.9 µg/mL with regression greater than 0.99.

(a)

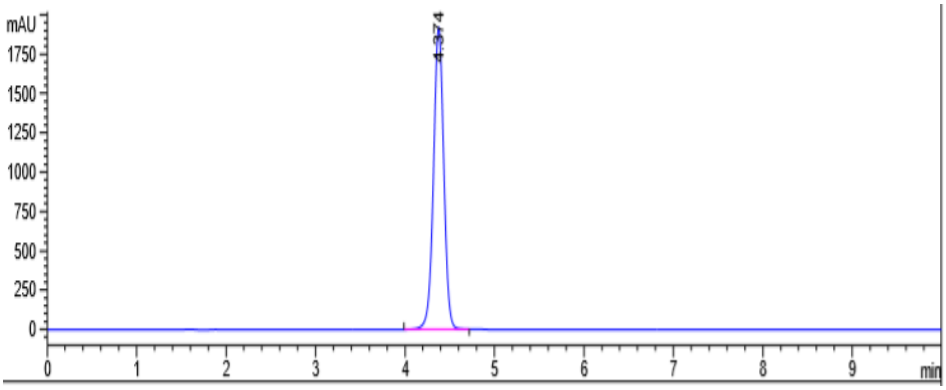

(b)

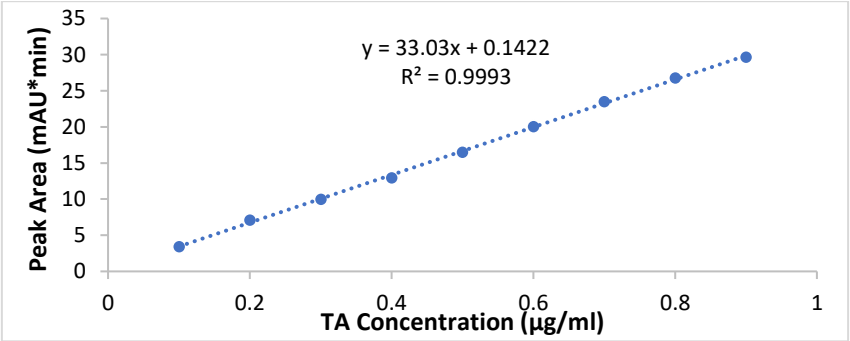

Figure 2.5: (a) HPLC peak of 0.5 mg/mL TA and (b) Calibration curve of TA at 240 nm.

Based on the calibration curve, LOD and LOQ of TA were calculated using equation 2.1 and equation 2.2 and found to be 0.026 µg/mL and 0.079 µg/mL respectively. Using the equation displayed on the calibration curve and the peak area of the sample, the concentration of the drug in the formulations was calculated [224].

In the screening experiment, to increase the solubility of the drug and the encapsulation efficiency, a combination of acetone and acetonitrile was used. The solvents in which the polymer and drug are soluble were selected as this solvent mixture showed better drug encapsulation with uniform distribution of nanoparticles in the next set of formulations. After the successful formation of the NPs in the screening experiments, DOE was used for further optimization of the NPs using Minitab software [352–354]. The drug, polymer and surfactant were selected as factors to identify their impact on the characteristics of the NPs. Taking one factor at a time when designing experiments consumes a huge number of resources and time whereas a systematic DOE utilises a multifactorial process to optimize the formulation methodology.

2.3.2 Optimization of chitosan-coated PLGA nanoparticles encapsulating triamcinolone acetonide

The TA encapsulated PLGA nanoparticles were prepared using acetone and acetonitrile as solvents using the experiments generated by the Plackett-Burman factorial DOE. In Plackett-Burman DOE, the main effects involved in the nanoparticles development are analysed with a less number of experiments compared to other models and hence prioritised for this study [355]. As the thin-film method for preparing NPs was a time consuming procedure, the experimental design which generated a smaller number of experiments for the chosen factors was selected [356]. A total of 26 experiments with 3 factors (drug, PLGA and surfactant) were obtained in the Minitab software using the Plackett-Burman DOE, with the aim of obtaining NPs with desired characteristics.

As highlighted in Chapter 1, in previous studies it was shown that particle size, PDI, zeta potential and encapsulation efficiency are considered as important parameters for ocular drug delivery. Dosing frequency can be reduced with increase in encapsulation efficiency and the smaller size helps in permeation across the ocular barriers and increases the bioavailability of the drug [357]. The zeta potential gives important information about the stability of NPs. As a result, these three key parameters were selected as the main particle characteristics with the findings summarised in the Table 2.3.

Table 2.3: Particle characteristics obtained from Plackett-Burman design of experiments.

Formulation Code	Particle Size (nm)	PDI	Zeta potential (mv)	%Encapsulation efficiency
AA 1,1	537	0.661	- 4.2	30.00
AA 1,2	485	0.125	- 2.4	28.77
AA 1,3	404	0.516	- 3.5	16.58
AA 1,4	434	0.101	- 5.9	28.81
AA 2,1	428	0.176	- 3.7	16.34
AA 2,2	406	0.091	- 4.2	23.99
AA 3,1	379	0.096	- 2.8	15.49
AA 3,2	407	0.085	- 1.5	20.43
AA 4,1	447	0.080	- 2.9	60.02
AA 4,2	410	0.385	- 3.0	71.91
AA 4,3	523	0.063	- 2.0	59.20
AA 4,4	448	0.147	- 4.0	56.78
AA 5,1	503	1.052	- 3.1	19.66
AA 5,2	403	0.146	- 2.4	21.72
AA 6,1	477	0.941	- 9.8	9.12
AA 6,2	235	0.106	- 3.6	9.42
AA 7,1	610	0.186	- 5.2	36.90
AA 7,2	807	0.085	- 2.7	36.19
AA 7,3	723	0.194	- 3.0	36.76
AA 7,4	614	0.099	- 4.0	28.34
AA 8,1	415	0.093	- 2.0	22.00
AA 8,2	363	0.217	- 8.2	16.74
AA 8,3	429	0.157	- 2.3	12.13
AA 8,4	413	0.099	- 2.0	16.60
AA 9,1	504	0.132	- 2.5	40.20
AA 9,2	408	0.165	- 2.5	40.59

The Plackett-Burman factorial design responses were analysed using Minitab software and the Pareto charts which represent the standardised effects based on *t*-statistics that tests the null hypothesis assuming the effect as 0 are represented in Figure 2.6.

(a)

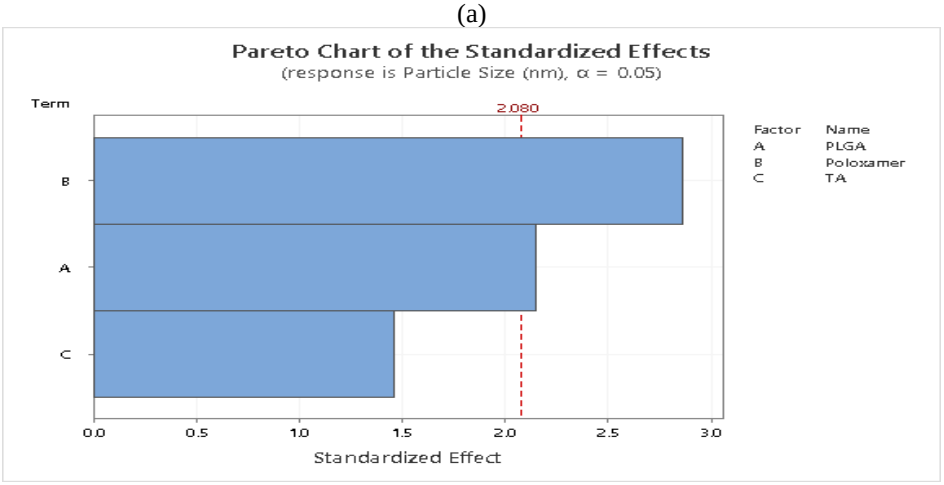

(b)

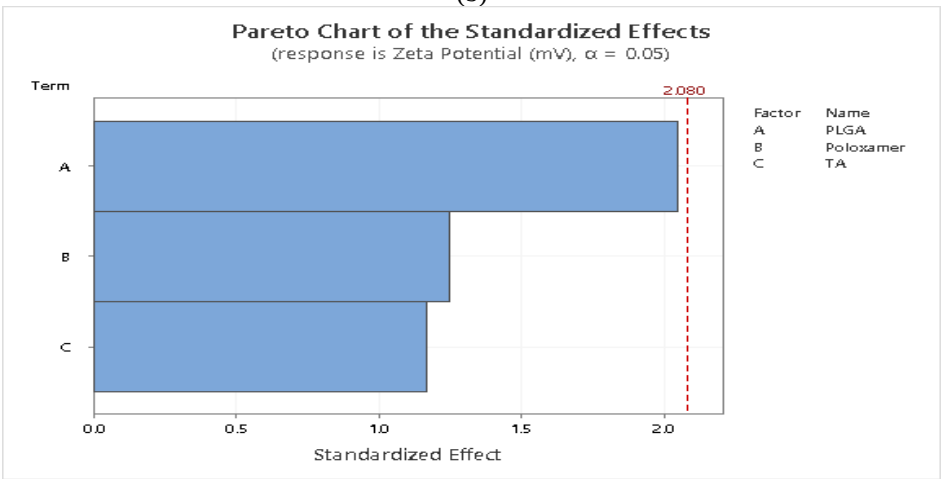

(c)

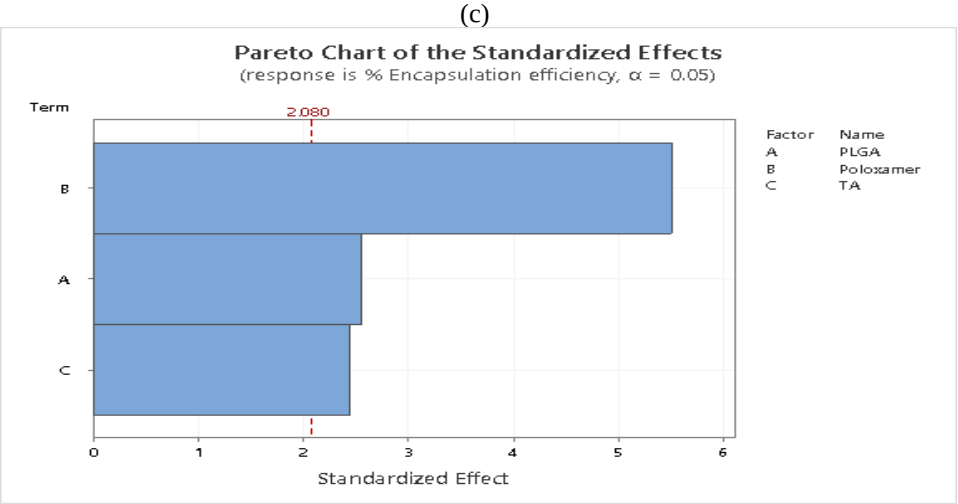

Figure 2.6: Pareto charts of the standardized effects of, (a) Particle size (b) Zeta potential and (c) %Encapsulation efficiency.

In Figure 2.6 (a), the effect of poloxamer, PLGA and drug concentration on the particle size was seen. The bars representing the poloxamer and PLGA have crossed the reference line, which means they have a statistically significant effect on size whereas variation in drug concentration has a statistically insignificant effect (significance/insignificance is considered at α=0.05 level with the model terms). Different ratios of drug, polymer and surfactant have no significant effect on zeta potential, and this may be due to the separation of unbound PLGA. Taghipour *et al.* formulated albumin-loaded PLGA nanoparticles using a solvent evaporation technique and optimized their NPs with a factorial DOE [358]. The results of their DOE showed no effect on ZP with increase in concentration of PLGA, but poloxamer increased the ZP slightly (-30 to -32 mV). The current study demonstrated a similar effect of PLGA on ZP but non-ionic poloxamer exhibited no effect on ZP.

All three factors demonstrated a significant effect on %encapsulation efficiency. The NPs with low drug concentration (2.5 mg) and high ratio of PLGA:Poloxamer (1:10) demonstrated greater drug entrapment (Table 2.4). At high concentrations of polymer, better drug encapsulation was seen due to the presence of more polymeric chains available for drug entrapment [359].

Table 2.4: Particle size, polydispersity index (PDI), zeta potential and %EE values for selected PLGA nanoparticle formulations, n=6 ± SD.

Formulation Code	Particle Size (nm)	PDI	Zeta potential (mV)	%Encapsulation efficiency
AA 4	467 ± 79.90	0.126 ± 0.133	-3.81 ± 2.05	62.21 ± 5.88
AA 7	538 ± 102.53	0.123 ± 0.058	-3.97 ± 1.32	39.01 ± 10.56
AA 9	456 ± 67.89	0.262 ± 0.191	-4.19 ± 2.12	30.75 ± 17.53

Based on the particle size, PDI, ZP and encapsulation efficiency values, three formulations with codes AA4, AA7 and AA9 were selected for further studies. The responses for these formulations with six repetitions are shown in the below Table 2.5.

2.3.3 Screening of chitosan concentration to coat PLGA nanoparticles:

The concentrations of chitosan used for screening have been considered from previously published research on chitosan-coated PLGA NPs [170,224,357,360,361]. Water-soluble

chitosan was used at 0.5, 1, 2 and 3% (w/v) to coat the prepared blank PLGA NPs and to investigate the effect on charge as represented in Figure 2.7. The 2% (w/v) chitosan concentration gave a zeta potential of +30.6 ± 1.84 mV and there was no increase in charge with an increase in chitosan concentration thereafter. This could be due to saturation of chitosan after adsorption on PLGA NPs with the excess chitosan removed using high speed centrifugation.

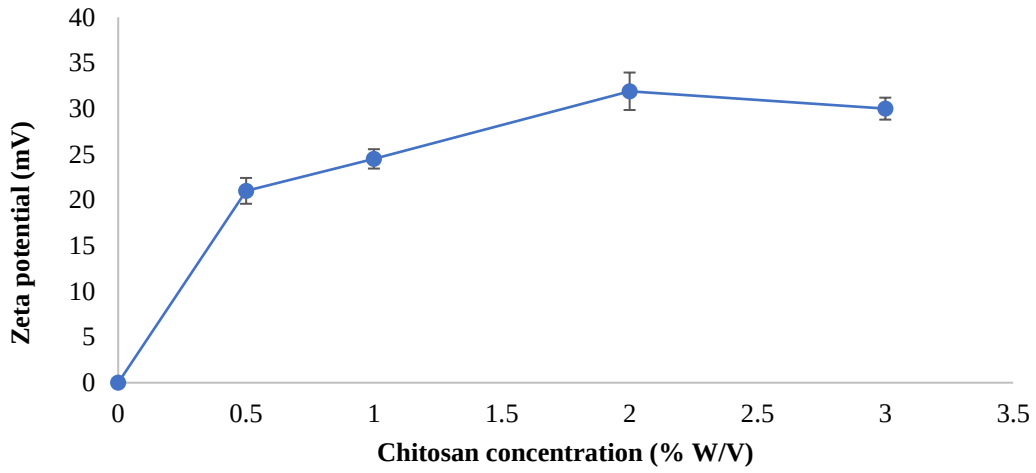

Figure 2.7: Effect of chitosan concentration on zeta potential of NPs.

2.3.4 Chitosan-coated PLGA nanoparticles

Based on the above observations, the PLGA nanoparticles with formulation codes AA4, AA7 and AA9 were coated with 2% (w/v) chitosan solution. To identify any statistical significance, the coefficient of variance (CV) of the replicates was calculated with a CV value of less than 1 observed for all the results indicating low variance. There was no significant change in particle size before and after coating the nanoparticles (411 – 538 nm), as shown in Table 2.5. Chronopoulou *et al*. also reported no significant change in particle size after coating PLGA NPs with chitosan [224]. This may be due to the absorption of chitosan onto porous PLGA NPs, where chitosan fills the pores and forms a thin layer around the NPs [340]. The ZP values before (-2.5 – -4.1 mV) and after coating (+41 - +50 mV) imply that the particles were stable as zeta potential values less than -30 mV and higher than +30 mV are considered to be highly stable [362].

Table 2.5: Particle size, zeta potential and encapsulation efficiency values for PLGA NPs (AA) and chitosan-coated PLGA NPs (CS AA), n=3 ± SD.

Formulation Code	Particle Size (nm)	CV	Zeta potential (mV)	CV	%Encapsulation efficiency	CV
AA 4	467 ± 79.90	0.17	-2.5 ± 0.70	0.28	63.13 ± 6.44	0.10
CS-AA 4	517 ± 231.22	0.44	+44.05 ± 5.02	0.11	24.16 ± 10.29	0.43
AA 7	538 ± 102.53	0.04	-4.1 ± 1.56	0.38	56.80 ± 21.24	0.37
CS-AA 7	452 ± 19.09	0.04	+50.4 ± 4.95	0.09	28.89 ± 3.01	0.10
AA 9	456 ± 67.89	0.15	-4.15 ± 2.33	0.56	40.46 ± 15.64	0.39
CS-AA 9	411 ± 2.83	0.01	+41.85 ± 5.30	0.13	25.48 ± 9.93	0.38

As seen in Table 2.5, the encapsulation efficiency of the NPs decreased after coating with chitosan for AA4 formulation it reduced from 63% to 24%. The coating might have affected the extraction of drug from the NPs as acetonitrile was used as an extraction solvent for HPLC analysis but the chitosan was not soluble in acetonitrile [224]. Also, during the separation of unbound chitosan using high speed centrifugation, there might have been a loss of some NPs due to the washing of the pellet and using repetitive centrifugation steps. There is a probability of some drug being released during the incubation process while coating the PLGA NPs. In a screening experiment a combination of solvents in which chitosan, PLGA, poloxamer and drug can be dissolved were tested. The solvent mixtures investigated along with the encapsulation efficiencies are shown in Table 2.6.

Table 2.6: Effect of solvents on drug extraction from NPs.

Solvent Mixture	Formulation	%Encapsulation efficiency
10% (v/v) Triton X + Acetonitrile	AA4	44.72
	CS-AA4	8.97
Acetonitrile + water	AA4	44.57
	CS-AA4	24.16
Acetonitrile	AA4	64.28
	CS-AA4	12.05
Methanol + acetonitrile + water	AA4	63.88
	CS-AA4	35.42
Methanol + Acetonitrile	AA4	65.07
	CS-AA4	35.04

The solvent mixture of methanol, acetonitrile and water exhibited better drug extraction from chitosan-coated PLGA nanoparticles, due to the high solubility of TA in methanol. As mentioned in the methods section for the preparation of PLGA nanoparticles, low-speed centrifugation was used to separate unbound drug. Whereas for chitosan-coated PLGA NPs, high-speed centrifugation was used to separate unreacted chitosan. Previous studies showed loss of NPs during this process [216,363]. This high-speed centrifugation along with the coating procedure of PLGA NPs might have resulted in low encapsulation efficiency values upon coating.

2.3.5 Thermal analysis of nanoparticles

Thermogravimetric analysis (TGA) was used to determine the degradation temperature of the nanoparticles. In TGA, materials are heated to a higher temperature while monitoring the mass loss, which generates a degradation curve [364]. The degradation temperature of PLGA and chitosan-coated PLGA NPs was higher compared to the individual components, as seen in Table 2.7 and Figure 2.8, which implies that the NPs are more stable [365].

Table 2.7: Degradation temperatures of individual components, coated and non-coated-NPs.

Sample name	Degradation temperature (°C)
PLGA	253
Poloxamer	350
Chitosan	190
Triamcinolone acetonide	289
PLGA NPs (AA4)	345
CS-PLGA NPs (CS-AA4)	363

Upon coating of the nanoparticles, the thermal stability of the drug, polymer, surfactant and PLGA NPs have been enhanced.

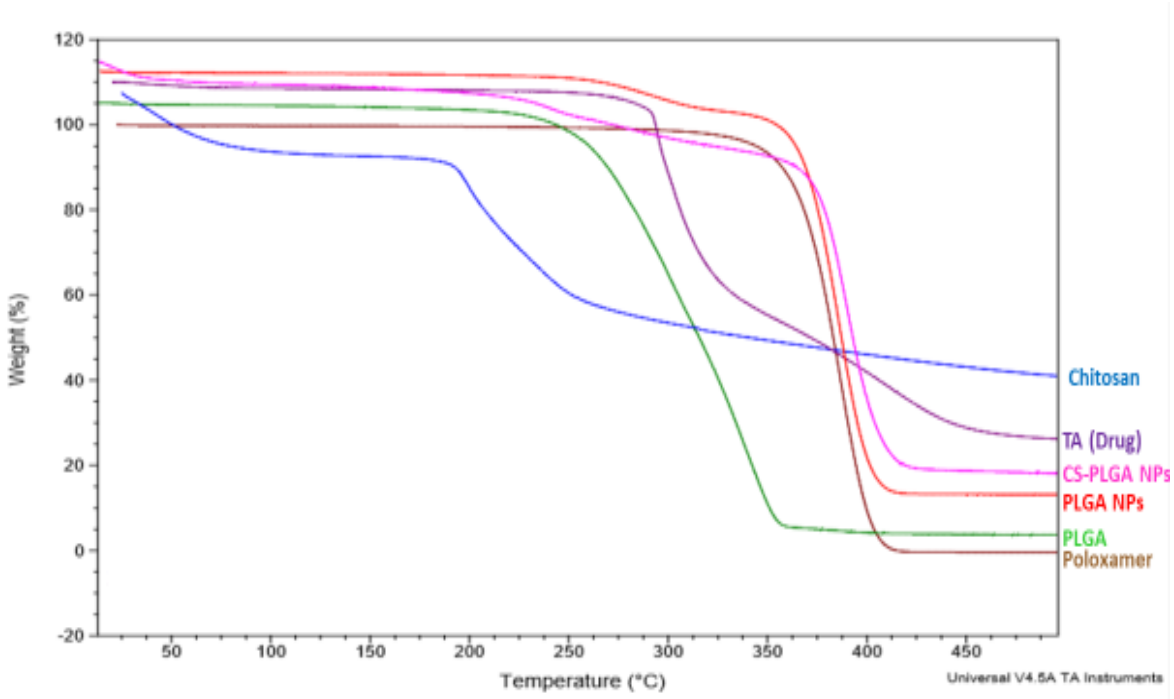

Figure 2.8: TGA thermograms of TA, PLGA, poloxamer, chitosan, PLGA and chitosan-coated PLGA NPs.

These TGA results are in agreement with the previous study by Xiao *et al*. on chitosan-coated PLGA microparticles containing orange essential oil [366]. Their chitosan-coated PLGA microparticles exhibited enhanced thermal stability when compared to excipients and PLGA microparticles. Current TGA results suggest that the drug and polymers present in the nanoparticles are more thermally stable when compared to the individual components this could be due to the stable structure of coated and non-coated NPs.

A differential scanning calorimeter (DSC) was used to examine the physical state of the drug in the NPs and also to examine the thermal behaviour of prepared NPs [367]. DSC analysis was performed for the NPs and the individual components (Figure 2.9).

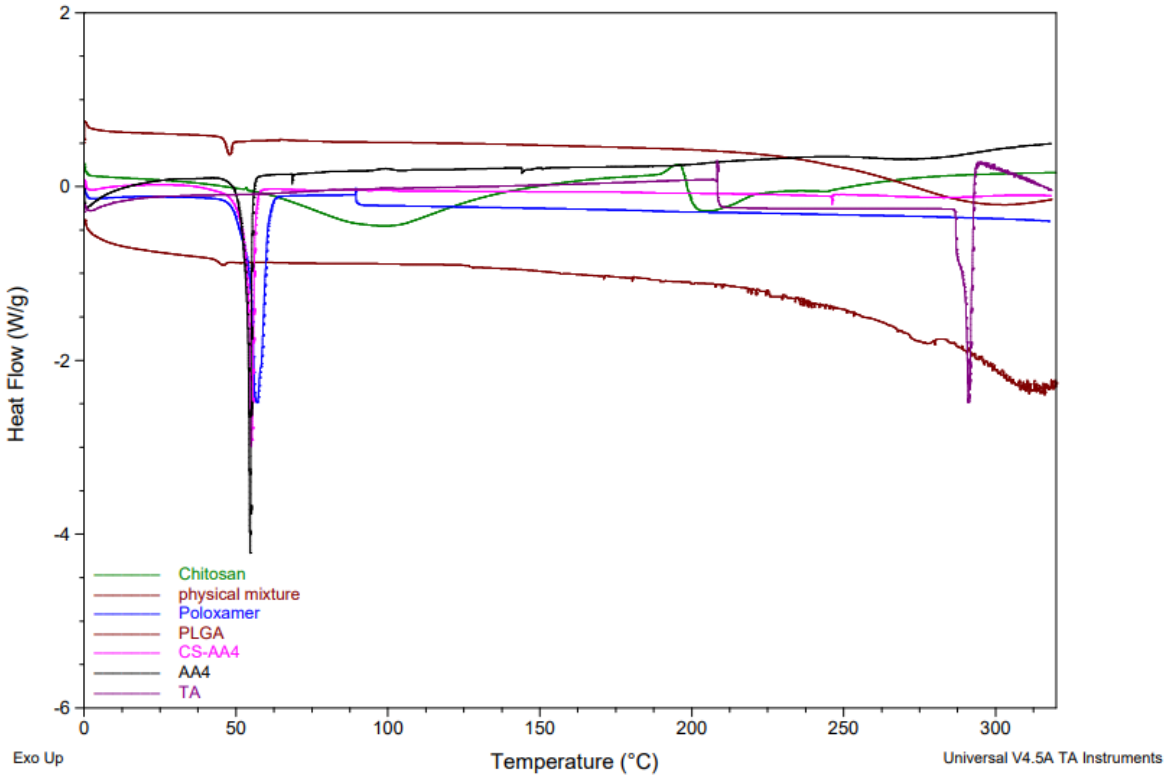

Figure 2.9: DSC thermograms of TA, PLGA, poloxamer, chitosan, physical mixture, PLGA and chitosan-coated PLGA NPs.

The endothermic peaks of poloxamer at 57.01 ℃ indicates the melting point (T_m) [368]. The fusion of glass transition peak (T_g) and polymer relaxation peak has been observed for PLGA at 48 ℃ and the second peak at 300 ℃ was due to the degradation of the polymer [369]. Chitosan displayed a broad endothermic peak at 100 ℃ which was due to the presence of water [370]. The drug, TA exhibited a sharp endothermic peak at 291.05 ℃ due to its crystalline nature (T_c).

Poloxamer and PLGA endothermic peaks were mixed and there was a shift of peak in the PLGA and chitosan-coated PLGA NPs, which shows the uniform mixture of the components in the formulation. The sharp crystalline peak of the drug (TA) was not seen in either of the formulations indicating the molecular dispersion of the drug in NPs leading to enhanced stability [371].

The DSC thermogram of PLGA shows a mix of T_g and polymer relaxation peaks. To separate these two peaks modulated DSC was performed, where the T_g and polymer relaxation peaks were seen to be separated at a heating rate of 0.5 ℃/min as shown in Figure 2.10.

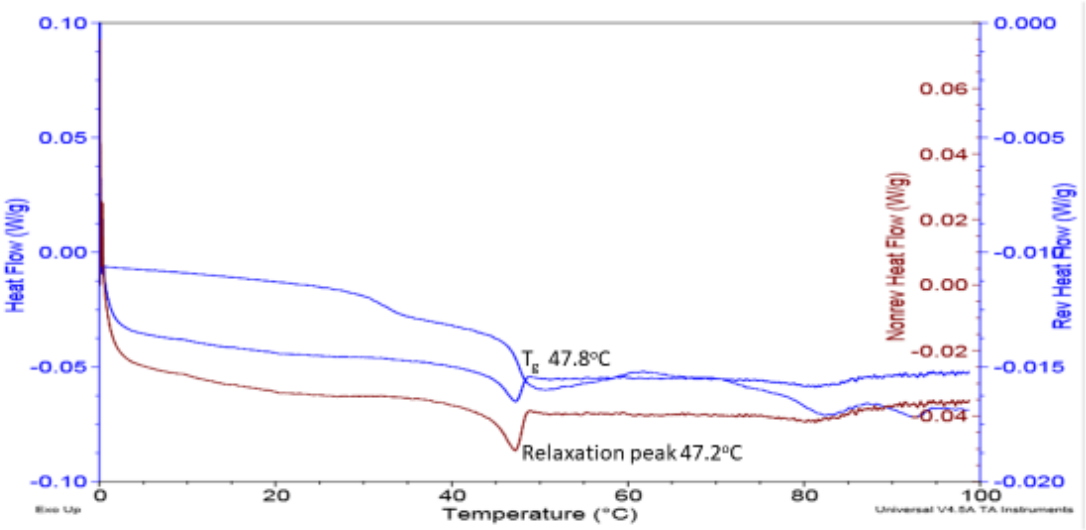

Figure 2.10: Modulated DSC thermogram of PLGA highlighting the glass transition and polymer relaxation peaks.

The T_g of PLGA was found to be 47.8 ℃ and the polymer relaxation peak was seen at 47.2 ℃ and the T_g temperature of the PLGA in the prepared NPs was above the physiological temperature. This is advantageous for the drug delivery application as at the T_g mobility of the PLGA polymeric chain will be increased leading to the escape of the drug molecules before reaching the target site. This could also affect the controlled release property of the nanoparticulate system.

Rouse *et al*. also reported the superimposed peaks of T_g and polymer relaxation peaks in their DSC scans and further performed modulated DSC to identify Tg [372]. In their study, the authors reported the T_g peak at 46 ℃ followed by a relaxation peak. Thermal analysis plays a vital role in establishing the compatibility of the components within the formulation and to identify the structural behaviour of the drug before and after preparation of NPs [373].

2.3.6 Cytotoxicity testing (MTT assay)

The MTT (3-(4, 5-Dimethylthiazol-2-yl)-2, 5-diphenyltetrazolium bromide) assay is a colorimetric assay that measures the reduction of MTT yellow dye by mitochondrial succinate dehydrogenase [374]. When MTT enters the cells and passes into the mitochondria, it is reduced to a dark purple formazan crystal. The duration of this enzymatic activity and the resulting purple colour was used as an indication to measure cellular viability and to determine any cytotoxicity caused by nanoparticles. The first barrier to topically administered NPs is the corneal epithelium, hence human corneal epithelial cells (HCECs) were used to evaluate the safety of the prepared NPs on ocular cells [375]. Future *in-vitro* cell experiments (permeation

and biomarker studies) were designed for these optimized NPs, with the concentrations of the drug and NPs ranging from 5 µM to 100 µM [302,376]. Similar concentrations were used to assess the toxicity of these NPs on HCECs. The cytotoxicity study performed for TA, PLGA NPs and TA-encapsulated NPs demonstrated that they were non-toxic (Figure 2.11). The concentration of TA inside the PLGA NPs was considered to prepare 5 µM to 100 µM. Blank NPs were prepared with the same concentrations of NPs material as drug-loaded NPs.

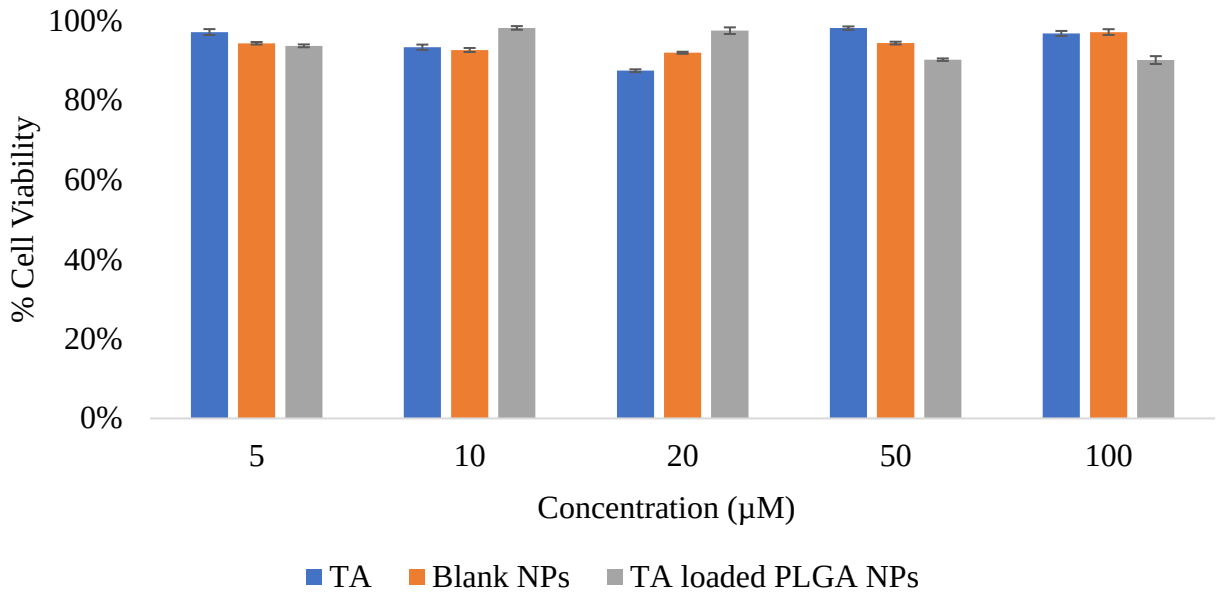

Figure 2.11: Cytotoxicity study of TA, PLGA NPs (without drug) and TA-encapsulated NPs on HCECs, n=3 ± SD.

The blank NPs and drug-loaded NPs exhibited more than 90% cell viability even with an increase in concentration from 5 µM to 100 µM. The drug on its own resulted in more than 87% cell viability with the same concentrations. PLGA NPs have previously shown non-toxic results on cell lines and animal eyes [377].

2.3.7: *In-vitro* drug release study

The %cumulative drug release was plotted against time (h) for the *in-vitro* drug release study performed using a dialysis membrane and PBS with 1% tween 80 as release media (Figure 2.12). The volume of release media was at least 3 times the drug solubility limit to avoid saturation. To increase the solubility of hydrophobic TA, tween 80 was used as a surfactant in the release medium [274]. The surfactant increased the solubility of drug from 21 ± 2.16 µg/mL to 102.05 ± 4.78 µg/mL. For the release study, formulation (AA4 and CS AA4) equivalent to 25 µg/mL of drug (even if 100% of drug was released, saturation was not possible as the release

media was four times greater than the solubility level) was taken, considering the volume of release media.

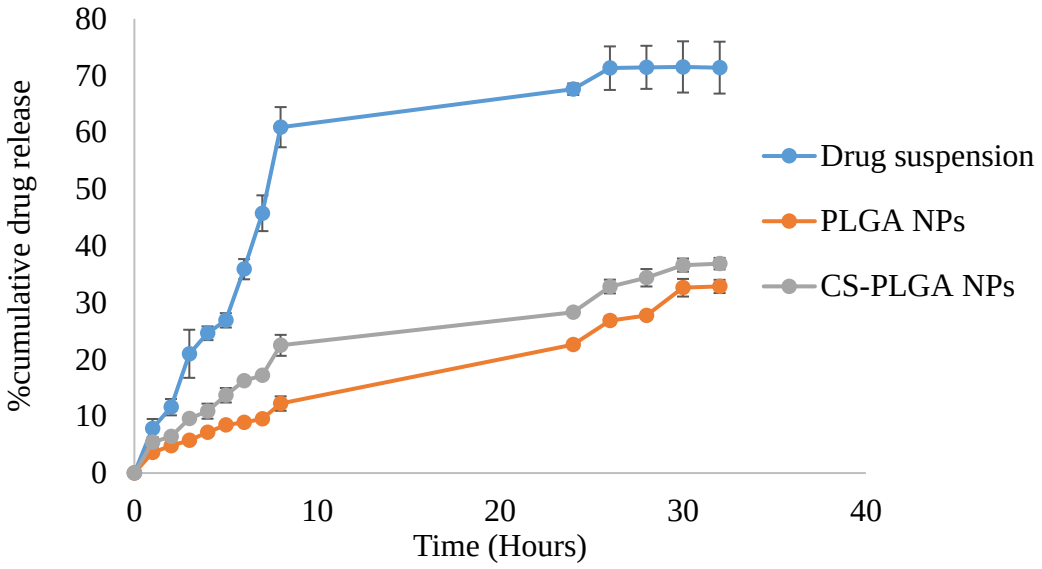

Figure 2.12: *In-vitro* drug release of PLGA NPs (AA4) and CS-PLGA NPs (CS AA4) using a dialysis membrane.

The PLGA NPs and chitosan-coated PLGA NPs demonstrated a biphasic release, burst release on Day 1 followed by controlled release; this release pattern is in agreement with previous investigations on similar particles [167,378]. The PLGA NPs showed 33% drug release (165 µg out of 500 µg) and chitosan-coated PLGA NPs released 37% drug release (185 µg out of 500 µg) in 33 h. The released drug is relevant to the therapeutic concentration considering the clearance mechanisms when applied topically. RETISERT® is a commercially available implant containing 0.59 mg of fluocinolone acetonide (similar corticosteroid as TA) with a release rate of 600 ng/day to treat inflammation at the back of the eye [70]. The anti-inflammatory potency of TA is 4.8 times higher than fluocinolone acetonide and dosage will be designed based on the bioavailability of TA at the retina [379]

In a previous study, where Pandit *et al.* formulated bevacizumab-loaded, chitosan-coated PLGA NPs they investigated the *in-vitro* drug release profile in PBS [160]. They observed a similar burst release of the drug in the first hour and obtained 25% drug release in 72 h, reaching a plateau. A similar pattern was observed in the current study. As highlighted in Chapter 1, PLGA exhibits controlled release of drug in many particulate systems due to its degradation mechanism. Chitosan coating did not significantly alter drug release ($P > 0.05$) and demonstrated a similar pattern of release when compared to PLGA NPs, which was also observed in previous studies [216].

For the dialysis membrane *in-vitro* drug release technique, the drug suspension on its own was released slowly instead of by rapid release. This may be due to the dialysis membrane barrier also impacting the transfer of released drug from inside the dialysis bag to the external release media (as mentioned in Section 1.4.5). As such, this experimental approach may affect the actual calculated release rate of the drug from the NPs [267]. Considering this, the next set of trial experiments was carried out (with PLGA NPs (AA4) with similar concentration used for the dialysis drug release method) in PBS with 1% tween 80 without a dialysis membrane using microcentrifuge tube and centrifugation drug release methods. The microcentrifugation tube method (Figure 2.13) showed a similar release pattern for TA compared to the dialysis method (Figure 2.12) with 27.5% drug released in 30 h. After the last time point of the microcentrifuge tube, the drug which is not released was quantified by extracting from NPs, which is 67.8%.

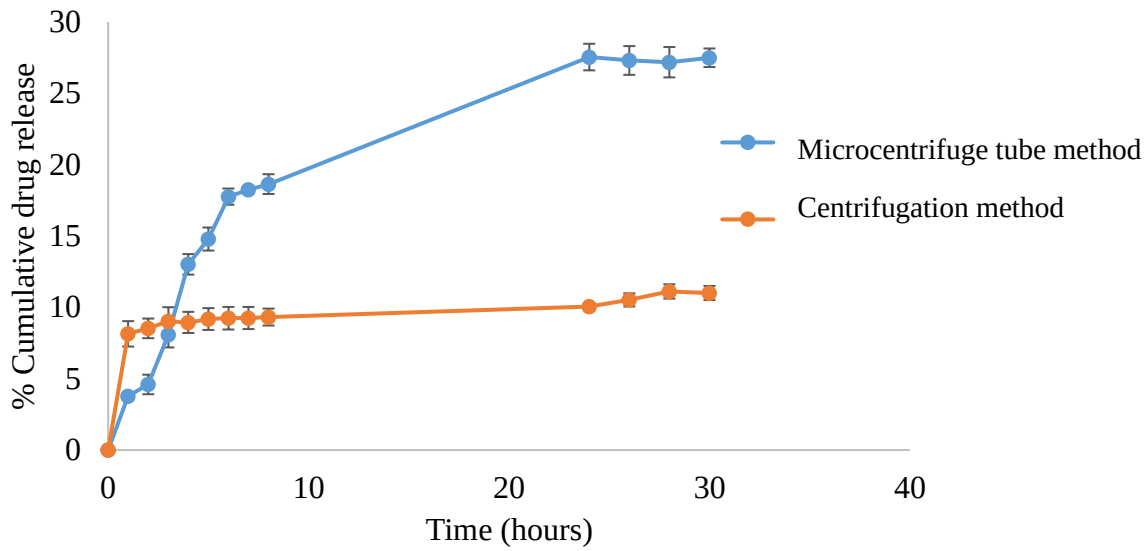

Figure 2.13: *In-vitro* drug release of PLGA NPs (AA4) using microcentrifuge tube and centrifugation drug release methods with PBS with 1% tween 80 as release media.

For the centrifugation method the drug release was very low compared to the other methods (11% of drug released in 30 h). This could be due to interruption of the drug release at every sampling point for centrifugation of the whole release media to separate the released drug [380]. Also, some of the NPs might have been lost in the supernatant during the repeated centrifugation steps. When comparing all three methods (dialysis, aliquot and centrifugation), drug release in PBS with 1% tween 80 using an aliquot method was found to be effective as there was no dialysis membrane barrier and the release was not interrupted at the sampling points (as fresh microcentrifuge tubes were taken at each time point) [381].

2.4 Conclusions

The chitosan-coated PLGA nanoparticles encapsulating TA were fabricated by a thin-film hydration technique and were optimized using factorial Plackett-Burman statistical design. Drug, polymer, and surfactant concentrations were considered as variables. The optimized formulation (AA4 and CS AA4) was selected based on the responses of particle size, PDI, ZP and %encapsulation efficiency. The optimized NPs before and after coating had a particle size of 467 nm and 517 nm with 64% and 35% of encapsulation efficiency, respectively. Thermal analysis revealed that the NPs exhibited prolonged thermal stability with molecular dispersion of the drug in the nanoparticulate system. The formulation showed 27.5% drug release in 30 h reaching a plateau suggesting the controlled release of the drug.

Considering the characteristics achieved these nanoparticulate systems may benefit ocular delivery to treat AMD [382–384]. As mentioned in previous sections the polymers used are biodegradable and biocompatible and the mucoadhesive property of chitosan along with the lipophilic nature of TA may help in better permeation across the barriers of the eye. The prepared NPs, when loaded in a suitable drug delivery platform may increase ocular bioavailability [385,386].

The following chapters outline the preparation of chitosan-coated PLGA nanoparticles using an oil-in-water emulsion method. NPs will be prepared with TA, Quercetin and in a combination of both the drugs. The final optimized dual therapy NPs will be studied on human retinal cell lines (biomarker studies) to evaluate their capability in treating the disease.

Chapter 3: Triamcinolone acetonide-loaded chitosan-coated PLGA nanoparticles prepared by emulsion formulation technique

3.1 Introduction

The work in this chapter was published as "Chitosan-Coated PLGA Nanoparticles Encapsulating Triamcinolone Acetonide as a Potential Candidate for Sustained Ocular Drug Delivery" [387]. As highlighted in previous chapters, active research is ongoing to develop improved controlled release drug delivery systems which can be given through topical routes like eye drops to treat AMD and other posterior segment eye diseases [388–390]. In recent times immense investigation is being done for the tailoring of nanoparticulate platforms to possess unique properties such as enhanced bioavailability with negligible toxicity. Synthetic and natural polymers with biodegradable and biocompatible characteristics are frequently utilised to fabricate ocular formulations to achieve these properties by delivering the therapeutic agent in a controlled manner with minimal toxicity [329]. The capacity of a drug to release from these polymeric systems largely depends on elements such as polymer molecular weight, degradation mechanism, polymer and drug compatibility and permeability, etc. [391]. When designing the topical formulation for ocular drug delivery, mucoadhesiveness and permeation enhancing properties play a vital role as the mucus, sclera and corneal membranes are negatively charged and intact. The positive charge of the particles with permeation enhancing polymers in the formulation aids in better retention in ocular tissues and also permeate across the ocular membranes with tight junctions [265].

A review paper on drug solubility highlighted that most of the new active pharmaceutical ingredients are hydrophobic or lipophilic agents [392]. The major issue with the use of these hydrophobic drugs, including triamcinolone acetonide (TA), is minimal aqueous solubility leading to substandard bioavailability. Loading of hydrophobic drugs like TA and quercetin into nanoparticulate systems can help overcome this complication [393]. In Chapter 2, TA-loaded nanoparticles were developed and optimised by using the thin-film hydration method. In the present chapter surface modified NPs were fabricated using an oil-in-water emulsion technique. In previous investigations NPs prepared by emulsion/solvent evaporation technique yielded monodisperse NPs with a smaller size; as it involves ultrasonication during the preparation process which could control the size of the NPs [394,395]. Both the methods (thin-film hydration and emulsion techniques) have been utilised to fabricate the surface modified NPs in the present study; the characteristics of the obtained NPs was compared, and ideal candidates were selected to achieve the suitable topical formulation. These optimised NPs will be selected to load the novel combination of drugs, TA (corticosteroid) and quercetin

(flavonoid) and their effect on multiple pathologies of AMD will be studied as mentioned in Chapter 1.

The present Chapter aims to develop a topically applied nanoparticulate system containing chitosan-coated PLGA nanoparticles prepared by an emulsion technique to exhibit extended drug release for the treatment of AMD. Optimization of the NPs was achieved using response surface design of experiments and Minitab software. The prepared NPs were investigated for particle size, polydispersity index (PDI), zeta potential, encapsulation efficiency and *in-vitro* release of the drug. Cytotoxicity assay will be performed to determine the toxicity profile of the formulations on the ocular cell lines. Optimized NPs will be combined with a suitable drug delivery platform like an eye drop with permeation enhancers to develop a multi-drug delivery system with added advantages of the nanoparticulate system and the drug delivery platform.

3.2 Experimental

3.2.1 Materials

As per Section 2.2.1 plus the following were used:

Poly (vinyl alcohol) (MW: 89-98K) were purchased from Sigma Aldrich, Ireland.

3.2.2 Equipment

As per Section 2.2.2.

3.3 Methods

3.3.1 Preparation of PLGA nanoparticles

The nanoparticles were prepared by the single emulsion technique which was a modification of a previously published double emulsion method [170]. PLGA (3.5 mg/mL) and TA (1 mg) were dissolved in 2 mL of dichloromethane (DCM) and this mixture was added dropwise to 10 mL of the aqueous solution containing surfactant (poloxamer and poly (vinyl alcohol) at 1% (w/v) and 0.25% (w/v), respectively, were tested as surfactants). The mixture was sonicated for 10 min, left to stir overnight to evaporate the organic solvent and finally the nanosuspension was centrifuged at 3000 rpm for 30 min at 4 ℃ to remove any unentrapped drug. The supernatant obtained was subjected to high-speed centrifugation at 15,000 rpm for 30 min at 4 ℃ to recover the NPs.

3.3.2 Chitosan coating of PLGA nanoparticles

The prepared PLGA NPs were incubated in chitosan solution (1:1 (v/v)) overnight by stirring at room temperature. Two different concentrations of chitosan, 0.25% (w/v) and 1% (w/v) were used. After the incubation, the NPs were collected by centrifugation at 15,000 rpm for 30 min.

3.3.3 Optimization of chitosan coated PLGA nanoparticles by emulsion technique

After the formation of the NPs in the screening experiments and considering the reproducibility, the formulation optimization was designed using design of experiments (DOE). For the nano emulsion optimization Box-Behnken, a surface-response DOE has been chosen. The three independent variables used are PLGA (3.5 – 4.5 mg/mL), Poloxamer (1-2% (w/v)) and chitosan (1-2% (w/v)). The experimental model generated by the Minitab software is summarised in Table 3.1.

Table 3.1: Design of experiments generated by Box-Behnken design statistical design in Minitab software.

StdOrder	RunOrder	PtType	Blocks	PLGA (mg/ml)	Poloxamer % (w/v)	Chitosan % (w/v)
12	1	2	1	4	2	2
23	2	2	1	4.5	1.5	2
7	3	2	1	3.5	1.5	2
22	4	2	1	3.5	1.5	2
18	5	2	1	3.5	2	1.5
9	6	2	1	4	1	1
5	7	2	1	3.5	1.5	1
17	8	2	1	4.5	1	1.5
4	9	2	1	4.5	2	1.5
20	10	2	1	3.5	1.5	1
2	11	2	1	4.5	1	1.5
28	12	0	1	4	1.5	1.5
19	13	2	1	4.5	2	1.5
16	14	2	1	3.5	1	1.5
6	15	2	1	4.5	1.5	1
25	16	2	1	4	2	1
10	17	2	1	4	2	1
1	18	2	1	3.5	1	1.5
29	19	0	1	4	1.5	1.5
11	20	2	1	4	1	2
15	21	0	1	4	1.5	1.5
27	22	2	1	4	2	2
24	23	2	1	4	1	1
8	24	2	1	4.5	1.5	2
3	25	2	1	3.5	2	1.5
30	26	0	1	4	1.5	1.5
13	27	0	1	4	1.5	1.5
14	28	0	1	4	1.5	1.5
26	29	2	1	4	1	2
21	30	2	1	4.5	1.5	1

The four dependant response variables are particles size, polydispersity index (PDI), zeta potential and encapsulation efficiency. The formulations with the same composition have been given one formulation code starting from E1 to E13 as seen in Table 3.2 for PLGA NPs and CS-E1 to CS-E13 for chitosan-coated NPs.

Table 3.2: Compositions of the emulsion codes for the experiments generated by DOE.

Emulsion Code	PLGA (mg/ml)	Poloxamer % (w/v)	Chitosan % (w/v)	No. of Runs
E1	4	2	2	2
E2	4.5	1.5	2	2
E3	3.5	1.5	2	2
E4	3.5	2	1.5	2
E5	4	1	1	2
E6	3.5	1.5	1	2
E7	4.5	1	1.5	2
E8	4.5	2	1.5	2
E9	4	1.5	1.5	6
E10	3.5	1	1.5	2
E11	4.5	1.5	1	2
E12	4	2	1	2
E13	4	1	2	2

3.3.4 Characterization of the nanoparticles

The characterization of NPs was done with the same procedure mentioned in Chapter 2. The %encapsulation efficiency of the PLGA NPs was analysed as mentioned in Chapter 2.

3.3.5 *In-vitro* drug release study

In-vitro drug release was performed using the microcentrifuge method outlined in Section 2.2.8.3. To avoid the bacterial contamination of the formulation and the release media over 70 h, 0.01% sodium azide was used as anti-bacterial agent [160].

3.4 Results and discussion

3.4.1 Screening of chitosan coated PLGA nanoparticles

The chitosan-coated PLGA nanoparticles were prepared by modifying two previously published methods [170,396]. PVA has shown promising results as the surfactant in the mentioned studies and was therefore considered for the screening experiments. In the previous chapter, poloxamer was used as the surfactant, which produced the stable NPs using the thin-film hydration technique and it has also shown promising results in the past [397]. The concentrations of the drug, polymer and surfactant have been selected based on previous studies and the work done in Chapter 2. The findings of the NPs prepared with 0.25% (w/v) PVA and 1% (w/v) poloxamer are represented in Table 3.3.

Table 3.3: Particle size, zeta potential, PDI and % encapsulation efficiency of the screening nano-emulsion. Results represent n=3 ± SD.

Emulsion Code	Surfactant % (w/v)	Particle Size (nm)	Zeta potential (mV)	PDI	%Encapsulation efficiency
A1	0.25% PVA	359 ± 76.37	-14 ± 5.44	0.15 ± 0.07	50 ± 8.25
CS-A1	0.25% PVA	346 ± 125.37	+18 ± 1.77	0.70 ± 0.53	27 ± 4.98
A2	1% Poloxamer	200 ± 61.16	-20 ± 9.26	0.07 ± 0.01	59 ± 5.37
CS-A2	1% Poloxamer	187 ± 23.55	+14 ± 5.44	0.06 ± 0.01	34 ± 3.85

The nanoparticles fabricated with poloxamer as surfactant yielded smaller NPs with low PDI and high encapsulation of the TA compared to NPs prepared with PVA. This was perhaps due to entanglement of PEO moieties of poloxamer with polymeric chains of PLGA leading to more compact and stable NPs with high drug protection [398–400]. Salama *et al*. formulated fluocinolone acetonide-loaded NPs using PLGA and poloxamer; they attained particle size of 203 ± 5 nm with 56 ± 4% of encapsulation efficiency [335]. Along with the smaller size, the NPs also released the drug in a controlled manner up to 24 h; those authors postulated that this was due to the interactions between PLGA and PEO groups of poloxamer (which could make the particle intact and protect the drug leading to more tailored drug release).

3.4.2 Optimization of nanoparticles using statistical experimental design

The Box-Behnken response surface statistical design consisting of 3 factors and 3 levels was prioritised for this study to optimize the NPs prepared by the emulsion method. The model

evaluates the main effects, interaction effects and quadratic effects of the variable factors on the NPs characteristics (Table 3.4).

Table 3.4: Investigated values of responses for the prepared NPs using Box-Behnken design.

Run Order	PLGA (mg/ml)	Poloxamer % (w/v)	Chitosan % (w/v)	Particle size (nm)	PDI	Zeta Potential (mV)	%Encapsulation efficiency
1	4	2	2	340.0	0.091	10.50	34.07
2	4.5	1.5	2	420.0	0.064	28.60	34.34
3	3.5	1.5	2	333.0	0.042	37.80	36.56
4	3.5	1.5	2	410.0	0.470	31.20	36.90
5	3.5	2	1.5	569.0	0.102	-46.40	51.92
6	4	1	1	340.0	0.118	31.50	48.95
7	3.5	1.5	1	819.0	0.120	46.90	28.79
8	4.5	1	1.5	414.0	0.145	22.70	53.40
9	4.5	2	1.5	337.0	0.117	-42.70	50.95
10	3.5	1.5	1	680.0	0.171	29.40	33.48
11	4.5	1	1.5	464.0	0.097	25.60	56.38
12	4	1.5	1.5	349.0	0.114	20.40	53.43
13	4.5	2	1.5	380.0	0.244	-38.20	52.15
14	3.5	1	1.5	286.9	0.109	19.60	57.79
15	4.5	1.5	1	410.0	0.157	36.89	30.94
16	4	2	1	350.0	0.236	-35.60	37.46
17	4	2	1	390.0	0.121	-28.40	34.37
18	3.5	1	1.5	383.0	0.071	33.70	52.56
19	4	1.5	1.5	465.0	0.118	25.52	50.67
20	4	1	2	480.0	0.283	57.70	33.41
21	4	1.5	1.5	390.0	0.084	31.50	56.26
22	4	2	2	370.7	0.220	18.20	31.98
23	4	1	1	525.0	0.134	48.80	49.51
24	4.5	1.5	2	257.7	0.088	18.90	31.16
25	3.5	2	1.5	420.0	0.112	-33.20	35.28
26	4	1.5	1.5	268.7	0.187	29.30	41.07
27	4	1.5	1.5	441.0	0.045	30.60	39.09
28	4	1.5	1.5	471.0	0.412	28.60	38.21
29	4	1	2	427.0	0.121	33.40	27.62
30	4.5	1.5	1	361.0	0.165	42.70	30.38

As expected, the PLGA nanoparticles coated with chitosan showed positive zeta potential. But the formulations having the highest concentration of poloxamer 2% (w/v) displayed negative zeta potential. This could be due to the formation of poloxamer micelles, these micelles are known to produce negatively charged particles [401].

It also identifies the combination of factors to obtain the predicted response based on the point prediction (response optimizer). The findings of the NPs with various combinations of the polymer, surfactant, and chitosan according to the DOE are represented in Table 3.4. The concentration of PLGA, chitosan and both combined have a significant effect on particle size (Figure 3.1). The low concentration of PLGA (3.5 mg/mL) and poloxamer (1% (w/v)) and medium concentration of chitosan (1.5% (w/v)) gave the smallest NPs (334.95 ± 67.95 nm).

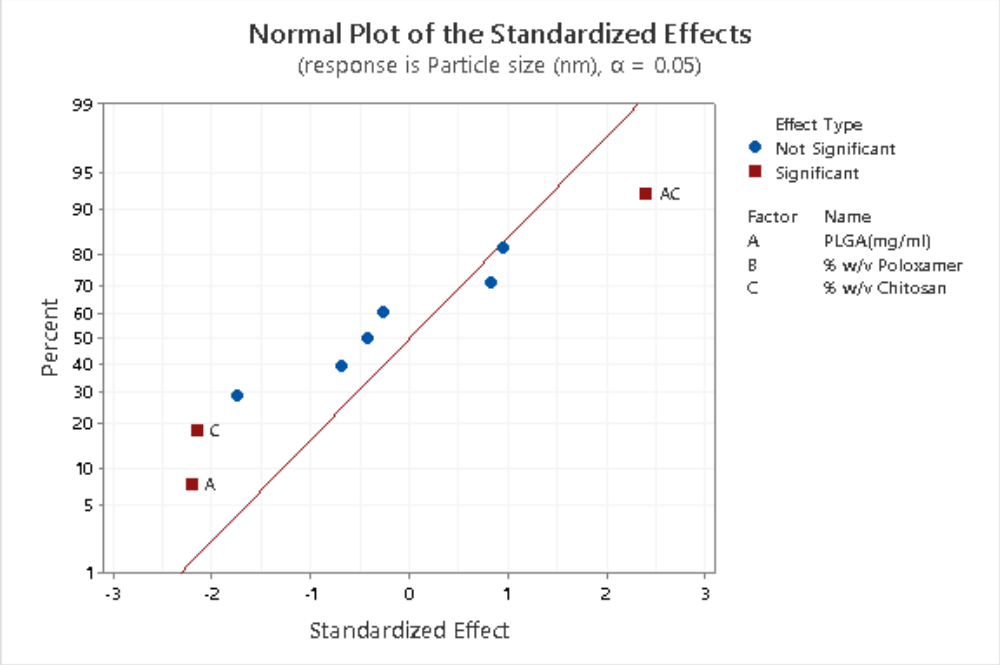

Figure 3.1: Effect of factors (PLGA, poloxamer and chitosan) on particle size.

In a previous study Madani *et al.* also observed an increase in nanoparticle size with an increase in PLGA concentration [402]. The authors postulated that in emulsion technique, increased PLGA concentration in organic solvent elevates the viscosity of dispersed medium resulting in reduced shear stress leading to formation of larger nanodroplets.

There was no statistically significant effect of all the three factors on PDI of the NPs as seen in Figure 3.2; the formulations prepared with a high concentration of surfactant (2% (w/v)) yielded low PDI NPs. As mentioned in Section 2.1, this could be due to the arrangement of poloxamer on nanoparticle surface with PEO group facing the aqueous solvent. Thus, providing a protective barrier around the particle preventing the aggregation.

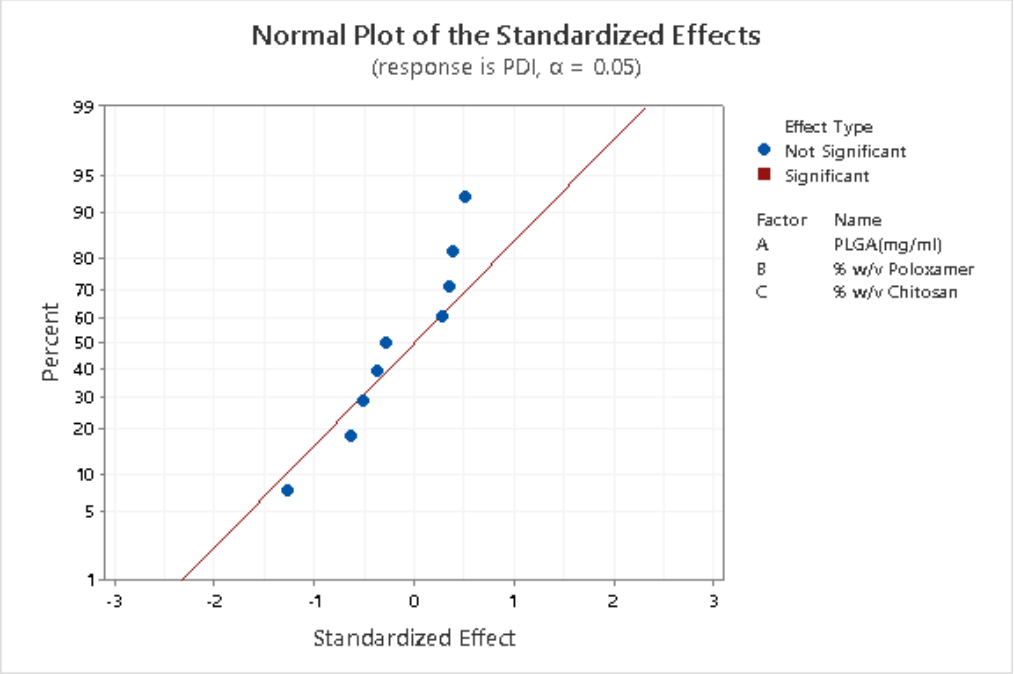

Figure 3.2: Effect of PLGA, poloxamer and chitosan on PDI of the prepared NPs.

The PDI values of all the formulations ranged from 0.04 to 0.47 (Table 3.4) indicating that NPs prepared from emulsion method were monodispersed (Figure 3.3) [403,404].

(a)

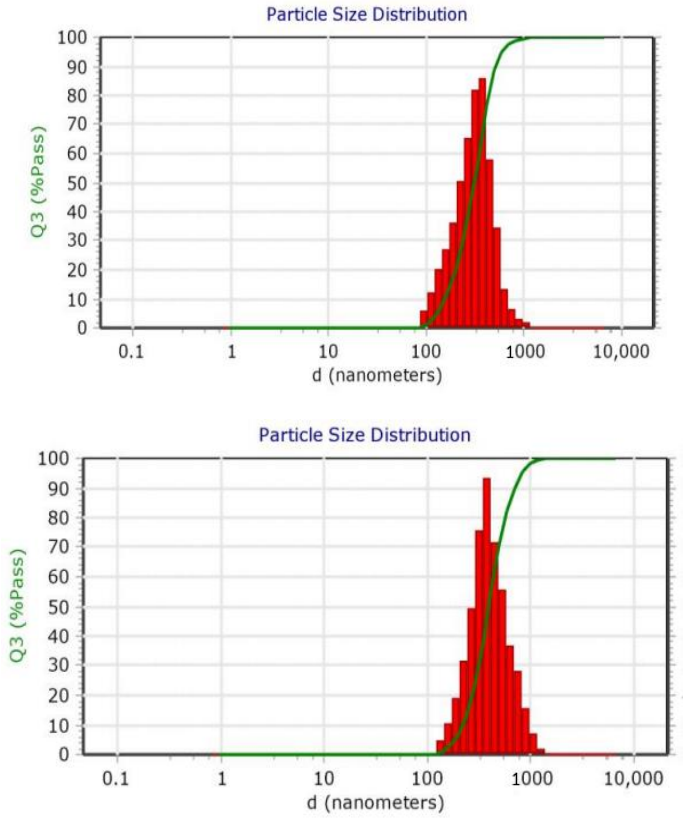

(b)

Figure 3.3: Particle size analysis of (a) PLGA NPs (E10) and chitosan-coated PLGA NPs (CS-E10) from DLS.

Effect of chitosan coating on PLGA nanoparticles

Even though the DOE was designed for chitosan-coated PLGA nanoparticles, NPs have been characterised before and after the coating to compare the difference in size, charge, and encapsulation efficiency. The effect on the particle size of the NPs before and after chitosan coating is seen in Figure 3.4.

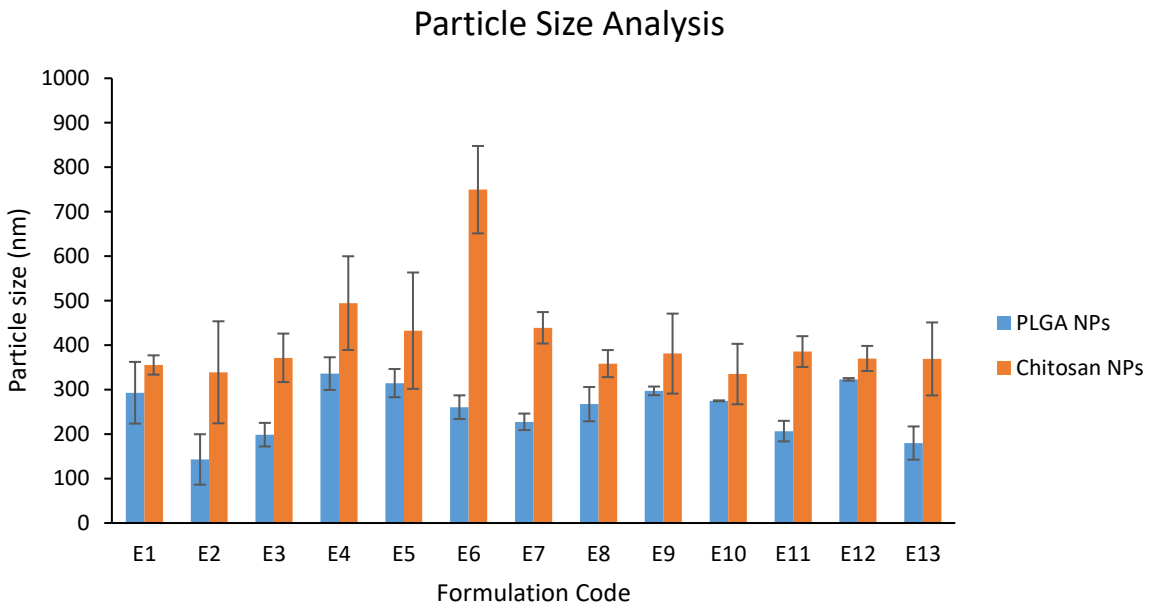

Figure 3.4: Comparison of particle size of the NPs (PLGA NPs) and after chitosan coating. Results represent n=3 ± SD.

The particle size of all the PLGA nanoparticles increased upon chitosan coating. This was maybe due to adsorption of the chitosan on the porous surface of the PLGA NPs. Guo *et al.* studied the adsorption mechanism of chitosan onto PLGA NPs prepared by oil-in-water emulsion technique [340]. In their study, they noticed the increase in particle size of PLGA NPs - 261.5 to -972.7 nm with an increasing chitosan concentration (0.12-2.4 g/L). The authors stated the adsorption of chitosan onto PLGA NPs depends on the chitosan cationic nature, high surface energy and non-uniform microporous surface of PLGA NPs based on their adsorption isotherms. Some formulations in Chapter 2 displayed a decrease in particle size upon chitosan coating, this could be due to a different preparation method (thin-film hydration) which is not involving high-speed centrifugation for the separation of PLGA NPs. To understand the detailed mechanism of chitosan coating and to know the difference between the NPs prepared by thin-film hydration and emulsion techniques, microscopic studies such as SEM and TEM will be useful.

The encapsulation efficiency of some NPs decreased upon chitosan coating as seen in Table 3.5, maybe due to the repeated centrifugation step after chitosan coating, which may lead to loss of some particles and surface bound drug.

Table 3.5: %Encapsulation efficiency of PLGA (E1-E13) and chitosan coated PLGA (CS-E1-CS-E13), n=3 ± SD.

Emulsion Code	%Encapsulation efficiency	Emulsion Code	%Encapsulation efficiency
E1	33.03 ± 1.48	CS-E1	26.71 ± 2.08
E2	32.75 ± 2.25	CS-E2	27.05 ± 1.32
E3	36.73 ± 0.24	CS-E3	28.19 ± 1.32
E4	50.97 ± 12.04	CS-E4	43.6 ± 11.77
E5	58.08 ± 1.60	CS-E5	49.23 ± 0.40
E6	31.13 ± 3.32	CS-E6	25.01 ± 1.35
E7	66.04 ± 2.60	CS-E7	54.89 ± 2.11
E8	59.09 ± 1.77	CS-E8	51.55 ± 0.85
E9	55.87 ± 10.12	CS-E9	47.23 ± 7.15
E10	63.38 ± 2.30	CS-E10	55.18 ± 3.70
E11	30.66 ± 0.40	CS-E11	30.25 ± 1.26
E12	35.91 ± 2.18	CS-E12	30.37 ± 1.57
E13	30.52 ± 4.09	CS-E13	24.09 ± 3.01

The PLGA nanoparticles with emulsion code E7 and E10 showed high encapsulation of drug, 66.04 ± 2.60% and 63.38 ± 2.30%, respectively. Upon chitosan coating the same formulations displayed higher encapsulation of the drug compared to other formulations (54.89 ± 2.11 and 55.18 ± 3.70%, respectively). Using the surface plots shown in Figure 3.5, the effect of PLGA, poloxamer and chitosan on the encapsulation efficiency of the NPs was represented.

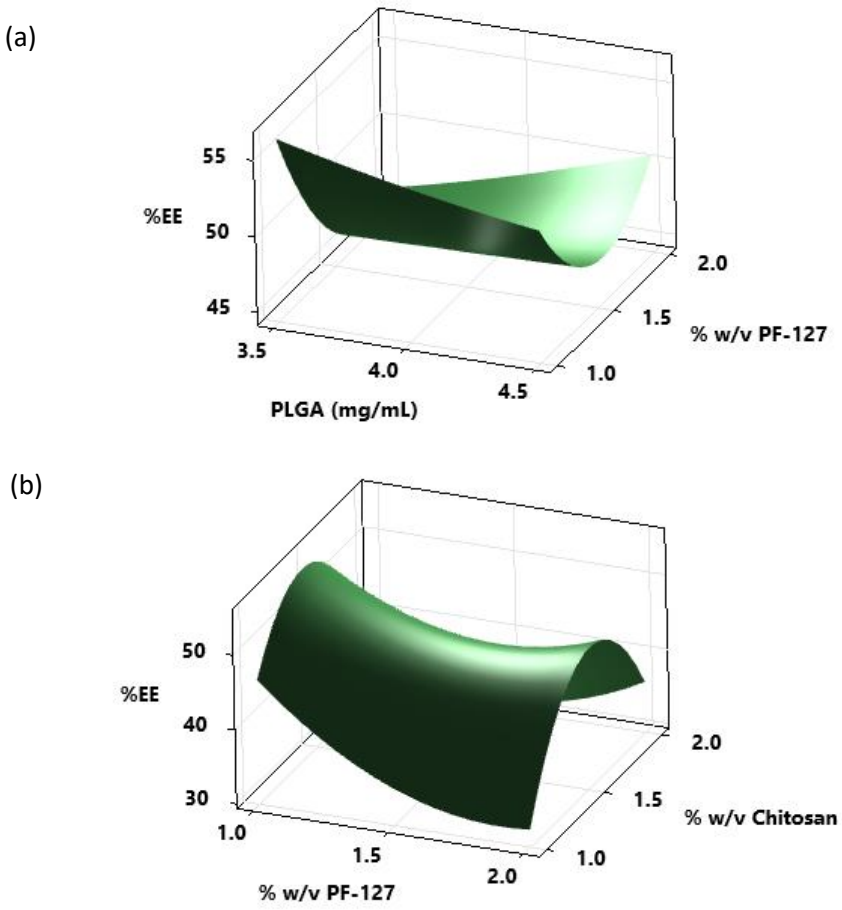

Figure 3.5: (a) Surface plot of %EE (encapsulation efficiency) Vs PLGA and poloxamer (b) Surface plot of % EE Vs % (w/v) chitosan and % (w/v) poloxamer.

For the PLGA NPs, the formulations prepared with a low concentration of poloxamer (1% (w/v)) showed high encapsulation efficiency whereas for chitosan-coated NPs medium concentration of chitosan (1.5% w/v) loaded more drug (Figure 3.5). In a previous study, poloxamer yielded better particles with good encapsulation at 1% (w/v) compared to other higher concentrations [397]. PLGA NPs, E7 and E10, showed smaller particle size with low PDI values: 227.55 and 274.80 nm with 0.12 and 0.11 PDI values, respectively. CS-E7 and CS-E10 measured particle size was 439 and 334 nm with 0.23 and 0.15 PDI values and zeta potential of +24.15 ± 2.05 mV and +26.65 ± 9.97 mV, respectively. According to previous research nanoparticulate system with the mentioned size ranges permeated through the corneal and retinal epithelial layer *in-vitro* [173,334].

3.4.3 Response optimization using response surface design

The response optimizer of this DOE model studies the input responses entered into the model from the combination of factors which are statistically designed. Based on these results the design estimates the coefficients using the mathematical model that best fits the experimental settings thereby predicting the desired responses. To confirm this prediction, it is recommended to perform the experiments using the suggested parameters. Two predictions were entered into the software, and they were coded as prediction emulsion 1 (NP1) and prediction emulsion 2 (NP2).

Prediction 1: Chitosan coated PLGA nanoparticles with smaller particle size and high encapsulation efficiency

In the response optimizer when the goal of achieving a smaller particle size of chitosan-coated nanoparticles with high encapsulation of the TA was entered, the following suggestion was generated (Table 3.6 and Figure 3.6).

Table 3.6: Predicted experimental conditions for low particle size and high encapsulation efficiency for CS-PLGA NPs.

Response	**Goal**	**Lower**	**Target**	**Upper**	**Weight**	**Importance**
%Encapsulation efficiency	Maximum	27.62	57.79		1	1
Particle size (nm)	Minimum		257.70	819	1	1
Solution	**PLGA (mg/mL)**	**Poloxamer % (w/v)**	**Chitosan % (w/v)**	**%Encapsulation efficiency Fit**	**Particle size (nm) Fit**	**Composite Desirability**
1	3.70	1	1.52	55.18	388.46	0.84
Response		**Fit**	**Standard Error of the Fit**	**95% CI**		**95% PI**
%Encapsulation efficiency		55.18	2.97	(48.98, 61.37)		(40.85, 69.50)
Particle size (nm)		388.5	46.70	(291.1, 485.8)		(163.2, 613.7)

The parameters and experimental conditions (PLGA-3.7 mg/mL, poloxamer-1% (w/v) and chitosan-1.5% (w/v)) generated by the response surface model are summarised above.

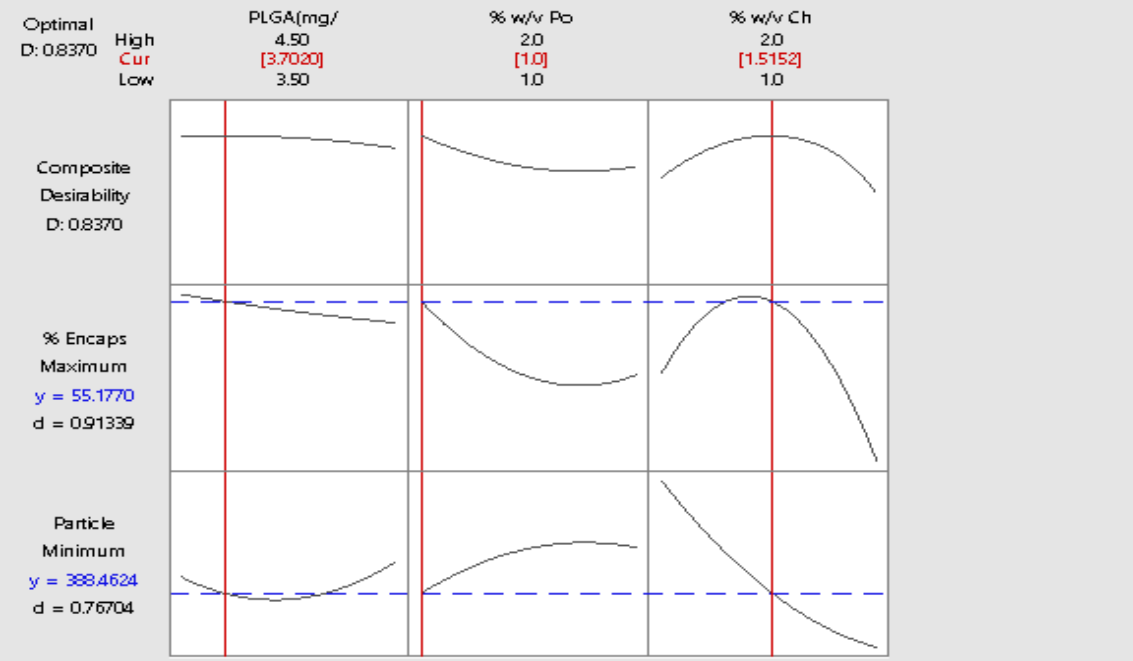

Figure 3.6: Response optimization parameters and predicted experimental conditions for low particle size and high encapsulation efficiency for CS-PLGA NPs.

The model has generated the composite desirability graphs for each parameter and factor to show the reason for selecting the particular concentrations of the factors to achieve desired result as seen in Figure 3.6. The composite desirability (CD) value was 0.84, if the CD value is close to one there are more chances of getting the prediction result. According to 95% confidence interval, the particle size and encapsulation efficiency will lie between 291.1 to 495.8 nm and 48.98 to 61.37%, respectively. If 95% prediction interval was considered the particle size and encapsulation efficiency will be between 163.2 to 613.7 nm and 40.85 to 69.50%, respectively. According to the response optimizer summary if the suggested combination was used, chitosan-coated PLGA NPs of size 388 nm with 55.18% encapsulation efficiency will be yielded.

Prediction 2: Chitosan-coated PLGA nanoparticles with smaller particle size and +25 mV zeta potential

Following the same procedure of generating the prediction 1 parameters, the response optimizer has generated composition to be used to get the NPs with smaller particle size and zeta potential of +25 mV.

Table 3.7: Predicted experimental conditions for low particle size and + 25 mV zeta potential efficiency for CS-PLGA NPs.

Response	Goal	Lower	Target	Upper	Weight	Importance
Zeta potential (mV)	+25	-46.4	+25	+48	1	1
Particle size (nm)	Minimum		257.70	819	1	1
Solution	**PLGA (mg/mL)**	**Poloxamer % (w/v)**	**Chitosan % (w/v)**	**Zeta potential (mV) Fit**	**Particle size (nm) Fit**	**Composite Desirability**
1	4.50	1.00	1.32	25.00	388.46	1.00
Response		**Fit**	**Standard Error of the Fit**	**95% CI**		**95% PI**
Zeta potential (mV)		25.00	8.16	(7.97, 42.03)		(-6.86, 56.86)
Particle size (nm)		388.5	46.7	(291.1, 485.8)		(163.2, 613.7)

Following the suggestions generated by the response optimizer, NPs prepared by prediction 1 and prediction 2 were named NP1, NP2 for the PLGA NPS and CS-NP1, CS-NP2 for the CS-coated PLGA NPs. The NPs were prepared with the same procedure mentioned in Section 3.3.1 and the characteristics obtained were represented in Table 3.8. Similar to the previous formulations prepared by the Box-Behnken DOE, the particle size increased upon chitosan-coating of the PLGA NPs. There was no significant difference in the particle size of the optimised formulations from DOE (CSE7 and CSE10) and the prediction emulsions (NP1 and NP2). However, the chitosan-coated prediction emulsions have lower PDI values (0.098-0.136) compared to CSE7 and CSE10 (0.15-0.23).

Table 3.8: Characteristics of the PLGA and chitosan-coated PLGA NPs prepared by point prediction using response surface DOE, n=3 ± SD.

Emulsion Code	Particle size (nm)	PDI	Zeta potential (mV)	%Encapsulation efficiency
NP1	318.23 ± 18.61	0.220 ± 0.08	-7.4 ± 2.43	64.80 ± 3.95
CS-NP1	386.67 ± 15.14	0.136 ± 0.05	33.3 ± 4.69	57.14 ± 3.81
NP2	240.47 ± 48.75	0.084 ± 0.05	-6.9 ± 3.08	60.31± 2.46
CS-NP2	351.33 ± 27.02	0.098 ± 0.04	31.97 ± 0.21	51.71 ± 1.82

The experimental response values of the prepared prediction nano-emulsions were similar to the predicted response values of the software (Table 3.9). Predicted particles size of the chitosan-coated NP1 and NP2 was 388.5 ± 46.7 nm and the obtained particle size was 386.67 ± 15.14 and 351.33 ± 27.02, respectively.

Table 3.9: Comparison of experimental and predicted values of CS-NP1, n=3 ± SD.

Emulsion Code	**Particle Size (nm)** Experimental value	**Particle Size (nm)** Predicted Value	**%Encapsulation efficiency** Experimental Value	**%Encapsulation efficiency** Predicted Value
CS-NP1	386.67 ± 15.14	388.5 ± 46.7	57.14 ± 3.81	55.18 ± 2.97
Emulsion Code	**Particle Size (nm)** Experimental value	**Particle Size (nm)** Predicted Value	**Zeta potential (mV)** Experimental Value	**Zeta potential (mV)** Predicted Value
CS-NP2	351.33 ± 27.02	388.5 ± 46.7	31.97 ± 0.21	25.00 ± 8.16

The obtained response values for both the predictions are within the standard error of the fit generated by the response optimizer. The two formulations from prediction experiments before and after coating, NP1, NP2, CS-NP1, CS-NP2 and the optimised formulation from the initial Box-Behnken design E10 and CS-E10, were used for further investigations. Both E10 and CS-E10 formulations were now named NP3 and CS-NP3, respectively.

3.4.4 Thermal Analysis

Similar to Section 2.6.6.3, thermal analysis was also performed for the nanoparticles fabricated using emulsion technique. To study the stability of the materials in the formulations and also to investigate the impact of the nanoparticle formation on their stability. Extended thermal stability was noticed in the PLGA NPs (NP1, NP2 and NP3) compared to drug, polymer, and surfactant (Figure 3.7). Gradual degradation of PLGA and TA was noticed in the TGA thermograms, but the NPs exhibited rapid degradation around 400 ℃.

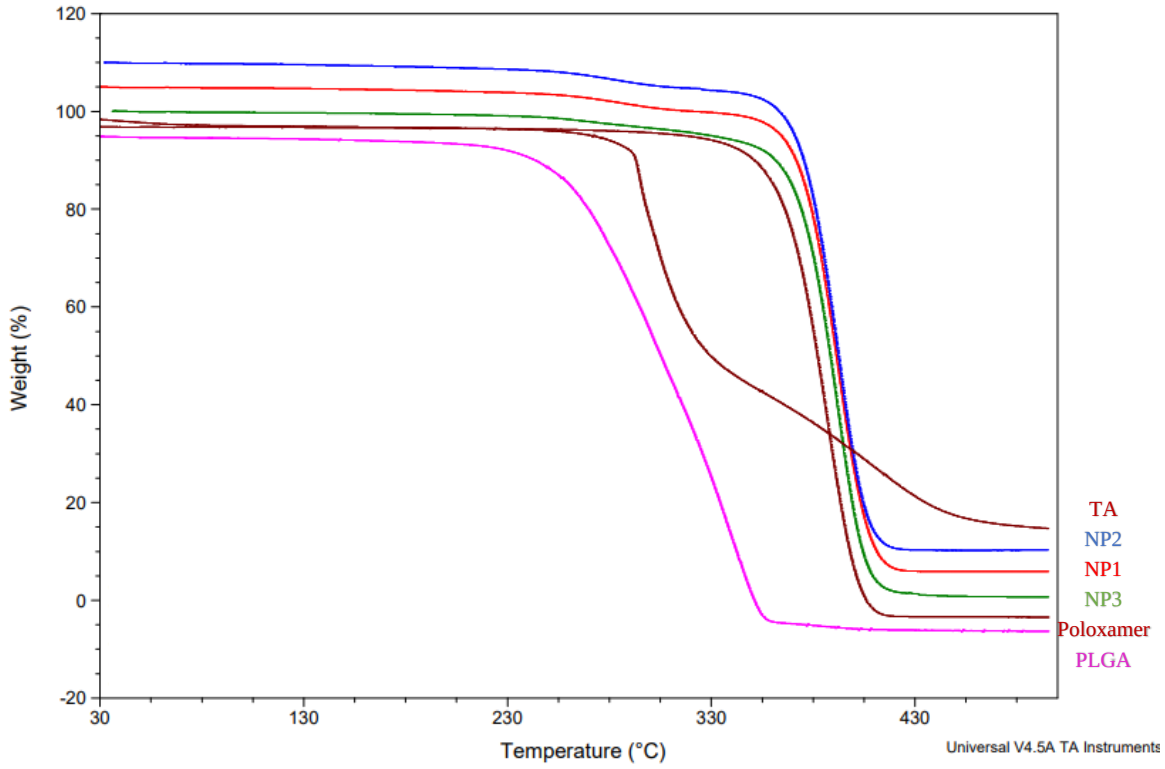

Figure 3.7: Thermal analysis of individual components and PLGA NPs (NP1, NP2 and NP3).

Mathew *et al*. formulated curcumin-loaded PLGA NPs using a single emulsion method to treat Alzheimer's disease [405]. They noticed similar thermal behaviour of PLGA NPs, the curcumin showed gradual thermal degradation, but the NPs displayed rapid degradation with increased thermal stability.

In the thermal analysis of chitosan-coated NPs (CS-NP1, CS-NP2, and CS-NP3), the thermograms of these NPs (Figure 3.8) exhibited weight loss around 300 ℃ due to the loss of water at the initial degradation of the surface adsorbed chitosan [406]. Increased thermal stability of the chitosan-coated formulations was noticed compared to polymers and drug, which was also noticed in thermograms of PLGA NPs.

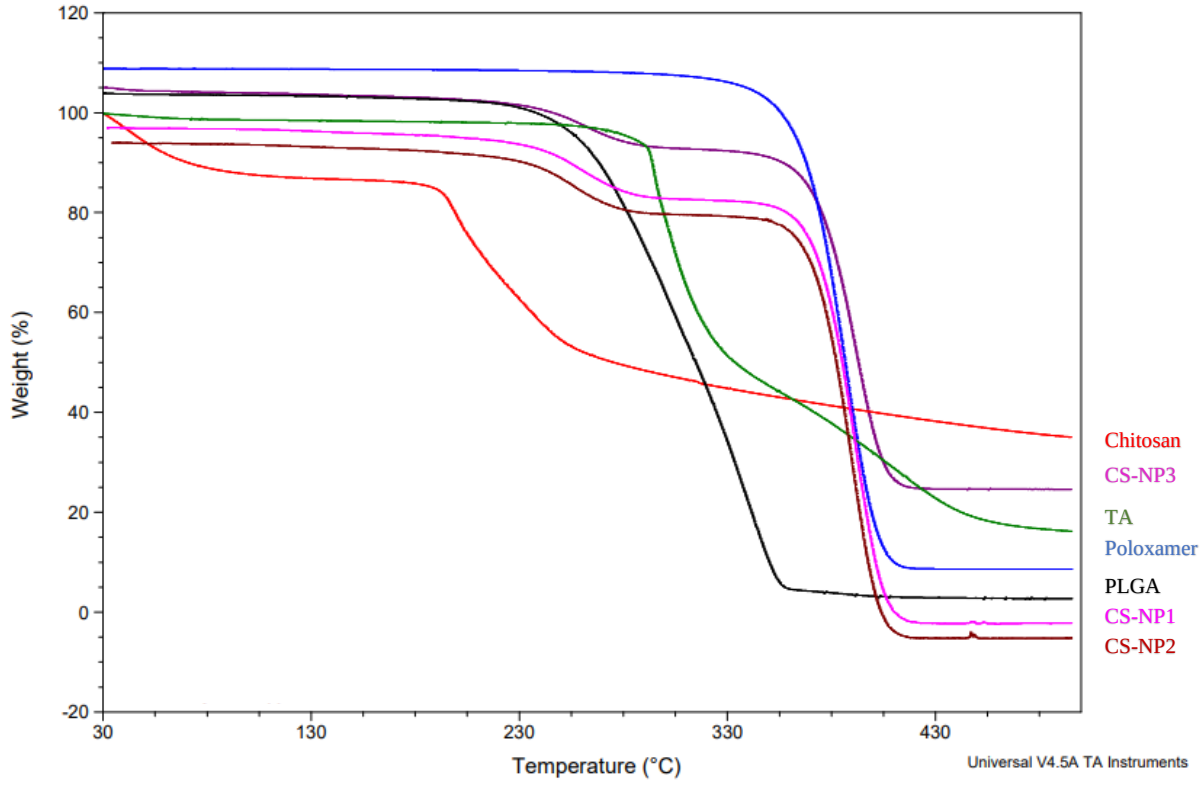

Figure 3.8: Thermal analysis of chitosan-coated NPs (CS-NP1, CS-NP2 and CS-NP3) and the individual components using TGA.

In previous studies similar thermal behaviour was noticed where the nanoparticles demonstrated extended thermal stability compared to the individual components probably due to their intact structure and monodispersion [407,408].

To know the physical state of the drug and the molecular dispersion in the NPs, DSC analysis was performed (Figure 3.9). PLGA displayed two endothermic peaks at 47.79 ℃ and 300.02 ℃ corresponding to glass transition/relaxation peak and degradation, respectively [369]. Poloxamer displayed endothermic peak at 56.39 ℃ due to the melting temperature [409]. The endothermic glass transition/relaxation peak of PLGA and melting peak of poloxamer were combined and shifted to 52.9 ℃ and 55.25 ℃ for NP1, NP2, and NP3 formulations, which suggests the interaction of the polymer and surfactant in the NPs. TA exhibited a sharp endothermic peak at 291 ℃ due to the melting point in the crystalline state [410]. Both the endothermic peaks of drug (melting peak) and PLGA (degradation peak) were seen at 311.85 ℃ in the physical mixture. Whereas the degradation peak of PLGA was not seen in any of the formulations due to the extended thermal stability which was observed in previous TGA results.

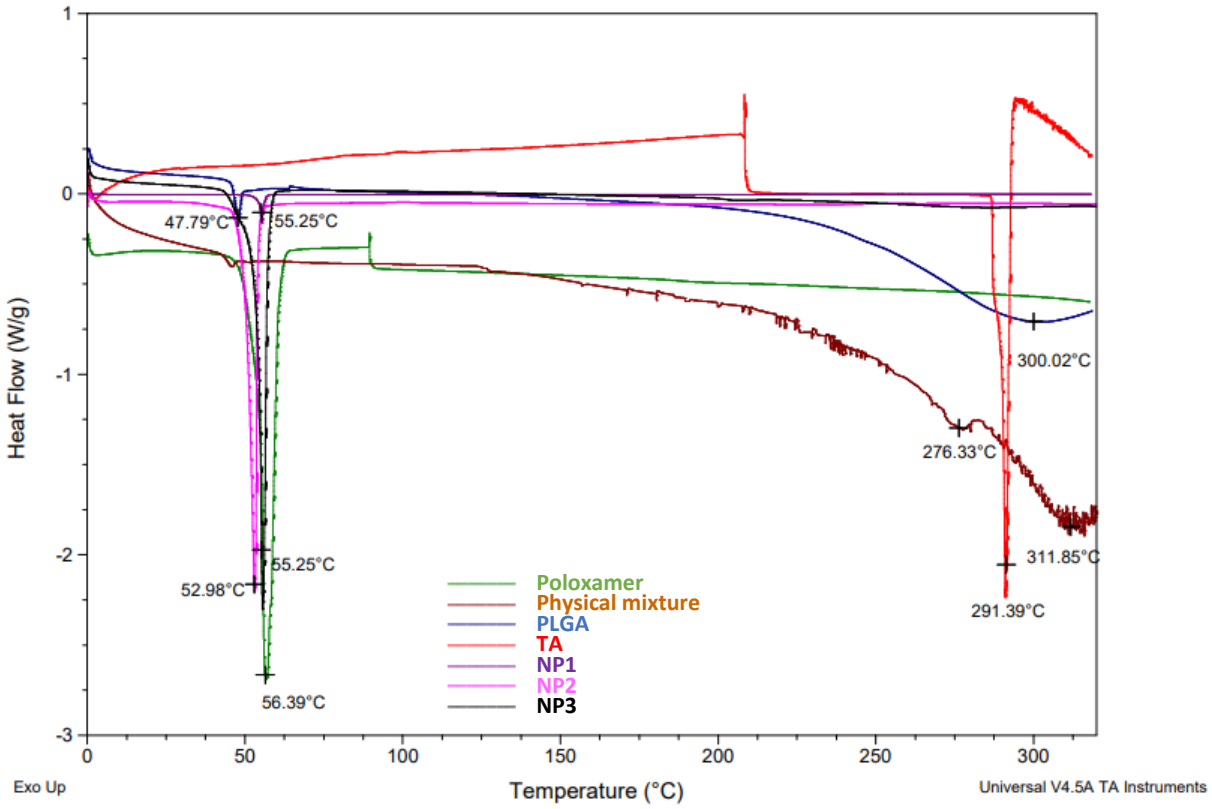

Figure 3.9: DSC thermograms of individual components, physical mixture and PLGA NPs (NP1, NP2 and NP3).

The sharp endothermic peak of the drug was not seen in the PLGA NPs (Figure 3.9) and chitosan-coated PLGA NPs (Figure 3.9) which indicates the change of drug to the amorphous form and molecular dispersion in the NPs system [410].

A similar shift and fusion of endothermic peaks of poloxamer and PLGA was observed in chitosan-coated PLGA NPs (CS-NP1, CS-NP2, and CS-NP3). Chitosan exhibited two endothermic peaks, at 96.45 ℃ and 203.58 ℃, with respect to loss of water and decomposition of amine groups. The exothermic peak of chitosan around 200 ℃ is due to phase inversion during the start of decomposition [411,412]. In all chitosan-coated formulations, the degradation endothermic peak of chitosan shifted to 233.70 ℃ due to the increased stability of chitosan within the nanoparticulate system.

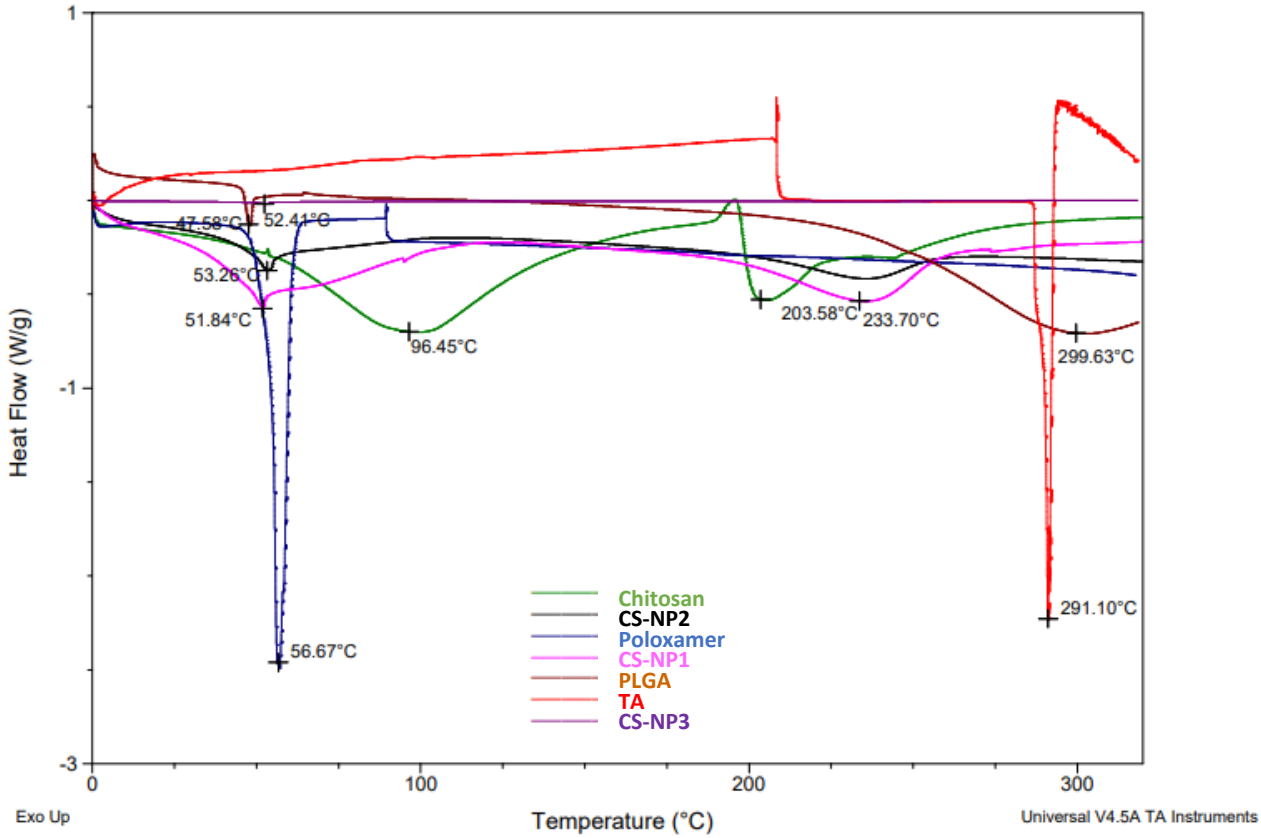

Figure 3.10: DSC thermograms of components and chitosan-coated NPs (CS-NP1, CS-NP2 and CS-NP3).

3.4.5 Fourier transform infra-red spectroscopy (FT-IR) analysis of excipients and NPs

FT-IR spectrums and functional groups of poloxamer, PLGA, TA, physical mixture and PLGA NPs (NP3) are presented in Figure 3.11 and Table 3.10. The comparison of chitosan and chitosan-coated PLGA NPs spectrums is shown in Figure 3.12 and Table 3.11. Drug and excipients functional groups were also present in the formulation with peaks at similar wavenumbers, which suggests that there was no interaction between the drug and the components [304].

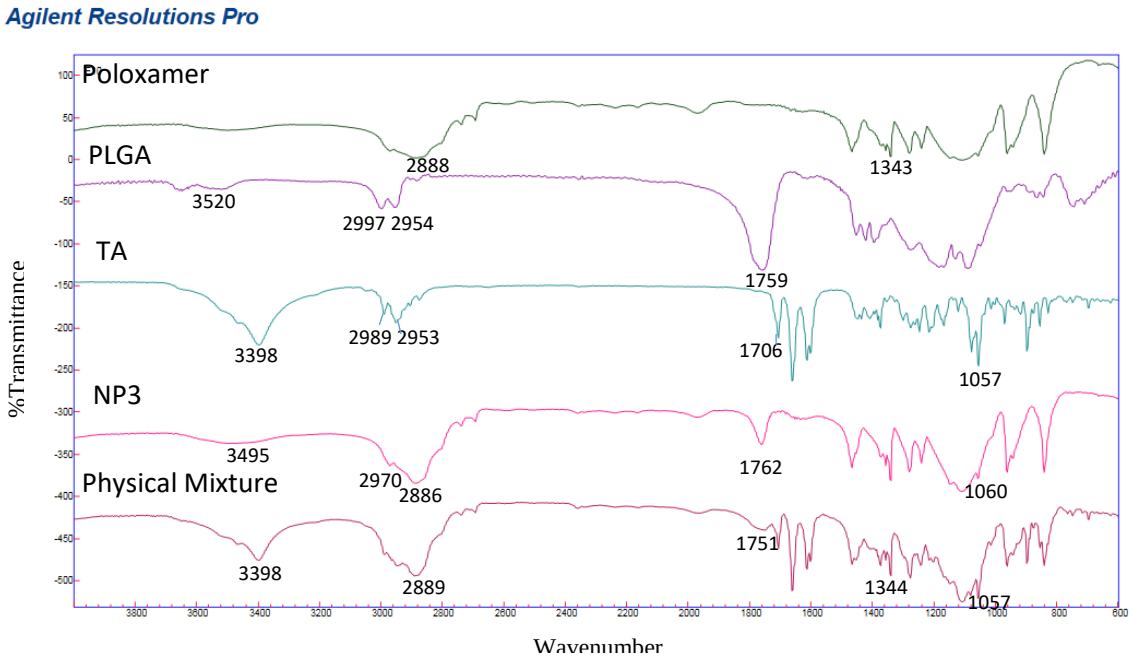

Figure 3.11: FT-IR analysis of the individual components, physical mixture and PLGA NPs (NP3).

Pure TA spectra displayed an infrared absorption band at 3398 cm^{-1} related to the hydrogen-bonded hydroxyl stretching vibration, at 1706 cm^{-1} associated with stretching vibration of the carbonyl group (at aliphatic ester bonds). Another typical absorption band of TA at 1056 cm^{-1} is due to the stretching vibration of C-F.

Table 3.10: Representation of FT-IR peaks and functional groups of the individual components and PLGA NPs (NP1).

Frequency (cm^{-1})	Functional group	Individual Components (cm^{-1})			Physical Mixture (cm^{-1})			NP3 (cm^{-1})			Ref.
		PLGA	Poloxamer	TA	PLGA	Poloxamer	TA	PLGA	Poloxamer	TA	
3510	OH	3520						3495			[413]
3398	OH			3398			3398				[414]
3000-2950	C-H	2997-2954						2970-2886			[413]
2891	C-H		2888			2889			2886		[415]
2985-2937	C-H			2989 - 2951						2970 - 2886	[414]
1705	C=O			1706						1762	[414]
1757	C=O	1759			1751			1762			[413]
1344	O-H		1343			1344					[415]
1055	C-F			1057			1057			1060	[410]

The physical mixture also showed the characteristic peaks of the TA in a similar wavelength range. In all the formulations, the blueshift of the ketonic carbonyl and C-F groups was observed at 1762 cm^{-1} and 1060 cm^{-1}, respectively.

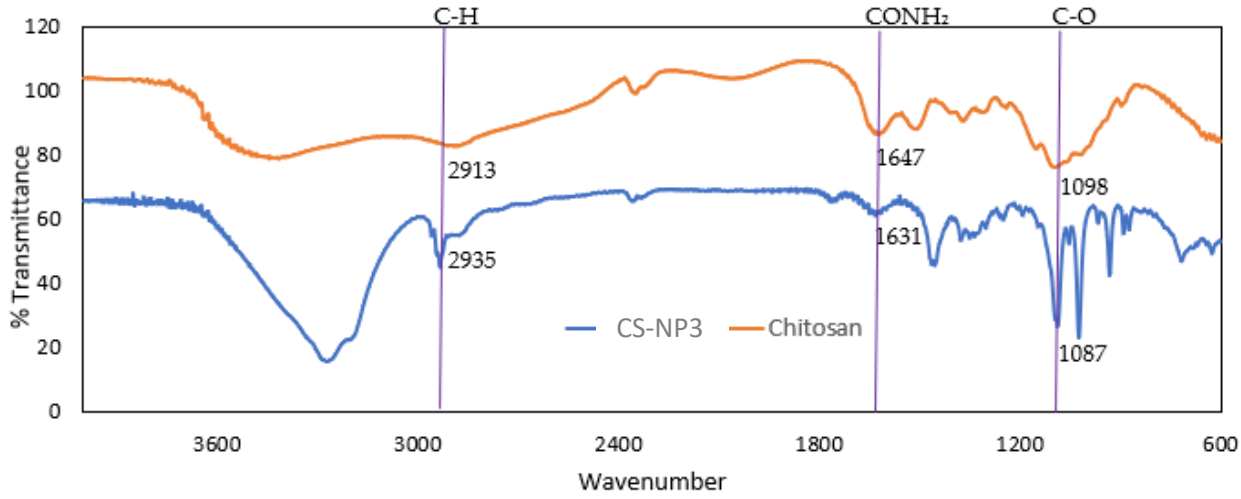

Figure 3.12: FTIR spectrums of chitosan and chitosan-coated PLGA NPs (CS-NP3).

The FT-IR spectra suggested the existence of chitosan coating on PLGA nanoparticles by the presence of characteristic functional group of chitosan ($CONH_2$) on CS-NP3 spectra with a slight shift in wavenumber, which is in agreement with previous studies [406].

Table 3.11: FTIR functional groups of chitosan and chitosan-coated PLGA NPs (CS-NP3).

Frequency (cm^{-1})	**Functional group**	**Chitosan (cm^{-1})**	**Chitosan-coated NP3 (cm^{-1})**	**Ref**
2924	C-H	2913	2934	[416]
1657	$CONH_2$	1630	1647	[417]
1070	C-O	1098	1088	[418]

The presence of chitosan functional groups on chitosan-coated PLGA NPs along with the conversion of ZP from negative to positive charge upon chitosan coating and the DSC thermogram changes of chitosan-coated NPs indicate the presence of chitosan on the surface of PLGA NPs.

3.4. *In-vitro* drug release study

The %cumulative drug release was plotted against time (h) for the *in-vitro* drug release study performed using PBS with 0.01% sodium azide and 1% tween 80 as release media as shown in

Figure 3.13). As mentioned in Section 2.3.7, to increase the solubility of hydrophobic TA and to maintain sink conditions, tween 80 was used as surfactant to increase the solubility in release medium [274].

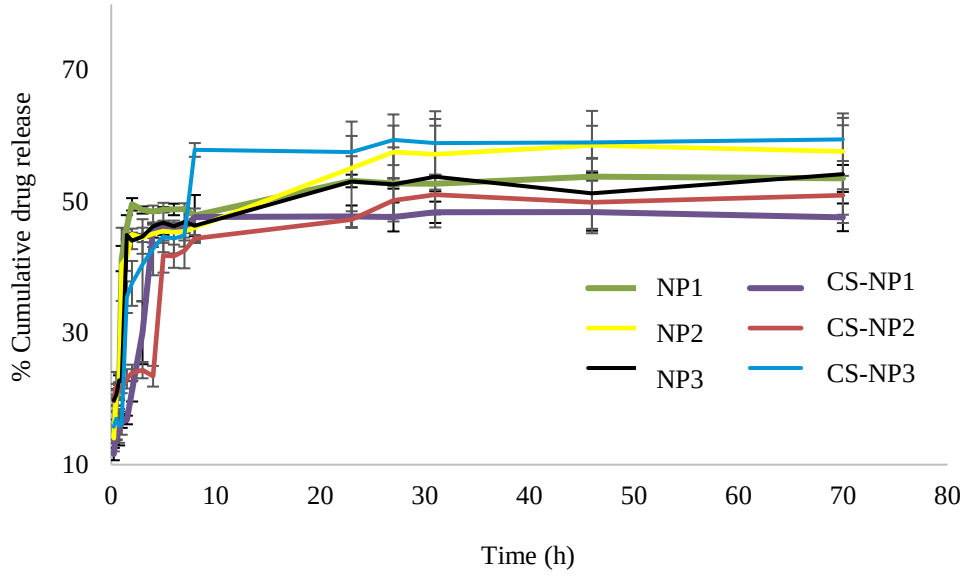

Figure 3.13: *In-vitro* drug release from NPs (NP1, NP2, NP3, CS-NP1, CS-NP2, and CS-NP3).

The drug release from the PLGA nano-formulations reached a plateau after 23 h (Figure 3.14 (a)) and the chitosan-coated nano-formulations reached a plateau at 27 h (Figure 3.14 (b)). Despite showing the controlled release at the initial stage, the non-coated NP2 formulation displayed high drug release (57.65% ± 5.77% at 70 h) similar to CS-NP3 but the CS-NP2 better-controlled release with 50.97% ± 2.95% at 70 h. Even though the release from all the three PLGA NPs was similar, chitosan-coated NP3 formulation showed more drug release compared to other formulations (59.47% ± 3.28%). This could be due to less concentration of PLGA in NP3 (3.5 mg/mL) compared to NP1 (3.7 mg/mL) and NP2 (4.5 mg/mL). With the increase in polymer concentration, the drug might have better protection leading to delay in the drug release [419]. The drug present in the nanoparticles, which was not released at the last time point from CS-NP3 was quantified and 37% ± 4.82% accounted out of 40.53% ± 3.28% of the drug remained in the NPs.

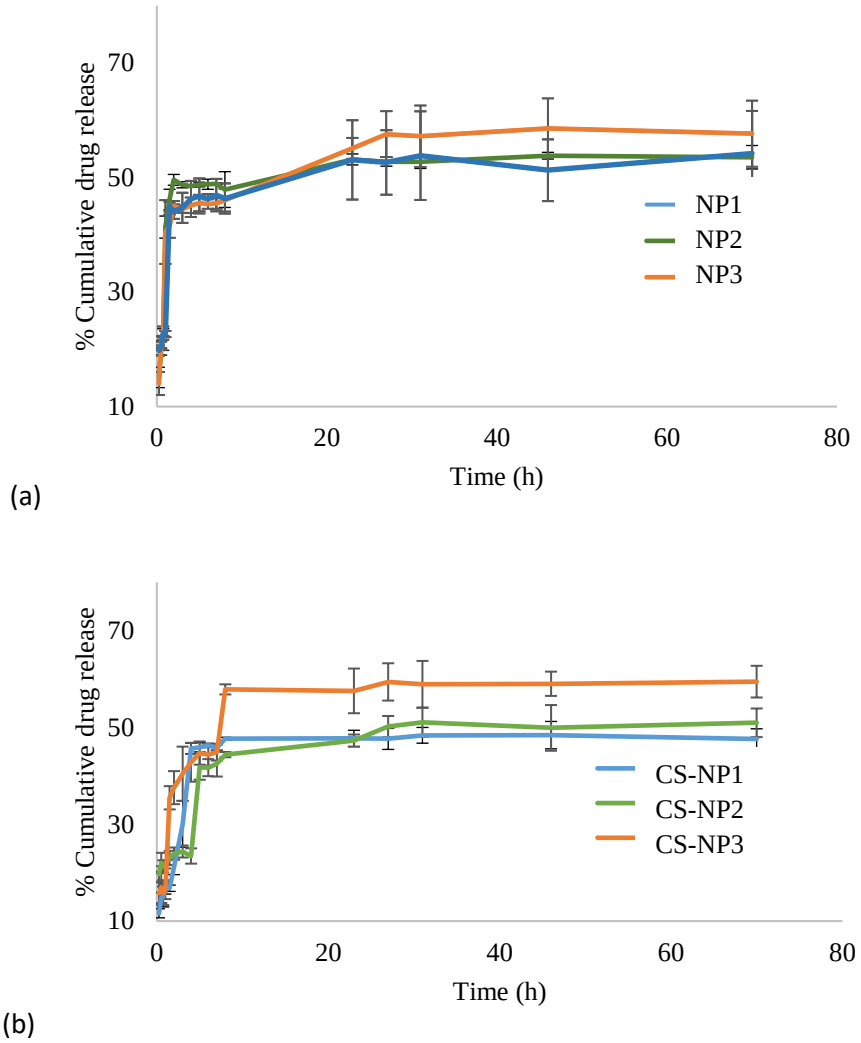

Figure 3.14: *In-vitro* drug release from (a) PLGA NPs and (b) chitosan-coated PLGA NPs.

In Chapter 2, the chitosan-coated nanoparticles prepared by thin-film hydration technique showed no effect on burst release, in contrast to that of chitosan-coated NPs fabricated using emulsion method controlled the initial burst release when compared to PLGA NPs. In the first 2 h, PLGA NPs released 44 – 40% of drug whereas chitosan-coated PLGA NPs released 21 – 37% of drug, which indicates the role of chitosan coating in controlling the initial burst release (Figure 3.15). Similar results were observed in previously published findings of NPs prepared with same materials [406,420].

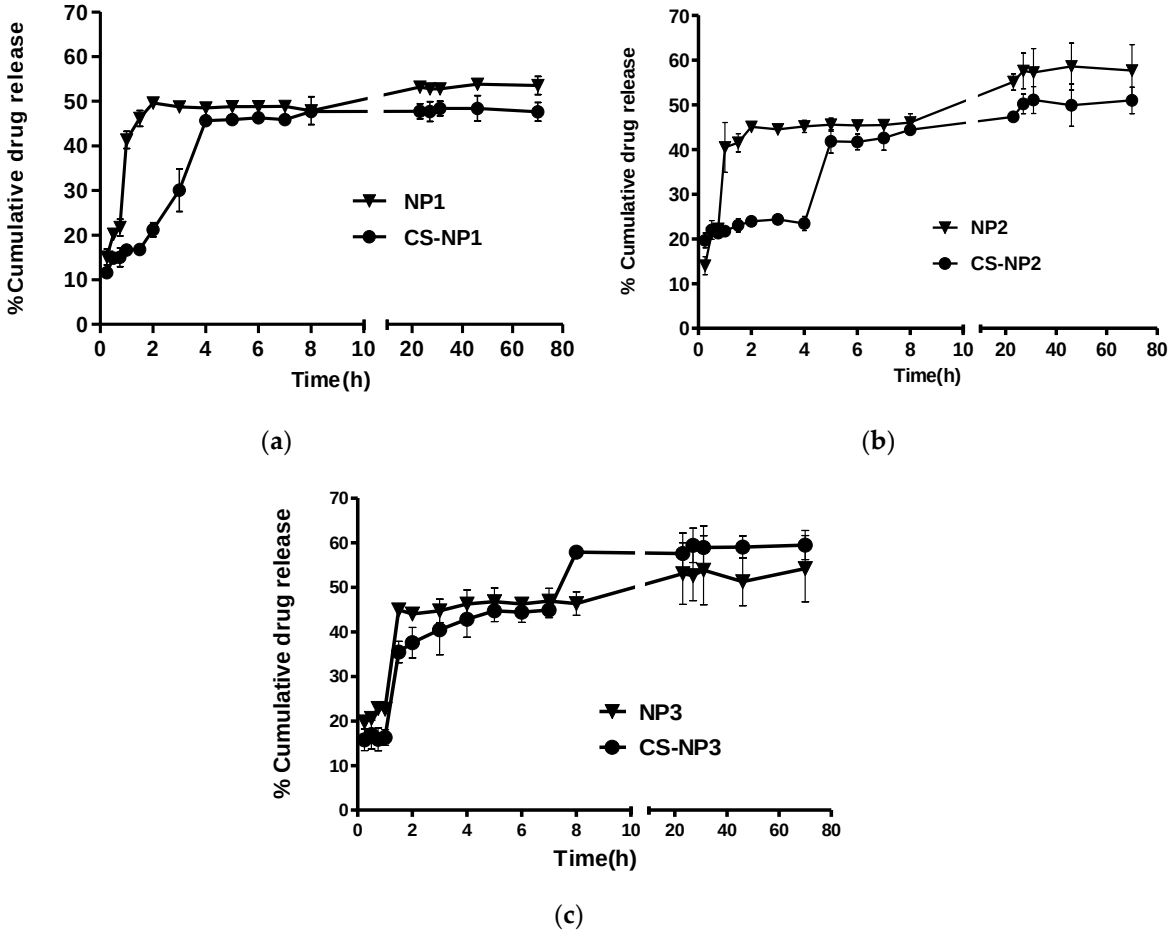

Figure 3.15: Comparison of *in-vitro* drug release of non-coated and coated NPs: (a) NP1 and CS-NP1, (b) NP2 and CS-NP2 and (c) NP3 and CS-NP3.

There was no statistical significance in drug release between before and after coating of the NP3 emulsion formulation ($p > 0.05$), whereas formulations NP1 and NP2 showed significant difference compared to CS-NP1 and CS-NP2 ($p < 0.01$). This difference is due to the significant control of initial burst release, which is mentioned previously in this section.

The curve fit of the *in-vitro* TA release was analysed with the mathematical models considering coefficient of determination (R^2) as represented in Table 3.12. Korsmeyer-Peppas is most fitting to the TA release from the NPs (R^2 between 0.621 and 0.894) when compared to other models, which suggests the sustained release of the TA. This model indicates that the release from the PLGA NPs involves multiple release mechanisms such as, diffusion, dissolution and swelling [421].

Table 3.12: In-vitro drug release mathematical model fitting concerning coefficient of determination (R^2).

Formulation Code	Coefficient of determination (R^2)				
	Zero-order	First-order	Hixson-Crowell	Higuchi	Korsmeyer-Peppas
PE 1	0.552	0.582	0.572	0.69	0.791
PE 2	0.756	0.767	0.763	0.893	0.894
E 10	0.338	0.41	0.386	0.464	0.621
CS-PE1	0.237	0.252	0.247	0.387	0.641
CS-PE2	0.503	0.541	0.528	0.676	0.845
CS-E10	0.504	0.586	0.56	0.681	0.853

All the three optimized nano-emulsions before and after chitosan coating exhibited controlled release of the drug (Figure 3.15) up to 70 h due to the degradation mechanism and controlled release properties of PLGA mentioned in Section 1.4.1.1.

3.5 Conclusion

Chitosan-coated PLGA nanoparticles were successfully optimized with a Box-Behnken response surface DOE and response optimizer. The optimized surface-modified NPs (CS-NP1, CS-NP2 and CS-NP3) were reproducible and stable with a particle size of 334 nm to 386 nm and PDI between 0.09 and 0.15, having a zeta potential between +26 and +33 mV. These NPs encapsulated 55% – 57% of TA and displayed a controlled release of the drug reaching a plateau in 27 h. This study highlighted the importance of poloxamer as a surfactant when compared to PVA in yielding smaller particles with uniform distribution. Secondly, the utilization of DOE and the use of a response optimizer added significantly in achieving the desired NPs. The prediction emulsions (CS-NP1 and CS-NP2) showed high %encapsulation efficiency and controlled release of the drug with monodispersed NPs.

Considering the characteristics of the surface-modified PLGA NPs, the emulsion method has produced NPs with low particle size and PDI values compared to the thin-film hydration technique. In the following chapters this technique will be used to encapsulate the second drug (QCN) and for the co-encapsulation of TA and QCN. Optimized NPs with the combination of drugs will be investigated on *in-vitro* ocular cell line (Human retinal epithelial cell lines) to assess the cytotoxicity. The impact of these dual drugs on the pathology of AMD will be studied by anti-inflammatory, antioxidant, and anti-angiogenic assays on cell lines.

Chapter 4: Investigation of a novel combination therapy for age-related macular degeneration

4.1 Introduction

As mentioned in the earlier chapters, age-related macular degeneration (AMD) is an accelerating blinding disease with no cure. Current available treatments can only slow down disease progression. Initial investigations led to wet AMD being considered as a vascular disease, primarily involving angiogenesis and choroidal neovascularization (CNV) [422]. However, it is now considered as a complicated multifactorial disorder with various non-vascular components [423]. Current anti-VEGF (vascular endothelial growth factor) agents control CNV which occurs in the later stages of AMD. At this stage, branching and development of new blood vessels evolve from the choroid, which later reach the RPE and damage central vision. Marketed anti-VEGF agents are brolucizumab, aflibercept, ranibizumab, pegaptanib sodium and faricimab-svoa. While current treatments are effective, they are associated with serious side effects, such as retinal detachment [424], retinal haemorrhage [9], endophthalmitis [10], an increase in intraocular pressure [11] and, as stated above, do not cure the condition. With increasing evidence supporting the complexity of AMD pathology, the investigation of new therapeutic targets and combination therapies that can target multiple pathologies of the disease has received increased attention (Figure 4.1).

A synergistic effect is observed when two or more drugs interact and produce an enhanced effect when compared to the sum of their individual effects [425]. A synergetic interaction allows for a lower dose of individual drugs, which may reduce adverse effects. Combination therapies such as anti-VEGF agents together with photodynamic therapy [426], and anti-VEGF agents along with corticosteroids [427] have been used previously and are known to be effective. As mentioned in earlier chapters, anti-VEGF injections have serious side effects, and monoclonal antibodies (current anti-VEGF agents) are expensive.

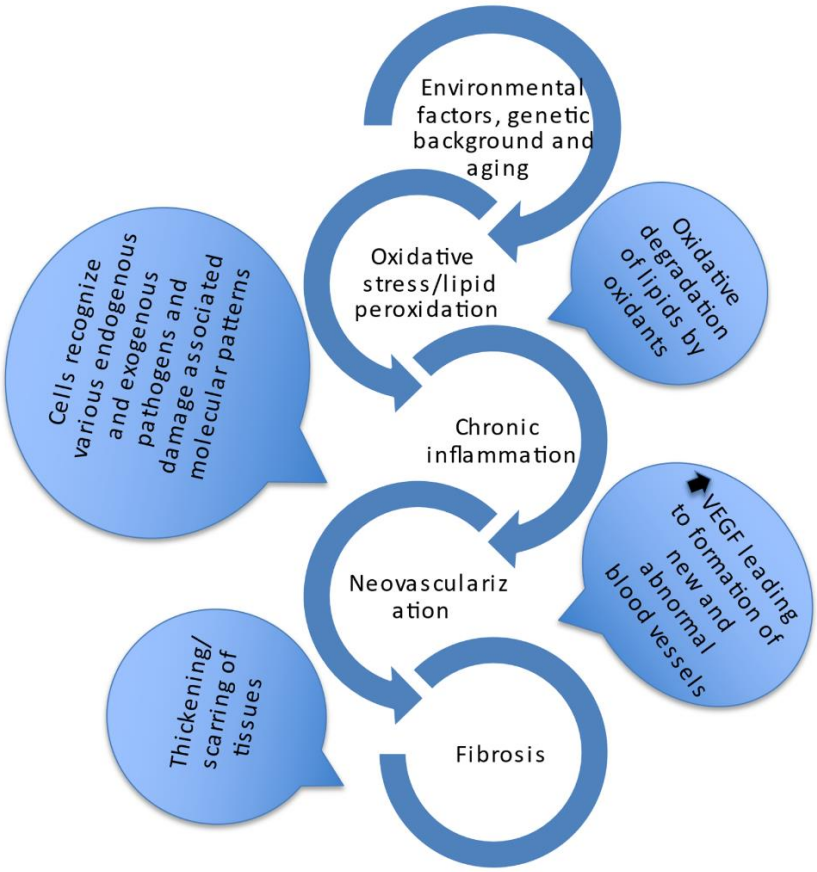

Figure 4.1: Schematic representation of the pathological conditions of wet age-related macular degeneration (WAMD) [428–430]**.**

There is an unmet need to develop non-invasive and effective treatment options for AMD, which can be self-administered by patients. In the current study, a novel combination of a corticosteroid (triamcinolone acetonide) and flavonoid (Quercetin) was investigated on human retinal epithelial cell lines to determine the potential pharmacological effect on AMD. Triamcinolone acetonide (TA) is one of the foremost compounds evaluated for the treatment for multiple back of the eye diseases such as, macular edema, uveitis, AMD, and vitreoretinopathy. The initial use of intravitreal TA to treat exudative AMD resulted in significant reduction of CNV but in long-term use, TA as a monotherapy had no effect on visual acuity loss (in spite of significant anti-angiogenic effects beyond 3 months of treatment). Hence a combination of TA and photodynamic therapy was performed, which acted synergistically and reduced the number of re-treatments [431]. In the present study, TA was investigated in combination with quercetin (QCN), considering its reported anti-oxidant and anti-VEGF properties [80,432]. Some of the crucial pathological conditions of AMD highlighted in Figure 1 were stimulated on human retinal cells (oxidative stress, inflammation, and VEGF secretion)

and exposed to different concentrations of TA and QCN both individually and in combination, in an attempt to investigate their potential for the treatment of AMD. Initially, non-toxic concentrations of the individual drugs and in combination were identified using the *in-vitro* cytotoxicity assay on ARPE-19. Following the cytotoxicity study ELISA (enzyme-linked immunosorbent assay) was performed to investigate the effect of treatments on the secretion of chosen inflammatory and angiogenic cytokines. The effect of drugs on oxidative stress and cell migration was observed in *in-vitro* conditions.

4.2 Materials and equipment

Adult retinal pigment epithelium-19 (CRL-2302™) and Fetal Bovine Serum (ATCC-30-2025, EU Approved, South American Origin) were purchased from LGC standards Ltd, UK. DMEM/F-12 cell culture media (Gibco™ 31330038), Trypsin (Gibco™ 25300054), Penicillin-Streptomycin (Gibco™ 15070063) and p-nitrophenyl phosphate (PNPP) were procured from Fisher Scientific, Ireland. Dichlorofluorescin diacetate (DCFH-DA) and 2,2-diphenyl-1-picryl-hydrazyl-hydrate (DPPH) were purchased from Sigma Aldrich, Ireland. IL-6, IL-8, MCP-1, and VEGF-C ELISA kits were purchased from Assay genie, Ireland. 96, 24 and 6 well plates and serological pipettes were procured from Greiner bio-one, Cruinn diagnostics, Ireland.

The following equipment was used throughout the experimental work: Refrigerated centrifuge (Sigma 3-18KS, Focus scientific, Ireland), plate reader (HTS Plate Reader-MSD Model 1250 Sector Imager, US), inCu safe cell culture incubator (Davidson and Hardy Ltd, Ireland), - 80 ℃ chest freezer (Medical supply company, Ltd, Ireland), flow cytometer (Cytomics FC500, Beckman Coulter, United States), Memmert – Water Bath (Mason technology, Ireland), Airstream® Class II Biological Safety Cabinet (ESCO, Mason technology, Ireland), and Classic Vortex Mixer (Fisherbrand™, Ireland).

4.3 Methods

4.3.1 Cell culture

ARPE-19 (adult retinal pigment epithelium-19) cell line was cultured using cell culture media containing a 1:1 mixture of DMEM and F-12 nutrient mixture. The media was supplemented with 10% FBS and 1% penicillin-streptomycin antibiotic mixture. During the culture, cells were maintained at 37 °C with 5% CO_2 in a humidified incubator and sub-cultured with trypsin upon confluency.

4.3.2 Cytotoxicity evaluation of individual drugs and drug combinations

Cytotoxicity evaluation of the drugs, both individually and in combination, was performed using the acid phosphatase assay (APA) [433]. Initial stock solutions of the drugs were prepared in DMSO, and the working solutions were prepared and diluted using cell culture media. The cytotoxicity assay was performed on TA and QCN from 5 to 250 µM and 1 to 250 µM, respectively. After investigating individual drugs, drug combinations were tested. Each concentration of TA at 10, 25, 50, 75 and 100 µM was tested in combination with all the concentrations of QCN (5, 10, 15 and 20 µM).

Initially ARPE-19 cells were seeded onto a 96-well plate at a seeding density of 5000 cells/well containing 100 µL of cell culture media and cultured for 24 h. After 24 h, treatments were added to the wells and incubated for the period of the study (24 h and 48 h). After the treatment period, media was removed, and cells were washed twice with PBS. Upon washing, 100 µL of 10 mM PNPP substrate dissolved in 0.1 M sodium acetate buffer was added to the wells and incubated for 2 h. Finally, 50 µL of stop solution (1 M sodium hydroxide) was added and the plate was analysed in the plate reader at 405 nm.

4.3.3 Anti-inflammatory and anti-VEGF activities on ARPE-19 using ELISA

The human IL-6, IL-8, MCP-1, and VEGF-C ELISA kits were used according to the manufacturer's protocol to investigate the cytokine secretions in the cell supernatants. Cells were seeded onto a 24-well plate at a seeding density of 3×10^4 cells/well with 500 µL of cell culture media and cultured for 24 h. Cells were kept overnight in low serum media (with 1% FBS) to synchronise their growth phase before stimulating inflammation. After 24 h cells were stimulated with 10 µg/mL LPS to induce inflammation for a duration of 24 h. Upon stimulation, cells were exposed to various treatments of drugs alone and in combination for 24 h. After the treatment duration media conditioned by treated cells were collected and analysed for the cytokines and VEGF-C secretions using the ELISA kits. ELISA was performed according to the manufacturer's protocol.

4.3.4 Scratch assay

For the scratch, or wound healing, assay cells were seeded onto six-well plates with a seeding density of 25×10^4 cells/well. Upon reaching 80-90% confluency, a sterile 200 µL pipette tip was used to scrape the confluent monolayer of cells in a horizontal line [434]. After creating the scratch, cell debris was washed with PBS and the cell culture media containing treatments

was added to each well. The scratch was photographed using an Olympus EP50 microscope at 10 X magnification at 0, 6, 9, 24, 27 and 30 h. “Image J” software was used to analyse the width of the scratch.

4.3.5 Antioxidant activity

4.3.5.1 DPPH assay

The DPPH assay was performed in a 96-well plate where 20 µL of methanolic DPPH solution was added to 180 µL of methanolic solutions of treatments [435]. Based on the outcome from anti-inflammatory studies, the higher concentrations of TA and QCN, both individually and in combination were investigated for antioxidant activity (TA 75, 100 µM and QCN 15, 20 µM). This reaction mixture was incubated for 30 min in darkness at room temperature and the absorbance was measured at 517 nm using a microplate reader.

4.3.5.2 DCFH-DA assay

ARPE-19 cells were seeded onto 6-well plates at a seeding density of 25×10^4 cells/well and incubated for 24 h. At the 24 h time point cells were stimulated to induce oxidative stress. The stimulants, LPS and hydrogen peroxide (H_2O_2) were tested at concentrations 10, 20, 40 µg/mL and 100, 200, 300 µM, respectively. Following stimulation, cells were exposed to similar concentrations of TA and QCN as used for the DPPH assay (both individually and in combination) for 24 h and after the treatment period cells were incubated with 20 µM DCFH-DA dye [436]. Upon incubation with dye, cells were detached using trypsin and resuspended in PBS for analysis using flow cytometry.

4.3.6 Statistics

Statistical differences between the treatments were assessed using student’s T test. The results were considered statistically significant if the P value was less than 0.05. All statistical analysis were performed using both excel and GraphPad® software .

4.4 Results and discussion

4.4.1 Drug cytotoxicity study

Cytotoxicity studies are the important first step to assess the safety of drug molecules during the developmental stage before testing them on animals. Before investigating the combination of drugs on ARPE-19 cells, individual drugs were studied. The concentrations were selected from previously published studies (with higher concentrations included to establish toxic and

non-toxic concentrations) [376,437–440]. Both TA and QCN were evaluated between 10 and 250 µM concentrations for 24 and 48 h periods (Figure 4.2 (a) and (b)).

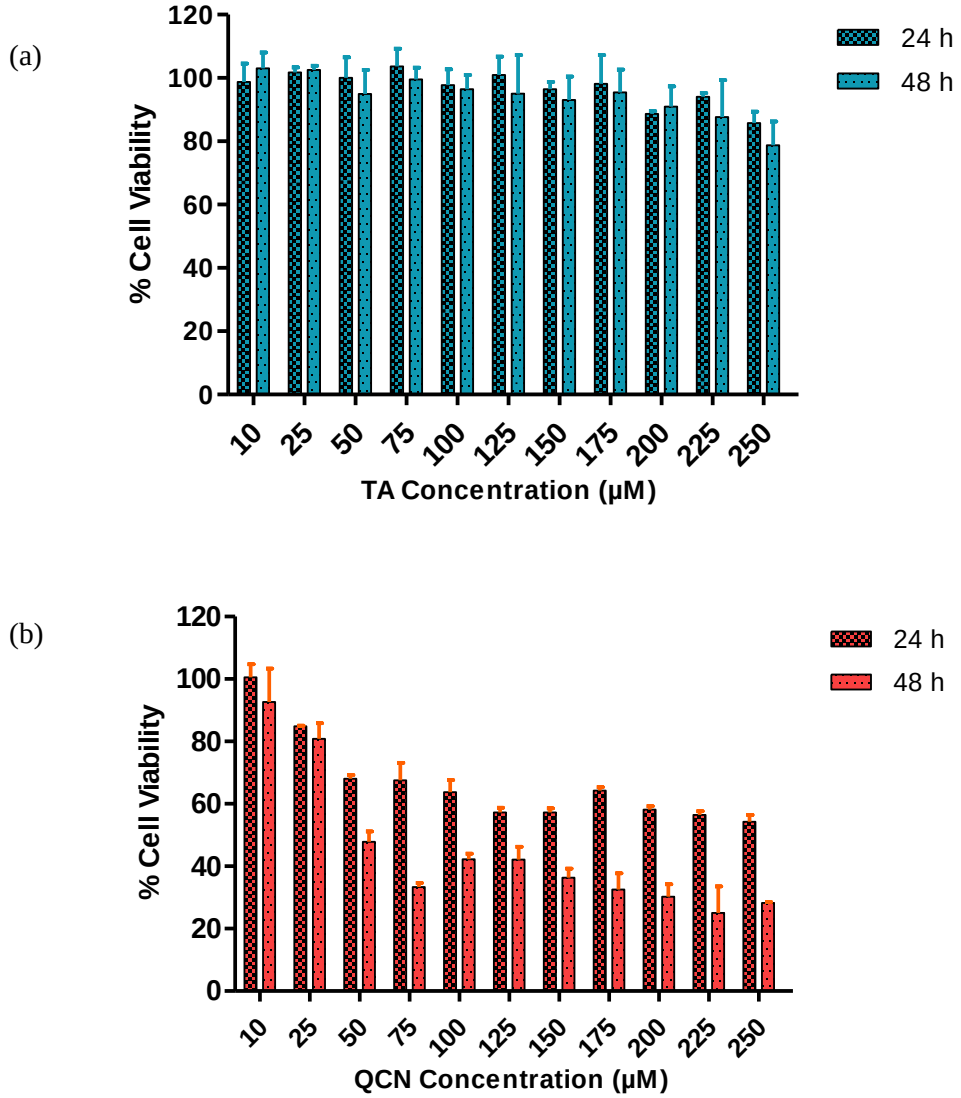

Figure 4.2: % Cell viability of (a) TA and (b) QCN for a range of concentrations between 10 and 250 µM. Data points represent the average ± SD of n = 3 biological replicates for (a) and technical replicates for (b).

The viability of cells was not affected with exposure to TA from 10 to 250 µM (cell viability >80%) and no changes in cell morphology were observed (Figure 4.2a). Whereas QCN exhibited a decrease in cell viability with increase in concentration, as depicted in Figure 2b. The QCN concentration up to 25 µM displayed more than 80% cell viability but the higher concentrations exhibited a toxic effect on cells. Given these results, a further study focused on lower concentrations of QCN, 1 - 100 µM.

The viability of the ARPE-19 cells was not significantly changed (P >0.05) by the treatment with QCN from 1 to 30 µM (Figure 4.3). Nonetheless, QCN concentrations from 40 to 100 µM significantly decreased the viability of cells with P value <0.05. These results relate to a previous study by Wang *et al*., they evaluated the effect of QCN on high glucose-induced injury in ARPE-19, the viability of the cells was decreased with QCN concentration greater than 30 µM [441]. Similar results were noticed by Cheng et al., who investigated the effect of QCN on inflammatory cytokines and chemokines in ARPE-19 cells [439]. According to the above-mentioned literature, QCN concentrations up to 20 µM proved to be non-toxic with an anti-inflammatory effect in *in-vitro* conditions. Previous investigations discovered that flavonoids such as QCN, luteolin, apigenin, etc., exhibited beneficial effects at low concentrations but are toxic at higher concentrations on human cell lines with the structure-cytotoxicity relationship still unclear [442].

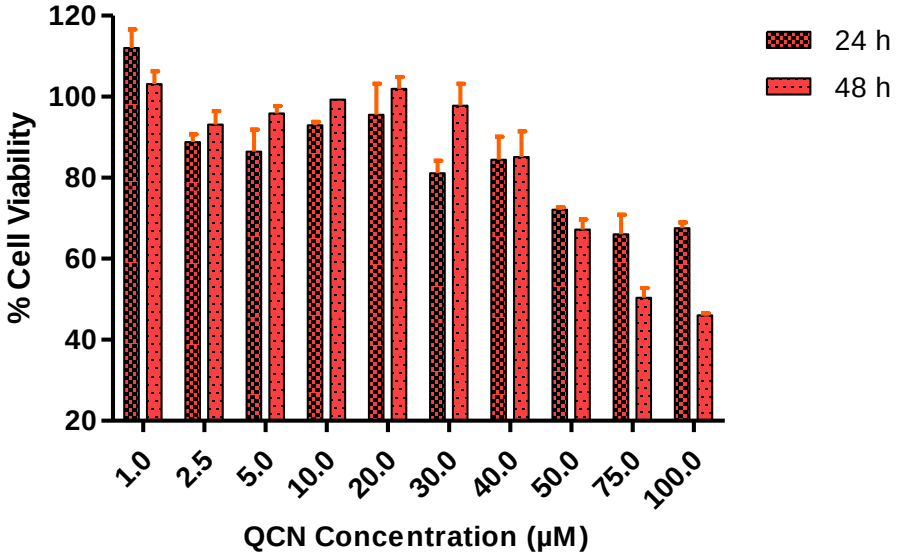

Figure 4.3: % Cell viability of QCN for a range of concentrations between 1 and 100 µM, data points represent the average ± SD of n = 3 biological replicates.

The QCN concentration from 1 to 20 µM demonstrated more than 90% cell viability (Figure 4.3) and proved to be safe on human retinal cells. Based on these results and effective concentrations of the drugs on the pathology of AMD in previous studies [438,439]; TA 10, 25, 50, 75 and 100 µM and QCN from 5, 10, 15 and 20 µM were chosen to be studied in combination.

Drug combinations, as listed in Section 4.3.2. showed no synergetic toxicity on ARPE-19 cells or changes to cell morphology (Figure 4.4). All the chosen combination concentrations demonstrated more than 85% cell viability, similar to the individual drugs.

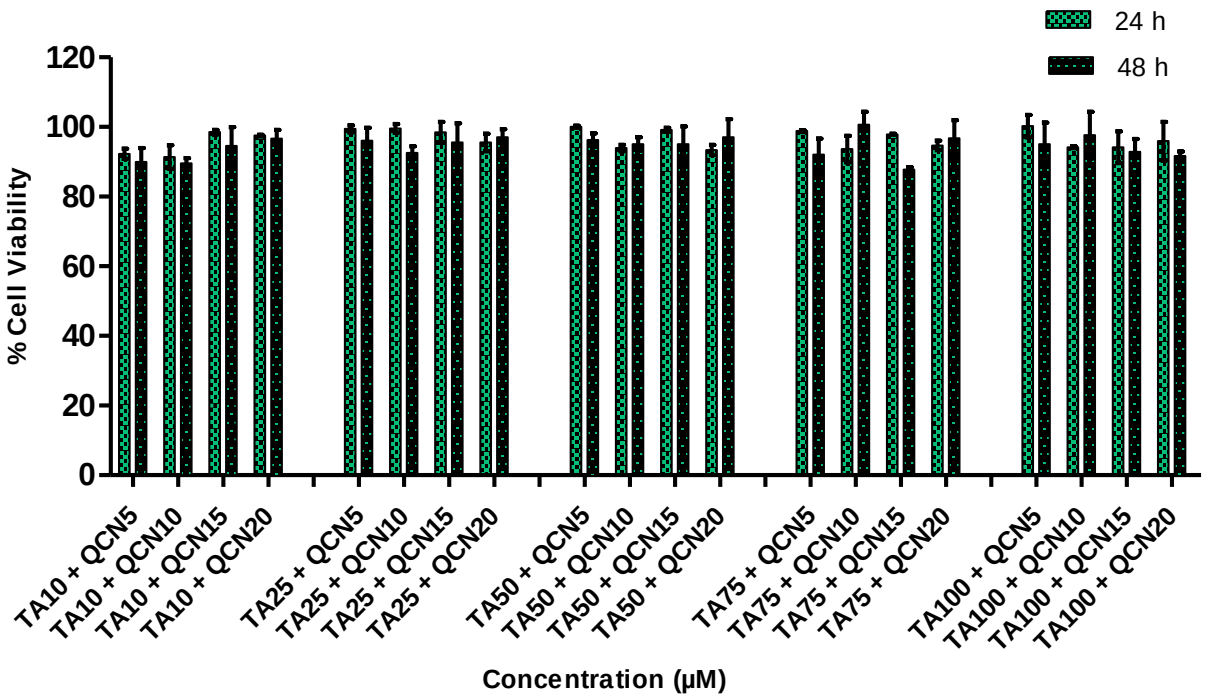

Figure 4.4: % Cell viability of a combination of drugs (TA and QCN: TA+QCN) on ARPE-19 cells. Data points represent the average ± SD of n = 3 biological replicates.

The cytotoxicity assay estimates the loss of cellular and intercellular functions or structure, which includes cytotoxicity effects. Hence, this provided insight into any potential tissue/cell injury and irritation during application. This *in-vitro* cytotoxicity study suggested that the individual drugs and in combination were safe on human retinal cell lines.

4.4.2 Anti-inflammatory activity studies using ARPE-19 cells

Multiple studies on biological samples from AMD patients and studies which assessed physiological conditions during the disease state supports the conclusion that AMD is a multifactorial disorder, which involves RPE dysfunction and damage to photoreceptor cells (mainly due to inflammatory conditions and oxidative stress) [443–445]. RPE play a crucial role in the formation of the blood-retinal barrier (BRB), establishment of ocular immune privilege and in secretion of immunomodulatory factors to monitor immunogenic inflammation. In the case of AMD, damage to RPE effects ocular immune tolerance distorting BRB, downregulating the immune and anti-inflammatory proteins, resulting in attack by T cells on autoantigens [63,446]. This process leads to stimulation of inflammatory mediators and

pathways resulting in the production of cytokines and chemokines, such as IL-4, 5, 6, 8, 10, 13, 17, TGF-beta, IFN-Y, MCP-1, and VEGF. Various inflammatory cytokines were reportedly raised in the serum, fluids, systematically, or in the ocular tissues of AMD patients. Investigations of blood samples of the AMD patients showed elevated levels of monocyte chemotactic protein-1 (MCP-1), IL-6 and IL-8 and that monocytes may lead to the progression of AMD [447,448]. Considering the previous findings and their role in AMD inflammation, IL-6, IL-8, and MCP-1 were prioritized for the current study. Suppression or inhibition of these cytokines and mediators is the key indicator for study of the anti-inflammatory properties of the chosen drug or treatment [449].

To induce inflammation, two stimulants were screened; lipopolysaccharide (LPS) and hydrogen peroxide (H_2O_2), which had worked effectively in previous studies. LPS is a molecule abundantly available on cell membranes of gram-negative bacteria that can cause inflammatory events by stimulating the release of several cytokines in a vast number of cell types. LPS binds to the CD14 receptor, which exists as membrane protein on ARPE-19 cells leading to the activation of Toll-like-receptor (TLRs) pathways resulting in secretion of inflammatory cytokines [450,451]. Elevated levels of intracellular ROS were observed in the cells exposed to H_2O_2 leading to oxidative stress. This reaction leads to the disruption of cellular balance resulting in chronic inflammation [452,453].

To investigate the anti-inflammatory effect of both individual drugs and drugs in combination on ARPE-19 cells, ELISAs were used to measure the inflammatory cytokines. Before exposing the cells to stimulants, a cytotoxicity study was carried out to identify any toxic effects of the stimulants on the cells. Based on the previous literature LPS from 0.5 to 100 µg/mL and H_2O_2 between 10 and 300 µM were tested (Figure 4.5 (a) and (b)).

(a)

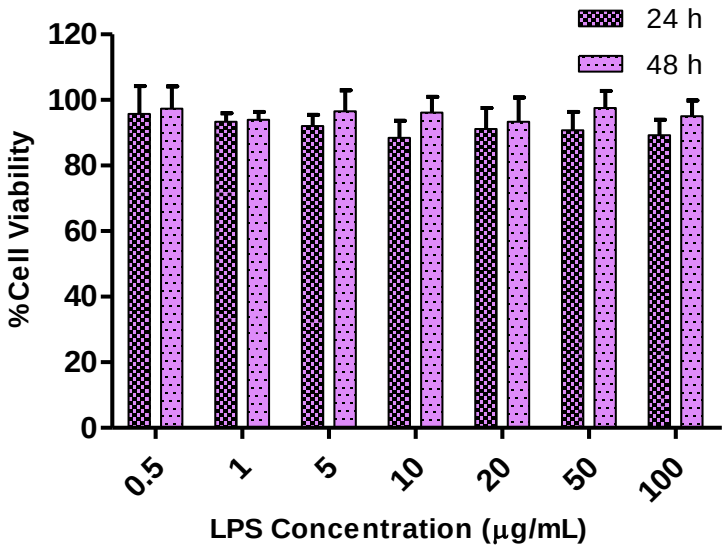

(b)

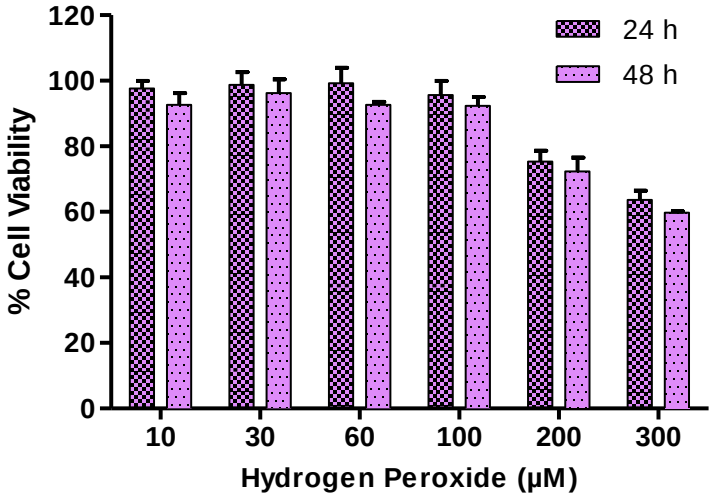

Figure 4.5: Assessment of cytotoxicity of (a) LPS and (b) hydrogen peroxide on ARPE-19 cells up to 48 h, n=3 ± SD.

Considering the current cytotoxicity study and the concentration used in literature [454,455], LPS between 0.5 and 50 µg/mL and H_2O_2 from 10 to 100 µM were chosen to induce inflammation (Figure 4.6). IL-6 and IL-8 inflammatory cytokines secreted by ARPE-19 were analysed by ELISA in order to select the stimulant and the concentration to be used for further studies to stimulate inflammation.

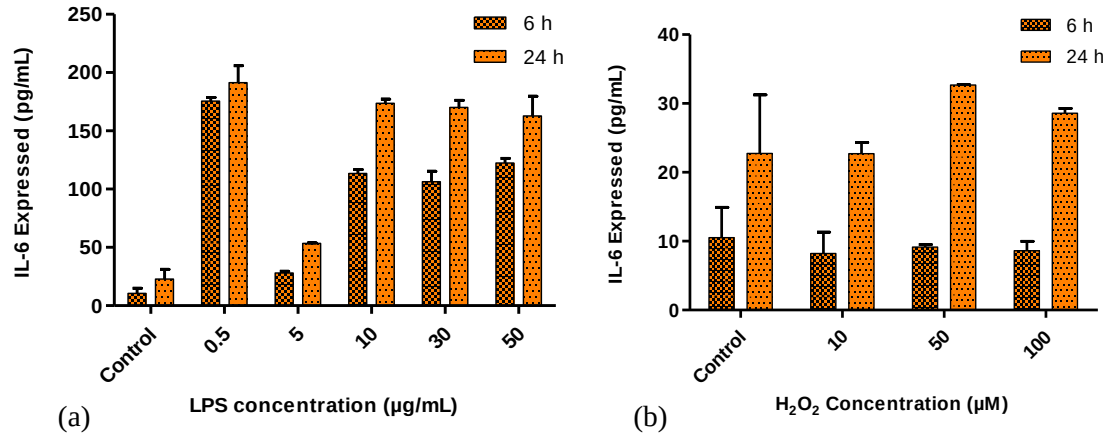

Figure 4.6: Secretion of IL-6 by ARPE-19 on stimulation with different concentrations of (a) LPS and (b) hydrogen peroxide, n=3 ± SD.

The IL-6 cytokine consistently increased with LPS stimulation from 10 to 50 µg/mL except for 0.5 µg/mL, the reason for increased secretion at this concentration needs to be further investigated. However, in the case of H_2O_2 the secretion of IL-6 at 6 and 24 h was similar to control cells. Gunawardena *et al*., claimed that H_2O_2 acts as an anti-inflammatory agent by acting as a messenger that can travel through extracellular space and then diffuse into adjacent cells [456]. In their study, the authors reported the conversion of H202 into water and oxygen in the extracellular space. Given the results observed in the current study, it is possible that H_2O_2 did not enter the next cell as a stimulant. Hence there was no significant increase in the secretion of IL-6 cytokine compared to control unstimulated cells (Figure 4.6 (b)). Therefore, for the next screening study on IL-8 ELISA, LPS alone was investigated (Figure 4.7).

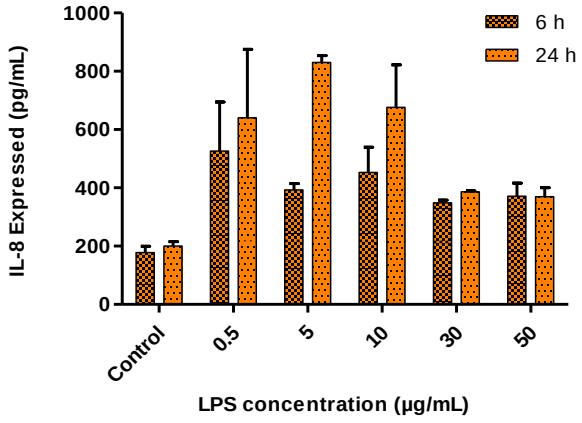

Figure 4.7: Levels of IL-8 expressed by ARPE-19 upon stimulation with LPS, n=2 ± SD.

As expected, LPS endotoxin induced inflammation on ARPE-19 led to the secretion of IL-6 and IL-8 cytokines. When compared to the control unstimulated cells, cells stimulated with LPS showed an increase in the secretion of cytokines with these results being in accordance with previous inflammatory studies on ARPE-19 [457]. The 10 µg/mL concentration of LPS consistently increased the secretion of IL-6 and IL-8 over 24 h period hence this condition was used for further studies. Similar results were observed by Paeng *et al.,* who investigated the activity of YCG063 (inhibitor of ROS) on inflammation in ARPE-19 [457]. They used LPS to induce the inflammation where LPS at 10 µg/mL consistently secreted IL-6, IL-8, MCP-1, and ICAM-1 cytokines for 24 h stimulation.

After stimulating the cells with the chosen concentration of LPS for 24 h (except for the control unstimulated cells), cells were exposed to different concentrations of TA and QCN individually and in combination to investigate any anti-inflammatory effect (Figure 4.8).

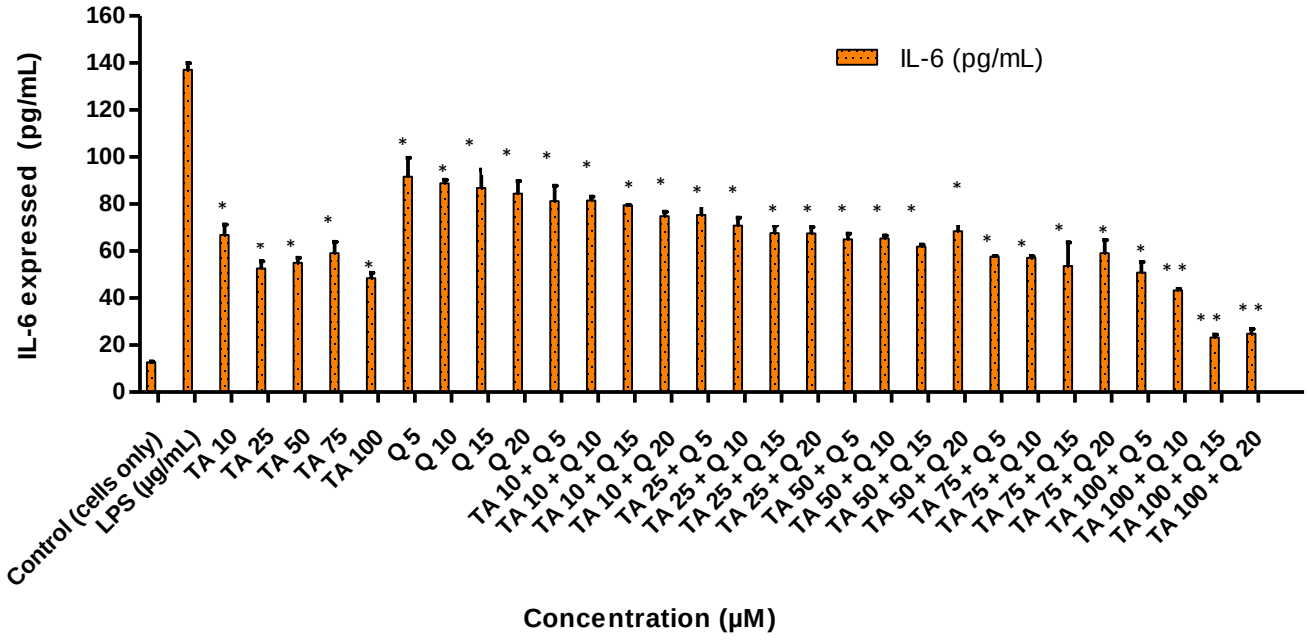

Figure 4.8: Investigating the anti-inflammatory effect of TA and QCN individually and in combination using IL-6 ELISA: ARPE-19 cells were stimulated using 10 µg/mL LPS for 24 h followed by 24 h treatments. ** P <0.01 (highly significant) * P <0.05 (significant), n=2 ± SD.

When compared to LPS stimulated cells, which expresses the maximum amount of IL-6, all the treatments exhibited a significant anti-inflammatory effect by lowering the secretion of cytokine in the ELISA study (P <0.05). This supports the conclusion that corticosteroids such

as TA show an anti-inflammatory effect by multiple signal transduction pathways [458,459]. In the current study TA consistently lowered the secretion of IL-6 and showed maximum inhibition at 100 μM. In accordance with previous studies on ARPE-19, QCN decreased the secretion of IL-6 with the maximum effect observed at 20 μM [376]. Cheng *et al.* also reported that QCN at 20 μM showed anti-inflammatory activity on ARPE-19 by lowering the secretion of inflammatory cytokines (IL-6, IL-8, MCP-1, and ICAM-1) [439]. They found the lowering of mRNA expression of these cytokines through reverse transcription-quantitative polymerase chain reaction (RT-qPCR) for quercetin treated cells. From the western blot studies, QCN was found to regulate the mitogen-activated protein kinase (MAPK) and nuclear factor kappa B (NF-kB) inflammatory signalling pathways. QCN has the potential to lower the inflammatory responses in retinal pigment epithelial cells and can be considered as a therapeutic agent for inflammation along with its antioxidant properties.

As mentioned previously, there is no treatment for multifactorial AMD and monotherapy is not completely effective in treating the disease. In the current study, the efficacy of a novel combination of corticosteroid and flavonoid (TA + QCN) was examined. In accordance with this, different concentrations of TA + QCN were tested for their anti-inflammatory effect. When compared to individual drugs, TA and QCN together displayed a synergetic decrease of IL-6 secretion at higher concentrations (TA 100 + QCN 15 μM and TA 100 + 20 μM) with P value <0.05.

Following a similar procedure as the IL-6 ELISA study, IL-8 secretion was studied with the individual drugs and in combination. All the treatments significantly reduced IL-8 cytokine secretion when compared to LPS stimulated cells (Figure 4.9). Whereas the higher concentrations of TA in combination with QCN (TA50 + Q20, TA75 + Q5, 10, 15, 20 and TA100 + Q5, 10, 15, 20) showed the higher anti-inflammatory effect compared to other treatments ($P < 0.001$).

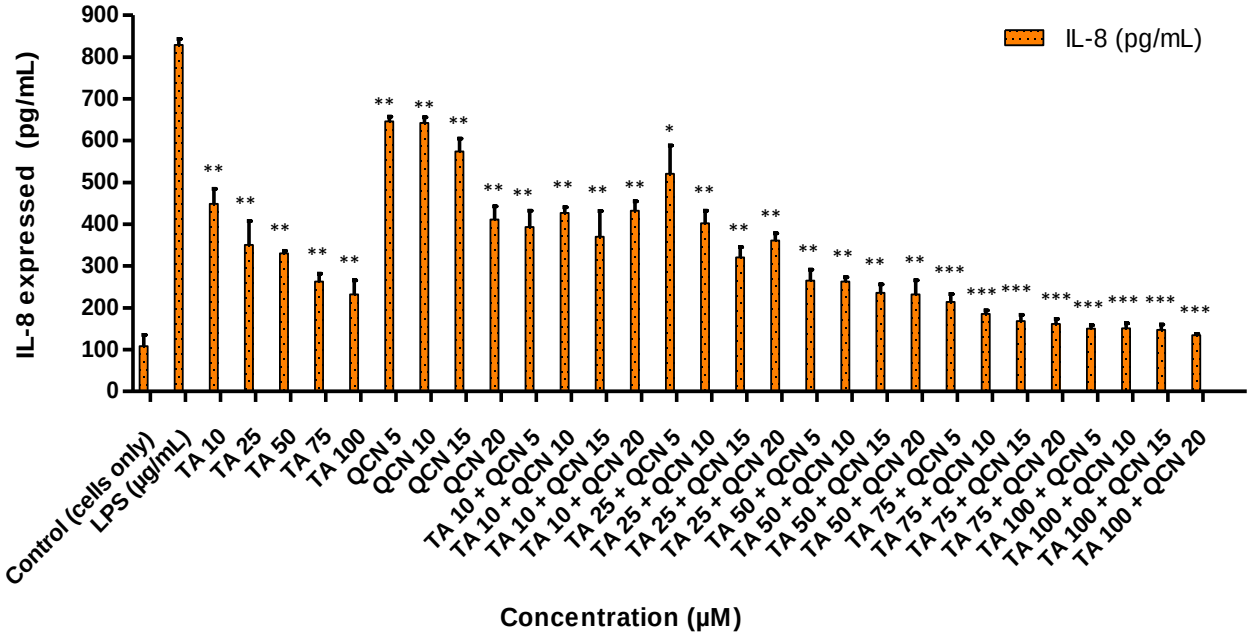

Figure 4.9: Investigating the anti-inflammatory effect of TA and QCN on their own and in combination using IL-8 ELISA: ARPE-19 cells were stimulated using 10 µg/mL LPS for 24 h followed by 24 h treatments. *** P <0.001 (very highly significant) ** P <0.01 (highly significant) * P <0.05 (significant), n=2 ± SD.

Similar to the IL-6 cytokine study, a synergistic effect was observed in some combination concentrations when compared to individual drugs. TA 50 µM and 75 µM in combination with QCN 10, 15, 20 µM and TA 100 µM + Q 5 µM significantly decreased IL-8 secretion and demonstrated an anti-inflammatory effect (P <0.05). The cells treated with individual drugs secreted IL-8 between 232 and 646 pg/mL, whereas the cells treated with combination drugs secreted between 135 and 521 pg/mL (quantified using ELISA).

Following on from the IL-6 and IL-8 cytokines study, MCP-1 was investigated following a similar procedure as a quantitative signal of inflammation (Section 4.3.3). The secretion of MCP-1 cytokine was lowered for all the treatments with the exception of QCN 5 µM, as seen in Figure 4.10, indicating anti-inflammatory activity. MCP-1 belongs to the chemokine family and acts as a proinflammatory protein which can activate T lymphocytes and monocytes and is reported to be an important indicator of inflammation [460].

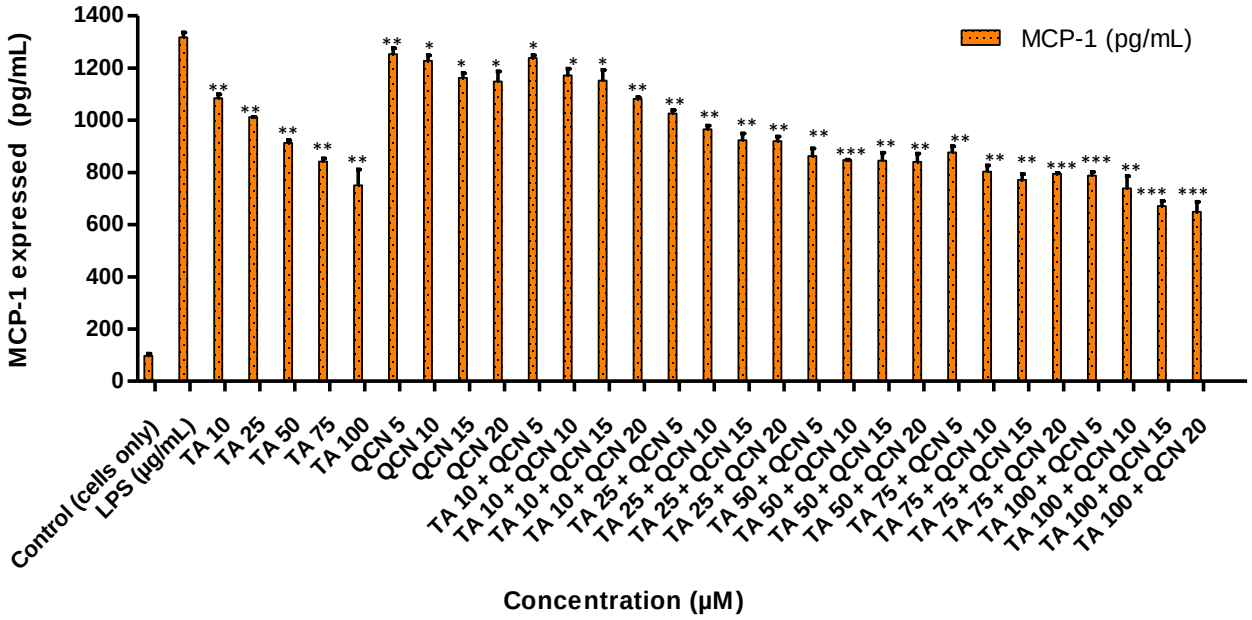

Figure 4.10: Investigating the anti-inflammatory effect of TA and QCN on their own and in combination using MCP-1 ELISA: ARPE-19 cells were stimulated using 10 µg/mL LPS for 24 h followed by 24 h treatments. *** P <0.001 (very highly significant) ** P <0.01 (highly significant) * P <0.05 (significant), n=2 ± SD.

Dose-dependent decrease of MCP-1 secretion was observed with increase in TA concentration from 10 to 100 µM. The cells treated with higher concentrations of TA 50, 75, and 100 µM secreted MCP-1 between 751 ± 61 to 913 ± 10 pg/mL and in combination with QCN 15 and 20 µM the secretion was further inhibited with a range of 650 ± 38 and 845 ± 30 pg/mL (quantified using MCP-1 ELIS). As mentioned previously, multiple studies demonstrated that QCN acts as an anti-inflammatory agent by regulating the MAPK pathway in different kinds of cells under various stimulants, whereas TA acts on key inflammatory transcription factors such as NF-κB (Nuclear factor kappa-light-chain-enhancer of activated B cells) [461–465]. As the two therapeutics have different major targets to combat inflammation, the combination therapy had effectively decreased the chosen cytokines secretion in the current study.

4.4.3 Anti-VEGF activity

Neovascularization plays a major role in the progression of AMD hence anti-angiogenic therapies are useful [466]. VEGF is identified to be the major factor in promoting vascular permeability and angiogenesis. This VEGF family includes: VEGF-A, VEGF-B, VEGF-C, VEGF-D, VEGF-E and placenta growth factor (PIGF) [467]. VEGF is secreted in the ocular environment by RPE, endothelial cells and photoreceptors. Elevated levels of VEGF in the vitreous were discovered in AMD patients with neovascularization [468]. This increase of

VEGF levels will lead to damage of the blood retinal barrier, branching of blood vessels and may also stimulate inflammation by induction of inflammatory mediators like intercellular adhesion molecule-1 [469]. Due to these factors VEGF is the target for current treatments and considered as a pharmaceutical target for identifying potential treatment for AMD [470].

Considering the findings from Section 4.4.2 (anti-inflammatory studies), the drug combination concentrations were filtered down and only higher concentrations of TA (75 and 100 µM) were tested in combination with higher concentrations of QCN (15 and 20 µM) on VEGF-C. Even though all the VEGF proteins in the VEGF family were raised in human plasma during AMD, significantly increased levels of VEGF-C is found in all the layers of the retina, and it correlates with other VEGF proteins (in terms of expression and suppression) [471,472]. Considering these findings for the current study, VEGF-C angiogenic cytokine was prioritised to assess the anti-VEGF activity of the combination therapy. The individual drugs, and combinations thereof, lowered the expression of VEGF-C when compared to LPS stimulated cells, as seen in Figure 4.11. However, for a few concentrations the decrease was not significant (TA 10 µM, QCN 5 µM, TA 75 µM and TA 100 µM in combination with QCN 5 µM).

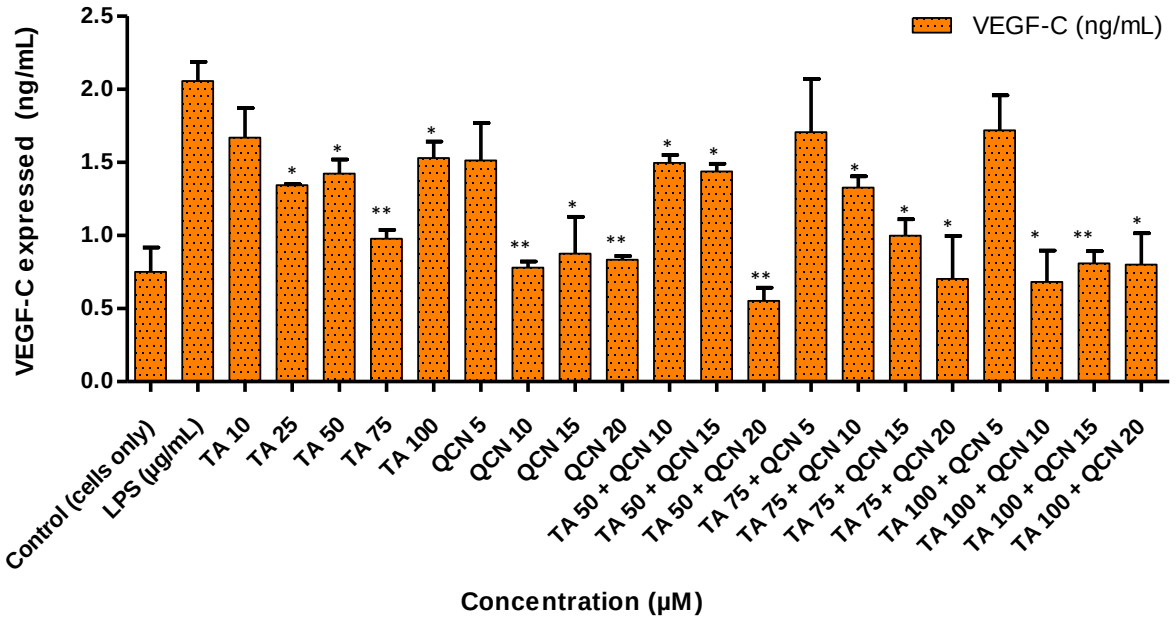

Figure 4.11: Investigating anti-VEGF activity of TA and QCN on their own and in combination using VEGF-C ELISA: ARPE-19 cells were stimulated using 10 µg/mL LPS for 24 h followed by 24 h treatments. ** P <0.01 (highly significant) * P <0.05 (significant), n=2 ± SD.

Compared to TA, QCN demonstrated better suppression of VEGF-C, by lowering the concentration from 2 ± 2 pg/mL (control - LPS stimulated) to 1 ± 0.02 pg/mL (QCN 20 µM).

In a previous study investigating the anti-cancer properties of QCN, it was shown to inhibit the pathways (protein kinase B (Akt), mammalian target of rapamycin (mTOR), and ribosomal protein S6 kinase (p70S6K)), which activates VEGF receptors [473]. This capability of QCN to act on the pathways which secrete VEGF proteins could be the reason for the significant suppression of VEGF-C at higher concentrations ($P < 0.05$). In a study on humans, upon oral administration of QCN it suppressed neovascularization, and the authors also reported visual and retinal restoration (similar to the currently available anti-VEGF therapies) [474,475]. The inflammatory pathways on which QCN acts was studied previously but the exact mechanism of action of anti-VEGF activity is still under investigation (the mechanism behind inhibiting VEGF signalling pathways). Similar to QCN, TA's anti-VEGF mechanism still needs elucidation but some studies report that it might decrease synthesis of VEGF by non-genomic destabilization of VEGF mRNA [476,477]. As observed in the anti-inflammatory study, combination treatment containing higher concentrations of TA and QCN were effective.

4.4.4 Antioxidant activity

Reactive oxygen species (ROS) levels are monitored to maintain homeostasis at a cellular level. Oxidative stress is a condition where these ROS levels elevate and gather to an extent that leads to the damage of cellular macromolecules and induced apoptosis [478]. The risk factors which lead to the progression of AMD include: genetics, aging, ethnicity and environmental factors such as high fat diet, smoking and light induced oxidative stress [479]. According to Harman's free radical theory of aging, the build-up of free radicals over a life time leads to oxidative damage of cellular macromolecules effecting the physiological condition of the organism [480]. Exposure to blue light and ultraviolet rays leads to the degeneration of mitochondria of RPE cells resulting in reduction of ATP generation and increase of ROS levels [481,482]. Rahman *et al.* reported that cigarette smoke is a powerful oxidant consisting of approximately 4700 chemical compounds such as ROS, peroxides, epoxides, nitric oxide, etc. [483]. The redox homeostasis of RPE depends on the stimulation of the transcription factor nuclear factor erythroid 2–related factor 2 (Nrf2) and NF-kB and this natural process is effected by the above mentioned factors leading to the oxidative stress observed in AMD [484]. Considering the role of oxidative stress in AMD, the potential therapeutics under investigation in the current study were tested to assess their antioxidant activity using DPPH and DCFH-DA assays.

4.4.4.1 DPPH Assay

The 1,1-diphenyl-2-picrylhydrazyl (DPPH) assay is one of the most commonly used colorimetric assays and gives an indication of the radical scavenging ability of the test compound. DPPH is a very stable free radical and when it comes in contact with an antioxidant it loses its free radical property resulting in a colour change from violet to yellow [485]. The higher concentrations of TA and QCN, and in combination, consistently lowered inflammatory cytokine expression and VEGF-C, hence these concentrations were selected to investigate their antioxidant activity (Figure 4.12).

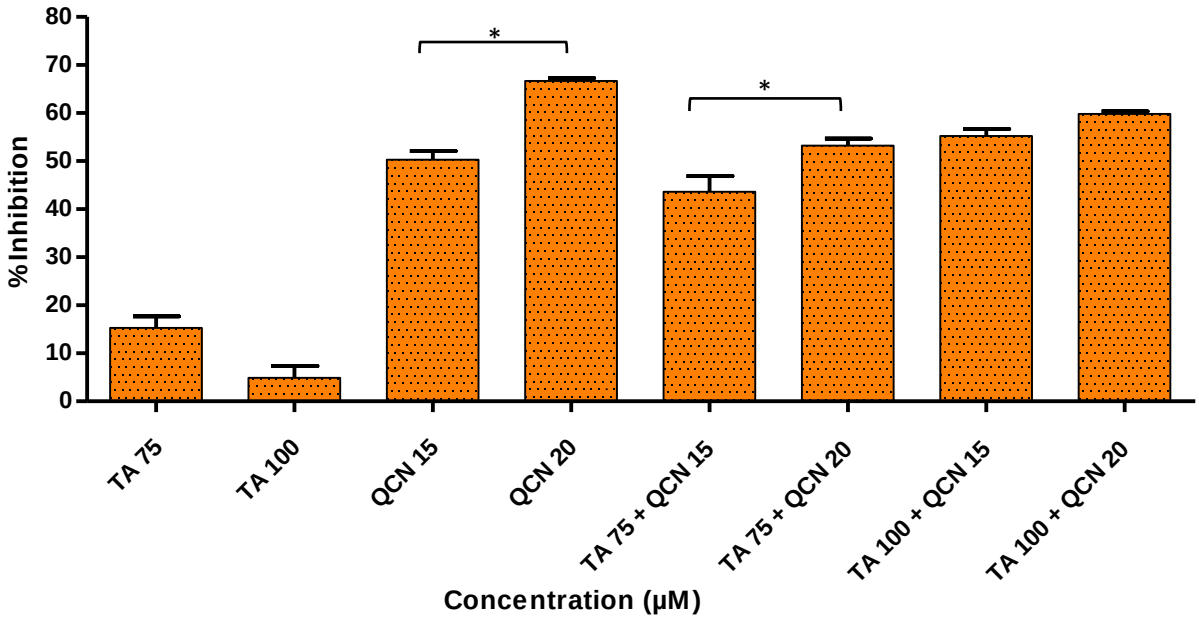

Figure 4.12: Investigation of antioxidant activity using a DPPH assay by considering the %inhibition of DPPH free radical agent. * P <0.05 (significant), n=2 ± SD.

As expected, QCN efficiently decreased the level of DPPH free radical and exhibited a strong anti-oxidant effect as observed in previous studies, whereas TA displayed a minimal anti-oxidant effect [486,487]. A higher concentration of QCN (20 µM) demonstrated better anti-oxidant effect compared to 15 µM by significantly inhibiting DPPH by 67%. QCN 20 µM in combination with TA 75 and 100 µM displayed better radical scavenging activity than QCN 15 µM in combination with TA 75 and 100 µM concentration. The anti-inflammatory effect of flavonoids like QCN primarily depends on their potential to scavenge ROS (Figure 4.13). This results in regulating of the Nrf2 and NF-kB pathways to maintain cellular homeostasis and prevent oxidative stress [488].

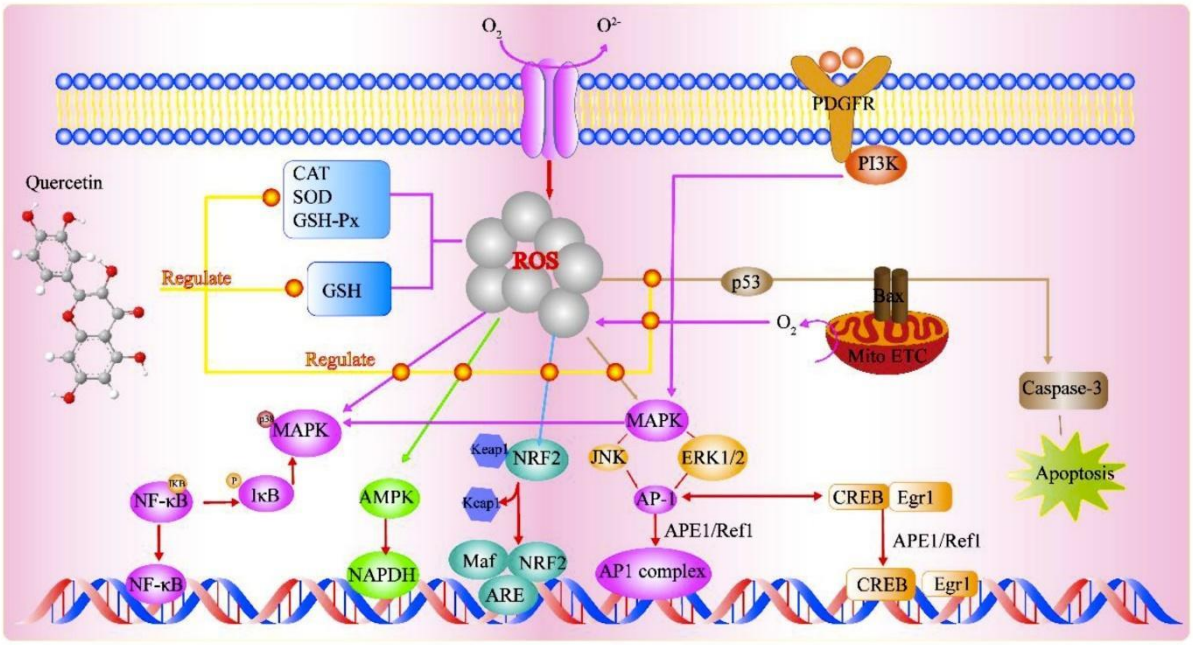

Figure 4.13: Representation of the anti-oxidant mechanism of QCN highlighting the pathways activated by the ROS [489]**.**

QCN on its own and in combination demonstrated better antioxidant activity when compared to TA. It can regulate both enzyme-mediated and non-enzyme-dependent antioxidant defence systems. It can also activate antioxidant defence systems and maintain oxidative balance by regulating signal pathways such as NRFB (nuclear factor E2-related factor), AMPK (AMP-activated protein kinase), and MAPK (Mitogen-activated protein kinase) as seen in Figure 4.13 [489].

4.4.4.2 DCFH-DA assay

Following the chemical antioxidant assay (DPPH), the intracellular antioxidant assay was studied to investigate the effectiveness of the treatments on the stressed ARPE-19 cells. For the 2',7'-dichlorodihydrofluorescein diacetate (DCFH-DA) assay, oxidative stress was induced to ARPE-19 cells using stimulants listed in Section 4.3.6.2. Upon stimulation and treatment, the intracellular ROS levels were measured using flow cytometry to assess the anti-oxidant effect of the treatments. The oxidation of DCFH-DA to 2'-7'dichlorofluorescein (DCF) was used for the detection of intracellular ROS levels including nitrogen dioxide and hydroxyl radicals. The cells will take up the DCFH-DA dye where cellular esterase cleaves off the acetyl groups, resulting in the formation of DCFH (2',7'-dichlorodihydrofluorescein). Oxidation of DCFH in the presence of intracellular ROS leads to the formation of DCF. This DCF fluorescent molecule can be detected using a flow cytometer by mean fluorescence intensity

(MFI). To induce oxidative stress, LPS and hydrogen peroxide (HP) were tested at concentrations 10, 20, 40 µg/mL and 100, 200, 300 µM, respectively. When compared to unstimulated cells, the cells stimulated with H_2O_2 at 300 µM induced oxidative stress, which is reflected by stained cells and MFI as depicted in Figure 4.14.

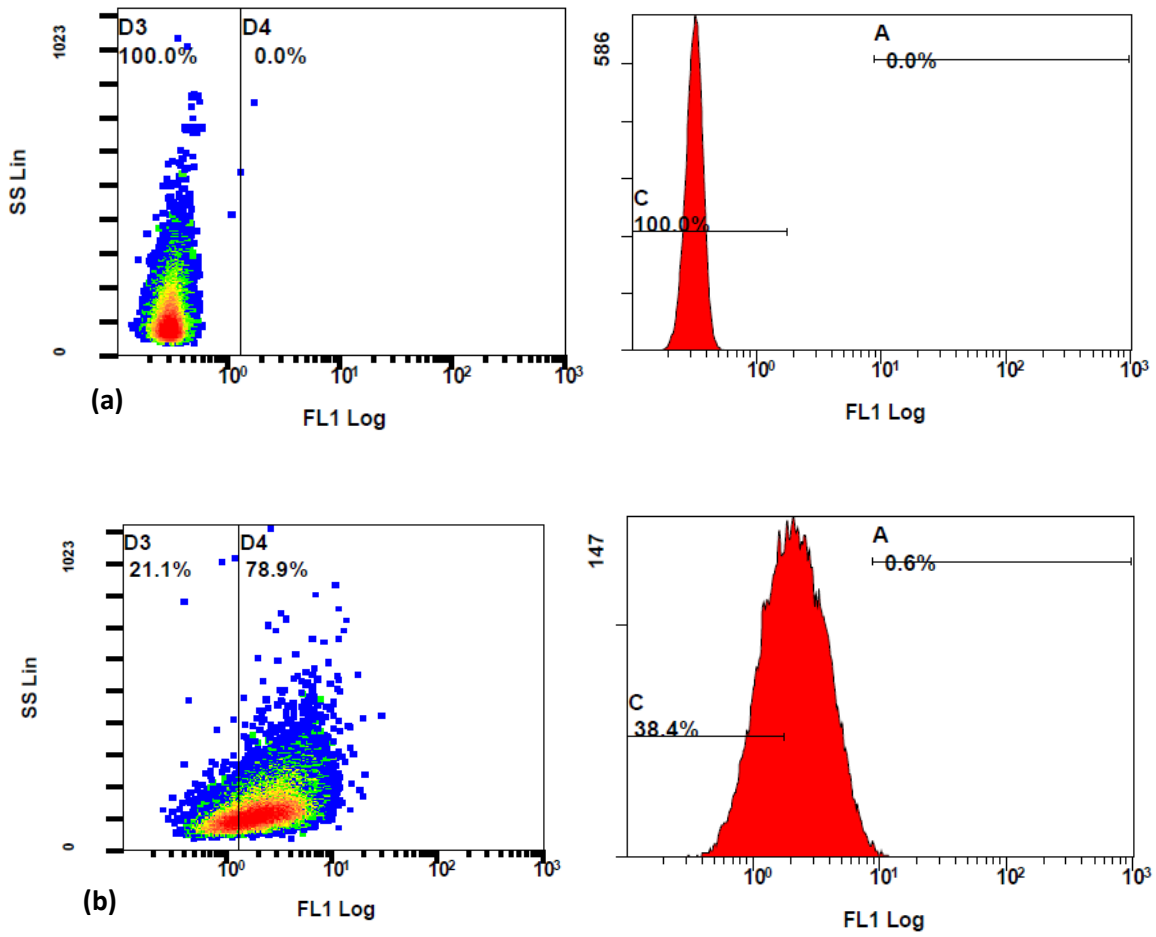

Figure 4.14: Flow cytometer analysis of ROS generation using DCFH-DA dye (a) unstimulated stained cells (b) stimulated stained cells with 300 M hydrogen peroxide.

The ROS levels of the cells stimulated with H_2O_2 at 300 µM had significantly increased when compared to unstimulated cells (MFI of unstimulated stained and stimulated stained cells was 2.01 ± 0.10 and 3.73 ± 0.29, respectively, with a P value <0.05). Considering the MFI value and the appearance of stained cells in the fluorescent gate, (D4) as seen in Figure 14 (b), a 300 µM concentration of H_2O_2 was selected for further investigation. To determine the effect of DCFH-DA dye on the morphology or the characteristics of the cells, flow cytometry analysis was performed on the control unstimulated unstained and control unstimulated stained cells. As depicted in Figure 4.15, no changes of the ARPE-19 cells were observed with the exposure

to the DCFH-DA dye. The forward and side scattered plots of flow cytometer analysis represent the population of ARPE-19 cells based on their size and density.

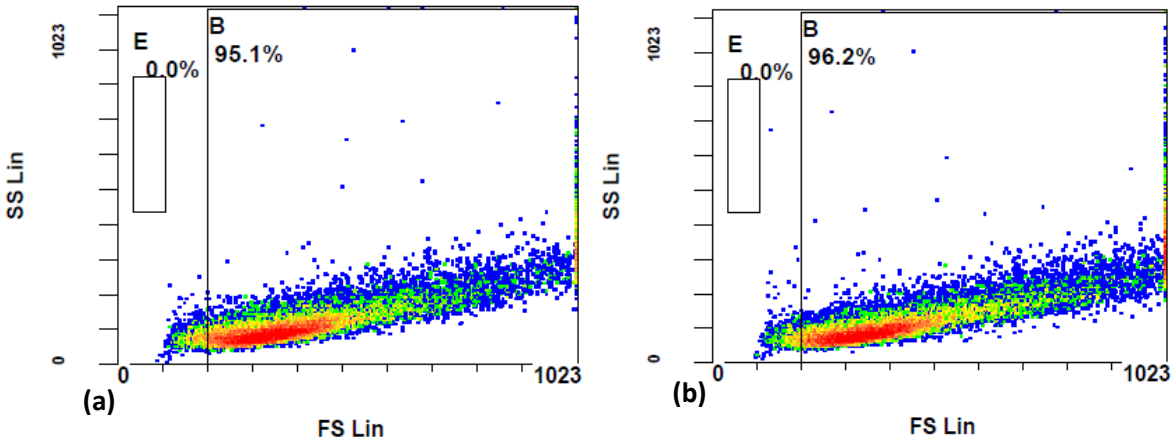

Figure 4.15: Comparison of unstimulated (a) stained and (b) unstained ARPE-19 cells using flow cytometer analysis.

The concentrations used for the DPPH assay were those used for the investigation of the intracellular ROS levels. When compared to the control stimulated stained, QCN and all the combination concentrations significantly suppressed the generated ROS (Figure 4.16). The findings of the DCFH-DA were similar to the DPPH anti-oxidant assay where TA did not lower the ROS levels. The combination drugs exhibited a synergetic anti-oxidant effect by significantly reducing the ROS, which was represented by lower MFI values (P value <0.05).

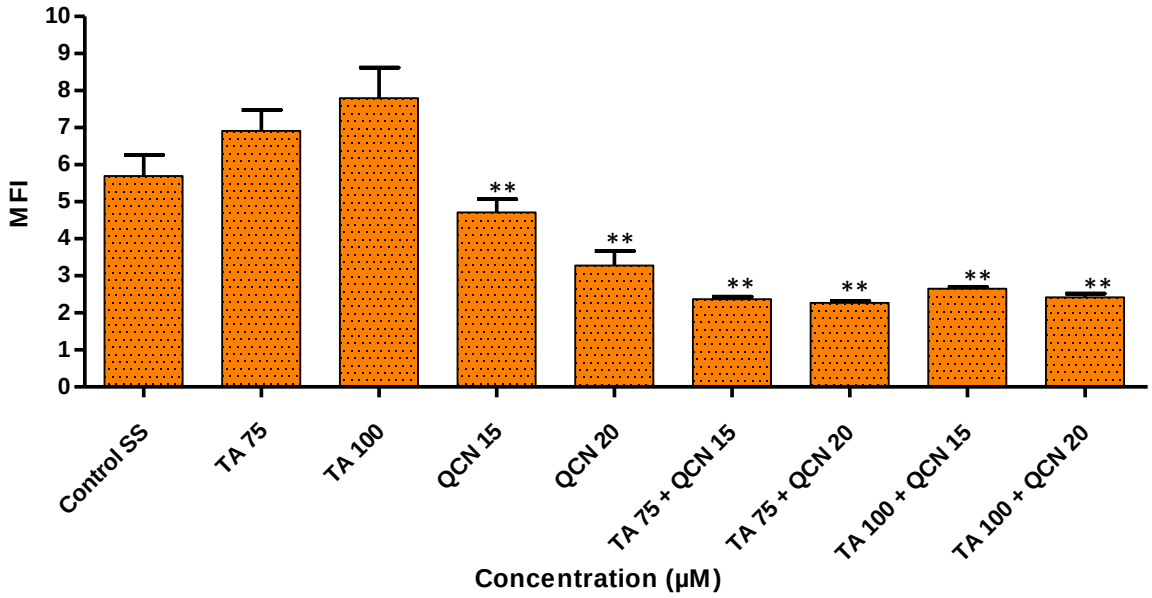

Figure 4.16: Investigation of intracellular ROS levels by estimating mean fluorescence intensity (MFI) using flow cytometer.) ** P <0.01 (highly significant) in comparison with control stimulated stained cells. n=3 ± SD.

The graphs in Figure 4.17 represent the stained cells with ROS in Gate D4 (fluorescent gate) and unstained cells in gate D3 (non-fluorescent gate). The control stimulated stained cells displayed 98.1% cell population in the fluorescent gate indicating the generation of ROS due to oxidative stress. Due to the synergetic antioxidant effect the stained cells containing ROS was significantly reduced, which is represented by a shift of cell population to the non-fluorescent gate. The cells containing ROS were reduced to 18-51%, which was also represented by the increase in non-stained cells between 49% and 82 %.

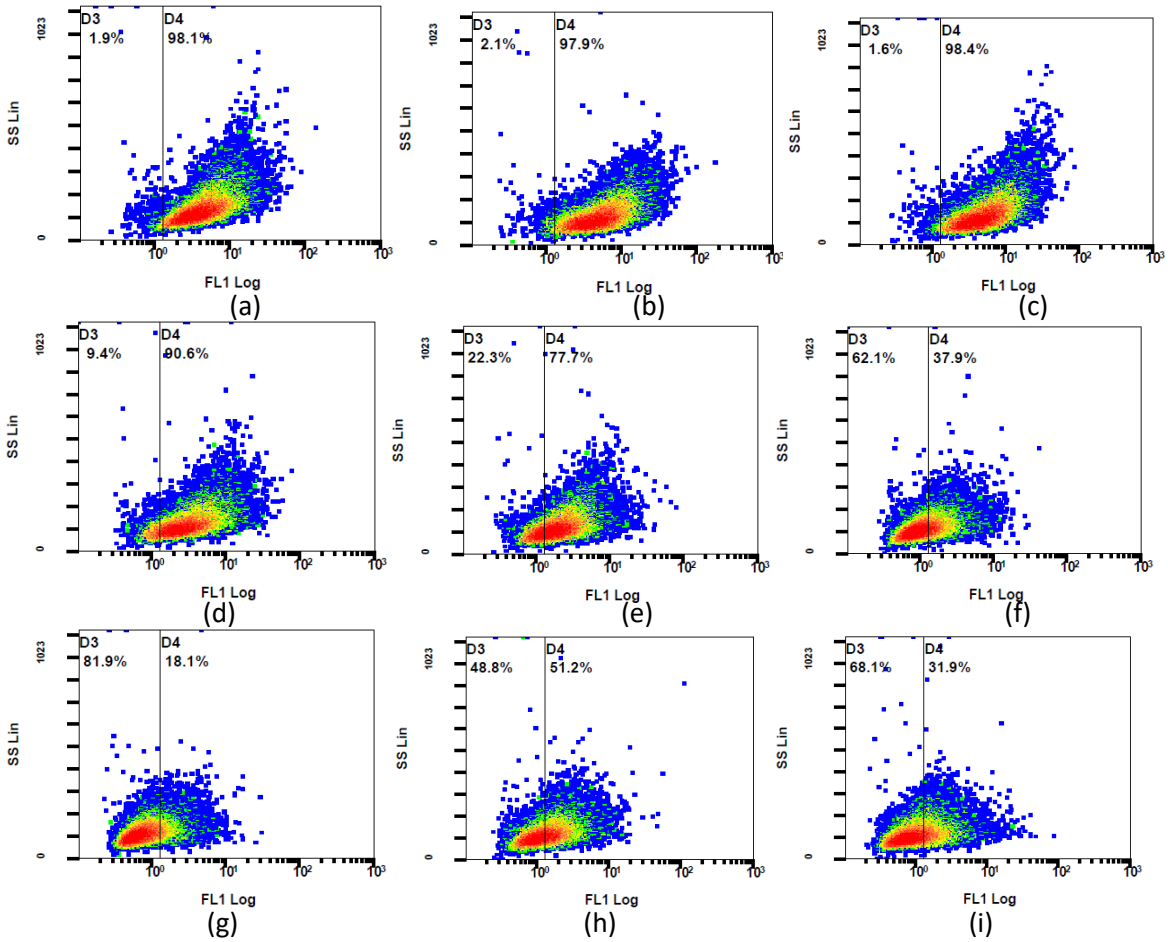

Figure 4.17: The fluorescent ARPE-19 cells were in gate D4 and the non-fluorescent cells in gate D3 (a) control stimulated (b) TA 75 µM (c) TA 100 µM (d) Q 15 µM (e) Q 20 µM (f) TA 75 + Q 15 µM (g) TA 75 + Q 20 µM (h) TA 100 + Q 15 µM, and (i) TA 100 + Q 20 µM.

Suntiparpluacha *et al.* studied the effect of TA and TA in combination with vitamin C supplementation on oxidative stress in human chondrocytes [490]. In their study, TA did not show any anti-oxidant effect and exhibited a slight increase in oxidative stress. When they combined TA with anti-oxidant (vitamin C), When they combined TA with an antioxidant (vitamin C), the oxidative stress was further decreased compared to the antioxidant alone. The outcome of the current study was similar to their findings, the addition of QCN could decrease the side effects of TA and enhance the anti-oxidant activity of QCN. In previous studies corticosteroids such as dexamethasone and cortisone have shown a decrease in antioxidant enzymes and mitochondrial activity in hippocampal neurons and rat pheochromocytoma cell lines [491,492]. These side effects of corticosteroids might be reduced with the addition of anti-oxidant agents such as QCN.

In accordance with the stained and unstained cell population in gates D4 and D3, the fluorescent peak shifts from 10^1 to 10^0 highlight the strong anti-oxidant effect by reducing the intracellular ROS (Figure 4.18).

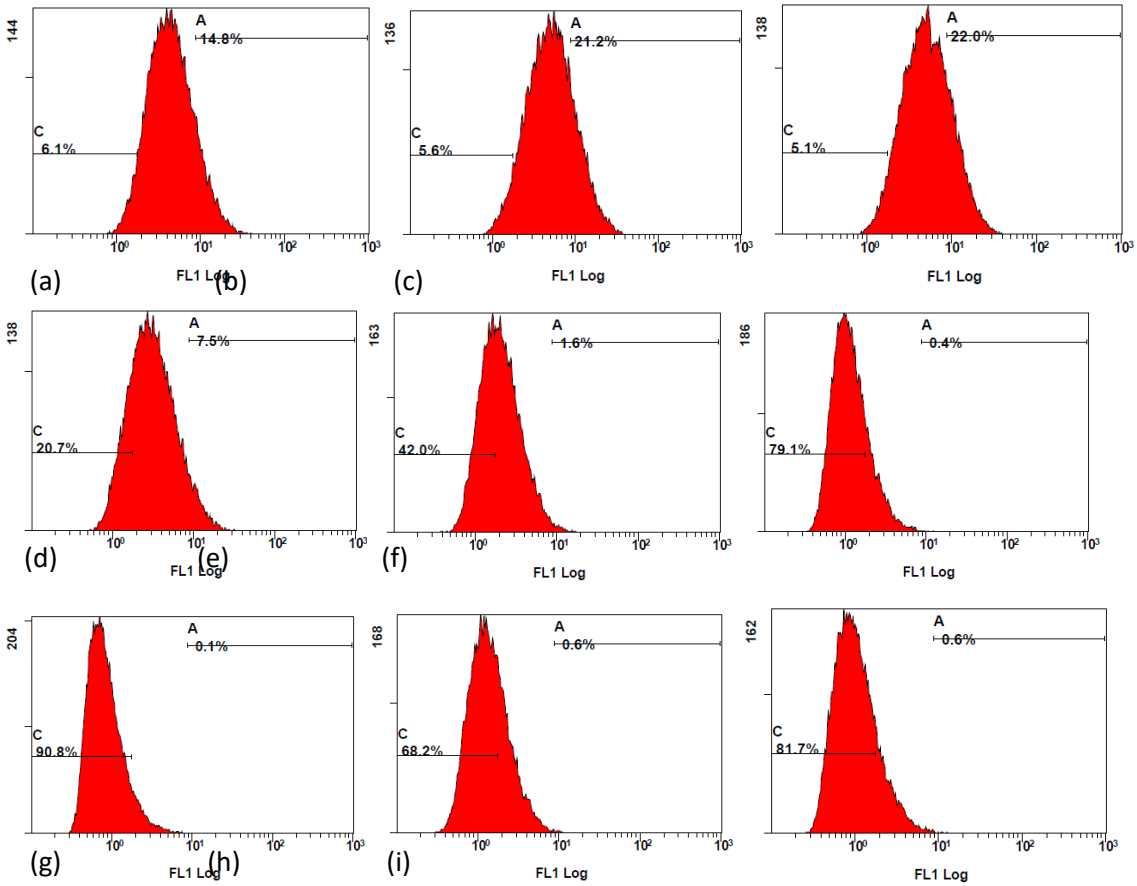

Figure 4.18: Examination of stained ROS species by mean fluorescence intensity (MFI) measured using flow cytometry. (a) control stimulated (b) TA 75 µM (c) TA 100 µM (d) Q 15 µM (e) Q 20 µM (f) TA 75 + Q 15 µM (g) TA 75 + Q 20 µM (h) TA 100 + Q 15 µM, and(i) TA 100 + Q 20 µM.

The retina has a high metabolism and the oxidative stress effects are high as the ROS are generated by the mitochondria of the cells. The generation of ROS hinders the physiological process of the cells leading to inflammation, autophagy, and apoptosis [493]. Monitoring the ROS levels is the key factor for retinal diseases, such as AMD, DR, and retinitis pigmentosa, etc. In both the antioxidant assays, QCN alone and in combination with TA showed effectiveness in reducing the ROS levels and proved to be an effective antioxidant agent.

4.4.5 Scratch Assay

The major cause of irreversible vision loss is the exudative form of AMD, which is characterized by CNV where the newly formed blood vessels protrude from the choroid to the retina through Bruch's membrane [494]. Even though the mechanism of CNV is not fully

understood, some pathological studies point to the connection between CNV and sub-RPE deposits [495,496]. Additionally, focal inflammation leads to focal thinning and damage of Bruch's membrane in patients of AMD. RPE cells are essential for the maintenance of photoreceptor cells as they provide nutrients [497]. But the contact between RPE and photoreceptor cells was seen to be disrupted due to the accumulation of sub-RPE deposits and the interference of branched blood vessels [498]. At this stage the migration of RPE towards the photoreceptor cells plays a vital role in protecting vision. Considering the role of migration, the scratch assay or cell migration assay was performed in the current study to assess the effect of treatments on RPE cell migration. As the scratch assay needs the cells to be fully confluent with high seeding density on 6 well plates, the concentrations were limited to higher concentration of TA and QCN and those in combination (Figure 4.19).

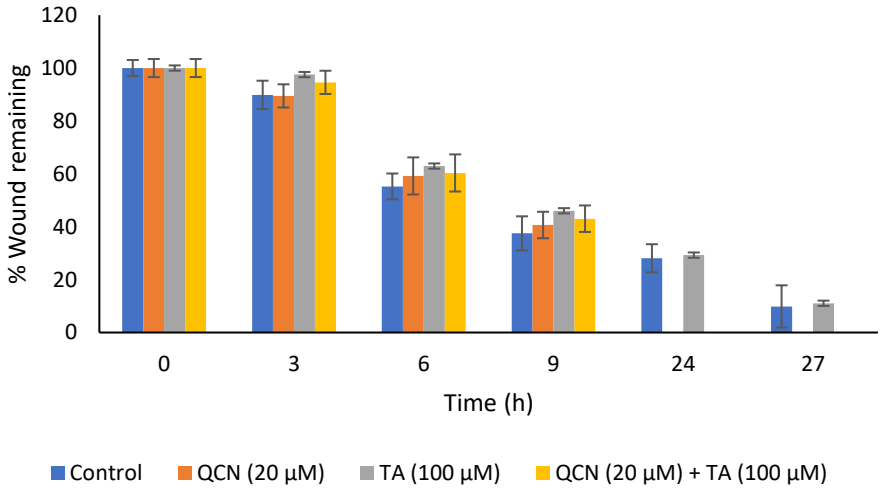

Figure 4.19: Assessment of cell migration using scratch assay at different time points. n=3 ± SD.

Upon seeding 25 × 10^4 cells/well and reaching around 90% confluency, the wounds were created and measured using image 'J' software. During the study the cells were serum starved (1% FBS was used instead of 10%) to ensure the assessment of cell migration and to demonstrate that the wound was not closed due to cell proliferation. QCN at 20 µM and in combination with TA 100 µM enhanced the migration of the cells and wound closure was observed by the 24 h time point (Figure 4.20).

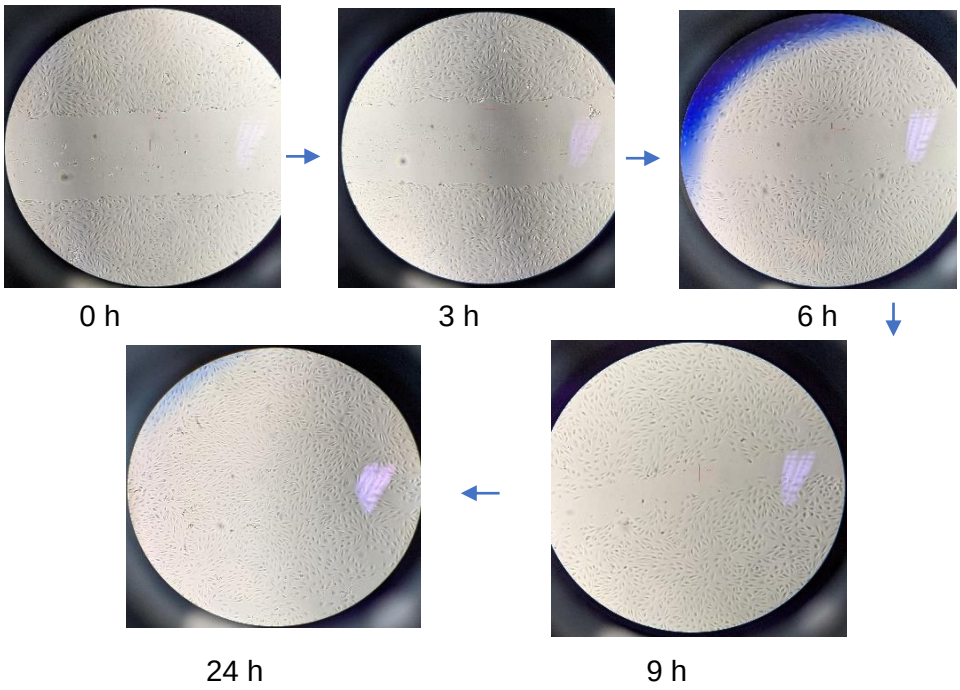

Figure 4.20: Microscopic pictures representing the wound closure process of the ARPE-19 cells treated with TA 100 + Q 20 µM at different time points.

A recent study by Irfan *et al.* investigated the effect of QCN and rutin on the closure of wounds created on mesenchymal stem cells, they observed complete wound closure for QCN treated cells at the 24 h time point [499]. The authors concluded that the anti-oxidant and anti-inflammatory properties of QCN aided in the closure of the wounds. These properties help in the regulation of growth factors and cytokines, which are involved in various phases of the wound healing process [500].

The control and TA exhibited similar pattern in the closure of the wound, TA did not enhance any cell migration (Figure 4.21). These finding were similar to previous study by Kim *et al.*, where they found that in the presence of nitric oxide, TA decreased cell migration [501]. During the wound creation, the ARPE-19 cells might be stressed leading to the release of ROS, such as nitric oxide, as TA alone did not display any antioxidant activity, therefore it is not as effective as QCN in closing wounds or in migrating the cells.

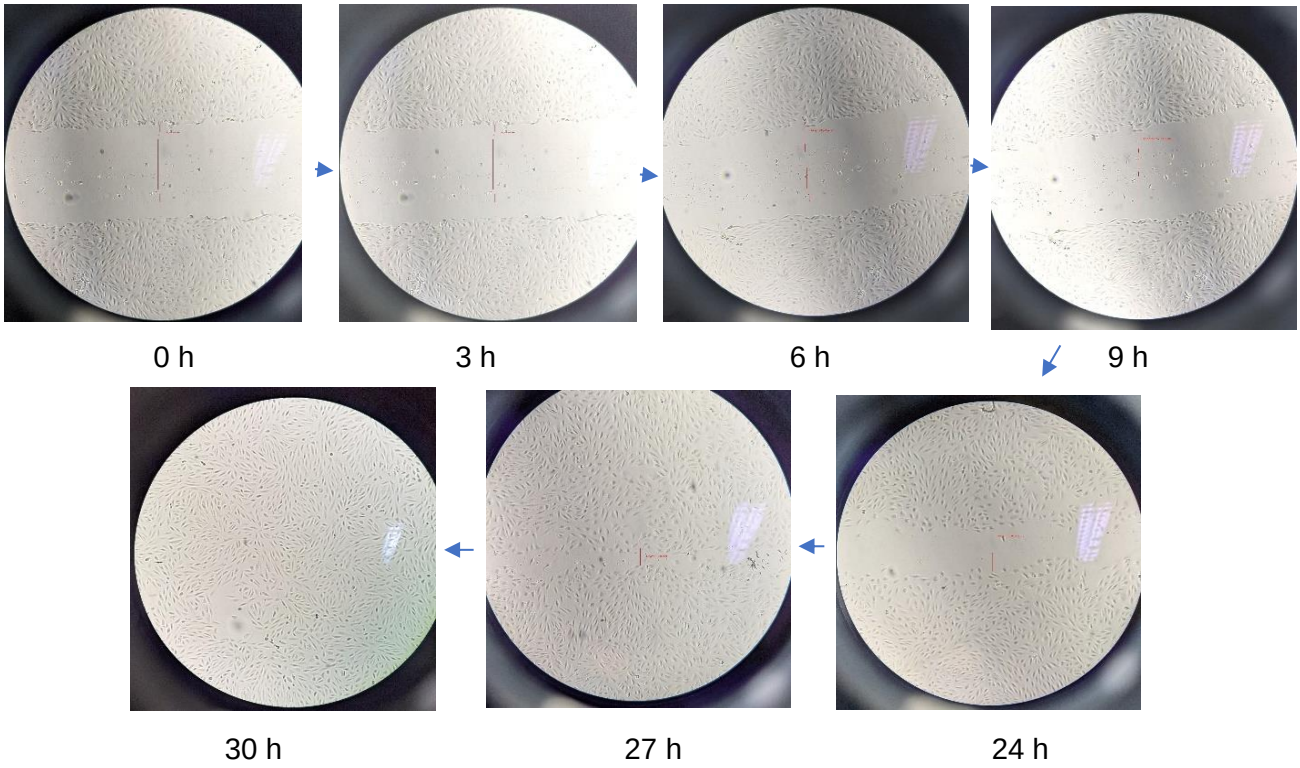

Figure 4.21: Microscopic pictures representing the wound closure process of the ARPE-19 cells treated with TA 100 µM at different time points.

4.5 Conclusions

The critical factor in AMD is its multifactorial nature, activation of inflammatory and VEGF signalling pathways leading to the secretion of cytokines with parallel oxidative stress affecting the physiological process by the generation of ROS. Treating these multiple conditions to protect the retina and restore the vision of people suffering from AMD is a great challenge for the scientific community. As mentioned in Section 1.1 although the current treatments are efficient in delaying the progression of the disease, they do not provide a cure. Hence investigating new therapeutics and delivering them through non-invasive routes is the aim of the current study.

Firstly, the individual drug concentrations (TA and QCN) and the combinations (TA + QCN) were safe on the retinal cell line and displayed no signs of synergetic toxicity or changes in morphology of the cells at the chosen concentrations. The combination exhibited a better anti-inflammatory effect as the TA and QCN act predominantly on different inflammatory signalling pathways (TA acts on NF kappa B and QCN on MAPK). In terms of anti-VEGF activity, both drugs act in a different way, QCN inhibits the kinase pathways leading to

deactivation of VEGF receptors whereas TA destabilises VEGF mRNA, which lead to the greater suppression of VEGF-C with the combination treatments. Both the anti-oxidant assays (DPPH and DCFH-DA) showed similar outcomes by exhibiting the synergetic effect in reducing ROS levels when treated with combination drugs (with reproducible results). QCN displayed enhanced retinal cell migration towards the wound on its own and in combination with TA.

All these findings suggest corticosteroid (TA) and flavonoid (QCN) as a potential combination therapy to target AMD. This novel combination of drugs encapsulated in the nanoparticulate system optimised in Chapter 3 could be delivered through a topical route. These dual drug loaded-nanoparticles have the potential to be an effective treatment strategy for AMD patients, which could significantly reduce healthcare costs. The proposed combination drugs are economical, easily available and have the potential to be administered at home by patients. Considering the outcome of the studies in this chapter, the following chapter is focused on fabricating and investigating the dual drug-loaded nanoparticles.

Chapter 5: Dual drug-loaded nanoparticles for the controlled release of a novel AMD therapeutic

5.1 Introduction

In Chapters 2 and 3, chitosan-coated PLGA nanoparticles encapsulating TA were prepared by two different techniques: thin-film hydration and oil-in-water emulsion methods. Considering the primary characteristics (low particle size, PDI and high %encapsulation efficiency) that play a major role in designing topical formulations for back of the eye diseases; NPs synthesised using an emulsion formulation technique were prioritised for further investigation. The optimized surface-modified NPs (CS-NP1, CS-NP2 and CS-NP3) using the emulsion technique were reproducible and stable with a particle size of 334 nm to 386 nm and PDI between 0.09 and 0.15, combined with a zeta potential between +26 and +33 mV. As mentioned previously, the smaller particle size of emulsion NPs with low PDI value indicates the mono-dispersion of NPs and a positive charge aid better permeation across ocular barriers. In Chapter 4, TA was investigated in combination with QCN, considering anti-inflammatory, antioxidant and anti-VEGF properties and proved to be effective for *in-vitro* conditions.

There is a clear unmet need to develop non-invasive and effective treatment options for AMD, which can be self-administered by patients, which remain a challenge for the scientific community [502]. The major problem with the use of hydrophobic drugs, including TA and QCN is poor aqueous solubility leading to low bioavailability. Loading hydrophobic drugs into polymeric NPs can help in overcoming this complication [393]. Developing a topical formulation is a great challenge, as the eye is complex with multiple anatomical, biochemical, and physiological barriers restricting the entry of drugs to the target site of action.

Considering the need and challenges associated, in the present study, the optimised formulation in Chapter 3 and the investigated novel drug combination in Chapter 4 were utilised to fabricate a dual drug-loaded nanoparticulate system as a potential treatment for AMD. In this Chapter, TA + QCN encapsulated PLGA and CS-PLGA nanoparticles were fabricated and characterised for particle size, PDI and zeta potential using DLS. *In-vitro* drug release of the optimized NPs was performed under physiological pH conditions while maintaining sink conditions. As the first step to assess the safety of the developed NPs, *in-vitro* cytotoxicity assays were performed on ARPE-19 cells. To investigate the difference in therapeutic activity of the drugs encapsulated and released from the particulate system, an anti-inflammatory study was performed using the released drugs on inflammation induced ARPE-19 cells.

5.2 Experimental

5.2.1 Materials

As per Section 2.2.1 and Section 4.2

5.2.2 Equipment

As per Section 2.2.2. and Section 4.2 plus the following were used:

Malvern Zetasizer pro (Particular sciences, Ireland)

5.2.3 Preparation of dual drug-loaded nanoparticles

The chitosan-coated and non-coated NPs encapsulating the dual drugs (TA and QCN) were prepared by the previously optimised emulsion technique in Chapter 3 (Section 3.3.1 and 3.3.2). The compositions of the drug, polymer, surfactant, and the coating material are listed in Table 5.1.

Table 5.1: Composition of nanoparticles fabricated by an emulsion formulation technique.

Formulation	TA (mg)	QCN (mg)	PLGA (mg/mL)	Poloxamer % (w/v)	Chitosan % (w/v)
NP1	1	1	3.7	1	-
CS-NP1	1	1	3.7	1	1.52
NP2	1	1	4.5	1	-
CS-NP2	1	1	4.5	1	1.32
NP3	1	1	3.5	1	-
CS-NP3	1	1	3.5	1	1.50

The blank nanoparticles of all the optimised formulations were prepared with the similar compositions without drug.

5.2.4 Characterisation of dual drug-loaded nanoparticles

The characterisation of the nanoparticles was performed with the same procedure outlined in Section 2.2.6. The particle size, PDI and ZP were determined using DLS and ZS xplorer software was used to determine the above characteristics. The drugs encapsulated in the NPs were quantified using the HPLC method outlined in Section 2.6.6.2, with a dual-wavelength detector to detect both TA and QCN at 240 nm and 310 nm, respectively.

5.2.5 *In-vitro* drug release study

The drug release study was carried out using the microcentrifuge method as described in Section 2.2.8.3.

5.2.6 *In-vitro* assessment of toxicity of the formulation

The cytotoxicity study of the blank and dual drug-loaded nanoparticles was performed for a duration of 24 h using the APA assay detailed in Section 4.3.2. NPs were sterilised in the biosafety cabinet under UV light for 30 min before treating the cells [503]. NP1, NP2, NP3, CS-NP1, CS-NP2, and CS-NP3 containing TA 50 μM and 100 μM were tested. These NPs contained QCN concentrations from 31 to 80 μM.

5.2.7 Anti-inflammatory activity of drug released from the nanoparticles

The anti-inflammatory activity of the drugs released from the NPs was assessed using the IL-8 ELISA following the procedure described in Section 4.3.3.

5.3 Results and discussion

5.3.1 Dual drug-loaded nanoparticles

The particle size of all three PLGA nanoparticles ranged between 212 nm and 231 nm and upon chitosan coating the particle size increased to 384 nm and 482 nm (Table 5.2). TA-loaded PLGA NPs optimised in Section 3.4.2 also showed an increase in particle size upon chitosan coating. This increase in particle size is due to the adsorption of chitosan on the surface of the negatively charged PLGA NPs [340]. As mentioned in Section 1.3.1.1, when the formulation is instilled topically, the permeation of the NPs across the ocular barriers is a considerable challenge. Tahara *et al.* fabricated PLGA NPs encapsulating coumarin-6 dye using emulsion solvent diffusion and also surface coated them with mucoadhesive polymers (chitosan and glycol chitosan) and polysorbate [504]. Their particle size of PLGA NPs was 200 nm and the surface-modified NPs ranged between 250 nm to 500 nm.When instilled on mouse eye after 30 min the entire eyeball (anterior segment, the cornea, iris/ciliary and the retina) was dyed, as observed with a fluorescent microscope. According to their fluorescent images, the topical formulation may enter the back of the eye via trans-corneal, trans-scleral and uveal routes. That study highlighted that topically applied nanoparticulate systems utilise multiple routes/pathways (trans-corneal, trans-scleral and uveal route) to travel to the back of the eye.

Table 5.2: Particle size, PDI, ZP and %encapsulation efficiency of the dual drug-loaded NPs prepared by an emulsion formulation technique, n=3 ± SD.

Formulation	Particle size (nm)	PDI	Zeta potential (mV)	%Encapsulation efficiency	
				TA	QCN
NP1	228 ± 18.55	0.48 ± 0.18	−05.98 ± 1.65	67.71 ± 6.01	52.36 ± 4.09
CS-NP1	400 ± 17.42	0.29 ± 0.03	+28.59 ± 7.29	57.88 ± 5.92	48.21 ± 3.34
NP2	231 ± 2.69	0.27 ± 0.23	−06.22 ± 1.82	63.93 ± 0.34	47.88 ± 1.34
CS-NP2	482 ± 12.95	0.37 ± 0.21	+43.50 ± 8.41	55.93 ± 0.02	34.90 ± 0.10
NP3	212.4 ± 8.60	0.23 ± 0.12	−07.61 ± 2.16	61.52 ± 2.86	49.16 ± 4.08
CS-NP3	384 ± 11.38	0.27 ± 0.02	+33.47 ± 5.78	58.74 ± 5.49	37.76 ± 7.40

The nanoparticles fabricated in the present study with the characteristics mention in the Table 5.2 have the potential to permeate through the ocular barriers. These NPs can utilise trans-corneal, periocular, or uveal routes to reach the target site of the retina [388]. The charge of the dual drug-loaded PLGA and CS-PLGA NPs were negative (−6 to −8 mV) and positive (+29 to +44 mV), respectively as expected due to the carboxyl groups of PLGA and the amine groups of chitosan. ZP values of the obtained NPs were either below −25 mV or above +25 mV, indicating that the formulations were colloidally stable suspensions [505]. The PDI values were less than 0.5 and the particles displayed narrow and monodispersion distribution curves on DLS (Figure 5.1). Larger particles (1.68%) were noticed for the formulation CS-NP3 in Figure 5.1 (f), which could be due to the presence of unreacted chitosan.

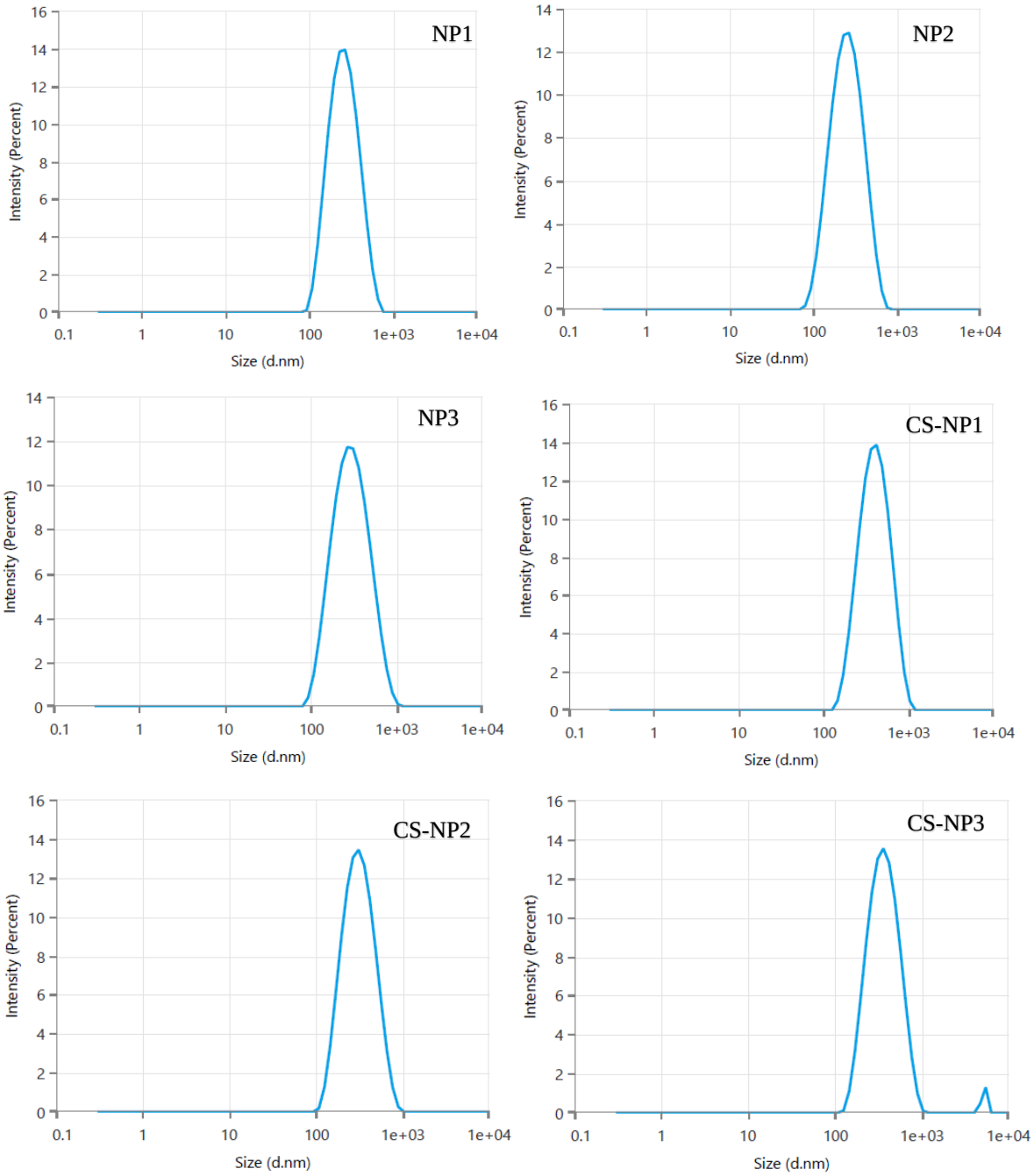

Figure 5.1: Particle size distribution profiles of the (a) NP1, (b) NP2, (c) NP3, (d) CS-NP1, (e) CS-NP2, and (f) CS-NP3 formulations.

Spherical and monodispersed nanoparticles up to 600 nm were found to have no effect on biological parameters of cells [506]. HPLC was used to quantify the drugs loaded in the NPs and the encapsulation efficiency of TA (between 56% and 68%) was higher than QCN (between 35% and 52%. The linear concentration range for both the drugs was 25 to 200 µg/mL and the linear regression correlation was greater than 0.99 (Figure 5.2).

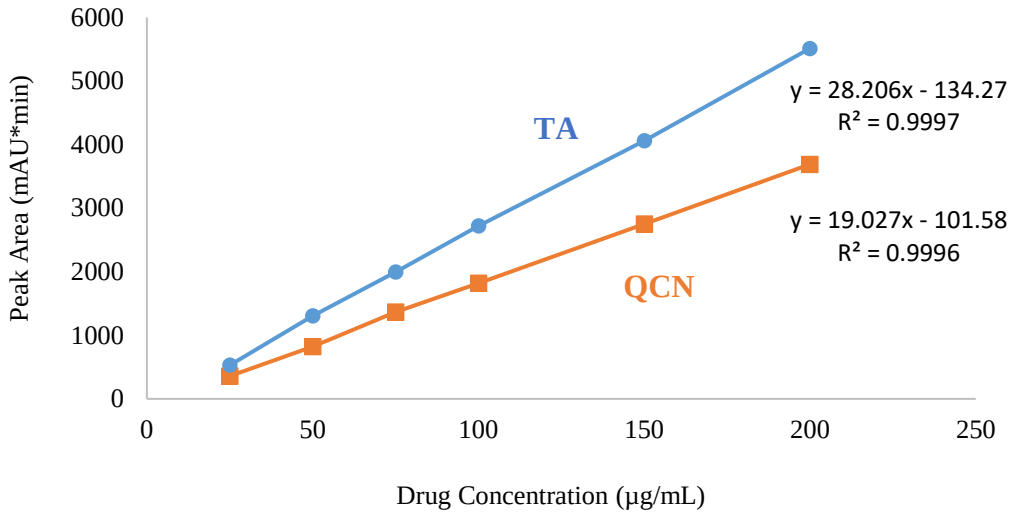

Figure 5.2: Calibration curve of TA and QCN.

Instead of single wavelength, dual-wavelength was used to detect both TA and quercetin at 240 nm and 370 nm respectively (Figure 5.3).

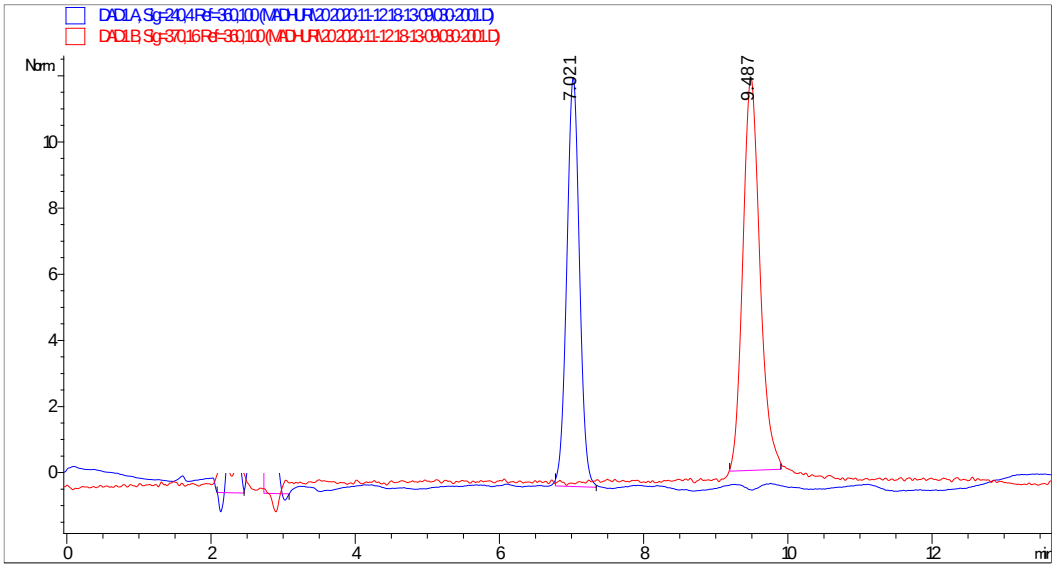

Figure 5.3: HPLC peaks of TA (blue) and quercetin (red) of CS-NP1 with retention times at 7.0 and 9.1 min were detected using wavelengths 240 and 370 nm, respectively.

5.3.2 *In-vitro* drug release study

In-vitro drug release of the dual drug-loaded nanoparticles was investigated in PBS with 1% tween 80 as release media using the microcentrifuge method. As mentioned in Section 2.3.7, tween 80 was used as a surfactant to increase the solubility of hydrophobic drugs to maintain sink conditions. In Section 3.4, TA-loaded NPs showed initial burst of 13 - 19% in the first 15 min whereas for the dual drug loaded-loaded NPs, TA displayed a controlled release of 1 - 3% at the 15 min time point (Figure 5.4).

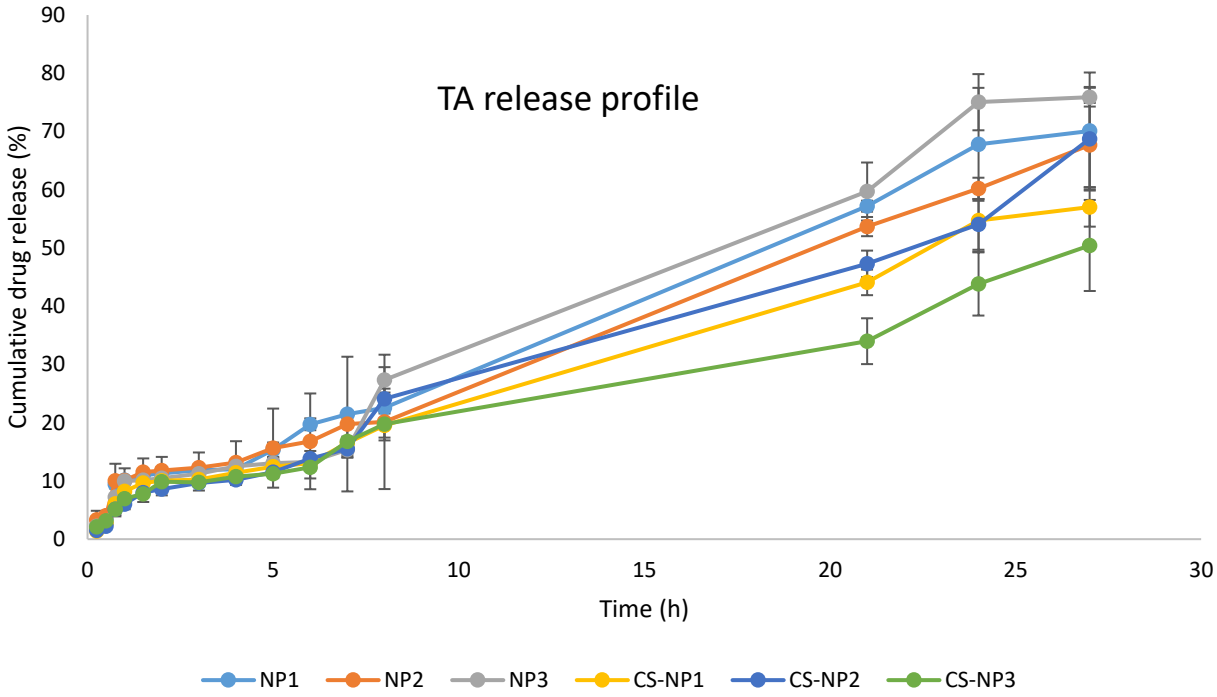

Figure 5.4: *In-vitro* drug release of TA from dual drug loaded-NPs (NP1, NP2, NP3, CS-NP1, CS-NP2 and CS-NP3), n=2 ± SD.

TA release (up to 27 h) from all the formulations of coated and non-coated nanoparticles showed controlled release of the drug. There was no significant difference in the drug release before and after coating the NPs with chitosan. PLGA NPs initially exhibit diffusion-based release followed by controlled release due to polymer degradation [507]. Long term release is suggested for future work to investigate the complete release profile of the dual drug-loaded NPs.

Curve fitting of the *in-vitro* TA release was analysed with the different mathematical models indicating coefficient of determination (R^2) as seen in Table 5.3. Zero-order showed a better curve fit for the TA release from the formulations with R^2 values between 0.9793 and 0.9901 when compared to other models. The model suggests a constant release rate of the drug, indicating the controlled release of the TA [508]. Even though the R^2 values were high for the zero-order model, the R^2 is >0.9 for the first-order, Hixson-Crowell, and Higuchi models also. The drug release from PLGA particles can follow mono, bi, or multiphase release due to the diffusion of the drug from the porous surface of the particles, drug diffusion through the polymer and the hydrolytic degradation of the polymer [509]. Mono-phasic controlled release was observed in the current study as the zero-order model is the best fit.

Table 5.3: *In-vitro* drug release mathematical model fitting for TA release from NPs with coefficient of determination (R^2).

Formulation Code	Coefficient of determination (R^2)				
	Zero-order	First-order	Hixson-Crowell	Higuchi	Korsmeyer-Peppas
NP1	0.9901	0.9796	0.9852	0.9362	0.7477
NP2	0.9898	0.9700	0.9827	0.9273	0.7333
NP3	0.9793	0.9585	0.9693	0.9074	0.7029
CS- NP1	0.9880	0.9803	0.9837	0.9352	0.7480
CS- NP2	0.9854	0.9528	0.9684	0.9268	0.7388
CS- NP3	0.9821	0.9739	0.9762	0.9447	0.7792

All the formulations displayed slow drug release for QCN with 16 – 27% release in 27 h (Figure 5.5). The NP2 formulation containing a high concentration of PLGA (4.5 mg/mL) released the least amount of the drug (16%).

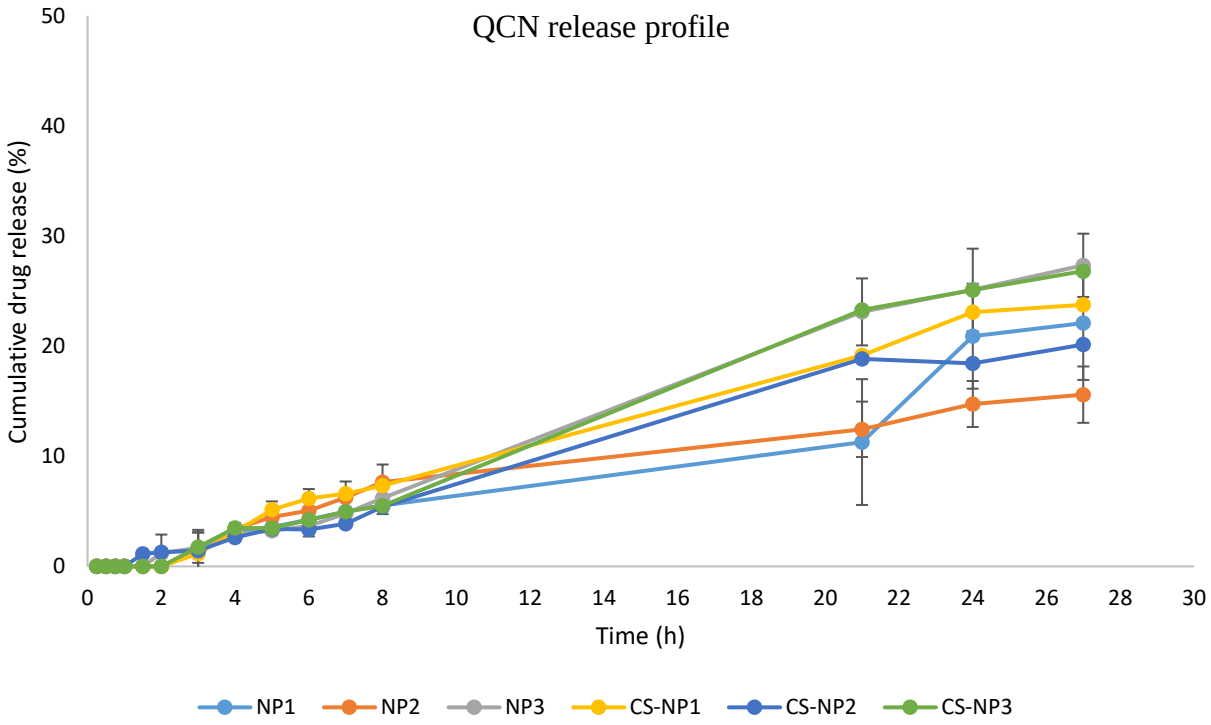

Figure 5.5: *In-vitro* drug release of QCN from dual drug loaded-NPs (NP1, NP2, NP3, CS-NP1, CS-NP2 and CS-NP3), n=3 ± SD.

Smita *et al.* loaded QCN dihydrate in PLGA NPs (100 - 200 nm) and investigated the release profile in PBS [510]. In that study, they reported the slow release of QCN with 38% drug release in 50 h with the reason attributed to drug diffusion from the PLGA surface, matrix, and polymer degradation (which are attributed to the controlled/prolonged drug release).

Similar to the TA release profile, the curve fit of the *in-vitro* QCN release was identified with the different mathematical models with the help of R^2 values as represented in Table 5.4. For QCN, the best curve fit was different for multiple formulations: NP1, NP3, CS-NP2, and CS-NP3 fitted a zero-order model with R^2 between 0.9572 and 0.9911, NP2 fitted a Higuchi model with R^2 0.9793, and CS-NP2 fitted a first-order model with R^2 of 0.9937. Similarly, to the TA drug release results, QCN R^2 values were also high for the four mathematical models (first-order, Hixson-Crowell, and Higuchi models) with R^2 >0.9.

Table 5.4: *In-vitro* drug release mathematical model fitting for QCN release with linear coefficients of determination (R^2).

Formulation Code	Coefficient of determination (R^2)				
	Zero-order	First-order	Hixson-Crowell	Higuchi	Korsmeyer-Peppas
NP1	0.9572	0.9492	0.9521	0.9063	0.7240
NP2	0.9542	0.9623	0.9597	0.9793	0.8716
NP3	0.9911	0.9883	0.9894	0.9144	0.8775
CS- NP1	0.9914	0.9937	0.9932	0.9545	0.7381
CS- NP2	0.9859	0.9844	0.9850	0.9257	0.9139
CS- NP3	0.9895	0.9872	0.9881	0.9164	0.7788

In Section 2.3.7 and Section 3.4, TA showed initial burst release compared to the TA released from the dual drug-loaded nanoparticles. Multiple previous studies reported the biphasic release of PLGA NPs with initial burst release followed by a controlled release [160,216,360]. For the *in-vitro* drug release performed in the present study on dual drug-loaded NPs, initial burst release was not observed for both drugs. Murugesan *et al.* formulated dual drug-loaded PLGA nanospheres encapsulating rutin and benzamide using an emulsion technique to evaluate the synergistic efficacy for breast cancer treatment [511]. They achieved a particle size between 150 and 200 nm with an encapsulation efficiency of 86% and 83% for rutin and benzamide, respectively. In the mentioned study, *in-vitro* drug release of the dual drug-loaded NPs was performed where initial burst release was not observed, demonstrating a single-phase

controlled release, which was in accordance with the results obtained in the present study. The impact of QCN on the release of TA can be known by formulating the QCN-loaded NPs and studying the release profile of QCN alone. Also, a prolonged drug release study of the single drug-loaded NPs and dual drug-loaded NPs will be beneficial in understanding the effect of co-encapsulation of drugs on the release mechanism. If release from the drug delivery system is not tailored, a higher concentration of the drug can be released than required leading to unwanted side effects. Hence, controlled release nanoparticulate systems are beneficial for maintaining *in-vivo* drug concentration at a constant rate to attain the desired therapeutic efficiency for a longer period, thus reducing the dosing frequency [512].

Commercially available corticosteroid implants for back of the eye inflammatory diseases like Ozurdex® (dexamethasone intravitreal implant) and Retisert® (Fluocinolone acetonide IVT implant) release about 0.2 µg of drug per day [513]. The anti-VEGF activity of TA was seen on human retinal epithelial cell lines at TA concentration of 4.34 µg [514]. TA release from the present study was more than the therapeutic dose of the marketed corticosteroid IVT implants, which is beneficial as TA has 12.5 times less anti-inflammatory potency than dexamethasone and 4.8 times more than fluocinolone acetonide [379]. Future *ex-vivo* and animal studies will provide information on the bioavailability of TA upon topical administration of the developed NPs with the drug dose regimen also depending on the pathological condition or disease state.

5.3.3 *In-vitro* assessment of toxicity of the formulation

The ARPE-19 cells were treated with blank nanoparticles and dual drug-loaded NPs at various concentrations. As the drugs were co-encapsulated in the NPs, selecting the particular concentrations of both drugs was not possible. Hence NPs containing TA at concentrations of 50 µM and 100 µM (medium and high concentrations) were chosen to study the cytotoxic effects. Even though the concentration of TA was mentioned in Figures 5.6 and 5.7, the selected NPs contained QCN from 31 µM to 80 µM for both coated and non-coated formulations. Blank NPs were prepared with the same concentrations of NPs material as drug-loaded NPs.

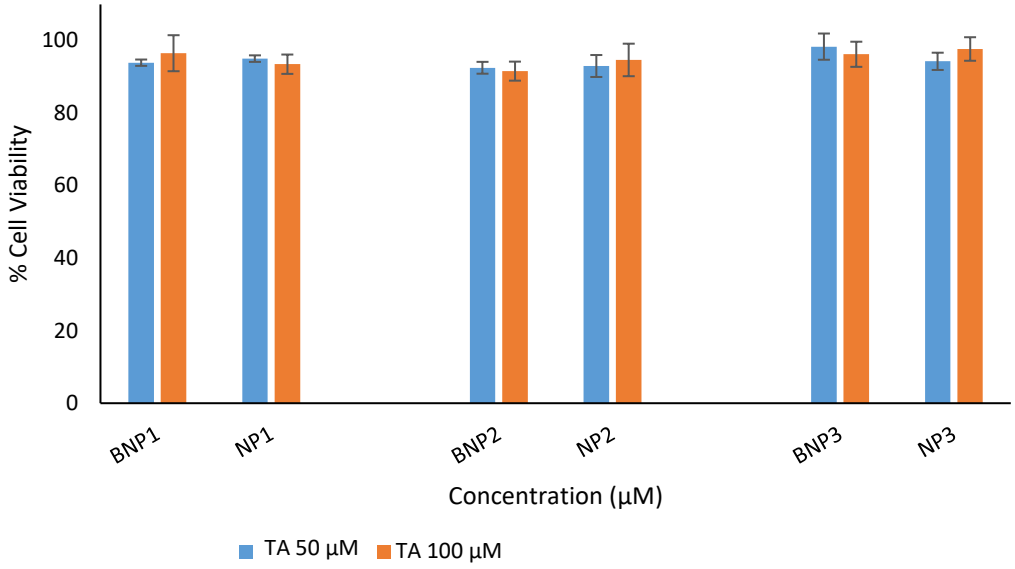

Figure 5.6: *In-vitro* cytotoxicity study of the blank and dual drug-loaded PLGA NPs (QCN concentration in the NPs ranging from 31 µM to 80 µM), n=3 ± SD.

All the PLGA nanoparticles displayed more than 90% cell viability and proved to be non-toxic on ARPE-19 cells. These results agree with a previous study by Hirani *et al.* where they prepared TA-loaded PLGA NPs using a nanoprecipitation method and attained a particle size of 208 nm with 42% TA encapsulation [514]. According to their study, TA-loaded NPs at concentrations, 1, 10 and 100 µM were non-toxic on ARPE-19 cells.

In Section 4.4.1, QCN at concentrations above 40 µM, showed a cytotoxic effect on ARPE-19 but when encapsulated in the PLGA and CS-PLGA NPs displayed no signs of cytotoxicity up to 80 µM (Figure 5.7). This is due to the protective nature of the nanoparticulate system and the slow release of the drug, which was seen in the *in-vitro* drug release study (Section 5.3.2).

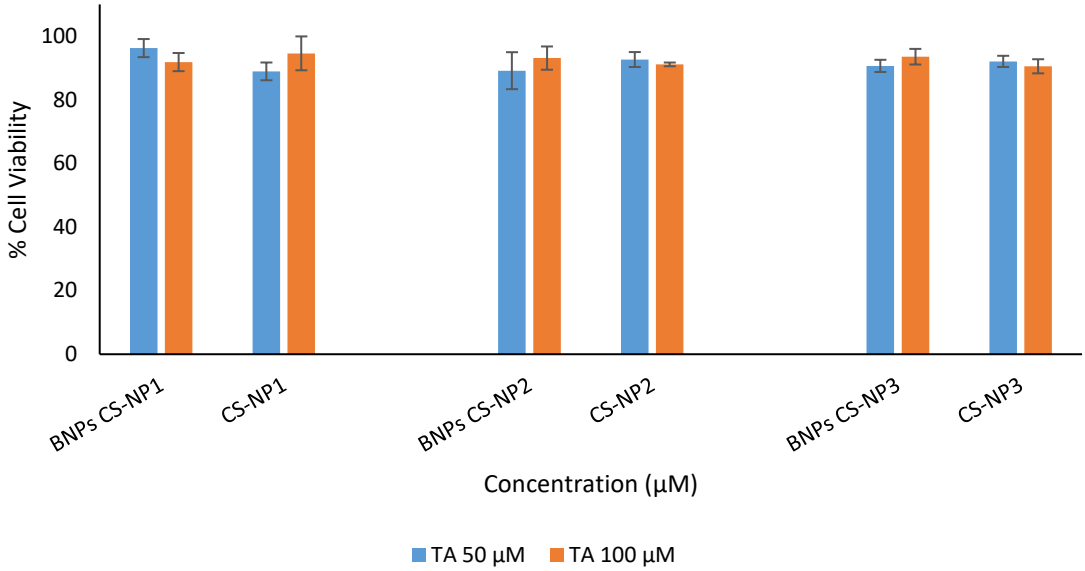

Figure 5.7: *In-vitro* cytotoxicity study of the blank and dual drug-loaded CS-PLGA NPs (QCN concentration in the NPs ranging from 31 µM to 80 µM), n=3 ± SD.

Guo et *al.* investigated the effectiveness of TA-loaded mPEG-PLGA nanoparticles in treating uveitis in rats [515]. In their study, TA and TA-loaded NPs were non-toxic on both ARPE-19 cells and rats with significant reduction in the inflammation (*in-vivo* conditions) displaying controlled *in-vitro* release of TA around 60% in 27 h. These results agree with the current study where TA and TA-loaded NPs (NP1, NP2, NP3, CS-NP1, CS-NP2 and CS-NP3) were proved to be non-cytotoxic on ARPE-19 cells with controlled release of TA over 27 h.

5.3.4 Anti-inflammatory activity of the drugs release from the nanoparticles

As mentioned in Chapter 4 (Section 4.4.2), inflammation was stimulated using LPS, which leads to the activation of TLR pathways resulting in the secretion of inflammatory cytokines. ARPE-19 cells were stimulated and treated with the drugs released from *in-vitro* drug release study (Section 5.3.2). TA 25 and 50 µM in combination with QCN from 14 – 40 µM were tested for anti-inflammatory activity using IL-8 ELISA (Figure 5.8).

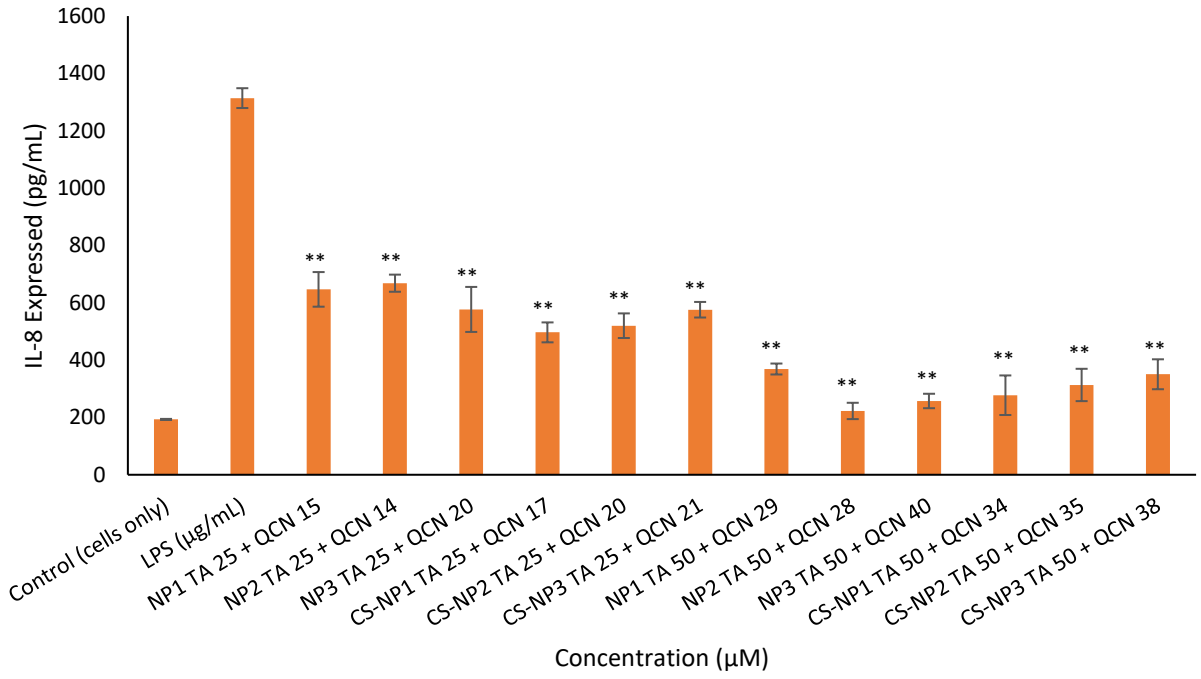

Figure 5.8: Investigating the drugs (TA + QCN) released from dual drug-loaded NPs on anti-inflammatory activity ** P <0.01 (highly significant), n=2 ± SD.

The drug combinations significantly lowered the secretion of IL-8 cytokine when compared to the control stimulated cells treated by LPS alone. These results agree with the dual drugs anti-inflammatory study on IL-8 cytokine in Section 4.4.2. The secretion and suppression of IL-8 cytokine are associated with IL-6 and MCP-1 cytokines; hence this alone was studied as a preliminary investigation. This indicates that the drugs encapsulated into the PLGA and CS-PLGA NPs did not show any difference in therapeutic activity after being released from the particles. As mentioned previously, multiple investigations showed QCN acts on the MAPK pathway in different human cells, whereas TA acts on key inflammatory transcription factors such as NF-κB [461–465]. As the two drugs have different primary targets to act on inflammation, the combination therapy had decreased the secretion of IL-8 in the current study.

5.4 Conclusion

The optimised dual drug-loaded PLGA and CS-PLGA nanoparticles have particle size between 212 nm and 482 nm with PDI of 0.2 – 0.4 and zeta potential of +44 and –6 mV. According to the literature, nanoparticulate systems that have similar size and charge, as obtained in the present study, showed effectiveness in permeating to the back of the eye when instilled topically (in *in-vivo* animal studies) [304,516]. PLGA NPs proved to have good stability with controlled release of the drug in many studies but they lack the property of mucoadhesion

[333]. This property improves the ocular surface retention time, which plays a crucial role when targeting the topical route of delivery for posterior segment as the clearance of NPs in tear drainage is a limitation [334,517,518]. The surface modification of PLGA NPs with natural, biocompatible and biodegradable polymers like chitosan has proven to be advantageous for ocular drug delivery [160,224,519]. Surface modification of PLGA NPs with chitosan did not show any effect on the release profile of drugs or the cytotoxic effects on ARPE-19.

The other challenge associated with permeation of drugs to the back of the eye is to identify new therapeutic agents or treatment options for AMD. As mentioned previously, the current treatments can only slow down the progression of diseases with invasive drug delivery. Active research is ongoing as the ageing population and the number of people suffering from AMD are increasing as stated in Section 1.1. The use of supplements in the Age-Related Eye Disease Study (AREDS) showed reduction in AMD progression [520]. However, the outcomes from AREDS demonstrated that 33% of the patients progressed to late stage AMD. Since the first use of intravitreal injection of anti-VEGF agents in 2008, developing a cure for the disease remains a challenge to the scientific community.

Through the literature search, two drugs were identified, with the dual drugs having multiple properties that could show effectiveness on the complex pathology of AMD. A novel combination of drugs (TA + QCN) was investigated on ARPE-19 cells with respect to cytotoxicity, inflammation, oxidative stress and on VEGF secretion in *in-vitro* conditions and proved to be effective. Research methodologies were designed to investigate new drug combinations at the preliminary level in *in-vitro* human cell lines. This research on a novel dual drug therapy will significantly add to the ongoing research of identifying therapeutics for AMD.

The investigated dual drug therapy was successfully co-encapsulated into the optimised PLGA and CS-PLGA NPs displaying controlled release of both drugs. This study highlights the importance of multidisciplinary research, combining formulation development and therapeutic efficiency studies. Results from this study identified a potential treatment for AMD, representing a step forward in the translation of this research. In future work the developed nanoparticles will be incorporated into a non-invasive topical platform leading to greater patient compliance, improved quality of life for people living with these conditions and a significant reduction in healthcare costs.

Chapter 6: Future work

6.1 Introduction

As mentioned in earlier chapters these anti-VEGF injections have serious side effects and monoclonal antibodies (current anti-VEGF agents) are expensive. There is an urgent need to develop non-invasive and effective treatment options for AMD, which can be self-administered by patients. In Chapters 4 and 5, the potential dual therapy for AMD was investigated on ARPE-19 cells and encapsulated into surface-modified PLGA nanoparticles to overcome the challenges associated with ocular barriers (Section 1.3.1). The characteristics achieved for the fabricated dual drug-loaded NPs are suitable for ocular drug delivery [216]. The polymeric matrix of PLGA helps in controlled delivery of the drugs through diffusion, while the mucoadhesive property of chitosan may enhance permeation by binding to the negatively charged corneal and retinal epithelial barriers of the eye [203]. The size of the NPs in conjunction with the biodegradable and biocompatible properties of the polymers suggest these particles might be promising for topical ocular drug delivery.

In future work, an investigation of freeze-dried nanoformulations and the application of different mathematical models for the release data was suggested. These optimized formulations will be fully investigated on *in-vitro* ocular cell lines (Human corneal and retinal cell lines) for their permeation capability through the ocular barriers and the ability to internalise in the cells. Upon investigating the permeation across ocular cell barriers, the formulation will be studied on *ex-vivo* porcine eyes. The porcine eyes are anatomically and physiologically similar to human eyes and the *ex-vivo* studies will enable an investigation into entrapment and bioavailability of the dual drugs and the dual drug-loaded NPs at each ocular barrier [521]. NPs and the drugs will be studied for cell internalisation or cell uptake as this plays a crucial role in assessing bioavailability (nanoparticle uptake by cells is related to the drug concentration) [522]. With these findings, the dual therapy NPs will be investigated to establish their stability and change in characteristics in physiologically related solutions such as, simulated tear fluid, vitreous humor, aqueous humor, FBS, etc. These studies will give important information about the safety assessment of NPs in the eye as it has been reported that NPs can be altered in some physiological conditions and cause adverse effects [523].

6.2 Cellular uptake and quantification of internalised nanoparticles

The cell internalization capability of the optimized formulations will be investigated using coumarin-6 as a fluorescent dye with confocal microscopy (to view the resultant images). Briefly, the cultured cell lines will be incubated with fluorescent dye loaded NPs and solutions

of dye. After incubation, cells will be washed and fixed with paraformaldehyde for examination under a fluorescent microscope [524]. For the quantification of internalised NPs, the cells are lysed with triton x-100 to release the internalised NPs and further quantified using HPLC [525].

A preliminary study was performed to investigate the cell internalisation of the drugs alone and in combination (Table 6.1). The ARPE19 cells were seeded at 15 x 10^4 density per well onto a six-well plate and incubated for a day to achieve 70-80% confluency. Upon which cells were incubated with TA (10 and 100 µM), QCN (5 and 20 µM) and higher concentrations in combination (TA 100 µM + QCN 20 µM) for 24 h. After the treatment time, the media on the cells was removed and cells were washed with PBS thrice. The cells were detached using trypsin and lysed to extract the drugs internalised. Ultimately the cell lysates were analysed using HPLC to determine the quantity of internalised drug.

Table 6.1: Quantification of the internalised TA, QCN and TA + QCN in the ARPE-19 cells.

Treatment		**Drug quantified in the cells (µMoles)**	**Drug quantified in the cell culture media (µMoles)**
µM	**µMoles**		
TA 10	TA 1.5 x 10^{-8}	9.2 x 10^{-9} (61%)	4.0 x 10^{-9} (27%)
TA 100	TA 1.5 x 10^{-7}	8.9 x 10^{-9} (6%)	8.0 x 10^{-8} (53%)
QCN 5	QCN 7.5 x 10^{-9}	4.0 x 10^{-9} (53%)	2.2 x 10^{-9} (29%)
QCN 20	QCN 3.0 x 10^{-8}	1.1 x 10^{-8} (37%)	1.4 x 10^{-8} (47%)
TA + QCN 100 + 20	TA + QCN 1.5 x 10^{-7} + 3.0 x 10^{-8}	TA + QCN 7.5 x 10^{-9} (5%) + 1.4 x 10^{-8} (47%)	TA + QCN 8.8 x 10^{-8} (59%) + 1.1 x 10^{-8} (37%)

Upon exposure of the drugs to ARPE-19 cells, TA was internalised at 10 and 100 µM concentrations by 61% and 6%, respectively. Around 60% of TA is not detected either in the cell culture media or inside the cells, further investigation needs to be carried out to establish the fate of the drug. QCN was internalised at 5 and 20 µM by 53% and 37%, respectively and the QCN uptake was increased by 10% when treated in combination with TA. In this study, treatments were incubated for 24 h, in future studies extended incubation can give a better idea of the drugs residence time inside the cells. Microscopic observations of the treated ARPE-19 cells showed no changed in the morphology and no floating dead cells were identified. The

drugs cell internalisation capability will enhance the bioavailability and permeation in *in-vivo* conditions [522].

6.3 Future permeation studies

6.3.1 Permeability of nanoparticles through an ocular monolayer

A monolayer of HCECs and ARPE-19 cells with tight junctions will be cultured on trans wells, which will have apical and basal compartments. The integrity of the corneal and retinal epithelial monolayers will be checked with a voltage meter by measuring transepithelial electrical resistance (TEER). At specific time intervals, the samples will be withdrawn from the basal compartment and quantified using HPLC to assess the permeated drug [526]. The TEER will also be monitored at those time points to investigate the permeation enhancing ability of surface-modified NPs compared to non-coated NPs [527].

6.3.2 *Ex-vivo* permeation of nanoparticles

Ex-vivo permeation experiments will be performed on porcine eyes as they are a validated model for human eyes and the isolation of cornea and sclera with retina can be easily done in the lab [528]. These excised tissues will be mounted on Franz diffusion cells with the drugs and nanoparticles loaded in the donor chamber. The drugs released into the release media in the receiver chamber will be quantified using the established HPLC method.

6.4 Stability of the nanoparticles

The stability and sterilisation techniques of the dual drug-loaded NPs in freeze dried form needs to be investigated to suggest better storage conditions. Upon identifying suitable storage conditions, stability in physiological conditions was suggested. NPs can be incubated in simulated fluids such as, tear fluid, lachrymal fluid, aqueous humor, vitreous humor, FBS, the media containing enzymes/proteins present *in-vivo* conditions, etc [325,529]. Upon incubation characteristics of the NPs such as, particle size, PDI, ZP and encapsulation efficiency can be monitored using DLS and HPLC.

6.5 Conclusions

In chapters 2, 3, 4, and 5, a new drug combination was identified as a potential treatment for AMD and encapsulated into PLGA and surface-modified PLGA NPs to enhance the permeation of the particles through ocular barriers and to control the drugs release. The suggested future work will give a better understanding of bioavailability and if therapeutically

enough concentration can reach to the back of the eye when applied topically. Through the stability studies performed in physiological solutions and fluids, the potential adverse effects of the NPs or change in the particles characteristics can be uncovered before proceeding to future animal studies.

References

[1] C. van de Pol, Basic anatomy and physiology of the human visual system, (2014).

[2] E. Morley, E. Morley, Blindness and Vision, Iris Murdoch Elias Canetti. (2018) 15–60. https://doi.org/10.4324/9781351191791-2.

[3] European Commission, Population structure and ageing, Eurostat. (2023) 1–10. https://ec.europa.eu/eurostat/statistics-explained/index.php?title=Population_structure_and_ageing#The_share_of_elderly_people_continues_to_increase.

[4] U.N. Das, Diabetic macular edema, retinopathy and age-related macular degeneration as inflammatory conditions, Arch. Med. Sci. (2016). https://doi.org/10.5114/aoms.2016.61918.

[5] W.S. Cheng, D.W. Lu, C.H. Chiang, C.J. Chang, Overview of clinical trials for dry age-related macular degeneration, J. Med. Sci. (2017). https://doi.org/10.4103/jmedsci.jmedsci_115_16.

[6] J.Q. Li, T. Welchowski, M. Schmid, M.M. Mauschitz, F.G. Holz, R.P. Finger, Prevalence and incidence of age-related macular degeneration in Europe: a systematic review and meta-analysis, Br. J. Ophthalmol. 104 (2020) 1077–1084. https://doi.org/10.1136/bjophthalmol-2019-314422.

[7] A.C. Pedrosa, T. Sousa, J. Pinheiro-Costa, J. Beato, M.S. Falcão, F. Falcão-Reis, A. Carneiro, Treatment of neovascular age-related macular degeneration with anti-VEGF agents: Predictive factors of long-term visual outcomes, J. Ophthalmol. 2017 (2017). https://doi.org/10.1155/2017/4263017.

[8] A. Miller, M.A. Wilneff, A. Yazji, E. Petrinec, M. Carbone, C. Miller, C. McCrossin, R. Donkor, D.G. Miller, Analysis of urgent follow up visits and complications after intravitreal injections: a retrospective cohort study, Int. J. Retin. Vitr. 8 (n.d.) 8. https://doi.org/10.1186/s40942-021-00358-w.

[9] S. Day, K. Acquah, P. Mruthyunjaya, D.S. Grossman, P.P. Lee, F.A. Sloan, Ocular complications after antivascular endothelial growth factor therapy in medicare patients with age-related macular degeneration, Am. J. Ophthalmol. (2011). https://doi.org/10.1016/j.ajo.2011.01.053.

[10] J.B. Fileta, I.U. Scott, H.W. Flynn, Meta-analysis of infectious endophthalmitis after intravitreal injection of anti-vascular endothelial growth factor agents, Ophthalmic Surg. Lasers Imaging Retin. (2014). https://doi.org/10.3928/23258160-20140306-08.

[11] A. Sternfeld, R. Ehrlich, D. Weinberger, A. Dotan, Effect of different lens status on intraocular pressure elevation in patients treated with anti-vascular endothelial growth factor injections, Int. J. Ophthalmol. 13 (2020) 79–84. https://doi.org/10.18240/ijo.2020.01.12.

[12] A. Obeid, X. Gao, F.S. Ali, C.M. Aderman, A. Shahlaee, M.K. Adam, S.K. Kasi, L. Hyman, A.C. Ho, J. Hsu, Loss to Follow-up among Patients with Neovascular Age-Related Macular Degeneration Who Received Intravitreal Anti-Vascular Endothelial Growth Factor Injections, JAMA Ophthalmol. 136 (2018) 1251–1259. https://doi.org/10.1001/jamaophthalmol.2018.3578.

[13] K.M. Droege, P.S. Muether, M.M. Hermann, A. Caramoy, U. Viebahn, B. Kirchhof, S. Fauser, Adherence to ranibizumab treatment for neovascular age-related macular degeneration in real life, Graefe's Arch. Clin. Exp. Ophthalmol. (2013). https://doi.org/10.1007/s00417-012-2177-3.

[14] Y. Ge, A. Zhang, R. Sun, J. Xu, T. Yin, H. He, J. Gou, J. Kong, Y. Zhang, X. Tang, Penetratin-

modified lutein nanoemulsion in-situ gel for the treatment of age-related macular degeneration, Expert Opin. Drug Deliv. (2020). https://doi.org/10.1080/17425247.2020.1735348.

[15] J. Yan, X. Peng, Y. Cai, W. Cong, Development of facile drug delivery platform of ranibizumab fabricated PLGA-PEGylated magnetic nanoparticles for age-related macular degeneration therapy, J. Photochem. Photobiol. B Biol. (2018). https://doi.org/10.1016/j.jphotobiol.2018.04.033.

[16] J.H. Jung, B. Chiang, H.E. Grossniklaus, M.R. Prausnitz, Ocular drug delivery targeted by iontophoresis in the suprachoroidal space using a microneedle, J Control Release. 277 (2018) 14–22. https://doi.org/10.1016/j.jconrel.2018.03.001.

[17] R. Bisht, J.K. Jaiswal, Y.-S. Chen, J. Jin, I.D. Rupenthal, Light-responsive in situ forming injectable implants for effective drug delivery to the posterior segment of the eye, Expert Opin. Drug Deliv. 13 (2016) 953–962. https://doi.org/10.1517/17425247.2016.1163334.

[18] Y. Yu, L.C. Lau, A.C. Lo, Y. Chau, Injectable Chemically Crosslinked Hydrogel for the Controlled Release of Bevacizumab in Vitreous: A 6-Month In Vivo Study, Transl Vis Sci Technol. 4 (2015) 5. https://doi.org/10.1167/tvst.4.2.5.

[19] Z. Shi, S.K. Li, P. Charoenputtakun, C.Y. Liu, D. Jasinski, P. Guo, RNA nanoparticle distribution and clearance in the eye after subconjunctival injection with and without thermosensitive hydrogels, J Control Release. 270 (2018) 14–22. https://doi.org/10.1016/j.jconrel.2017.11.028.

[20] C. Huang, Adeno-associated virus-mediated expression of growth-associated protein-43 aggravates retinal ganglion cell death in experimental chronic glaucomatous injury, Mol. Vis. 19 (2013) 1422–1432.

[21] A.K. Mitra, Ocular transporters and receptors: Their role in drug delivery, 2013. https://doi.org/10.1533/9781908818317.

[22] K. Cholkar, A. Patel, A.D. Vadlapudi, A.K. Mitra, Novel Nanomicellar Formulation Approaches for Anterior and Posterior Novel Nanomicellar Formulation Approaches for Anterior and Posterior Segment Ocular Drug Delivery, (2012). https://doi.org/10.2174/1877912311202020082.

[23] WHO, Blindness And Vision Impairment Prevention, (2019) 22–24. https://www.who.int/news-room/fact-sheets/detail/blindness-and-visual-impairment.

[24] E. Ünsal, K. Eltutar, İ.K. Muftuoglu, Morphologic changes in the anterior segment using ultrasound biomicroscopy after cataract surgery and intraocular lens implantation, Eur. J. Ophthalmol. (2017). https://doi.org/10.5301/ejo.5000812.

[25] Q. Fu, Z. Mo, D. Lyu, L. Zhang, Z. Qin, Q. Tang, H. Yin, P. Xu, L. Wu, X. Lou, Z. Chen, K. Yao, Air pollution and outpatient visits for conjunctivitis: A case-crossover study in Hangzhou, China, Environ. Pollut. (2017). https://doi.org/10.1016/j.envpol.2017.08.109.

[26] J. Vehof, N. Sillevis Smitt-Kamminga, S.A. Nibourg, C.J. Hammond, Predictors of Discordance between Symptoms and Signs in Dry Eye Disease, Ophthalmology. (2017). https://doi.org/10.1016/j.ophtha.2016.11.008.

[27] J. Randazzo, Orally Active Multi-Functional Antioxidants Delay Cataract Formation in Streptozotocin (Type 1) Diabetic and Gamma-Irradiated Rats, PLoS One. 6 (2011). https://doi.org/10.1371/journal.pone.0018980.g001.

[28] L. Lee, F. D'Esposito, J. Garap, G. Wabulembo, S.P. Koim, D. Keys, A.T. Cama, H. Limburg, A. Burnett, Rapid assessment of avoidable blindness in Papua New Guinea: A nationwide survey, Br. J. Ophthalmol. (2019). https://doi.org/10.1136/bjophthalmol-2017-311802.

[29] B. Srilatha, A Review on Age Related Eye Diseases and their Preventive Measures, J. Clin. Exp. Ophthalmol. 2 (2011). https://doi.org/10.4172/21559570.1000196.

[30] K.K. Nichols, G.N. Foulks, A.J. Bron, B.J. Glasgow, M. Dogru, K. Tsubota, M.A. Lemp, D.A. Sullivan, The international workshop on meibomian gland dysfunction: Executive summary, Investig. Ophthalmol. Vis. Sci. (2011). https://doi.org/10.1167/iovs.10-6997a.

[31] M.T.M. Wang, A. Muntz, J. Lim, J.S. Kim, L. Lacerda, A. Arora, J.P. Craig, Ageing and the natural history of dry eye disease: A prospective registry-based cross-sectional study, Ocul. Surf. (2020). https://doi.org/10.1016/j.jtos.2020.07.003.

[32] M.A. Lemp, L.A. Crews, A.J. Bron, G.N. Foulks, B.D. Sullivan, Distribution of aqueous-deficient and evaporative dry eye in a clinic-based patient cohort: A retrospective study, Cornea. (2012). https://doi.org/10.1097/ICO.0b013e318225415a.

[33] Y. Wei, P.A. Asbell, The core mechanism of dry eye disease is inflammation, Eye Contact Lens. (2014). https://doi.org/10.1097/ICL.0000000000000042.

[34] M. Brill, Spontaneous eye blinks as an alternative measure for spatial presence experiences, University of Wuerzburg, 2019. https://www.researchgate.net/publication/333994733_Spontaneous_eye_blinks_as_an_alternative_measure_for_spatial_presence_experiences.

[35] B.W. Jones, R.L. Pfeiffer, W.D. Ferrell, C.B. Watt, M. Marmor, R.E. Marc, Retinal remodeling in human retinitis pigmentosa, Exp. Eye Res. (2016). https://doi.org/10.1016/j.exer.2016.03.018.

[36] S. Nakakura, Y. Kobayashi, K. Matsuya, E. Terao, Y. Kiuchi, Iris thickness and severity of neovascular glaucoma determined using swept-source anterior-segment optical coherence tomography, J. Glaucoma. (2018). https://doi.org/10.1097/IJG.0000000000000921.

[37] A. Das, P.G. McGuire, S. Rangasamy, Diabetic Macular Edema: Pathophysiology and Novel Therapeutic Targets, Ophthalmology. (2015). https://doi.org/10.1016/j.ophtha.2015.03.024.

[38] M.M. Nentwich, Diabetic retinopathy - ocular complications of diabetes mellitus, World J. Diabetes. (2015). https://doi.org/10.4239/wjd.v6.i3.489.

[39] E.K. De Jong, M.J. Geerlings, A.I. Den Hollander, Age-related macular degeneration, Genetics and Genomics of Eye Disease, (2020) 155–180. https://doi.org/10.1016/B978-0-12-816222-4.00010-1.

[40] R.N. Weinreb, T. Aung, F.A. Medeiros, The pathophysiology and treatment of glaucoma: a review, JAMA. 311 (2014) 1901–1911. https://doi.org/10.1001/jama.2014.3192.

[41] V. Krishnaswami, R. Kandasamy, S. Alagarsamy, R. Palanisamy, S. Natesan, Biological macromolecules for ophthalmic drug delivery to treat ocular diseases, Int J Biol Macromol. 110 (2018) 7–16. https://doi.org/10.1016/j.ijbiomac.2018.01.120.

[42] Y. Shan, Y. Xu, X. Lin, L. Lou, Y. Wang, J. Ye, Burden of vision loss due to diabetic retinopathy in China from 1990 to 2017: findings from the global burden of disease study, Acta Ophthalmol. (2020). https://doi.org/10.1111/aos.14573.

[43] D.S. Fong, L.P. Aiello, F.L. Ferris, R. Klein, Diabetic retinopathy, Diabetes Care. (2004). https://doi.org/10.2337/diacare.27.10.2540.

[44] N. Ban, T.J. Lee, A. Sene, M. Choudhary, M. Lekwuwa, Z. Dong, A. Santeford, J.B. Lin, G. Malek, D.S. Ory, R.S. Apte, Impaired monocyte cholesterol clearance initiates age-related retinal degeneration and vision loss, JCI Insight. (2018). https://doi.org/10.1172/jci.insight.120824.

[45] World Health Organization, World report on vision, 2019.

[46] P. Mitchell, G. Liew, B. Gopinath, T.Y. Wong, Age-related macular degeneration, Lancet. (2018). https://doi.org/10.1016/S0140-6736(18)31550-2.

[47] A. Bhuiyan, A Review of Disease Grading and Remote Diagnosis for Sight Threatening Eye Condition: Age Related Macular Degeneration, J. Comput. Sci. Syst. Biol. (2014). https://doi.org/10.4172/jcsb.1000139.

[48] D.J. Taylor, L. Jones, A.M. Binns, D.P. Crabb, 'You've got dry macular degeneration, end of story': a qualitative study into the experience of living with non-neovascular age-related macular degeneration, Eye. (2020). https://doi.org/10.1038/s41433-019-0445-8.

[49] D.G. Birch, Age-related macular degeneration: a target for nanotechnology derived medicines, Int. J. Nanomedicine. 2 (2007) 65–77.

[50] N. Ferrara, Vascular endothelial growth factor and age-related macular degeneration: From basic science to therapy, Nat. Med. 16 (2010) 1107–1111. https://doi.org/10.1038/nm1010-1107.

[51] M. N, Routes of Oxidative Stress in Age-Related Macular Degeneration, Int. J. Ophthalmol. Clin. Res. (2016). https://doi.org/10.23937/2378-346x/1410049.

[52] T.A. Eye, AREDS Report No. 8, Arch Ophthalmol. 119 (2001) 1417–1436.

[53] M. Xu, R. Fan, X. Fan, Y. Shao, X. Li, Progress and Challenges of Anti-VEGF Agents and Their Sustained-Release Strategies for Retinal Angiogenesis, Drug Des. Devel. Ther. 16 (2022) 3241–3262. https://doi.org/10.2147/DDDT.S383101.

[54] H.A. Khaqan, T. Khan, H. Tayyab, T.K. Marwat, M.Q. Lateef, H.A. Khaqan, Complications VEGF Injections at Multiple Centers Observing Different Protocols, 35 (2019) 1–6.

[55] X. Gao, A. Obeid, C.M. Aderman, K.E. Talcott, F.S. Ali, M.K. Adam, B.W. Rovner, L. Hyman, A.C. Ho, J. Hsu, Loss to Follow-up After Intravitreal Anti–Vascular Endothelial Growth Factor Injections in Patients with Diabetic Macular Edema, Ophthalmol. Retin. (2019). https://doi.org/10.1016/j.oret.2018.11.002.

[56] G. Xin, M. Zhang, Z. Zhong, L. Tang, Y. Feng, Z. Wei, S. Li, Y. Li, J. Zhang, B. Zhang, M. Zhang, N. Rowell, Z. Chen, H. Niu, K. Yu, W. Huang, Ophthalmic Drops with Nanoparticles Derived from a Natural Product for Treating Age-Related Macular Degeneration, ACS Appl. Mater. Interfaces. (2020). https://doi.org/10.1021/acsami.0c17296.

[57] G. Adamus, Are anti-retinal autoantibodies a cause or a consequence of retinal degeneration in autoimmune retinopathies?, Front. Immunol. (2018). https://doi.org/10.3389/fimmu.2018.00765.

[58] R.S. Sulaiman, M. Kadmiel, J.A. Cidlowski, Glucocorticoid receptor signaling in the eye, Steroids. 133 (2018) 60–66. https://doi.org/10.1016/j.steroids.2017.11.002.

[59] D.A. Copland, S. Theodoropoulou, J. Liu, A.D. Dick, A perspective of AMD through the eyes of immunology, Investig. Ophthalmol. Vis. Sci. (2018). https://doi.org/10.1167/iovs.18-23893.

[60] K. Jiang, E. To, J. Z. Cui, S. Cao, Drusen and Pro-inflammatory Mediators in the Post-Mortem

Human Eye, J. Clin. Exp. Ophthalmol. (2012). https://doi.org/10.4172/2155-9570.1000208.

[61] V. Behnke, A. Wolf, T. Langmann, The role of lymphocytes and phagocytes in age-related macular degeneration (AMD), Cell. Mol. Life Sci. (2020). https://doi.org/10.1007/s00018-019-03419-4.

[62] J.C. ten Berge, Z. Fazil, I. van den Born, R.C.W. Wolfs, M.W.J. Schreurs, W.A. Dik, A. Rothova, Intraocular cytokine profile and autoimmune reactions in retinitis pigmentosa, age-related macular degeneration, glaucoma and cataract, Acta Ophthalmol. (2019). https://doi.org/10.1111/aos.13899.

[63] K. Morohoshi, A.M. Goodwin, M. Ohbayashi, S.J. Ono, Autoimmunity in retinal degeneration: autoimmune retinopathy and age-related macular degeneration, J Autoimmun. 33 (2009) 247–254. https://doi.org/10.1016/j.jaut.2009.09.003.

[64] J.A. Olson, E.H. Steffensen, R.W. Smith, R.R. Margulis, E.L. Whitney, Use of adrenocorticotropic hormone and cortisone in ocular disease, AMA. Arch. Ophthalmol. (1951). https://doi.org/10.1001/archopht.1951.01700010280004.

[65] L.I. Mckay, J.A. Cidlowski, Physiologic and Pharmacologic Effects of Corticosteroids, Holland-Frei Cancer Med. (2003).

[66] R. Machemer, G. Sugita, Y. Tano, Treatment of intraocular proliferations with intravitreal steroids, Trans. Am. Ophthalmol. Soc. (1979).

[67] J. Vandewalle, A. Luypaert, K. De Bosscher, C. Libert, Therapeutic Mechanisms of Glucocorticoids, Trends Endocrinol. Metab. (2018). https://doi.org/10.1016/j.tem.2017.10.010.

[68] S.M. Whitcup, J.A. Cidlowski, K.G. Csaky, J. Ambati, Pharmacology of corticosteroids for diabetic macular edema, Investig. Ophthalmol. Vis. Sci. (2018). https://doi.org/10.1167/iovs.17-22259.

[69] K. Papangkorn, E. Prendergast, J.W. Higuchi, B. Brar, W.I. Higuchi, Noninvasive Ocular Drug Delivery System of Dexamethasone Sodium Phosphate in the Treatment of Experimental Uveitis Rabbit, J. Ocul. Pharmacol. Ther. (2017). https://doi.org/10.1089/jop.2017.0053.

[70] V.S. Sangwan, P.A. Pearson, H. Paul, T.L. Comstock, Use of the Fluocinolone Acetonide Intravitreal Implant for the Treatment of Noninfectious Posterior Uveitis: 3-Year Results of a Randomized Clinical Trial in a Predominantly Asian Population, Ophthalmol. Ther. (2015). https://doi.org/10.1007/s40123-014-0027-6.

[71] S.A. Gaballa, U.B. Kompella, O. Elgarhy, A.M. Alqahtani, B. Pierscionek, R.G. Alany, H. Abdelkader, Corticosteroids in ophthalmology: drug delivery innovations, pharmacology, clinical applications, and future perspectives, Drug Deliv. Transl. Res. (2020). https://doi.org/10.1007/s13346-020-00843-z.

[72] J.B. Jonas, ntravitreal triamcinolone acetonide for exudative age related macular degeneration, Br J Ophthalmol. 87 (2003) 462–468.

[73] Pei-Qiang Huang, Efficiency in Natural Product Total Synthesis, Wiley, 2018. https://www.wiley.com/en-ie/Efficiency+in+Natural+Product+Total+Synthesis-p-9781118605400.

[74] M.C. Wani, H.L. Taylor, M.E. Wall, P. Coggon, A.T. Mcphail, Plant Antitumor Agents.VI.The Isolation and Structure of Taxol, a Novel Antileukemic and Antitumor Agent from Taxus brevifolia2, J. Am. Chem. Soc. (1971). https://doi.org/10.1021/ja00738a045.

[75] E. Chain, The early years of the penicillin discovery, Trends Pharmacol. Sci. (1979). https://doi.org/10.1016/0165-6147(79)90004-X.

[76] B.D. Kahan, Cyclosporine: The agent and its actions, Transplant. Proc. (1985).

[77] E. Kellenberger, A. Hofmann, R.J. Quinn, Similar interactions of natural products with biosynthetic enzymes and therapeutic targets could explain why nature produces such a large proportion of existing drugs, Nat. Prod. Rep. (2011). https://doi.org/10.1039/c1np00026h.

[78] A. Francisco, J. B. HARBORNE (ED.) The flavonoids–Advances in research since 1986 Chapman & Hall, London, U.K. 1994, £195.00, 676 pp. ISBN 0-412-48070-0, Phytochem. Anal. (1995). https://doi.org/10.1002/pca.2800060109.

[79] M. Lesjak, I. Beara, N. Simin, D. Pintać, T. Majkić, K. Bekvalac, D. Orčić, N. Mimica-Dukić, Antioxidant and anti-inflammatory activities of quercetin and its derivatives, J. Funct. Foods. (2018). https://doi.org/10.1016/j.jff.2017.10.047.

[80] F. Li, Y. Bai, M. Zhao, L. Huang, S. Li, X. Li, Y. Chen, Quercetin inhibits vascular endothelial growth factor-induced choroidal and retinal angiogenesis in vitro, Ophthalmic Res. (2015). https://doi.org/10.1159/000369824.

[81] M. Lee, S. Yun, H. Lee, J. Yang, Quercetin mitigates inflammatory responses induced by vascular endothelial growth factor in mouse retinal photoreceptor cells through suppression of nuclear factor Kappa B, Int. J. Mol. Sci. (2017). https://doi.org/10.3390/ijms18112497.

[82] P. Zhuang, Y. Shen, B.Q. i. Lin, W.Y. u. Zhang, G.C.Y. Chiou, Effect of quercetin on formation of choroidal neovascularization (CNV) in age-related macular degeneration(AMD), Eye Sci. (2011). https://doi.org/10.3969/j.issn.1000-4432.2011.01.006.

[83] Y. Wang, L. Zhao, C. Wang, J. Hu, X. Guo, D. Zhang, W. Wu, F. Zhou, B. Ji, Protective effect of quercetin and chlorogenic acid, two polyphenols widely present in edible plant varieties, on visible light-induced retinal degeneration in vivo, J. Funct. Foods. (2017). https://doi.org/10.1016/j.jff.2017.02.034.

[84] M.C. Foti, R. Amorati, A. Baschieri, C. Rocco, Singlet oxygen quenching- and chain-breaking antioxidant-properties of a quercetin dimer able to prevent age-related macular degeneration, Biophys. Chem. (2018). https://doi.org/10.1016/j.bpc.2018.10.001.

[85] Y. Chen, X. xin Li, N. zeng Xing, X. guang Cao, Quercetin inhibits choroidal and retinal angiogenesis in vitro, Graefe's Arch. Clin. Exp. Ophthalmol. (2008). https://doi.org/10.1007/s00417-007-0728-9.

[86] T.B. McKay, D. Lyon, A. Sarker-Nag, S. Priyadarsini, J.M. Asara, D. Karamichos, Quercetin Attenuates Lactate Production and Extracellular Matrix Secretion in Keratoconus, Sci. Rep. (2015). https://doi.org/10.1038/srep09003.

[87] L. Jia, S. Huang, X. Yin, Y. Zan, Y. Guo, L. Han, Quercetin suppresses the mobility of breast cancer by suppressing glycolysis through Akt-mTOR pathway mediated autophagy induction, Life Sci. (2018). https://doi.org/10.1016/j.lfs.2018.07.027.

[88] G.L. Russo, M. Russo, C. Spagnuolo, The pleiotropic flavonoid quercetin: From its metabolism to the inhibition of protein kinases in chronic lymphocytic leukemia, Food Funct. (2014). https://doi.org/10.1039/c4fo00413b.

[89] K. Gupta, D. Panda, Perturbation of microtubule polymerization by quercetin through tubulin binding: A novel mechanism of its antiproliferative activity, Biochemistry. (2002). https://doi.org/10.1021/bi025952r.

[90] Y. Kong, K. Li, T. Fu, C. Wan, D. Zhang, H. Song, Y. Zhang, N. Liu, Z. Gan, L. Yuan, Quercetin ameliorates Aβ toxicity in Drosophila AD model by modulating cell cycle-related protein expression, Oncotarget. (2016). https://doi.org/10.18632/ONCOTARGET.11963.

[91] D.L. Li, L. Mao, Q. Gu, F. Wei, Y.Y. Gong, Quercetin protects retina external barrier from oxidative stress injury by promoting autophagy, Cutan. Ocul. Toxicol. (2020). https://doi.org/10.1080/15569527.2020.1860082.

[92] V.K. Yellepeddi, S. Palakurthi, Recent Advances in Topical Ocular Drug Delivery, J. Ocul. Pharmacol. Ther. (2016). https://doi.org/10.1089/jop.2015.0047.

[93] J. V. Forrester, A.D. Dick, P.G. McMenamin, F. Roberts, E. Pearlman, J. V. Forrester, A.D. Dick, P.G. McMenamin, F. Roberts, E. Pearlman, General and ocular pharmacology, Eye. (2016) 338-369.e1. https://doi.org/10.1016/B978-0-7020-5554-6.00006-X.

[94] C.Y. Chen, T.Y. Wong, W.J. Heriot, Intravitreal Bevacizumab (Avastin) for Neovascular Age-related Macular Degeneration: A Short-term Study, Am. J. Ophthalmol. (2007). https://doi.org/10.1016/j.ajo.2006.10.004.

[95] H.A. Leder, D.A. Jabs, A. Galor, J.P. Dunn, J.E. Thorne, Periocular triamcinolone acetonide injections for cystoid macular edema complicating noninfectious uveitis, Am. J. Ophthalmol. (2011). https://doi.org/10.1016/j.ajo.2011.02.009.

[96] Fluocinolone acetonide ophthalmic - Bausch & Lomb: Fluocinolone acetonide envision TD implant, Drugs R D. (2005). https://doi.org/10.2165/00126839-200506020-00007.

[97] C.H. Tsai, P.Y. Wang, I.C. Lin, H. Huang, G.S. Liu, C.L. Tseng, Ocular Drug Delivery: Role of Degradable Polymeric Nanocarriers for Ophthalmic Application, Int J Mol Sci. 19 (2018). https://doi.org/10.3390/ijms19092830.

[98] J.C. Lang, Ocular drug delivery conventional ocular formulations, Adv. Drug Deliv. Rev. (1995). https://doi.org/10.1016/0169-409X(95)00012-V.

[99] J. Araújo, E. Gonzalez, M.A. Egea, M.L. Garcia, E.B. Souto, Nanomedicines for ocular NSAIDs: safety on drug delivery, Nanomedicine Nanotechnology, Biol. Med. (2009). https://doi.org/10.1016/j.nano.2009.02.003.

[100] J. Alvarez-Trabado, Y. Diebold, A. Sanchez, Designing lipid nanoparticles for topical ocular drug delivery, Int J Pharm. 532 (2017) 204–217. https://doi.org/10.1016/j.ijpharm.2017.09.017.

[101] G.A. Rodrigues, D. Lutz, J. Shen, X. Yuan, H. Shen, J. Cunningham, H.M. Rivers, Topical Drug Delivery to the Posterior Segment of the Eye: Addressing the Challenge of Preclinical to Clinical Translation, Pharm. Res. 35 (2018). https://doi.org/10.1007/s11095-018-2519-x.

[102] C. Bucolo, F. Drago, S. Salomone, Ocular drug delivery: a clue from nanotechnology, Front Pharmacol. 3 (2012) 188. https://doi.org/10.3389/fphar.2012.00188.

[103] A. Subrizi, E.M. del Amo, V. Korzhikov-Vlakh, T. Tennikova, M. Ruponen, A. Urtti, Design principles of ocular drug delivery systems: importance of drug payload, release rate, and material properties, Drug Discov. Today. (2019). https://doi.org/10.1016/j.drudis.2019.02.001.

[104] N. Djebli, S. Khier, F. Griguer, A.L. Coutant, A. Tavernier, G. Fabre, C. Leriche, D. Fabre, Ocular Drug Distribution After Topical Administration: Population Pharmacokinetic Model in Rabbits, Eur. J. Drug Metab. Pharmacokinet. (2017). https://doi.org/10.1007/s13318-016-0319-4.

[105] Y. Shirasaki, Molecular Design for Enhancement of Ocular Penetration, J. Pharm. Sci. 97

(2008) 2462–2496. https://doi.org/https://doi.org/10.1002/jps.21200.

[106] A.J. Bron, J.M. Tiffany, S.M. Gouveia, N. Yokoi, L.W. Voon, Functional aspects of the tear film lipid layer, Exp. Eye Res. 78 (2004) 347–360. https://doi.org/https://doi.org/10.1016/j.exer.2003.09.019.

[107] C.E. Willoughby, D. Ponzin, S. Ferrari, A. Lobo, K. Landau, Y. Omidi, Anatomy and physiology of the human eye: effects of mucopolysaccharidoses disease on structure and function - a review, Clin. Experiment. Ophthalmol. 38 (2010) 2–11. https://doi.org/10.1111/j.1442-9071.2010.02363.x.

[108] O.P. Sharma, V. Patel, T. Mehta, Nanocrystal for ocular drug delivery: hope or hype, Drug Deliv. Transl. Res. (2016). https://doi.org/10.1007/s13346-016-0292-0.

[109] A. Edwards, M.R. Prausnitz, Predicted permeability of the cornea to topical drugs, Pharm. Res. (2001). https://doi.org/10.1023/A:1013061926851.

[110] J. Ban, Y. Zhang, X. Huang, G. Deng, D. Hou, Y. Chen, Z. lu, Corneal permeation properties of a charged lipid nanoparticle carrier containing dexamethasone, Int. J. Nanomedicine. (2017). https://doi.org/10.2147/IJN.S126199.

[111] J. Liaw, Y. Rojanasakul, J.R. Robinson, The effect of drug charge type and charge density on corneal transport, Int. J. Pharm. (1992). https://doi.org/10.1016/0378-5173(92)90308-O.

[112] P. Nirbhavane, G. Sharma, B. Singh, G. Begum, M.C. Jones, S. Rauz, R. Vincent, A.K. Denniston, L.J. Hill, O.P. Katare, Triamcinolone acetonide loaded-cationic nano-lipoidal formulation for uveitis: Evidences of improved biopharmaceutical performance and anti-inflammatory activity, Colloids Surfaces B Biointerfaces. (2020). https://doi.org/10.1016/j.colsurfb.2020.110902.

[113] N.A. Abdul Nasir, P. Agarwal, R. Agarwal, I. Iezhitsa, R. Alyautdin, N.N. Nukolova, V.P. Chekhonin, N. Mohd Ismail, Intraocular distribution of topically applied hydrophilic and lipophilic substances in rat eyes, Drug Deliv. (2016). https://doi.org/10.3109/10717544.2015.1077292.

[114] E.D. Donnenfeld, T.L. Comstock, J.W. Proksch, Human aqueous humor concentrations of besifloxacin, moxifloxacin, and gatifloxacin after topical ocular application, J. Cataract Refract. Surg. (2011). https://doi.org/10.1016/j.jcrs.2010.12.046.

[115] J.L. Chung, E.H. Lim, S.W. Song, B.Y. Kim, J.H. Lee, F.S. Mah, K.Y. Seo, Comparative intraocular penetration of 4 fluoroquinolones after topical instillation, Cornea. (2013). https://doi.org/10.1097/ICO.0b013e31828d6d9e.

[116] D. Huang, Y.S. Chen, I.D. Rupenthal, Overcoming ocular drug delivery barriers through the use of physical forces, Adv Drug Deliv Rev. 126 (2018) 96–112. https://doi.org/10.1016/j.addr.2017.09.008.

[117] E. Ramsay, M. Ruponen, T. Picardat, U. Tengvall, M. Tuomainen, S. Auriola, E. Toropainen, A. Urtti, E.M. del Amo, Impact of Chemical Structure on Conjunctival Drug Permeability: Adopting Porcine Conjunctiva and Cassette Dosing for Construction of In Silico Model, J. Pharm. Sci. (2017). https://doi.org/10.1016/j.xphs.2017.04.061.

[118] S.J. Lee, W. He, S.B. Robinson, M.R. Robinson, K.G. Csaky, H. Kim, Evaluation of clearance mechanisms with transscleral drug delivery, Investig. Ophthalmol. Vis. Sci. (2010). https://doi.org/10.1167/iovs.10-5337.

[119] L. Rodriguez-Peralta, The blood-aqueous barrier in five species, Am. J. Ophthalmol. (1975).

https://doi.org/10.1016/0002-9394(75)90405-5.

[120] R.T. Addo, Ocular drug delivery: Advances, challenges and applications, 2016. https://doi.org/10.1007/978-3-319-47691-9.

[121] N.P.S. Cheruvu, U.B. Kompella, Bovine and porcine transscleral solute transport: Influence of lipophilicity and the choroid-Bruch's layer, Investig. Ophthalmol. Vis. Sci. (2006). https://doi.org/10.1167/iovs.06-0404.

[122] J. Ambati, C.S. Canakis, J.W. Miller, E.S. Gragoudas, A. Edwards, D.J. Weissgold, I. Kim, F.C. Delori, A.P. Adamis, Diffusion of high molecular weight compounds through sclera, Investig. Ophthalmol. Vis. Sci. (2000).

[123] D.L. Nickla, J. Wallman, The multifunctional choroid, Prog. Retin. Eye Res. (2010). https://doi.org/10.1016/j.preteyeres.2009.12.002.

[124] R.S. Kadam, U.B. Kompella, Influence of lipophilicity on drug partitioning into sclera, choroid-retinal pigment epithelium, retina, trabecular meshwork, and optic nerve, J. Pharmacol. Exp. Ther. (2010). https://doi.org/10.1124/jpet.109.161570.

[125] E.M. Del Amo, A.K. Rimpela, E. Heikkinen, O.K. Kari, E. Ramsay, T. Lajunen, M. Schmitt, L. Pelkonen, M. Bhattacharya, D. Richardson, A. Subrizi, T. Turunen, M. Reinisalo, J. Itkonen, E. Toropainen, M. Casteleijn, H. Kidron, M. Antopolsky, K.S. Vellonen, M. Ruponen, A. Urtti, Pharmacokinetic aspects of retinal drug delivery, Prog Retin Eye Res. 57 (2017) 134–185. https://doi.org/10.1016/j.preteyeres.2016.12.001.

[126] M. Campbell, P. Humphries, The blood-retina barrier tight junctions and barrier modulation, Adv. Exp. Med. Biol. (2013). https://doi.org/10.1007/978-1-4614-4711-5_3.

[127] L. Pitkänen, V.P. Ranta, H. Moilanen, A. Urtti, Permeability of retinal pigment epithelium: Effects of permeant molecular weight and lipophilicity, Investig. Ophthalmol. Vis. Sci. (2005). https://doi.org/10.1167/iovs.04-1051.

[128] C.T. Supuran, Agents for the prevention and treatment of age-related macular degeneration and macular edema: a literature and patent review, Expert Opin. Ther. Pat. (2019). https://doi.org/10.1080/13543776.2019.1671353.

[129] M. Yuzawa, K. Fujita, K.U. Wittrup-Jensen, C. Norenberg, O. Zeitz, K. Adachi, E.C.Y. Wang, J. Heier, P. Kaiser, V. Chong, J.F. Korobelnik, Improvement in vision-related function with intravitreal aflibercept: Data from phase 3 studies in wet age-related macular degeneration, Ophthalmology. (2015). https://doi.org/10.1016/j.ophtha.2014.09.024.

[130] S.C. Böhni, M. Bittner, J.P. Howell, L.M. Bachmann, L. Faes, M.K. Schmid, Comparison of Eylea® with Lucentis® as first-line therapy in patients with treatment-naïve neovascular age-related macular degeneration in real-life clinical practice: Retrospective case-series analysis, BMC Ophthalmol. (2015). https://doi.org/10.1186/s12886-015-0101-4.

[131] A.J. Augustin, B.D. Kuppermann, P. Lanzetta, A. Loewenstein, X.Y. Li, H. Cui, Y. Hashad, S.M. Whitcup, S. Abujamra, J. Acton, F. Ali, A. Antoszyk, C.C. Awh, A. Barak, K.U. Bartz-Schmidt, C.R. Baumal, R. Belfort, M. Bhende, D.S. Boyer, W.Z. Bridges, D.M. Brown, T. Carmichael, K. Carnevale, A.M. Casella, T. Chang, D. Chechik, S.N. Chen, L.P. Chong, V. Chong, J. Corwin, C. Creuzot-Garcher, A. Cruess, M. Daniell, M.P. De Avila, H.V. De Moraes, R.G. Devenyi, B.H. Doft, M. Donaldson, R. Dreyer, D. Eliott, H.M. Engel, J. Ernest, T.F. Essman, P.M. Falcone, S. Fekrat, J.R. Ferencz, J.L. Ferreira, J. Figueira, I. Fiser, B. Foster, G.M. Fox, W.R. Freeman, S.P. Garg, M. Gillies, D. Glaser, B.G. Goldstein, A.M.V. Gomes, J.R. Gonder, L. Gopal, P. Gous, A. Gupta, A. Gupta, L. Halperin, D. Han, S.M. Hariprasad, F.G. Holz, P. Kaiser, B. Kalvodova, B.

Katz, R.S. Katz, D. Kecik, J. Kellaway, I. Klemperer, R. Lattanzio, W.K. Lee, J. Lehr, M. Leys, I. Loose, A. Lotery, D.W. Lu, P. McCartney, A.B. Majji, J.A. Martinez, P. Massin, R.K. Maturi, U. Menchini, G. Menon, M. Michels, E. Midena, J. Miller, P. Mitchell, J. Moisseiev, L. Morse, R. Navarro, J. Nemeth, H. Newland, R. Newsom, J. Nichols, J. Orellana, N. Orzalesi, A. Paranhos, R. Park, S. Park, M.B. Parodi, P.R. Pavan, J. Peace, D.J. Perez-Ortiz, A. Pollack, K. Ramaswamy, R. Ratnakaram, G. Ravalico, J. Rehak, K. Rezaei, S. Rizzo, F.J. Rodriguez-Alvira, J.P. Romanet, S. Rose, R.B. Rosen, L. Rossetti, J.M. Ruiz-Moreno, S.V. Sadda, K. Sall, D. Sandner, A.F.V. Sanz, G. Sartani, S. Schmickler, S.D. Schwartz, Y.R. Sharma, S.J. Sheu, M. Singer, S. Sivaprasad, G. Soubrane, P. Soucek, E.H. Souied, G. Staurenghi, J. Studnicka, M. Suarez-Figueroa, W.Y. Takahashi, D. Tognetto, P.L. Tsai, L.J. Ulanski, H.S. Uy, M. Varano, M. Veith, I. Vicha, F. Viola, L. Visser, D. Weinberger, G.L. Wing, E. Wong, T.Y. Wong, E. Wylegala, J. Yan, Y.H. Yoon, L.H. Young, H.G. Yu, I.E. Zimmer-Galler, Dexamethasone intravitreal implant in previously treated patients with diabetic macular edema: Subgroup analysis of the MEAD study, BMC Ophthalmol. (2015). https://doi.org/10.1186/s12886-015-0148-2.

[132] S.A. Horowitz, N.P. Damasceno, E.F. Damasceno, Treatment of radiation retinopathy with intravitreal injection of ranibizumab (Lucentis®), Int. Med. Case Rep. J. (2020). https://doi.org/10.2147/IMCRJ.S191654.

[133] S.R. Singh, M.W. Stewart, G. Chattannavar, M. Ashraf, A. Souka, M. ElDardeery, N. Wadhwa, C. Sarvaiya, A.M. Mansour, A. Marashi, S. Ramchandani, I.Z. Braimah, M.H.J. Bonyadi, A. Ramezani, M. Soheilian, J.R. De Oliveira Dias, G.C. De Andrade, A. Maia, E.B. Rodrigues, M.E. Farah, A. Banker, J. Chhablani, Safety of 5914 intravitreal ziv-aflibercept injections, Br. J. Ophthalmol. (2019). https://doi.org/10.1136/bjophthalmol-2018-312453.

[134] R. Neumann, D. Barequet, The gap between the need for novel retinal drug delivery methods, technologies in R&D phase, and approved ocular drug delivery technologies, Drug Discov. Today. (2019). https://doi.org/10.1016/j.drudis.2019.03.018.

[135] I. Kozak, O.R. Kayikcioglu, L. Cheng, I. Falkenstein, G.A. Silva, D.X. Yu, W.R. Freeman, The effect of recombinant human hyaluronidase on dexamethasone penetration into the posterior segment of the eye after sub-tenon's injection, J. Ocul. Pharmacol. Ther. (2006). https://doi.org/10.1089/jop.2006.22.362.

[136] R. Anker, N. Kaur, Regional anaesthesia for ophthalmic surgery, BJA Educ. (2017). https://doi.org/10.1093/bjaed/mkw078.

[137] C.W. Wong, B. Czarny, J.M. Metselaar, C. Ho, S.R. Ng, A.V. Barathi, G. Storm, T.T. Wong, Evaluation of subconjunctival liposomal steroids for the treatment of experimental uveitis, Sci. Rep. (2018). https://doi.org/10.1038/s41598-018-24545-2.

[138] P. Tyagi, R.S. Kadam, U.B. Kompella, Comparison of Suprachoroidal Drug Delivery with Subconjunctival and Intravitreal Routes Using Noninvasive Fluorophotometry, PLoS One. (2012). https://doi.org/10.1371/journal.pone.0048188.

[139] B. Bhushan, Introduction to nanotechnology, Springer Handbooks. (2017). https://doi.org/10.1007/978-3-662-54357-3_1.

[140] C. Li, R. Chen, M. Xu, J. Qiao, L. Yan, X.D. Guo, Hyaluronic acid modified MPEG-b-PAE block copolymer aqueous micelles for efficient ophthalmic drug delivery of hydrophobic genistein, Drug Deliv. 25 (2018) 1258–1265. https://doi.org/10.1080/10717544.2018.1474972.

[141] H.S.M. Ali, A stable hydrocortisone nanosuspension for improved dissolution: Preparation, characterization and in vitro evaluation, Pak. J. Pharm. Sci. 30 (2017) 1635–1643.

[142] G. Tan, S. Yu, H. Pan, J. Li, D. Liu, K. Yuan, X. Yang, W. Pan, Bioadhesive chitosan-loaded

liposomes: A more efficient and higher permeable ocular delivery platform for timolol maleate, Int J Biol Macromol. 94 (2017) 355–363. https://doi.org/10.1016/j.ijbiomac.2016.10.035.

[143] M. Lancina, Fast Dissolving Dendrimer Nanofiber (DNF) Mats as Alternative to Eye Drops for More Efficient Topical Antiglaucoma Drug Delivery, ACS Biomater. Sci. Eng. 3 (2017) 1861–1868.

[144] M.Y. Bin Sahadan, W.Y. Tong, W.N. Tan, C.R. Leong, M.N. Bin Misri, M. Chan, S.Y. Cheng, S. Shaharuddin, Phomopsidione nanoparticles coated contact lenses reduce microbial keratitis causing pathogens, Exp Eye Res. 178 (2018) 10–14. https://doi.org/10.1016/j.exer.2018.09.011.

[145] K. McAvoy, D. Jones, R.R.S. Thakur, Synthesis and Characterisation of Photocrosslinked poly(ethylene glycol) diacrylate Implants for Sustained Ocular Drug Delivery, Pharm Res. 35 (2018) 36. https://doi.org/10.1007/s11095-017-2298-9.

[146] J. Kreuter, Nanoparticles-a historical perspective, Int. J. Pharm. (2007). https://doi.org/10.1016/j.ijpharm.2006.10.021.

[147] R.C. Nagarwal, S. Kant, P.N. Singh, P. Maiti, J.K. Pandit, Polymeric nanoparticulate system: a potential approach for ocular drug delivery, J Control Release. 136 (2009) 2–13. https://doi.org/10.1016/j.jconrel.2008.12.018.

[148] Y. Bin Choy, W.M. Ryu, S.N. Kim, C.H. Min, Dry tablet formulation of plga nanoparticles with a preocular applicator for topical drug delivery to the eye, Pharmaceutics. (2019). https://doi.org/10.3390/pharmaceutics11120651.

[149] M. Singh, A. Guzman-Aranguez, A. Hussain, C.S. Srinivas, I.P. Kaur, Solid lipid nanoparticles for ocular delivery of isoniazid: Evaluation, proof of concept and in vivo safety & kinetics, Nanomedicine. (2019). https://doi.org/10.2217/nnm-2018-0278.

[150] P. Suwannoi, M. Chomnawang, A. Tunsirikongkon, A. Phongphisutthinan, C.C. Müller-Goymann, N. Sarisuta, TAT-surface modified acyclovir-loaded albumin nanoparticles as a novel ocular drug delivery system, J. Drug Deliv. Sci. Technol. (2019). https://doi.org/10.1016/j.jddst.2019.05.029.

[151] R. Bisht, J.K. Jaiswal, V.F. Oliver, C. Eurtivong, J. Reynisson, I.D. Rupenthal, Preparation and evaluation of PLGA nanoparticle-loaded biodegradable light-responsive injectable implants as a promising platform for intravitreal drug delivery, J. Drug Deliv. Sci. Technol. (2017). https://doi.org/10.1016/j.jddst.2017.06.006.

[152] H. Almeida, P. Lobão, C. Frigerio, J. Fonseca, R. Silva, J.M. Sousa Lobo, M.H. Amaral, Preparation, characterization and biocompatibility studies of thermoresponsive eyedrops based on the combination of nanostructured lipid carriers (NLC) and the polymer Pluronic F-127 for controlled delivery of ibuprofen, Pharm. Dev. Technol. 22 (2017) 336–349. https://doi.org/10.3109/10837450.2015.1125922.

[153] S.P. Balguri, G.R. Adelli, S. Majumdar, Topical ophthalmic lipid nanoparticle formulations (SLN, NLC) of indomethacin for delivery to the posterior segment ocular tissues, Eur J Pharm Biopharm. 109 (2016) 224–235. https://doi.org/10.1016/j.ejpb.2016.10.015.

[154] A. Yu, H. Shi, H. Liu, Z. Bao, M. Dai, D. Lin, D. Lin, X. Xu, X. Li, Y. Wang, Mucoadhesive dexamethasone-glycol chitosan nanoparticles for ophthalmic drug delivery, Int. J. Pharm. (2020). https://doi.org/10.1016/j.ijpharm.2019.118943.

[155] J. Alvarez-Trabado, A. Lopez-Garcia, M. Martin-Pastor, Y. Diebold, A. Sanchez, Sorbitan ester

nanoparticles (SENS) as a novel topical ocular drug delivery system: Design, optimization, and in vitro/ex vivo evaluation, Int J Pharm. 546 (2018) 20–30. https://doi.org/10.1016/j.ijpharm.2018.05.015.

[156] A.T. Ogunjimi, S.M.G. Melo, C.G. Vargas-Rechia, F.S. Emery, R.F. V Lopez, Hydrophilic polymeric nanoparticles prepared from Delonix galactomannan with low cytotoxicity for ocular drug delivery, Carbohydr Polym. 157 (2017) 1065–1075. https://doi.org/10.1016/j.carbpol.2016.10.076.

[157] R. Zhao, J. Li, J. Wang, Z. Yin, Y. Zhu, W. Liu, Development of Timolol-Loaded Galactosylated Chitosan Nanoparticles and Evaluation of Their Potential for Ocular Drug Delivery, AAPS PharmSciTech. 18 (2017) 997–1008. https://doi.org/10.1208/s12249-016-0669-x.

[158] V.G. Llera-Rojas, M. Hernández-Salgado, D. Quintanar-Guerrero, G. Leyva-Gómez, S. Mendoza-Elvira, R. Villalobos-García, Comparative study of the release profiles of ibuprofen from polymeric nanocapsules and nanospheres, J. Mex. Chem. Soc. (2019). https://doi.org/10.29356/jmcs.v63i2.943.

[159] K. Ghosal, A. Manakhov, L. Zajíčková, S. Thomas, Structural and Surface Compatibility Study of Modified Electrospun Poly(ε-caprolactone) (PCL) Composites for Skin Tissue Engineering, AAPS PharmSciTech. (2017). https://doi.org/10.1208/s12249-016-0500-8.

[160] J. Pandit, Y. Sultana, M. Aqil, Chitosan-coated PLGA nanoparticles of bevacizumab as novel drug delivery to target retina: optimization, characterization, and in vitro toxicity evaluation, Artif. Cells, Nanomedicine, Biotechnol. 45 (2017) 1397–1407. https://doi.org/10.1080/21691401.2016.1243545.

[161] D. Zhu, W. Tao, H. Zhang, G. Liu, T. Wang, L. Zhang, X. Zeng, L. Mei, Acta Biomaterialia Docetaxel (DTX) -loaded polydopamine-modified TPGS-PLA nanoparticles as a targeted drug delivery system for the treatment of liver cancer, Acta Biomater. 30 (2016) 144–154. https://doi.org/10.1016/j.actbio.2015.11.031.

[162] F.H. Nasr, S. Khoee, M.M. Dehghan, S.S. Chaleshtori, A. Shafiee, Preparation and Evaluation of Contact Lenses Embedded with Polycaprolactone-Based Nanoparticles for Ocular Drug Delivery, Biomacromolecules. 17 (2016) 485–495. https://doi.org/10.1021/acs.biomac.5b01387.

[163] H. Saade, Preparation and Loading with Rifampicin of Sub-50 nmPoly(ethyl cyanoacrylate) Nanoparticles by SemicontinuousHeterophase Polymerization, J. Nanomater. (2016). https://doi.org/10.1155/2016/8384973.

[164] H. Tian, Z. Tang, X. Zhuang, X. Chen, X. Jing, Biodegradable synthetic polymers: Preparation, functionalization and biomedical application, Prog. Polym. Sci. 37 (2012) 237–280. https://doi.org/10.1016/j.progpolymsci.2011.06.004.

[165] G.M. Fernandes-Cunha, S.L. Fialho, G.R. da Silva, A. Silva-Cunha, M. Zhao, F. Behar-Cohen, Ocular safety of Intravitreal Clindamycin Hydrochloride Released by PLGA Implants, Pharm. Res. (2017). https://doi.org/10.1007/s11095-017-2118-2.

[166] P.S. Chan, J.W. Xian, Q. Li, C.W. Chan, S.S.Y. Leung, K.K.W. To, Biodegradable Thermosensitive PLGA-PEG-PLGA Polymer for Non-irritating and Sustained Ophthalmic Drug Delivery, AAPS J. (2019). https://doi.org/10.1208/s12248-019-0326-x.

[167] X. Yang, H.M. Trinh, V. Agrahari, Y. Sheng, D. Pal, A.K. Mitra, Nanoparticle-Based Topical Ophthalmic Gel Formulation for Sustained Release of Hydrocortisone Butyrate, AAPS PharmSciTech. (2016). https://doi.org/10.1208/s12249-015-0354-5.

[168] X.S. Wu, N. Wang, Synthesis, characterization, biodegradation, and drug delivery application of biodegradable lactic/glycolic acid polymers. Part II: Biodegradation, J. Biomater. Sci. Polym. Ed. (2001). https://doi.org/10.1163/156856201744425.

[169] H.S. Yoo, Biodegradable Nanoparticles Containing Doxorubicin-PLGA Conjugate for Sustained Release, Pharm Res. 16 (1990) 1114–1118.

[170] J. Pandit, Y. Sultana, M. Aqil, Chitosan-coated PLGA nanoparticles of bevacizumab as novel drug delivery to target retina: optimization, characterization, and in vitro toxicity evaluation, Artif. Cells, Nanomedicine Biotechnol. 45 (2017) 1397–1407. https://doi.org/10.1080/21691401.2016.1243545.

[171] A.L. Goffin, J.M. Raquez, E. Duquesne, G. Siqueira, Y. Habibi, A. Dufresne, P. Dubois, From interfacial ring-opening polymerization to melt processing of cellulose nanowhisker-filled polylactide-based nanocomposites, Biomacromolecules. (2011). https://doi.org/10.1021/bm200581h.

[172] B. Tyler, D. Gullotti, A. Mangraviti, T. Utsuki, H. Brem, Polylactic acid (PLA) controlled delivery carriers for biomedical applications, Adv Drug Deliv Rev. 107 (2016) 163–175. https://doi.org/10.1016/j.addr.2016.06.018.

[173] J.-L. Bourges, S.E. Gautier, F. Delie, R.A. Bejjani, J.-C. Jeanny, R. Gurny, D. BenEzra, F.F. Behar-Cohen, Ocular Drug Delivery Targeting the Retina and Retinal Pigment Epithelium Using Polylactide Nanoparticles, Investig. Opthalmology Vis. Sci. 44 (2003) 3562. https://doi.org/10.1167/iovs.02-1068.

[174] S.M. Li, X.H. Chen, R.A. Gross, S.P. Mccarthy, Hydrolytic degradation of PCL/PEO copolymers in alkaline media, J. Mater. Sci. Mater. Med. 11 (2000) 227–233. https://doi.org/10.1023/A:1008920326988.

[175] Chih-Hung Lee, Poly(ε-caprolactone) nanocapsule carriers with sustained drug release: single dose for long-term glaucoma treatment, Nanoscale. 9 (2017) 11754–11764. https://doi.org/10.1039/C7NR03221H10.1039/x0xx00000x.

[176] D. Akilbekova, M. Shaimerdenova, S. Adilov, D. Berillo, Biocompatible scaffolds based on natural polymers for regenerative medicine, Int. J. Biol. Macromol. (2018). https://doi.org/10.1016/j.ijbiomac.2018.03.116.

[177] G.Z. Papageorgiou, Thinking green: Sustainable polymers from renewable resources, Polymers (Basel). (2018). https://doi.org/10.3390/polym10090952.

[178] M. Henke, J. Tessmar, A. Göpferich, Biomimetic Polymers (for Biomedical Applications), in: Polym. Sci. A Compr. Ref. 10 Vol. Set, 2012. https://doi.org/10.1016/B978-0-444-53349-4.00222-3.

[179] H.B. Eral, V. López-Mejías, M. O'Mahony, B.L. Trout, A.S. Myerson, P.S. Doyle, Biocompatible alginate microgel particles as heteronucleants and encapsulating vehicles for hydrophilic and hydrophobic drugs, Cryst. Growth Des. (2014). https://doi.org/10.1021/cg500250e.

[180] B. Gao, L. Chen, Y. Zhao, X. Yan, X. Wang, C. Zhou, Y. Shi, W. Xue, Methods to prepare dopamine/polydopamine modified alginate hydrogels and their special improved properties for drug delivery, Eur. Polym. J. 110 (2019) 192–201. https://doi.org/10.1016/j.eurpolymj.2018.11.025.

[181] F.S.Y. Wong, K.K. Tsang, A.M.W. Chu, B.P. Chan, K.M. Yao, A.C.Y. Lo, Injectable cell-encapsulating composite alginate-collagen platform with inducible termination switch for safer ocular drug delivery, Biomaterials. 201 (2019) 53–67.

https://doi.org/10.1016/j.biomaterials.2019.01.032.

[182] R. Silva, R. Singh, B. Sarker, D.G. Papageorgiou, J.A. Juhasz-Bortuzzo, J.A. Roether, I. Cicha, J. Kaschta, D.W. Schubert, K. Chrissafis, R. Detsch, A.R. Boccaccini, Hydrogel matrices based on elastin and alginate for tissue engineering applications, Int. J. Biol. Macromol. (2018). https://doi.org/10.1016/j.ijbiomac.2018.03.091.

[183] R.C. Nagarwal, R. Kumar, J.K. Pandit, Chitosan coated sodium alginate-chitosan nanoparticles loaded with 5-FU for ocular delivery: In vitro characterization and in vivo study in rabbit eye, Eur. J. Pharm. Sci. (2012). https://doi.org/10.1016/j.ejps.2012.08.008.

[184] F.S.Y. Wong, K.K. Tsang, A.M.W. Chu, B.P. Chan, K.M. Yao, A.C.Y. Lo, Injectable cell-encapsulating composite alginate-collagen platform with inducible termination switch for safer ocular drug delivery, Biomaterials. (2019). https://doi.org/10.1016/j.biomaterials.2019.01.032.

[185] S. Noreen, S.A. Ghumman, F. Batool, B. Ijaz, M. Basharat, S. Noureen, T. Kausar, S. Iqbal, Terminalia arjuna gum/alginate in situ gel system with prolonged retention time for ophthalmic drug delivery, Int. J. Biol. Macromol. 152 (2020) 1056–1067. https://doi.org/10.1016/j.ijbiomac.2019.10.193.

[186] M.M. Ibrahim, A.H. Abd-Elgawad, O.A. Soliman, M.M. Jablonski, Natural Bioadhesive Biodegradable Nanoparticle-Based Topical Ophthalmic Formulations for Management of Glaucoma, Transl Vis Sci Technol. 4 (2015) 12. https://doi.org/10.1167/tvst.4.3.12.

[187] S. Balkani, S. Shamekhi, R. Raoufinia, R. Parvan, J. Abdolalizadeh, Purification and characterization of bovine serum albumin using chromatographic method, Adv. Pharm. Bull. (2016). https://doi.org/10.15171/apb.2016.080.

[188] M.M. Pereira, R.A.P. Cruz, M.R. Almeida, Á.S. Lima, J.A.P. Coutinho, M.G. Freire, Single-step purification of ovalbumin from egg white using aqueous biphasic systems, Process Biochem. (2016). https://doi.org/10.1016/j.procbio.2016.03.002.

[189] L. Yang, J. Zheng, Z. Zou, H. Cai, P. Qi, Z. Qing, Q. Yan, L. Qiu, W. Tan, R. Yang, Human serum albumin as an intrinsic signal amplification amplifier for ultrasensitive assays of the prostate-specific antigen in human plasma, Chem. Commun. (2020). https://doi.org/10.1039/c9cc08501g.

[190] B. Meloun, L. Morávek, V. Kostka, Complete amino acid sequence of human serum albumin, FEBS Lett. (1975). https://doi.org/10.1016/0014-5793(75)80242-0.

[191] J.M. Llabot, I. Luis de Redin, M. Agüeros, M.J. Dávila Caballero, C. Boiero, J.M. Irache, D. Allemandi, In vitro characterization of new stabilizing albumin nanoparticles as a potential topical drug delivery system in the treatment of corneal neovascularization (CNV), J. Drug Deliv. Sci. Technol. (2019). https://doi.org/10.1016/j.jddst.2019.04.042.

[192] D. Huang, Y. Chen, I.D. Rupenthal, Hyaluronic Acid Coated Albumin Nanoparticles for Targeted Peptide Delivery to the Retina Hyaluronic Acid Coated Albumin Nanoparticles for Targeted Peptide Delivery to the Retina, (2016). https://doi.org/10.1021/acs.molpharmaceut.6b01029.

[193] A. Tzameret, H. Ketter-Katz, V. Edelshtain, I. Sher, E. Corem-Salkmon, I. Levy, D. Last, D. Guez, Y. Mardor, S. Margel, Y. Rotenstrich, In vivo MRI assessment of bioactive magnetic iron oxide/human serum albumin nanoparticle delivery into the posterior segment of the eye in a rat model of retinal degeneration, J. Nanobiotechnology. 17 (2019) 1–11. https://doi.org/10.1186/s12951-018-0438-y.

[194] I. Luis de Redin, C. Boiero, M.C. Martinez-Oharriz, M. Agueros, R. Ramos, I. Penuelas, D. Allemandi, J.M. Llabot, J.M. Irache, Human serum albumin nanoparticles for ocular delivery of bevacizumab, Int J Pharm. 541 (2018) 214–223. https://doi.org/10.1016/j.ijpharm.2018.02.003.

[195] J. Lizardi-mendoza, W.M.A. Monal, F.M.G. Valencia, Chemical Characteristics and Functional Properties of Chitosan, Elsevier Inc., 2016. https://doi.org/10.1016/B978-0-12-802735-6/00001-X.

[196] A. Enriquez de Salamanca, Y. Diebold, M. Calonge, C. Garcia-Vazquez, S. Callejo, A. Vila, M.J. Alonso, Chitosan nanoparticles as a potential drug delivery system for the ocular surface: toxicity, uptake mechanism and in vivo tolerance, Invest Ophthalmol Vis Sci. 47 (2006) 1416–1425. https://doi.org/10.1167/iovs.05-0495.

[197] F.A. Oyarzun-Ampuero, J. Brea, M.I. Loza, D. Torres, M.J. Alonso, Chitosan-hyaluronic acid nanoparticles loaded with heparin for the treatment of asthma, Int J Pharm. 381 (2009) 122–129. https://doi.org/10.1016/j.ijpharm.2009.04.009.

[198] N.A. Fletcher, M.D. Krebs, RSC Advances Sustained delivery of anti-VEGF from injectable hydrogel systems provides a prolonged decrease of endothelial cell proliferation and angiogenesis in vitro, RSC Adv. 8 (2018) 8999–9005. https://doi.org/10.1039/C7RA13014G.

[199] M. Rodríguez-Vázquez, B. Vega-Ruiz, R. Ramos-Zúñiga, D.A. Saldaña-Koppel, L.F. Quiñones-Olvera, Chitosan and Its Potential Use as a Scaffold for Tissue Engineering in Regenerative Medicine, Biomed Res. Int. 2015 (2015) 1–15. https://doi.org/10.1155/2015/821279.

[200] W. Chaiyasan, S.P. Srinivas, W. Tiyaboonchai, Crosslinked chitosan-dextran sulfate nanoparticle for improved topical ocular drug delivery, (2015) 1224–1234.

[201] S. Natesan, S. Pandian, C. Ponnusamy, R. Palanichamy, S. Muthusamy, R. Kandasamy, Co-encapsulated resveratrol and quercetin in chitosan and peg modified chitosan nanoparticles: For efficient intra ocular pressure reduction, Int. J. Biol. Macromol. (2017). https://doi.org/10.1016/j.ijbiomac.2017.04.117.

[202] N. Elsaid, T.L. Jackson, Z. Elsaid, A. Alqathama, S. Somavarapu, PLGA microparticles entrapping chitosan-based nanoparticles for the ocular delivery of ranibizumab, Mol. Pharm. (2016). https://doi.org/10.1021/acs.molpharmaceut.6b00335.

[203] H.W. Sung, K. Sonaje, Z.X. Liao, L.W. Hsu, E.Y. Chuang, PH-responsive nanoparticles shelled with chitosan for oral delivery of insulin: From mechanism to therapeutic applications, Acc. Chem. Res. 45 (2012) 619–629. https://doi.org/10.1021/ar200234q.

[204] W. Chaiyasan, S.P. Srinivas, W. Tiyaboonchai, Mucoadhesive chitosan-dextran sulfate nanoparticles for sustained drug delivery to the ocular surface, J Ocul Pharmacol Ther. 29 (2013) 200–207. https://doi.org/10.1089/jop.2012.0193.

[205] P. Aksungur, M. Demirbilek, E.B. Denkbaş, J. Vandervoort, A. Ludwig, N. Ünlü, Development and characterization of Cyclosporine A loaded nanoparticles for ocular drug delivery: Cellular toxicity, uptake, and kinetic studies, J. Control. Release. (2011). https://doi.org/10.1016/j.jconrel.2011.01.010.

[206] A. Siddiqua Gazi, A.K. Sailaja, Preparation and Characterization of Paracetamol Loaded Eudragit S100 Nanoparticles by Salting Out Technique, J. Dev. Drugs. (2018). https://doi.org/10.4172/2329-6631.1000183.

[207] S. V. Dalvi, M.A. Azad, R. Dave, Precipitation and stabilization of ultrafine particles of Fenofibrate in aqueous suspensions by RESOLV, Powder Technol. (2013).

https://doi.org/10.1016/j.powtec.2012.05.038.

[208] F. Shakeri, S. Shakeri, M. Hojjatoleslami, Preparation and Characterization of Carvacrol Loaded Polyhydroxybutyrate Nanoparticles by Nanoprecipitation and Dialysis Methods, J. Food Sci. (2014). https://doi.org/10.1111/1750-3841.12406.

[209] A.L.M. Cavalcanti, M.Y.F.A. Reis, G.C.L. Silva, Í.M.M. Ramalho, G.P. Guimarães, J.A. Silva, K.L.A. Saraiva, B.P.G.L. Damasceno, Microemulsion for topical application of pentoxifylline: In vitro release and in vivo evaluation, Int. J. Pharm. (2016). https://doi.org/10.1016/j.ijpharm.2016.04.065.

[210] S.D. Desai, J. Blanchard, Pluronic® F127-based ocular delivery system containing biodegradable polyisobutylcyanoacrylate nanocapsules of pilocarpine, Drug Deliv. J. Deliv. Target. Ther. Agents. (2000). https://doi.org/10.1080/107175400455128.

[211] M.S. Baig, A. Ahad, M. Aslam, S.S. Imam, M. Aqil, A. Ali, Application of Box-Behnken design for preparation of levofloxacin-loaded stearic acid solid lipid nanoparticles for ocular delivery: Optimization, in vitro release, ocular tolerance, and antibacterial activity, Int. J. Biol. Macromol. (2016). https://doi.org/10.1016/j.ijbiomac.2015.12.077.

[212] J. Li, X. Guo, Z. Liu, C.I. Okeke, N. Li, H. Zhao, M.O. Aggrey, W. Pan, T. Wu, Preparation and evaluation of charged solid lipid nanoparticles of tetrandrine for ocular drug delivery system: Pharmacokinetics, cytotoxicity and cellular uptake studies, Drug Dev. Ind. Pharm. (2014). https://doi.org/10.3109/03639045.2013.795582.

[213] B. Balzus, F.F. Sahle, S. Hönzke, C. Gerecke, F. Schumacher, S. Hedtrich, B. Kleuser, R. Bodmeier, Formulation and ex vivo evaluation of polymeric nanoparticles for controlled delivery of corticosteroids to the skin and the corneal epithelium, Eur. J. Pharm. Biopharm. (2017). https://doi.org/10.1016/j.ejpb.2017.02.001.

[214] A.K. Sah, P.K. Suresh, V.K. Verma, PLGA nanoparticles for ocular delivery of loteprednol etabonate: a corneal penetration study, Artif. Cells, Nanomedicine Biotechnol. (2017). https://doi.org/10.1080/21691401.2016.1203794.

[215] A.H. Salama, M.M. AbouSamra, G.E.A. Awad, S.S. Mansy, Promising bioadhesive ofloxacin-loaded polymeric nanoparticles for the treatment of ocular inflammation: formulation and in vivo evaluation, Drug Deliv. Transl. Res. (2020). https://doi.org/10.1007/s13346-020-00856-8.

[216] A.H. Salama, A.A. Mahmoud, R. Kamel, A Novel Method for Preparing Surface-Modified Fluocinolone Acetonide Loaded PLGA Nanoparticles for Ocular Use: In Vitro and In Vivo Evaluations, AAPS PharmSciTech. 17 (2016) 1159–1172. https://doi.org/10.1208/s12249-015-0448-0.

[217] S. Salatin, J. Barar, M. Barzegar-Jalali, K. Adibkia, F. Kiafar, M. Jelvehgari, Development of a nanoprecipitation method for the entrapment of a very water soluble drug into Eudragit RL nanoparticles, Res. Pharm. Sci. (2017). https://doi.org/10.4103/1735-5362.199041.

[218] S. Tyagi, nanoparticles-an-overview-of-preparation, Res. Rev. J. Pharm. Nanotechnol. 4 (2016).

[219] M. Ahuja, P. Verma, M. Bhatia, Preparation and evaluation of chitosan–itraconazole co-precipitated nanosuspension for ocular delivery, J. Exp. Nanosci. (2015). https://doi.org/10.1080/17458080.2013.822108.

[220] D. Patiño-Ruiz, L. Marrugo, N. Reyes, M. Acevedo-Morantes, A. Herrera, Ionotropic Gelation Synthesis of Chitosan-Alginate Nanodisks for Delivery System and in Vitro Assessment of Prostate Cancer Cytotoxicity, Int. J. Polym. Sci. (2020).

https://doi.org/10.1155/2020/5329747.

[221] J.P. Rao, K.E. Geckeler, Polymer nanoparticles: Preparation techniques and size-control parameters, Prog. Polym. Sci. 36 (2011) 887–913. https://doi.org/10.1016/j.progpolymsci.2011.01.001.

[222] N.C. Silva, S. Silva, B. Sarmento, M. Pintado, Chitosan nanoparticles for daptomycin delivery in ocular treatment of bacterial endophthalmitis, Drug Deliv. 22 (2015) 885–893. https://doi.org/10.3109/10717544.2013.858195.

[223] E. Chiellini, C. Errico, C. Bartoli, F. Chiellini, Poly(hydroxyalkanoates)-based polymeric nanoparticles for drug delivery, J. Biomed. Biotechnol. 2009 (2009). https://doi.org/10.1155/2009/571702.

[224] L. Chronopoulou, M. Massimi, M.F. Giardi, C. Cametti, L.C. Devirgiliis, M. Dentini, C. Palocci, Chitosan-coated PLGA nanoparticles: A sustained drug release strategy for cell cultures, Colloids Surfaces B Biointerfaces. 103 (2013) 310–317. https://doi.org/10.1016/j.colsurfb.2012.10.063.

[225] P. Pattanayak, S.K. Singh, M. Gulati, S. Vishwas, B. Kapoor, D.K. Chellappan, K. Anand, G. Gupta, N.K. Jha, P.K. Gupta, P. Prasher, K. Dua, H. Dureja, D. Kumar, V. Kumar, Microfluidic chips: recent advances, critical strategies in design, applications and future perspectives, Microfluid. Nanofluidics. 25 (2021) 99. https://doi.org/10.1007/s10404-021-02502-2.

[226] S. Xu, Z. Nie, M. Seo, P. Lewis, E. Kumacheva, H.A. Stone, P. Garstecki, D.B. Weibel, I. Gitlin, G.M. Whitesides, Generation of monodisperse particles by using microfluidics: Control over size, shape, and composition, Angew. Chemie - Int. Ed. 44 (2005) 724–728. https://doi.org/10.1002/anie.200462226.

[227] C. Yousry, P.M. Zikry, H.M. Salem, E.B. Basalious, O.N. El-Gazayerly, Integrated nanovesicular/self-nanoemulsifying system (INV/SNES) for enhanced dual ocular drug delivery: statistical optimization, in vitro and in vivo evaluation, Drug Deliv. Transl. Res. (2020). https://doi.org/10.1007/s13346-020-00716-5.

[228] X. Xu, L. Sun, L. Zhou, Y. Cheng, F. Cao, Functional chitosan oligosaccharide nanomicelles for topical ocular drug delivery of dexamethasone, Carbohydr. Polym. (2020). https://doi.org/10.1016/j.carbpol.2019.115356.

[229] J.F. Fangueiro, T. Andreani, M.A. Egea, M.L. Garcia, S.B. Souto, A.M. Silva, E.B. Souto, Design of cationic lipid nanoparticles for ocular delivery: Development, characterization and cytotoxicity, Int. J. Pharm. (2014). https://doi.org/10.1016/j.ijpharm.2013.11.025.

[230] M.J. Masarudin, S.M. Cutts, B.J. Evison, D.R. Phillips, P.J. Pigram, Factors determining the stability, size distribution, and cellular accumulation of small, monodisperse chitosan nanoparticles as candidate vectors for anticancer drug delivery: Application to the passive encapsulation of [14C]-doxorubicin, Nanotechnol. Sci. Appl. (2015). https://doi.org/10.2147/NSA.S91785.

[231] U.K. Sharma, A. Verma, S.K. Prajapati, H. Pandey, A.C. Pandey, In vitro, in vivo and pharmacokinetic assessment of amikacin sulphate laden polymeric nanoparticles meant for controlled ocular drug delivery, Appl. Nanosci. (2015). https://doi.org/10.1007/s13204-014-0300-y.

[232] J. McMillan, E. Batrakova, H.E. Gendelman, Cell delivery of therapeutic nanoparticles, in: Prog. Mol. Biol. Transl. Sci., 2011. https://doi.org/10.1016/B978-0-12-416020-0.00014-0.

[233] M. Bouchoucha, M.F. Côté, R. C-Gaudreault, M.A. Fortin, F. Kleitz, Size-Controlled

Functionalized Mesoporous Silica Nanoparticles for Tunable Drug Release and Enhanced Anti-Tumoral Activity, Chem. Mater. (2016). https://doi.org/10.1021/acs.chemmater.6b00877.

[234] S. Soltani, P. Zakeri-Milani, M. Barzegar-Jalali, M. Jelvehgari, Design of eudragit RL nanoparticles by nanoemulsion method as carriers for ophthalmic drug delivery of ketotifen fumarate, Iran. J. Basic Med. Sci. (2016). https://doi.org/10.22038/ijbms.2016.6940.

[235] Z. Ali, P.K. Sharma, M.H. Warsi, Fabrication and evaluation of Ketorolac loaded cubosome for ocular drug delivery, J. Appl. Pharm. Sci. (2016). https://doi.org/10.7324/JAPS.2016.60930.

[236] M. Filella, J. Zhang, M.E. Newman, J. Buffle, Analytical applications of photon correlation spectroscopy for size distribution measurements of natural colloidal suspensions: Capabilities and limitations, Colloids Surfaces A Physicochem. Eng. Asp. (1997). https://doi.org/10.1016/S0927-7757(96)03677-1.

[237] M. Danaei, M. Dehghankhold, S. Ataei, F. Hasanzadeh Davarani, R. Javanmard, A. Dokhani, S. Khorasani, M.R. Mozafari, Impact of particle size and polydispersity index on the clinical applications of lipidic nanocarrier systems, Pharmaceutics. (2018). https://doi.org/10.3390/pharmaceutics10020057.

[238] S. Amin, G. V. Barnett, J.A. Pathak, C.J. Roberts, P.S. Sarangapani, Protein aggregation, particle formation, characterization & rheology, Curr. Opin. Colloid Interface Sci. 19 (2014) 438–449. https://doi.org/10.1016/j.cocis.2014.10.002.

[239] S. Bhattacharjee, DLS and zeta potential - What they are and what they are not?, J. Control. Release. 235 (2016) 337–351. https://doi.org/10.1016/j.jconrel.2016.06.017.

[240] C. Bantz, O. Koshkina, T. Lang, H.J. Galla, C.J. Kirkpatrick, R.H. Stauber, M. Maskos, The surface properties of nanoparticles determine the agglomeration state and the size of the particles under physiological conditions, Beilstein J. Nanotechnol. (2014). https://doi.org/10.3762/bjnano.5.188.

[241] Chapter 10 Microfluidic methods for measuring zeta potential, in: Interface Sci. Technol., 2004. https://doi.org/10.1016/S1573-4285(04)80032-2.

[242] D.J. Shaw, Introduction to Colloid and Surface Chemistry: Fourth Edition, 2013. https://doi.org/10.1016/C2009-0-24070-0.

[243] T. Tadros, Zeta potential in colloid science. Principles and application, Colloids and Surfaces. (1982). https://doi.org/10.1016/0166-6622(82)80060-7.

[244] X. Zhu, M. Su, S. Tang, L. Wang, X. Liang, F. Meng, Y. Hong, Z. Xu, Synthesis of thiolated chitosan and preparation nanoparticles with sodium alginate for ocular drug delivery, Mol. Vis. (2012).

[245] M.A. Kalam, Development of chitosan nanoparticles coated with hyaluronic acid for topical ocular delivery of dexamethasone, Int J Biol Macromol. 89 (2016) 127–136. https://doi.org/10.1016/j.ijbiomac.2016.04.070.

[246] P. Verma, S.K. Maheshwari, Preparation of Sliver and Selenium Nanoparticles and Its Characterization by Dynamic Light Scattering and Scanning Electron Microscopy., J. Microsc. Ultrastruct. (2018). https://doi.org/10.4103/JMAU.JMAU_3_18.

[247] B.J. Inkson, 2 - Scanning electron microscopy (SEM) and transmission electron microscopy (TEM) for materials characterization, Elsevier Ltd, 2016. https://doi.org/10.1016/B978-0-08-100040-3.00002-X.

[248] J.H. Park, H. Jeong, J. Hong, M. Chang, M. Kim, R.S. Chuck, J.K. Lee, C.Y. Park, The Effect of

Silica Nanoparticles on Human Corneal Epithelial Cells, Sci Rep. 6 (2016) 37762. https://doi.org/10.1038/srep37762.

[249] Y. Zhao, X. Sun, G. Zhang, B.G. Trewyn, I.I. Slowing, V.S.Y. Lin, Interaction of mesoporous silica nanoparticles with human red blood cell membranes: Size and surface effects, ACS Nano. (2011). https://doi.org/10.1021/nn103077k.

[250] I.Y. Kim, E. Joachim, H. Choi, K. Kim, Toxicity of silica nanoparticles depends on size, dose, and cell type, Nanomedicine Nanotechnology, Biol. Med. (2015). https://doi.org/10.1016/j.nano.2015.03.004.

[251] K. Greish, G. Thiagarajan, H. Herd, R. Price, H. Bauer, D. Hubbard, A. Burckle, S. Sadekar, T. Yu, A. Anwar, A. Ray, H. Ghandehari, Size and surface charge significantly influence the toxicity of silica and dendritic nanoparticles, Nanotoxicology. (2012). https://doi.org/10.3109/17435390.2011.604442.

[252] B.J. Inkson, Scanning Electron Microscopy (SEM) and Transmission Electron Microscopy (TEM) for Materials Characterization, in: Mater. Charact. Using Nondestruct. Eval. Methods, 2016. https://doi.org/10.1016/B978-0-08-100040-3.00002-X.

[253] Ameeduzzafar, S.S. Imam, S.N. Abbas Bukhari, J. Ahmad, A. Ali, Formulation and optimization of levofloxacin loaded chitosan nanoparticle for ocular delivery: In-vitro characterization, ocular tolerance and antibacterial activity, Int J Biol Macromol. 108 (2018) 650–659. https://doi.org/10.1016/j.ijbiomac.2017.11.170.

[254] Y. Gokce, B. Cengiz, N. Yildiz, A. Calimli, Z. Aktas, Ultrasonication of chitosan nanoparticle suspension: Influence on particle size, Colloids Surfaces A Physicochem. Eng. Asp. (2014). https://doi.org/10.1016/j.colsurfa.2014.08.028.

[255] L. V. Stebounova, E. Guio, V.H. Grassian, Silver nanoparticles in simulated biological media: A study of aggregation, sedimentation, and dissolution, J. Nanoparticle Res. (2011). https://doi.org/10.1007/s11051-010-0022-3.

[256] K. Burapapadh, H. Takeuchi, P. Sriamornsak, Development of pectin nanoparticles through mechanical homogenization for dissolution enhancement of itraconazole, Asian J. Pharm. Sci. (2016). https://doi.org/10.1016/j.ajps.2015.07.003.

[257] G.A. Morris, J. Castile, A. Smith, G.G. Adams, S.E. Harding, The effect of prolonged storage at different temperatures on the particle size distribution of tripolyphosphate (TPP)-chitosan nanoparticles, Carbohydr. Polym. (2011). https://doi.org/10.1016/j.carbpol.2011.01.044.

[258] G. Behl, J. Iqbal, N.J. O'Reilly, P. McLoughlin, L. Fitzhenry, Synthesis and Characterization of Poly(2-hydroxyethylmethacrylate) Contact Lenses Containing Chitosan Nanoparticles as an Ocular Delivery System for Dexamethasone Sodium Phosphate, Pharm. Res. (2016). https://doi.org/10.1007/s11095-016-1903-7.

[259] W.F. Huang, C.P. Tsui, C.Y. Tang, M. Yang, L. Gu, Surface charge switchable and pH-responsive chitosan/polymer core-shell composite nanoparticles for drug delivery application, Compos. Part B Eng. 121 (2017) 83–91. https://doi.org/10.1016/j.compositesb.2017.03.028.

[260] X.-Y. Lu, D.-C. Wu, Z.-J. Li, G.-Q. Chen, Chpater 7 – Polymer Nanoparticles, in: Prog. Mol. Biol. Transl. Sci., 2011.

[261] N. Rescignano, L. Tarpani, A. Romani, I. Bicchi, S. Mattioli, C. Emiliani, L. Torre, J.M. Kenny, S. Martino, L. Latterini, I. Armentano, In-vitro degradation of PLGA nanoparticles in aqueous medium and in stem cell cultures by monitoring the cargo fluorescence spectrum, Polym. Degrad. Stab. (2016). https://doi.org/10.1016/j.polymdegradstab.2016.10.017.

[262] R. Scaffaro, F. Lopresti, L. Botta, Preparation, characterization and hydrolytic degradation of PLA/PCL co-mingled nanofibrous mats prepared via dual-jet electrospinning, Eur. Polym. J. 96 (2017) 266–277. https://doi.org/10.1016/j.eurpolymj.2017.09.016.

[263] F.A. Maulvi, H.H. Choksi, A.R. Desai, A.S. Patel, K.M. Ranch, B.A. Vyas, D.O. Shah, pH triggered controlled drug delivery from contact lenses: Addressing the challenges of drug leaching during sterilization and storage, Colloids Surfaces B Biointerfaces. (2017). https://doi.org/10.1016/j.colsurfb.2017.05.064.

[264] Y. Zhou, A. Fang, F. Wang, H. Li, Q. Jin, L. Huang, C. Fu, J. Zeng, Z. Jin, X. Song, Core-shell lipid-polymer nanoparticles as a promising ocular drug delivery system to treat glaucoma, Chinese Chem. Lett. (2020). https://doi.org/10.1016/j.cclet.2019.04.048.

[265] J. Li, X. Jin, Y. Yang, L. Zhang, R. Liu, Z. Li, Trimethyl chitosan nanoparticles for ocular baicalein delivery: Preparation, optimization, in vitro evaluation, in vivo pharmacokinetic study and molecular dynamics simulation, Int. J. Biol. Macromol. (2020). https://doi.org/10.1016/j.ijbiomac.2020.04.115.

[266] R. Kesarla, T. Tank, P.A. Vora, T. Shah, S. Parmar, A. Omri, Preparation and evaluation of nanoparticles loaded ophthalmic in situ gel, Drug Deliv. (2016). https://doi.org/10.3109/10717544.2014.987333.

[267] Y. Zambito, E. Pedreschi, G. Di Colo, Is dialysis a reliable method for studying drug release from nanoparticulate systems? - A case study, Int. J. Pharm. (2012). https://doi.org/10.1016/j.ijpharm.2012.05.020.

[268] S. Modi, B.D. Anderson, Determination of drug release kinetics from nanoparticles: Overcoming pitfalls of the dynamic dialysis method, Mol. Pharm. (2013). https://doi.org/10.1021/mp400154a.

[269] M. Yu, W. Yuan, D. Li, A. Schwendeman, S.P. Schwendeman, Predicting drug release kinetics from nanocarriers inside dialysis bags, J. Control. Release. (2019). https://doi.org/10.1016/j.jconrel.2019.09.016.

[270] B. Yavuz, S.B. Pehlivan, İ. Vural, N. Ünlü, In Vitro/In Vivo Evaluation of Dexamethasone—PAMAM Dendrimer Complexes for Retinal Drug Delivery, J. Pharm. Sci. 104 (2015) 3814–3823. https://doi.org/10.1002/JPS.24588.

[271] W. Sun, S. Mao, Y. Shi, L.C. Li, L. Fang, Nanonization of itraconazole by high pressure homogenization: Stabilizer optimization and effect of particle size on oral absorption, J. Pharm. Sci. (2011). https://doi.org/10.1002/jps.22587.

[272] W.T. Huang, M. Larsson, Y.C. Lee, D.M. Liu, G.Y. Chiou, Dual drug-loaded biofunctionalized amphiphilic chitosan nanoparticles: Enhanced synergy between cisplatin and demethoxycurcumin against multidrug-resistant stem-like lung cancer cells, Eur. J. Pharm. Biopharm. (2016). https://doi.org/10.1016/j.ejpb.2016.10.014.

[273] R.N. Wadetwar, A.R. Agrawal, P.S. Kanojiya, In situ gel containing Bimatoprost solid lipid nanoparticles for ocular delivery: In-vitro and ex-vivo evaluation, J. Drug Deliv. Sci. Technol. (2020). https://doi.org/10.1016/j.jddst.2020.101575.

[274] S.A. Abouelmagd, B. Sun, A.C. Chang, Y.J. Ku, Y. Yeo, Release kinetics study of poorly water-soluble drugs from nanoparticles: Are we doing it right?, Mol. Pharm. (2015). https://doi.org/10.1021/mp500817h.

[275] G. Di Prima, F. Bongiovì, F.S. Palumbo, G. Pitarresi, M. Licciardi, G. Giammona, Mucoadhesive PEGylated inulin-based self-assembling nanoparticles: In vitro and ex vivo transcorneal

permeation enhancement of corticosteroids, J. Drug Deliv. Sci. Technol. (2019). https://doi.org/10.1016/j.jddst.2018.10.028.

[276] D. Huang, Y.S. Chen, S.S. Thakur, I.D. Rupenthal, Ultrasound-mediated nanoparticle delivery across ex vivo bovine retina after intravitreal injection, Eur. J. Pharm. Biopharm. (2017). https://doi.org/10.1016/j.ejpb.2017.06.009.

[277] X. Xu, Z. Xu, J. Liu, Z. Zhang, H. Chen, X. Li, S. Shi, Visual tracing of diffusion and biodistribution for amphiphilic cationic nanoparticles using photoacoustic imaging after ex vivo intravitreal injections, Int. J. Nanomedicine. (2016). https://doi.org/10.2147/IJN.S109986.

[278] Q. Bao, B. Newman, Y. Wang, S. Choi, D.J. Burgess, In vitro and ex vivo correlation of drug release from ophthalmic ointments, J. Control. Release. (2018). https://doi.org/10.1016/j.jconrel.2018.03.003.

[279] G.A. Abdelbary, M.M. Amin, M.Y. Zakaria, Ocular ketoconazole-loaded proniosomal gels: Formulation, ex vivo corneal permeation and in vivo studies, Drug Deliv. (2017). https://doi.org/10.1080/10717544.2016.1247928.

[280] A.E. Eldeeb, S. Salah, M. Ghorab, Formulation and evaluation of cubosomes drug delivery system for treatment of glaucoma: Ex-vivo permeation and in-vivo pharmacodynamic study, J. Drug Deliv. Sci. Technol. (2019). https://doi.org/10.1016/j.jddst.2019.04.036.

[281] F.A. Maulvi, M.A. Mangukiya, P.A. Patel, R.J. Vaidya, A.R. Koli, K.M. Ranch, D.O. Shah, Extended release of ketotifen from silica shell nanoparticle-laden hydrogel contact lenses: in vitro and in vivo evaluation, J. Mater. Sci. Mater. Med. (2016). https://doi.org/10.1007/s10856-016-5724-3.

[282] E. Sanchez-Lopez, M.A. Egea, A. Cano, M. Espina, A.C. Calpena, M. Ettcheto, A. Camins, E.B. Souto, A.M. Silva, M.L. Garcia, PEGylated PLGA nanospheres optimized by design of experiments for ocular administration of dexibuprofen-in vitro, ex vivo and in vivo characterization, Colloids Surf B Biointerfaces. 145 (2016) 241–250. https://doi.org/10.1016/j.colsurfb.2016.04.054.

[283] J. Liu, X. Zhang, G. Li, F. Xu, S. Li, L. Teng, Y. Li, F. Sun, Anti-angiogenic activity of bevacizumab-bearing dexamethasone-loaded PLGA nanoparticles for potential intravitreal applications, Int. J. Nanomedicine. (2019). https://doi.org/10.2147/IJN.S217038.

[284] R. Bisht, J.K. Jaiswal, I.D. Rupenthal, Nanoparticle-loaded biodegradable light-responsive in situ forming injectable implants for effective peptide delivery to the posterior segment of the eye, Med. Hypotheses. (2017). https://doi.org/10.1016/j.mehy.2017.03.033.

[285] M. Khalil, U. Hashmi, R. Riaz, S. Rukh Abbas, Chitosan coated liposomes (CCL) containing triamcinolone acetonide for sustained delivery: A potential topical treatment for posterior segment diseases, Int. J. Biol. Macromol. (2020). https://doi.org/10.1016/j.ijbiomac.2019.10.256.

[286] C. Puglia, D. Santonocito, C. Ostacolo, E.M. Sommella, P. Campiglia, C. Carbone, F. Drago, R. Pignatello, C. Bucolo, Ocular formulation based on palmitoylethanolamide-loaded nanostructured lipid carriers: Technological and pharmacological profile, Nanomaterials. (2020). https://doi.org/10.3390/nano10020287.

[287] I. Ahmad, J. Pandit, Y. Sultana, A.K. Mishra, P.P. Hazari, M. Aqil, Optimization by design of etoposide loaded solid lipid nanoparticles for ocular delivery: Characterization, pharmacokinetic and deposition study, Mater. Sci. Eng. C. (2019). https://doi.org/10.1016/j.msec.2019.03.060.

[288] W. Li, L. Chen, Z. Gu, Z. Chen, H. Li, Z. Cheng, H. Li, L. Zou, Co-delivery of microRNA-150 and quercetin by lipid nanoparticles (LNPs) for the targeted treatment of age-related macular degeneration (AMD), J. Control. Release. 355 (2023) 358–370. https://doi.org/https://doi.org/10.1016/j.jconrel.2023.01.080.

[289] R. Varshochian, M. Riazi-Esfahani, M. Jeddi-Tehrani, A.R. Mahmoudi, S. Aghazadeh, M. Mahbod, M. Movassat, F. Atyabi, A. Sabzevari, R. Dinarvand, Albuminated PLGA nanoparticles containing bevacizumab intended for ocular neovascularization treatment, J Biomed Mater Res A. 103 (2015) 3148–3156. https://doi.org/10.1002/jbm.a.35446.

[290] S. Patel, C. Garapati, P. Chowdhury, H. Gupta, J. Nesamony, S. Nauli, S.H. Boddu, Development and evaluation of dexamethasone nanomicelles with potential for treating posterior uveitis after topical application, J Ocul Pharmacol Ther. 31 (2015) 215–227. https://doi.org/10.1089/jop.2014.0152.

[291] M.L. Lovett, X. Wang, T. Yucel, L. York, M. Keirstead, L. Haggerty, D.L. Kaplan, Silk hydrogels for sustained ocular delivery of anti-vascular endothelial growth factor (anti-VEGF) therapeutics, Eur J Pharm Biopharm. 95 (2015) 271–278. https://doi.org/10.1016/j.ejpb.2014.12.029.

[292] B. Xie, L. Jin, Z. Luo, J. Yu, S. Shi, Z. Zhang, M. Shen, H. Chen, X. Li, Z. Song, An injectable thermosensitive polymeric hydrogel for sustained release of Avastin(R) to treat posterior segment disease, Int J Pharm. 490 (2015) 375–383. https://doi.org/10.1016/j.ijpharm.2015.05.071.

[293] B.M. Davis, E.M. Normando, L. Guo, L.A. Turner, S. Nizari, P. O'Shea, S.E. Moss, S. Somavarapu, M.F. Cordeiro, Topical delivery of Avastin to the posterior segment of the eye in vivo using annexin A5-associated liposomes, Small. 10 (2014) 1575–1584. https://doi.org/10.1002/smll.201303433.

[294] R.D. Vaishya, M. Gokulgandhi, S. Patel, M. Minocha, A.K. Mitra, Novel dexamethasone-loaded nanomicelles for the intermediate and posterior segment uveitis, AAPS PharmSciTech. 15 (2014) 1238–1251. https://doi.org/10.1208/s12249-014-0100-4.

[295] W. Wu, Z. He, Z. Zhang, X. Yu, Z. Song, X. Li, Intravitreal injection of rapamycin-loaded polymeric micelles for inhibition of ocular inflammation in rat model, Int J Pharm. 513 (2016) 238–246. https://doi.org/10.1016/j.ijpharm.2016.09.013.

[296] J. Araujo, S. Nikolic, M.A. Egea, E.B. Souto, M.L. Garcia, Nanostructured lipid carriers for triamcinolone acetonide delivery to the posterior segment of the eye, Colloids Surf B Biointerfaces. 88 (2011) 150–157. https://doi.org/10.1016/j.colsurfb.2011.06.025.

[297] Q. Li, K.L. Lai, P.S. Chan, S.C. Leung, H.Y. Li, Y. Fang, K.K.W. To, C.H.J. Choi, Q.Y. Gao, T.W.Y. Lee, Micellar delivery of dasatinib for the inhibition of pathologic cellular processes of the retinal pigment epithelium, Colloids Surf B Biointerfaces. 140 (2016) 278–286. https://doi.org/10.1016/j.colsurfb.2015.12.053.

[298] K. Kauper, C. McGovern, S. Sherman, P. Heatherton, R. Rapoza, P. Stabila, B. Dean, A. Lee, S. Borges, B. Bouchard, W. Tao, Two-year intraocular delivery of ciliary neurotrophic factor by encapsulated cell technology implants in patients with chronic retinal degenerative diseases, Investig. Ophthalmol. Vis. Sci. (2012). https://doi.org/10.1167/iovs.12-9970.

[299] A. Solanki, R. Smalling, A.H. Parola, I. Nathan, R. Kasher, Y. Pathak, V. Sutariya, Humanin Nanoparticles for Reducing Pathological Factors Characteristic of Age-Related Macular Degeneration, Curr. Drug Deliv. (2018). https://doi.org/10.2174/1567201815666181031163111.

[300] C. Chittasupho, P. Posritong, P. Ariyawong, Stability, Cytotoxicity, and Retinal Pigment Epithelial Cell Binding of Hyaluronic Acid-Coated PLGA Nanoparticles Encapsulating Lutein, AAPS PharmSciTech. (2019). https://doi.org/10.1208/s12249-018-1256-0.

[301] V. Agrahari, A. Mandal, V. Agrahari, H.M. Trinh, M. Joseph, A. Ray, H. Hadji, R. Mitra, D. Pal, A.K. Mitra, A comprehensive insight on ocular pharmacokinetics, Drug Deliv. Transl. Res. (2016). https://doi.org/10.1007/s13346-016-0339-2.

[302] A. Hirani, A. Grover, Y.W. Lee, Y. Pathak, V. Sutariya, Triamcinolone acetonide nanoparticles incorporated in thermoreversible gels for age-related macular degeneration, Pharm Dev Technol. 21 (2016) 61–67. https://doi.org/10.3109/10837450.2014.965326.

[303] D. Park, V. Shah, B.M. Rauck, T.R. Friberg, Y. Wang, An Anti-angiogenic Reverse Thermal Gel as a Drug-Delivery System for Age-Related Wet Macular Degeneration, Macromol. Biosci. (2013). https://doi.org/10.1002/mabi.201200384.

[304] A. Tatke, N. Dudhipala, K.Y. Janga, S.P. Balguri, B. Avula, M.M. Jablonski, S. Majumdar, In situ gel of triamcinolone acetonide-loaded solid lipid nanoparticles for improved topical ocular delivery: Tear kinetics and ocular disposition studies, Nanomaterials. (2019). https://doi.org/10.3390/nano9010033.

[305] S.B. Makwana, V.A. Patel, S.J. Parmar, Development and characterization of in-situ gel for ophthalmic formulation containing ciprofloxacin hydrochloride, Results Pharma Sci. (2016). https://doi.org/10.1016/j.rinphs.2015.06.001.

[306] P. Upadhayay, M. Kumar, K. Pathak, Norfloxacin loaded pH triggered nanoparticulate in-situ gel for extraocular bacterial infections: Optimization, ocular irritancy and corneal toxicity, Iran. J. Pharm. Res. (2016). https://doi.org/10.22037/ijpr.2016.1795.

[307] M. Kouchak, M. Mahmoodzadeh, F. Farrahi, Designing of a pH-Triggered Carbopol®/HPMC In Situ Gel for Ocular Delivery of Dorzolamide HCl: In Vitro, In Vivo, and Ex Vivo Evaluation, AAPS PharmSciTech. (2019). https://doi.org/10.1208/s12249-019-1431-y.

[308] M.J. Coffey, H.H. Decory, S.S. Lane, Development of a non-settling gel formulation of 0.5% loteprednol etabonate for anti-inflammatory use as an ophthalmic drop, Clin. Ophthalmol. (2013). https://doi.org/10.2147/OPTH.S40588.

[309] N.J. Kim, A. Harris, A. Elghouche, W. Gama, B. Siesky, Ocular Permeation Enhancers, in: Nano-Biomaterials Ophthalmic Drug Deliv., 2016. https://doi.org/10.1007/978-3-319-29346-2_9.

[310] P. Mehta, A.A. Al-Kinani, O. Qutachi, M.S. Arshad, A. Alqahtani, M.-W. Chang, W.M. Amoaku, R.G. Alany, Z. Ahmad, Assessing the ex vivo permeation behaviour of functionalised contact lens coatings engineered using an electrohydrodynamic technique , J. Phys. Mater. (2018). https://doi.org/10.1088/2515-7639/aaf263.

[311] P. Van Der Bijl, A.D. Van Eyk, D. Meyer, Effects of three penetration enhancers on transcorneal permeation of cyclosporine, Cornea. (2001). https://doi.org/10.1097/00003226-200107000-00013.

[312] Y. Wang, C.H. Liu, T. Ji, M. Mehta, W. Wang, E. Marino, J. Chen, D.S. Kohane, Intravenous treatment of choroidal neovascularization by photo-targeted nanoparticles, Nat. Commun. (2019). https://doi.org/10.1038/s41467-019-08690-4.

[313] A. Gawin-Mikołajewicz, K.P. Nartowski, A.J. Dyba, A.M. Gołkowska, K. Malec, B. Karolewicz, Ophthalmic Nanoemulsions: From Composition to Technological Processes and Quality Control, Mol. Pharm. 18 (2021) 3719–3740. https://doi.org/10.1021/acs.molpharmaceut.1c00650.

[314] J.A. Beutler, Natural Products as a Foundation for Drug Discovery, Curr. Protoc. Pharmacol. 46 (2009) 9.11.1-9.11.21. https://doi.org/https://doi.org/10.1002/0471141755.ph0911s46.

[315] J. Zhang, K. Hu, L. Di, P. Wang, Z. Liu, J. Zhang, P. Yue, W. Song, J. Zhang, T. Chen, Z. Wang, Y. Zhang, X. Wang, C. Zhan, Y.-C. Cheng, X. Li, Q. Li, J.-Y. Fan, Y. Shen, J.-Y. Han, H. Qiao, Traditional herbal medicine and nanomedicine: Converging disciplines to improve therapeutic efficacy and human health, Adv. Drug Deliv. Rev. 178 (2021) 113964. https://doi.org/https://doi.org/10.1016/j.addr.2021.113964.

[316] D. Jorgensen, Clinical Study Protocol, 2020. https://doi.org/https://clinicaltrials.gov/ct2/show/NCT03785340.

[317] S. Silverstein, E. Yeu, J. Tauber, M. Guillon, L. Jones, D. Galarreta, S. Srinivasan, V. Manoj, Symptom relief following a single dose of propylene glycol-hydroxypropyl guar nanoemulsion in patients with dry eye disease: A phase IV, multicenter trial, Clin. Ophthalmol. 14 (2020) 3167–3177. https://doi.org/10.2147/OPTH.S263362.

[318] M. Korenfeld, J. Gira, K. Jong, J. Martel, S. Vold, T. Walters, D. Usner, E. Donnenfeld, OCS-01 (Novel Topical Dexamethasone Formulation) in Inflammation and Pain Post Cataract Surgery: A Randomized, Double-Masked, Vehicle-Controlled Study, Clin. Ther. 44 (2022) 1577–1587. https://doi.org/10.1016/j.clinthera.2022.11.003.

[319] M.M. Momin, S.D. Afreen, Nanoformulations and highlights of clinical studies for ocular drug delivery systems: An overview, Crit. Rev. Ther. Drug Carrier Syst. 38 (2021) 79–107. https://doi.org/10.1615/CritRevTherDrugCarrierSyst.2021035767.

[320] A.L. Onugwu, C.S. Nwagwu, O.S. Onugwu, A.C. Echezona, C.P. Agbo, S.A. Ihim, P. Emeh, P.O. Nnamani, A.A. Attama, V. V Khutoryanskiy, Nanotechnology based drug delivery systems for the treatment of anterior segment eye diseases, J. Control. Release. 354 (2023) 465–488. https://doi.org/https://doi.org/10.1016/j.jconrel.2023.01.018.

[321] G. Birrenbach, P.P. Speiser, Polymerized micelles and their use as adjuvants in immunology, J. Pharm. Sci. (1976). https://doi.org/10.1002/jps.2600651217.

[322] M. Yadav, N. Schiavone, A.I.G. Aranguez, F. Giansanti, L. Papucci, M.J. Perez de Lara, M. Singh, I.P. Kaur, Atorvastatin-loaded solid lipid nanoparticles as eye drops: proposed treatment option for age-related macular degeneration (AMD)., Drug Deliv. Transl. Res. (2020). https://doi.org/10.1007/s13346-020-00733-4.

[323] C. Chittasupho, K. Kengtrong, S. Chalermnithiwong, N. Sarisuta, Anti-angiogenesis by dual action of R5K peptide conjugated itraconazole nanoparticles, AAPS PharmSciTech. (2020). https://doi.org/10.1208/s12249-019-1568-8.

[324] H.M. Eid, M.H. Elkomy, S.F. El Menshawe, H.F. Salem, Development, Optimization, and In Vitro/In Vivo Characterization of Enhanced Lipid Nanoparticles for Ocular Delivery of Ofloxacin: the Influence of Pegylation and Chitosan Coating, AAPS PharmSciTech. (2019). https://doi.org/10.1208/s12249-019-1371-6.

[325] M. Alkholief, H. Albasit, A. Alhowyan, S. Alshehri, M. Raish, M. Abul Kalam, A. Alshamsan, Employing a PLGA-TPGS based nanoparticle to improve the ocular delivery of Acyclovir, Saudi Pharm. J. (2019). https://doi.org/10.1016/j.jsps.2018.11.011.

[326] E. Sánchez-López, G. Esteruelas, A. Ortiz, M. Espina, J. Prat, M. Muñoz, A. Cano, A.C. Calpena, M. Ettcheto, A. Camins, Z. Alsafi, E.B. Souto, M.L. García, M. Pujol, Article dexibuprofen biodegradable nanoparticles: One step closer towards a better ocular interaction study, Nanomaterials. (2020). https://doi.org/10.3390/nano10040720.

[327] S. Liu, M.D. Dozois, C.N. Chang, A. Ahmad, D.L.T. Ng, D. Hileeto, H. Liang, M.M. Reyad, S. Boyd, L.W. Jones, F.X. Gu, Prolonged ocular retention of mucoadhesive nanoparticle eye drop formulation enables treatment of eye diseases using significantly reduced dosage, Mol. Pharm. (2016). https://doi.org/10.1021/acs.molpharmaceut.6b00445.

[328] R. Sheshala, G.C. Hong, W.P. Yee, V.S. Meka, R.R.S. Thakur, In situ forming phase-inversion implants for sustained ocular delivery of triamcinolone acetonide, Drug Deliv Transl Res. (2018). https://doi.org/10.1007/s13346-018-0491-y.

[329] N. Khan, Ameeduzzafar, K. Khanna, A. Bhatnagar, F.J. Ahmad, A. Ali, Chitosan coated PLGA nanoparticles amplify the ocular hypotensive effect of forskolin: Statistical design, characterization and in vivo studies, Int J Biol Macromol. 116 (2018) 648–663. https://doi.org/10.1016/j.ijbiomac.2018.04.122.

[330] B. Şenel, A.A. Öztürk, New approaches to tumor therapy with siRNA-decorated and chitosan-modified PLGA nanoparticles, Drug Dev. Ind. Pharm. (2019). https://doi.org/10.1080/03639045.2019.1665061.

[331] B.J. Thompson, P.T. Ronaldson, Drug delivery to the ischemic brain, Adv. Pharmacol. 71 (2014) 165–202. https://doi.org/10.1016/bs.apha.2014.06.013.

[332] S.W. Tan, N. Billa, C.R. Roberts, J.C. Burley, Surfactant effects on the physical characteristics of Amphotericin B-containing nanostructured lipid carriers, Colloids Surfaces A Physicochem. Eng. Asp. (2010). https://doi.org/10.1016/j.colsurfa.2010.09.030.

[333] S. Akhter, F. Ramazani, M.Z. Ahmad, F.J. Ahmad, Z. Rahman, A. Bhatnagar, G. Storm, Ocular pharmacoscintigraphic and aqueous humoral drug availability of ganciclovir-loaded mucoadhesive nanoparticles in rabbits, Eur. J. Nanomedicine. (2013). https://doi.org/10.1515/ejnm-2013-0012.

[334] B. Silva, J. Marto, B.S. Braz, E. Delgado, A.J. Almeida, L. Gonçalves, New nanoparticles for topical ocular delivery of erythropoietin, Int. J. Pharm. (2020). https://doi.org/10.1016/j.ijpharm.2020.119020.

[335] A.H. Salama, A.A. Mahmoud, R. Kamel, A Novel Method for Preparing Surface-Modified Fluocinolone Acetonide Loaded PLGA Nanoparticles for Ocular Use: In Vitro and In Vivo Evaluations, AAPS PharmSciTech. (2016). https://doi.org/10.1208/s12249-015-0448-0.

[336] S.A. Khan, P.S. Doyle, D. Ding, S. Vijayan, B. Kundukad, A. Somasundar, Design of Mucoadhesive PLGA Microparticles for Ocular Drug Delivery, ACS Appl. Bio Mater. 1 (2018) 561–571. https://doi.org/10.1021/acsabm.8b00041.

[337] A.R.N. Pontillo, A. Detsi, Nanoparticles for ocular drug delivery: Modified and non-modified chitosan as a promising biocompatible carrier, Nanomedicine. (2019). https://doi.org/10.2217/nnm-2019-0040.

[338] A. Seyfoddin, T. Sherwin, D. V. Patel, C. N. McGhee, I. D. Rupenthal, J. A. Taylor, R. Al-Kassas, Ex vivo and In vivo Evaluation of Chitosan Coated Nanostructured Lipid Carriers for Ocular Delivery of Acyclovir, Curr. Drug Deliv. (2016). https://doi.org/10.2174/1567201813666151116142752.

[339] J. Kirch, A. Schneider, B. Abou, A. Hopf, U.F. Schaefer, M. Schneider, C. Schall, C. Wagner, C.M. Lehr, Optical tweezers reveal relationship between microstructure and nanoparticle penetration of pulmonary mucus, Proc Natl Acad Sci U S A. 109 (2012) 18355–18360. https://doi.org/10.1073/pnas.1214066109.

[340] C. Guo, R.A. Gemeinhart, Understanding the adsorption mechanism of chitosan onto

poly(lactide-co-glycolide) particles, Eur J Pharm Biopharm. 70 (2008) 597–604. https://doi.org/10.1016/j.ejpb.2008.06.008.

[341] Q. Xu, N.J. Boylan, J.S. Suk, Y.-Y. Wang, E.A. Nance, J.-C. Yang, P.J. McDonnell, R.A. Cone, E.J. Duh, J. Hanes, Nanoparticle diffusion in, and microrheology of, the bovine vitreous ex vivo, J. Control. Release. 167 (2013) 76–84. https://doi.org/https://doi.org/10.1016/j.jconrel.2013.01.018.

[342] D. Chen, H. Yu, H. Mu, G. Li, Y. Shen, Novel multicore niosomes based on double pH-sensitive mixed micelles for Ginsenoside Rh2 delivery, Artif. Cells, Nanomedicine Biotechnol. (2014). https://doi.org/10.3109/21691401.2013.794358.

[343] S.K. Yadav, G. Khan, M. Bansal, H. Vardhan, B. Mishra, Screening of ionically crosslinked chitosan-tripolyphosphate microspheres using Plackett–Burman factorial design for the treatment of intrapocket infections, Drug Dev. Ind. Pharm. (2017). https://doi.org/10.1080/03639045.2017.1349782.

[344] J.N. Betts, M.G. Johnson, P.T. Rygiewicz, G.A. King, C.P. Andersen, Potential for metal contamination by direct sonication of nanoparticle suspensions, Environ. Toxicol. Chem. (2013). https://doi.org/10.1002/etc.2123.

[345] M.J. Santander-Ortega, N. Csaba, L. González, D. Bastos-González, J.L. Ortega-Vinuesa, M.J. Alonso, Protein-loaded PLGA-PEO blend nanoparticles: Encapsulation, release and degradation characteristics, Colloid Polym. Sci. (2010). https://doi.org/10.1007/s00396-009-2131-z.

[346] P.N. Gupta, S. Jain, C. Nehate, N. Alam, V. Khare, R.D. Dubey, A. Saneja, S. Kour, S.K. Singh, Development and evaluation of paclitaxel loaded PLGA: Poloxamer blend nanoparticles for cancer chemotherapy, Int. J. Biol. Macromol. (2014). https://doi.org/10.1016/j.ijbiomac.2014.05.067.

[347] V.V.S.N.L. Andra, S.V.N. Pammi, L.V.K.P. Bhatraju, L.K. Ruddaraju, A Comprehensive Review on Novel Liposomal Methodologies, Commercial Formulations, Clinical Trials and Patents, Bionanoscience. 12 (2022) 274–291. https://doi.org/10.1007/s12668-022-00941-x.

[348] D. Hou, R. Gui, S. Hu, Y. Huang, Z. Feng, Q. Ping, Preparation and Characterization of Novel Drug-Inserted-Montmorillonite Chitosan Carriers for Ocular Drug Delivery, Adv. Nanoparticles. (2015). https://doi.org/10.4236/anp.2015.43009.

[349] A.M. Bodratti, P. Alexandridis, Formulation of poloxamers for drug delivery, J. Funct. Biomater. (2018). https://doi.org/10.3390/jfb9010011.

[350] J.U. Menon, S. Kona, A.S. Wadajkar, F. Desai, A. Vadla, K.T. Nguyen, Effects of surfactants on the properties of PLGA nanoparticles, J. Biomed. Mater. Res. - Part A. (2012). https://doi.org/10.1002/jbm.a.34040.

[351] S. Streck, H. Neumann, H.M. Nielsen, T. Rades, A. McDowell, Comparison of bulk and microfluidics methods for the formulation of poly-lactic-co-glycolic acid (PLGA) nanoparticles modified with cell-penetrating peptides of different architectures, Int. J. Pharm. X. (2019). https://doi.org/10.1016/j.ijpx.2019.100030.

[352] T.A. Ahmed, Preparation of transfersomes encapsulating sildenafil aimed for transdermal drug delivery: Plackett-Burman design and characterization, J. Liposome Res. (2015). https://doi.org/10.3109/08982104.2014.950276.

[353] Z. Rahman, A.S. Zidan, M.J. Habib, M.A. Khan, Understanding the quality of protein loaded PLGA nanoparticles variability by Plackett-Burman design, Int. J. Pharm. (2010).

https://doi.org/10.1016/j.ijpharm.2009.12.040.

[354] S. Dhat, S. Pund, C. Kokare, P. Sharma, B. Shrivastava, Risk management and statistical multivariate analysis approach for design and optimization of satranidazole nanoparticles, Eur. J. Pharm. Sci. (2017). https://doi.org/10.1016/j.ejps.2016.09.035.

[355] A.K. Das, S. Dewanjee, Chapter 3 - Optimization of Extraction Using Mathematical Models and Computation, in: S.D. Sarker, L.B.T.-C.P. Nahar (Eds.), Elsevier, 2018: pp. 75–106. https://doi.org/https://doi.org/10.1016/B978-0-12-812364-5.00003-1.

[356] P. Benjasirimongkol, S. Piriyaprasarth, K. Moribe, P. Sriamornsak, Use of Risk Assessment and Plackett–Burman Design for Developing Resveratrol Spray-Dried Emulsions: a Quality-by-Design Approach, AAPS PharmSciTech. 20 (2019) 1–10. https://doi.org/10.1208/s12249-018-1220-z.

[357] N. Khan, Ameeduzzafar, K. Khanna, A. Bhatnagar, F.J. Ahmad, A. Ali, Chitosan coated PLGA nanoparticles amplify the ocular hypotensive effect of forskolin: Statistical design, characterization and in vivo studies, Int. J. Biol. Macromol. (2018). https://doi.org/10.1016/j.ijbiomac.2018.04.122.

[358] B. Taghipour, M. Yakhchali, I. Haririan, A.M. Tamaddon, S.M. Samani, The effects of technical and compositional variables on the size and release profile of bovine serum albumin from PLGA based particulate systems, Res. Pharm. Sci. (2014).

[359] S. Jose, S. Sowmya, T.A. Cinu, N.A. Aleykutty, S. Thomas, E.B. Souto, Surface modified PLGA nanoparticles for brain targeting of Bacoside-A, Eur. J. Pharm. Sci. (2014). https://doi.org/10.1016/j.ejps.2014.06.024.

[360] K. Yoncheva, J. Vandervoort, A. Ludwig, Development of mucoadhesive poly(lactide-co-glycolide) nanoparticles for ocular application, Pharm. Dev. Technol. 16 (2011) 29–35. https://doi.org/10.3109/10837450903479954.

[361] B. Semete, L.I.J. Booysen, L. Kalombo, J.D. Venter, L. Katata, B. Ramalapa, J.A. Verschoor, H. Swai, In vivo uptake and acute immune response to orally administered chitosan and PEG coated PLGA nanoparticles, Toxicol. Appl. Pharmacol. (2010). https://doi.org/10.1016/j.taap.2010.09.002.

[362] A. Kumar, C.K. Dixit, U. States, Methods for characterization of nanoparticles 3, (2017). https://doi.org/10.1016/B978-0-08-100557-6.00003-1.

[363] G. Dalwadi, H.A.E. Benson, Y. Chen, Comparison of diafiltration and tangential flow filtration for purification of nanoparticle suspensions, Pharm. Res. (2005). https://doi.org/10.1007/s11095-005-7781-z.

[364] S. Loganathan, R.B. Valapa, R.K. Mishra, G. Pugazhenthi, S. Thomas, Thermogravimetric Analysis for Characterization of Nanomaterials, in: Therm. Rheol. Meas. Tech. Nanomater. Charact., 2017. https://doi.org/10.1016/B978-0-323-46139-9.00004-9.

[365] M.F. Silva, A.A.W. Hechenleitner, J.M. Irache, A.J.A. De Oliveira, E.A.G. Pineda, Study of thermal degradation of PLGA, PLGA nanospheres and PLGA/maghemite superparamagnetic nanospheres, Mater. Res. 18 (2015) 1400–1406. https://doi.org/10.1590/1516-1439.045415.

[366] Z. Xiao, S. Wan, Y. Niu, X. Kou, Effect of preparation parameters on microparticles with high loading capacity and adsorption property adsorbed on functional paper, Coatings. (2019). https://doi.org/10.3390/coatings9110704.

[367] S. Bandopadhyay, N. Bandyopadhyay, P.K. Deb, C. Singh, R.K. Tekade, Preformulation Studies

of Drug Substances, Protein, and Peptides: Role in Drug Discovery and Pharmaceutical Product Development. Role in Drug Discovery and Pharmaceutical Product Development., in: Dos. Form Des. Considerations Vol. I, 2018. https://doi.org/10.1016/B978-0-12-814423-7.00012-5.

[368] T.Z. Fermino, C.M. Awano, L.X. Moreno, D.R. Vollet, F.S. de Vicente, Structure and thermal stability in hydrophobic Pluronic F127-modified silica aerogels, Microporous Mesoporous Mater. (2018). https://doi.org/10.1016/j.micromeso.2018.03.039.

[369] C. D'Avila Carvalho Erbetta, Synthesis and Characterization of Poly(D,L-Lactide-co-Glycolide) Copolymer, J. Biomater. Nanobiotechnol. (2012). https://doi.org/10.4236/jbnb.2012.32027.

[370] N. Elsaid, T.L. Jackson, M. Gunic, S. Somavarapu, Positively charged amphiphilic chitosan derivative for the transscleral delivery of rapamycin, Investig. Ophthalmol. Vis. Sci. (2012). https://doi.org/10.1167/iovs.12-10717.

[371] M.K. Oo, S. Mahmood, W.T. Wui, U.K. Mandal, B. Chatterjee, Effects of Different Formulation Methods on Drug Crystallinity, Drug-Carrier Interaction, and Ex Vivo Permeation of a Ternary Solid Dispersion Containing Nisoldipine, J. Pharm. Innov. (2019). https://doi.org/10.1007/s12247-019-09415-2.

[372] J.J. Rouse, F. Mohamed, C.F. van der Walle, Physical ageing and thermal analysis of PLGA microspheres encapsulating protein or DNA, Int. J. Pharm. 339 (2007) 112–120. https://doi.org/10.1016/j.ijpharm.2007.02.026.

[373] M.K. Anwer, M.A. Al-Mansoor, S. Jamil, R. Al-Shdefat, M.N. Ansari, F. Shakeel, Development and evaluation of PLGA polymer based nanoparticles of quercetin, Int. J. Biol. Macromol. (2016). https://doi.org/10.1016/j.ijbiomac.2016.07.002.

[374] Ö. Şen, M. Emanet, M. Çulha, Biocompatibility evaluation of boron nitride nanotubes, in: Boron Nitride Nanotub. Nanomedicine, 2016. https://doi.org/10.1016/B978-0-323-38945-7.00003-1.

[375] J.H. Park, H. Jeong, J. Hong, M. Chang, M. Kim, R.S. Chuck, J.K. Lee, C.Y. Park, The Effect of Silica Nanoparticles on Human Corneal Epithelial Cells, Sci. Rep. (2016). https://doi.org/10.1038/srep37762.

[376] M. Hytti, N. Piippo, A. Salminen, P. Honkakoski, K. Kaarniranta, A. Kauppinen, Quercetin alleviates 4-hydroxynonenal-induced cytotoxicity and inflammation in ARPE-19 cells, Exp. Eye Res. (2015). https://doi.org/10.1016/j.exer.2015.02.001.

[377] C. Cañadas, H. Alvarado, A.C. Calpena, A.M. Silva, E.B. Souto, M.L. García, G. Abrego, In vitro, ex vivo and in vivo characterization of PLGA nanoparticles loading pranoprofen for ocular administration, Int. J. Pharm. (2016). https://doi.org/10.1016/j.ijpharm.2016.07.055.

[378] P.J.T. Reardon, M. Parhizkar, A.H. Harker, R.J. Browning, V. Vassileva, E. Stride, R.B. Pedley, M. Edirisinghe, J.C. Knowles, Electrohydrodynamic fabrication of core-shell PLGA nanoparticles with controlled release of cisplatin for enhanced cancer treatment, Int. J. Nanomedicine. (2017). https://doi.org/10.2147/IJN.S134833.

[379] B.D. Kuppermann, L.C. Zacharias, M.C. Kenney, Steroid differentiation: The safety profile of various steroids on retinal cells in vitro and their implications for clinical use (an American ophthalmological society thesis), Trans. Am. Ophthalmol. Soc. 112 (2014) 116–141.

[380] C. Altmeyer, T.K. Karam, N.M. Khalil, R.M. Mainardes, Tamoxifen-loaded poly (L-lactide) nanoparticles : Development , characterization and in vitro evaluation of cytotoxicity, Mater. Sci. Eng. C. 60 (2016) 135–142. https://doi.org/10.1016/j.msec.2015.11.019.

[381] J. Mosafer, K. Abnous, M. Tafaghodi, A. Mokhtarzadeh, M. Ramezani, European Journal of Pharmaceutics and Biopharmaceutics In vitro and in vivo evaluation of anti-nucleolin-targeted magnetic PLGA nanoparticles loaded with doxorubicin as a theranostic agent for enhanced targeted cancer imaging and therapy, Eur. J. Pharm. Biopharm. 113 (2017) 60–74. https://doi.org/10.1016/j.ejpb.2016.12.009.

[382] R. Kaskoos, Investigation of moxifloxacin loaded chitosan-dextran nanoparticles for topical instillation into eye: In-vitro and ex-vivo evaluation, Int. J. Pharm. Investig. (2014). https://doi.org/10.4103/2230-973x.143114.

[383] T. Abdullah, N. Ibrahim, M. Warsi, Chondroitin sulfate-chitosan nanoparticles for ocular delivery of bromfenac sodium: Improved permeation, retention, and penetration, Int. J. Pharm. Investig. (2016). https://doi.org/10.4103/2230-973x.177823.

[384] F. Wang, L. Chen, S. Jiang, J. He, X. Zhang, J. Peng, Q. Xu, R. Li, Optimization of methazolamide-loaded solid lipid nanoparticles for ophthalmic delivery using Box-Behnken design, J. Liposome Res. (2014). https://doi.org/10.3109/08982104.2014.891231.

[385] M. Paulsamy, C. Ponnusamy, M. Palanisami, G. Nackeeran, S.S. Paramasivam, A. Sugumaran, R. Kandasamy, S. Natesan, R. Palanichamy, Nepafenac loaded silica nanoparticles dispersed in-situ gel systems: Development and characterization, Int. J. Biol. Macromol. (2018). https://doi.org/10.1016/j.ijbiomac.2018.01.123.

[386] R. Gonzalez-Pizarro, P. Carvajal-Vidal, L. Halbault Bellowa, A.C. Calpena, M. Espina, M.L. García, In-situ forming gels containing fluorometholone-loaded polymeric nanoparticles for ocular inflammatory conditions, Colloids Surfaces B Biointerfaces. (2019). https://doi.org/10.1016/j.colsurfb.2018.11.065.

[387] M. Dandamudi, P. McLoughlin, G. Behl, S. Rani, L. Coffey, A. Chauhan, D. Kent, L. Fitzhenry, Chitosan-coated plga nanoparticles encapsulating triamcinolone acetonide as a potential candidate for sustained ocular drug delivery, Pharmaceutics. 13 (2021) 1–20. https://doi.org/10.3390/pharmaceutics13101590.

[388] K. Tahara, K. Karasawa, R. Onodera, H. Takeuchi, Feasibility of drug delivery to the eye's posterior segment by topical instillation of PLGA nanoparticles, Asian J. Pharm. Sci. 12 (2017). https://doi.org/10.1016/j.ajps.2017.03.002.

[389] Y. Wang, X. Xu, Y. Gu, Y. Cheng, F. Cao, Recent advance of nanoparticle-based topical drug delivery to the posterior segment of the eye, Expert Opin. Drug Deliv. (2018). https://doi.org/10.1080/17425247.2018.1496080.

[390] M.M. Ibrahim, A.E.H. Abd-Elgawad, O.A.E. Soliman, M.M. Jablonski, Nanoparticle-based topical ophthalmic formulations for sustained celecoxib release, J. Pharm. Sci. (2013). https://doi.org/10.1002/jps.23417.

[391] O. Pillai, R. Panchagnula, Polymers in drug delivery, Curr. Opin. Chem. Biol. (2001). https://doi.org/10.1016/S1367-5931(00)00227-1.

[392] K.T. Savjani, A.K. Gajjar, J.K. Savjani, Drug Solubility: Importance and Enhancement Techniques, ISRN Pharm. (2012). https://doi.org/10.5402/2012/195727.

[393] A. Sabzevari, K. Adibkia, H. Hashemi, A. Hedayatfar, N. Mohsenzadeh, F. Atyabi, M.H. Ghahremani, R. Dinarvand, Polymeric triamcinolone acetonide nanoparticles as a new alternative in the treatment of uveitis: In vitro and in vivo studies, Eur. J. Pharm. Biopharm. (2013). https://doi.org/10.1016/j.ejpb.2012.12.010.

[394] L. Álvarez-Álvarez, L. Barral, R. Bouza, Y. Farrag, F. Otero-Espinar, S. Feijóo-Bandín, F. Lago,

Hydrocortisone loaded poly-(3-hydroxybutyrate-co-3-hydroxyvalerate) nanoparticles for topical ophthalmic administration: Preparation, characterization and evaluation of ophthalmic toxicity, Int. J. Pharm. (2019). https://doi.org/10.1016/j.ijpharm.2019.118519.

[395] A. El Shaer, S. Mustafa, M. Kasar, S. Thapa, B. Ghatora, R.G. Alany, Nanoparticle-laden contact lens for controlled ocular delivery of prednisolone: Formulation optimization using statistical experimental design, Pharmaceutics. (2016). https://doi.org/10.3390/pharmaceutics8020014.

[396] I.A. de Lima, N.M. Khalil, T.T. Tominaga, A. Lechanteur, B. Sarmento, R.M. Mainardes, Mucoadhesive chitosan-coated PLGA nanoparticles for oral delivery of ferulic acid, Artif. Cells, Nanomedicine Biotechnol. (2018). https://doi.org/10.1080/21691401.2018.1477788.

[397] T. Feczk, Comparison of the preparation of PLGA – BSA nano- and microparticles by PVA , poloxamer and PVP, 319 (2008) 188–195. https://doi.org/10.1016/j.colsurfa.2007.07.011.

[398] L. Mayol, C. Serri, C. Menale, S. Crispi, M.T. Piccolo, L. Mita, S. Giarra, M. Forte, A. Saija, M. Biondi, D.G. Mita, Curcumin loaded PLGA-poloxamer blend nanoparticles induce cell cycle arrest in mesothelioma cells, Eur. J. Pharm. Biopharm. (2015). https://doi.org/10.1016/j.ejpb.2015.03.005.

[399] S. Giarra, C. Serri, L. Russo, S. Zeppetelli, G. De Rosa, A. Borzacchiello, M. Biondi, L. Ambrosio, L. Mayol, Spontaneous arrangement of a tumor targeting hyaluronic acid shell on irinotecan loaded PLGA nanoparticles, Carbohydr. Polym. (2016). https://doi.org/10.1016/j.carbpol.2015.12.031.

[400] M.J. Santander-Ortega, D. Bastos-González, J.L. Ortega-Vinuesa, M.J. Alonso, Insulin-loaded PLGA nanoparticles for oral administration: An in vitro physico-chemical characterization, J. Biomed. Nanotechnol. (2009). https://doi.org/10.1166/jbn.2009.022.

[401] S. Shaarani, S.S. Hamid, N.H.M. Kaus, The Influence of Pluronic F68 and F127 Nanocarrier on Physicochemical Properties, In vitro Release, and Antiproliferative Activity of Thymoquinone Drug, Pharmacognosy Res. 9 (2017) 12–20. https://doi.org/10.4103/0974-8490.199774.

[402] F. Madani, S.S. Esnaashari, B. Mujokoro, F. Dorkoosh, M. Khosravani, M. Adabi, Investigation of effective parameters on size of paclitaxel loaded PLGA nanoparticles, Adv. Pharm. Bull. 8 (2018) 77–84. https://doi.org/10.15171/apb.2018.010.

[403] R. Kumar, R.C. Nagarwal, M. Dhanawat, J.K. Pandit, In-Vitro and In-Vivo study of indomethacin loaded gelatin nanoparticles, J. Biomed. Nanotechnol. (2011). https://doi.org/10.1166/jbn.2011.1290.

[404] K.J. Sreeram, M. Nidhin, R. Indumathy, B.U. Nair, Synthesis of iron oxide nanoparticles of narrow size distribution on polysaccharide templates, Bull. Mater. Sci. (2008). https://doi.org/10.1007/s12034-008-0016-2.

[405] A. Mathew, T. Fukuda, Y. Nagaoka, T. Hasumura, H. Morimoto, Y. Yoshida, T. Maekawa, K. Venugopal, D.S. Kumar, Curcumin loaded-PLGA nanoparticles conjugated with Tet-1 peptide for potential use in Alzheimer's disease, PLoS One. (2012). https://doi.org/10.1371/journal.pone.0032616.

[406] B. Lu, X. Lv, Y. Le, Chitosan-modified PLGA nanoparticles for control-released drug delivery, Polymers (Basel). (2019). https://doi.org/10.3390/polym11020304.

[407] F. Hu, W. Liu, L. Yan, F. Kong, K. Wei, Optimization and characterization of poly(lactic-co-glycolic acid) nanoparticles loaded with astaxanthin and evaluation of anti-photodamage effect in vitro, R. Soc. Open Sci. (2019). https://doi.org/10.1098/rsos.191184.

[408] W.N. Omwoyo, B. Ogutu, F. Oloo, H. Swai, L. Kalombo, P. Melariri, G.M. Mahanga, J.W. Gathirwa, Preparation, characterization, and optimization of primaquine-loaded solid lipid nanoparticles, Int. J. Nanomedicine. (2014). https://doi.org/10.2147/IJN.S62630.

[409] V. Kunasekaran, K. Krishnamoorthy, Compatibility studies of rasagiline mesylate with selected excipients for an effective solid lipid nanoparticles formulation, Int. J. Pharm. Pharm. Sci. (2015).

[410] E. García-Millán, M. Quintáns-Carballo, F.J. Otero-Espinar, Solid-state characterization of triamcinolone acetonide nanosuspensiones by X-ray spectroscopy, ATR Fourier transforms infrared spectroscopy and differential scanning calorimetry analysis, Data Br. (2017). https://doi.org/10.1016/j.dib.2017.09.002.

[411] M. Kaya, S. Khadem, Y.S. Cakmak, M. Mujtaba, S. Ilk, L. Akyuz, A.M. Salaberria, J. Labidi, A.H. Abdulqadir, E. Deligöz, Antioxidative and antimicrobial edible chitosan films blended with stem, leaf and seed extracts of Pistacia terebinthus for active food packaging, RSC Adv. (2018). https://doi.org/10.1039/c7ra12070b.

[412] F. Ferrero, M. Periolatto, Antimicrobial finish of textiles by chitosan UV-curing, J. Nanosci. Nanotechnol. (2012). https://doi.org/10.1166/jnn.2012.4902.

[413] Z. Zhang, X. Wang, R. Zhu, Y. Wang, B. Li, Y. Ma, Y. Yin, Synthesis and characterization of serial random and block-copolymers based on lactide and glycolide, Polym. Sci. - Ser. B. (2016). https://doi.org/10.1134/S1560090416060191.

[414] M. Abou-ElNour, R.A.H. Ishak, M. Tiboni, G. Bonacucina, M. Cespi, L. Casettari, M.E. Soliman, A.S. Geneidi, Triamcinolone acetonide-loaded PLA/PEG-PDL microparticles for effective intra-articular delivery: synthesis, optimization, in vitro and in vivo evaluation, J. Control. Release. 309 (2019) 125–144. https://doi.org/10.1016/j.jconrel.2019.07.030.

[415] T. Al Kayal, D. Panetta, B. Canciani, P. Losi, M. Tripodi, S. Burchielli, P. Ottoni, P.A. Salvadori, G. Soldani, Evaluation of the effect of a gamma irradiated DBM-Pluronic F127 composite on bone regeneration in wistar rat, PLoS One. (2015). https://doi.org/10.1371/journal.pone.0125110.

[416] S. Yasmeen, M. Kabiraz, B. Saha, M. Qadir, M. Gafur, S. Masum, Chromium (VI) Ions Removal from Tannery Effluent using Chitosan-Microcrystalline Cellulose Composite as Adsorbent, Int. Res. J. Pure Appl. Chem. (2016). https://doi.org/10.9734/irjpac/2016/23315.

[417] C. Lustriane, F.M. Dwivany, V. Suendo, M. Reza, Effect of chitosan and chitosan-nanoparticles on post harvest quality of banana fruits, J. Plant Biotechnol. (2018). https://doi.org/10.5010/JPB.2018.45.1.036.

[418] G. Dennis, W. Harrison, K. Agnes, G. Erastus, Effect of Biological Control Antagonists Adsorbed on Chitosan Immobilized Silica Nanocomposite on Ralstonia solanacearum and Growth of Tomato Seedlings, Adv. Res. (2016). https://doi.org/10.9734/air/2016/22742.

[419] N. Kamaly, B. Yameen, J. Wu, O.C. Farokhzad, Degradable controlled-release polymers and polymeric nanoparticles: Mechanisms of controlling drug release, Chem. Rev. (2016). https://doi.org/10.1021/acs.chemrev.5b00346.

[420] J.M. Chae, I.J. Oh, Sustained Release of All-trans Retinoic Acid from Chitosan-coated Poly(DL-lactide-co-glycolide) Nanoparticles, Yakhak Hoeji. (2019). https://doi.org/10.17480/psk.2019.63.6.367.

[421] M.L. Bruschi, ed., 5 - Mathematical models of drug release, in: Strateg. to Modify Drug Release from Pharm. Syst., Woodhead Publishing, 2015: pp. 63–86.

https://doi.org/https://doi.org/10.1016/B978-0-08-100092-2.00005-9.

[422] D.M. Brown, J.S. Heier, T. Ciulla, M. Benz, P. Abraham, G. Yancopoulos, N. Stahl, A. Ingerman, R. Vitti, A.J. Berliner, K. Yang, Q.D. Nguyen, Primary endpoint results of a phase II study of vascular endothelial growth factor trap-eye in wet age-related macular degeneration, Ophthalmology. 118 (2011) 1089–1097. https://doi.org/10.1016/j.ophtha.2011.02.039.

[423] M.P. Rozing, J.A. Durhuus, M. Krogh Nielsen, Y. Subhi, T.B.L. Kirkwood, R.G.J. Westendorp, T.L. Sørensen, Age-related macular degeneration: A two-level model hypothesis, Prog. Retin. Eye Res. 76 (2020) 100825. https://doi.org/https://doi.org/10.1016/j.preteyeres.2019.100825.

[424] M. Saito, M. Kano, K. Itagaki, Y. Oguchi, T. Sekiryu, Retinal pigment epithelium tear after intravitreal aflibercept injection, Clin. Ophthalmol. (2013). https://doi.org/10.2147/OPTH.S47735.

[425] J. Foucquier, M. Guedj, Analysis of drug combinations: current methodological landscape, Pharmacol. Res. \& Perspect. 3 (2015) e00149. https://doi.org/https://doi.org/10.1002/prp2.149.

[426] K. Hatz, U. Schneider, B. Henrich, B. Braun, S. Sacu, C. Prünte, Comparing ranibizumab monotherapy and combination with single photodynamic therapy in wet AMD: Retreatment and morphologic results, Eur. J. Ophthalmol. (2017). https://doi.org/10.5301/ejo.5000886.

[427] B.D. Kuppermann, M. Goldstein, R.K. Maturi, A. Pollack, M. Singer, A. Tufail, D. Weinberger, X.Y. Li, C.C. Liu, J. Lou, S.M. Whitcup, Dexamethasone Intravitreal Implant as Adjunctive Therapy to Ranibizumab in Neovascular Age-Related Macular Degeneration: A Multicenter Randomized Controlled Trial, Ophthalmologica. (2015). https://doi.org/10.1159/000381865.

[428] P. Zhou, X.-X. Li, Role of genetic factors in the pathogenesis of exudative age-related macular degeneration, Taiwan J. Ophthalmol. 4 (2014) 152–155. https://doi.org/https://doi.org/10.1016/j.tjo.2014.03.007.

[429] K.-H. Wong, H.-Y. Nam, S.-Y. Lew, M. Naidu, P. David, T.A. Kamalden, S.N.H. Hadie, L.-W. Lim, Discovering the Potential of Natural Antioxidants in Age-Related Macular Degeneration: A Review, Pharmaceuticals. 15 (2022). https://doi.org/10.3390/ph15010101.

[430] K. Kaarniranta, D. Sinha, J. Blasiak, A. Kauppinen, Z. Veréb, A. Salminen, M.E. Boulton, G. Petrovski, Autophagy and heterophagy dysregulation leads to retinal pigment epithelium dysfunction and development of age-related macular degeneration, Autophagy. 9 (2013) 973–984. https://doi.org/10.4161/auto.24546.

[431] V. Sarao, D. Veritti, F. Boscia, P. Lanzetta, Intravitreal steroids for the treatment of retinal diseases, Sci. World J. 2014 (2014). https://doi.org/10.1155/2014/989501.

[432] Y. Shao, H. Yu, Y. Yang, M. Li, L. Hang, X. Xu, A Solid Dispersion of Quercetin Shows Enhanced Nrf2 Activation and Protective Effects against Oxidative Injury in a Mouse Model of Dry Age-Related Macular Degeneration, Oxid. Med. Cell. Longev. 2019 (2019) 1479571. https://doi.org/10.1155/2019/1479571.

[433] J. Bojarska, M. Breza, M. Remko, M. Czyz, A. Gajos-Michniewicz, M. Zimecki, K. Kaczmarek, I.D. Madura, J.M. Wojciechowski, W.M. Wolf, Structural and Biofunctional Insights into the Cyclo(Pro-Pro-Phe-Phe-) Scaffold from Experimental and In Silico Studies: Melanoma and Beyond, Int. J. Mol. Sci. 23 (2022). https://doi.org/10.3390/ijms23137173.

[434] N. Cormier, A. Yeo, E. Fiorentino, J. Paxson, Optimization of the wound scratch assay to detect changes in murine mesenchymal stromal cell migration after damage by soluble

cigarette smoke extract, J. Vis. Exp. 2015 (2015) 1–9. https://doi.org/10.3791/53414.

[435] R. Skouta, K. Morán-Santibañez, C.A. Valenzuela, A.H. Vasquez, K. Fenelon, Assessing the Antioxidant Properties of Larrea tridentata Extract as a Potential Molecular Therapy against Oxidative Stress, Molecules. 23 (2018). https://doi.org/10.3390/molecules23071826.

[436] G. Behl, M. Sharma, M. Sikka, S. Dahiya, A. Chhikara, M. Chopra, Gallic acid loaded disulfide cross-linked biocompatible polymeric nanogels as controlled release system: Synthesis, characterization, and antioxidant activity, J. Biomater. Sci. Polym. Ed. 24 (2013) 865–881. https://doi.org/10.1080/09205063.2012.723958.

[437] A. Hirani, A. Grover, Y.W. Lee, Y. Pathak, V. Sutariya, Triamcinolone acetonide nanoparticles incorporated in thermoreversible gels for age-related macular degeneration, Pharm. Dev. Technol. 21 (2016) 61–67. https://doi.org/10.3109/10837450.2014.965326.

[438] C.C. HSIAO, Y.C. CHANG, Y.T. HSIAO, P.H. CHEN, M.C. HSIEH, W.C. WU, Y.H. KAO, Triamcinolone acetonide modulates TGF-β2-induced angiogenic and tissue-remodeling effects in cultured human retinal pigment epithelial cells, Mol. Med. Rep. 24 (2021) 1–10. https://doi.org/10.3892/mmr.2021.12442.

[439] S.C. Cheng, W.C. Huang, J.H.S. Pang, Y.H. Wu, C.Y. Cheng, Quercetin inhibits the production of il-1β-induced inflammatory cytokines and chemokines in arpe-19 cells via the mapk and nf-κb signaling pathways, Int. J. Mol. Sci. (2019). https://doi.org/10.3390/ijms20122957.

[440] N.M.M. Saviranta, L. Veeroos, L.J. Granlund, V.H. Hassinen, K. Kaarniranta, R.O. Karjalainen, Plant flavonol quercetin and isoflavone biochanin A differentially induce protection against oxidative stress and inflammation in ARPE-19 cells, Food Res. Int. (2011). https://doi.org/10.1016/j.foodres.2010.10.056.

[441] X. Wang, H. Li, H. Wang, J. Shi, Quercetin attenuates high glucose-induced injury in human retinal pigment epithelial cell line ARPE-19 by up-regulation of miR-29b, J. Biochem. 167 (2020) 495–502. https://doi.org/10.1093/jb/mvaa001.

[442] M.M. Atsuo, N.S. Asaki, K.S. Aga, T.K. Aneko, Cytotoxicity of Flavonoids toward Cultured Normal Human Cells, 28 (2005) 253–259.

[443] Y. Deng, L. Qiao, M. Du, C. Qu, L. Wan, J. Li, L. Huang, Age-related macular degeneration: Epidemiology, genetics, pathophysiology, diagnosis, and targeted therapy, Genes Dis. 9 (2022) 62–79. https://doi.org/10.1016/j.gendis.2021.02.009.

[444] L.G. Fritsche, R.N. Fariss, D. Stambolian, G.R. Abecasis, C.A. Curcio, A. Swaroop, Age-related macular degeneration: Genetics and biology coming together, Annu. Rev. Genomics Hum. Genet. 15 (2014) 151–171. https://doi.org/10.1146/annurev-genom-090413-025610.

[445] N. Singh, A. Swaroop, R. Ratnapriya, Making Biological Sense of Genetic Studies of Age-Related Macular Degeneration, in: E.Y. Chew, A. Swaroop (Eds.), Age-Related Macular Degener. From Clin. to Genes Back to Patient Manag., Springer International Publishing, Cham, 2021: pp. 201–219. https://doi.org/10.1007/978-3-030-66014-7_8.

[446] H. Keino, S. Horie, S. Sugita, Immune Privilege and Eye-Derived T-Regulatory Cells, J. Immunol. Res. 2018 (2018) 1679197. https://doi.org/10.1155/2018/1679197.

[447] M. Grunin, B. Rinsky, Y. Smith, I. Chowers, Transcriptome Analysis on Monocytes from Patients with Neovascular Age-Related Macular Degeneration, Nat. Publ. Gr. (2016) 1–13. https://doi.org/10.1038/srep29046.

[448] U. Chakravarthy, H. Xu, STAT3 Activation in Circulating Monocytes Contributes to Neovascular

Age-Related Macular Degeneration, (2016) 412–423.

[449] J.E. Knickelbein, C.C. Chan, H.N. Sen, F.L. Ferris, R.B. Nussenblatt, Inflammatory mechanisms of age-related macular degeneration, Int. Ophthalmol. Clin. 55 (2015) 63–78. https://doi.org/10.1097/IIO.0000000000000073.

[450] V.M. Elner, S.G. Elner, Z.-M. Bian, A.L. Kindezelskii, A. Yoshida, H.R. Petty, RPE CD14 immunohistochemical, genetic, and functional expression, Exp. Eye Res. 76 (2003) 321–331. https://doi.org/https://doi.org/10.1016/S0014-4835(02)00310-X.

[451] S.P. Kambhampati, M.K. Mishra, P. Mastorakos, Y. Oh, G.A. Lutty, R.M. Kannan, Intracellular delivery of dendrimer triamcinolone acetonide conjugates into microglial and human retinal pigment epithelial cells, Eur J Pharm Biopharm. 95 (2015) 239–249. https://doi.org/10.1016/j.ejpb.2015.02.013.

[452] X. Zhang, L. Wang, H. Lu, Z. Zong, Z. Chen, Y. Li, X. Luo, Y. Li, Preservation of hydrogen peroxide-induced oxidative damage in HepG-2 cells by rice protein hydrolysates pretreated with electron beams, Sci. Rep. 10 (2020) 8415. https://doi.org/10.1038/s41598-020-64814-7.

[453] T. Hussain, B. Tan, Y. Yin, F. Blachier, M.C.B. Tossou, N. Rahu, Oxidative Stress and Inflammation : What Polyphenols Can Do for Us ?, 2016 (2016). https://doi.org/10.1155/2016/7432797.

[454] X. Zhang, F. Jia, W. Ma, X. Li, X. Zhou, DAD3 targets ACE2 to inhibit the MAPK and NF-κB signalling pathways and protect against LPS-induced inflammation in bovine mammary epithelial cells, Vet. Res. 53 (2022) 104. https://doi.org/10.1186/s13567-022-01122-0.

[455] C. Park, J.S. Noh, Y. Jung, S.-H. Leem, J.W. Hyun, Y.-C. Chang, T.K. Kwon, G.-Y. Kim, H. Lee, Y.H. Choi, Fisetin Attenuated Oxidative Stress-Induced Cellular Damage in ARPE-19 Human Retinal Pigment Epithelial Cells Through Nrf2-Mediated Activation of Heme Oxygenase-1, Front. Pharmacol. 13 (2022). https://doi.org/10.3389/fphar.2022.927898.

[456] D. Gunawardena, R. Raju, G. Münch, Hydrogen peroxide mediates pro-inflammatory cell-to-cell signaling: A new therapeutic target for inflammation?, Neural Regen. Res. 14 (2019) 1430–1437. https://doi.org/10.4103/1673-5374.253529.

[457] S. Paeng Hwa, W. Park Sun, W.-K. Jung, D.-S. Lee, G.-Y. Kim, Y. Choi Hyun, S.-K. Seo, W. Jang Hee, J. Choi Sik, Y.-M. Lee, S. Park, I.-W. Choi, YCG063 inhibits Pseudomonas aeruginosa LPS-induced inflammation in human retinal pigment epithelial cells through the TLR2-mediated AKT/NF-κB pathway and ROS-independent pathways, Int J Mol Med. 36 (2015) 808–816. https://doi.org/10.3892/ijmm.2015.2266.

[458] S. Imai, T. Otsuka, A. Naito, M.S. and H. Hara, Triamcinolone Acetonide Suppresses Inflammation and Facilitates Vascular Barrier Function in Human Retinal Microvascular Endothelial Cells, Curr. Neurovasc. Res. 14 (2017) 232–241. https://doi.org/http://dx.doi.org/10.2174/1567202614666170619081929.

[459] P.J. Barnes, How corticosteroids control inflammation: Quintiles Prize Lecture 2005, Br. J. Pharmacol. 148 (2006) 245–254. https://doi.org/10.1038/sj.bjp.0706736.

[460] U. Klueh, C. Czajkowski, I. Ludzinska, Y. Qiao, J. Frailey, D.L. Kreutzer, Impact of CCL2 and CCR2 chemokine/receptor deficiencies on macrophage recruitment and continuous glucose monitoring in vivo, Biosens. Bioelectron. 86 (2016) 262–269. https://doi.org/https://doi.org/10.1016/j.bios.2016.06.026.

[461] L.Q. Meng, F.Y. Yang, M.S. Wang, B.K. Shi, D.X. Chen, D. Chen, Q. Zhou, Q.B. He, L.X. Ma, W.L. Cheng, N.Z. Xing, Quercetin protects against chronic prostatitis in rat model through NF-κB

and MAPK signaling pathways, Prostate. 78 (2018) 790–800. https://doi.org/10.1002/pros.23536.

[462] Y.-D. Min, C.-H. Choi, H. Bark, H.-Y. Son, H.-H. Park, S. Lee, J.-W. Park, E.-K. Park, H.-I. Shin, S.-H. Kim, Quercetin inhibits expression of inflammatory cytokines through attenuation of NF-κB and p38 MAPK in HMC-1 human mast cell line, Inflamm. Res. 56 (2007) 210–215. https://doi.org/10.1007/s00011-007-6172-9.

[463] Y. Bian, P. Liu, J. Zhong, Y. Hu, S. Zhuang, K. Fan, Z. Liu, Quercetin Attenuates Adhesion Molecule Expression in Intestinal Microvascular Endothelial Cells by Modulating Multiple Pathways, Dig. Dis. Sci. 63 (2018) 3297–3304. https://doi.org/10.1007/s10620-018-5221-2.

[464] C. Li, W.-J. Zhang, B. Frei, Quercetin inhibits LPS-induced adhesion molecule expression and oxidant production in human aortic endothelial cells by p38-mediated Nrf2 activation and antioxidant enzyme induction, Redox Biol. 9 (2016) 104–113. https://doi.org/https://doi.org/10.1016/j.redox.2016.06.006.

[465] K. Pitarokoili, M. Sgodzai, T. Grüter, H. Bachir, J. Motte, B. Ambrosius, X. Pedreiturria, M.S. Yoon, R. Gold, Intrathecal triamcinolone acetonide exerts anti-inflammatory effects on Lewis rat experimental autoimmune neuritis and direct anti-oxidative effects on Schwann cells, J. Neuroinflammation. 16 (2019) 1–12. https://doi.org/10.1186/s12974-019-1445-0.

[466] A. Pugazhendhi, M. Hubbell, P. Jairam, B. Ambati, Neovascular Macular Degeneration: A Review of Etiology, Risk Factors, and Recent Advances in Research and Therapy, Int. J. Mol. Sci. 22 (2021). https://doi.org/10.3390/ijms22031170.

[467] C.S. Melincovici, A.B. Boşca, S. Şuşman, M. Mărginean, C. Mihu, M. Istrate, I.M. Moldovan, A.L. Roman, C.M. Mihu, Vascular endothelial growth factor (VEGF) – key factor in normal and pathological angiogenesis, Rom. J. Morphol. Embryol. 59 (2018) 455–467.

[468] M. Nobl, M. Reich, I. Dacheva, J. Siwy, W. Mullen, J.P. Schanstra, C.Y. Choi, J. Kopitz, F.T.A. Kretz, G.U. Auffarth, F. Koch, M.J. Koss, Proteomics of vitreous in neovascular age-related macular degeneration, Exp. Eye Res. 146 (2016) 107–117. https://doi.org/https://doi.org/10.1016/j.exer.2016.01.001.

[469] J.S. Penn, A. Madan, R.B. Caldwell, M. Bartoli, R.W. Caldwell, M.E. Hartnett, Vascular endothelial growth factor in eye disease, Prog. Retin. Eye Res. 27 (2008) 331–371. https://doi.org/10.1016/j.preteyeres.2008.05.001.

[470] S.M. Kaiser, S. Arepalli, J.P. Ehlers, Current and future anti-VEGF agents for neovascular age-related macular degeneration, J. Exp. Pharmacol. 13 (2021) 905–912. https://doi.org/10.2147/JEP.S259298.

[471] G.C. Teague, W. Johnson, M. Shatos, M.E. Baldwin, K. Lashkari, Plasma Levels of VEGF-C and Soluble VEGF Receptor-3 are Elevated in Neovascular AMD, Invest. Ophthalmol. Vis. Sci. 58 (2017) 2327.

[472] G.C. Teague, J. Ma, W. Johnson, M.E. Baldwin, K. Lashkari, Expression of VEGF-A, VEGF-C, VEGF-D and soluble receptors in Clinical Age-Related Macular Degeneration, Invest. Ophthalmol. Vis. Sci. 57 (2016) 3698.

[473] P. Pratheeshkumar, A. Budhraja, Y.O. Son, X. Wang, Z. Zhang, S. Ding, L. Wang, A. Hitron, J.C. Lee, M. Xu, G. Chen, J. Luo, X. Shi, Quercetin Inhibits Angiogenesis Mediated Human Prostate Tumor Growth by Targeting VEGFR- 2 Regulated AKT/mTOR/P70S6K Signaling Pathways, PLoS One. 7 (2012) 1–10. https://doi.org/10.1371/journal.pone.0047516.

[474] S. Richer, W. Stiles, L. Ulanski, D. Carroll, C. Podella, Observation of Human Retinal

Remodeling in Octogenarians with a Resveratrol Based Nutritional Supplement, Nutrients. 5 (2013) 1989–2005. https://doi.org/10.3390/nu5061989.

[475] S. Richer, S. Patel, S. Sockanathan, L.J. Ulanski, L. Miller, C. Podella, Resveratrol Based Oral Nutritional Supplement Produces Long-Term Beneficial Effects on Structure and Visual Function in Human Patients, Nutrients. 6 (2014) 4404–4420. https://doi.org/10.3390/nu6104404.

[476] H. Zhou, L. Yang, H. Li, H. Gong, L. Cheng, H. Zheng, L.M. Zhang, Y. Lan, Downregulation of VEGF mRNA expression by triamcinolone acetonide acetate-loaded chitosan derivative nanoparticles in human retinal pigment epithelial cells, Int. J. Nanomedicine. 7 (2012) 4649–4660. https://doi.org/10.2147/IJN.S29690.

[477] J.E. Sears, G. Hoppe, Triamcinolone Acetonide Destabilizes VEGF mRNA in Müller Cells under Continuous Cobalt Stimulation, Invest. Ophthalmol. Vis. Sci. 46 (2005) 4336–4341. https://doi.org/10.1167/iovs.05-0565.

[478] E. Birben, U.M. Sahiner, C. Sackesen, S. Erzurum, O. Kalayci, Oxidative Stress and Antioxidant Defense, World Allergy Organ. J. 5 (2012) 9–19. https://doi.org/10.1097/WOX.0b013e3182439613.

[479] S. Datta, M. Cano, K. Ebrahimi, L. Wang, J.T. Handa, The impact of oxidative stress and inflammation on RPE degeneration in non-neovascular AMD, Prog. Retin. Eye Res. 60 (2017) 201–218. https://doi.org/https://doi.org/10.1016/j.preteyeres.2017.03.002.

[480] D. Harman, Lawrence Berkeley National Laboratory Recent Work Title AGING: A THEORY BASED ON FREE RADICAL AND RADIATION CHEMISTRY, (1955) Lawrence Berkeley National Laboratory. https://escholarship.org/uc/item/3w86c4g7.

[481] I. V Ivanov, T. Mappes, P. Schaupp, C. Lappe, S. Wahl, Ultraviolet radiation oxidative stress affects eye health, J. Biophotonics. 11 (2018) e201700377. https://doi.org/https://doi.org/10.1002/jbio.201700377.

[482] W.K. Noell, V.S. Walker, B.S. Kang, S. Berman, Retinal damage by light in rats., Invest. Ophthalmol. 5 (1966) 450–473.

[483] I. Rahman, W. MacNee, Role of oxidants/antioxidants in smoking-induced lung diseases, Free Radic. Biol. Med. 21 (1996) 669–681. https://doi.org/https://doi.org/10.1016/0891-5849(96)00155-4.

[484] I. Bellezza, I. Giambanco, A. Minelli, R. Donato, Nrf2-Keap1 signaling in oxidative and reductive stress, Biochim. Biophys. Acta - Mol. Cell Res. 1865 (2018) 721–733. https://doi.org/https://doi.org/10.1016/j.bbamcr.2018.02.010.

[485] A.C. Gonçalves, C. Bento, F. Jesus, G. Alves, L.R. Silva, Chapter 2 - Sweet Cherry Phenolic Compounds: Identification, Characterization, and Health Benefits, in: Atta-ur-Rahman (Ed.), Elsevier, 2018: pp. 31–78. https://doi.org/https://doi.org/10.1016/B978-0-444-64179-3.00002-5.

[486] C. Caddeo, M. Gabriele, X. Fernàndez-Busquets, D. Valenti, A.M. Fadda, L. Pucci, M. Manconi, Antioxidant activity of quercetin in Eudragit-coated liposomes for intestinal delivery, Int. J. Pharm. 565 (2019) 64–69. https://doi.org/https://doi.org/10.1016/j.ijpharm.2019.05.007.

[487] T. Hatahet, M. Morille, A. Shamseddin, A. Aubert-Pouëssel, J.M. Devoisselle, S. Bégu, Dermal quercetin lipid nanocapsules: Influence of the formulation on antioxidant activity and cellular protection against hydrogen peroxide, Int. J. Pharm. 518 (2017) 167–176. https://doi.org/https://doi.org/10.1016/j.ijpharm.2016.12.043.

[488] Y. Murakami, A. Kawata, S. Ito, T. Katayama, S. Fujisawa, Radical-scavenging and anti-inflammatory activity of quercetin and related compounds and their combinations against RAW264.7 cells stimulated with porphyromonas gingivalis fimbriae. relationships between anti-inflammatory activity and quantum chemical par, In Vivo (Brooklyn). (2015).

[489] D. Xu, M.-J. Hu, Y.-Q. Wang, Y.-L. Cui, Antioxidant Activities of Quercetin and Its Complexes for Medicinal Application, Molecules. 24 (2019). https://doi.org/10.3390/molecules24061123.

[490] M. Suntiparpluacha, N. Tammachote, R. Tammachote, Triamcinolone acetonide reduces viability, induces Oxidative Stress , and Alters Gene Expressions of Human Chondrocytes, Eur Rev Med Pharmacol Sci. 20 (2016) 4985–4992.

[491] J.-M. You, S.-J. Yun, K.N. Nam, C. Kang, R. Won, E.H. Lee, Mechanism of glucocorticoid-induced oxidative stress in rat hippocampal slice cultures, Can. J. Physiol. Pharmacol. 87 (2009) 440–447. https://doi.org/10.1139/Y09-027.

[492] V.M. Tang, A.H. Young, H. Tan, C. Beasley, J.F. Wang, Glucocorticoids increase protein carbonylation and mitochondrial dysfunction, Horm. Metab. Res. 45 (2013) 709–715. https://doi.org/10.1055/s-0033-1345119.

[493] A. Tisi, M. Feligioni, M. Passacantando, M. Ciancaglini, R. Maccarone, The Impact of Oxidative Stress on Blood-Retinal Barrier Physiology in Age-Related Macular Degeneration, Cells. 10 (2021). https://doi.org/10.3390/cells10010064.

[494] A. Stahl, Diagnostik und Therapie der altersabhängigen Makuladegeneration, Dtsch. Arztebl. Int. 117 (2020) 513–520. https://doi.org/10.3238/arztebl.2020.0513.

[495] S.H. Sarks, New vessel formation beneath the retinal pigment epithelium in senile eyes, Br. J. Ophthalmol. 57 (1973) 951–965. https://doi.org/10.1136/bjo.57.12.951.

[496] S.H. Sarks, Ageing and degeneration in the macular region: a clinico-pathological study., Br. J. Ophthalmol. 60 (1976) 324 LP – 341. https://doi.org/10.1136/bjo.60.5.324.

[497] R. Simó, M. Villarroel, L. Corraliza, C. Hernández, M. Garcia-Ramírez, The Retinal Pigment Epithelium: Something More than a Constituent of the Blood-Retinal Barrier—Implications for the Pathogenesis of Diabetic Retinopathy, J. Biomed. Biotechnol. 2010 (2010) 190724. https://doi.org/10.1155/2010/190724.

[498] J.H.C. Wong, J.Y.W. Ma, A.I. Jobling, A. Brandli, U. Greferath, E.L. Fletcher, K.A. Vessey, Exploring the pathogenesis of age-related macular degeneration: A review of the interplay between retinal pigment epithelium dysfunction and the innate immune system, Front. Neurosci. 16 (2022) 1–21. https://doi.org/10.3389/fnins.2022.1009599.

[499] F. Irfan, F. Jameel, I. Khan, R. Aslam, S. Faizi, A. Salim, Role of quercetin and rutin in enhancing the therapeutic potential of mesenchymal stem cells for cold induced burn wound, Regen. Ther. 21 (2022) 225–238. https://doi.org/10.1016/j.reth.2022.07.011.

[500] A. Gopalakrishnan, M. Ram, S. Kumawat, S.K. Tandan, D. Kumar, Quercetin accelerated cutaneous wound healing in rats by increasing levels of VEGF and TGF-β1, Indian J. Exp. Biol. 54 (2016) 187–195.

[501] L.S.H. Kim Jae Woo Lee Jae Hyung, Role of Nitric Oxide in the Proliferative and Migratory Effect of Triamcinolone in RPE Cells, Jkos. 51 (2010) 120–125. https://doi.org/10.3341/jkos.2010.51.1.120.

[502] C.N. Thomas, D.A. Sim, W.H. Lee, N. Alfahad, A.D. Dick, A.K. Denniston, L.J. Hill, Emerging

therapies and their delivery for treating age-related macular degeneration, Br. J. Pharmacol. 179 (2022) 1908–1937. https://doi.org/https://doi.org/10.1111/bph.15459.

[503] H. Lin, Y. Yue, D.E. Maidana, P. Bouzika, A. Atik, H. Matsumoto, J.W. Miller, D.G. Vavvas, Drug Delivery Nanoparticles: Toxicity Comparison in Retinal Pigment Epithelium and Retinal Vascular Endothelial Cells, Semin. Ophthalmol. 31 (2016) 1–9. https://doi.org/10.3109/08820538.2015.1114865.

[504] K. Tahara, K. Karasawa, R. Onodera, H. Takeuchi, Feasibility of drug delivery to the eye's posterior segment by topical instillation of PLGA nanoparticles, Asian J. Pharm. Sci. (2017). https://doi.org/10.1016/j.ajps.2017.03.002.

[505] Y. Tsugita, S. Maeda, Colloidal stability of polypyrrole-ITO conducting inks, Jpn. J. Appl. Phys. 61 (2022). https://doi.org/10.35848/1347-4065/ac564f.

[506] M. Kersting, M. Olejnik, N. Rosenkranz, K. Loza, M. Breisch, A. Rostek, G. Westphal, J. Bünger, N. Ziegler, A. Ludwig, M. Köller, C. Sengstock, M. Epple, Subtoxic cell responses to silica particles with different size and shape, Sci. Rep. 10 (2020) 1–17. https://doi.org/10.1038/s41598-020-78550-5.

[507] S. Fredenberg, M. Wahlgren, M. Reslow, A. Axelsson, The mechanisms of drug release in poly(lactic-co-glycolic acid)-based drug delivery systems—A review, Int. J. Pharm. 415 (2011) 34–52. https://doi.org/https://doi.org/10.1016/j.ijpharm.2011.05.049.

[508] N.S. Heredia, K. Vizuete, M. Flores-Calero, K. Pazmiño V., F. Pilaquinga, B. Kumar, A. Debut, Comparative statistical analysis of the release kinetics models for nanoprecipitated drug delivery systems based on poly(lactic-co-glycolic acid), PLoS One. 17 (2022) e0264825. https://doi.org/10.1371/journal.pone.0264825.

[509] Y. Xu, C.-S. Kim, D.M. Saylor, D. Koo, Polymer degradation and drug delivery in PLGA-based drug–polymer applications: A review of experiments and theories, J. Biomed. Mater. Res. Part B Appl. Biomater. 105 (2017) 1692–1716. https://doi.org/https://doi.org/10.1002/jbm.b.33648.

[510] S. Pimple, A.S. Manjappa, M. Ukawala, R.S.R. Murthy, PLGA nanoparticles loaded with etoposide and quercetin dihydrate individually: in vitro cell line study to ensure advantage of combination therapy, Cancer Nanotechnol. 3 (2012) 25–36. https://doi.org/10.1007/s12645-012-0027-y.

[511] M.S. Deepika, R. Thangam, T.S. Sheena, R.T.V. Vimala, S. Sivasubramanian, K. Jeganathan, R. Thirumurugan, Dual drug loaded PLGA nanospheres for synergistic efficacy in breast cancer therapy, Mater. Sci. Eng. C. 103 (2019) 109716. https://doi.org/10.1016/j.msec.2019.05.001.

[512] A. Hardenia, N. Maheshwari, S.S. Hardenia, S.K. Dwivedi, R. Maheshwari, R.K. Tekade, Chapter 1 - Scientific Rationale for Designing Controlled Drug Delivery Systems, in: R.K.B.T.-B.F. of D.D. Tekade (Ed.), Adv. Pharm. Prod. Dev. Res., Academic Press, 2019: pp. 1–28. https://doi.org/https://doi.org/10.1016/B978-0-12-817909-3.00001-7.

[513] L.R. Steeples, N.P. Jones, I. Leal, Evaluating the Safety , Efficacy and Patient Acceptability of Intravitreal Fluocinolone Acetonide (0 . 2mcg / Day) Implant in the Treatment of Non-Infectious Uveitis Affecting the Posterior Segment, (2021).

[514] A. Hirani, A. Grover, Y.W. Lee, Y. Pathak, V. Sutariya, Triamcinolone acetonide nanoparticles incorporated in thermoreversible gels for age-related macular degeneration, Pharm. Dev. Technol. (2016). https://doi.org/10.3109/10837450.2014.965326.

[515] D. Guo, Q. Li, Y. Sun, J. Guo, Q. Zhao, X. Yin, H. Wei, S. Wu, H. Bi, Evaluation of controlled-

release triamcinolone acetonide-loaded mPEG-PLGA nanoparticles in treating experimental autoimmune uveitis, Nanotechnology. 30 (2019) 165702.

[516] L.R. Schopf, A.M. Popov, E.M. Enlow, J.L. Bourassa, W.Z. Ong, P. Nowak, H. Chen, Topical ocular drug delivery to the back of the eye by mucus-penetrating particles, Transl. Vis. Sci. Technol. (2015). https://doi.org/10.1167/tvst.4.3.11.

[517] T. Bíró, Z. Aigner, Current approaches to use cyclodextrins and mucoadhesive polymers in ocular drug delivery-a mini-review, Sci. Pharm. 87 (2019). https://doi.org/10.3390/scipharm87030015.

[518] S. Akhter, M. Anwar, M.A. Siddiqui, I. Ahmad, J. Ahmad, M.Z. Ahmad, A. Bhatnagar, F.J. Ahmad, Improving the topical ocular pharmacokinetics of an immunosuppressant agent with mucoadhesive nanoemulsions: Formulation development, in-vitro and in-vivo studies, Colloids Surfaces B Biointerfaces. 148 (2016) 19–29. https://doi.org/10.1016/j.colsurfb.2016.08.048.

[519] A.H. Salama, A.A. Mahmoud, R. Kamel, A Novel Method for Preparing Surface-Modified Fluocinolone Acetonide Loaded PLGA Nanoparticles for Ocular Use: In Vitro and In Vivo Evaluations, AAPS PharmSciTech. 17 (2015) 1159–1172. https://doi.org/10.1208/s12249-015-0448-0.

[520] E. Agrón, J. Mares, T.E. Clemons, A. Swaroop, E.Y. Chew, T.D.L. Keenan, Dietary Nutrient Intake and Progression to Late Age-Related Macular Degeneration in the Age-Related Eye Disease Studies 1 and 2, Ophthalmology. 128 (2021) 425–442. https://doi.org/https://doi.org/10.1016/j.ophtha.2020.08.018.

[521] K. Peynshaert, J. Devoldere, S.C. De Smedt, K. Remaut, In vitro and ex vivo models to study drug delivery barriers in the posterior segment of the eye, Adv Drug Deliv Rev. 126 (2018) 44–57. https://doi.org/10.1016/j.addr.2017.09.007.

[522] R. Zhang, X. Qin, F. Kong, P. Chen, G. Pan, Improving cellular uptake of therapeutic entities through interaction with components of cell membrane, Drug Deliv. 26 (2019) 328–342. https://doi.org/10.1080/10717544.2019.1582730.

[523] S. Zhu, L. Gong, Y. Li, H. Xu, Z. Gu, Y. Zhao, Safety Assessment of Nanomaterials to Eyes: An Important but Neglected Issue, Adv. Sci. 6 (2019) 1802289. https://doi.org/https://doi.org/10.1002/advs.201802289.

[524] P. Bhatt, P. Narvekar, R. Lalani, M.B. Chougule, Y. Pathak, V. Sutariya, An in vitro Assessment of Thermo-Reversible Gel Formulation Containing Sunitinib Nanoparticles for Neovascular Age-Related Macular Degeneration, AAPS PharmSciTech. 20 (2019). https://doi.org/10.1208/s12249-019-1474-0.

[525] W.L.L. Suen, Y. Chau, Specific uptake of folate-decorated triamcinolone-encapsulating nanoparticles by retinal pigment epithelium cells enhances and prolongs antiangiogenic activity, J. Control. Release. (2013). https://doi.org/10.1016/j.jconrel.2013.01.004.

[526] L. Hellinen, H. Hongisto, E. Ramsay, K. Kaarniranta, K.S. Vellonen, H. Skottman, M. Ruponen, Drug flux across RPE cell models: The hunt for an appropriate outer blood–retinal barrier model for use in early drug discovery, Pharmaceutics. (2020). https://doi.org/10.3390/pharmaceutics12020176.

[527] J.R. Costa, N.C. Silva, B. Sarmento, M. Pintado, Potential chitosan-coated alginate nanoparticles for ocular delivery of daptomycin, Eur. J. Clin. Microbiol. Infect. Dis. (2015). https://doi.org/10.1007/s10096-015-2344-7.

[528] S. Pescina, P. Govoni, A. Potenza, C. Padula, P. Santi, S. Nicoli, Development of a Convenient ex vivo Model for the Study of the Transcorneal Permeation of Drugs: Histological and Permeability Evaluation, J. Pharm. Sci. 104 (2015) 63–71. https://doi.org/10.1002/jps.24231.

[529] M.R. Mulenos, H. Lujan, L.R. Pitts, C.M. Sayes, Silver Nanoparticles Agglomerate Intracellularly Depending on the Stabilizing Agent: Implications for Nanomedicine Efficacy, Nanomaterials. 10 (2020). https://doi.org/10.3390/nano10101953.

Appendix A

pharmaceutics

MDPI

Article

Chitosan-Coated PLGA Nanoparticles Encapsulating Triamcinolone Acetonide as a Potential Candidate for Sustained Ocular Drug Delivery

Madhuri Dandamudi [1,*], Peter McLoughlin [1], Gautam Behl [1], Sweta Rani [1], Lee Coffey [1], Anuj Chauhan [2], David Kent [3] and Laurence Fitzhenry [1]

[1] Ocular Therapeutics Research Group, Pharmaceutical and Molecular Biotechnology Research Centre, Waterford Institute of Technology, X91 K0EK Waterford, Ireland; pmcloughlin@wit.ie (P.M.); gbehl@wit.ie (G.B.); srani@wit.ie (S.R.); LCOFFEY@wit.ie (L.C.); LFITZHENRY@wit.ie (L.F.)

[2] Department of Chemical and Biological Engineering, Colorado School of Mines, Colorado, CO 80401, USA; chauhan@mines.edu

[3] The Vision Clinic, R95 XC98 Kilkenny, Ireland; dkent@liverpool.ac.uk

* Correspondence: madhuri.dandamudi@postgrad.wit.ie

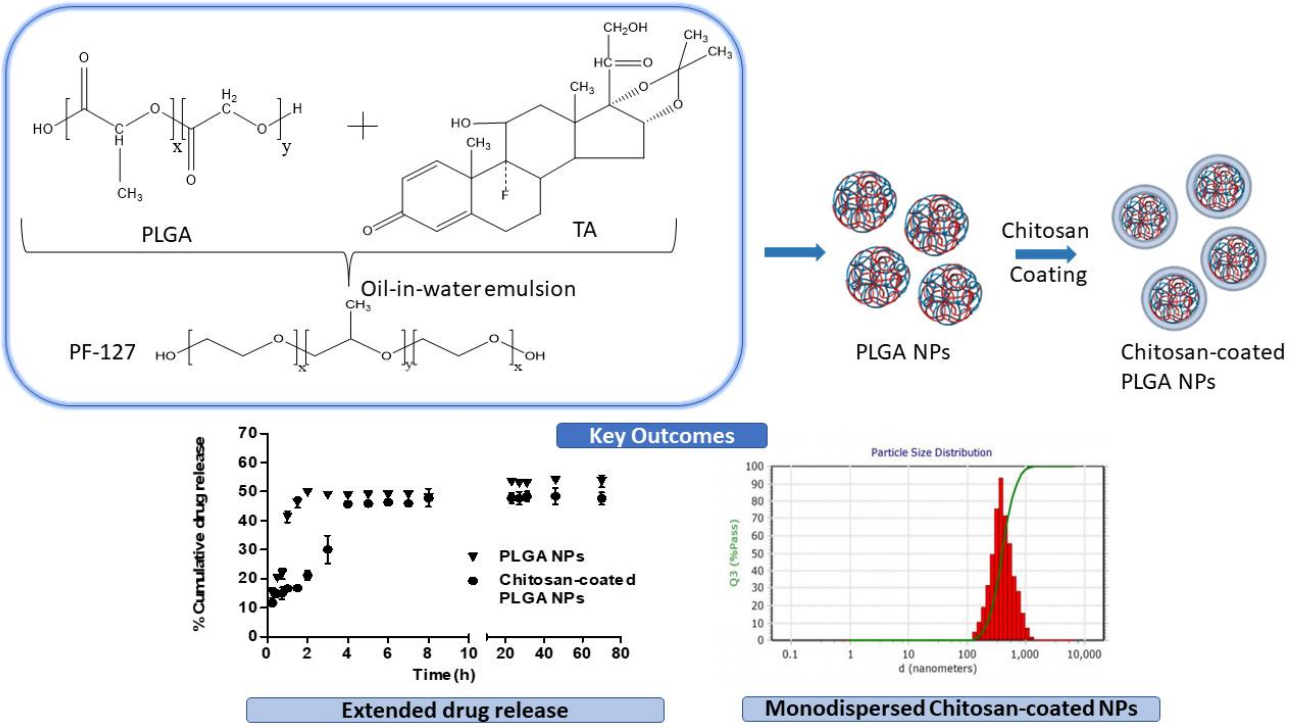

Citation: Dandamudi, M.; McLoughlin, P.; Behl, G.; Rani, S.; Coffey, L.; Chauhan, A.; Kent, D.; Fitzhenry, L. Chitosan-Coated PLGA Nanoparticles Encapsulating Triamcinolone Acetonide as a Potential Candidate for Sustained Ocular Drug Delivery. *Pharmaceutics* **2021**, *13*, 1590. https://doi.org/10.3390/pharmaceutics13101590

Academic Editor: Charles M. Heard

Received: 30 July 2021

Accepted: 24 September 2021

Published: 30 September 2021

Abstract: The current treatment for the acquired retinal vasculopathies involves lifelong repeated intravitreal injections of either anti-vascular endothelial growth factor (VEGF) therapy or modulation of inflammation with steroids. Consequently, any treatment modification that decreases this treatment burden for patients and doctors alike would be a welcome intervention. To that end, this research aims to develop a topically applied nanoparticulate system encapsulating a corticosteroid for extended drug release. Poly (lactic-co-glycolic acid) (PLGA) nanoparticles (NPs) supports the controlled release of the encapsulated drug, while surface modification of these NPs with chitosan might prolong the mucoadhesion ability leading to improved bioavailability of the drug. Triamcinolone acetonide (TA)-loaded chitosan-coated PLGA NPs were fabricated using the oil-in-water emulsion technique. The optimized surface-modified NPs obtained using Box-Behnken response surface statistical design were reproducible with a particle diameter of 334 ± 67.95 to 386 ± 15.14 nm and PDI between 0.09 and 0.15. These NPs encapsulated 55–57% of TA and displayed a controlled release of the drug reaching a plateau in 27 h. Fourier-transform infrared spectroscopic (FTIR) analysis demonstrated characteristic peaks for chitosan (C-H, CONH2 and C-O at 2935, 1631 and 1087 cm^{-1}, respectively) in chitosan-coated PLGA NPs. This result data, coupled with positive zeta potential values (ranged between +26 and +33 mV), suggests the successful coating of chitosan onto PLGA NPs. Upon coating of the NPs, the thermal stability of the drug, polymer, surfactant and PLGA NPs have been enhanced. The characteristics of the surface-modified NPs supports their use as potential candidates for topical ocular drug delivery for acquired retinal vasculopathies.

Keywords: nanoparticles; posterior segment eye diseases; PLGA; chitosan; chitosan-coated nanoparticles; triamcinolone acetonide; corticosteroid; ocular drug delivery

1. Introduction

According to the World Health Organisation (WHO), the majority of people with vision loss and vision impairment are aged over 50 [1]. As the percentage of aging in the global population continues to increase, the number of people suffering from acquired ocular diseases will also significantly rise (~20% of Europe's population are now over 65) [2]. The acquired retinal vasculopathies, including diabetic retinopathy (DR), venous occlusive disease (VOD) and age-related macular degeneration (AMD) are the most common causes of vision loss in the elderly [3]. All of these conditions are typically treated by regular intravitreal injections that are expensive and can be associated with serious side effects such as cataracts, retinal detachment and endophthalmitis [4]. Together with an increased

financial burden, clinical level of anxiety and depression was seen in patients receiving intravitreal injections, which is hindering the patients' quality of life [5]. As such, there is a compelling necessity to develop a patient friendly treatment with negligible side effects such as topical formulation or controlled release drug delivery system which could reduce or negate the need for current intravitreal eye injections. The main pathological factors contributing to AMD, DR, VOD and macular edema appear to be inflammation, retinal fluid accumulation with a higher vascular permeability [6]. Synthetic glucocorticosteroids (GCs) are commonly used drugs to treat a wide variety of inflammatory diseases in the eye [7]. They are mainly used for their immunosuppressive and anti-inflammatory properties, which are regulated through signal transduction by glucocorticoid receptors. Triamcinolone acetonide (TA), a member of the GCs family, has been shown to inhibit the secretion of VEGF, the production of cytokines and decrease vascular permeability [8,9].

The major issue with the use of hydrophobic drugs, including TA, is minimal aqueous solubility leading to suboptimal bioavailability. Loading hydrophobic drugs into nanoparticulate systems can help overcome this complication [10]. Developing a topical formulation is a significant challenge, as the eye is a complex organ with multiple anatomical, biochemical, and physiological barriers restricting the entry of drug molecules to the site of action. Since the initial use of nanoparticulate systems in medicine to date, they have revolutionized drug delivery and have also shown promising research outcomes for treating complex ocular diseases [11–13]. Different forms of nanomaterials being tested for anterior and posterior segment eye diseases include NPs [14], nano-micelles [15], liposomes [16], dendrimers [17], nanoparticle-loaded contact lenses [18] and sub-conjunctival implants with nanostructures [19], etc. Liposomes and micelles have limitations such as low stability, leakage of entrapped drug and premature release of the loaded drug [20,21]. The changes in NPs-loaded contact lenses during the storage period like burst release of the drug before administration, swelling and optical transparency, etc., still need to be addressed [22]. For elderly patients wearing contact lenses and inserting implants with minor surgery leads to poor patient compliance. Recently, polymeric NPs has been studied for topical ocular delivery and shown promising results [23–25]. Considering the size of NPs, they are likely to have greater diffusivity through biological membranes like the corneal epithelium compared to a suspension of hydrophobic drugs. Previous research on NPs for ocular drug delivery has demonstrated an increase in corneal permeability of the incorporated drugs when compared to their drug suspension [26–28]. Additionally, the higher surface area of nanoparticulate systems enables enhanced interaction with the epithelial layers of the eye leading to the increased retention time of topically administered drug delivery systems [29].

The biodegradable polymer, poly lactic-co-glycolic acid (PLGA), is approved by the United States food and drug administration (FDA) and European Medicines Agency (EMA) and proved its suitability for drug delivery [30]. Additionally, there is a commercial PLGA based formulation called Ozurdex® to treat VOD, DR and posterior uveitis which highlights the ocular tolerance of PLGA [31]. PLGA NPs have shown good stability with prolonged release of the drug in many studies but they lack mucoadhesion [32]. This property enhances the ocular surface retention time, which plays a vital role when targeting the topical route for posterior segment diseases as the loss of NPs in tear drainage is the major limitation [33–35]. The surface modification of PLGA NPs with natural and biodegradable polymers like chitosan has proven to be beneficial for ocular drug delivery [23,36,37]. Polymers with mucoadhesive properties bind to mucin through various mechanisms such as hydrogen bonds, electrostatic interactions, polymer chain inter-diffusion and van der Waal forces [38]. These surface modified NPs may have the potential to increase the stability of the encapsulated drug, reducing the initial burst release of the drug and the in vivo targeting ligands may conjugate with free amine groups of chitosan [39,40]. Conversion of charge from negative to positive may enhance cellular adhesion and retention time of the

formulation at the target site [41]. The adsorption of chitosan onto PLGA NPs follows a multilayer behavior with the reason for adsorption being found to be the cationic nature of chitosan and also the non-uniform porous surface of PLGA NPs [42]. Considering these parameters, the current research was focused on developing a topically applied nanoparticulate system exhibiting extended drug release for the treatment of posterior segment disease. This system consists of TA-loaded chitosan-coated PLGA NPs prepared by an emulsion technique. Emulsifier or stabilizer, such as Pluronic® F-127 (PF-127), used in the nanoparticle preparation forms a steric barrier around the nanoparticle with both PEO (polyethylene oxide) and PPO (polypropylene oxide) moieties, thus keeping the NPs uniformly dispersed [43]. Optimization of the NPs was achieved using a response surface design of experiments. The prepared NPs were investigated for particle size, polydispersity index (PDI), zeta potential (ZP) and percent drug encapsulation efficiency (EE). The NPs were investigated for thermal stability, characterized by FT-IR, and examined for in vitro drug release to assess their suitability as drug carriers. As the research on nanoparticulate systems continues with ocular use, the scalability, safety, and robustness of these systems will be established leading to a new and highly efficient nanoparticulate system available for patient use.

2. Materials and Methods

2.1. Materials

Triamcinolone acetonide (TA) (MW: 434.50 g/mol with purity >99%) and water-soluble chitosan (MW: 10–100 KDa with a deacetylation degree >90%) were procured from Carbosynth Ltd., Berkshire, UK. PLGA (DL-lactide/Glycolide copolymer, ratio M/M%: 50/50, MW: 38,000–54,000), Pluronic® F-127 (MW: ~12,600 g/mol), poly (vinyl alcohol) (MW: 89,000–98,000), dichloromethane (purity ≥99.8%), tween® 80, sodium azide (purity >99.5%) and phosphate buffer saline tablets (0.01 M phosphate buffer), were purchased from Sigma Aldrich, Arklow, Ireland.

2.2. Methods

2.2.1. Preparation and Optimization of Chitosan-Coated PLGA Nanoparticles

The NPs were prepared by a single emulsion technique which was a modification of a previously published double emulsion method [36]. PLGA (3.5 mg/mL) and TA (1 mg) were dissolved in 2 mL of dichloromethane (DCM) and this mixture was added dropwise to 10 mL of the aqueous solution containing stabilizer (0.25% (*w*/*v*) PVA or 1% (*w*/*v*) PF-127). Upon which, the mixture was sonicated for 10 min and left stirring overnight to evaporate the organic solvent. Finally, the nanosuspension was centrifuged at 3000 rpm for 15 min at 4 °C to remove any unentrapped drug. The supernatant obtained was subjected to high-speed centrifugation at 15,000 rpm for 30 min at 4 °C to recover the NPs. Chitosan-coated PLGA NPs were obtained by incubating PLGA NPs in chitosan solution (1:1 (*v*/*v*)) overnight by stirring at room temperature. After the incubation, the NPs were collected by centrifugation at 15,000 rpm for 30 min (NPs redispersed in Milli-Q® water with pH 7). Considering the reproducibility of the NPs in the screening experiments, the formulation optimization experiments were designed using the design of experiments (DOE). For the optimization of NPs, a Box-Behnken, surface-response DOE was chosen. The three independent variables used were PLGA (3.5–4.5 mg/mL), PF-127 (1–2% (*w*/*v*)) and chitosan (1–2% (*w*/*v*)), while the four dependent response variables were particle size, PDI, ZP and %EE. This DOE generated 30 formulations (Table S1 in Supplementary Materials), and the NPs with the same composition were given one formulation code starting from E1 to E13 for PLGA NPs (prepared with the same composition as Table 1 without chitosan) and CS-E1 to CS-E13 for chitosan-coated NPs as represented in Table 1.

Table 1. Compositions of the chitosan-coated PLGA NPs with formulation codes for the experiments generated by DOE.

Emulsion Code	PLGA (mg/mL)	PF-127% (*w*/*v*)	Chitosan% (*w*/*v*)
CS-E1	4	2	2
CS-E2	4.5	1.5	2
CS-E3	3.5	1.5	2
CS-E4	3.5	2	1.5
CS-E5	4	1	1
CS-E6	3.5	1.5	1
CS-E7	4.5	1	1.5
CS-E8	4.5	2	1.5
CS-E9	4	1.5	1.5
CS-E10	3.5	1	1.5
CS-E11	4.5	1.5	1
CS-E12	4	2	1
CS-E13	4	1	2

The ideal concentrations of independent variables were selected based on the responses obtained. Additionally, two formulations were chosen using point prediction and the experimental values obtained were compared to predicted values to verify the experimental model chosen.

2.2.2. Particle Size, Polydispersity Index and Zeta Potential

The particle size, PDI and ZP were determined using dynamic light scattering (DLS), where analysis was performed at 25 °C with an angle of detection of 180° with the heterodyne-backscatter arrangement. A total of 1 mL of nanosuspension was placed in a sample cell and the FLEX software was used to analyze electrophoretic mobility (for ZP) and particle size distribution using Brownian motion. For each nanosuspension sample, the mean value was recorded as an average of three measurements.

2.2.3. Encapsulation Efficiency

The encapsulated drug was quantified by high-performance liquid chromatography (HPLC) using a C18 column, mobile phase of pH 3 phosphoric acid buffer: acetonitrile (50:50 (*v*/*v*)), a 1.2 mL/min isocratic flow rate, an injection volume of 20 µL and a 240 nm detection wavelength. TA was quantified using a calibration curve with demonstrated linearity in the range of 0.1–0.9 µg/mL. Based on the standard deviation (Sy) and slope (S) of the calibration curve, the limit of detection (LOD) and limit of quantification (LOQ) of TA was determined using the Equations (1) and (2).

$$\text{LOD} = 3.3 \frac{Sy}{S} \quad (1)$$

$$\text{LOQ} = 10 \frac{Sy}{S} \quad (2)$$

A fixed volume of drug-loaded NPs suspension was diluted with mobile phase and the encapsulation efficiency was calculated using the following Equation (3):

$$\text{Encapsulation efficiency (\%)} = \frac{\text{Drug present in nanoparticles}}{\text{total drug added}} \times 100 \quad (3)$$

2.2.4. Freeze-Drying of Nanoparticles

The NPs in suspension form containing 1% trehalose as cryoprotectant was pre-cooled at −20 °C overnight. Upon pre-cooling, the samples were placed in the freeze dryer (Freezone 2.5, LABCONCO, Kansas city, MO, USA) at 6 Pa for 72 h maintained at −50 °C. These freeze-dried NPs were used for thermal studies and FTIR analysis.

2.2.5. Thermal Analysis

The thermal behavior of the formulation materials, PLGA and chitosan-coated PLGA NPs was investigated using thermal gravimetric analysis (TGA) and differential scanning calorimetry (DSC). Thermal analysis was performed using a nitrogen gas flow rate of 50 mL/min and a heating rate of 10 °C/min. Thermal decomposition analysis was performed from room temperature to 500 °C with a sample weight between 5 and 10 mg. The weight loss and onset of degradation were simultaneously recorded as a function of temperature/time. Resulting TGA thermograms were analyzed using TA universal analysis software. Calibration using indium was performed to ensure the accuracy and precision of the DSC thermograms obtained. Accurately weighed samples of 5–10 mg were loaded in T zero aluminum pans with a pinhole lid. The analysis was performed up to 350 °C under a nitrogen atmosphere at a heating rate of 10 °C/min.

2.2.6. Fourier-Transform Infrared Spectroscopy Analysis

FTIR was performed on a Varian 600 IR using potassium bromide (KBr) disc with the spectra obtained in the region of 4000–600 cm^{-1} at a resolution of 2.0 cm^{-1} and 64 scans per run. The raw materials and freeze-dried nanoparticles were mixed with KBr in 1:10 ratios and compressed into a disc for analysis.

2.2.7. In Vitro Drug Release

The drug release study was carried out using phosphate buffered saline (PBS (pH 7.4)) with 1% Tween® 80 and 0.01% sodium azide as release medium. Before performing the drug release study, the solubility of TA in the release medium was determined, where 2 and 10 mg of TA was incubated in 5 mL of PBS and PBS with 1% Tween® 80 at 37 °C with agitation. After 24 h the samples were centrifuged at 10,000 rpm and the supernatant was syringe filtered prior to HPLC analysis. Initially, release media containing nanosuspension with a drug concentration of 25 µg/mL was taken. The release medium was distributed into 2 mL microcentrifuge tubes containing nanosuspension equivalent to 50 µg of TA. These microcentrifuge tubes were placed in a shaker with continuous agitation at 37 °C. At every sampling point, a new microcentrifuge tube was taken and centrifuged at 15,000 rpm for 15 min and the drug present in the supernatant was quantified. The %drug release and %cumulative drug release were calculated by using the following Equations (4) and (5).

$$\text{Drug release (\%)} = \frac{\text{Released drug}}{\text{total drug}} \times 100 \quad (4)$$

$$\text{Cumulative drug release (\%)} = \frac{\text{Volume of sample withdrawn}}{\text{bath Volume}} \times P(t-1) \quad (5)$$

P = %release at time 't'.

P (t − 1) = %release previous to 't'.

The best curve fit of the in vitro TA release was analyzed with the mathematical models: zero and first order, Hixson–Crowell, Higuchi and Korsmeyer–Peppas based on regression coefficient (R^2) values.

2.2.8. Statistical Analysis

All the data were presented as mean ± SD. Minitab statistical software was used to analyze the design of experiments responses.

3. Results

3.1. Screening of Chitosan-Coated PLGA Nanoparticles

This study is focused on developing a nanoparticulate system encapsulating a corticosteroid for topical ocular drug delivery to treat acquired retinal vasculopathies. PLGA NPs are potential candidates for drug delivery to the back of the eye diseases following topical instillation [25]. The surface modification of these NPs with mucoadhesive polymers would enhance the ocular residence time and hence increasing the drug's bioavailability [44]. PLGA undergoes biodegradation by hydrolysis resulting in glycolic and lactic acids, which further enter the tricarboxylic acid cycle and is metabolized into carbon dioxide, energy, and water; this process makes PLGA in vivo degradable [45]. Biodegradation of chitosan occurs through hydrolysis by proteases (primarily lysozyme). The degradation products are monosaccharides or oligosaccharides and glycosaminoglycan or glycol-amino proteins, which are natural metabolites [46]. The goal of the current study is to optimize the formulation variables to attain the NPs with the smallest size possible, which can encapsulate the appropriate amounts of drug to suit the ocular application. Chitosan-coated PLGA NPs were prepared using a single emulsion technique by modifying two previously published methods [36,47]. Initially, screening experiments were performed to study the reproducibility of the chosen method and to test the effectiveness of PVA and PF-127 as stabilizers. The findings of the blank PLGA (A1 and A2) and chitosan-coated PLGA NPs (CS-A1 and CS-A2) prepared with 0.25% (*w*/*v*) PVA or 1% (*w*/*v*) PF-127 are represented in Table 2. PVA showed promising results as the stabilizer in these studies and was therefore considered for the screening experiments [36]. In our previous (unpublished) studies, PF-127 was used as the stabilizer, which produced stable NPs. It has also shown promising results in the past [48].

Table 2. Particle size, zeta potential, PDI and % encapsulation efficiency of the NPs from screening experiments. Particle size is the representation of the diameter of the particle (nm). Data = mean ± std (n = 3).

Emulsion Code	Stabilizer (% (*w*/*v*))	Particle Size (nm)	Zeta Potential (mV)	PDI
A1	PVA (0.25)	359 ± 76.37	−14 ± 5.44	0.15 ± 0.07
CS-A1	PVA (0.25)	346 ± 125.37	+18 ± 1.77	0.70 ± 0.53
A2	PF-127 (1)	200 ± 61.16	−20 ± 9.26	0.07 ± 0.01
CS-A2	PF-127 (1)	187 ± 23.55	+14 ± 5.44	0.06 ± 0.01

The NPs fabricated with PF-127 as stabilizer yielded smaller NPs of 200 ± 61.16 nm and 187 ± 23.55 nm with low PDI (0.06–0.07) and high encapsulation of the TA (34–59%) compared to NPs prepared with PVA (27–50%). This was perhaps due to the entanglement of PEO moieties of PF-127 with polymeric chains of PLGA leading to more compact NPs with high drug protection [49–51]. Salama et al. formulated fluocinolone acetonide-loaded NPs using PLGA and PF-127; they attained a particle size of 203 ± 5 nm with 56 ± 4% EE [23]. Along with the smaller size, the NPs also released the drug in a controlled manner up to 24 h; the authors postulated this was due to the interactions between PLGA and PEO groups of PF-127, which increases the stability of NPs (the entanglement of PLGA chains and PEO moieties could make the particle more compact and protect the drug leading to extended drug release). The encapsulation efficiency of the NPs decreased upon chitosan coating due to the repeated centrifugation step after chitosan coating, which may lead to loss of some particles and surface bound drug.

3.2. Optimization of Nanoparticles Using Statistical Experimental Design

DOE is widely used in the pharmaceutical industry and academia to investigate the factors that control the drug delivery system. An experimental design is important to study several factors at multiple levels using predefined experiments which can be applied to design a product or process [52]. DOE has proved to be a powerful tool for designing nanoparticulate systems, which can identify the effect of individual factors and interaction between factors on the characteristics of the NPs [53]. Box-Behnken design is more efficient and cost-effective than a central composite design with the same parameters due to fewer design points [54]. The central composite design usually consists of design points outside the region of interest (axial points outside the cube), in contrast the Box-Behnken design points lie in the selected region of interest (region of interest is selected based on screening experiments). The Box-Behnken, response surface statistical design consisting of three factors with three levels prioritized for this study to optimize the NPs prepared by the emulsion method. The model evaluates the main effects, interaction effects and quadratic effects of the variable factors on the NPs characteristics. It also identifies the combination of factors to obtain the predicted response based on the point prediction (response optimizer). Trabado et al. used a Box-Behnken response surface DOE to optimize the characteristics (particle size, ZP, PDI, %EE and %drug loading) of cyclosporin-loaded sorbitan ester NPs for topical ocular drug delivery [55]. In their study, the optimized formulation of 170.5 nm with a ZP of +33.9 mV and a drug loading capacity of 19.66% was achieved by using the response optimizer feature of the Box-Behnken DOE (by using the prediction composition generated by DOE they got the required responses for the chosen application). As mentioned in Section 2.2.1, in the present study, the three independent variables used were PLGA (3.5–4.5 mg/mL), PF-127 (1–2% (*w*/*v*)) and chitosan (1–2% (*w*/*v*)); the responses taken were particle size, polydispersity index (PDI), ZP and %EE. The lack of fit value of all the four responses generated by the DOE model used was $p > 0.05$ (insignificant), indicating the fit of experimental values to the model. The concentration of PLGA, chitosan and both combined have a significant effect on particle size (Figure 1). The low concentration of PLGA (3.5 mg/mL) and PF-127 (1% (*w*/*v*)) and medium concentration of chitosan (1.5% (*w*/*v*)) gave the smallest NPs of 334.95 ± 67.95 nm (Table S2 in Supplementary Material).

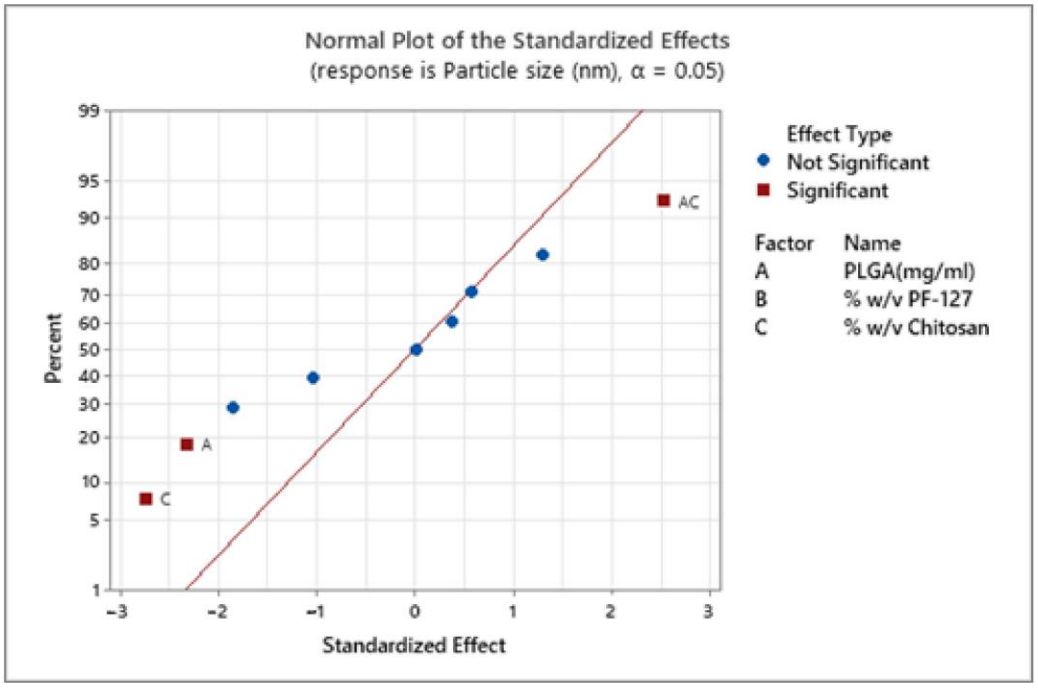

Figure 1. Effect of factors (PLGA, PF-127 and chitosan) on the particle size of chitosan-coated PLGA nanoparticles. The blue points represent the insignificant factors, and the red points represent significant factors.

In a previous study, Madani et al. also observed an increase in nanoparticle size with the increase in PLGA concentration [56]. The authors postulated that in an emulsion technique, increased PLGA concentration in organic solvent elevates the viscosity of dispersed medium resulting in reduced shear stress leading to the formation of larger nanodroplets. There was no statistically significant effect of all three factors on the PDI of the NPs (Figure 2).

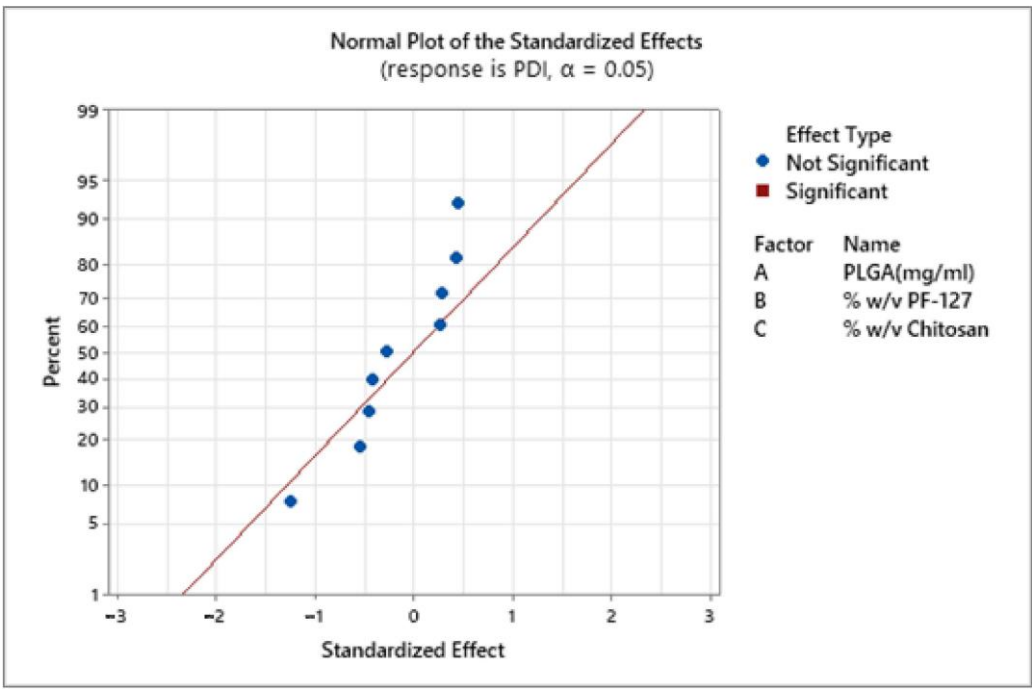

Figure 2. Effect of PLGA, PF-127 and chitosan on PDI of the prepared chitosan-coated PLGA nanoparticles. The blue points represent the insignificant factors.

The PDI values of all the formulations ranged from 0.04 and 0.47 indicating that NPs

prepared from an emulsion method were monodispersed (Figure 3). These results agree with recent study by Canioni et al., who formulated dexamethasone palmitate NPs to treat AMD via intravitreal injections [57]. They studied the influence of PEG-40- sterate, Pluronic® F-168 and F-127 on NPs stability and monodispersion, the PF-127 at 1.5–2% (*w*/*v*) had shown best PDI values (0.02–0.12) with good stability compared to the other two surfactants (PDI: 0.03–0.5). This could be due to the arrangement of PF-127 on the nanoparticle surface with the PEO group facing the aqueous solvent creating steric stabilization. Thus, providing a protective barrier around the particle and preventing aggregation. The suitability of nanoformulations for specific drug delivery applications largely depends on average particle size and their dispersity. PDI is an important variable for studying the distribution of NPs or estimating their permeation efficiency across ocular barriers [58].

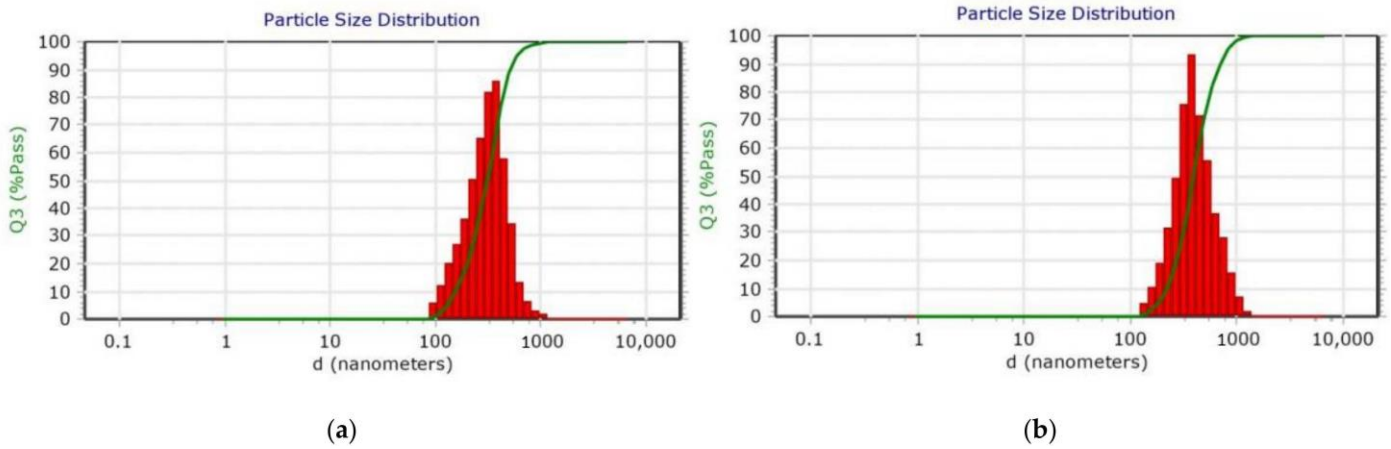

Figure 3. Dynamic light scattering (DLS) particle size distribution of (**a**) PLGA nanoparticles (E10) and (**b**) chitosan-coated PLGA nanoparticles (CS-E10). The graph represents the volume distribution of the nanoparticles, %Volume passing (Q3%pass) vs. diameter (*d*).

The particle size of all the PLGA NPs increased upon chitosan coating (Figure S1 in Supplementary Materials), this is potentially due to adsorption of the chitosan on the porous surface of the PLGA NPs. Guo et al. studied the adsorption mechanism of chitosan onto PLGA NPs prepared by an oil-in-water emulsion technique [42]. In their study, they noticed the increase in particle size of PLGA NPs from 261.5 to 972.7 nm with an increase in chitosan concentration (0.12–2.4 g/L). Based on adsorption isotherms, the authors proposed that the adsorption of chitosan onto PLGA NPs depends on the chitosan cationic nature, high surface energy and non-uniform microporous surface of PLGA NPs. The amount of TA present in NPs was determined using HPLC and TA showed linearity between 0.1 and 0.9 µg/mL with regression greater than 0.999. Based on the calibration curve, LOD and LOQ of TA were calculated using Equations (1) and (2) and found to be 0.026 and 0.079 µg/mL, respectively. In the present work, PLGA NPs with the emulsion codes E7 and E10 showed high encapsulation of drug, 66.04 ± 2.60% and 63.38 ± 2.30%, respectively. Upon chitosan coating, the same formulations displayed higher encapsulation of the drug compared to other formulations (54.89 ± 2.11 and 55.18 ± 3.70%, respectively). Using the surface plots shown in Figure 4, the effect of PLGA, PF-127 and chitosan on the %EE of the NPs was represented.

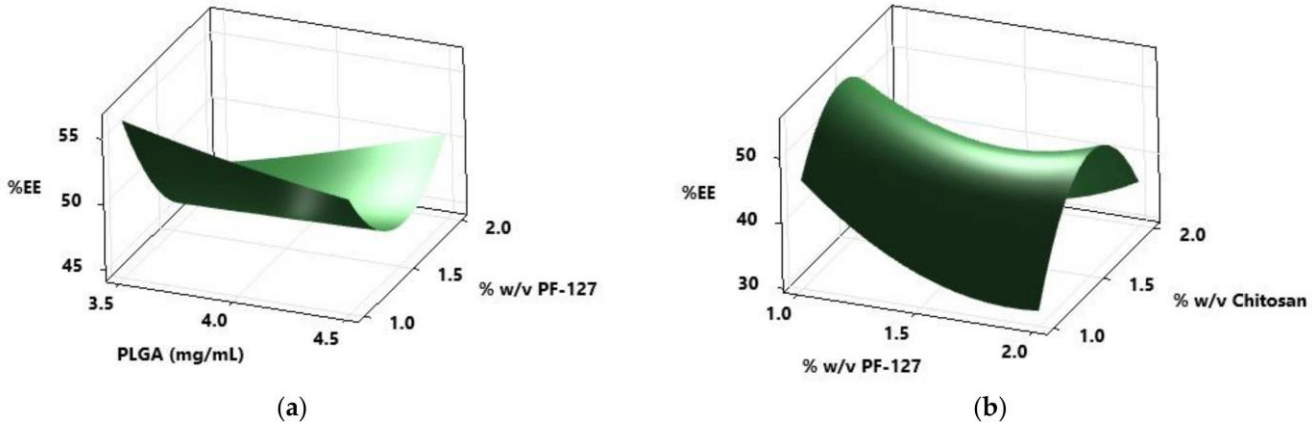

Figure 4. Response surface plots of (**a**) %EE (encapsulation efficiency) vs. PLGA and PF-127 (**b**) % EE vs. % (*w*/*v*) chitosan and % (*w*/*v*) PF-127.

The formulations prepared with a low concentration of PF-127 (1% (*w*/*v*)) showed high encapsulation efficiency (66.04 ± 2.60%) whereas for chitosan-coated NPs, medium concentrations of chitosan (1.5% *w*/*v*) displayed a high %EE of 55.18 ± 3.70% (Figure 4). PLGA NPs, E7 and E10, showed smaller particle size (227.55 ± 18.60 and 274.80 ± 0.99 nm) with low PDI values (0.12 and 0.11). The particle size of CS-E7 and CS-E10 was 439 ± 35.36 and 334 ± 67.95 nm with PDI values of 0.23 and 0.15 and ZP of +24.15 ± 2.05 mV and +26.65 ± 9.97 mV, respectively. Tahara et al. fabricated PLGA NPs encapsulating coumarin-6 dye using emulsion solvent diffusion and also surface coated them with chitosan, glycol chitosan and polysorbate [25]. Their particle size of PLGA NPs was 200 nm and the surface-modified NPs ranged between 250 and 500 nm. When these formulations were applied topically on the mouse eye, after 30 min the entire eyeball (anterior segment, the cornea, iris/ciliary and the retina) was dyed, which was observed under the fluorescent microscope. According to their fluorescent images, the topical formulation may enter the back of the eye via trans-corneal, trans-scleral and uveal routes. This study highlights that topically applied nanoparticulate systems utilize multiple routes (trans-corneal, trans-scleral and uveal routes) to travel to the back of the eye. According to previously published research, the nanoparticulate systems having similar characteristics obtained in the present study permeated to the back of the eye when instilled topically [59,60].

3.3. Response Optimization Using Response Surface Design

Based on the responses of the DOE, the response optimizer predicts the combination of variables to get the desired responses of particle size, ZP and %EE for the NPs. Two predictions were entered into the software, and they were coded as PE1, PE2 and CS-PE1 and CS-PE2 for PLGA NPs and chitosan-coated PLGA NPs, respectively. For prediction one (PE1 and CS-PE1), the goal of achieving a smaller particle size of chitosan-coated NPs with high encapsulation of TA was entered (Table S3 in Supplementary Materials). Whereas for prediction two (PE2 and CS-PE2) NPs with smaller particle size and ZP of +25 mV was considered as desired responses (Table S4 in Supplementary Materials). The DOE model generated the composite desirability (CD) graphs for each factor and response to show the reason for selecting the specific concentrations of the factors to achieve the desired result (Figure S2 in Supplementary Material). The CD value was 0.84 and 1 for predictions 1 and 2, if the CD value is close to one there are more chances of getting the prediction result. The NPs were prepared with the same procedure summarized in Section 2.2.1 and the characteristics obtained are represented in Table 3. Similar to the previous formulations prepared by the Box-Behnken DOE, the particle size increased upon chitosan-coating of the PLGA NPs. There was no significant difference in the particle size of the optimized formulations from DOE (CSE7 and CSE10) and the prediction emulsions (PE1 and PE2). However, the chitosan-coated prediction emulsions have lower PDI values (0.09–0.13)

compared to CSE7 and CSE10 (0.15–0.23).

Table 3. Characteristics of the PLGA and chitosan-coated PLGA nanoparticles prepared by point prediction using response surface DOE. Particle size is the representation of the diameter of the particle (nm). Data = mean ± std (n = 3).

Emulsion Code	Particle size (nm)	PDI	Zeta potential (mV)	%Encapsulation efficiency
PE1	318.23 ± 18.61	0.220 ± 0.08	-7.4 ± 2.43	64.80 ± 3.95
CS-PE1	386.67 ± 15.14	0.136 ± 0.05	+33.3 ± 4.69	57.14 ± 3.81
PE2	240.47 ± 48.75	0.084 ± 0.05	-6.9 ± 3.08	60.31± 2.46
CS-PE2	351.33 ± 27.02	0.098 ± 0.04	+31.97 ± 0.21	51.71 ± 1.82

The experimental response values of the prepared prediction nano-emulsions were similar to the predicted response values of the software. The predicted particles size of the chitosan-coated PE1 and PE2 was 388.5 ± 46.7 nm, and the obtained particle size was 386.67 ± 15.14 and 351.33 ± 27.02, respectively (Tables S3 and S4 in Supplementary Materials). The obtained response values for both the predictions are within the standard error of the fit generated by the response optimizer suggesting the validity and fit of the model. The two prediction formulations and E10 formulation, before and after chitosan coating were selected for further studies based on their particle size, PDI, %EE and ZP. The great challenge with topical ocular drug delivery is to increase the drug's bioavailability. The TA-loaded NPs fabricated in the current study might show enhanced bioavailability with an increase in the ocular residence compared to the free TA. Recently, Xing et al. prepared TA-loaded PLGA-chitosan NPs using an emulsion technique to treat ocular inflammation [61]. They investigated the pharmacokinetic profile of the free TA and TA-loaded NPs on the albino rabbits upon administration into the conjunctival sac. The maximum concentration of TA observed for free TA and TA-loaded NPs was 15.8 ± 0.57 and 43.2 ± 0.57 µg/L at 1 and 6 h, respectively in the aqueous humor. The free TA cleared after 6 h, whereas the TA-loaded NPs maintained the concentration until the end of the study (24 h). This study highlights the effectiveness of nanoformulations in increasing the bioavailability of TA.

3.4. Thermal Analysis

Thermal analysis was also performed for the NPs fabricated using an emulsion technique. This was carried out in order to study the stability of the materials in the formulations and to investigate the impact of nanoparticle formation on their stability (Figure 5). Extended thermal stability was noticed in the PLGA NPs (E10, PE1 and PE2) compared to drug, polymer, and surfactant (Figure S3 in Supplementary Materials).

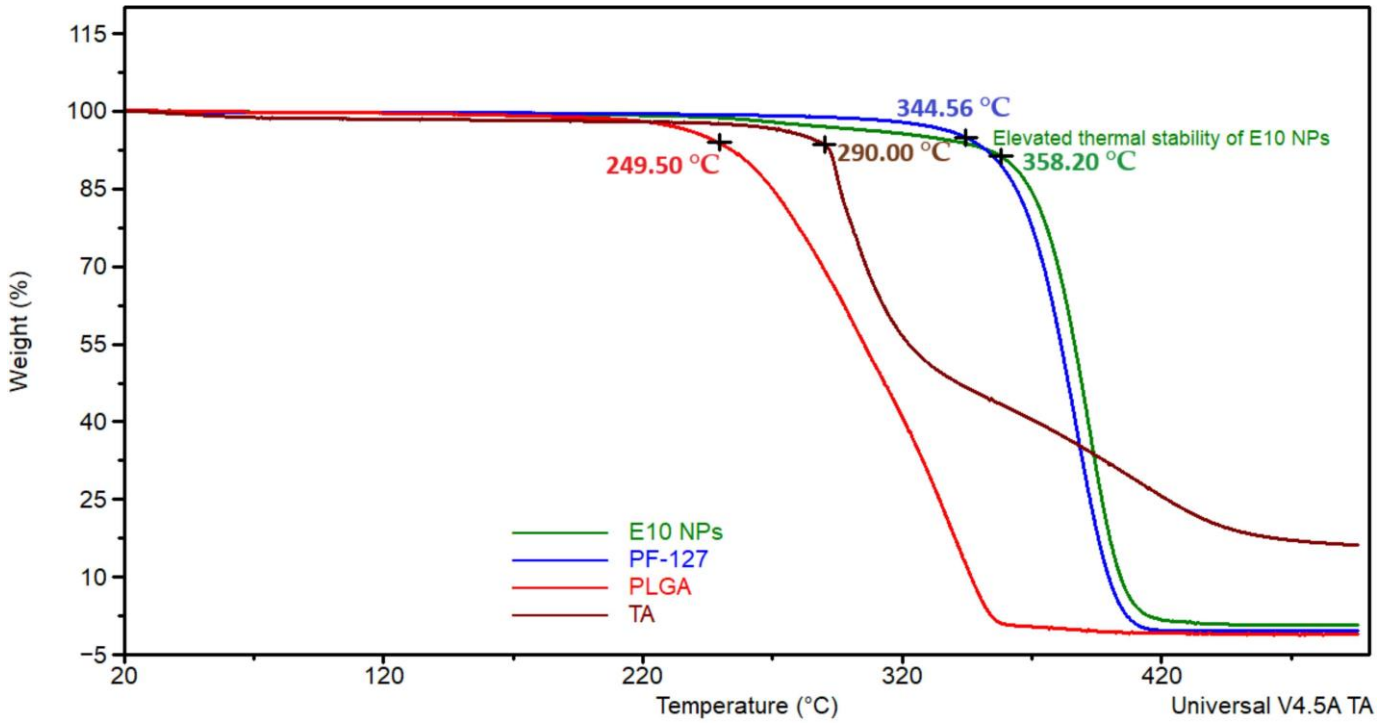

Figure 5. Thermogravimetric analysis (TGA) curves exhibiting the extended thermal stability of PLGA NPs (E10) compared to individual components (TA, PLGA and PF-127).

In the thermal analysis of chitosan-coated NPs (CSE10, PE1 and PE2), the thermograms of these NPs (Figure S4 in Supplementary Materials) exhibited weight loss around 300 °C due to the loss of water at the initial degradation of the surface adsorbed chitosan [62]. Increased thermal stability of the chitosan-coated formulations was observed compared to polymer and drug alone, which was also noticed in the thermograms of PLGA NPs. In previous studies, similar thermal behavior was noticed where the NPs demonstrated enhanced thermal stability compared to the individual components probably due to their intact structure and molecular dispersion [63,64].

To examine the physical state of the drug and the molecular dispersion in the NPs, DSC analysis was performed (Figure 6). PLGA displayed two endothermic peaks at 47.58 and 299.91 °C corresponding to glass transition/relaxation and degradation, respectively [65]. PF-127 displayed an endothermic peak at 56.96 °C associated with the melting temperature [66]. The endothermic glass transition/relaxation peak of PLGA and melting peak of PF-127 were combined and shifted to 55.54 °C for E10 formulations, which suggests the interaction of the polymer and surfactant in the NPs. TA exhibited a sharp endothermic peak at 291.10 °C due to the melting point of the crystalline state [67]. Both the endothermic peaks of the drug (melting peak) and PLGA (degradation peak) displayed at 312.13 °C in the physical mixture, the intensity of the drug peak decreased in the physical mixture may be due to the dilution effect of polymer and surfactant (a similar amount of TA and PLGA was present in the formulation and the physical mixture). However, the degradation peak of PLGA was not seen in any of the formulations due to the enhanced thermal stability which was observed in the TGA results (Figure S2 in Supplementary Materials).

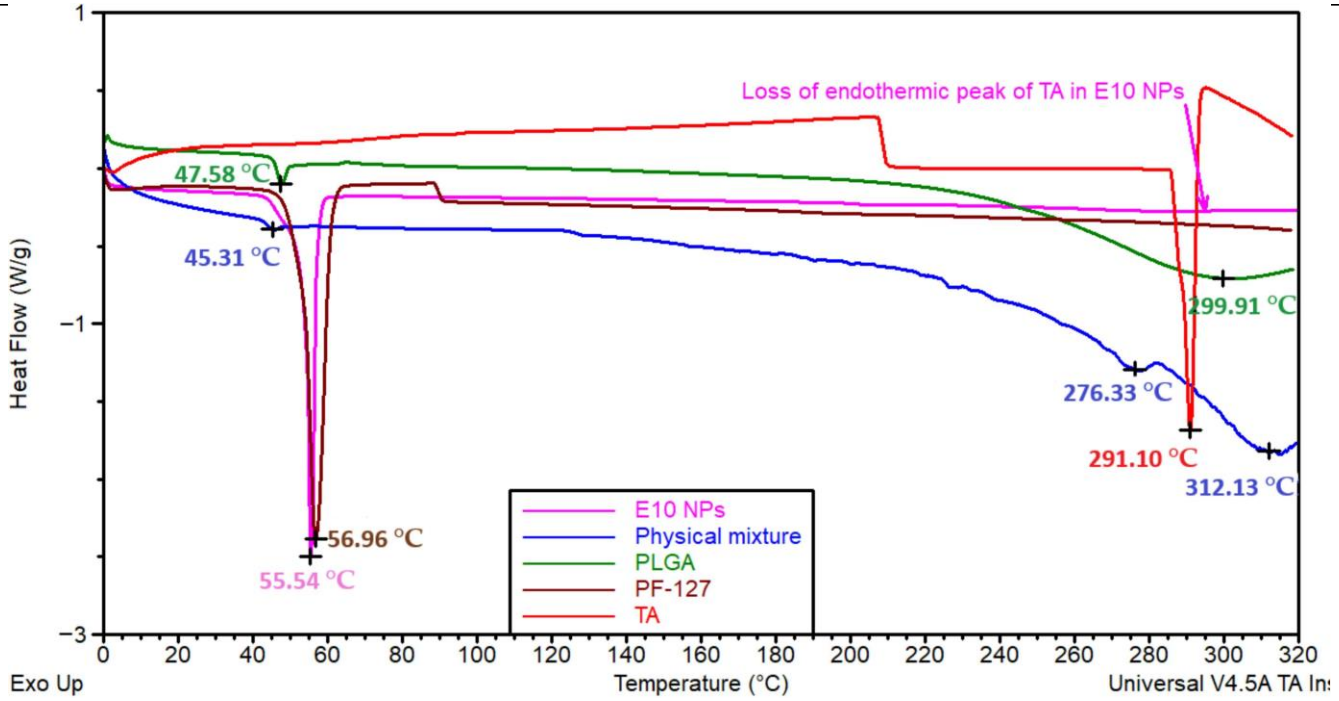

Figure 6. Differential scanning calorimetry (DSC) thermograms of physical mixture, individual components (TA, PLGA and PF-127) and PLGA NPs (E10).

The sharp endothermic peak of the drug was not seen in any of the PLGA NPs (Figure S5 in Supplementary Materials), which indicates the change of the drug to the amor- phous form leading to enhanced aqueous solubility of the drug and molecular dispersion in the nanoparticulate system [67]. These findings agree with Salama et al. where fluocinolone acetonide-loaded nanoparticles were prepared using PLGA and PF-127 [23]. They noticed the conversion of corticosteroid to amorphous form by loss of characteristic endothermic peak of the drug in formulations (which is present in pure drug thermogram due to its crystalline state). The fusion of endothermic peaks of PLGA and PF-127 highlights the entanglement of PLGA chains and PF-127 moieties indicating the formation of intact NPs as mentioned in Section 3.1.

3.5. Fourier Transform Infra-Red Spectroscopy (FT-IR) Analysis

FT-IR spectra and functional groups of PF-127, PLGA, TA, physical mixture and PLGA NPs (E10) are presented in Figure 7 and Table 4. Drug and excipients functional groups were present in the formulation with peaks at similar wavenumbers, which suggests that there was no interaction between the drug and the components [59].

Pure TA spectra displayed an infrared absorption band at 3398 cm^{-1} related to the hydrogen-bonded hydroxyl stretching vibration, at 1706 cm^{-1} associated with stretching vibration of the carbonyl group (in the aliphatic ester bonds). Another typical absorption band of TA at 1057 cm^{-1} is due to the stretching vibration of C–F. The physical mixture also showed the characteristic peaks of the TA in a similar wavelength range. Blueshift of the ketonic carbonyl and C–F groups was observed in the formulation at 1762 and 1060 cm^{-1}, respectively.

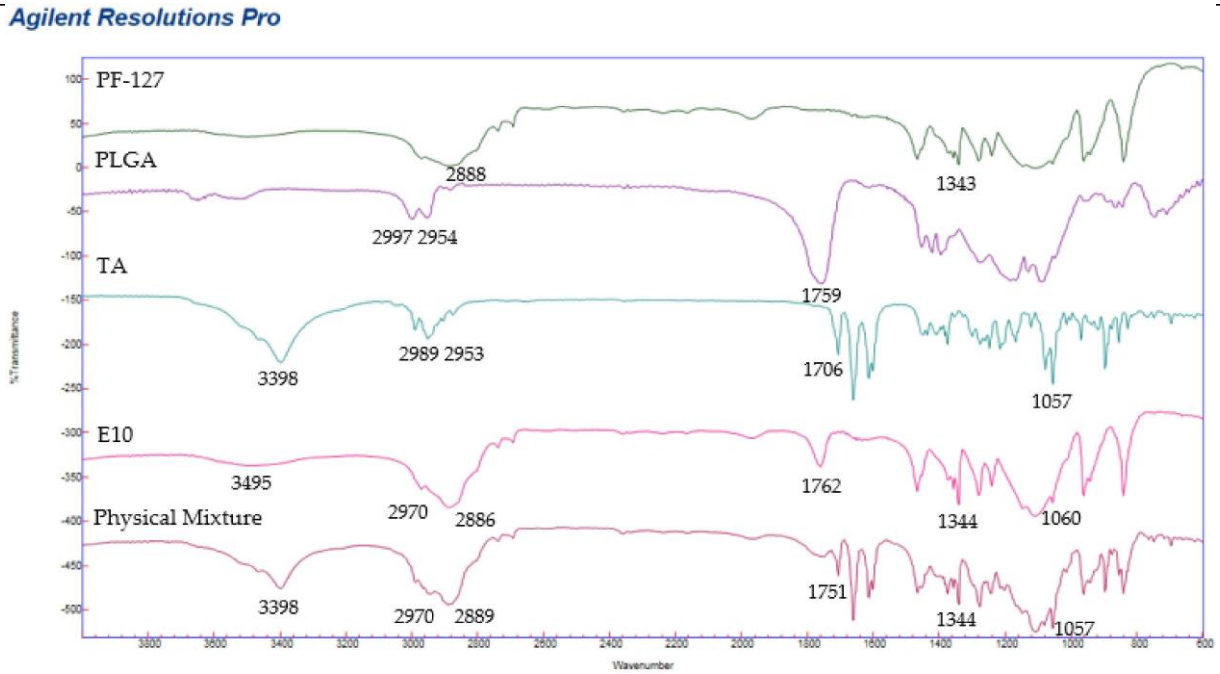

Figure 7. FTIR spectrums of individual components (TA, PLGA and PF-127), physical mixture and PLGA nanoparticles (E10).

Table 4. Representation of FT-IR peaks and functional groups of the individual components, physical mixture and PLGA NPs (E10).

Frequency (cm^{-1})	Functional Group	Individual Components (cm^{-1})			Physical Mixture (cm^{-1})			E10-Nanoparticles (cm^{-1})			Ref.
		PLGA	PF-127	TA	PLGA	PF-127	TA	PLGA	PF-127	TA	
3510	OH	3520						3495			[68]
3398	OH			3398			3398				[69]
3000–2950	C–H	2997–2954		2989–2953			2970–2889	2970–2886			[68]
2891	C–H		2888			2889			2886		[70]
2985–2937	C–H			2989–2951			2970–2889			2970–2886	[69]
1705	C=O			1706						1762	[69]
1757	C=O	1759			1751			1762			[68]
1344	O–H		1343			1344			1344		[70]
1055	C–F			1057			1057			1060	[67]

The FT-IR spectra (Figure 8) suggested the existence of chitosan coating on PLGA NPs by the presence of characteristics functional group of chitosan; C–H, $CONH_2$ and C–O on CS-E10 spectra at 2935, 1631 and 1087 cm^{-1}, respectively, with a slight shift in wavenumber [62,71–73].

The FTIR characteristic peaks of chitosan together with the conversion of negative ZP to positive ZP and the thermogram changes of coated NPs suggest the successful coating of chitosan onto PLGA NPs. The characteristic negative charge of the eye structures can be utilized to enhance drug bioavailability by introducing oppositely charged polymer for surface coating [74].

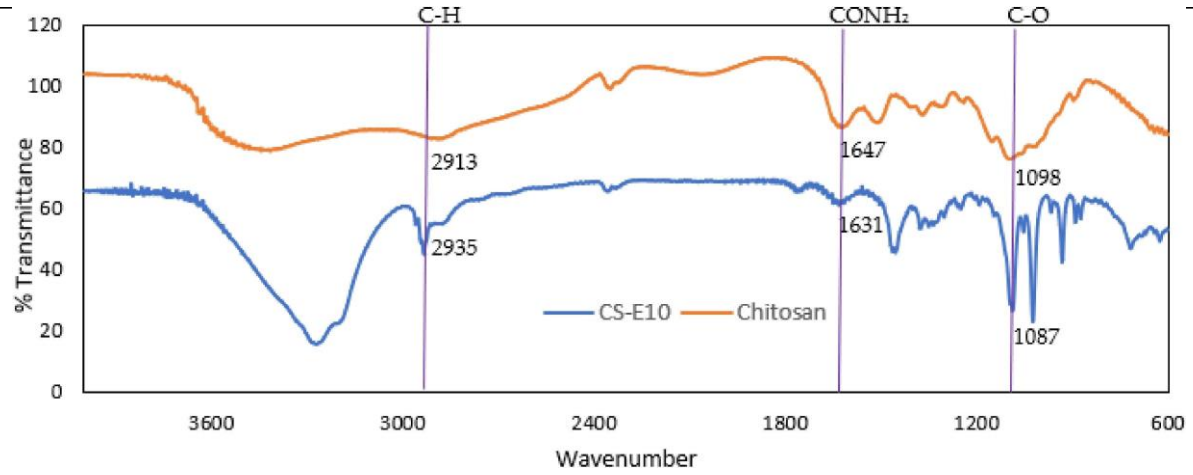

Figure 8. FTIR spectra of chitosan and chitosan-coated PLGA NPs (CS-E10) highlighting the functional groups.

3.6. In Vitro Drug Release Study

The %cumulative drug release was plotted against time (h) for the in vitro drug release study performed using PBS (pH 7.4) with 0.01% sodium azide and 1% Tween® 80 as release media. To increase the solubility of hydrophobic TA, Tween® 80 was used as a surfactant in the release medium [75]. The surfactant increased the solubility of the drug from 21 ± 2.16 to 102.05 ± 4.78 µg/mL. To avoid bacterial contamination of the formulation and the release media over 70 h, 0.01% sodium azide was used as an antibacterial agent [36].

The drug release from the PLGA nano-formulations reached a plateau after 23 h and the chitosan-coated nano-formulations reached a plateau at 27 h. Even though the release from all the three PLGA NPs was similar, the CS-E10 formulation showed more drug release compared to other formulations (59.47 ± 3.28%). This could be due to a lower concentration of PLGA in E10 (3.5 mg/mL) compared to PE1 (3.7 mg/mL) and PE2 (4.5 mg/mL). With the increase in polymer concentration, the drug might have better protection leading to a delay in the drug release [76]. The chitosan-coated NPs fabricated using an emulsion method controlled the initial burst release when compared to PLGA NPs. In the first 2 h, PLGA NPs released 44–40% of the drug (potentially due to the release of the drug close to the pores of the PLGA NPs) whereas chitosan-coated PLGA NPs released 21–37% of the drug, which indicates the role of chitosan coating in controlling the initial burst release (Figure 9). Similar control of initial burst release was observed in previously published findings of NPs prepared with the same polymers [62,77].

The NPs demonstrated a biphasic release, burst release on Day 1 followed by controlled release; this release pattern is in agreement with previous investigations [78–80]. Pandit et al. formulated bevacizumab-loaded, chitosan-coated PLGA NPs using emulsion technique and investigated the in vitro drug release profile in PBS [36]. They observed a similar burst release of the drug in the first day followed by controlled release over 72 h reaching a plateau. The curve fit of the in vitro TA release was analyzed with the mathematical models considering regression coefficient (R^2) as represented in Table 5. Korsmeyer–Peppas is most fitting to the TA release from the NPs (R^2 between 0.621 and 0.894) when compared to other models, which suggests the sustained release of the TA. This model indicates that the release from the PLGA NPs involves multiple release mechanisms, such as diffusion, dissolution and swelling [81].

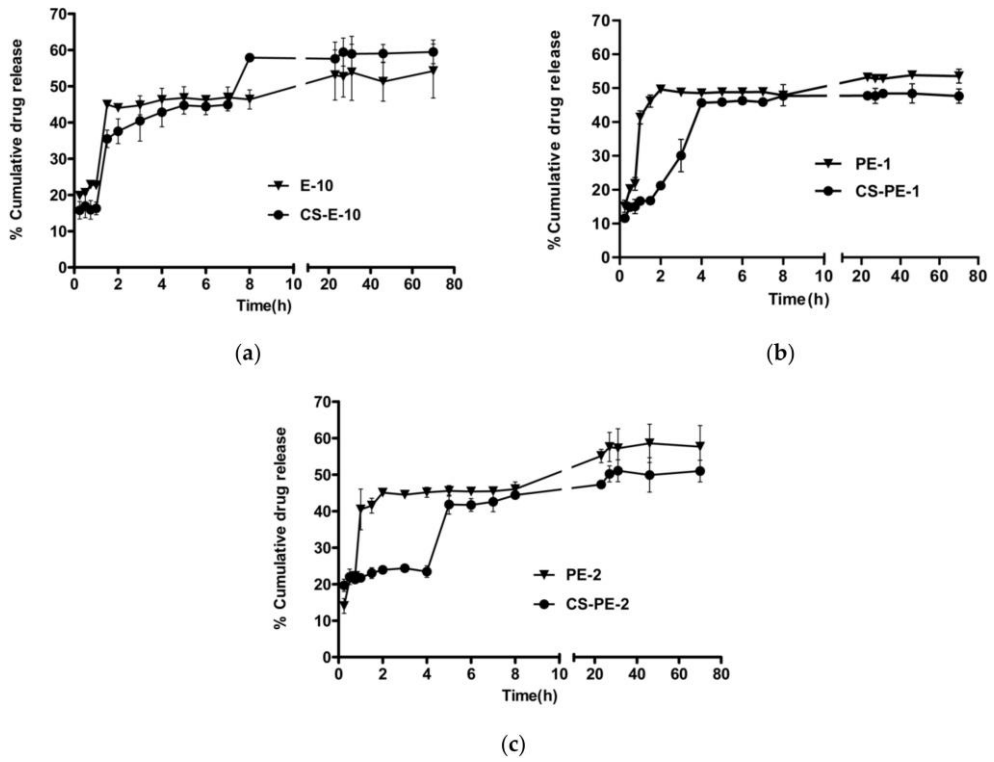

Figure 9. Comparison of in vitro drug release of non-coated and coated NPs: (**a**) E-10 and CS-E10, (**b**) PE-1 and CS-PE-1 and (**c**) PE-2 and CS-PE-2. The concentration of TA-loaded NPs in release media was 25 µg/mL for all formulations. Data = mean ± std (n = 3).

Table 5. In vitro drug release mathematical model fitting concerning coefficient of determination (R^2).

Formulation Code	Coefficient of determination (R^2)				
	Zero-Order	First-Order	Hixson–Crowell	Higuchi	Korsmeyer–Peppas
PE 1	0.552	0.582	0.572	0.69	0.791
PE 2	0.756	0.767	0.763	0.893	0.894
E 10	0.338	0.41	0.386	0.464	0.621
CS-PE1	0.237	0.252	0.247	0.387	0.641
CS-PE2	0.503	0.541	0.528	0.676	0.845
CS-E10	0.504	0.586	0.56	0.681	0.853

Commercially available corticosteroid implants for posterior inflammation like Ozurdex® (dexamethasone intravitreal implant) and Retisert® (fluocinolone acetonide intravitreal implant) release about 0.2 µg of drug per day [82]. The anti-VEGF activity of TA was observed on human retinal epithelial cell lines from a concentration of 4.34 µg [9]. In the present study, around 25 µg of TA was released in the first two days leading to a sustained release. The released drug is more than the therapeutic dose of the similar corticosteroid intravitreal implants, which is advantageous considering the loss of the drug during the transport from the front of the eye to the posterior segment. The drug dose regimen depends on the pathological condition of the disease. All three optimized

nano-emulsions (E10, PE1 and PE2) before and after chitosan coating exhibited controlled release of the drug over the duration of the experiment (70 h) due to the release mechanism of PLGA NPs.

4. Conclusions

The formulation of chitosan-coated PLGA NPs was successfully optimized with a Box-Behnken response surface DOE and a response optimizer. The optimized surface- modified NPs (CS-E10, CS-PE1 and CS-PE-2) were reproducible and colloidally stable with a particle size of 334 ± 67.95 to 386 ± 15.14 nm and PDI between 0.09 ± 0.04 and 0.15 ± 0.08, having a ZP between +26 ± 9.97 and +33 ± 4.69 mV. These NPs encapsulated 55–57% of TA and displayed a controlled release of the drug reaching a plateau in 27 h.

This study highlighted the importance of PF-127 as a surfactant in yielding smaller particles with uniform distribution and the utilization of DOE and response optimizer in achieving the desired NPs. The prediction formulations (CS-PE1 and CS-PE2) obtained from the response optimizer showed high %EE and controlled release of the drug with monodispersed NPs. The polymeric matrix of PLGA supports controlled diffusion of encapsulated drug, while the mucoadhesive property of chitosan may enhance permeation across the barriers of the eye. The size of the NPs in conjunction with the biodegradable and biocompatible properties of the polymers suggest these particles might be promising for topical ocular drug delivery, which could improve patient comfort and outcomes while reducing healthcare expenses by negating or reducing the need for intravitreal injections.

Supplementary Materials: The following are available online at https://www.mdpi.com/article/10

.3390/pharmaceutics13101590/s1, Table S1: Design of experiments generated by Box-Behnken design statistical design in Minitab software. Table S2: Investigated values of responses for the prepared nanoparticles using Box-Behnken design. Figure S1: Comparison of particle size (nm) of PLGA NPs before and after coating with chitosan. Table S3: Predicted experimental conditions for low particle size and high encapsulation efficiency for CS-PLGA nanoparticles. Figure S2: Response optimization parameters and predicted experimental conditions for low particle size and high encapsulation efficiency for CS-PLGA nanoparticles. Table S4: Predicted experimental conditions for low particle size and +25 mV zeta potential efficiency for CS-PLGA nanoparticles. Figure S3: Thermal analysis of individual components and PLGA NPs (PE1, PE2 and E10). Figure S4: Thermal analysis of chitosan- coated NPs (CS-E10, CS-PE1 and CS-PE2) and the individual components using TGA. Figure S5: DSC thermograms of components and PLGA NPs (E10, PE1 and PE2).

Author Contributions: Conceptualization, M.D. and L.F.; methodology, M.D., A.C., G.B., P.M. and L.F.; writing—original draft preparation, M.D. and L.F.; writing—review and editing, M.D., P.M., A.C., G.B., D.K., S.R., L.C. and L.F.; supervision, A.C., G.B., P.M. and L.F.; project administration, L.F.; funding acquisition, L.F. All authors have read and agreed to the published version of the manuscript.

Funding: This research was funded by the WIT PhD scholarship (project code: WD2017_PhD_023). The APC was funded by Research Connexions, WIT.

Institutional Review Board Statement: Not applicable.

Informed Consent Statement: Not applicable.

Conflicts of Interest: All other authors declare no conflict of interest.

References

[1] C. van de Pol, Basic anatomy and physiology of the human visual system, (2014).

[2] E. Morley, E. Morley, Blindness and Vision, Iris Murdoch Elias Canetti. (2018) 15–60. https://doi.org/10.4324/9781351191791-2.

[3] European Commission, Population structure and ageing, Eurostat. (2023) 1–10. https://ec.europa.eu/eurostat/statistics-explained/index.php?title=Population_structure_and_ageing#The_share_of_elderly_people_continues_to_increase.

[4] U.N. Das, Diabetic macular edema, retinopathy and age-related macular degeneration as inflammatory conditions, Arch. Med. Sci. (2016). https://doi.org/10.5114/aoms.2016.61918.

[5] W.S. Cheng, D.W. Lu, C.H. Chiang, C.J. Chang, Overview of clinical trials for dry age-related macular degeneration, J. Med. Sci. (2017). https://doi.org/10.4103/jmedsci.jmedsci_115_16.

[6] J.Q. Li, T. Welchowski, M. Schmid, M.M. Mauschitz, F.G. Holz, R.P. Finger, Prevalence and incidence of age-related macular degeneration in Europe: a systematic review and meta-analysis, Br. J. Ophthalmol. 104 (2020) 1077–1084. https://doi.org/10.1136/bjophthalmol-2019-314422.

[7] A.C. Pedrosa, T. Sousa, J. Pinheiro-Costa, J. Beato, M.S. Falcão, F. Falcão-Reis, A. Carneiro, Treatment of neovascular age-related macular degeneration with anti-VEGF agents: Predictive factors of long-term visual outcomes, J. Ophthalmol. 2017 (2017). https://doi.org/10.1155/2017/4263017.

[8] A. Miller, M.A. Wilneff, A. Yazji, E. Petrinec, M. Carbone, C. Miller, C. McCrossin, R. Donkor, D.G. Miller, Analysis of urgent follow up visits and complications after intravitreal injections: a retrospective cohort study, Int. J. Retin. Vitr. 8 (n.d.) 8. https://doi.org/10.1186/s40942-021-00358-w.

[9] S. Day, K. Acquah, P. Mruthyunjaya, D.S. Grossman, P.P. Lee, F.A. Sloan, Ocular complications after antivascular endothelial growth factor therapy in medicare patients with age-related macular degeneration, Am. J. Ophthalmol. (2011). https://doi.org/10.1016/j.ajo.2011.01.053.

[10] J.B. Fileta, I.U. Scott, H.W. Flynn, Meta-analysis of infectious endophthalmitis after intravitreal injection of anti-vascular endothelial growth factor agents, Ophthalmic Surg. Lasers Imaging Retin. (2014). https://doi.org/10.3928/23258160-20140306-08.

[11] A. Sternfeld, R. Ehrlich, D. Weinberger, A. Dotan, Effect of different lens status on intraocular pressure elevation in patients treated with anti-vascular endothelial growth factor injections, Int. J. Ophthalmol. 13 (2020) 79–84. https://doi.org/10.18240/ijo.2020.01.12.

[12] A. Obeid, X. Gao, F.S. Ali, C.M. Aderman, A. Shahlaee, M.K. Adam, S.K. Kasi, L. Hyman, A.C. Ho, J. Hsu, Loss to Follow-up among Patients with Neovascular Age-Related Macular Degeneration Who Received Intravitreal Anti-Vascular Endothelial Growth Factor Injections, JAMA Ophthalmol. 136 (2018) 1251–1259. https://doi.org/10.1001/jamaophthalmol.2018.3578.

[13] K.M. Droege, P.S. Muether, M.M. Hermann, A. Caramoy, U. Viebahn, B. Kirchhof, S. Fauser, Adherence to ranibizumab treatment for neovascular age-related macular degeneration in real life, Graefe's Arch. Clin. Exp. Ophthalmol. (2013). https://doi.org/10.1007/s00417-012-2177-3.

[14] Y. Ge, A. Zhang, R. Sun, J. Xu, T. Yin, H. He, J. Gou, J. Kong, Y. Zhang, X. Tang, Penetratin-modified lutein nanoemulsion in-situ gel for the treatment of age-related macular degeneration, Expert Opin. Drug Deliv. (2020). https://doi.org/10.1080/17425247.2020.1735348.

[15] J. Yan, X. Peng, Y. Cai, W. Cong, Development of facile drug delivery platform of ranibizumab fabricated PLGA-PEGylated magnetic nanoparticles for age-related macular degeneration therapy, J. Photochem. Photobiol. B Biol. (2018). https://doi.org/10.1016/j.jphotobiol.2018.04.033.

[16] J.H. Jung, B. Chiang, H.E. Grossniklaus, M.R. Prausnitz, Ocular drug delivery targeted by iontophoresis in the suprachoroidal space using a microneedle, J Control Release. 277 (2018) 14–22. https://doi.org/10.1016/j.jconrel.2018.03.001.

[17] R. Bisht, J.K. Jaiswal, Y.-S. Chen, J. Jin, I.D. Rupenthal, Light-responsive in situ forming injectable implants for effective drug delivery to the posterior segment of the eye, Expert Opin. Drug Deliv. 13 (2016) 953–962. https://doi.org/10.1517/17425247.2016.1163334.

[18] Y. Yu, L.C. Lau, A.C. Lo, Y. Chau, Injectable Chemically Crosslinked Hydrogel for the Controlled Release of Bevacizumab in Vitreous: A 6-Month In Vivo Study, Transl Vis Sci Technol. 4 (2015) 5.

https://doi.org/10.1167/tvst.4.2.5.

[19] Z. Shi, S.K. Li, P. Charoenputtakun, C.Y. Liu, D. Jasinski, P. Guo, RNA nanoparticle distribution and clearance in the eye after subconjunctival injection with and without thermosensitive hydrogels, J Control Release. 270 (2018) 14–22. https://doi.org/10.1016/j.jconrel.2017.11.028.

[20] C. Huang, Adeno-associated virus-mediated expression of growth-associated protein-43 aggravates retinal ganglion cell death in experimental chronic glaucomatous injury, Mol. Vis. 19 (2013) 1422–1432.

[21] A.K. Mitra, Ocular transporters and receptors: Their role in drug delivery, 2013. https://doi.org/10.1533/9781908818317.

[22] K. Cholkar, A. Patel, A.D. Vadlapudi, A.K. Mitra, Novel Nanomicellar Formulation Approaches for Anterior and Posterior Novel Nanomicellar Formulation Approaches for Anterior and Posterior Segment Ocular Drug Delivery, (2012). https://doi.org/10.2174/1877912311202020082.

[23] WHO, Blindness And Vision Impairment Prevention, (2019) 22–24. https://www.who.int/news-room/fact-sheets/detail/blindness-and-visual-impairment.

[24] E. Ünsal, K. Eltutar, İ.K. Muftuoglu, Morphologic changes in the anterior segment using ultrasound biomicroscopy after cataract surgery and intraocular lens implantation, Eur. J. Ophthalmol. (2017). https://doi.org/10.5301/ejo.5000812.

[25] Q. Fu, Z. Mo, D. Lyu, L. Zhang, Z. Qin, Q. Tang, H. Yin, P. Xu, L. Wu, X. Lou, Z. Chen, K. Yao, Air pollution and outpatient visits for conjunctivitis: A case-crossover study in Hangzhou, China, Environ. Pollut. (2017). https://doi.org/10.1016/j.envpol.2017.08.109.

[26] J. Vehof, N. Sillevis Smitt-Kamminga, S.A. Nibourg, C.J. Hammond, Predictors of Discordance between Symptoms and Signs in Dry Eye Disease, Ophthalmology. (2017). https://doi.org/10.1016/j.ophtha.2016.11.008.

[27] J. Randazzo, Orally Active Multi-Functional Antioxidants Delay Cataract Formation in Streptozotocin (Type 1) Diabetic and Gamma-Irradiated Rats, PLoS One. 6 (2011). https://doi.org/10.1371/journal.pone.0018980.g001.

[28] L. Lee, F. D'Esposito, J. Garap, G. Wabulembo, S.P. Koim, D. Keys, A.T. Cama, H. Limburg, A. Burnett, Rapid assessment of avoidable blindness in Papua New Guinea: A nationwide survey, Br. J. Ophthalmol. (2019). https://doi.org/10.1136/bjophthalmol-2017-311802.

[29] B. Srilatha, A Review on Age Related Eye Diseases and their Preventive Measures, J. Clin. Exp. Ophthalmol. 2 (2011). https://doi.org/10.4172/21559570.1000196.

[30] K.K. Nichols, G.N. Foulks, A.J. Bron, B.J. Glasgow, M. Dogru, K. Tsubota, M.A. Lemp, D.A. Sullivan, The international workshop on meibomian gland dysfunction: Executive summary, Investig. Ophthalmol. Vis. Sci. (2011). https://doi.org/10.1167/iovs.10-6997a.

[31] M.T.M. Wang, A. Muntz, J. Lim, J.S. Kim, L. Lacerda, A. Arora, J.P. Craig, Ageing and the natural history of dry eye disease: A prospective registry-based cross-sectional study, Ocul. Surf. (2020). https://doi.org/10.1016/j.jtos.2020.07.003.

[32] M.A. Lemp, L.A. Crews, A.J. Bron, G.N. Foulks, B.D. Sullivan, Distribution of aqueous-deficient and evaporative dry eye in a clinic-based patient cohort: A retrospective study, Cornea. (2012). https://doi.org/10.1097/ICO.0b013e318225415a.

[33] Y. Wei, P.A. Asbell, The core mechanism of dry eye disease is inflammation, Eye Contact Lens. (2014). https://doi.org/10.1097/ICL.0000000000000042.

[34] M. Brill, Spontaneous eye blinks as an alternative measure for spatial presence experiences, University of Wuerzburg, 2019. https://www.researchgate.net/publication/333994733_Spontaneous_eye_blinks_as_an_alternative_measure_for_spatial_presence_experiences.

[35] B.W. Jones, R.L. Pfeiffer, W.D. Ferrell, C.B. Watt, M. Marmor, R.E. Marc, Retinal remodeling in human retinitis pigmentosa, Exp. Eye Res. (2016). https://doi.org/10.1016/j.exer.2016.03.018.

[36] S. Nakakura, Y. Kobayashi, K. Matsuya, E. Terao, Y. Kiuchi, Iris thickness and severity of neovascular glaucoma determined using swept-source anterior-segment optical coherence tomography, J. Glaucoma. (2018). https://doi.org/10.1097/IJG.0000000000000921.

[37] A. Das, P.G. McGuire, S. Rangasamy, Diabetic Macular Edema: Pathophysiology and Novel Therapeutic Targets, Ophthalmology. (2015). https://doi.org/10.1016/j.ophtha.2015.03.024.

[38] M.M. Nentwich, Diabetic retinopathy - ocular complications of diabetes mellitus, World J. Diabetes. (2015). https://doi.org/10.4239/wjd.v6.i3.489.

[39] E.K. De Jong, M.J. Geerlings, A.I. Den Hollander, Age-related macular degeneration, Genetics and Genomics of Eye Disease, (2020) 155–180. https://doi.org/10.1016/B978-0-12-816222-4.00010-1.

[40] R.N. Weinreb, T. Aung, F.A. Medeiros, The pathophysiology and treatment of glaucoma: a review,

JAMA. 311 (2014) 1901–1911. https://doi.org/10.1001/jama.2014.3192.
[41] V. Krishnaswami, R. Kandasamy, S. Alagarsamy, R. Palanisamy, S. Natesan, Biological macromolecules for ophthalmic drug delivery to treat ocular diseases, Int J Biol Macromol. 110 (2018) 7–16. https://doi.org/10.1016/j.ijbiomac.2018.01.120.
[42] Y. Shan, Y. Xu, X. Lin, L. Lou, Y. Wang, J. Ye, Burden of vision loss due to diabetic retinopathy in China from 1990 to 2017: findings from the global burden of disease study, Acta Ophthalmol. (2020). https://doi.org/10.1111/aos.14573.
[43] D.S. Fong, L.P. Aiello, F.L. Ferris, R. Klein, Diabetic retinopathy, Diabetes Care. (2004). https://doi.org/10.2337/diacare.27.10.2540.
[44] N. Ban, T.J. Lee, A. Sene, M. Choudhary, M. Lekwuwa, Z. Dong, A. Santeford, J.B. Lin, G. Malek, D.S. Ory, R.S. Apte, Impaired monocyte cholesterol clearance initiates age-related retinal degeneration and vision loss, JCI Insight. (2018). https://doi.org/10.1172/jci.insight.120824.
[45] World Health Organization, World report on vision, 2019.
[46] P. Mitchell, G. Liew, B. Gopinath, T.Y. Wong, Age-related macular degeneration, Lancet. (2018). https://doi.org/10.1016/S0140-6736(18)31550-2.
[47] A. Bhuiyan, A Review of Disease Grading and Remote Diagnosis for Sight Threatening Eye Condition: Age Related Macular Degeneration, J. Comput. Sci. Syst. Biol. (2014). https://doi.org/10.4172/jcsb.1000139.
[48] D.J. Taylor, L. Jones, A.M. Binns, D.P. Crabb, 'You've got dry macular degeneration, end of story': a qualitative study into the experience of living with non-neovascular age-related macular degeneration, Eye. (2020). https://doi.org/10.1038/s41433-019-0445-8.
[49] D.G. Birch, Age-related macular degeneration: a target for nanotechnology derived medicines, Int. J. Nanomedicine. 2 (2007) 65–77.
[50] N. Ferrara, Vascular endothelial growth factor and age-related macular degeneration: From basic science to therapy, Nat. Med. 16 (2010) 1107–1111. https://doi.org/10.1038/nm1010-1107.
[51] M. N, Routes of Oxidative Stress in Age-Related Macular Degeneration, Int. J. Ophthalmol. Clin. Res. (2016). https://doi.org/10.23937/2378-346x/1410049.
[52] T.A. Eye, AREDS Report No. 8, Arch Ophthalmol. 119 (2001) 1417–1436.
[53] M. Xu, R. Fan, X. Fan, Y. Shao, X. Li, Progress and Challenges of Anti-VEGF Agents and Their Sustained-Release Strategies for Retinal Angiogenesis, Drug Des. Devel. Ther. 16 (2022) 3241–3262. https://doi.org/10.2147/DDDT.S383101.
[54] H.A. Khaqan, T. Khan, H. Tayyab, T.K. Marwat, M.Q. Lateef, H.A. Khaqan, Complications VEGF Injections at Multiple Centers Observing Different Protocols, 35 (2019) 1–6.
[55] X. Gao, A. Obeid, C.M. Aderman, K.E. Talcott, F.S. Ali, M.K. Adam, B.W. Rovner, L. Hyman, A.C. Ho, J. Hsu, Loss to Follow-up After Intravitreal Anti–Vascular Endothelial Growth Factor Injections in Patients with Diabetic Macular Edema, Ophthalmol. Retin. (2019). https://doi.org/10.1016/j.oret.2018.11.002.
[56] G. Xin, M. Zhang, Z. Zhong, L. Tang, Y. Feng, Z. Wei, S. Li, Y. Li, J. Zhang, B. Zhang, M. Zhang, N. Rowell, Z. Chen, H. Niu, K. Yu, W. Huang, Ophthalmic Drops with Nanoparticles Derived from a Natural Product for Treating Age-Related Macular Degeneration, ACS Appl. Mater. Interfaces. (2020). https://doi.org/10.1021/acsami.0c17296.
[57] G. Adamus, Are anti-retinal autoantibodies a cause or a consequence of retinal degeneration in autoimmune retinopathies?, Front. Immunol. (2018). https://doi.org/10.3389/fimmu.2018.00765.
[58] R.S. Sulaiman, M. Kadmiel, J.A. Cidlowski, Glucocorticoid receptor signaling in the eye, Steroids. 133 (2018) 60–66. https://doi.org/10.1016/j.steroids.2017.11.002.
[59] D.A. Copland, S. Theodoropoulou, J. Liu, A.D. Dick, A perspective of AMD through the eyes of immunology, Investig. Ophthalmol. Vis. Sci. (2018). https://doi.org/10.1167/iovs.18-23893.
[60] K. Jiang, E. To, J. Z. Cui, S. Cao, Drusen and Pro-inflammatory Mediators in the Post-Mortem Human Eye, J. Clin. Exp. Ophthalmol. (2012). https://doi.org/10.4172/2155-9570.1000208.
[61] V. Behnke, A. Wolf, T. Langmann, The role of lymphocytes and phagocytes in age-related macular degeneration (AMD), Cell. Mol. Life Sci. (2020). https://doi.org/10.1007/s00018-019-03419-4.
[62] J.C. ten Berge, Z. Fazil, I. van den Born, R.C.W. Wolfs, M.W.J. Schreurs, W.A. Dik, A. Rothova, Intraocular cytokine profile and autoimmune reactions in retinitis pigmentosa, age-related macular degeneration, glaucoma and cataract, Acta Ophthalmol. (2019). https://doi.org/10.1111/aos.13899.
[63] K. Morohoshi, A.M. Goodwin, M. Ohbayashi, S.J. Ono, Autoimmunity in retinal degeneration: autoimmune retinopathy and age-related macular degeneration, J Autoimmun. 33 (2009) 247–254. https://doi.org/10.1016/j.jaut.2009.09.003.
[64] J.A. Olson, E.H. Steffensen, R.W. Smith, R.R. Margulis, E.L. Whitney, Use of adrenocorticotropic hormone and cortisone in ocular disease, AMA. Arch. Ophthalmol. (1951).

https://doi.org/10.1001/archopht.1951.01700010280004.
[65] L.I. Mckay, J.A. Cidlowski, Physiologic and Pharmacologic Effects of Corticosteroids, Holland-Frei Cancer Med. (2003).
[66] R. Machemer, G. Sugita, Y. Tano, Treatment of intraocular proliferations with intravitreal steroids, Trans. Am. Ophthalmol. Soc. (1979).
[67] J. Vandewalle, A. Luypaert, K. De Bosscher, C. Libert, Therapeutic Mechanisms of Glucocorticoids, Trends Endocrinol. Metab. (2018). https://doi.org/10.1016/j.tem.2017.10.010.
[68] S.M. Whitcup, J.A. Cidlowski, K.G. Csaky, J. Ambati, Pharmacology of corticosteroids for diabetic macular edema, Investig. Ophthalmol. Vis. Sci. (2018). https://doi.org/10.1167/iovs.17-22259.
[69] K. Papangkorn, E. Prendergast, J.W. Higuchi, B. Brar, W.I. Higuchi, Noninvasive Ocular Drug Delivery System of Dexamethasone Sodium Phosphate in the Treatment of Experimental Uveitis Rabbit, J. Ocul. Pharmacol. Ther. (2017). https://doi.org/10.1089/jop.2017.0053.
[70] V.S. Sangwan, P.A. Pearson, H. Paul, T.L. Comstock, Use of the Fluocinolone Acetonide Intravitreal Implant for the Treatment of Noninfectious Posterior Uveitis: 3-Year Results of a Randomized Clinical Trial in a Predominantly Asian Population, Ophthalmol. Ther. (2015). https://doi.org/10.1007/s40123-014-0027-6.
[71] S.A. Gaballa, U.B. Kompella, O. Elgarhy, A.M. Alqahtani, B. Pierscionek, R.G. Alany, H. Abdelkader, Corticosteroids in ophthalmology: drug delivery innovations, pharmacology, clinical applications, and future perspectives, Drug Deliv. Transl. Res. (2020). https://doi.org/10.1007/s13346-020-00843-z.
[72] J.B. Jonas, ntravitreal triamcinolone acetonide for exudative age related macular degeneration, Br J Ophthalmol. 87 (2003) 462–468.
[73] Pei-Qiang Huang, Efficiency in Natural Product Total Synthesis, Wiley, 2018. https://www.wiley.com/en-ie/Efficiency+in+Natural+Product+Total+Synthesis-p-9781118605400.
[74] M.C. Wani, H.L. Taylor, M.E. Wall, P. Coggon, A.T. Mcphail, Plant Antitumor Agents.VI.The Isolation and Structure of Taxol, a Novel Antileukemic and Antitumor Agent from Taxus brevifolia2, J. Am. Chem. Soc. (1971). https://doi.org/10.1021/ja00738a045.
[75] E. Chain, The early years of the penicillin discovery, Trends Pharmacol. Sci. (1979). https://doi.org/10.1016/0165-6147(79)90004-X.
[76] B.D. Kahan, Cyclosporine: The agent and its actions, Transplant. Proc. (1985).
[77] E. Kellenberger, A. Hofmann, R.J. Quinn, Similar interactions of natural products with biosynthetic enzymes and therapeutic targets could explain why nature produces such a large proportion of existing drugs, Nat. Prod. Rep. (2011). https://doi.org/10.1039/c1np00026h.
[78] A. Francisco, J. B. HARBORNE (ED.) The flavonoids–Advances in research since 1986 Chapman & Hall, London, U.K. 1994, £195.00, 676 pp. ISBN 0-412-48070-0, Phytochem. Anal. (1995). https://doi.org/10.1002/pca.2800060109.
[79] M. Lesjak, I. Beara, N. Simin, D. Pintać, T. Majkić, K. Bekvalac, D. Orčić, N. Mimica-Dukić, Antioxidant and anti-inflammatory activities of quercetin and its derivatives, J. Funct. Foods. (2018). https://doi.org/10.1016/j.jff.2017.10.047.
[80] F. Li, Y. Bai, M. Zhao, L. Huang, S. Li, X. Li, Y. Chen, Quercetin inhibits vascular endothelial growth factor-induced choroidal and retinal angiogenesis in vitro, Ophthalmic Res. (2015). https://doi.org/10.1159/000369824.
[81] M. Lee, S. Yun, H. Lee, J. Yang, Quercetin mitigates inflammatory responses induced by vascular endothelial growth factor in mouse retinal photoreceptor cells through suppression of nuclear factor Kappa B, Int. J. Mol. Sci. (2017). https://doi.org/10.3390/ijms18112497.
[82] P. Zhuang, Y. Shen, B.Q. i. Lin, W.Y. u. Zhang, G.C.Y. Chiou, Effect of quercetin on formation of choroidal neovascularization (CNV) in age-related macular degeneration(AMD), Eye Sci. (2011). https://doi.org/10.3969/j.issn.1000-4432.2011.01.006.
[83] Y. Wang, L. Zhao, C. Wang, J. Hu, X. Guo, D. Zhang, W. Wu, F. Zhou, B. Ji, Protective effect of quercetin and chlorogenic acid, two polyphenols widely present in edible plant varieties, on visible light-induced retinal degeneration in vivo, J. Funct. Foods. (2017). https://doi.org/10.1016/j.jff.2017.02.034.
[84] M.C. Foti, R. Amorati, A. Baschieri, C. Rocco, Singlet oxygen quenching- and chain-breaking antioxidant-properties of a quercetin dimer able to prevent age-related macular degeneration, Biophys. Chem. (2018). https://doi.org/10.1016/j.bpc.2018.10.001.
[85] Y. Chen, X. xin Li, N. zeng Xing, X. guang Cao, Quercetin inhibits choroidal and retinal angiogenesis in vitro, Graefe's Arch. Clin. Exp. Ophthalmol. (2008). https://doi.org/10.1007/s00417-007-0728-9.
[86] T.B. McKay, D. Lyon, A. Sarker-Nag, S. Priyadarsini, J.M. Asara, D. Karamichos, Quercetin Attenuates Lactate Production and Extracellular Matrix Secretion in Keratoconus, Sci. Rep. (2015).

https://doi.org/10.1038/srep09003.

[87] L. Jia, S. Huang, X. Yin, Y. Zan, Y. Guo, L. Han, Quercetin suppresses the mobility of breast cancer by suppressing glycolysis through Akt-mTOR pathway mediated autophagy induction, Life Sci. (2018). https://doi.org/10.1016/j.lfs.2018.07.027.

[88] G.L. Russo, M. Russo, C. Spagnuolo, The pleiotropic flavonoid quercetin: From its metabolism to the inhibition of protein kinases in chronic lymphocytic leukemia, Food Funct. (2014). https://doi.org/10.1039/c4fo00413b.

[89] K. Gupta, D. Panda, Perturbation of microtubule polymerization by quercetin through tubulin binding: A novel mechanism of its antiproliferative activity, Biochemistry. (2002). https://doi.org/10.1021/bi025952r.

[90] Y. Kong, K. Li, T. Fu, C. Wan, D. Zhang, H. Song, Y. Zhang, N. Liu, Z. Gan, L. Yuan, Quercetin ameliorates Aβ toxicity in Drosophila AD model by modulating cell cycle-related protein expression, Oncotarget. (2016). https://doi.org/10.18632/ONCOTARGET.11963.

[91] D.L. Li, L. Mao, Q. Gu, F. Wei, Y.Y. Gong, Quercetin protects retina external barrier from oxidative stress injury by promoting autophagy, Cutan. Ocul. Toxicol. (2020). https://doi.org/10.1080/15569527.2020.1860082.

[92] V.K. Yellepeddi, S. Palakurthi, Recent Advances in Topical Ocular Drug Delivery, J. Ocul. Pharmacol. Ther. (2016). https://doi.org/10.1089/jop.2015.0047.

[93] J. V. Forrester, A.D. Dick, P.G. McMenamin, F. Roberts, E. Pearlman, J. V. Forrester, A.D. Dick, P.G. McMenamin, F. Roberts, E. Pearlman, General and ocular pharmacology, Eye. (2016) 338-369.e1. https://doi.org/10.1016/B978-0-7020-5554-6.00006-X.

[94] C.Y. Chen, T.Y. Wong, W.J. Heriot, Intravitreal Bevacizumab (Avastin) for Neovascular Age-related Macular Degeneration: A Short-term Study, Am. J. Ophthalmol. (2007). https://doi.org/10.1016/j.ajo.2006.10.004.

[95] H.A. Leder, D.A. Jabs, A. Galor, J.P. Dunn, J.E. Thorne, Periocular triamcinolone acetonide injections for cystoid macular edema complicating noninfectious uveitis, Am. J. Ophthalmol. (2011). https://doi.org/10.1016/j.ajo.2011.02.009.

[96] Fluocinolone acetonide ophthalmic - Bausch & Lomb: Fluocinolone acetonide envision TD implant, Drugs R D. (2005). https://doi.org/10.2165/00126839-200506020-00007.

[97] C.H. Tsai, P.Y. Wang, I.C. Lin, H. Huang, G.S. Liu, C.L. Tseng, Ocular Drug Delivery: Role of Degradable Polymeric Nanocarriers for Ophthalmic Application, Int J Mol Sci. 19 (2018). https://doi.org/10.3390/ijms19092830.

[98] J.C. Lang, Ocular drug delivery conventional ocular formulations, Adv. Drug Deliv. Rev. (1995). https://doi.org/10.1016/0169-409X(95)00012-V.

[99] J. Araújo, E. Gonzalez, M.A. Egea, M.L. Garcia, E.B. Souto, Nanomedicines for ocular NSAIDs: safety on drug delivery, Nanomedicine Nanotechnology, Biol. Med. (2009). https://doi.org/10.1016/j.nano.2009.02.003.

[100] J. Alvarez-Trabado, Y. Diebold, A. Sanchez, Designing lipid nanoparticles for topical ocular drug delivery, Int J Pharm. 532 (2017) 204–217. https://doi.org/10.1016/j.ijpharm.2017.09.017.

[101] G.A. Rodrigues, D. Lutz, J. Shen, X. Yuan, H. Shen, J. Cunningham, H.M. Rivers, Topical Drug Delivery to the Posterior Segment of the Eye: Addressing the Challenge of Preclinical to Clinical Translation, Pharm. Res. 35 (2018). https://doi.org/10.1007/s11095-018-2519-x.

[102] C. Bucolo, F. Drago, S. Salomone, Ocular drug delivery: a clue from nanotechnology, Front Pharmacol. 3 (2012) 188. https://doi.org/10.3389/fphar.2012.00188.

[103] A. Subrizi, E.M. del Amo, V. Korzhikov-Vlakh, T. Tennikova, M. Ruponen, A. Urtti, Design principles of ocular drug delivery systems: importance of drug payload, release rate, and material properties, Drug Discov. Today. (2019). https://doi.org/10.1016/j.drudis.2019.02.001.

[104] N. Djebli, S. Khier, F. Griguer, A.L. Coutant, A. Tavernier, G. Fabre, C. Leriche, D. Fabre, Ocular Drug Distribution After Topical Administration: Population Pharmacokinetic Model in Rabbits, Eur. J. Drug Metab. Pharmacokinet. (2017). https://doi.org/10.1007/s13318-016-0319-4.

[105] Y. Shirasaki, Molecular Design for Enhancement of Ocular Penetration, J. Pharm. Sci. 97 (2008) 2462–2496. https://doi.org/https://doi.org/10.1002/jps.21200.

[106] A.J. Bron, J.M. Tiffany, S.M. Gouveia, N. Yokoi, L.W. Voon, Functional aspects of the tear film lipid layer, Exp. Eye Res. 78 (2004) 347–360. https://doi.org/https://doi.org/10.1016/j.exer.2003.09.019.

[107] C.E. Willoughby, D. Ponzin, S. Ferrari, A. Lobo, K. Landau, Y. Omidi, Anatomy and physiology of the human eye: effects of mucopolysaccharidoses disease on structure and function - a review, Clin. Experiment. Ophthalmol. 38 (2010) 2–11. https://doi.org/10.1111/j.1442-9071.2010.02363.x.

[108] O.P. Sharma, V. Patel, T. Mehta, Nanocrystal for ocular drug delivery: hope or hype, Drug Deliv. Transl. Res. (2016). https://doi.org/10.1007/s13346-016-0292-0.
[109] A. Edwards, M.R. Prausnitz, Predicted permeability of the cornea to topical drugs, Pharm. Res. (2001). https://doi.org/10.1023/A:1013061926851.
[110] J. Ban, Y. Zhang, X. Huang, G. Deng, D. Hou, Y. Chen, Z. lu, Corneal permeation properties of a charged lipid nanoparticle carrier containing dexamethasone, Int. J. Nanomedicine. (2017). https://doi.org/10.2147/IJN.S126199.
[111] J. Liaw, Y. Rojanasakul, J.R. Robinson, The effect of drug charge type and charge density on corneal transport, Int. J. Pharm. (1992). https://doi.org/10.1016/0378-5173(92)90308-O.
[112] P. Nirbhavane, G. Sharma, B. Singh, G. Begum, M.C. Jones, S. Rauz, R. Vincent, A.K. Denniston, L.J. Hill, O.P. Katare, Triamcinolone acetonide loaded-cationic nano-lipoidal formulation for uveitis: Evidences of improved biopharmaceutical performance and anti-inflammatory activity, Colloids Surfaces B Biointerfaces. (2020). https://doi.org/10.1016/j.colsurfb.2020.110902.
[113] N.A. Abdul Nasir, P. Agarwal, R. Agarwal, I. Iezhitsa, R. Alyautdin, N.N. Nukolova, V.P. Chekhonin, N. Mohd Ismail, Intraocular distribution of topically applied hydrophilic and lipophilic substances in rat eyes, Drug Deliv. (2016). https://doi.org/10.3109/10717544.2015.1077292.
[114] E.D. Donnenfeld, T.L. Comstock, J.W. Proksch, Human aqueous humor concentrations of besifloxacin, moxifloxacin, and gatifloxacin after topical ocular application, J. Cataract Refract. Surg. (2011). https://doi.org/10.1016/j.jcrs.2010.12.046.
[115] J.L. Chung, E.H. Lim, S.W. Song, B.Y. Kim, J.H. Lee, F.S. Mah, K.Y. Seo, Comparative intraocular penetration of 4 fluoroquinolones after topical instillation, Cornea. (2013). https://doi.org/10.1097/ICO.0b013e31828d6d9e.
[116] D. Huang, Y.S. Chen, I.D. Rupenthal, Overcoming ocular drug delivery barriers through the use of physical forces, Adv Drug Deliv Rev. 126 (2018) 96–112. https://doi.org/10.1016/j.addr.2017.09.008.
[117] E. Ramsay, M. Ruponen, T. Picardat, U. Tengvall, M. Tuomainen, S. Auriola, E. Toropainen, A. Urtti, E.M. del Amo, Impact of Chemical Structure on Conjunctival Drug Permeability: Adopting Porcine Conjunctiva and Cassette Dosing for Construction of In Silico Model, J. Pharm. Sci. (2017). https://doi.org/10.1016/j.xphs.2017.04.061.
[118] S.J. Lee, W. He, S.B. Robinson, M.R. Robinson, K.G. Csaky, H. Kim, Evaluation of clearance mechanisms with transscleral drug delivery, Investig. Ophthalmol. Vis. Sci. (2010). https://doi.org/10.1167/iovs.10-5337.
[119] L. Rodriguez-Peralta, The blood-aqueous barrier in five species, Am. J. Ophthalmol. (1975). https://doi.org/10.1016/0002-9394(75)90405-5.
[120] R.T. Addo, Ocular drug delivery: Advances, challenges and applications, 2016. https://doi.org/10.1007/978-3-319-47691-9.
[121] N.P.S. Cheruvu, U.B. Kompella, Bovine and porcine transscleral solute transport: Influence of lipophilicity and the choroid-Bruch's layer, Investig. Ophthalmol. Vis. Sci. (2006). https://doi.org/10.1167/iovs.06-0404.
[122] J. Ambati, C.S. Canakis, J.W. Miller, E.S. Gragoudas, A. Edwards, D.J. Weissgold, I. Kim, F.C. Delori, A.P. Adamis, Diffusion of high molecular weight compounds through sclera, Investig. Ophthalmol. Vis. Sci. (2000).
[123] D.L. Nickla, J. Wallman, The multifunctional choroid, Prog. Retin. Eye Res. (2010). https://doi.org/10.1016/j.preteyeres.2009.12.002.
[124] R.S. Kadam, U.B. Kompella, Influence of lipophilicity on drug partitioning into sclera, choroid-retinal pigment epithelium, retina, trabecular meshwork, and optic nerve, J. Pharmacol. Exp. Ther. (2010). https://doi.org/10.1124/jpet.109.161570.
[125] E.M. Del Amo, A.K. Rimpela, E. Heikkinen, O.K. Kari, E. Ramsay, T. Lajunen, M. Schmitt, L. Pelkonen, M. Bhattacharya, D. Richardson, A. Subrizi, T. Turunen, M. Reinisalo, J. Itkonen, E. Toropainen, M. Casteleijn, H. Kidron, M. Antopolsky, K.S. Vellonen, M. Ruponen, A. Urtti, Pharmacokinetic aspects of retinal drug delivery, Prog Retin Eye Res. 57 (2017) 134–185. https://doi.org/10.1016/j.preteyeres.2016.12.001.
[126] M. Campbell, P. Humphries, The blood-retina barrier tight junctions and barrier modulation, Adv. Exp. Med. Biol. (2013). https://doi.org/10.1007/978-1-4614-4711-5_3.
[127] L. Pitkänen, V.P. Ranta, H. Moilanen, A. Urtti, Permeability of retinal pigment epithelium: Effects of permeant molecular weight and lipophilicity, Investig. Ophthalmol. Vis. Sci. (2005). https://doi.org/10.1167/iovs.04-1051.
[128] C.T. Supuran, Agents for the prevention and treatment of age-related macular degeneration and macular

edema: a literature and patent review, Expert Opin. Ther. Pat. (2019). https://doi.org/10.1080/13543776.2019.1671353.

[129] M. Yuzawa, K. Fujita, K.U. Wittrup-Jensen, C. Norenberg, O. Zeitz, K. Adachi, E.C.Y. Wang, J. Heier, P. Kaiser, V. Chong, J.F. Korobelnik, Improvement in vision-related function with intravitreal aflibercept: Data from phase 3 studies in wet age-related macular degeneration, Ophthalmology. (2015). https://doi.org/10.1016/j.ophtha.2014.09.024.

[130] S.C. Böhni, M. Bittner, J.P. Howell, L.M. Bachmann, L. Faes, M.K. Schmid, Comparison of Eylea® with Lucentis® as first-line therapy in patients with treatment-naïve neovascular age-related macular degeneration in real-life clinical practice: Retrospective case-series analysis, BMC Ophthalmol. (2015). https://doi.org/10.1186/s12886-015-0101-4.

[131] A.J. Augustin, B.D. Kuppermann, P. Lanzetta, A. Loewenstein, X.Y. Li, H. Cui, Y. Hashad, S.M. Whitcup, S. Abujamra, J. Acton, F. Ali, A. Antoszyk, C.C. Awh, A. Barak, K.U. Bartz-Schmidt, C.R. Baumal, R. Belfort, M. Bhende, D.S. Boyer, W.Z. Bridges, D.M. Brown, T. Carmichael, K. Carnevale, A.M. Casella, T. Chang, D. Chechik, S.N. Chen, L.P. Chong, V. Chong, J. Corwin, C. Creuzot-Garcher, A. Cruess, M. Daniell, M.P. De Avila, H.V. De Moraes, R.G. Devenyi, B.H. Doft, M. Donaldson, R. Dreyer, D. Eliott, H.M. Engel, J. Ernest, T.F. Essman, P.M. Falcone, S. Fekrat, J.R. Ferencz, J.L. Ferreira, J. Figueira, I. Fiser, B. Foster, G.M. Fox, W.R. Freeman, S.P. Garg, M. Gillies, D. Glaser, B.G. Goldstein, A.M.V. Gomes, J.R. Gonder, L. Gopal, P. Gous, A. Gupta, A. Gupta, L. Halperin, D. Han, S.M. Hariprasad, F.G. Holz, P. Kaiser, B. Kalvodova, B. Katz, R.S. Katz, D. Kecik, J. Kellaway, I. Klemperer, R. Lattanzio, W.K. Lee, J. Lehr, M. Leys, I. Loose, A. Lotery, D.W. Lu, P. McCartney, A.B. Majji, J.A. Martinez, P. Massin, R.K. Maturi, U. Menchini, G. Menon, M. Michels, E. Midena, J. Miller, P. Mitchell, J. Moisseiev, L. Morse, R. Navarro, J. Nemeth, H. Newland, R. Newsom, J. Nichols, J. Orellana, N. Orzalesi, A. Paranhos, R. Park, S. Park, M.B. Parodi, P.R. Pavan, J. Peace, D.J. Perez-Ortiz, A. Pollack, K. Ramaswamy, R. Ratnakaram, G. Ravalico, J. Rehak, K. Rezaei, S. Rizzo, F.J. Rodriguez-Alvira, J.P. Romanet, S. Rose, R.B. Rosen, L. Rossetti, J.M. Ruiz-Moreno, S.V. Sadda, K. Sall, D. Sandner, A.F.V. Sanz, G. Sartani, S. Schmickler, S.D. Schwartz, Y.R. Sharma, S.J. Sheu, M. Singer, S. Sivaprasad, G. Soubrane, P. Soucek, E.H. Souied, G. Staurenghi, J. Studnicka, M. Suarez-Figueroa, W.Y. Takahashi, D. Tognetto, P.L. Tsai, L.J. Ulanski, H.S. Uy, M. Varano, M. Veith, I. Vicha, F. Viola, L. Visser, D. Weinberger, G.L. Wing, E. Wong, T.Y. Wong, E. Wylegala, J. Yan, Y.H. Yoon, L.H. Young, H.G. Yu, I.E. Zimmer-Galler, Dexamethasone intravitreal implant in previously treated patients with diabetic macular edema: Subgroup analysis of the MEAD study, BMC Ophthalmol. (2015). https://doi.org/10.1186/s12886-015-0148-2.

[132] S.A. Horowitz, N.P. Damasceno, E.F. Damasceno, Treatment of radiation retinopathy with intravitreal injection of ranibizumab (Lucentis®), Int. Med. Case Rep. J. (2020). https://doi.org/10.2147/IMCRJ.S191654.

[133] S.R. Singh, M.W. Stewart, G. Chattannavar, M. Ashraf, A. Souka, M. ElDardeery, N. Wadhwa, C. Sarvaiya, A.M. Mansour, A. Marashi, S. Ramchandani, I.Z. Braimah, M.H.J. Bonyadi, A. Ramezani, M. Soheilian, J.R. De Oliveira Dias, G.C. De Andrade, A. Maia, E.B. Rodrigues, M.E. Farah, A. Banker, J. Chhablani, Safety of 5914 intravitreal ziv-aflibercept injections, Br. J. Ophthalmol. (2019). https://doi.org/10.1136/bjophthalmol-2018-312453.

[134] R. Neumann, D. Barequet, The gap between the need for novel retinal drug delivery methods, technologies in R&D phase, and approved ocular drug delivery technologies, Drug Discov. Today. (2019). https://doi.org/10.1016/j.drudis.2019.03.018.

[135] I. Kozak, O.R. Kayikcioglu, L. Cheng, I. Falkenstein, G.A. Silva, D.X. Yu, W.R. Freeman, The effect of recombinant human hyaluronidase on dexamethasone penetration into the posterior segment of the eye after sub-tenon's injection, J. Ocul. Pharmacol. Ther. (2006). https://doi.org/10.1089/jop.2006.22.362.

[136] R. Anker, N. Kaur, Regional anaesthesia for ophthalmic surgery, BJA Educ. (2017). https://doi.org/10.1093/bjaed/mkw078.

[137] C.W. Wong, B. Czarny, J.M. Metselaar, C. Ho, S.R. Ng, A.V. Barathi, G. Storm, T.T. Wong, Evaluation of subconjunctival liposomal steroids for the treatment of experimental uveitis, Sci. Rep. (2018). https://doi.org/10.1038/s41598-018-24545-2.

[138] P. Tyagi, R.S. Kadam, U.B. Kompella, Comparison of Suprachoroidal Drug Delivery with Subconjunctival and Intravitreal Routes Using Noninvasive Fluorophotometry, PLoS One. (2012). https://doi.org/10.1371/journal.pone.0048188.

[139] B. Bhushan, Introduction to nanotechnology, Springer Handbooks. (2017). https://doi.org/10.1007/978-3-662-54357-3_1.

[140] C. Li, R. Chen, M. Xu, J. Qiao, L. Yan, X.D. Guo, Hyaluronic acid modified MPEG-b-PAE block copolymer aqueous micelles for efficient ophthalmic drug delivery of hydrophobic genistein, Drug Deliv.

25 (2018) 1258–1265. https://doi.org/10.1080/10717544.2018.1474972.
[141] H.S.M. Ali, A stable hydrocortisone nanosuspension for improved dissolution: Preparation, characterization and in vitro evaluation, Pak. J. Pharm. Sci. 30 (2017) 1635–1643.
[142] G. Tan, S. Yu, H. Pan, J. Li, D. Liu, K. Yuan, X. Yang, W. Pan, Bioadhesive chitosan-loaded liposomes: A more efficient and higher permeable ocular delivery platform for timolol maleate, Int J Biol Macromol. 94 (2017) 355–363. https://doi.org/10.1016/j.ijbiomac.2016.10.035.
[143] M. Lancina, Fast Dissolving Dendrimer Nanofiber (DNF) Mats as Alternative to Eye Drops for More Efficient Topical Antiglaucoma Drug Delivery, ACS Biomater. Sci. Eng. 3 (2017) 1861–1868.
[144] M.Y. Bin Sahadan, W.Y. Tong, W.N. Tan, C.R. Leong, M.N. Bin Misri, M. Chan, S.Y. Cheng, S. Shaharuddin, Phomopsidione nanoparticles coated contact lenses reduce microbial keratitis causing pathogens, Exp Eye Res. 178 (2018) 10–14. https://doi.org/10.1016/j.exer.2018.09.011.
[145] K. McAvoy, D. Jones, R.R.S. Thakur, Synthesis and Characterisation of Photocrosslinked poly(ethylene glycol) diacrylate Implants for Sustained Ocular Drug Delivery, Pharm Res. 35 (2018) 36. https://doi.org/10.1007/s11095-017-2298-9.
[146] J. Kreuter, Nanoparticles-a historical perspective, Int. J. Pharm. (2007). https://doi.org/10.1016/j.ijpharm.2006.10.021.
[147] R.C. Nagarwal, S. Kant, P.N. Singh, P. Maiti, J.K. Pandit, Polymeric nanoparticulate system: a potential approach for ocular drug delivery, J Control Release. 136 (2009) 2–13. https://doi.org/10.1016/j.jconrel.2008.12.018.
[148] Y. Bin Choy, W.M. Ryu, S.N. Kim, C.H. Min, Dry tablet formulation of plga nanoparticles with a preocular applicator for topical drug delivery to the eye, Pharmaceutics. (2019). https://doi.org/10.3390/pharmaceutics11120651.
[149] M. Singh, A. Guzman-Aranguez, A. Hussain, C.S. Srinivas, I.P. Kaur, Solid lipid nanoparticles for ocular delivery of isoniazid: Evaluation, proof of concept and in vivo safety & kinetics, Nanomedicine. (2019). https://doi.org/10.2217/nnm-2018-0278.
[150] P. Suwannoi, M. Chomnawang, A. Tunsirikongkon, A. Phongphisutthinan, C.C. Müller-Goymann, N. Sarisuta, TAT-surface modified acyclovir-loaded albumin nanoparticles as a novel ocular drug delivery system, J. Drug Deliv. Sci. Technol. (2019). https://doi.org/10.1016/j.jddst.2019.05.029.
[151] R. Bisht, J.K. Jaiswal, V.F. Oliver, C. Eurtivong, J. Reynisson, I.D. Rupenthal, Preparation and evaluation of PLGA nanoparticle-loaded biodegradable light-responsive injectable implants as a promising platform for intravitreal drug delivery, J. Drug Deliv. Sci. Technol. (2017). https://doi.org/10.1016/j.jddst.2017.06.006.
[152] H. Almeida, P. Lobão, C. Frigerio, J. Fonseca, R. Silva, J.M. Sousa Lobo, M.H. Amaral, Preparation, characterization and biocompatibility studies of thermoresponsive eyedrops based on the combination of nanostructured lipid carriers (NLC) and the polymer Pluronic F-127 for controlled delivery of ibuprofen, Pharm. Dev. Technol. 22 (2017) 336–349. https://doi.org/10.3109/10837450.2015.1125922.
[153] S.P. Balguri, G.R. Adelli, S. Majumdar, Topical ophthalmic lipid nanoparticle formulations (SLN, NLC) of indomethacin for delivery to the posterior segment ocular tissues, Eur J Pharm Biopharm. 109 (2016) 224–235. https://doi.org/10.1016/j.ejpb.2016.10.015.
[154] A. Yu, H. Shi, H. Liu, Z. Bao, M. Dai, D. Lin, D. Lin, X. Xu, X. Li, Y. Wang, Mucoadhesive dexamethasone-glycol chitosan nanoparticles for ophthalmic drug delivery, Int. J. Pharm. (2020). https://doi.org/10.1016/j.ijpharm.2019.118943.
[155] J. Alvarez-Trabado, A. Lopez-Garcia, M. Martin-Pastor, Y. Diebold, A. Sanchez, Sorbitan ester nanoparticles (SENS) as a novel topical ocular drug delivery system: Design, optimization, and in vitro/ex vivo evaluation, Int J Pharm. 546 (2018) 20–30. https://doi.org/10.1016/j.ijpharm.2018.05.015.
[156] A.T. Ogunjimi, S.M.G. Melo, C.G. Vargas-Rechia, F.S. Emery, R.F. V Lopez, Hydrophilic polymeric nanoparticles prepared from Delonix galactomannan with low cytotoxicity for ocular drug delivery, Carbohydr Polym. 157 (2017) 1065–1075. https://doi.org/10.1016/j.carbpol.2016.10.076.
[157] R. Zhao, J. Li, J. Wang, Z. Yin, Y. Zhu, W. Liu, Development of Timolol-Loaded Galactosylated Chitosan Nanoparticles and Evaluation of Their Potential for Ocular Drug Delivery, AAPS PharmSciTech. 18 (2017) 997–1008. https://doi.org/10.1208/s12249-016-0669-x.
[158] V.G. Llera-Rojas, M. Hernández-Salgado, D. Quintanar-Guerrero, G. Leyva-Gómez, S. Mendoza-Elvira, R. Villalobos-García, Comparative study of the release profiles of ibuprofen from polymeric nanocapsules and nanospheres, J. Mex. Chem. Soc. (2019). https://doi.org/10.29356/jmcs.v63i2.943.
[159] K. Ghosal, A. Manakhov, L. Zajíčková, S. Thomas, Structural and Surface Compatibility Study of Modified Electrospun Poly(ε-caprolactone) (PCL) Composites for Skin Tissue Engineering, AAPS PharmSciTech. (2017). https://doi.org/10.1208/s12249-016-0500-8.

[160] J. Pandit, Y. Sultana, M. Aqil, Chitosan-coated PLGA nanoparticles of bevacizumab as novel drug delivery to target retina: optimization, characterization, and in vitro toxicity evaluation, Artif. Cells, Nanomedicine, Biotechnol. 45 (2017) 1397–1407. https://doi.org/10.1080/21691401.2016.1243545.

[161] D. Zhu, W. Tao, H. Zhang, G. Liu, T. Wang, L. Zhang, X. Zeng, L. Mei, Acta Biomaterialia Docetaxel (DTX) -loaded polydopamine-modified TPGS-PLA nanoparticles as a targeted drug delivery system for the treatment of liver cancer, Acta Biomater. 30 (2016) 144–154. https://doi.org/10.1016/j.actbio.2015.11.031.

[162] F.H. Nasr, S. Khoee, M.M. Dehghan, S.S. Chaleshtori, A. Shafiee, Preparation and Evaluation of Contact Lenses Embedded with Polycaprolactone-Based Nanoparticles for Ocular Drug Delivery, Biomacromolecules. 17 (2016) 485–495. https://doi.org/10.1021/acs.biomac.5b01387.

[163] H. Saade, Preparation and Loading with Rifampicin of Sub-50 nmPoly(ethyl cyanoacrylate) Nanoparticles by SemicontinuousHeterophase Polymerization, J. Nanomater. (2016). https://doi.org/10.1155/2016/8384973.

[164] H. Tian, Z. Tang, X. Zhuang, X. Chen, X. Jing, Biodegradable synthetic polymers: Preparation, functionalization and biomedical application, Prog. Polym. Sci. 37 (2012) 237–280. https://doi.org/10.1016/j.progpolymsci.2011.06.004.

[165] G.M. Fernandes-Cunha, S.L. Fialho, G.R. da Silva, A. Silva-Cunha, M. Zhao, F. Behar-Cohen, Ocular safety of Intravitreal Clindamycin Hydrochloride Released by PLGA Implants, Pharm. Res. (2017). https://doi.org/10.1007/s11095-017-2118-2.

[166] P.S. Chan, J.W. Xian, Q. Li, C.W. Chan, S.S.Y. Leung, K.K.W. To, Biodegradable Thermosensitive PLGA-PEG-PLGA Polymer for Non-irritating and Sustained Ophthalmic Drug Delivery, AAPS J. (2019). https://doi.org/10.1208/s12248-019-0326-x.

[167] X. Yang, H.M. Trinh, V. Agrahari, Y. Sheng, D. Pal, A.K. Mitra, Nanoparticle-Based Topical Ophthalmic Gel Formulation for Sustained Release of Hydrocortisone Butyrate, AAPS PharmSciTech. (2016). https://doi.org/10.1208/s12249-015-0354-5.

[168] X.S. Wu, N. Wang, Synthesis, characterization, biodegradation, and drug delivery application of biodegradable lactic/glycolic acid polymers. Part II: Biodegradation, J. Biomater. Sci. Polym. Ed. (2001). https://doi.org/10.1163/156856201744425.

[169] H.S. Yoo, Biodegradable Nanoparticles Containing Doxorubicin-PLGA Conjugate for Sustained Release, Pharm Res. 16 (1990) 1114–1118.

[170] J. Pandit, Y. Sultana, M. Aqil, Chitosan-coated PLGA nanoparticles of bevacizumab as novel drug delivery to target retina: optimization, characterization, and in vitro toxicity evaluation, Artif. Cells, Nanomedicine Biotechnol. 45 (2017) 1397–1407. https://doi.org/10.1080/21691401.2016.1243545.

[171] A.L. Goffin, J.M. Raquez, E. Duquesne, G. Siqueira, Y. Habibi, A. Dufresne, P. Dubois, From interfacial ring-opening polymerization to melt processing of cellulose nanowhisker-filled polylactide-based nanocomposites, Biomacromolecules. (2011). https://doi.org/10.1021/bm200581h.

[172] B. Tyler, D. Gullotti, A. Mangraviti, T. Utsuki, H. Brem, Polylactic acid (PLA) controlled delivery carriers for biomedical applications, Adv Drug Deliv Rev. 107 (2016) 163–175. https://doi.org/10.1016/j.addr.2016.06.018.

[173] J.-L. Bourges, S.E. Gautier, F. Delie, R.A. Bejjani, J.-C. Jeanny, R. Gurny, D. BenEzra, F.F. Behar-Cohen, Ocular Drug Delivery Targeting the Retina and Retinal Pigment Epithelium Using Polylactide Nanoparticles, Investig. Opthalmology Vis. Sci. 44 (2003) 3562. https://doi.org/10.1167/iovs.02-1068.

[174] S.M. Li, X.H. Chen, R.A. Gross, S.P. Mccarthy, Hydrolytic degradation of PCL/PEO copolymers in alkaline media, J. Mater. Sci. Mater. Med. 11 (2000) 227–233. https://doi.org/10.1023/A:1008920326988.

[175] Chih-Hung Lee, Poly(ε-caprolactone) nanocapsule carriers with sustained drug release: single dose for long-term glaucoma treatment, Nanoscale. 9 (2017) 11754–11764. https://doi.org/10.1039/C7NR03221H10.1039/x0xx00000x.

[176] D. Akilbekova, M. Shaimerdenova, S. Adilov, D. Berillo, Biocompatible scaffolds based on natural polymers for regenerative medicine, Int. J. Biol. Macromol. (2018). https://doi.org/10.1016/j.ijbiomac.2018.03.116.

[177] G.Z. Papageorgiou, Thinking green: Sustainable polymers from renewable resources, Polymers (Basel). (2018). https://doi.org/10.3390/polym10090952.

[178] M. Henke, J. Tessmar, A. Göpferich, Biomimetic Polymers (for Biomedical Applications), in: Polym. Sci. A Compr. Ref. 10 Vol. Set, 2012. https://doi.org/10.1016/B978-0-444-53349-4.00222-3.

[179] H.B. Eral, V. López-Mejías, M. O'Mahony, B.L. Trout, A.S. Myerson, P.S. Doyle, Biocompatible alginate microgel particles as heteronucleants and encapsulating vehicles for hydrophilic and hydrophobic drugs, Cryst. Growth Des. (2014). https://doi.org/10.1021/cg500250e.

[180] B. Gao, L. Chen, Y. Zhao, X. Yan, X. Wang, C. Zhou, Y. Shi, W. Xue, Methods to prepare dopamine/polydopamine modified alginate hydrogels and their special improved properties for drug delivery, Eur. Polym. J. 110 (2019) 192–201. https://doi.org/10.1016/j.eurpolymj.2018.11.025.

[181] F.S.Y. Wong, K.K. Tsang, A.M.W. Chu, B.P. Chan, K.M. Yao, A.C.Y. Lo, Injectable cell-encapsulating composite alginate-collagen platform with inducible termination switch for safer ocular drug delivery, Biomaterials. 201 (2019) 53–67. https://doi.org/10.1016/j.biomaterials.2019.01.032.

[182] R. Silva, R. Singh, B. Sarker, D.G. Papageorgiou, J.A. Juhasz-Bortuzzo, J.A. Roether, I. Cicha, J. Kaschta, D.W. Schubert, K. Chrissafis, R. Detsch, A.R. Boccaccini, Hydrogel matrices based on elastin and alginate for tissue engineering applications, Int. J. Biol. Macromol. (2018). https://doi.org/10.1016/j.ijbiomac.2018.03.091.

[183] R.C. Nagarwal, R. Kumar, J.K. Pandit, Chitosan coated sodium alginate-chitosan nanoparticles loaded with 5-FU for ocular delivery: In vitro characterization and in vivo study in rabbit eye, Eur. J. Pharm. Sci. (2012). https://doi.org/10.1016/j.ejps.2012.08.008.

[184] F.S.Y. Wong, K.K. Tsang, A.M.W. Chu, B.P. Chan, K.M. Yao, A.C.Y. Lo, Injectable cell-encapsulating composite alginate-collagen platform with inducible termination switch for safer ocular drug delivery, Biomaterials. (2019). https://doi.org/10.1016/j.biomaterials.2019.01.032.

[185] S. Noreen, S.A. Ghumman, F. Batool, B. Ijaz, M. Basharat, S. Noureen, T. Kausar, S. Iqbal, Terminalia arjuna gum/alginate in situ gel system with prolonged retention time for ophthalmic drug delivery, Int. J. Biol. Macromol. 152 (2020) 1056–1067. https://doi.org/10.1016/j.ijbiomac.2019.10.193.

[186] M.M. Ibrahim, A.H. Abd-Elgawad, O.A. Soliman, M.M. Jablonski, Natural Bioadhesive Biodegradable Nanoparticle-Based Topical Ophthalmic Formulations for Management of Glaucoma, Transl Vis Sci Technol. 4 (2015) 12. https://doi.org/10.1167/tvst.4.3.12.

[187] S. Balkani, S. Shamekhi, R. Raoufinia, R. Parvan, J. Abdolalizadeh, Purification and characterization of bovine serum albumin using chromatographic method, Adv. Pharm. Bull. (2016). https://doi.org/10.15171/apb.2016.080.

[188] M.M. Pereira, R.A.P. Cruz, M.R. Almeida, Á.S. Lima, J.A.P. Coutinho, M.G. Freire, Single-step purification of ovalbumin from egg white using aqueous biphasic systems, Process Biochem. (2016). https://doi.org/10.1016/j.procbio.2016.03.002.

[189] L. Yang, J. Zheng, Z. Zou, H. Cai, P. Qi, Z. Qing, Q. Yan, L. Qiu, W. Tan, R. Yang, Human serum albumin as an intrinsic signal amplification amplifier for ultrasensitive assays of the prostate-specific antigen in human plasma, Chem. Commun. (2020). https://doi.org/10.1039/c9cc08501g.

[190] B. Meloun, L. Morávek, V. Kostka, Complete amino acid sequence of human serum albumin, FEBS Lett. (1975). https://doi.org/10.1016/0014-5793(75)80242-0.

[191] J.M. Llabot, I. Luis de Redin, M. Agüeros, M.J. Dávila Caballero, C. Boiero, J.M. Irache, D. Allemandi, In vitro characterization of new stabilizing albumin nanoparticles as a potential topical drug delivery system in the treatment of corneal neovascularization (CNV), J. Drug Deliv. Sci. Technol. (2019). https://doi.org/10.1016/j.jddst.2019.04.042.

[192] D. Huang, Y. Chen, I.D. Rupenthal, Hyaluronic Acid Coated Albumin Nanoparticles for Targeted Peptide Delivery to the Retina Hyaluronic Acid Coated Albumin Nanoparticles for Targeted Peptide Delivery to the Retina, (2016). https://doi.org/10.1021/acs.molpharmaceut.6b01029.

[193] A. Tzameret, H. Ketter-Katz, V. Edelshtain, I. Sher, E. Corem-Salkmon, I. Levy, D. Last, D. Guez, Y. Mardor, S. Margel, Y. Rotenstrich, In vivo MRI assessment of bioactive magnetic iron oxide/human serum albumin nanoparticle delivery into the posterior segment of the eye in a rat model of retinal degeneration, J. Nanobiotechnology. 17 (2019) 1–11. https://doi.org/10.1186/s12951-018-0438-y.

[194] I. Luis de Redin, C. Boiero, M.C. Martinez-Oharriz, M. Agueros, R. Ramos, I. Penuelas, D. Allemandi, J.M. Llabot, J.M. Irache, Human serum albumin nanoparticles for ocular delivery of bevacizumab, Int J Pharm. 541 (2018) 214–223. https://doi.org/10.1016/j.ijpharm.2018.02.003.

[195] J. Lizardi-mendoza, W.M.A. Monal, F.M.G. Valencia, Chemical Characteristics and Functional Properties of Chitosan, Elsevier Inc., 2016. https://doi.org/10.1016/B978-0-12-802735-6/00001-X.

[196] A. Enriquez de Salamanca, Y. Diebold, M. Calonge, C. Garcia-Vazquez, S. Callejo, A. Vila, M.J. Alonso, Chitosan nanoparticles as a potential drug delivery system for the ocular surface: toxicity, uptake mechanism and in vivo tolerance, Invest Ophthalmol Vis Sci. 47 (2006) 1416–1425. https://doi.org/10.1167/iovs.05-0495.

[197] F.A. Oyarzun-Ampuero, J. Brea, M.I. Loza, D. Torres, M.J. Alonso, Chitosan-hyaluronic acid nanoparticles loaded with heparin for the treatment of asthma, Int J Pharm. 381 (2009) 122–129. https://doi.org/10.1016/j.ijpharm.2009.04.009.

[198] N.A. Fletcher, M.D. Krebs, RSC Advances Sustained delivery of anti-VEGF from injectable hydrogel

systems provides a prolonged decrease of endothelial cell proliferation and angiogenesis in vitro, RSC Adv. 8 (2018) 8999–9005. https://doi.org/10.1039/C7RA13014G.

[199] M. Rodríguez-Vázquez, B. Vega-Ruiz, R. Ramos-Zúñiga, D.A. Saldaña-Koppel, L.F. Quiñones-Olvera, Chitosan and Its Potential Use as a Scaffold for Tissue Engineering in Regenerative Medicine, Biomed Res. Int. 2015 (2015) 1–15. https://doi.org/10.1155/2015/821279.

[200] W. Chaiyasan, S.P. Srinivas, W. Tiyaboonchai, Crosslinked chitosan-dextran sulfate nanoparticle for improved topical ocular drug delivery, (2015) 1224–1234.

[201] S. Natesan, S. Pandian, C. Ponnusamy, R. Palanichamy, S. Muthusamy, R. Kandasamy, Co-encapsulated resveratrol and quercetin in chitosan and peg modified chitosan nanoparticles: For efficient intra ocular pressure reduction, Int. J. Biol. Macromol. (2017). https://doi.org/10.1016/j.ijbiomac.2017.04.117.

[202] N. Elsaid, T.L. Jackson, Z. Elsaid, A. Alqathama, S. Somavarapu, PLGA microparticles entrapping chitosan-based nanoparticles for the ocular delivery of ranibizumab, Mol. Pharm. (2016). https://doi.org/10.1021/acs.molpharmaceut.6b00335.

[203] H.W. Sung, K. Sonaje, Z.X. Liao, L.W. Hsu, E.Y. Chuang, PH-responsive nanoparticles shelled with chitosan for oral delivery of insulin: From mechanism to therapeutic applications, Acc. Chem. Res. 45 (2012) 619–629. https://doi.org/10.1021/ar200234q.

[204] W. Chaiyasan, S.P. Srinivas, W. Tiyaboonchai, Mucoadhesive chitosan-dextran sulfate nanoparticles for sustained drug delivery to the ocular surface, J Ocul Pharmacol Ther. 29 (2013) 200–207. https://doi.org/10.1089/jop.2012.0193.

[205] P. Aksungur, M. Demirbilek, E.B. Denkbaş, J. Vandervoort, A. Ludwig, N. Ünlü, Development and characterization of Cyclosporine A loaded nanoparticles for ocular drug delivery: Cellular toxicity, uptake, and kinetic studies, J. Control. Release. (2011). https://doi.org/10.1016/j.jconrel.2011.01.010.

[206] A. Siddiqua Gazi, A.K. Sailaja, Preparation and Characterization of Paracetamol Loaded Eudragit S100 Nanoparticles by Salting Out Technique, J. Dev. Drugs. (2018). https://doi.org/10.4172/2329-6631.1000183.

[207] S. V. Dalvi, M.A. Azad, R. Dave, Precipitation and stabilization of ultrafine particles of Fenofibrate in aqueous suspensions by RESOLV, Powder Technol. (2013). https://doi.org/10.1016/j.powtec.2012.05.038.

[208] F. Shakeri, S. Shakeri, M. Hojjatoleslami, Preparation and Characterization of Carvacrol Loaded Polyhydroxybutyrate Nanoparticles by Nanoprecipitation and Dialysis Methods, J. Food Sci. (2014). https://doi.org/10.1111/1750-3841.12406.

[209] A.L.M. Cavalcanti, M.Y.F.A. Reis, G.C.L. Silva, Í.M.M. Ramalho, G.P. Guimarães, J.A. Silva, K.L.A. Saraiva, B.P.G.L. Damasceno, Microemulsion for topical application of pentoxifylline: In vitro release and in vivo evaluation, Int. J. Pharm. (2016). https://doi.org/10.1016/j.ijpharm.2016.04.065.

[210] S.D. Desai, J. Blanchard, Pluronic® F127-based ocular delivery system containing biodegradable polyisobutylcyanoacrylate nanocapsules of pilocarpine, Drug Deliv. J. Deliv. Target. Ther. Agents. (2000). https://doi.org/10.1080/107175400455128.

[211] M.S. Baig, A. Ahad, M. Aslam, S.S. Imam, M. Aqil, A. Ali, Application of Box-Behnken design for preparation of levofloxacin-loaded stearic acid solid lipid nanoparticles for ocular delivery: Optimization, in vitro release, ocular tolerance, and antibacterial activity, Int. J. Biol. Macromol. (2016). https://doi.org/10.1016/j.ijbiomac.2015.12.077.

[212] J. Li, X. Guo, Z. Liu, C.I. Okeke, N. Li, H. Zhao, M.O. Aggrey, W. Pan, T. Wu, Preparation and evaluation of charged solid lipid nanoparticles of tetrandrine for ocular drug delivery system: Pharmacokinetics, cytotoxicity and cellular uptake studies, Drug Dev. Ind. Pharm. (2014). https://doi.org/10.3109/03639045.2013.795582.

[213] B. Balzus, F.F. Sahle, S. Hönzke, C. Gerecke, F. Schumacher, S. Hedtrich, B. Kleuser, R. Bodmeier, Formulation and ex vivo evaluation of polymeric nanoparticles for controlled delivery of corticosteroids to the skin and the corneal epithelium, Eur. J. Pharm. Biopharm. (2017). https://doi.org/10.1016/j.ejpb.2017.02.001.

[214] A.K. Sah, P.K. Suresh, V.K. Verma, PLGA nanoparticles for ocular delivery of loteprednol etabonate: a corneal penetration study, Artif. Cells, Nanomedicine Biotechnol. (2017). https://doi.org/10.1080/21691401.2016.1203794.

[215] A.H. Salama, M.M. AbouSamra, G.E.A. Awad, S.S. Mansy, Promising bioadhesive ofloxacin-loaded polymeric nanoparticles for the treatment of ocular inflammation: formulation and in vivo evaluation, Drug Deliv. Transl. Res. (2020). https://doi.org/10.1007/s13346-020-00856-8.

[216] A.H. Salama, A.A. Mahmoud, R. Kamel, A Novel Method for Preparing Surface-Modified Fluocinolone Acetonide Loaded PLGA Nanoparticles for Ocular Use: In Vitro and In Vivo Evaluations, AAPS PharmSciTech. 17 (2016) 1159–1172. https://doi.org/10.1208/s12249-015-0448-0.

[217] S. Salatin, J. Barar, M. Barzegar-Jalali, K. Adibkia, F. Kiafar, M. Jelvehgari, Development of a

nanoprecipitation method for the entrapment of a very water soluble drug into Eudragit RL nanoparticles, Res. Pharm. Sci. (2017). https://doi.org/10.4103/1735-5362.199041.
[218] S. Tyagi, nanoparticles-an-overview-of-preparation, Res. Rev. J. Pharm. Nanotechnol. 4 (2016).
[219] M. Ahuja, P. Verma, M. Bhatia, Preparation and evaluation of chitosan–itraconazole co-precipitated nanosuspension for ocular delivery, J. Exp. Nanosci. (2015). https://doi.org/10.1080/17458080.2013.822108.
[220] D. Patiño-Ruiz, L. Marrugo, N. Reyes, M. Acevedo-Morantes, A. Herrera, Ionotropic Gelation Synthesis of Chitosan-Alginate Nanodisks for Delivery System and in Vitro Assessment of Prostate Cancer Cytotoxicity, Int. J. Polym. Sci. (2020). https://doi.org/10.1155/2020/5329747.
[221] J.P. Rao, K.E. Geckeler, Polymer nanoparticles: Preparation techniques and size-control parameters, Prog. Polym. Sci. 36 (2011) 887–913. https://doi.org/10.1016/j.progpolymsci.2011.01.001.
[222] N.C. Silva, S. Silva, B. Sarmento, M. Pintado, Chitosan nanoparticles for daptomycin delivery in ocular treatment of bacterial endophthalmitis, Drug Deliv. 22 (2015) 885–893. https://doi.org/10.3109/10717544.2013.858195.
[223] E. Chiellini, C. Errico, C. Bartoli, F. Chiellini, Poly(hydroxyalkanoates)-based polymeric nanoparticles for drug delivery, J. Biomed. Biotechnol. 2009 (2009). https://doi.org/10.1155/2009/571702.
[224] L. Chronopoulou, M. Massimi, M.F. Giardi, C. Cametti, L.C. Devirgiliis, M. Dentini, C. Palocci, Chitosan-coated PLGA nanoparticles: A sustained drug release strategy for cell cultures, Colloids Surfaces B Biointerfaces. 103 (2013) 310–317. https://doi.org/10.1016/j.colsurfb.2012.10.063.
[225] P. Pattanayak, S.K. Singh, M. Gulati, S. Vishwas, B. Kapoor, D.K. Chellappan, K. Anand, G. Gupta, N.K. Jha, P.K. Gupta, P. Prasher, K. Dua, H. Dureja, D. Kumar, V. Kumar, Microfluidic chips: recent advances, critical strategies in design, applications and future perspectives, Microfluid. Nanofluidics. 25 (2021) 99. https://doi.org/10.1007/s10404-021-02502-2.
[226] S. Xu, Z. Nie, M. Seo, P. Lewis, E. Kumacheva, H.A. Stone, P. Garstecki, D.B. Weibel, I. Gitlin, G.M. Whitesides, Generation of monodisperse particles by using microfluidics: Control over size, shape, and composition, Angew. Chemie - Int. Ed. 44 (2005) 724–728. https://doi.org/10.1002/anie.200462226.
[227] C. Yousry, P.M. Zikry, H.M. Salem, E.B. Basalious, O.N. El-Gazayerly, Integrated nanovesicular/self-nanoemulsifying system (INV/SNES) for enhanced dual ocular drug delivery: statistical optimization, in vitro and in vivo evaluation, Drug Deliv. Transl. Res. (2020). https://doi.org/10.1007/s13346-020-00716-5.
[228] X. Xu, L. Sun, L. Zhou, Y. Cheng, F. Cao, Functional chitosan oligosaccharide nanomicelles for topical ocular drug delivery of dexamethasone, Carbohydr. Polym. (2020). https://doi.org/10.1016/j.carbpol.2019.115356.
[229] J.F. Fangueiro, T. Andreani, M.A. Egea, M.L. Garcia, S.B. Souto, A.M. Silva, E.B. Souto, Design of cationic lipid nanoparticles for ocular delivery: Development, characterization and cytotoxicity, Int. J. Pharm. (2014). https://doi.org/10.1016/j.ijpharm.2013.11.025.
[230] M.J. Masarudin, S.M. Cutts, B.J. Evison, D.R. Phillips, P.J. Pigram, Factors determining the stability, size distribution, and cellular accumulation of small, monodisperse chitosan nanoparticles as candidate vectors for anticancer drug delivery: Application to the passive encapsulation of [14C]-doxorubicin, Nanotechnol. Sci. Appl. (2015). https://doi.org/10.2147/NSA.S91785.
[231] U.K. Sharma, A. Verma, S.K. Prajapati, H. Pandey, A.C. Pandey, In vitro, in vivo and pharmacokinetic assessment of amikacin sulphate laden polymeric nanoparticles meant for controlled ocular drug delivery, Appl. Nanosci. (2015). https://doi.org/10.1007/s13204-014-0300-y.
[232] J. McMillan, E. Batrakova, H.E. Gendelman, Cell delivery of therapeutic nanoparticles, in: Prog. Mol. Biol. Transl. Sci., 2011. https://doi.org/10.1016/B978-0-12-416020-0.00014-0.
[233] M. Bouchoucha, M.F. Côté, R. C-Gaudreault, M.A. Fortin, F. Kleitz, Size-Controlled Functionalized Mesoporous Silica Nanoparticles for Tunable Drug Release and Enhanced Anti-Tumoral Activity, Chem. Mater. (2016). https://doi.org/10.1021/acs.chemmater.6b00877.
[234] S. Soltani, P. Zakeri-Milani, M. Barzegar-Jalali, M. Jelvehgari, Design of eudragit RL nanoparticles by nanoemulsion method as carriers for ophthalmic drug delivery of ketotifen fumarate, Iran. J. Basic Med. Sci. (2016). https://doi.org/10.22038/ijbms.2016.6940.
[235] Z. Ali, P.K. Sharma, M.H. Warsi, Fabrication and evaluation of Ketorolac loaded cubosome for ocular drug delivery, J. Appl. Pharm. Sci. (2016). https://doi.org/10.7324/JAPS.2016.60930.
[236] M. Filella, J. Zhang, M.E. Newman, J. Buffle, Analytical applications of photon correlation spectroscopy for size distribution measurements of natural colloidal suspensions: Capabilities and limitations, Colloids Surfaces A Physicochem. Eng. Asp. (1997). https://doi.org/10.1016/S0927-7757(96)03677-1.
[237] M. Danaei, M. Dehghankhold, S. Ataei, F. Hasanzadeh Davarani, R. Javanmard, A. Dokhani, S. Khorasani, M.R. Mozafari, Impact of particle size and polydispersity index on the clinical applications of lipidic nanocarrier systems, Pharmaceutics. (2018). https://doi.org/10.3390/pharmaceutics10020057.

[238] S. Amin, G. V. Barnett, J.A. Pathak, C.J. Roberts, P.S. Sarangapani, Protein aggregation, particle formation, characterization & rheology, Curr. Opin. Colloid Interface Sci. 19 (2014) 438–449. https://doi.org/10.1016/j.cocis.2014.10.002.

[239] S. Bhattacharjee, DLS and zeta potential - What they are and what they are not?, J. Control. Release. 235 (2016) 337–351. https://doi.org/10.1016/j.jconrel.2016.06.017.

[240] C. Bantz, O. Koshkina, T. Lang, H.J. Galla, C.J. Kirkpatrick, R.H. Stauber, M. Maskos, The surface properties of nanoparticles determine the agglomeration state and the size of the particles under physiological conditions, Beilstein J. Nanotechnol. (2014). https://doi.org/10.3762/bjnano.5.188.

[241] Chapter 10 Microfluidic methods for measuring zeta potential, in: Interface Sci. Technol., 2004. https://doi.org/10.1016/S1573-4285(04)80032-2.

[242] D.J. Shaw, Introduction to Colloid and Surface Chemistry: Fourth Edition, 2013. https://doi.org/10.1016/C2009-0-24070-0.

[243] T. Tadros, Zeta potential in colloid science. Principles and application, Colloids and Surfaces. (1982). https://doi.org/10.1016/0166-6622(82)80060-7.

[244] X. Zhu, M. Su, S. Tang, L. Wang, X. Liang, F. Meng, Y. Hong, Z. Xu, Synthesis of thiolated chitosan and preparation nanoparticles with sodium alginate for ocular drug delivery, Mol. Vis. (2012).

[245] M.A. Kalam, Development of chitosan nanoparticles coated with hyaluronic acid for topical ocular delivery of dexamethasone, Int J Biol Macromol. 89 (2016) 127–136. https://doi.org/10.1016/j.ijbiomac.2016.04.070.

[246] P. Verma, S.K. Maheshwari, Preparation of Sliver and Selenium Nanoparticles and Its Characterization by Dynamic Light Scattering and Scanning Electron Microscopy., J. Microsc. Ultrastruct. (2018). https://doi.org/10.4103/JMAU.JMAU_3_18.

[247] B.J. Inkson, 2 - Scanning electron microscopy (SEM) and transmission electron microscopy (TEM) for materials characterization, Elsevier Ltd, 2016. https://doi.org/10.1016/B978-0-08-100040-3.00002-X.

[248] J.H. Park, H. Jeong, J. Hong, M. Chang, M. Kim, R.S. Chuck, J.K. Lee, C.Y. Park, The Effect of Silica Nanoparticles on Human Corneal Epithelial Cells, Sci Rep. 6 (2016) 37762. https://doi.org/10.1038/srep37762.

[249] Y. Zhao, X. Sun, G. Zhang, B.G. Trewyn, I.I. Slowing, V.S.Y. Lin, Interaction of mesoporous silica nanoparticles with human red blood cell membranes: Size and surface effects, ACS Nano. (2011). https://doi.org/10.1021/nn103077k.

[250] I.Y. Kim, E. Joachim, H. Choi, K. Kim, Toxicity of silica nanoparticles depends on size, dose, and cell type, Nanomedicine Nanotechnology, Biol. Med. (2015). https://doi.org/10.1016/j.nano.2015.03.004.

[251] K. Greish, G. Thiagarajan, H. Herd, R. Price, H. Bauer, D. Hubbard, A. Burckle, S. Sadekar, T. Yu, A. Anwar, A. Ray, H. Ghandehari, Size and surface charge significantly influence the toxicity of silica and dendritic nanoparticles, Nanotoxicology. (2012). https://doi.org/10.3109/17435390.2011.604442.

[252] B.J. Inkson, Scanning Electron Microscopy (SEM) and Transmission Electron Microscopy (TEM) for Materials Characterization, in: Mater. Charact. Using Nondestruct. Eval. Methods, 2016. https://doi.org/10.1016/B978-0-08-100040-3.00002-X.

[253] Ameeduzzafar, S.S. Imam, S.N. Abbas Bukhari, J. Ahmad, A. Ali, Formulation and optimization of levofloxacin loaded chitosan nanoparticle for ocular delivery: In-vitro characterization, ocular tolerance and antibacterial activity, Int J Biol Macromol. 108 (2018) 650–659. https://doi.org/10.1016/j.ijbiomac.2017.11.170.

[254] Y. Gokce, B. Cengiz, N. Yildiz, A. Calimli, Z. Aktas, Ultrasonication of chitosan nanoparticle suspension: Influence on particle size, Colloids Surfaces A Physicochem. Eng. Asp. (2014). https://doi.org/10.1016/j.colsurfa.2014.08.028.

[255] L. V. Stebounova, E. Guio, V.H. Grassian, Silver nanoparticles in simulated biological media: A study of aggregation, sedimentation, and dissolution, J. Nanoparticle Res. (2011). https://doi.org/10.1007/s11051-010-0022-3.

[256] K. Burapapadh, H. Takeuchi, P. Sriamornsak, Development of pectin nanoparticles through mechanical homogenization for dissolution enhancement of itraconazole, Asian J. Pharm. Sci. (2016). https://doi.org/10.1016/j.ajps.2015.07.003.

[257] G.A. Morris, J. Castile, A. Smith, G.G. Adams, S.E. Harding, The effect of prolonged storage at different temperatures on the particle size distribution of tripolyphosphate (TPP)-chitosan nanoparticles, Carbohydr. Polym. (2011). https://doi.org/10.1016/j.carbpol.2011.01.044.

[258] G. Behl, J. Iqbal, N.J. O'Reilly, P. McLoughlin, L. Fitzhenry, Synthesis and Characterization of Poly(2-hydroxyethylmethacrylate) Contact Lenses Containing Chitosan Nanoparticles as an Ocular Delivery

System for Dexamethasone Sodium Phosphate, Pharm. Res. (2016). https://doi.org/10.1007/s11095-016-1903-7.

[259] W.F. Huang, C.P. Tsui, C.Y. Tang, M. Yang, L. Gu, Surface charge switchable and pH-responsive chitosan/polymer core-shell composite nanoparticles for drug delivery application, Compos. Part B Eng. 121 (2017) 83–91. https://doi.org/10.1016/j.compositesb.2017.03.028.

[260] X.-Y. Lu, D.-C. Wu, Z.-J. Li, G.-Q. Chen, Chpater 7 – Polymer Nanoparticles, in: Prog. Mol. Biol. Transl. Sci., 2011.

[261] N. Rescignano, L. Tarpani, A. Romani, I. Bicchi, S. Mattioli, C. Emiliani, L. Torre, J.M. Kenny, S. Martino, L. Latterini, I. Armentano, In-vitro degradation of PLGA nanoparticles in aqueous medium and in stem cell cultures by monitoring the cargo fluorescence spectrum, Polym. Degrad. Stab. (2016). https://doi.org/10.1016/j.polymdegradstab.2016.10.017.

[262] R. Scaffaro, F. Lopresti, L. Botta, Preparation, characterization and hydrolytic degradation of PLA/PCL co-mingled nanofibrous mats prepared via dual-jet electrospinning, Eur. Polym. J. 96 (2017) 266–277. https://doi.org/10.1016/j.eurpolymj.2017.09.016.

[263] F.A. Maulvi, H.H. Choksi, A.R. Desai, A.S. Patel, K.M. Ranch, B.A. Vyas, D.O. Shah, pH triggered controlled drug delivery from contact lenses: Addressing the challenges of drug leaching during sterilization and storage, Colloids Surfaces B Biointerfaces. (2017). https://doi.org/10.1016/j.colsurfb.2017.05.064.

[264] Y. Zhou, A. Fang, F. Wang, H. Li, Q. Jin, L. Huang, C. Fu, J. Zeng, Z. Jin, X. Song, Core-shell lipid-polymer nanoparticles as a promising ocular drug delivery system to treat glaucoma, Chinese Chem. Lett. (2020). https://doi.org/10.1016/j.cclet.2019.04.048.

[265] J. Li, X. Jin, Y. Yang, L. Zhang, R. Liu, Z. Li, Trimethyl chitosan nanoparticles for ocular baicalein delivery: Preparation, optimization, in vitro evaluation, in vivo pharmacokinetic study and molecular dynamics simulation, Int. J. Biol. Macromol. (2020). https://doi.org/10.1016/j.ijbiomac.2020.04.115.

[266] R. Kesarla, T. Tank, P.A. Vora, T. Shah, S. Parmar, A. Omri, Preparation and evaluation of nanoparticles loaded ophthalmic in situ gel, Drug Deliv. (2016). https://doi.org/10.3109/10717544.2014.987333.

[267] Y. Zambito, E. Pedreschi, G. Di Colo, Is dialysis a reliable method for studying drug release from nanoparticulate systems? - A case study, Int. J. Pharm. (2012). https://doi.org/10.1016/j.ijpharm.2012.05.020.

[268] S. Modi, B.D. Anderson, Determination of drug release kinetics from nanoparticles: Overcoming pitfalls of the dynamic dialysis method, Mol. Pharm. (2013). https://doi.org/10.1021/mp400154a.

[269] M. Yu, W. Yuan, D. Li, A. Schwendeman, S.P. Schwendeman, Predicting drug release kinetics from nanocarriers inside dialysis bags, J. Control. Release. (2019). https://doi.org/10.1016/j.jconrel.2019.09.016.

[270] B. Yavuz, S.B. Pehlivan, İ. Vural, N. Ünlü, In Vitro/In Vivo Evaluation of Dexamethasone—PAMAM Dendrimer Complexes for Retinal Drug Delivery, J. Pharm. Sci. 104 (2015) 3814–3823. https://doi.org/10.1002/JPS.24588.

[271] W. Sun, S. Mao, Y. Shi, L.C. Li, L. Fang, Nanonization of itraconazole by high pressure homogenization: Stabilizer optimization and effect of particle size on oral absorption, J. Pharm. Sci. (2011). https://doi.org/10.1002/jps.22587.

[272] W.T. Huang, M. Larsson, Y.C. Lee, D.M. Liu, G.Y. Chiou, Dual drug-loaded biofunctionalized amphiphilic chitosan nanoparticles: Enhanced synergy between cisplatin and demethoxycurcumin against multidrug-resistant stem-like lung cancer cells, Eur. J. Pharm. Biopharm. (2016). https://doi.org/10.1016/j.ejpb.2016.10.014.

[273] R.N. Wadetwar, A.R. Agrawal, P.S. Kanojiya, In situ gel containing Bimatoprost solid lipid nanoparticles for ocular delivery: In-vitro and ex-vivo evaluation, J. Drug Deliv. Sci. Technol. (2020). https://doi.org/10.1016/j.jddst.2020.101575.

[274] S.A. Abouelmagd, B. Sun, A.C. Chang, Y.J. Ku, Y. Yeo, Release kinetics study of poorly water-soluble drugs from nanoparticles: Are we doing it right?, Mol. Pharm. (2015). https://doi.org/10.1021/mp500817h.

[275] G. Di Prima, F. Bongiovì, F.S. Palumbo, G. Pitarresi, M. Licciardi, G. Giammona, Mucoadhesive PEGylated inulin-based self-assembling nanoparticles: In vitro and ex vivo transcorneal permeation enhancement of corticosteroids, J. Drug Deliv. Sci. Technol. (2019). https://doi.org/10.1016/j.jddst.2018.10.028.

[276] D. Huang, Y.S. Chen, S.S. Thakur, I.D. Rupenthal, Ultrasound-mediated nanoparticle delivery across ex vivo bovine retina after intravitreal injection, Eur. J. Pharm. Biopharm. (2017). https://doi.org/10.1016/j.ejpb.2017.06.009.

[277] X. Xu, Z. Xu, J. Liu, Z. Zhang, H. Chen, X. Li, S. Shi, Visual tracing of diffusion and biodistribution for amphiphilic cationic nanoparticles using photoacoustic imaging after ex vivo intravitreal injections, Int. J.

Nanomedicine. (2016). https://doi.org/10.2147/IJN.S109986.
[278] Q. Bao, B. Newman, Y. Wang, S. Choi, D.J. Burgess, In vitro and ex vivo correlation of drug release from ophthalmic ointments, J. Control. Release. (2018). https://doi.org/10.1016/j.jconrel.2018.03.003.
[279] G.A. Abdelbary, M.M. Amin, M.Y. Zakaria, Ocular ketoconazole-loaded proniosomal gels: Formulation, ex vivo corneal permeation and in vivo studies, Drug Deliv. (2017). https://doi.org/10.1080/10717544.2016.1247928.
[280] A.E. Eldeeb, S. Salah, M. Ghorab, Formulation and evaluation of cubosomes drug delivery system for treatment of glaucoma: Ex-vivo permeation and in-vivo pharmacodynamic study, J. Drug Deliv. Sci. Technol. (2019). https://doi.org/10.1016/j.jddst.2019.04.036.
[281] F.A. Maulvi, M.A. Mangukiya, P.A. Patel, R.J. Vaidya, A.R. Koli, K.M. Ranch, D.O. Shah, Extended release of ketotifen from silica shell nanoparticle-laden hydrogel contact lenses: in vitro and in vivo evaluation, J. Mater. Sci. Mater. Med. (2016). https://doi.org/10.1007/s10856-016-5724-3.
[282] E. Sanchez-Lopez, M.A. Egea, A. Cano, M. Espina, A.C. Calpena, M. Ettcheto, A. Camins, E.B. Souto, A.M. Silva, M.L. Garcia, PEGylated PLGA nanospheres optimized by design of experiments for ocular administration of dexibuprofen-in vitro, ex vivo and in vivo characterization, Colloids Surf B Biointerfaces. 145 (2016) 241–250. https://doi.org/10.1016/j.colsurfb.2016.04.054.
[283] J. Liu, X. Zhang, G. Li, F. Xu, S. Li, L. Teng, Y. Li, F. Sun, Anti-angiogenic activity of bevacizumab-bearing dexamethasone-loaded PLGA nanoparticles for potential intravitreal applications, Int. J. Nanomedicine. (2019). https://doi.org/10.2147/IJN.S217038.
[284] R. Bisht, J.K. Jaiswal, I.D. Rupenthal, Nanoparticle-loaded biodegradable light-responsive in situ forming injectable implants for effective peptide delivery to the posterior segment of the eye, Med. Hypotheses. (2017). https://doi.org/10.1016/j.mehy.2017.03.033.
[285] M. Khalil, U. Hashmi, R. Riaz, S. Rukh Abbas, Chitosan coated liposomes (CCL) containing triamcinolone acetonide for sustained delivery: A potential topical treatment for posterior segment diseases, Int. J. Biol. Macromol. (2020). https://doi.org/10.1016/j.ijbiomac.2019.10.256.
[286] C. Puglia, D. Santonocito, C. Ostacolo, E.M. Sommella, P. Campiglia, C. Carbone, F. Drago, R. Pignatello, C. Bucolo, Ocular formulation based on palmitoylethanolamide-loaded nanostructured lipid carriers: Technological and pharmacological profile, Nanomaterials. (2020). https://doi.org/10.3390/nano10020287.
[287] I. Ahmad, J. Pandit, Y. Sultana, A.K. Mishra, P.P. Hazari, M. Aqil, Optimization by design of etoposide loaded solid lipid nanoparticles for ocular delivery: Characterization, pharmacokinetic and deposition study, Mater. Sci. Eng. C. (2019). https://doi.org/10.1016/j.msec.2019.03.060.
[288] W. Li, L. Chen, Z. Gu, Z. Chen, H. Li, Z. Cheng, H. Li, L. Zou, Co-delivery of microRNA-150 and quercetin by lipid nanoparticles (LNPs) for the targeted treatment of age-related macular degeneration (AMD), J. Control. Release. 355 (2023) 358–370. https://doi.org/https://doi.org/10.1016/j.jconrel.2023.01.080.
[289] R. Varshochian, M. Riazi-Esfahani, M. Jeddi-Tehrani, A.R. Mahmoudi, S. Aghazadeh, M. Mahbod, M. Movassat, F. Atyabi, A. Sabzevari, R. Dinarvand, Albuminated PLGA nanoparticles containing bevacizumab intended for ocular neovascularization treatment, J Biomed Mater Res A. 103 (2015) 3148–3156. https://doi.org/10.1002/jbm.a.35446.
[290] S. Patel, C. Garapati, P. Chowdhury, H. Gupta, J. Nesamony, S. Nauli, S.H. Boddu, Development and evaluation of dexamethasone nanomicelles with potential for treating posterior uveitis after topical application, J Ocul Pharmacol Ther. 31 (2015) 215–227. https://doi.org/10.1089/jop.2014.0152.
[291] M.L. Lovett, X. Wang, T. Yucel, L. York, M. Keirstead, L. Haggerty, D.L. Kaplan, Silk hydrogels for sustained ocular delivery of anti-vascular endothelial growth factor (anti-VEGF) therapeutics, Eur J Pharm Biopharm. 95 (2015) 271–278. https://doi.org/10.1016/j.ejpb.2014.12.029.
[292] B. Xie, L. Jin, Z. Luo, J. Yu, S. Shi, Z. Zhang, M. Shen, H. Chen, X. Li, Z. Song, An injectable thermosensitive polymeric hydrogel for sustained release of Avastin(R) to treat posterior segment disease, Int J Pharm. 490 (2015) 375–383. https://doi.org/10.1016/j.ijpharm.2015.05.071.
[293] B.M. Davis, E.M. Normando, L. Guo, L.A. Turner, S. Nizari, P. O'Shea, S.E. Moss, S. Somavarapu, M.F. Cordeiro, Topical delivery of Avastin to the posterior segment of the eye in vivo using annexin A5-associated liposomes, Small. 10 (2014) 1575–1584. https://doi.org/10.1002/smll.201303433.
[294] R.D. Vaishya, M. Gokulgandhi, S. Patel, M. Minocha, A.K. Mitra, Novel dexamethasone-loaded nanomicelles for the intermediate and posterior segment uveitis, AAPS PharmSciTech. 15 (2014) 1238–1251. https://doi.org/10.1208/s12249-014-0100-4.
[295] W. Wu, Z. He, Z. Zhang, X. Yu, Z. Song, X. Li, Intravitreal injection of rapamycin-loaded polymeric micelles for inhibition of ocular inflammation in rat model, Int J Pharm. 513 (2016) 238–246. https://doi.org/10.1016/j.ijpharm.2016.09.013.

[296] J. Araujo, S. Nikolic, M.A. Egea, E.B. Souto, M.L. Garcia, Nanostructured lipid carriers for triamcinolone acetonide delivery to the posterior segment of the eye, Colloids Surf B Biointerfaces. 88 (2011) 150–157. https://doi.org/10.1016/j.colsurfb.2011.06.025.

[297] Q. Li, K.L. Lai, P.S. Chan, S.C. Leung, H.Y. Li, Y. Fang, K.K.W. To, C.H.J. Choi, Q.Y. Gao, T.W.Y. Lee, Micellar delivery of dasatinib for the inhibition of pathologic cellular processes of the retinal pigment epithelium, Colloids Surf B Biointerfaces. 140 (2016) 278–286. https://doi.org/10.1016/j.colsurfb.2015.12.053.

[298] K. Kauper, C. McGovern, S. Sherman, P. Heatherton, R. Rapoza, P. Stabila, B. Dean, A. Lee, S. Borges, B. Bouchard, W. Tao, Two-year intraocular delivery of ciliary neurotrophic factor by encapsulated cell technology implants in patients with chronic retinal degenerative diseases, Investig. Ophthalmol. Vis. Sci. (2012). https://doi.org/10.1167/iovs.12-9970.

[299] A. Solanki, R. Smalling, A.H. Parola, I. Nathan, R. Kasher, Y. Pathak, V. Sutariya, Humanin Nanoparticles for Reducing Pathological Factors Characteristic of Age-Related Macular Degeneration, Curr. Drug Deliv. (2018). https://doi.org/10.2174/1567201815666181031163111.

[300] C. Chittasupho, P. Posritong, P. Ariyawong, Stability, Cytotoxicity, and Retinal Pigment Epithelial Cell Binding of Hyaluronic Acid-Coated PLGA Nanoparticles Encapsulating Lutein, AAPS PharmSciTech. (2019). https://doi.org/10.1208/s12249-018-1256-0.

[301] V. Agrahari, A. Mandal, V. Agrahari, H.M. Trinh, M. Joseph, A. Ray, H. Hadji, R. Mitra, D. Pal, A.K. Mitra, A comprehensive insight on ocular pharmacokinetics, Drug Deliv. Transl. Res. (2016). https://doi.org/10.1007/s13346-016-0339-2.

[302] A. Hirani, A. Grover, Y.W. Lee, Y. Pathak, V. Sutariya, Triamcinolone acetonide nanoparticles incorporated in thermoreversible gels for age-related macular degeneration, Pharm Dev Technol. 21 (2016) 61–67. https://doi.org/10.3109/10837450.2014.965326.

[303] D. Park, V. Shah, B.M. Rauck, T.R. Friberg, Y. Wang, An Anti-angiogenic Reverse Thermal Gel as a Drug-Delivery System for Age-Related Wet Macular Degeneration, Macromol. Biosci. (2013). https://doi.org/10.1002/mabi.201200384.

[304] A. Tatke, N. Dudhipala, K.Y. Janga, S.P. Balguri, B. Avula, M.M. Jablonski, S. Majumdar, In situ gel of triamcinolone acetonide-loaded solid lipid nanoparticles for improved topical ocular delivery: Tear kinetics and ocular disposition studies, Nanomaterials. (2019). https://doi.org/10.3390/nano9010033.

[305] S.B. Makwana, V.A. Patel, S.J. Parmar, Development and characterization of in-situ gel for ophthalmic formulation containing ciprofloxacin hydrochloride, Results Pharma Sci. (2016). https://doi.org/10.1016/j.rinphs.2015.06.001.

[306] P. Upadhayay, M. Kumar, K. Pathak, Norfloxacin loaded pH triggered nanoparticulate in-situ gel for extraocular bacterial infections: Optimization, ocular irritancy and corneal toxicity, Iran. J. Pharm. Res. (2016). https://doi.org/10.22037/ijpr.2016.1795.

[307] M. Kouchak, M. Mahmoodzadeh, F. Farrahi, Designing of a pH-Triggered Carbopol®/HPMC In Situ Gel for Ocular Delivery of Dorzolamide HCl: In Vitro, In Vivo, and Ex Vivo Evaluation, AAPS PharmSciTech. (2019). https://doi.org/10.1208/s12249-019-1431-y.

[308] M.J. Coffey, H.H. Decory, S.S. Lane, Development of a non-settling gel formulation of 0.5% loteprednol etabonate for anti-inflammatory use as an ophthalmic drop, Clin. Ophthalmol. (2013). https://doi.org/10.2147/OPTH.S40588.

[309] N.J. Kim, A. Harris, A. Elghouche, W. Gama, B. Siesky, Ocular Permeation Enhancers, in: Nano-Biomaterials Ophthalmic Drug Deliv., 2016. https://doi.org/10.1007/978-3-319-29346-2_9.

[310] P. Mehta, A.A. Al-Kinani, O. Qutachi, M.S. Arshad, A. Alqahtani, M.-W. Chang, W.M. Amoaku, R.G. Alany, Z. Ahmad, Assessing the ex vivo permeation behaviour of functionalised contact lens coatings engineered using an electrohydrodynamic technique , J. Phys. Mater. (2018). https://doi.org/10.1088/2515-7639/aaf263.

[311] P. Van Der Bijl, A.D. Van Eyk, D. Meyer, Effects of three penetration enhancers on transcorneal permeation of cyclosporine, Cornea. (2001). https://doi.org/10.1097/00003226-200107000-00013.

[312] Y. Wang, C.H. Liu, T. Ji, M. Mehta, W. Wang, E. Marino, J. Chen, D.S. Kohane, Intravenous treatment of choroidal neovascularization by photo-targeted nanoparticles, Nat. Commun. (2019). https://doi.org/10.1038/s41467-019-08690-4.

[313] A. Gawin-Mikołajewicz, K.P. Nartowski, A.J. Dyba, A.M. Gołkowska, K. Malec, B. Karolewicz, Ophthalmic Nanoemulsions: From Composition to Technological Processes and Quality Control, Mol. Pharm. 18 (2021) 3719–3740. https://doi.org/10.1021/acs.molpharmaceut.1c00650.

[314] J.A. Beutler, Natural Products as a Foundation for Drug Discovery, Curr. Protoc. Pharmacol. 46 (2009) 9.11.1-9.11.21. https://doi.org/https://doi.org/10.1002/0471141755.ph0911s46.

[315] J. Zhang, K. Hu, L. Di, P. Wang, Z. Liu, J. Zhang, P. Yue, W. Song, J. Zhang, T. Chen, Z. Wang, Y. Zhang, X. Wang, C. Zhan, Y.-C. Cheng, X. Li, Q. Li, J.-Y. Fan, Y. Shen, J.-Y. Han, H. Qiao, Traditional herbal medicine and nanomedicine: Converging disciplines to improve therapeutic efficacy and human health, Adv. Drug Deliv. Rev. 178 (2021) 113964. https://doi.org/https://doi.org/10.1016/j.addr.2021.113964.

[316] D. Jorgensen, Clinical Study Protocol, 2020. https://doi.org/https://clinicaltrials.gov/ct2/show/NCT03785340.

[317] S. Silverstein, E. Yeu, J. Tauber, M. Guillon, L. Jones, D. Galarreta, S. Srinivasan, V. Manoj, Symptom relief following a single dose of propylene glycol-hydroxypropyl guar nanoemulsion in patients with dry eye disease: A phase IV, multicenter trial, Clin. Ophthalmol. 14 (2020) 3167–3177. https://doi.org/10.2147/OPTH.S263362.

[318] M. Korenfeld, J. Gira, K. Jong, J. Martel, S. Vold, T. Walters, D. Usner, E. Donnenfeld, OCS-01 (Novel Topical Dexamethasone Formulation) in Inflammation and Pain Post Cataract Surgery: A Randomized, Double-Masked, Vehicle-Controlled Study, Clin. Ther. 44 (2022) 1577–1587. https://doi.org/10.1016/j.clinthera.2022.11.003.

[319] M.M. Momin, S.D. Afreen, Nanoformulations and highlights of clinical studies for ocular drug delivery systems: An overview, Crit. Rev. Ther. Drug Carrier Syst. 38 (2021) 79–107. https://doi.org/10.1615/CritRevTherDrugCarrierSyst.2021035767.

[320] A.L. Onugwu, C.S. Nwagwu, O.S. Onugwu, A.C. Echezona, C.P. Agbo, S.A. Ihim, P. Emeh, P.O. Nnamani, A.A. Attama, V. V Khutoryanskiy, Nanotechnology based drug delivery systems for the treatment of anterior segment eye diseases, J. Control. Release. 354 (2023) 465–488. https://doi.org/https://doi.org/10.1016/j.jconrel.2023.01.018.

[321] G. Birrenbach, P.P. Speiser, Polymerized micelles and their use as adjuvants in immunology, J. Pharm. Sci. (1976). https://doi.org/10.1002/jps.2600651217.

[322] M. Yadav, N. Schiavone, A.I.G. Aranguez, F. Giansanti, L. Papucci, M.J. Perez de Lara, M. Singh, I.P. Kaur, Atorvastatin-loaded solid lipid nanoparticles as eye drops: proposed treatment option for age-related macular degeneration (AMD)., Drug Deliv. Transl. Res. (2020). https://doi.org/10.1007/s13346-020-00733-4.

[323] C. Chittasupho, K. Kengtrong, S. Chalermnithiwong, N. Sarisuta, Anti-angiogenesis by dual action of R5K peptide conjugated itraconazole nanoparticles, AAPS PharmSciTech. (2020). https://doi.org/10.1208/s12249-019-1568-8.

[324] H.M. Eid, M.H. Elkomy, S.F. El Menshawe, H.F. Salem, Development, Optimization, and In Vitro/In Vivo Characterization of Enhanced Lipid Nanoparticles for Ocular Delivery of Ofloxacin: the Influence of Pegylation and Chitosan Coating, AAPS PharmSciTech. (2019). https://doi.org/10.1208/s12249-019-1371-6.

[325] M. Alkholief, H. Albasit, A. Alhowyan, S. Alshehri, M. Raish, M. Abul Kalam, A. Alshamsan, Employing a PLGA-TPGS based nanoparticle to improve the ocular delivery of Acyclovir, Saudi Pharm. J. (2019). https://doi.org/10.1016/j.jsps.2018.11.011.

[326] E. Sánchez-López, G. Esteruelas, A. Ortiz, M. Espina, J. Prat, M. Muñoz, A. Cano, A.C. Calpena, M. Ettcheto, A. Camins, Z. Alsafi, E.B. Souto, M.L. García, M. Pujol, Article dexibuprofen biodegradable nanoparticles: One step closer towards a better ocular interaction study, Nanomaterials. (2020). https://doi.org/10.3390/nano10040720.

[327] S. Liu, M.D. Dozois, C.N. Chang, A. Ahmad, D.L.T. Ng, D. Hileeto, H. Liang, M.M. Reyad, S. Boyd, L.W. Jones, F.X. Gu, Prolonged ocular retention of mucoadhesive nanoparticle eye drop formulation enables treatment of eye diseases using significantly reduced dosage, Mol. Pharm. (2016). https://doi.org/10.1021/acs.molpharmaceut.6b00445.

[328] R. Sheshala, G.C. Hong, W.P. Yee, V.S. Meka, R.R.S. Thakur, In situ forming phase-inversion implants for sustained ocular delivery of triamcinolone acetonide, Drug Deliv Transl Res. (2018). https://doi.org/10.1007/s13346-018-0491-y.

[329] N. Khan, Ameeduzzafar, K. Khanna, A. Bhatnagar, F.J. Ahmad, A. Ali, Chitosan coated PLGA nanoparticles amplify the ocular hypotensive effect of forskolin: Statistical design, characterization and in vivo studies, Int J Biol Macromol. 116 (2018) 648–663. https://doi.org/10.1016/j.ijbiomac.2018.04.122.

[330] B. Şenel, A.A. Öztürk, New approaches to tumor therapy with siRNA-decorated and chitosan-modified PLGA nanoparticles, Drug Dev. Ind. Pharm. (2019). https://doi.org/10.1080/03639045.2019.1665061.

[331] B.J. Thompson, P.T. Ronaldson, Drug delivery to the ischemic brain, Adv. Pharmacol. 71 (2014) 165–202. https://doi.org/10.1016/bs.apha.2014.06.013.

[332] S.W. Tan, N. Billa, C.R. Roberts, J.C. Burley, Surfactant effects on the physical characteristics of Amphotericin B-containing nanostructured lipid carriers, Colloids Surfaces A Physicochem. Eng. Asp. (2010). https://doi.org/10.1016/j.colsurfa.2010.09.030.

[333] S. Akhter, F. Ramazani, M.Z. Ahmad, F.J. Ahmad, Z. Rahman, A. Bhatnagar, G. Storm, Ocular pharmacoscintigraphic and aqueous humoral drug availability of ganciclovir-loaded mucoadhesive nanoparticles in rabbits, Eur. J. Nanomedicine. (2013). https://doi.org/10.1515/ejnm-2013-0012.

[334] B. Silva, J. Marto, B.S. Braz, E. Delgado, A.J. Almeida, L. Gonçalves, New nanoparticles for topical ocular delivery of erythropoietin, Int. J. Pharm. (2020). https://doi.org/10.1016/j.ijpharm.2020.119020.

[335] A.H. Salama, A.A. Mahmoud, R. Kamel, A Novel Method for Preparing Surface-Modified Fluocinolone Acetonide Loaded PLGA Nanoparticles for Ocular Use: In Vitro and In Vivo Evaluations, AAPS PharmSciTech. (2016). https://doi.org/10.1208/s12249-015-0448-0.

[336] S.A. Khan, P.S. Doyle, D. Ding, S. Vijayan, B. Kundukad, A. Somasundar, Design of Mucoadhesive PLGA Microparticles for Ocular Drug Delivery, ACS Appl. Bio Mater. 1 (2018) 561–571. https://doi.org/10.1021/acsabm.8b00041.

[337] A.R.N. Pontillo, A. Detsi, Nanoparticles for ocular drug delivery: Modified and non-modified chitosan as a promising biocompatible carrier, Nanomedicine. (2019). https://doi.org/10.2217/nnm-2019-0040.

[338] A. Seyfoddin, T. Sherwin, D. V. Patel, C. N. McGhee, I. D. Rupenthal, J. A. Taylor, R. Al-Kassas, Ex vivo and In vivo Evaluation of Chitosan Coated Nanostructured Lipid Carriers for Ocular Delivery of Acyclovir, Curr. Drug Deliv. (2016). https://doi.org/10.2174/1567201813666151116142752.

[339] J. Kirch, A. Schneider, B. Abou, A. Hopf, U.F. Schaefer, M. Schneider, C. Schall, C. Wagner, C.M. Lehr, Optical tweezers reveal relationship between microstructure and nanoparticle penetration of pulmonary mucus, Proc Natl Acad Sci U S A. 109 (2012) 18355–18360. https://doi.org/10.1073/pnas.1214066109.

[340] C. Guo, R.A. Gemeinhart, Understanding the adsorption mechanism of chitosan onto poly(lactide-co-glycolide) particles, Eur J Pharm Biopharm. 70 (2008) 597–604. https://doi.org/10.1016/j.ejpb.2008.06.008.

[341] Q. Xu, N.J. Boylan, J.S. Suk, Y.-Y. Wang, E.A. Nance, J.-C. Yang, P.J. McDonnell, R.A. Cone, E.J. Duh, J. Hanes, Nanoparticle diffusion in, and microrheology of, the bovine vitreous ex vivo, J. Control. Release. 167 (2013) 76–84. https://doi.org/https://doi.org/10.1016/j.jconrel.2013.01.018.

[342] D. Chen, H. Yu, H. Mu, G. Li, Y. Shen, Novel multicore niosomes based on double pH-sensitive mixed micelles for Ginsenoside Rh2 delivery, Artif. Cells, Nanomedicine Biotechnol. (2014). https://doi.org/10.3109/21691401.2013.794358.

[343] S.K. Yadav, G. Khan, M. Bansal, H. Vardhan, B. Mishra, Screening of ionically crosslinked chitosan-tripolyphosphate microspheres using Plackett–Burman factorial design for the treatment of intrapocket infections, Drug Dev. Ind. Pharm. (2017). https://doi.org/10.1080/03639045.2017.1349782.

[344] J.N. Betts, M.G. Johnson, P.T. Rygiewicz, G.A. King, C.P. Andersen, Potential for metal contamination by direct sonication of nanoparticle suspensions, Environ. Toxicol. Chem. (2013). https://doi.org/10.1002/etc.2123.

[345] M.J. Santander-Ortega, N. Csaba, L. González, D. Bastos-González, J.L. Ortega-Vinuesa, M.J. Alonso, Protein-loaded PLGA-PEO blend nanoparticles: Encapsulation, release and degradation characteristics, Colloid Polym. Sci. (2010). https://doi.org/10.1007/s00396-009-2131-z.

[346] P.N. Gupta, S. Jain, C. Nehate, N. Alam, V. Khare, R.D. Dubey, A. Saneja, S. Kour, S.K. Singh, Development and evaluation of paclitaxel loaded PLGA: Poloxamer blend nanoparticles for cancer chemotherapy, Int. J. Biol. Macromol. (2014). https://doi.org/10.1016/j.ijbiomac.2014.05.067.

[347] V.V.S.N.L. Andra, S.V.N. Pammi, L.V.K.P. Bhatraju, L.K. Ruddaraju, A Comprehensive Review on Novel Liposomal Methodologies, Commercial Formulations, Clinical Trials and Patents, Bionanoscience. 12 (2022) 274–291. https://doi.org/10.1007/s12668-022-00941-x.

[348] D. Hou, R. Gui, S. Hu, Y. Huang, Z. Feng, Q. Ping, Preparation and Characterization of Novel Drug-Inserted-Montmorillonite Chitosan Carriers for Ocular Drug Delivery, Adv. Nanoparticles. (2015). https://doi.org/10.4236/anp.2015.43009.

[349] A.M. Bodratti, P. Alexandridis, Formulation of poloxamers for drug delivery, J. Funct. Biomater. (2018). https://doi.org/10.3390/jfb9010011.

[350] J.U. Menon, S. Kona, A.S. Wadajkar, F. Desai, A. Vadla, K.T. Nguyen, Effects of surfactants on the properties of PLGA nanoparticles, J. Biomed. Mater. Res. - Part A. (2012). https://doi.org/10.1002/jbm.a.34040.

[351] S. Streck, H. Neumann, H.M. Nielsen, T. Rades, A. McDowell, Comparison of bulk and microfluidics methods for the formulation of poly-lactic-co-glycolic acid (PLGA) nanoparticles modified with cell-penetrating peptides of different architectures, Int. J. Pharm. X. (2019). https://doi.org/10.1016/j.ijpx.2019.100030.

[352] T.A. Ahmed, Preparation of transfersomes encapsulating sildenafil aimed for transdermal drug delivery: Plackett-Burman design and characterization, J. Liposome Res. (2015). https://doi.org/10.3109/08982104.2014.950276.

[353] Z. Rahman, A.S. Zidan, M.J. Habib, M.A. Khan, Understanding the quality of protein loaded PLGA nanoparticles variability by Plackett-Burman design, Int. J. Pharm. (2010). https://doi.org/10.1016/j.ijpharm.2009.12.040.

[354] S. Dhat, S. Pund, C. Kokare, P. Sharma, B. Shrivastava, Risk management and statistical multivariate analysis approach for design and optimization of satranidazole nanoparticles, Eur. J. Pharm. Sci. (2017). https://doi.org/10.1016/j.ejps.2016.09.035.

[355] A.K. Das, S. Dewanjee, Chapter 3 - Optimization of Extraction Using Mathematical Models and Computation, in: S.D. Sarker, L.B.T.-C.P. Nahar (Eds.), Elsevier, 2018: pp. 75–106. https://doi.org/https://doi.org/10.1016/B978-0-12-812364-5.00003-1.

[356] P. Benjasirimongkol, S. Piriyaprasarth, K. Moribe, P. Sriamornsak, Use of Risk Assessment and Plackett–Burman Design for Developing Resveratrol Spray-Dried Emulsions: a Quality-by-Design Approach, AAPS PharmSciTech. 20 (2019) 1–10. https://doi.org/10.1208/s12249-018-1220-z.

[357] N. Khan, Ameeduzzafar, K. Khanna, A. Bhatnagar, F.J. Ahmad, A. Ali, Chitosan coated PLGA nanoparticles amplify the ocular hypotensive effect of forskolin: Statistical design, characterization and in vivo studies, Int. J. Biol. Macromol. (2018). https://doi.org/10.1016/j.ijbiomac.2018.04.122.

[358] B. Taghipour, M. Yakhchali, I. Haririan, A.M. Tamaddon, S.M. Samani, The effects of technical and compositional variables on the size and release profile of bovine serum albumin from PLGA based particulate systems, Res. Pharm. Sci. (2014).

[359] S. Jose, S. Sowmya, T.A. Cinu, N.A. Aleykutty, S. Thomas, E.B. Souto, Surface modified PLGA nanoparticles for brain targeting of Bacoside-A, Eur. J. Pharm. Sci. (2014). https://doi.org/10.1016/j.ejps.2014.06.024.

[360] K. Yoncheva, J. Vandervoort, A. Ludwig, Development of mucoadhesive poly(lactide-co-glycolide) nanoparticles for ocular application, Pharm. Dev. Technol. 16 (2011) 29–35. https://doi.org/10.3109/10837450903479954.

[361] B. Semete, L.I.J. Booysen, L. Kalombo, J.D. Venter, L. Katata, B. Ramalapa, J.A. Verschoor, H. Swai, In vivo uptake and acute immune response to orally administered chitosan and PEG coated PLGA nanoparticles, Toxicol. Appl. Pharmacol. (2010). https://doi.org/10.1016/j.taap.2010.09.002.

[362] A. Kumar, C.K. Dixit, U. States, Methods for characterization of nanoparticles 3, (2017). https://doi.org/10.1016/B978-0-08-100557-6.00003-1.

[363] G. Dalwadi, H.A.E. Benson, Y. Chen, Comparison of diafiltration and tangential flow filtration for purification of nanoparticle suspensions, Pharm. Res. (2005). https://doi.org/10.1007/s11095-005-7781-z.

[364] S. Loganathan, R.B. Valapa, R.K. Mishra, G. Pugazhenthi, S. Thomas, Thermogravimetric Analysis for Characterization of Nanomaterials, in: Therm. Rheol. Meas. Tech. Nanomater. Charact., 2017. https://doi.org/10.1016/B978-0-323-46139-9.00004-9.

[365] M.F. Silva, A.A.W. Hechenleitner, J.M. Irache, A.J.A. De Oliveira, E.A.G. Pineda, Study of thermal degradation of PLGA, PLGA nanospheres and PLGA/maghemite superparamagnetic nanospheres, Mater. Res. 18 (2015) 1400–1406. https://doi.org/10.1590/1516-1439.045415.

[366] Z. Xiao, S. Wan, Y. Niu, X. Kou, Effect of preparation parameters on microparticles with high loading capacity and adsorption property adsorbed on functional paper, Coatings. (2019). https://doi.org/10.3390/coatings9110704.

[367] S. Bandopadhyay, N. Bandyopadhyay, P.K. Deb, C. Singh, R.K. Tekade, Preformulation Studies of Drug Substances, Protein, and Peptides: Role in Drug Discovery and Pharmaceutical Product Development. Role in Drug Discovery and Pharmaceutical Product Development., in: Dos. Form Des. Considerations Vol. I, 2018. https://doi.org/10.1016/B978-0-12-814423-7.00012-5.

[368] T.Z. Fermino, C.M. Awano, L.X. Moreno, D.R. Vollet, F.S. de Vicente, Structure and thermal stability in hydrophobic Pluronic F127-modified silica aerogels, Microporous Mesoporous Mater. (2018). https://doi.org/10.1016/j.micromeso.2018.03.039.

[369] C. D'Avila Carvalho Erbetta, Synthesis and Characterization of Poly(D,L-Lactide-co-Glycolide) Copolymer, J. Biomater. Nanobiotechnol. (2012). https://doi.org/10.4236/jbnb.2012.32027.

[370] N. Elsaid, T.L. Jackson, M. Gunic, S. Somavarapu, Positively charged amphiphilic chitosan derivative for the transscleral delivery of rapamycin, Investig. Ophthalmol. Vis. Sci. (2012). https://doi.org/10.1167/iovs.12-10717.

[371] M.K. Oo, S. Mahmood, W.T. Wui, U.K. Mandal, B. Chatterjee, Effects of Different Formulation Methods on Drug Crystallinity, Drug-Carrier Interaction, and Ex Vivo Permeation of a Ternary Solid Dispersion Containing Nisoldipine, J. Pharm. Innov. (2019). https://doi.org/10.1007/s12247-019-09415-2.

[372] J.J. Rouse, F. Mohamed, C.F. van der Walle, Physical ageing and thermal analysis of PLGA microspheres encapsulating protein or DNA, Int. J. Pharm. 339 (2007) 112–120.

https://doi.org/10.1016/j.ijpharm.2007.02.026.
[373] M.K. Anwer, M.A. Al-Mansoor, S. Jamil, R. Al-Shdefat, M.N. Ansari, F. Shakeel, Development and evaluation of PLGA polymer based nanoparticles of quercetin, Int. J. Biol. Macromol. (2016). https://doi.org/10.1016/j.ijbiomac.2016.07.002.
[374] Ö. Şen, M. Emanet, M. Çulha, Biocompatibility evaluation of boron nitride nanotubes, in: Boron Nitride Nanotub. Nanomedicine, 2016. https://doi.org/10.1016/B978-0-323-38945-7.00003-1.
[375] J.H. Park, H. Jeong, J. Hong, M. Chang, M. Kim, R.S. Chuck, J.K. Lee, C.Y. Park, The Effect of Silica Nanoparticles on Human Corneal Epithelial Cells, Sci. Rep. (2016). https://doi.org/10.1038/srep37762.
[376] M. Hytti, N. Piippo, A. Salminen, P. Honkakoski, K. Kaarniranta, A. Kauppinen, Quercetin alleviates 4-hydroxynonenal-induced cytotoxicity and inflammation in ARPE-19 cells, Exp. Eye Res. (2015). https://doi.org/10.1016/j.exer.2015.02.001.
[377] C. Cañadas, H. Alvarado, A.C. Calpena, A.M. Silva, E.B. Souto, M.L. García, G. Abrego, In vitro, ex vivo and in vivo characterization of PLGA nanoparticles loading pranoprofen for ocular administration, Int. J. Pharm. (2016). https://doi.org/10.1016/j.ijpharm.2016.07.055.
[378] P.J.T. Reardon, M. Parhizkar, A.H. Harker, R.J. Browning, V. Vassileva, E. Stride, R.B. Pedley, M. Edirisinghe, J.C. Knowles, Electrohydrodynamic fabrication of core-shell PLGA nanoparticles with controlled release of cisplatin for enhanced cancer treatment, Int. J. Nanomedicine. (2017). https://doi.org/10.2147/IJN.S134833.
[379] B.D. Kuppermann, L.C. Zacharias, M.C. Kenney, Steroid differentiation: The safety profile of various steroids on retinal cells in vitro and their implications for clinical use (an American ophthalmological society thesis), Trans. Am. Ophthalmol. Soc. 112 (2014) 116–141.
[380] C. Altmeyer, T.K. Karam, N.M. Khalil, R.M. Mainardes, Tamoxifen-loaded poly (L-lactide) nanoparticles : Development , characterization and in vitro evaluation of cytotoxicity, Mater. Sci. Eng. C. 60 (2016) 135–142. https://doi.org/10.1016/j.msec.2015.11.019.
[381] J. Mosafer, K. Abnous, M. Tafaghodi, A. Mokhtarzadeh, M. Ramezani, European Journal of Pharmaceutics and Biopharmaceutics In vitro and in vivo evaluation of anti-nucleolin-targeted magnetic PLGA nanoparticles loaded with doxorubicin as a theranostic agent for enhanced targeted cancer imaging and therapy, Eur. J. Pharm. Biopharm. 113 (2017) 60–74. https://doi.org/10.1016/j.ejpb.2016.12.009.
[382] R. Kaskoos, Investigation of moxifloxacin loaded chitosan-dextran nanoparticles for topical instillation into eye: In-vitro and ex-vivo evaluation, Int. J. Pharm. Investig. (2014). https://doi.org/10.4103/2230-973x.143114.
[383] T. Abdullah, N. Ibrahim, M. Warsi, Chondroitin sulfate-chitosan nanoparticles for ocular delivery of bromfenac sodium: Improved permeation, retention, and penetration, Int. J. Pharm. Investig. (2016). https://doi.org/10.4103/2230-973x.177823.
[384] F. Wang, L. Chen, S. Jiang, J. He, X. Zhang, J. Peng, Q. Xu, R. Li, Optimization of methazolamide-loaded solid lipid nanoparticles for ophthalmic delivery using Box-Behnken design, J. Liposome Res. (2014). https://doi.org/10.3109/08982104.2014.891231.
[385] M. Paulsamy, C. Ponnusamy, M. Palanisami, G. Nackeeran, S.S. Paramasivam, A. Sugumaran, R. Kandasamy, S. Natesan, R. Palanichamy, Nepafenac loaded silica nanoparticles dispersed in-situ gel systems: Development and characterization, Int. J. Biol. Macromol. (2018). https://doi.org/10.1016/j.ijbiomac.2018.01.123.
[386] R. Gonzalez-Pizarro, P. Carvajal-Vidal, L. Halbault Bellowa, A.C. Calpena, M. Espina, M.L. García, In-situ forming gels containing fluorometholone-loaded polymeric nanoparticles for ocular inflammatory conditions, Colloids Surfaces B Biointerfaces. (2019). https://doi.org/10.1016/j.colsurfb.2018.11.065.
[387] M. Dandamudi, P. McLoughlin, G. Behl, S. Rani, L. Coffey, A. Chauhan, D. Kent, L. Fitzhenry, Chitosan-coated plga nanoparticles encapsulating triamcinolone acetonide as a potential candidate for sustained ocular drug delivery, Pharmaceutics. 13 (2021) 1–20. https://doi.org/10.3390/pharmaceutics13101590.
[388] K. Tahara, K. Karasawa, R. Onodera, H. Takeuchi, Feasibility of drug delivery to the eye's posterior segment by topical instillation of PLGA nanoparticles, Asian J. Pharm. Sci. 12 (2017). https://doi.org/10.1016/j.ajps.2017.03.002.
[389] Y. Wang, X. Xu, Y. Gu, Y. Cheng, F. Cao, Recent advance of nanoparticle-based topical drug delivery to the posterior segment of the eye, Expert Opin. Drug Deliv. (2018). https://doi.org/10.1080/17425247.2018.1496080.
[390] M.M. Ibrahim, A.E.H. Abd-Elgawad, O.A.E. Soliman, M.M. Jablonski, Nanoparticle-based topical ophthalmic formulations for sustained celecoxib release, J. Pharm. Sci. (2013). https://doi.org/10.1002/jps.23417.

[391] O. Pillai, R. Panchagnula, Polymers in drug delivery, Curr. Opin. Chem. Biol. (2001). https://doi.org/10.1016/S1367-5931(00)00227-1.
[392] K.T. Savjani, A.K. Gajjar, J.K. Savjani, Drug Solubility: Importance and Enhancement Techniques, ISRN Pharm. (2012). https://doi.org/10.5402/2012/195727.
[393] A. Sabzevari, K. Adibkia, H. Hashemi, A. Hedayatfar, N. Mohsenzadeh, F. Atyabi, M.H. Ghahremani, R. Dinarvand, Polymeric triamcinolone acetonide nanoparticles as a new alternative in the treatment of uveitis: In vitro and in vivo studies, Eur. J. Pharm. Biopharm. (2013). https://doi.org/10.1016/j.ejpb.2012.12.010.
[394] L. Álvarez-Álvarez, L. Barral, R. Bouza, Y. Farrag, F. Otero-Espinar, S. Feijóo-Bandín, F. Lago, Hydrocortisone loaded poly-(3-hydroxybutyrate-co-3-hydroxyvalerate) nanoparticles for topical ophthalmic administration: Preparation, characterization and evaluation of ophthalmic toxicity, Int. J. Pharm. (2019). https://doi.org/10.1016/j.ijpharm.2019.118519.
[395] A. El Shaer, S. Mustafa, M. Kasar, S. Thapa, B. Ghatora, R.G. Alany, Nanoparticle-laden contact lens for controlled ocular delivery of prednisolone: Formulation optimization using statistical experimental design, Pharmaceutics. (2016). https://doi.org/10.3390/pharmaceutics8020014.
[396] I.A. de Lima, N.M. Khalil, T.T. Tominaga, A. Lechanteur, B. Sarmento, R.M. Mainardes, Mucoadhesive chitosan-coated PLGA nanoparticles for oral delivery of ferulic acid, Artif. Cells, Nanomedicine Biotechnol. (2018). https://doi.org/10.1080/21691401.2018.1477788.
[397] T. Feczk, Comparison of the preparation of PLGA – BSA nano- and microparticles by PVA , poloxamer and PVP, 319 (2008) 188–195. https://doi.org/10.1016/j.colsurfa.2007.07.011.
[398] L. Mayol, C. Serri, C. Menale, S. Crispi, M.T. Piccolo, L. Mita, S. Giarra, M. Forte, A. Saija, M. Biondi, D.G. Mita, Curcumin loaded PLGA-poloxamer blend nanoparticles induce cell cycle arrest in mesothelioma cells, Eur. J. Pharm. Biopharm. (2015). https://doi.org/10.1016/j.ejpb.2015.03.005.
[399] S. Giarra, C. Serri, L. Russo, S. Zeppetelli, G. De Rosa, A. Borzacchiello, M. Biondi, L. Ambrosio, L. Mayol, Spontaneous arrangement of a tumor targeting hyaluronic acid shell on irinotecan loaded PLGA nanoparticles, Carbohydr. Polym. (2016). https://doi.org/10.1016/j.carbpol.2015.12.031.
[400] M.J. Santander-Ortega, D. Bastos-González, J.L. Ortega-Vinuesa, M.J. Alonso, Insulin-loaded PLGA nanoparticles for oral administration: An in vitro physico-chemical characterization, J. Biomed. Nanotechnol. (2009). https://doi.org/10.1166/jbn.2009.022.
[401] S. Shaarani, S.S. Hamid, N.H.M. Kaus, The Influence of Pluronic F68 and F127 Nanocarrier on Physicochemical Properties, In vitro Release, and Antiproliferative Activity of Thymoquinone Drug, Pharmacognosy Res. 9 (2017) 12–20. https://doi.org/10.4103/0974-8490.199774.
[402] F. Madani, S.S. Esnaashari, B. Mujokoro, F. Dorkoosh, M. Khosravani, M. Adabi, Investigation of effective parameters on size of paclitaxel loaded PLGA nanoparticles, Adv. Pharm. Bull. 8 (2018) 77–84. https://doi.org/10.15171/apb.2018.010.
[403] R. Kumar, R.C. Nagarwal, M. Dhanawat, J.K. Pandit, In-Vitro and In-Vivo study of indomethacin loaded gelatin nanoparticles, J. Biomed. Nanotechnol. (2011). https://doi.org/10.1166/jbn.2011.1290.
[404] K.J. Sreeram, M. Nidhin, R. Indumathy, B.U. Nair, Synthesis of iron oxide nanoparticles of narrow size distribution on polysaccharide templates, Bull. Mater. Sci. (2008). https://doi.org/10.1007/s12034-008-0016-2.
[405] A. Mathew, T. Fukuda, Y. Nagaoka, T. Hasumura, H. Morimoto, Y. Yoshida, T. Maekawa, K. Venugopal, D.S. Kumar, Curcumin loaded-PLGA nanoparticles conjugated with Tet-1 peptide for potential use in Alzheimer's disease, PLoS One. (2012). https://doi.org/10.1371/journal.pone.0032616.
[406] B. Lu, X. Lv, Y. Le, Chitosan-modified PLGA nanoparticles for control-released drug delivery, Polymers (Basel). (2019). https://doi.org/10.3390/polym11020304.
[407] F. Hu, W. Liu, L. Yan, F. Kong, K. Wei, Optimization and characterization of poly(lactic-co-glycolic acid) nanoparticles loaded with astaxanthin and evaluation of anti-photodamage effect in vitro, R. Soc. Open Sci. (2019). https://doi.org/10.1098/rsos.191184.
[408] W.N. Omwoyo, B. Ogutu, F. Oloo, H. Swai, L. Kalombo, P. Melariri, G.M. Mahanga, J.W. Gathirwa, Preparation, characterization, and optimization of primaquine-loaded solid lipid nanoparticles, Int. J. Nanomedicine. (2014). https://doi.org/10.2147/IJN.S62630.
[409] V. Kunasekaran, K. Krishnamoorthy, Compatibility studies of rasagiline mesylate with selected excipients for an effective solid lipid nanoparticles formulation, Int. J. Pharm. Pharm. Sci. (2015).
[410] E. García-Millán, M. Quintáns-Carballo, F.J. Otero-Espinar, Solid-state characterization of triamcinolone acetonide nanosuspensiones by X-ray spectroscopy, ATR Fourier transforms infrared spectroscopy and differential scanning calorimetry analysis, Data Br. (2017). https://doi.org/10.1016/j.dib.2017.09.002.
[411] M. Kaya, S. Khadem, Y.S. Cakmak, M. Mujtaba, S. Ilk, L. Akyuz, A.M. Salaberria, J. Labidi, A.H.

Abdulqadir, E. Deligöz, Antioxidative and antimicrobial edible chitosan films blended with stem, leaf and seed extracts of Pistacia terebinthus for active food packaging, RSC Adv. (2018). https://doi.org/10.1039/c7ra12070b.

[412] F. Ferrero, M. Periolatto, Antimicrobial finish of textiles by chitosan UV-curing, J. Nanosci. Nanotechnol. (2012). https://doi.org/10.1166/jnn.2012.4902.

[413] Z. Zhang, X. Wang, R. Zhu, Y. Wang, B. Li, Y. Ma, Y. Yin, Synthesis and characterization of serial random and block-copolymers based on lactide and glycolide, Polym. Sci. - Ser. B. (2016). https://doi.org/10.1134/S1560090416060191.

[414] M. Abou-ElNour, R.A.H. Ishak, M. Tiboni, G. Bonacucina, M. Cespi, L. Casettari, M.E. Soliman, A.S. Geneidi, Triamcinolone acetonide-loaded PLA/PEG-PDL microparticles for effective intra-articular delivery: synthesis, optimization, in vitro and in vivo evaluation, J. Control. Release. 309 (2019) 125–144. https://doi.org/10.1016/j.jconrel.2019.07.030.

[415] T. Al Kayal, D. Panetta, B. Canciani, P. Losi, M. Tripodi, S. Burchielli, P. Ottoni, P.A. Salvadori, G. Soldani, Evaluation of the effect of a gamma irradiated DBM-Pluronic F127 composite on bone regeneration in wistar rat, PLoS One. (2015). https://doi.org/10.1371/journal.pone.0125110.

[416] S. Yasmeen, M. Kabiraz, B. Saha, M. Qadir, M. Gafur, S. Masum, Chromium (VI) Ions Removal from Tannery Effluent using Chitosan-Microcrystalline Cellulose Composite as Adsorbent, Int. Res. J. Pure Appl. Chem. (2016). https://doi.org/10.9734/irjpac/2016/23315.

[417] C. Lustriane, F.M. Dwivany, V. Suendo, M. Reza, Effect of chitosan and chitosan-nanoparticles on post harvest quality of banana fruits, J. Plant Biotechnol. (2018). https://doi.org/10.5010/JPB.2018.45.1.036.

[418] G. Dennis, W. Harrison, K. Agnes, G. Erastus, Effect of Biological Control Antagonists Adsorbed on Chitosan Immobilized Silica Nanocomposite on Ralstonia solanacearum and Growth of Tomato Seedlings, Adv. Res. (2016). https://doi.org/10.9734/air/2016/22742.

[419] N. Kamaly, B. Yameen, J. Wu, O.C. Farokhzad, Degradable controlled-release polymers and polymeric nanoparticles: Mechanisms of controlling drug release, Chem. Rev. (2016). https://doi.org/10.1021/acs.chemrev.5b00346.

[420] J.M. Chae, I.J. Oh, Sustained Release of All-trans Retinoic Acid from Chitosan-coated Poly(DL-lactide-co-glycolide) Nanoparticles, Yakhak Hoeji. (2019). https://doi.org/10.17480/psk.2019.63.6.367.

[421] M.L. Bruschi, ed., 5 - Mathematical models of drug release, in: Strateg. to Modify Drug Release from Pharm. Syst., Woodhead Publishing, 2015: pp. 63–86. https://doi.org/https://doi.org/10.1016/B978-0-08-100092-2.00005-9.

[422] D.M. Brown, J.S. Heier, T. Ciulla, M. Benz, P. Abraham, G. Yancopoulos, N. Stahl, A. Ingerman, R. Vitti, A.J. Berliner, K. Yang, Q.D. Nguyen, Primary endpoint results of a phase II study of vascular endothelial growth factor trap-eye in wet age-related macular degeneration, Ophthalmology. 118 (2011) 1089–1097. https://doi.org/10.1016/j.ophtha.2011.02.039.

[423] M.P. Rozing, J.A. Durhuus, M. Krogh Nielsen, Y. Subhi, T.B.L. Kirkwood, R.G.J. Westendorp, T.L. Sørensen, Age-related macular degeneration: A two-level model hypothesis, Prog. Retin. Eye Res. 76 (2020) 100825. https://doi.org/https://doi.org/10.1016/j.preteyeres.2019.100825.

[424] M. Saito, M. Kano, K. Itagaki, Y. Oguchi, T. Sekiryu, Retinal pigment epithelium tear after intravitreal aflibercept injection, Clin. Ophthalmol. (2013). https://doi.org/10.2147/OPTH.S47735.

[425] J. Foucquier, M. Guedj, Analysis of drug combinations: current methodological landscape, Pharmacol. Res. \& Perspect. 3 (2015) e00149. https://doi.org/https://doi.org/10.1002/prp2.149.

[426] K. Hatz, U. Schneider, B. Henrich, B. Braun, S. Sacu, C. Prünte, Comparing ranibizumab monotherapy and combination with single photodynamic therapy in wet AMD: Retreatment and morphologic results, Eur. J. Ophthalmol. (2017). https://doi.org/10.5301/ejo.5000886.

[427] B.D. Kuppermann, M. Goldstein, R.K. Maturi, A. Pollack, M. Singer, A. Tufail, D. Weinberger, X.Y. Li, C.C. Liu, J. Lou, S.M. Whitcup, Dexamethasone Intravitreal Implant as Adjunctive Therapy to Ranibizumab in Neovascular Age-Related Macular Degeneration: A Multicenter Randomized Controlled Trial, Ophthalmologica. (2015). https://doi.org/10.1159/000381865.

[428] P. Zhou, X.-X. Li, Role of genetic factors in the pathogenesis of exudative age-related macular degeneration, Taiwan J. Ophthalmol. 4 (2014) 152–155. https://doi.org/https://doi.org/10.1016/j.tjo.2014.03.007.

[429] K.-H. Wong, H.-Y. Nam, S.-Y. Lew, M. Naidu, P. David, T.A. Kamalden, S.N.H. Hadie, L.-W. Lim, Discovering the Potential of Natural Antioxidants in Age-Related Macular Degeneration: A Review, Pharmaceuticals. 15 (2022). https://doi.org/10.3390/ph15010101.

[430] K. Kaarniranta, D. Sinha, J. Blasiak, A. Kauppinen, Z. Veréb, A. Salminen, M.E. Boulton, G. Petrovski, Autophagy and heterophagy dysregulation leads to retinal pigment epithelium dysfunction and

development of age-related macular degeneration, Autophagy. 9 (2013) 973–984. https://doi.org/10.4161/auto.24546.

[431] V. Sarao, D. Veritti, F. Boscia, P. Lanzetta, Intravitreal steroids for the treatment of retinal diseases, Sci. World J. 2014 (2014). https://doi.org/10.1155/2014/989501.

[432] Y. Shao, H. Yu, Y. Yang, M. Li, L. Hang, X. Xu, A Solid Dispersion of Quercetin Shows Enhanced Nrf2 Activation and Protective Effects against Oxidative Injury in a Mouse Model of Dry Age-Related Macular Degeneration, Oxid. Med. Cell. Longev. 2019 (2019) 1479571. https://doi.org/10.1155/2019/1479571.

[433] J. Bojarska, M. Breza, M. Remko, M. Czyz, A. Gajos-Michniewicz, M. Zimecki, K. Kaczmarek, I.D. Madura, J.M. Wojciechowski, W.M. Wolf, Structural and Biofunctional Insights into the Cyclo(Pro-Pro-Phe-Phe-) Scaffold from Experimental and In Silico Studies: Melanoma and Beyond, Int. J. Mol. Sci. 23 (2022). https://doi.org/10.3390/ijms23137173.

[434] N. Cormier, A. Yeo, E. Fiorentino, J. Paxson, Optimization of the wound scratch assay to detect changes in murine mesenchymal stromal cell migration after damage by soluble cigarette smoke extract, J. Vis. Exp. 2015 (2015) 1–9. https://doi.org/10.3791/53414.

[435] R. Skouta, K. Morán-Santibañez, C.A. Valenzuela, A.H. Vasquez, K. Fenelon, Assessing the Antioxidant Properties of Larrea tridentata Extract as a Potential Molecular Therapy against Oxidative Stress, Molecules. 23 (2018). https://doi.org/10.3390/molecules23071826.

[436] G. Behl, M. Sharma, M. Sikka, S. Dahiya, A. Chhikara, M. Chopra, Gallic acid loaded disulfide cross-linked biocompatible polymeric nanogels as controlled release system: Synthesis, characterization, and antioxidant activity, J. Biomater. Sci. Polym. Ed. 24 (2013) 865–881. https://doi.org/10.1080/09205063.2012.723958.

[437] A. Hirani, A. Grover, Y.W. Lee, Y. Pathak, V. Sutariya, Triamcinolone acetonide nanoparticles incorporated in thermoreversible gels for age-related macular degeneration, Pharm. Dev. Technol. 21 (2016) 61–67. https://doi.org/10.3109/10837450.2014.965326.

[438] C.C. HSIAO, Y.C. CHANG, Y.T. HSIAO, P.H. CHEN, M.C. HSIEH, W.C. WU, Y.H. KAO, Triamcinolone acetonide modulates TGF-β2-induced angiogenic and tissue-remodeling effects in cultured human retinal pigment epithelial cells, Mol. Med. Rep. 24 (2021) 1–10. https://doi.org/10.3892/mmr.2021.12442.

[439] S.C. Cheng, W.C. Huang, J.H.S. Pang, Y.H. Wu, C.Y. Cheng, Quercetin inhibits the production of il-1β-induced inflammatory cytokines and chemokines in arpe-19 cells via the mapk and nf-κb signaling pathways, Int. J. Mol. Sci. (2019). https://doi.org/10.3390/ijms20122957.

[440] N.M.M. Saviranta, L. Veeroos, L.J. Granlund, V.H. Hassinen, K. Kaarniranta, R.O. Karjalainen, Plant flavonol quercetin and isoflavone biochanin A differentially induce protection against oxidative stress and inflammation in ARPE-19 cells, Food Res. Int. (2011). https://doi.org/10.1016/j.foodres.2010.10.056.

[441] X. Wang, H. Li, H. Wang, J. Shi, Quercetin attenuates high glucose-induced injury in human retinal pigment epithelial cell line ARPE-19 by up-regulation of miR-29b, J. Biochem. 167 (2020) 495–502. https://doi.org/10.1093/jb/mvaa001.

[442] M.M. Atsuo, N.S. Asaki, K.S. Aga, T.K. Aneko, Cytotoxicity of Flavonoids toward Cultured Normal Human Cells, 28 (2005) 253–259.

[443] Y. Deng, L. Qiao, M. Du, C. Qu, L. Wan, J. Li, L. Huang, Age-related macular degeneration: Epidemiology, genetics, pathophysiology, diagnosis, and targeted therapy, Genes Dis. 9 (2022) 62–79. https://doi.org/10.1016/j.gendis.2021.02.009.

[444] L.G. Fritsche, R.N. Fariss, D. Stambolian, G.R. Abecasis, C.A. Curcio, A. Swaroop, Age-related macular degeneration: Genetics and biology coming together, Annu. Rev. Genomics Hum. Genet. 15 (2014) 151–171. https://doi.org/10.1146/annurev-genom-090413-025610.

[445] N. Singh, A. Swaroop, R. Ratnapriya, Making Biological Sense of Genetic Studies of Age-Related Macular Degeneration, in: E.Y. Chew, A. Swaroop (Eds.), Age-Related Macular Degener. From Clin. to Genes Back to Patient Manag., Springer International Publishing, Cham, 2021: pp. 201–219. https://doi.org/10.1007/978-3-030-66014-7_8.

[446] H. Keino, S. Horie, S. Sugita, Immune Privilege and Eye-Derived T-Regulatory Cells, J. Immunol. Res. 2018 (2018) 1679197. https://doi.org/10.1155/2018/1679197.

[447] M. Grunin, B. Rinsky, Y. Smith, I. Chowers, Transcriptome Analysis on Monocytes from Patients with Neovascular Age-Related Macular Degeneration, Nat. Publ. Gr. (2016) 1–13. https://doi.org/10.1038/srep29046.

[448] U. Chakravarthy, H. Xu, STAT3 Activation in Circulating Monocytes Contributes to Neovascular Age-Related Macular Degeneration, (2016) 412–423.

[449] J.E. Knickelbein, C.C. Chan, H.N. Sen, F.L. Ferris, R.B. Nussenblatt, Inflammatory mechanisms of age-related macular degeneration, Int. Ophthalmol. Clin. 55 (2015) 63–78.

https://doi.org/10.1097/IIO.0000000000000073.

[450] V.M. Elner, S.G. Elner, Z.-M. Bian, A.L. Kindezelskii, A. Yoshida, H.R. Petty, RPE CD14 immunohistochemical, genetic, and functional expression, Exp. Eye Res. 76 (2003) 321–331. https://doi.org/https://doi.org/10.1016/S0014-4835(02)00310-X.

[451] S.P. Kambhampati, M.K. Mishra, P. Mastorakos, Y. Oh, G.A. Lutty, R.M. Kannan, Intracellular delivery of dendrimer triamcinolone acetonide conjugates into microglial and human retinal pigment epithelial cells, Eur J Pharm Biopharm. 95 (2015) 239–249. https://doi.org/10.1016/j.ejpb.2015.02.013.

[452] X. Zhang, L. Wang, H. Lu, Z. Zong, Z. Chen, Y. Li, X. Luo, Y. Li, Preservation of hydrogen peroxide-induced oxidative damage in HepG-2 cells by rice protein hydrolysates pretreated with electron beams, Sci. Rep. 10 (2020) 8415. https://doi.org/10.1038/s41598-020-64814-7.

[453] T. Hussain, B. Tan, Y. Yin, F. Blachier, M.C.B. Tossou, N. Rahu, Oxidative Stress and Inflammation : What Polyphenols Can Do for Us ?, 2016 (2016). https://doi.org/10.1155/2016/7432797.

[454] X. Zhang, F. Jia, W. Ma, X. Li, X. Zhou, DAD3 targets ACE2 to inhibit the MAPK and NF-κB signalling pathways and protect against LPS-induced inflammation in bovine mammary epithelial cells, Vet. Res. 53 (2022) 104. https://doi.org/10.1186/s13567-022-01122-0.

[455] C. Park, J.S. Noh, Y. Jung, S.-H. Leem, J.W. Hyun, Y.-C. Chang, T.K. Kwon, G.-Y. Kim, H. Lee, Y.H. Choi, Fisetin Attenuated Oxidative Stress-Induced Cellular Damage in ARPE-19 Human Retinal Pigment Epithelial Cells Through Nrf2-Mediated Activation of Heme Oxygenase-1, Front. Pharmacol. 13 (2022). https://doi.org/10.3389/fphar.2022.927898.

[456] D. Gunawardena, R. Raju, G. Münch, Hydrogen peroxide mediates pro-inflammatory cell-to-cell signaling: A new therapeutic target for inflammation?, Neural Regen. Res. 14 (2019) 1430–1437. https://doi.org/10.4103/1673-5374.253529.

[457] S. Paeng Hwa, W. Park Sun, W.-K. Jung, D.-S. Lee, G.-Y. Kim, Y. Choi Hyun, S.-K. Seo, W. Jang Hee, J. Choi Sik, Y.-M. Lee, S. Park, I.-W. Choi, YCG063 inhibits Pseudomonas aeruginosa LPS-induced inflammation in human retinal pigment epithelial cells through the TLR2-mediated AKT/NF-κB pathway and ROS-independent pathways, Int J Mol Med. 36 (2015) 808–816. https://doi.org/10.3892/ijmm.2015.2266.

[458] S. Imai, T. Otsuka, A. Naito, M.S. and H. Hara, Triamcinolone Acetonide Suppresses Inflammation and Facilitates Vascular Barrier Function in Human Retinal Microvascular Endothelial Cells, Curr. Neurovasc. Res. 14 (2017) 232–241. https://doi.org/http://dx.doi.org/10.2174/1567202614666170619081929.

[459] P.J. Barnes, How corticosteroids control inflammation: Quintiles Prize Lecture 2005, Br. J. Pharmacol. 148 (2006) 245–254. https://doi.org/10.1038/sj.bjp.0706736.

[460] U. Klueh, C. Czajkowski, I. Ludzinska, Y. Qiao, J. Frailey, D.L. Kreutzer, Impact of CCL2 and CCR2 chemokine/receptor deficiencies on macrophage recruitment and continuous glucose monitoring in vivo, Biosens. Bioelectron. 86 (2016) 262–269. https://doi.org/https://doi.org/10.1016/j.bios.2016.06.026.

[461] L.Q. Meng, F.Y. Yang, M.S. Wang, B.K. Shi, D.X. Chen, D. Chen, Q. Zhou, Q.B. He, L.X. Ma, W.L. Cheng, N.Z. Xing, Quercetin protects against chronic prostatitis in rat model through NF-κB and MAPK signaling pathways, Prostate. 78 (2018) 790–800. https://doi.org/10.1002/pros.23536.

[462] Y.-D. Min, C.-H. Choi, H. Bark, H.-Y. Son, H.-H. Park, S. Lee, J.-W. Park, E.-K. Park, H.-I. Shin, S.-H. Kim, Quercetin inhibits expression of inflammatory cytokines through attenuation of NF-κB and p38 MAPK in HMC-1 human mast cell line, Inflamm. Res. 56 (2007) 210–215. https://doi.org/10.1007/s00011-007-6172-9.

[463] Y. Bian, P. Liu, J. Zhong, Y. Hu, S. Zhuang, K. Fan, Z. Liu, Quercetin Attenuates Adhesion Molecule Expression in Intestinal Microvascular Endothelial Cells by Modulating Multiple Pathways, Dig. Dis. Sci. 63 (2018) 3297–3304. https://doi.org/10.1007/s10620-018-5221-2.

[464] C. Li, W.-J. Zhang, B. Frei, Quercetin inhibits LPS-induced adhesion molecule expression and oxidant production in human aortic endothelial cells by p38-mediated Nrf2 activation and antioxidant enzyme induction, Redox Biol. 9 (2016) 104–113. https://doi.org/https://doi.org/10.1016/j.redox.2016.06.006.

[465] K. Pitarokoili, M. Sgodzai, T. Grüter, H. Bachir, J. Motte, B. Ambrosius, X. Pedreiturria, M.S. Yoon, R. Gold, Intrathecal triamcinolone acetonide exerts anti-inflammatory effects on Lewis rat experimental autoimmune neuritis and direct anti-oxidative effects on Schwann cells, J. Neuroinflammation. 16 (2019) 1–12. https://doi.org/10.1186/s12974-019-1445-0.

[466] A. Pugazhendhi, M. Hubbell, P. Jairam, B. Ambati, Neovascular Macular Degeneration: A Review of Etiology, Risk Factors, and Recent Advances in Research and Therapy, Int. J. Mol. Sci. 22 (2021). https://doi.org/10.3390/ijms22031170.

[467] C.S. Melincovici, A.B. Boşca, S. Şuşman, M. Mărginean, C. Mihu, M. Istrate, I.M. Moldovan, A.L. Roman, C.M. Mihu, Vascular endothelial growth factor (VEGF) – key factor in normal and pathological angiogenesis, Rom. J. Morphol. Embryol. 59 (2018) 455–467.

[468] M. Nobl, M. Reich, I. Dacheva, J. Siwy, W. Mullen, J.P. Schanstra, C.Y. Choi, J. Kopitz, F.T.A. Kretz, G.U. Auffarth, F. Koch, M.J. Koss, Proteomics of vitreous in neovascular age-related macular degeneration, Exp. Eye Res. 146 (2016) 107–117. https://doi.org/https://doi.org/10.1016/j.exer.2016.01.001.

[469] J.S. Penn, A. Madan, R.B. Caldwell, M. Bartoli, R.W. Caldwell, M.E. Hartnett, Vascular endothelial growth factor in eye disease, Prog. Retin. Eye Res. 27 (2008) 331–371. https://doi.org/10.1016/j.preteyeres.2008.05.001.

[470] S.M. Kaiser, S. Arepalli, J.P. Ehlers, Current and future anti-VEGF agents for neovascular age-related macular degeneration, J. Exp. Pharmacol. 13 (2021) 905–912. https://doi.org/10.2147/JEP.S259298.

[471] G.C. Teague, W. Johnson, M. Shatos, M.E. Baldwin, K. Lashkari, Plasma Levels of VEGF-C and Soluble VEGF Receptor-3 are Elevated in Neovascular AMD, Invest. Ophthalmol. Vis. Sci. 58 (2017) 2327.

[472] G.C. Teague, J. Ma, W. Johnson, M.E. Baldwin, K. Lashkari, Expression of VEGF-A, VEGF-C, VEGF-D and soluble receptors in Clinical Age-Related Macular Degeneration, Invest. Ophthalmol. Vis. Sci. 57 (2016) 3698.

[473] P. Pratheeshkumar, A. Budhraja, Y.O. Son, X. Wang, Z. Zhang, S. Ding, L. Wang, A. Hitron, J.C. Lee, M. Xu, G. Chen, J. Luo, X. Shi, Quercetin Inhibits Angiogenesis Mediated Human Prostate Tumor Growth by Targeting VEGFR- 2 Regulated AKT/mTOR/P70S6K Signaling Pathways, PLoS One. 7 (2012) 1–10. https://doi.org/10.1371/journal.pone.0047516.

[474] S. Richer, W. Stiles, L. Ulanski, D. Carroll, C. Podella, Observation of Human Retinal Remodeling in Octogenarians with a Resveratrol Based Nutritional Supplement, Nutrients. 5 (2013) 1989–2005. https://doi.org/10.3390/nu5061989.

[475] S. Richer, S. Patel, S. Sockanathan, L.J. Ulanski, L. Miller, C. Podella, Resveratrol Based Oral Nutritional Supplement Produces Long-Term Beneficial Effects on Structure and Visual Function in Human Patients, Nutrients. 6 (2014) 4404–4420. https://doi.org/10.3390/nu6104404.

[476] H. Zhou, L. Yang, H. Li, H. Gong, L. Cheng, H. Zheng, L.M. Zhang, Y. Lan, Downregulation of VEGF mRNA expression by triamcinolone acetonide acetate-loaded chitosan derivative nanoparticles in human retinal pigment epithelial cells, Int. J. Nanomedicine. 7 (2012) 4649–4660. https://doi.org/10.2147/IJN.S29690.

[477] J.E. Sears, G. Hoppe, Triamcinolone Acetonide Destabilizes VEGF mRNA in Müller Cells under Continuous Cobalt Stimulation, Invest. Ophthalmol. Vis. Sci. 46 (2005) 4336–4341. https://doi.org/10.1167/iovs.05-0565.

[478] E. Birben, U.M. Sahiner, C. Sackesen, S. Erzurum, O. Kalayci, Oxidative Stress and Antioxidant Defense, World Allergy Organ. J. 5 (2012) 9–19. https://doi.org/10.1097/WOX.0b013e3182439613.

[479] S. Datta, M. Cano, K. Ebrahimi, L. Wang, J.T. Handa, The impact of oxidative stress and inflammation on RPE degeneration in non-neovascular AMD, Prog. Retin. Eye Res. 60 (2017) 201–218. https://doi.org/https://doi.org/10.1016/j.preteyeres.2017.03.002.

[480] D. Harman, Lawrence Berkeley National Laboratory Recent Work Title AGING: A THEORY BASED ON FREE RADICAL AND RADIATION CHEMISTRY, (1955) Lawrence Berkeley National Laboratory. https://escholarship.org/uc/item/3w86c4g7.

[481] I. V Ivanov, T. Mappes, P. Schaupp, C. Lappe, S. Wahl, Ultraviolet radiation oxidative stress affects eye health, J. Biophotonics. 11 (2018) e201700377. https://doi.org/https://doi.org/10.1002/jbio.201700377.

[482] W.K. Noell, V.S. Walker, B.S. Kang, S. Berman, Retinal damage by light in rats., Invest. Ophthalmol. 5 (1966) 450–473.

[483] I. Rahman, W. MacNee, Role of oxidants/antioxidants in smoking-induced lung diseases, Free Radic. Biol. Med. 21 (1996) 669–681. https://doi.org/https://doi.org/10.1016/0891-5849(96)00155-4.

[484] I. Bellezza, I. Giambanco, A. Minelli, R. Donato, Nrf2-Keap1 signaling in oxidative and reductive stress, Biochim. Biophys. Acta - Mol. Cell Res. 1865 (2018) 721–733. https://doi.org/https://doi.org/10.1016/j.bbamcr.2018.02.010.

[485] A.C. Gonçalves, C. Bento, F. Jesus, G. Alves, L.R. Silva, Chapter 2 - Sweet Cherry Phenolic Compounds: Identification, Characterization, and Health Benefits, in: Atta-ur-Rahman (Ed.), Elsevier, 2018: pp. 31–78. https://doi.org/https://doi.org/10.1016/B978-0-444-64179-3.00002-5.

[486] C. Caddeo, M. Gabriele, X. Fernàndez-Busquets, D. Valenti, A.M. Fadda, L. Pucci, M. Manconi, Antioxidant activity of quercetin in Eudragit-coated liposomes for intestinal delivery, Int. J. Pharm. 565 (2019) 64–69. https://doi.org/https://doi.org/10.1016/j.ijpharm.2019.05.007.

[487] T. Hatahet, M. Morille, A. Shamseddin, A. Aubert-Pouëssel, J.M. Devoisselle, S. Bégu, Dermal quercetin lipid nanocapsules: Influence of the formulation on antioxidant activity and cellular protection against hydrogen peroxide, Int. J. Pharm. 518 (2017) 167–176. https://doi.org/https://doi.org/10.1016/j.ijpharm.2016.12.043.

[488] Y. Murakami, A. Kawata, S. Ito, T. Katayama, S. Fujisawa, Radical-scavenging and anti-inflammatory activity of quercetin and related compounds and their combinations against RAW264.7 cells stimulated with porphyromonas gingivalis fimbriae. relationships between anti-inflammatory activity and quantum chemical par, In Vivo (Brooklyn). (2015).

[489] D. Xu, M.-J. Hu, Y.-Q. Wang, Y.-L. Cui, Antioxidant Activities of Quercetin and Its Complexes for Medicinal Application, Molecules. 24 (2019). https://doi.org/10.3390/molecules24061123.

[490] M. Suntiparpluacha, N. Tammachote, R. Tammachote, Triamcinolone acetonide reduces viability, induces Oxidative Stress , and Alters Gene Expressions of Human Chondrocytes, Eur Rev Med Pharmacol Sci. 20 (2016) 4985–4992.

[491] J.-M. You, S.-J. Yun, K.N. Nam, C. Kang, R. Won, E.H. Lee, Mechanism of glucocorticoid-induced oxidative stress in rat hippocampal slice cultures, Can. J. Physiol. Pharmacol. 87 (2009) 440–447. https://doi.org/10.1139/Y09-027.

[492] V.M. Tang, A.H. Young, H. Tan, C. Beasley, J.F. Wang, Glucocorticoids increase protein carbonylation and mitochondrial dysfunction, Horm. Metab. Res. 45 (2013) 709–715. https://doi.org/10.1055/s-0033-1345119.

[493] A. Tisi, M. Feligioni, M. Passacantando, M. Ciancaglini, R. Maccarone, The Impact of Oxidative Stress on Blood-Retinal Barrier Physiology in Age-Related Macular Degeneration, Cells. 10 (2021). https://doi.org/10.3390/cells10010064.

[494] A. Stahl, Diagnostik und Therapie der altersabhängigen Makuladegeneration, Dtsch. Arztebl. Int. 117 (2020) 513–520. https://doi.org/10.3238/arztebl.2020.0513.

[495] S.H. Sarks, New vessel formation beneath the retinal pigment epithelium in senile eyes, Br. J. Ophthalmol. 57 (1973) 951–965. https://doi.org/10.1136/bjo.57.12.951.

[496] S.H. Sarks, Ageing and degeneration in the macular region: a clinico-pathological study., Br. J. Ophthalmol. 60 (1976) 324 LP – 341. https://doi.org/10.1136/bjo.60.5.324.

[497] R. Simó, M. Villarroel, L. Corraliza, C. Hernández, M. Garcia-Ramírez, The Retinal Pigment Epithelium: Something More than a Constituent of the Blood-Retinal Barrier—Implications for the Pathogenesis of Diabetic Retinopathy, J. Biomed. Biotechnol. 2010 (2010) 190724. https://doi.org/10.1155/2010/190724.

[498] J.H.C. Wong, J.Y.W. Ma, A.I. Jobling, A. Brandli, U. Greferath, E.L. Fletcher, K.A. Vessey, Exploring the pathogenesis of age-related macular degeneration: A review of the interplay between retinal pigment epithelium dysfunction and the innate immune system, Front. Neurosci. 16 (2022) 1–21. https://doi.org/10.3389/fnins.2022.1009599.

[499] F. Irfan, F. Jameel, I. Khan, R. Aslam, S. Faizi, A. Salim, Role of quercetin and rutin in enhancing the therapeutic potential of mesenchymal stem cells for cold induced burn wound, Regen. Ther. 21 (2022) 225–238. https://doi.org/10.1016/j.reth.2022.07.011.

[500] A. Gopalakrishnan, M. Ram, S. Kumawat, S.K. Tandan, D. Kumar, Quercetin accelerated cutaneous wound healing in rats by increasing levels of VEGF and TGF-β1, Indian J. Exp. Biol. 54 (2016) 187–195.

[501] L.S.H. Kim Jae Woo Lee Jae Hyung, Role of Nitric Oxide in the Proliferative and Migratory Effect of Triamcinolone in RPE Cells, Jkos. 51 (2010) 120–125. https://doi.org/10.3341/jkos.2010.51.1.120.

[502] C.N. Thomas, D.A. Sim, W.H. Lee, N. Alfahad, A.D. Dick, A.K. Denniston, L.J. Hill, Emerging therapies and their delivery for treating age-related macular degeneration, Br. J. Pharmacol. 179 (2022) 1908–1937. https://doi.org/https://doi.org/10.1111/bph.15459.

[503] H. Lin, Y. Yue, D.E. Maidana, P. Bouzika, A. Atik, H. Matsumoto, J.W. Miller, D.G. Vavvas, Drug Delivery Nanoparticles: Toxicity Comparison in Retinal Pigment Epithelium and Retinal Vascular Endothelial Cells, Semin. Ophthalmol. 31 (2016) 1–9. https://doi.org/10.3109/08820538.2015.1114865.

[504] K. Tahara, K. Karasawa, R. Onodera, H. Takeuchi, Feasibility of drug delivery to the eye's posterior segment by topical instillation of PLGA nanoparticles, Asian J. Pharm. Sci. (2017). https://doi.org/10.1016/j.ajps.2017.03.002.

[505] Y. Tsugita, S. Maeda, Colloidal stability of polypyrrole-ITO conducting inks, Jpn. J. Appl. Phys. 61 (2022). https://doi.org/10.35848/1347-4065/ac564f.

[506] M. Kersting, M. Olejnik, N. Rosenkranz, K. Loza, M. Breisch, A. Rostek, G. Westphal, J. Bünger, N. Ziegler, A. Ludwig, M. Köller, C. Sengstock, M. Epple, Subtoxic cell responses to silica particles with different size and shape, Sci. Rep. 10 (2020) 1–17. https://doi.org/10.1038/s41598-020-78550-5.

[507] S. Fredenberg, M. Wahlgren, M. Reslow, A. Axelsson, The mechanisms of drug release in poly(lactic-co-glycolic acid)-based drug delivery systems—A review, Int. J. Pharm. 415 (2011) 34–52. https://doi.org/https://doi.org/10.1016/j.ijpharm.2011.05.049.

[508] N.S. Heredia, K. Vizuete, M. Flores-Calero, K. Pazmiño V., F. Pilaquinga, B. Kumar, A. Debut, Comparative statistical analysis of the release kinetics models for nanoprecipitated drug delivery

systems based on poly(lactic-co-glycolic acid), PLoS One. 17 (2022) e0264825. https://doi.org/10.1371/journal.pone.0264825.

[509] Y. Xu, C.-S. Kim, D.M. Saylor, D. Koo, Polymer degradation and drug delivery in PLGA-based drug–polymer applications: A review of experiments and theories, J. Biomed. Mater. Res. Part B Appl. Biomater. 105 (2017) 1692–1716. https://doi.org/https://doi.org/10.1002/jbm.b.33648.

[510] S. Pimple, A.S. Manjappa, M. Ukawala, R.S.R. Murthy, PLGA nanoparticles loaded with etoposide and quercetin dihydrate individually: in vitro cell line study to ensure advantage of combination therapy, Cancer Nanotechnol. 3 (2012) 25–36. https://doi.org/10.1007/s12645-012-0027-y.

[511] M.S. Deepika, R. Thangam, T.S. Sheena, R.T.V. Vimala, S. Sivasubramanian, K. Jeganathan, R. Thirumurugan, Dual drug loaded PLGA nanospheres for synergistic efficacy in breast cancer therapy, Mater. Sci. Eng. C. 103 (2019) 109716. https://doi.org/10.1016/j.msec.2019.05.001.

[512] A. Hardenia, N. Maheshwari, S.S. Hardenia, S.K. Dwivedi, R. Maheshwari, R.K. Tekade, Chapter 1 - Scientific Rationale for Designing Controlled Drug Delivery Systems, in: R.K.B.T.-B.F. of D.D. Tekade (Ed.), Adv. Pharm. Prod. Dev. Res., Academic Press, 2019: pp. 1–28. https://doi.org/https://doi.org/10.1016/B978-0-12-817909-3.00001-7.

[513] L.R. Steeples, N.P. Jones, I. Leal, Evaluating the Safety , Efficacy and Patient Acceptability of Intravitreal Fluocinolone Acetonide (0 . 2mcg / Day) Implant in the Treatment of Non-Infectious Uveitis Affecting the Posterior Segment, (2021).

[514] A. Hirani, A. Grover, Y.W. Lee, Y. Pathak, V. Sutariya, Triamcinolone acetonide nanoparticles incorporated in thermoreversible gels for age-related macular degeneration, Pharm. Dev. Technol. (2016). https://doi.org/10.3109/10837450.2014.965326.

[515] D. Guo, Q. Li, Y. Sun, J. Guo, Q. Zhao, X. Yin, H. Wei, S. Wu, H. Bi, Evaluation of controlled-release triamcinolone acetonide-loaded mPEG-PLGA nanoparticles in treating experimental autoimmune uveitis, Nanotechnology. 30 (2019) 165702.

[516] L.R. Schopf, A.M. Popov, E.M. Enlow, J.L. Bourassa, W.Z. Ong, P. Nowak, H. Chen, Topical ocular drug delivery to the back of the eye by mucus-penetrating particles, Transl. Vis. Sci. Technol. (2015). https://doi.org/10.1167/tvst.4.3.11.

[517] T. Bíró, Z. Aigner, Current approaches to use cyclodextrins and mucoadhesive polymers in ocular drug delivery-a mini-review, Sci. Pharm. 87 (2019). https://doi.org/10.3390/scipharm87030015.

[518] S. Akhter, M. Anwar, M.A. Siddiqui, I. Ahmad, J. Ahmad, M.Z. Ahmad, A. Bhatnagar, F.J. Ahmad, Improving the topical ocular pharmacokinetics of an immunosuppressant agent with mucoadhesive nanoemulsions: Formulation development, in-vitro and in-vivo studies, Colloids Surfaces B Biointerfaces. 148 (2016) 19–29. https://doi.org/10.1016/j.colsurfb.2016.08.048.

[519] A.H. Salama, A.A. Mahmoud, R. Kamel, A Novel Method for Preparing Surface-Modified Fluocinolone Acetonide Loaded PLGA Nanoparticles for Ocular Use: In Vitro and In Vivo Evaluations, AAPS PharmSciTech. 17 (2015) 1159–1172. https://doi.org/10.1208/s12249-015-0448-0.

[520] E. Agrón, J. Mares, T.E. Clemons, A. Swaroop, E.Y. Chew, T.D.L. Keenan, Dietary Nutrient Intake and Progression to Late Age-Related Macular Degeneration in the Age-Related Eye Disease Studies 1 and 2, Ophthalmology. 128 (2021) 425–442. https://doi.org/https://doi.org/10.1016/j.ophtha.2020.08.018.

[521] K. Peynshaert, J. Devoldere, S.C. De Smedt, K. Remaut, In vitro and ex vivo models to study drug delivery barriers in the posterior segment of the eye, Adv Drug Deliv Rev. 126 (2018) 44–57. https://doi.org/10.1016/j.addr.2017.09.007.

[522] R. Zhang, X. Qin, F. Kong, P. Chen, G. Pan, Improving cellular uptake of therapeutic entities through interaction with components of cell membrane, Drug Deliv. 26 (2019) 328–342. https://doi.org/10.1080/10717544.2019.1582730.

[523] S. Zhu, L. Gong, Y. Li, H. Xu, Z. Gu, Y. Zhao, Safety Assessment of Nanomaterials to Eyes: An Important but Neglected Issue, Adv. Sci. 6 (2019) 1802289. https://doi.org/https://doi.org/10.1002/advs.201802289.

[524] P. Bhatt, P. Narvekar, R. Lalani, M.B. Chougule, Y. Pathak, V. Sutariya, An in vitro Assessment of Thermo-Reversible Gel Formulation Containing Sunitinib Nanoparticles for Neovascular Age-Related Macular Degeneration, AAPS PharmSciTech. 20 (2019). https://doi.org/10.1208/s12249-019-1474-0.

[525] W.L.L. Suen, Y. Chau, Specific uptake of folate-decorated triamcinolone-encapsulating nanoparticles by retinal pigment epithelium cells enhances and prolongs antiangiogenic activity, J. Control. Release. (2013). https://doi.org/10.1016/j.jconrel.2013.01.004.

[526] L. Hellinen, H. Hongisto, E. Ramsay, K. Kaarniranta, K.S. Vellonen, H. Skottman, M. Ruponen, Drug flux across RPE cell models: The hunt for an appropriate outer blood–retinal barrier model for use in early drug discovery, Pharmaceutics. (2020). https://doi.org/10.3390/pharmaceutics12020176.

[527] J.R. Costa, N.C. Silva, B. Sarmento, M. Pintado, Potential chitosan-coated alginate nanoparticles for

ocular delivery of daptomycin, Eur. J. Clin. Microbiol. Infect. Dis. (2015). https://doi.org/10.1007/s10096-015-2344-7.

[528] S. Pescina, P. Govoni, A. Potenza, C. Padula, P. Santi, S. Nicoli, Development of a Convenient ex vivo Model for the Study of the Transcorneal Permeation of Drugs: Histological and Permeability Evaluation, J. Pharm. Sci. 104 (2015) 63–71. https://doi.org/10.1002/jps.24231.

[529] M.R. Mulenos, H. Lujan, L.R. Pitts, C.M. Sayes, Silver Nanoparticles Agglomerate Intracellularly Depending on the Stabilizing Agent: Implications for Nanomedicine Efficacy, Nanomaterials. 10 (2020). https://doi.org/10.3390/nano10101953.